User guide for the **SASfit** software package

A program for fitting elementary structural models
to small angle scattering data

April 30, 2013

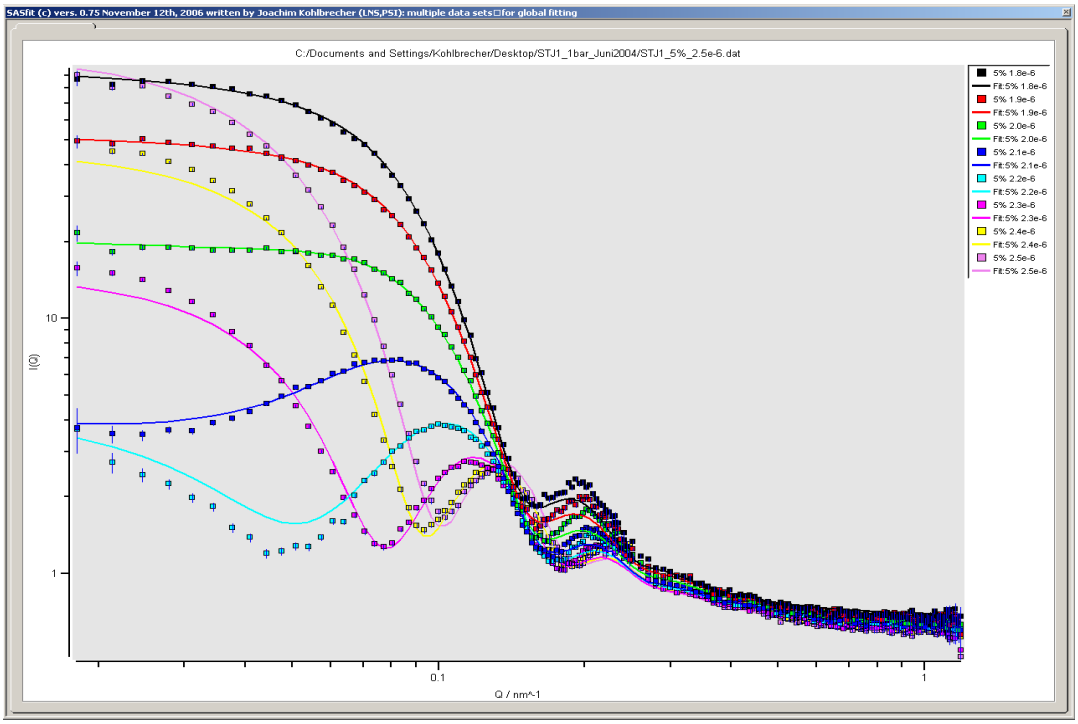

SASfit: A program for fitting simple structural models to small angle scattering data

Joachim Kohlbrecher

Paul Scherrer Institute
Laboratory for Neutron Scattering (LNS)
CH-5232 Villigen PSI
joachim.kohlbrecher@psi.ch

April 30, 2013

Abstract. SASfit has been written for analyzing and plotting small angle scattering data. It can calculate integral structural parameters like radius of gyration, scattering invariant, Porod constant. Furthermore it can fit size distributions together with several form factors including different structure factors. Additionally an algorithm has been implemented, which allows to simultaneously fit several scattering curves with a common set of (global) parameters. This last option is especially important in contrast variation experiments or measurements with polarised neutrons. The global fit helps to determine fit parameters unambiguously which by analyzing a single curve would be otherwise strongly correlated. The program has been written to fulfill the needs at the small angle neutron scattering facility at PSI (http://kur.web.psi.ch). The numerical routines have been written in C whereas the menu interface has been written in tcl/tk and the plotting routine with the extension blt. The newest SASfit version can be downloaded from http://kur.web.psi.ch/sans1/SANSSoft/sasfit.html.

Contents

CHAPTER 1

Introduction to the data analysis program SASfit

Small-angle scattering (SAS) is one of the powerful techniques to investigate the structure of materials on a mesoscopic length scale (10 - 10000 Å). It is used to study the shapes and sizes of the particles dispersed in a homogenous medium. The materials could be a macromolecule (biological molecule, polymer, micelle, etc) in a solvent, a precipitate of material A in a matrix of another material B, a microvoid in certain metal or a magnetic inhomogeneity in a nonmoagnetic material. This technique is also used to study the spatial distribution of particles in a medium, thus providing the information about the inter-particle interactions. The small angle scattering methods includes small angle neutron, x-ray or light scattering. The type of samples that can be studied by scattering techniques, the sample environment that can be applied, the actual length scale probed and the information that can be obtained, all depend on the nature of the radiation employed. The advantage of small-angle neutron scattering (SANS) over other SAS methods is the deuteration method. This consists in using deuterium labeled components in the sample in order to enhance their contrast. Whereas SANS has disadvantaged over small-angle x-ray scattering (SAXS) by the intrinsically low flux of neutron sources compared to the orders of magnitude higher fluxes of x-ray sources. Neutron scattering in general is sensitive to fluctuations in the density of nuclei in the sample. X-ray scattering is sensitive to inhomogeneities in electron densities whereas light scattering is sensitive to fluctuations in polarizability (refractive index). In general, irrespective of the type of radiation, they also share several similarities. Perhaps the most important of these is the fact that, with minor adjustments to account for the different types of radiation, the same basic equations and laws can be used to analyze data from these techniques. The small-angle scattering data can contain information concerning both the structure and interaction within the sytem. This information can be obtained by either performing model-independent analysis or detailed model dependent analysis. `SASfit` is such a software package built for analysis of small-angle neutron scattering data concerning soft matter. The main emphasis of the software is to provide easy to use visual interface for the new as well as for an expert user. The software package contains most of the tools to treat large range of scientific problems and large volume of data produced on a SAS instrument. It allows users to derive useful information from the SAS scattering data.

1.1. System Requirements And Software Installation

`SASfit` is a program for analyzing small angle scattering data. The numerical fitting routines are written in C and the menu interface in `tcl/tk`. For the plotting of the data the `tcl` extension `blt` has been used. The last version 0.85 of `SASfit` has been

tested with the tcl/tk version 8.3 and the blt version 2.4s.

SASfit is available for users analysing data taken at PSI.
SASfit has been developed at the Paul Scherrer Institute (PSI) and remains © of PSI.
SASfit is provided to users of the PSI facilities.
SASfit is provided "as is", and with no warranty.

1.1.1. Installation Procedure.

SASfit has has been compiled with tcl/tk 8.4 and Blt 2.4. To install the SASfit package one has to do the following:

(1) Download the zip-file "sasfit.zip" from the SASfit-home page
    http://kur.web.psi.ch/sans1/SANSSoft/sasfit.html
(2) extract the contents of the zip file. A new subdirectory called sasfit will be generated, which contains all required files.
(3) Execute the program ./sasfit/sasfit.exe

CHAPTER 2

Quick Start Tour

2.1. User Interface Window

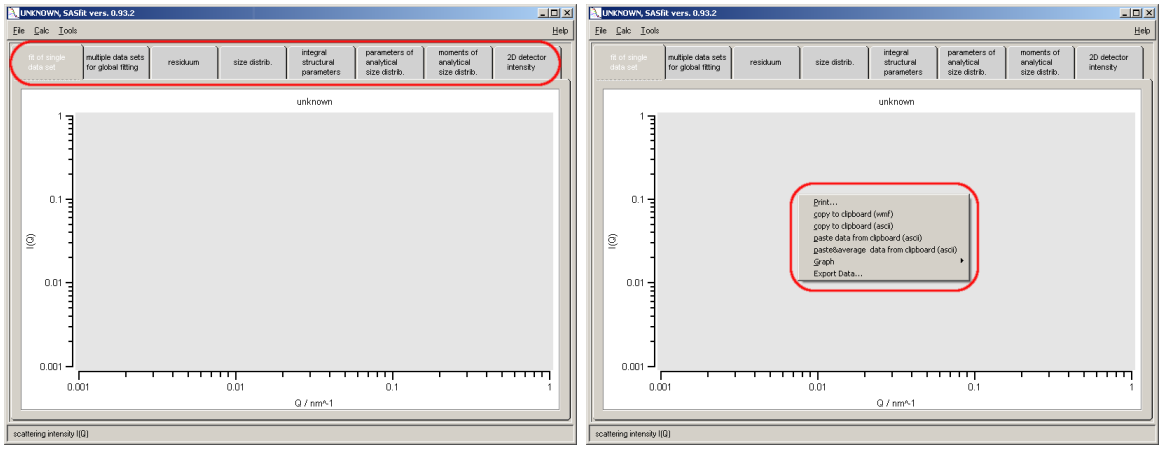

(a) main window (b) popup menu

FIGURE 2.1. Main `SASfit` graphical user interface window

The core `SASfit` window consists of various tabs (shown in the oval marking in the figure 2.1(a), they are "`fit of single data set`", "`multiple data sets for global fitting`", "`residuum`", "`size distrib.`", "`integral structural parameters`", "`parameters of analytical size distrib.`", "`moments of analytical size distrib.`", and "`2D detector intensity`" as shown in the red oval selection. The tabs for single data set and multiple data sets are used to plot single or multiple data files and view the plotted graphs along with the operations to perform during fitting. Residuum shows the difference between the experimental and theoretical fits. Size distributions give the plotted view of the number density v/s radius of the particle. Integral structural parameters are obtained using model independent fitting, such as Guinier approximation, Porod law etc. Parameters of analytical size distributions provides with details of size distributions used and the numbers obtained, whereas moments of analytical size distribution shows the contribution of scattering from different size distribution. The final tab 2D detector intensity is used in case of anisotropic scattering data. The window were the graphs are generated has options of printing the graph plotted view, copying the data in the ASCII format or as an image (wmf) format for further processing or presenting (figure 2.1(b)). `SASfit` accepts the

isotropic data in the ASCII format. The data can be imported as a single data set or for multiple data sets (several scattering curves).

2.2. Importing data files for a single data set

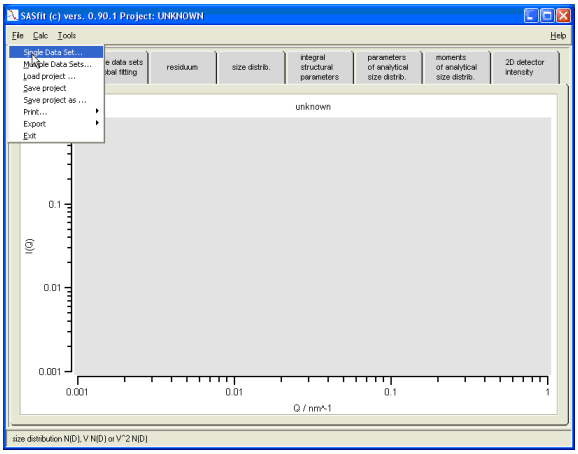

FIGURE 2.2. Menu interface for input single data set

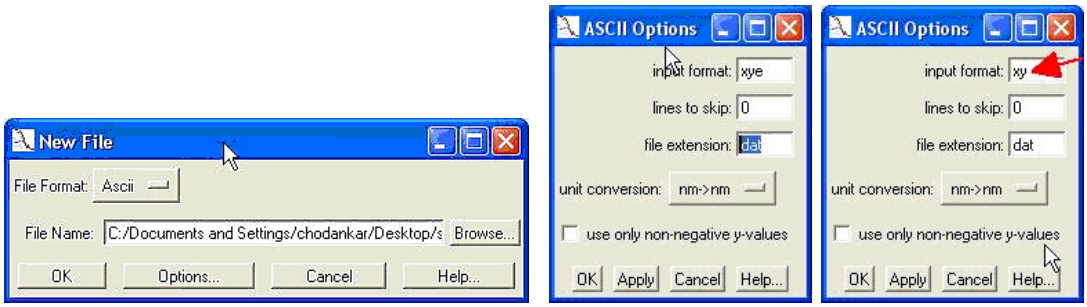

(a) Path and format selection for new file (b) Selecting the format columns of the file

FIGURE 2.3. Importing single data sets

The single data set option allows the user to perform operation on a single data file only. The file is imported via, `[File|Single Data Set...]` (Figure 2.2). This will open a new file window as shown in figure 2.3(a). The location of the file could be browsed and respectively selected. The options buttons is supplied to select the input format, which is performed by supplying a string such as `xye`. Where `x`, `y` and `e` stands for the scattering vector Q, scattering intensity $I(Q)$, `e` signifies the error bar $\Delta I(Q)$ on the measured scattering intensity. The error bars are required during the fitting operation and for files which do not contain the error bar column it would be calculated by default from the smoothing of the curve. There is an option to skip lines at the beginning of the data, which is intended to be used to skip header information in a data file , which could be misinterpreted as data. The number n specified in the menu defines the number

of lines skipped at the beginning of the data file. Furthermore a file extension can be provided, unit conversions can be performed as well as only non-negative y-values could be selected for plotting and performing further analysis. On pressing ok the data is loaded and the graph is plotted, with a new window labeled merge files being opened.

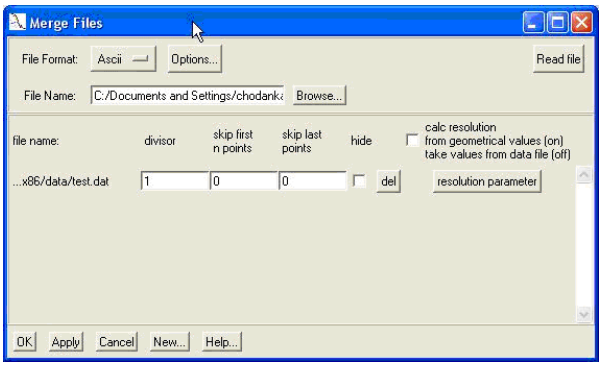

(a) Merge window for merging different Q scales into a single profile

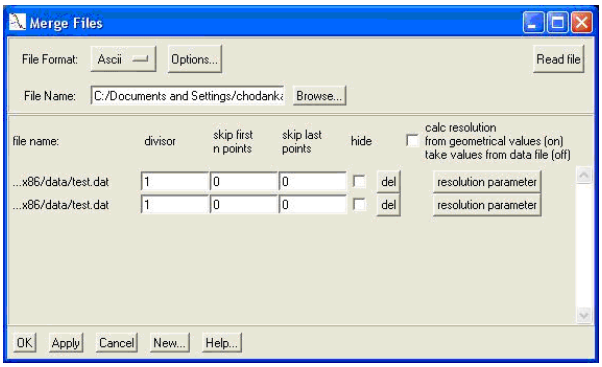

(b) An example showing merged data files

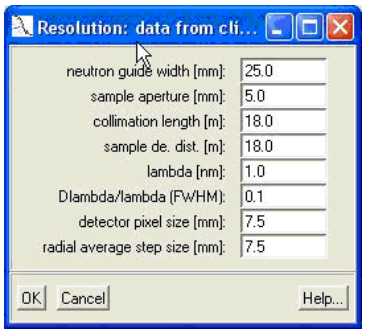

(c) resolution parameter interface

FIGURE 2.4. Merging many data files to one data set

In SAS, data can be collected at different collimator and sample to detector distances to correspond for a wide Q scale. Thus for a single sample at a given condition there can be more than one data files, to merge all of them together for completing the scattering profile, the above shown window comes into play. As shown in the merge files window, the new file could be browsed and selected; it has to be read using the read file button. The newly read file is listed below the first file, if it's a wrong selection it could be deleted back, also one can scale the different files measured at different Q windows, using the divisor column to have a continuous scattering profile. After scaling all the data profiles into one single profile, the statistically bad and unwanted data points can be removed by skipping the points at the beginning and at the end of the data files. The resolution parameters can be provided by pressing the resolution button and the required

information such as sample to detector distance, collimation distance, cross section of the guide etc as shown in figure (c) has to be entered to use resolution smearing during the fitting. The new button is use to discard all the current selections and plotted data files and starts a new session. The file could also be imported by pasting the clipboard data on the graph view as shown in the figure below. The conditions for columns are same as that for reading the file via browse method.

2.3. Importing data files for multiple data sets

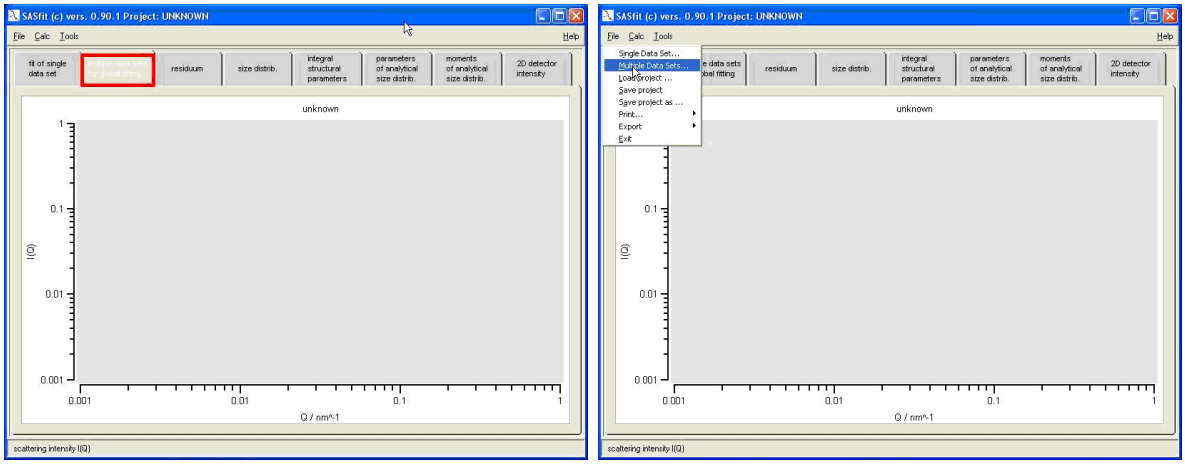

FIGURE 2.5. Procedure for importing data files for multiple data sets

The multiple data set option allows the user to perform operation on multiple data files by using common set of (global) parameters. This option is especially important in contrast variation experiments or measurements with polarized neutrons. The global fit helps to determine the fit parameters unambiguously which by analyzing a single curve would be otherwise strongly correlated. The file is imported by first going to multiple data sets for global fitting (red box in Figure 2.5) and then via, `[File|Multiple Data Set...]`. This will open a new window as was the case for importing single data set as shown below. The procedure for importing the first file is same as was the case for single file. On reading the first file the merge file window opens, which has additional buttons as compared to the merge file window in single data set (shown in the red rectangular box in figure 2.6(c)). In multiple data fitting, almost any number of data files could be loaded. The present active number of data is shown next to the data set in the merge file window. One can switch over from one data file to another by clicking previous or next. Add and remove buttons are used to add or remove another file. The addition of curves for different Q scales is performed similar to as mentioned in the Input single data set introduction.

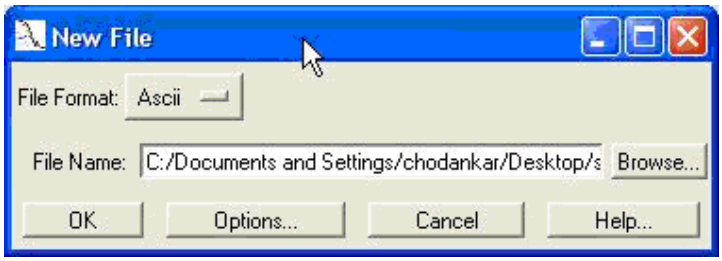

(a) Path and format selection for new file

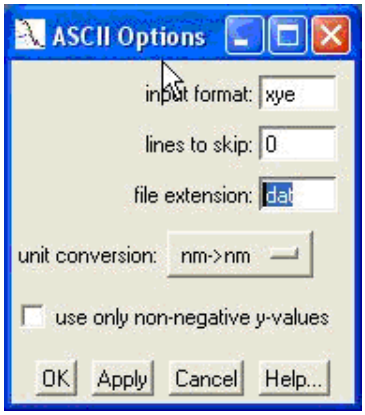

(b) Selecting the format of the file

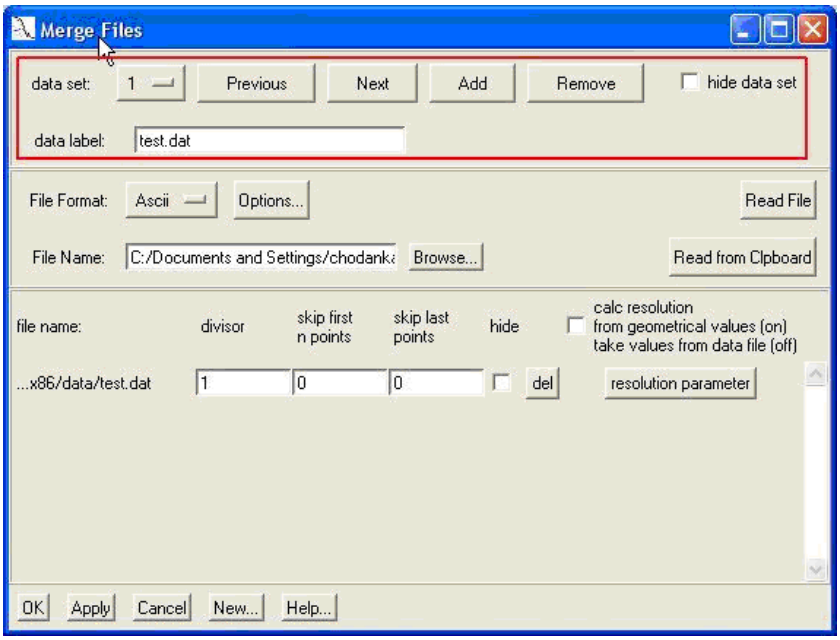

(c) Merge window for input of multiple data sets. Red box shows the buttons from which additional data files could be imported. Whereas the features of merging the data set for different Q scales is similar to that for importing single data set

FIGURE 2.6. Procedure for importing data files for multiple data sets

2.4. Simulating scattering curves

In addition to reading and loading data set, one can also have a realistic view of the experimental scattering data for a known structure by simulating the scattering profile beforehand to get a feel of the actual experiment scattering profile. The simulation can be performed either for a single data set or for multiple data sets using global parameters. To generate theoretical scattering profile, follow `[Calc|Single Data Set...|simulate]` or `[Calc|Multiple Data Sets...|simulate]`, either of them to generate a single data set or multiple data sets varied by changing the global parameter. The data can be generated for vast number of form factors and structure factor included in the software. The simulation is calculated using physically relevant parameters, this is useful to plan the experiment and to know whether a given concentration and contrast would produce a measurable signal.

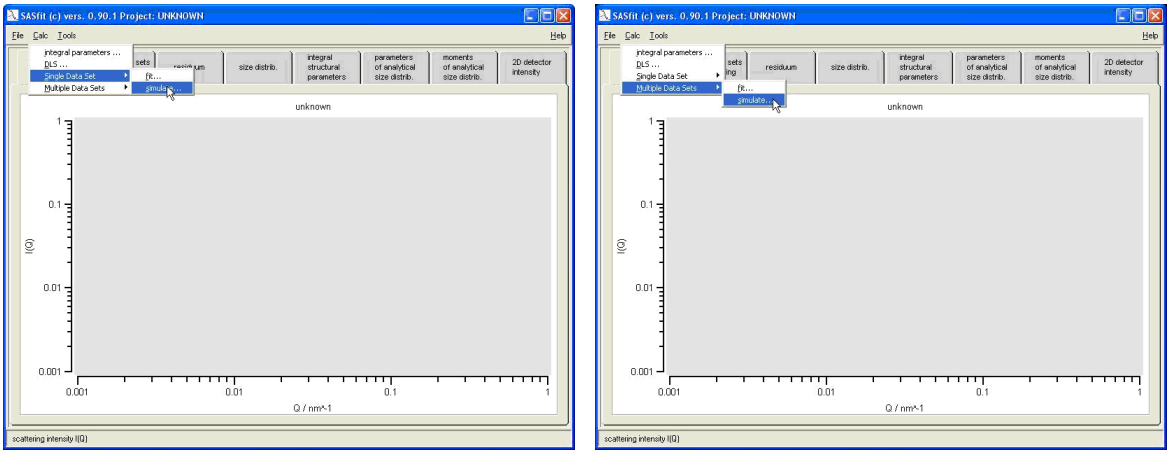

(a) simulation of a single curve (b) simulation of multiple curves

FIGURE 2.7. Procedure for simulating data profiles for single as well as multiple data files

2.5. Fitting

`SASfit` can analyse the data using both model-independent analysis and using a non-linear least square method to fit models. The model-independent analysis is a preliminary process of analyzing SAS data and does not require any advanced knowledge of the system to extract structural information this includes fittings (Guinier, Kratky, Porod, power-laws, etc.). On the other hand in case of non-linear least square methods a detailed fitting to the experimental data is performed using a wide variety of form factors and structure factors. The `SASfit` model library consists of large number of such functions, which can be readily used for the analysis. Moreover it can also fit different size distributions.

2.5.1. Model Independent Fitting (Integral parameters).

Model independent analysis requires no advanced knowledge about the sample and most importantly no experimental bias of assumed structure. It includes linearized fitting (Guinier, Porod and Zimm plot) to extract structural information. Model independent analysis are performed via `[Cals|integral parameters]`. In `SASfit` there are basically three functions available to do the analysis; they are Guinier, Zimm and Porod approximations (shown in the blue box in Figure 2.8(b). The number of data points to be included in the analysis can be accordingly varied and the resulting fit and the available parameters can be viewed instantaneously. For a large number of data a small script can be return to automate the process. This is performed by using the lower section of the integral structural parameters window (shown in red box). Prename indicates a character or string of characters with which all the data file names to be analysed starts with followed by certain numbers. The number of digits/characters in the filename could be given in the digits submission box, whereas the start number and the last file number are provided in their respective submission boxes. The step box indicates the incremental step of the file names which has to be analysed. The fitted parameters can be saved in the custom file to be viewed later. Load next file does step by step analysis of different files, whereas Do all would perform calculations on the entire file list, to be saved in the custom file for later viewing.

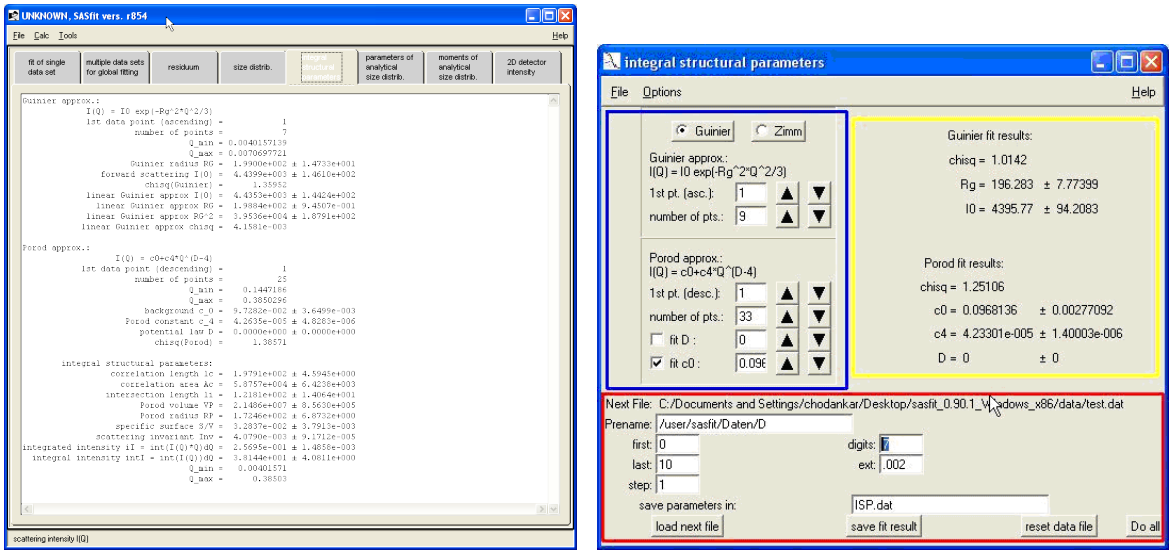

(a) data with fit results (b) entry menu with fitted parameters

FIGURE 2.8. Integral fit parameters

A set of valuable size and integrated parameters that can be calculated directly from the scattering curves $I(Q)$ [**17, 90, 18, 102, 65, 37**] consists of

$$\tilde{Q}_{\text{inv}} = \int_0^\infty Q^2 I(Q) \mathrm{d}Q \text{ (scattering invariant)} \tag{2.1a}$$

$$\frac{S}{V} = \frac{\pi}{\tilde{Q}_{\text{inv}}} \lim_{Q\to\infty} \left\{Q^4 I(Q)\right\} \text{ (specific surface)} \tag{2.1b}$$

$$\langle R_G \rangle^2 = 3\left(-\lim_{Q\to 0}\left\{\frac{\mathrm{d}[\ln I(Q)]}{\mathrm{d}(Q^2)}\right\}\right) \text{ (squared Guinier radius)} \tag{2.1c}$$

$$\langle d \rangle = \frac{4}{\pi}\frac{\int_0^\infty Q^2 I(Q)\mathrm{d}Q}{\lim\limits_{Q\to\infty}\left\{Q^4 I(Q)\right\}} \text{ (average intersection length)} \tag{2.1d}$$

$$\langle l \rangle = \frac{\pi}{\tilde{Q}_{\text{inv}}} \int_0^\infty Q I(Q) \mathrm{d}Q \text{ (correlation length)} \tag{2.1e}$$

$$\langle A \rangle = \frac{2\pi}{\tilde{Q}_{\text{inv}}} \int_0^\infty I(Q) \mathrm{d}Q \text{ (correlation surface)} \tag{2.1f}$$

$$\langle V \rangle = \frac{2\pi^2}{\tilde{Q}_{\text{inv}}} I(0) \text{ (correlation volume, Porod volume)} \tag{2.1g}$$

2.5.2. Model dependent analysis.

2.5.2.1. *Modeling a single data set.*

For Modeling a SANS data set the `SASfit` -programm allows to describe experimental data with an arbitrary number of scattering objects types. Each of them can have a size distribution, whereby the user can choose over which parameter a_i of the form factor the integration will be performed. For example in case of a spherical shell with a core radius of R and a shell thickness of ΔR `SASfit` allows to integrate either over the core radius $x = R$ or the shell thickness $x = \Delta R$ by marking the corresponding parameter (see option `distr` in Fig . 2.9(b)). Furthermore an additional structure factor can be included for each scattering object. Several ways to account for the structure factor have been implemented like the monodisperse approximation (4.1.1), decoupling approach (4.1.2), local monodisperse approximation (4.1.3), partial structure factor (4.1.4) and scaling approximation of partial structure factors (4.1.5). The details are described in chapter 4.

Implemented size distributions, form factors and structure factors are described in chapters 3, 4 and 5. Optional an additional smearing of this function with the instrument resolution function $R_{av}(Q, \langle Q \rangle)$ can be activated so that

$$I(\langle Q \rangle) = \int_0^\infty R_{av}(Q, \langle Q \rangle) \frac{d\sigma}{d\Omega}(Q)\, dQ \tag{2.2}$$

A user interface shown in Fig. 2.9 is supplied to choose between the number of scattering objects and to define parameter for each of them. Next to varying the different

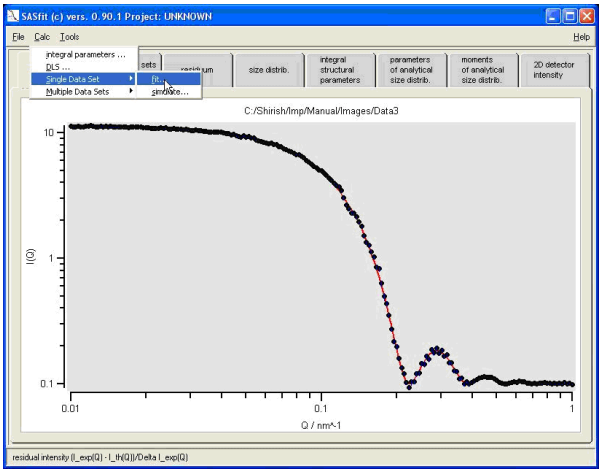

(a) Menu through which fitting procedure is initiated

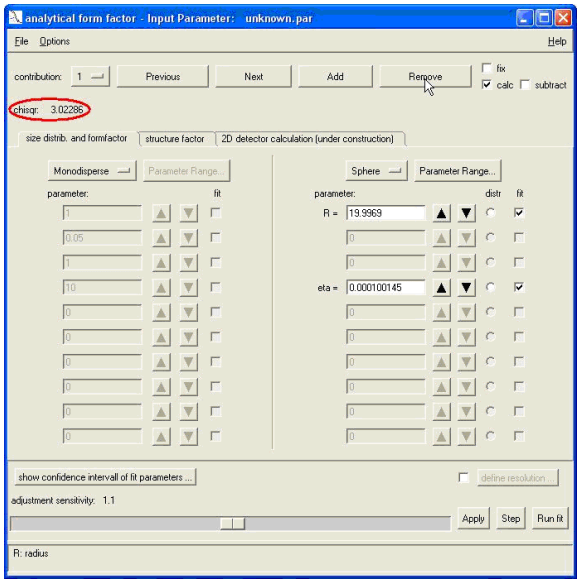

(b) User interface for fitting, containing different form factors and structure factor

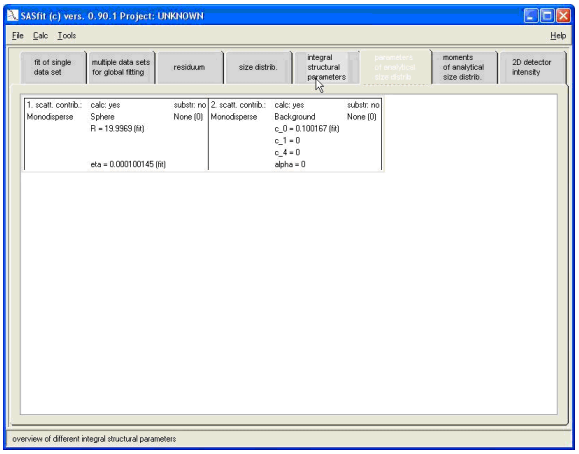

(c) Tab summarizing the analyzed parameters

FIGURE 2.9. Menus for fitting a single data set

parameters one can mark those, which one would like to fix or to vary in a fitting procedure (see option `fit` in Fig. **??**(b)) Model dependent analysis for single files are performed via `[Calc|Single Data Set|Fit...]`.

2.5.2.2. *Modeling multiple data sets.*

The multiple data set option allows the user to perform operation on multiple data file by using common set (global) parameters. This option is especially important in contrast variation experiments or measurements with polarized neutrons. The global

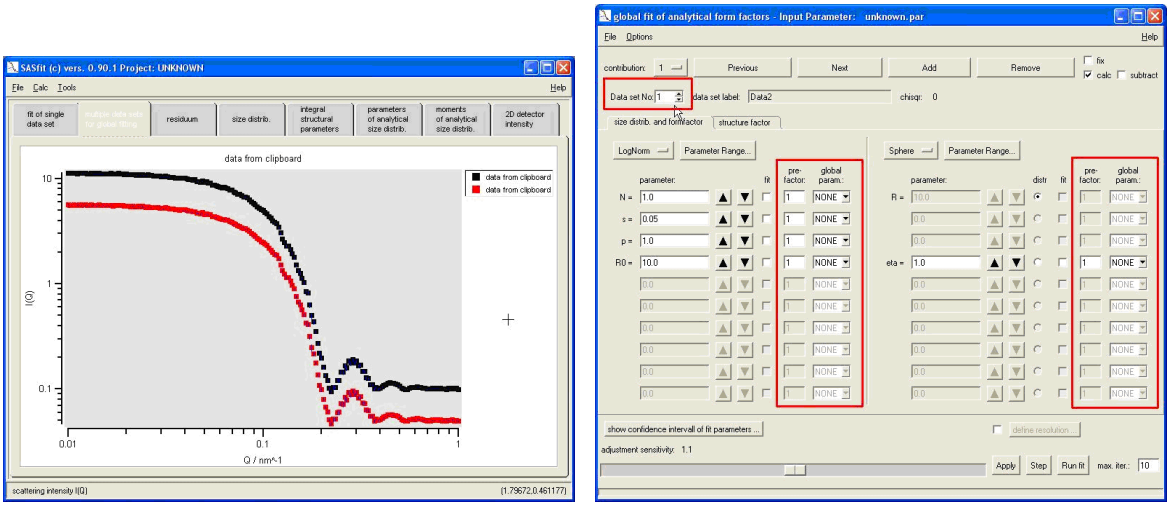

(a) Imported multiple data sets

(b) Uuser interface for fitting multiple data files

FIGURE 2.10. Menus for fitting a simultaneously multiple data sets

fitting helps the user to analyse large number of data which has a similar form or structure factor however different scaling constant. The data shown in the figure below is for a spherical monodispersed system both the data profile has identical features, except that the scaling factor between the two is of a factor of two. The data are called by the procedure explained in the input multiple data file section. The fitting of the data is performed by calling the fitting function via `[Calc|Multiple Data Sets|Fit...]`. The user interface for multiple data fitting has additional feature than to that for single data fitting, they are pre-factor and global parameters as shown in figure 2.10(b) red markings.

The procedure for fitting the data set is similar to that mentioned in the earlier section. The only difference is to include the global parameters for each function included. The scattering profile shown in the figure 2.10(a) is for a spherical monodispersed particle, both the profiles have identical features with a scaling factor of two. The user interface for fitting shows the following window in figures 2.11. The data set number shows the active data file, whereas contribution indicates the number of scattering objects. We have selected the form factor for a spherical particle. In the global parameter a new variable is produced for both radius and `eta` (scattering contrast). The pre-factor is kept constant at 1. A second contribution is added to the data set one by pressing add. In this case it is a background contribution, a new global parameter is introduced for it (`P3`). A similar procedure is done for second data set where the global parameter for the radius is kept same to that for data set one, whereas new global parameters are defined for scattering contrast and background. The fitting procedure can then be started by pressing Run fit. The figures 2.12 show the graphs during the fitting process. The parameters of fitting for all the contribution can be viewed by pressing parameters of analytical size distributions (figure 2.12(d)).

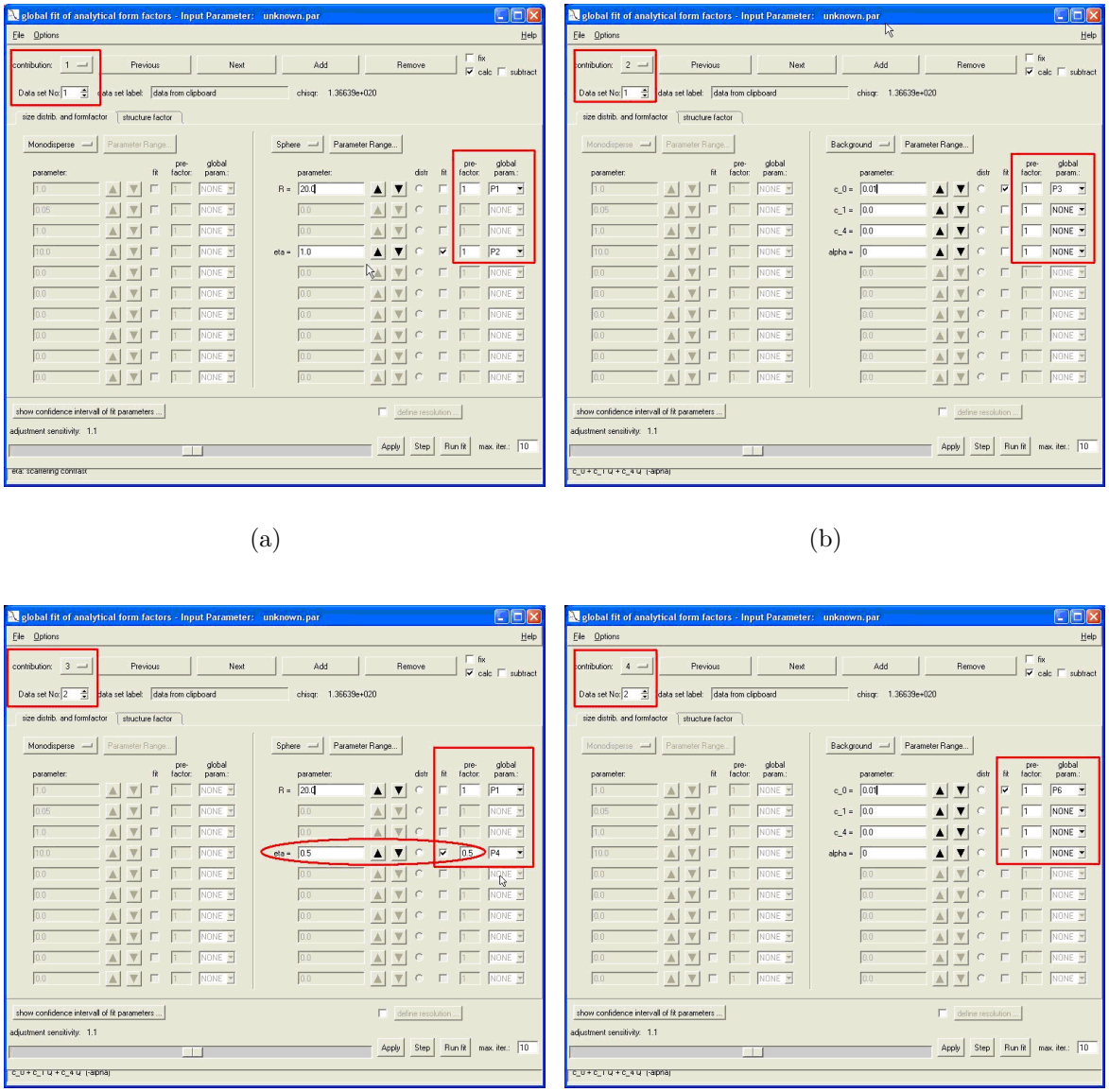

FIGURE 2.11. Different windows showing different controlling parameters during multiple data fitting.

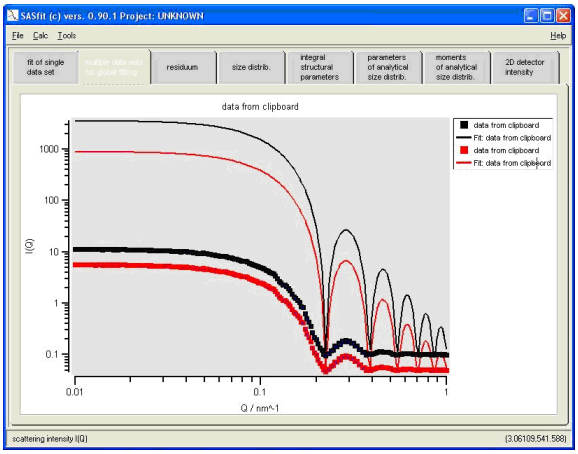

(a)

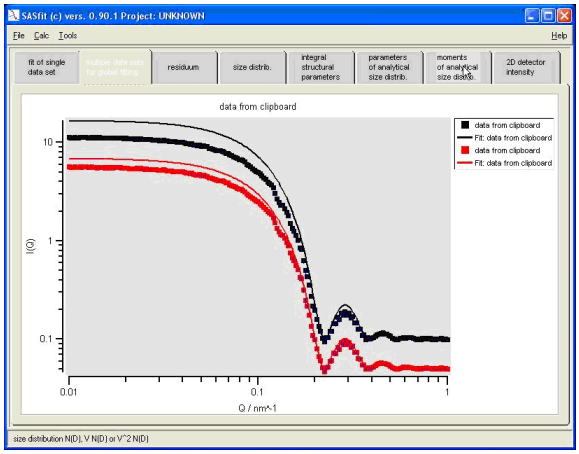

(b)

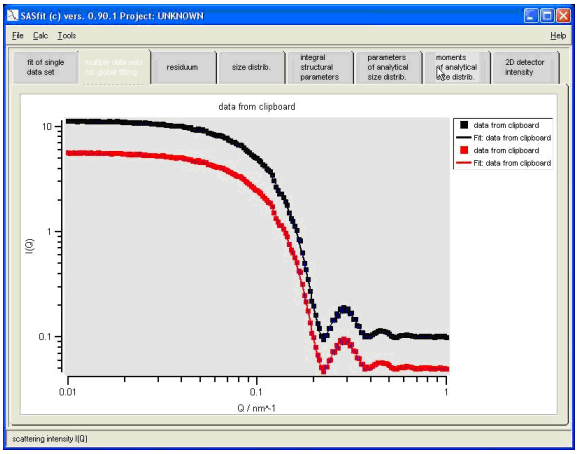

(c)

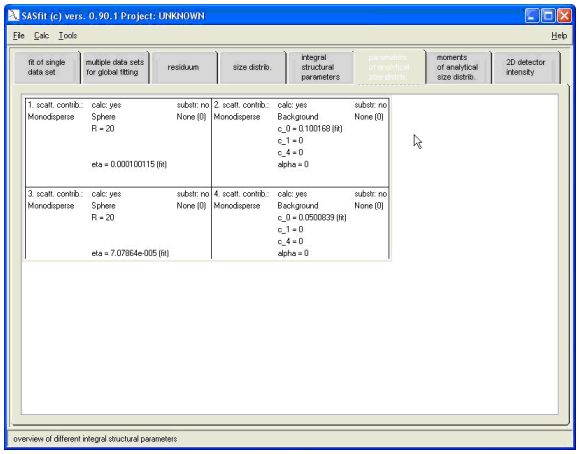

(d)

FIGURE 2.12. The scattering data profile and the analytical parameters obtained during the fitting process.

2.6. Fitting strategies

2.7. Criteria for goodness-of-fit

All criteria shown below for testing the goodness of a fit should be considered with caution [**10, 81**]. When you get data on a SAS instrument the the measured intensities are measured with some statistical uncertainties. Normally one assumes Poisson statistics to determine the uncertainty in the counting statistics. The data reduction software should than perform a proper error propagation analysis for all succeeding data treatment operations. However, by this procedure only statistical uncertainties are taken into account. All systematic uncertainties are than hopefully covered during the data treatment, as fir example background correction, transmission correction etc 12.

2.7.1. chi square test.

The method of least squares is built on the hypothesis that the optimum description of a set of data is one which minimizes the weighted sum of squares of deviations, between the data, $I_{\exp}(q_i)$, and the fitting function $I_{\text{th}}(q_i)$:

$$\chi^2 = \sum_{i=1}^{N} \left(\frac{I_{\exp}(q_i) - I_{\text{th}}(q_i)}{\Delta I(q_i)} \right)^2 \tag{2.3}$$

As a rule of thumb for chi-square fitting is the statement that a good fit is achieved when the reduced chi-square equals one. The reduced chi-square value, which equals the residual sum of square divided by the degree of freedom can be computed by

$$\chi^2_\nu = \frac{1}{N-m} \sum_{i=1}^{N} \left(\frac{I_{\exp}(q_i) - I_{\text{th}}(q_i)}{\Delta I(q_i)} \right)^2 = \frac{\chi^2}{N-m} \tag{2.4}$$

where N is the number of data points and m the number of fit parameters. $\nu = N - m$ is called the "number of degree of freedom". The reduced chi-square is closely related to the variance of the fit s^2 by

$$s^2 = \chi^2_\nu \left(\frac{1}{N} \sum_{i=1}^{N} \frac{1}{(\Delta I_i^{\exp})^2} \right)^{-1} \tag{2.5}$$

In the theory of hypothesis testing χ^2 can be used to test for goodness of a fit. The probability that a random set of N data points would yield a value of χ^2 equal or greater than the measured one is given by

$$Q_{\text{factor}} = Q\left(\frac{N-m}{2}, \frac{\chi^2}{2} \right) = \frac{\Gamma\left(\frac{N-m}{2}, \frac{\chi^2}{2} \right)}{\Gamma\left(\frac{N-m}{2} \right)} \text{ with } \Gamma(a,x) = \int_x^\infty t^{s-1} e^{-t} dt \tag{2.6}$$

For a fitting function being a good approximation to the data the experimental value of χ^2_ν should be close to one and the probability Q_{factor} somewhere between 0.01 and 0.5. For probability values close to one the fit seems to be too good to be true.

2.7.2. R-factor.

The crystallographers have introduced another parameter for the goodness of a fit. They use the R factor [**68, 38**] as a measure of model quality which is defines as

$$= \frac{\sum_{i=1}^{N} |I_{\exp}(q_i) - I_{\text{th}}(q_i)|}{\sum_{i=1}^{N} |I_{\exp}(q_i)|} \tag{2.7}$$

Theoretical values of R range from zero (perfect agreement of calculated and observed intensities) to infinity. R factors greater than 0.5 indicate in crystallography very poor agreement between observed and calculated intensities. Models refining to $R < 0.05$ are often considered to be good. However, the R factor must always be treated with caution, only as an indicator of precision and not accuracy. In Crystallography partially incorrect structures have been reported with R values below 0.1; many imprecise but essentially correct structures have been reported with higher R values.

In practice, weighted R factors R_{w} are more often used to track least-squares refinement, since the functions minimized are weighted according to estimates of the precision of the measured quantity. The weighted residuals are defined as:

$$R_w = \sqrt{\frac{\sum_{i=1}^{N} \left(\frac{I_{\exp}(q_i) - I_{\text{th}}(q_i)}{\Delta I(q_i)} \right)^2}{\sum_{i=1}^{N} \frac{I_{\exp}^2(q_i)}{\Delta I(q_i)}}} \tag{2.8}$$

2.8. Data I/O Formats

2.8.1. Input Format.

`SASfit` supports a simple ASCII format. Options for reading ASCII data can be set in the corresponding menu, where one can set an input format and the number of lines to be skipped at the beginning of the data file. To set an input format one has to supply a string like "`xyer`". Each line which does not contain valid float numbers are skipped automatically. Each line further should at least contain as many valid numbers as the supplied format string characters. That means if the line contains only three numbers but the format string is 4 or more characters long the line will be ignored. Separators between numbers can be "white space", "tabulator", or ",". For identifying the columns the characters and their position in the string are interpreted. `x`, `y` and `e` stands for the scattering vector Q, scattering intensity $I(Q)$ and its error $\Delta I(Q)$, respectively. `r` defines the column for a resolution parameter σ. The position of the character in the string defines which data column is assigned to Q, $I(Q)$, $\Delta I(Q)$, and σ. In case of double occurrence of a character the position of the last one is the significant position. Any characters not belonging to {`x`,`y`,`e`,`r`} can be used to skip a column. A definition string need to contain at least the two characters `x` and `y`.

Example 1 (HMI-BerSANS format):

```
%File
FileName=D0002831.200 FileDate=28-Jun-99 FileTime=11:57:16
Type=SANSDIso Title=IMF
%Counts
 2.651E-02, 2.372E+02, 4.650E+00
 3.240E-02, 2.170E+02, 2.291E+00
 3.829E-02, 1.898E+02, 1.713E+00
 4.418E-02, 1.743E+02, 1.479E+00
 5.007E-02, 1.528E+02, 1.318E+00
 5.596E-02, 1.361E+02, 1.153E+00
                    ⋮
```

As the first lines start with a string, they will be automatically ignored. To interpret the three columns as Q, $I(Q)$, $\Delta I(Q)$ the format string should be simply `xyz`. The HMI-BerSANS format can also be read in by explicitly selecting instead of the "ASCII"-format the "HMI"-format button in the menu.

Example 2:

```
⌈      19         0         0         0         0         0         0         6
  0.100000E+01   0.100000E+04   0.000000E+00   0.100000E+01   0.120000E+01
  0.000000E+00   0.000000E+00   0.000000E+00   0.000000E+00   0.000000E+00 ⌋
teflon              instrument tests
1  2.617993E-04   3.700000E+01   4.301163E+00
2  1.062462E-03   6.412500E+01   1.634587E+00
3  2.107973E-03   1.410135E+03   5.207492E+00
4  3.167636E-03   1.752197E+03   4.801586E+00
5  4.189463E-03   7.581771E+02   2.810281E+00
                   :
```

```
                :
45  1.255376E-02   1.486688E+01   2.197023E-01
46  1.360724E-02   1.204012E+01   1.927716E-01
47  1.466810E-02   1.026648E+01   1.679423E-01
```

A definition string `ixye` would ignore the leading line number at the beginning of each data line, but in the present example also the first 3 lines would also be interpreted as data points. To skip them one has to use the option for skipping leading lines in a data file. In the above case the number should be set to 3 or 4. As the 4$^{\text{th}}$ line is anyway ignore a value of 3 is sufficient to skip non data points.

Example 3: ILL data files from regrouped treatment (`gnnnnnn.eee`).

```
 Sample - d corrs    TEST prot/deutr. ellipt. chs  44 lines+(Q, I(Q), errI(Q))
  ILL  SAN D11

[        8303         1        37         1        42        38
            14        32         0         3         1 ]

  spol 20-Oct-1995  9:16:09
   AvA1 0.0000E+00 AsA2 9.5000E-01 XvA3 1.0000E+00 XsA4 1.0000E+00 XfA5 0.0000E+00
  S...  8303  0  1.00E+00 P100 0.5% 221   Sbak  8309  0  2.00E+00 Blank523 193
  V...  8301  0  1.00E+00 Hhaps 911

    0.0000 ! Theta-0 Detector offset angle
   32.5000 ! X0 cms Beam centre
   32.5000 ! Y0 cms Beam centre
    1.0000 ! Delta-R cms regrouping step
    2.5000 ! SD m Sample-detector distance
   10.5400 ! Angstroms incident wavelength
    5.6000 ! m collimation distance
    1.0000 ! concentration
       -3. ! ISUM central window sum
        1. ! flux monitor counts
  180.0000 ! degrees detector sector width
    0.0000 ! degrees sector orientation
   10.0000 ! % wavelength spread
   20.0000 ! mm source slit width x
    0.0000 ! mm source slit height y
   10.0000 ! mm sample width x
    0.0000 ! mm sample height y
   10.0000 ! mm detector x pixel size
   10.0000 ! mm detector y pixel size
    0.0000 ! degrees sample normal/beam
    0.0000 ! K sample temperature
    0.0000 ! sample transmission
    1.0000 ! mm sample thickness
  900.0000 ! secs counting time
    0.0000 ! reserved
    0.0000 ! reserved
    0.0000 ! reserved
    0.0000 ! reserved
    0.0000 ! reserved
    0.0000 ! reserved
    0.0000 ! reserved
    0.0000 ! reserved
```

```
⌈         37         0         0         0         0         0         0         6
     0.100000E+01   0.250000E+03   0.000000E+00   0.100000E+01   0.105400E+01
     0.000000E+00   0.000000E+00   0.000000E+00   0.000000E+00   0.000000E+00
 0.000000E+00   0.000000E+00   0.000000E+00 ⌋
   2.194656E-03   3.442688E-01   8.329221E-02
   5.466116E-03   3.000000E-01   5.008947E-02
   8.480323E-03   3.877941E-01   4.232426E-02
   1.189216E-02   6.498784E-01   1.519078E-02
   1.497785E-02   7.493181E-01   1.173622E-02
                        ⋮
```

To read in a regrouped ILL data file one has to use the definition string `xye` and secondly one has to skip the first 44 lines in the data file to ignore also the lines marked with ⌈ ⌋. If one does not skip the first 44 lines the marked lines are interpreted erroneously also as data points. The other lines at the beginning of the data file are ignored as they do not fulfill the condition that they have 3 columns containing only valid numbers.

2.8.2. Error bar.

In case no error bar is supplied `SASfit` will try to guess one. To do this an polynomial $y_p(Q)$ of degree p

$$y_p(Q) = \sum_{k=0}^{p} c_k Q^k \tag{2.9}$$

is fitted to the data point i and its n^{th} neighbors, i.e. is fitted to $2n+1$ points from $I_{i-n}(Q_{i-n})$ to $I_{i+n}(Q_{i+n})$. After the fit χ_i^2 is calculated

$$\chi_i^2 = \sum_{j=i-n}^{i+n} \left(I_j(Q_j) - y_P(Q_j)\right)^2 \tag{2.10}$$

The error bar ΔI_i for Q_i is than defined as

$$\Delta I_i = \sqrt{\frac{\chi_i^2}{2n-p}} \tag{2.11}$$

`SASfit` is using two nearest neighbors $n = 2$ and fitting a polynomial of degree $p = 2$ to it to guess an error bar.

2.8.3. Export Format.

Example for an exported data file:

```
0.00401571,     3497.47,     90.7282,          0,   0.00401571,      260294,         -1,          0,
0.00454087,        3340,     84.9531,          0,   0.00454087,      254548,         -1,          0,
 0.0050096,     3322.47,     79.6313,          0,    0.0050096,      248833,         -1,          0,
0.00552335,     2983.23,     73.7254,          0,   0.00552335,      241949,         -1,          0,
0.00598495,     2737.17,     68.4395,          0,   0.00598495,      235226,         -1,          0,
 0.0065309,     2598.76,     62.3109,          0,    0.0065309,      226647,         -1,          0,
0.00706977,      2233.9,     56.4829,          0,   0.00706977,      217551,         -1,          0,
0.00764207,     2080.96,     50.6186,          0,   0.00764207,      207264,         -1,          0,
```

```
0.00815988,     1882.88,     45.6557,          0,   0.00815988,      197459,         -1,          0,
                             ⋮                                ⋮
         ,           ,           ,          ,    0.0445634,     1535.14,         -1,          0,
         ,           ,           ,          ,    0.0453557,     1473.71,         -1,          0,
         ,           ,           ,          ,    0.0470219,     1340.34,         -1,          0,
         ,           ,           ,          ,    0.0490017,     1192.64,         -1,          0,
         ,           ,           ,          ,    0.0510837,     1055.44,         -1,          0,
```

If one like to export the data of an xy-plot all curves are stored in a single data file. Each curve will occupy four columns (Q, $I(Q)$, $\Delta I(Q)$, σ). If an error $\Delta I(Q)$ is not available, e.g. for theoretical data curves, the corresponding column will be filled with -1. Similar is valid for the resolution parameter σ which will be set to 0 in case it is not available. The individual columns are separated by ",". If the curve have different amount of data points the column will be filled with empty space for the missing data. This comma separated data format has been chosen as it can be imported easily by many commercial plotting softwares. The drawback of this format is, however, that `SASfit` cannot read it correctly, if the individual curves are of different length.

2.9. Scattering length density calculator

The `SLD calculator` is using thermal neutron cross-sections only to calculate neutron scattering length density. For x-rays the energy dependent scattering coefficients f' and f'' are derived using the theoretical approximation developed by Cromer and Liberman. This theory gives accurate values far from an absorption edge but does not account for the effects of neighboring atoms, which can be very substantial near an absorption edge. Before conducting an anomalous scattering experiment close to an absorption edge it is therefore advisable to determine the actual scattering behavior of the sample. The x-ray data have been taken from `http://skuld.bmsc.washington.edu/scatter/AS_periodic.html` and those for neutrons from `http://www.ncnr.nist.gov/resources/n-lengths/list.html`. The menu in-

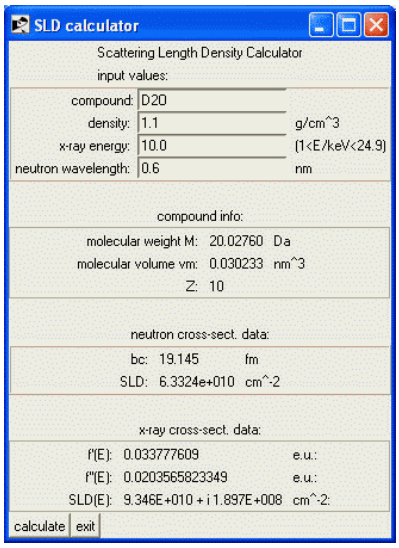

FIGURE 2.13. Input menu for the scattering length density calculator

terface in Fig. 2.13 has for input parameters, the sum formulae of the compound, its mass density in g/cm^3, the x-ray energy in keV and the neutron wave length in nm. In the compound name non-integer stoichiometry is supported, e.g. H0.2O0.1 and H2O will calculate the same scattering length density. However, the molecular volume v_m and the molecular weight M of cause depend on such differences. The elements in the compound name are case sensitive. Therefore you have to use `SiO2` instead of `SIO2`. Also isotopes are handled like `C(13)` (Carbon-13), `H(2)` (Deuterium), or `O(18)` (Oxygen-18). For Deuterium next to `H(2)` also `D` can be used.

Examples of how to format the compound name:

- Magnetite: `Fe3O4`, 5.15 g/cm^3
- Eucryptite: `LiAlSiO4`, 2.67 g/cm^3
- protonated toluene, `C7H8`, 0.865 g/cm^3
- deuterated toluene, `C7D8` or `C7H(2)8`, 0.94 g/cm^3
- mixture of 65/35 heavy water/light water, `(D2O)0.65(H2O)0.35`, 1.065 g/cm^3

From the compound name and the density first the molecular weight M, molecular volume v_m, and total number of electrons Z are calculated. Together with

the tabulated neutron scattering length and tabulated energy dependent scattering coefficient $f'(E)$ and $f''(E)$ the corresponding coherent neutron scattering length $b_c = \sum_i b_i$, coherent neutron scattering length density $\eta_{n,SLD} = b_c/v_m$ and for x-rays the complex energy dependent scattering scattering length density $\eta_{x,SLD} = (Z - (Z/82.5)^{2.37} + f'(E) + \imath f''(E))/v_m$ of the compound are calculated.

2.10. Resolution Function [72]

$$\langle k\rangle = 2\pi/\lambda \tag{2.12}$$

$$\langle\theta\rangle = \arcsin(\langle Q_{av}/(2\langle k\rangle)) \tag{2.13}$$

$$a_1 = \frac{r_1}{L + l/\cos^2(2\langle\theta\rangle)} \tag{2.14}$$

$$a_2 = r_2\cos^2(2\langle\theta\rangle)/l \tag{2.15}$$

$$\Delta\beta_1 = \begin{cases} a_1 \geq a_2: & \dfrac{2r_1}{L} - \dfrac{r_2^2}{2r_1}\dfrac{\cos^4(2\langle\theta\rangle)}{l^2 L}\left(L + \dfrac{l}{\cos^2(2\langle\theta\rangle)}\right)^2 \\ a_1 < a_2: & 2r_2\left(\dfrac{1}{L} + \dfrac{\cos^2(2\langle\theta\rangle)}{l}\right) - \dfrac{r_1^2}{2r_2}\dfrac{l}{L} \\ & \times\dfrac{1}{\cos^2(2\langle\theta\rangle)\left(L + \frac{l}{\cos^2(2\langle\theta\rangle)}\right)} \end{cases} \tag{2.16}$$

$$\sigma_W = \langle Q\rangle\frac{\Delta\lambda}{\lambda}\frac{1}{2\sqrt{2\ln(2)}} \tag{2.17}$$

$$\sigma_{C1} = \langle k\rangle\cos(\langle\theta\rangle)\frac{\Delta\beta_1}{2\sqrt{2\ln(2)}} \tag{2.18}$$

$$\sigma_{D1} = \langle k\rangle\cos(\langle\theta\rangle)\cos^2(2\langle\theta\rangle)\frac{D}{l\,2\sqrt{2\ln(2)}} \tag{2.19}$$

$$\sigma_{av} = \langle k\rangle\cos(\langle\theta\rangle)\cos^2(2\langle\theta\rangle)\frac{\Delta D}{l\,2\sqrt{2\ln(2)}} \tag{2.20}$$

$$\sigma = \sqrt{\sigma_W^2 + \sigma_{C1}^2 + \sigma_{D1}^2 + \sigma_{av}^2} \tag{2.21}$$

$$R_{av}\left(Q, \langle Q\rangle\right) = \frac{Q}{\sigma^2}\exp\left(-\frac{1}{2}\left(Q^2 + \langle Q\rangle^2\right)/\sigma^2\right) I_0(Q\langle Q\rangle/\sigma^2) \tag{2.22}$$

$$I(\langle Q\rangle) = \int_0^\infty R_{av}\left(Q, \langle Q\rangle\right)\frac{d\sigma}{d\Omega}(Q)\,dQ \tag{2.23}$$

$$\frac{d\sigma}{d\Omega}(Q) = \int_0^\infty N(R)F^2(Q,R)\,dR \tag{2.24}$$

CHAPTER 3

Form Factors

The different types of form factors are selected in the different submenus. Below one finds how they are ordered. The definitions of the individual form factors are defined below. Under the submenu `other functions` all form factors under development and those functions, which are not at all form factors but which have been implemented for some other purposes are listed.

- Background
- auxiliary and transition functions
  - `p(r) -> 4 pi r^2 sin(qr)/(qr)`
  - `gamma(r) -> 4 pi sin(qr)/(qr)`
- Spheres & Shells (3.1)
  - `Sphere` (3.1.1)
  - `Spherical Shell i` (3.1.2)
  - `Spherical Shell ii` (3.1.3)
  - `Spherical Shell iii` (3.1.4)
  - `MultiLamellarVesicle` (3.1.7)
  - `RNDMultiLamellarVesicle`
  - `RNDMultiLamellarVesicle2`
  - `BiLayeredVesicle` (3.1.5)
  - `LinShell` (7.3.2.1)
  - `LinShell2` (7.3.2.2)
  - `ExpShell` (7.3.2.3)
- ellipsoidal obj. (3.2)
  - `Ellipsoid i` 3.2.2
  - `Ellipsoid ii` 3.2.1
  - `EllipsoidalCoreShell` 3.2.3
  - `triaxEllShell1` 3.2.4
- polymers & micelles (3.3)
  - polymer chains
    - `Gauss` (3.3.1)
    - `Gauss2` (3.3.1)
    - `Gauss3` (3.3.1)
    - `GaussPoly` (3.3.1)
    - `generalized Gaussian coil` (3.3.1.5)
    - `generalized Gaussian coil 2` (3.3.1.6)
    - `generalized Gaussian coil 3` (3.3.1.7)
  - polymer stars
    - `BenoitStar` (3.3.2)

    * PolydisperseStar (3.3.3)
    * Dozier (3.3.4.1)
    * Dozier2 (3.3.4.2)
- polymer rings
    * FlexibleRingPolymer (3.3.5)
    * mMemberedTwistedRing (3.3.6)
    * DaisyLikeRing (3.3.7)
- spherical & ellipsoidal micelles
    * SPHERE+Chains(RW)_Nagg (3.3.11.2)
    * SPHERE+Chains(RW)_Rc (3.3.11.2)
    * SPHERE+Chains(RW) (3.3.11.2)
    * SPHERE+Chains(SAW)_Nagg
    * SPHERE+Chains(SAW)_Rc
    * SPHERE+Chains(SAW)
    * SPHERE+R^-a_Nagg (3.3.11.8)
    * SPHERE+R^-a_Rc (3.3.11.8)
    * SPHERE+R^-a (3.3.11.8)
    * SPHERE_smooth_interface+R^-a_Nagg
    * SPHERE_smooth_interface+R^-a_Rc
    * ELL+Chains(RW)_Nagg (3.3.11.3)
    * ELL+Chains(RW)_Rc (3.3.11.3)
    * ELL+Chains(RW) (3.3.11.3)
    * SphereWithGaussChains
    * BlockCopolymerMicelle
- cylindrical & rod-like micelles
    * CYL+Chains(RW)_Nagg (3.3.11.4)
    * CYL+Chains(RW)_Rc (3.3.11.4)
    * CYL+Chains(RW) (3.3.11.4)
    * WORM+Chains(RW)_nagg (3.3.11.5)
    * WORM+Chains(RW)_Rc (3.3.11.5)
    * WORM+Chains(RW)(3.3.11.5)
    * ROD+Chains(RW)_nagg (3.3.11.6)
    * ROD+Chains(RW)_Rc (3.3.11.6)
    * ROD+Chains(RW) (3.3.11.6)
    * ROD+R^-a_nagg (3.3.11.9)
    * ROD+R^-a_Rc (3.3.11.9)
    * ROD+R^-a (3.3.11.9)
    * ROD+Exp_nagg
    * ROD+Exp_Rc
    * ROD+Exp
- local planar micelles (sheets, ULV)
    * DISC+Chains(RW)_nagg
    * DISC+Chains(RW)_Lc
    * DISC+Chains(RW)
    * SphULV+Chains(RW)_nagg
    * SphULV+Chains(RW)_tc

        * SphULV+Chains(RW)
        * EllULV+Chains(RW)_nagg
        * EllULV+Chains(RW)_tc
        * EllULV+Chains(RW)
        * CylULV+Chains(RW)_nagg
        * CylULV+Chains(RW)_tc
        * CylULV+Chains(RW)
    - wormlike structures
        * WormLikeChainEXV (3.3.9)
        * KholodenkoWorm (3.3.10)
- cluster obj. (3.5)
    - Fisher-Burford (3.5.1)
    - MassFractExp(3.5.1)
    - MassFractGauss (3.5.1)
    - Aggregate (Exp(-x^a) Cut-Off) (3.5.1)
    - Aggregate (OverlapSph Cut-Off) (3.5.1)
    - DLCAggregation (3.5.1)
    - RLCAggregation (3.5.1)
    - MassFractOverlappingSph (3.5.1)
    - StackDiscs (3.5.2)
    - DumbbellShell (3.5.3)
    - two_attached_spheres
    - DoubleShellChain (3.5.4)
    - TetrahedronDoubleShell (3.5.5)
- non-particular structures
    - OrnsteinZernike (3.4.4)
    - BroadPeak (3.4.5)
    - TeubnerStrey (3.4.1)
    - DAB (3.4.2)
    - Spinodal (3.4.3)
    - BeacaugeExpPowLaw (3.3.8)
    - BeacaugeExpPowLaw2 (3.3.8)
    - Guinier 3.4.6
- cylindrical obj. (3.6)
    - Disc (3.6.1)
    - Rod (3.6.2)
    - EllCylShell
    - PorodCylinder (3.6.5)
    - LongCylinder (3.6.3)
    - FlatCylinder (3.6.4)
    - Cylinder (3.6.6)
    - LongCylShell (3.6.7)
    - CylShell1 (3.6.7)
    - CylShell2 (3.6.7)
    - ellCylShell1 (3.6.8)
    - ellCylShell2 (3.6.8)

  - alignedCylShell
  - partly aligned CylShell
  - Torus (3.6.11)
  - anisotropic obj.
    * Pcs(Q) for planar obj.
      · Pcs:homogenousXS (3.7.2.1)
      · Pcs:TwoInfinitelyThinPlates (3.7.3)
      · Pcs:LayeredCentroSymmetricXS(3.7.4)
      · Pcs:BiLayerGauss (3.7.5)
      · Pcs:Plate+Chains(RW)
    * Pcs(Q) for cylindrical obj.
      · Pcs:homogeneousXS
      · Pcs:CylindricalShell
      · Pcs:Rod+Chains(RW)
      · Pcs:ellCylSh
- plane obj.
  - homogenousXS (3.7.2.1)
  - SphSh+SD+homoXS
  - EllSh+SD+homoXS
  - EllSh+SD+homoXS(S)
  - CylSh+SD+homoXS
  - Disc+homoXS
  - TwoInfinitelyThinPlates (3.7.3)
  - LayeredCentroSymmetricXS (3.7.4)
  - BiLayerGauss (3.7.5)
- sheared objects
  - ShearedCylinder (3.8.1)
  - ShearedCylGauss (3.8.3)
- magnetic objects (3.9)
  - MagneticShellPsi (3.9.1.3)
  - MagneticShellAniso (3.9.1.1)
  - MagneticShellCrossTerm (3.9.1.2)
  - SuperparamagneticFFpsi (3.9.2.1)
  - SuperparamagneticFFAniso (3.9.2.2)
  - SuperparamagneticFFIso (3.9.2.3)
  - SuperparamagneticFFCrossTerm (3.9.2.4)
- Mie FF for SLS (3.10)
  - MieSphere (3.10.1)
  - MieShell (3.10.2)
- Peaks (6)
  - Amplitude Functions
    * Beta (Amplitude) (6.1.1)
    * Chi-squared (Amplitude) (6.2.1)
    * Erfc (Amplitude) (6.3.1
    * Error (Amplitude) (6.4.1)
    * exponentially modified Gaussian (Amplitude) (6.5.1)

        * `LogNormal, 4 parameters (Area)` (6.23.2)
        * `LogNormal (Area)` (6.24.2)
        * `Lorentzian (Area)` (6.25.2)
        * `Pearson IV (Area)` (6.27.2)
        * `Pearson VII (Area)` (6.28.2)
        * `pulse (Area)` (6.29.2)
        * `pulse with 2nd width (Area)` (6.30.2)
        * `pulse with power term (Area)` (6.31.2)
        * `Student-t (Area)` (6.32.2)
        * `Voigt (Area)` (6.33.2)
        * `Weibull (Area)` (6.33.5)
- other functions
  - Langevin
  - DoubleShell_withSD
  - SuperparStroboPsi
  - SuperparStroboPsi2
  - SuperparStroboPsiSQ
  - SuperparStroboPsiBt1
  - SuperparStroboPsiLx
  - SuperparStroboPsiL2x
  - DLS_Sphere_RDG
  - Robertus1
  - JülichMicelle

3.1. Spheres & Shells

3.1.1. Sphere.

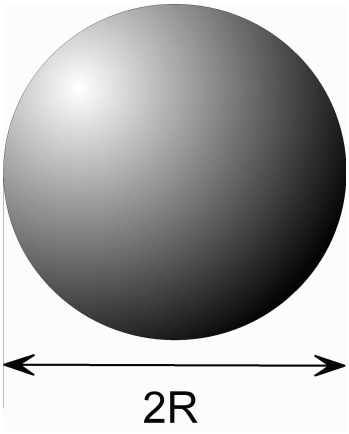

FIGURE 3.1. Sphere with diameter $2R$

$$I_{\text{Sphere}}(Q,R) = K^2(Q,R,\Delta\eta) \tag{3.1a}$$

with

$$K(Q,R,\Delta\eta) = \frac{4}{3}\pi R^3 \Delta\eta\, 3\frac{\sin QR - QR\cos QR}{(QR)^3} \tag{3.1b}$$

The forward scattering for $Q = 0$ is given by

$$\lim_{Q=0} I_{\text{Sphere}}(Q,R) = \left(\frac{4}{3}\pi R^3 \Delta\eta\right)^2$$

Input Parameters for model `Sphere`:

`R:` radius of sphere R
`- - -:` not used
`- - -:` not used
`eta:` scattering length density difference between particle and matrix $\Delta\eta$

Note:

- The parameters `param.p[1]` and `param.p[2]` are not used.

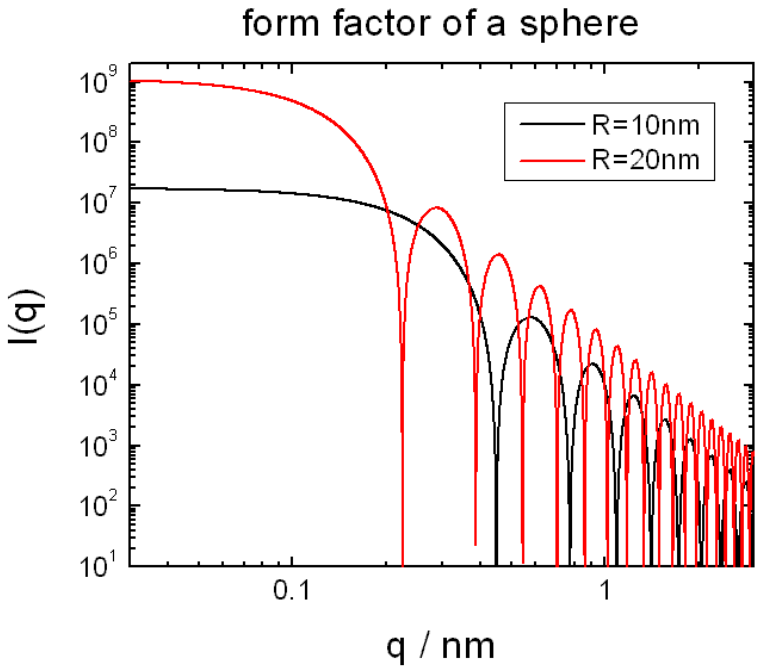

FIGURE 3.2. Scattering intensity of spheres with radii $R = 10$nm and $R = 20$nm. The scattering length density contrast is set to 1.

3.1.2. Spherical Shell i.

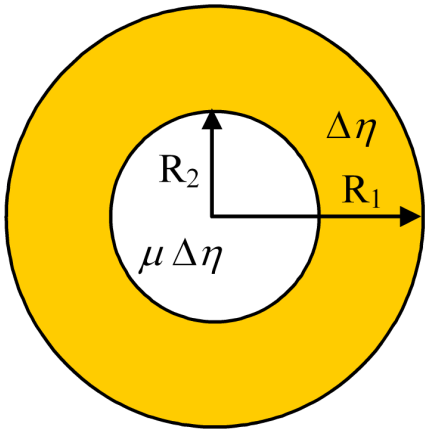

FIGURE 3.3. Spherical Shell i

This implementation of a spherical shell is parametrised with an inner radius R_2 and outer radius R_1. The scattering contrast relative to the matrix of the core is $\mu\Delta\eta$ and the one of the shell $\Delta\eta$.

$$I_{\text{Shell1}}(Q, R_1, R_2, \Delta\eta, \mu) = \left[K(Q, R_1, \Delta\eta) - K(Q, R_2, \Delta\eta(1-\mu))\right]^2 \tag{3.2}$$

with

$$K(Q, R, \Delta\eta) = \frac{4}{3}\pi R^3 \Delta\eta \, 3\frac{\sin QR - QR\cos QR}{(QR)^3} \tag{3.3}$$

The forward scattering for $Q = 0$ is given by

$$\lim_{Q=0} I_{\text{Shell1}}(Q, R_1, R_2, \Delta\eta, \mu) = \left(\frac{4}{3}\pi\Delta\eta\left[R_1^3 - R_2^3(1-\mu)\right]\right)^2$$

Input Parameters for model `Spherical Shell i`:

`R1:` overall radius of spherical shell R_1
`R2:` radius of core R_2
`eta:` scattering length density difference between shell and matrix $\Delta\eta$
`mu:` scattering length density difference between core and matrix relative to the shell contrast μ

Note:

None

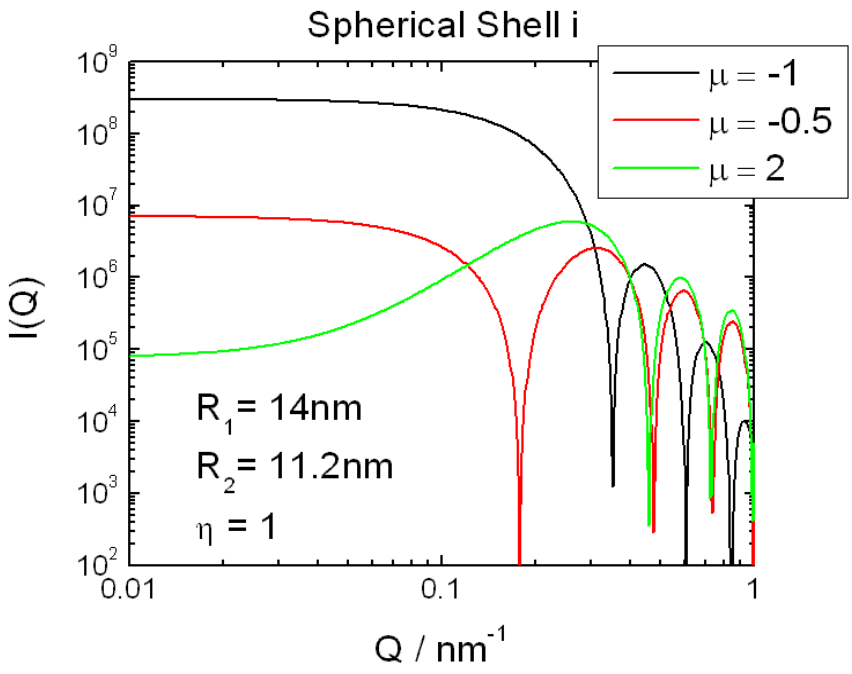

FIGURE 3.4. Scattering intensity of spherical shell with outer radius of $R_1 = 14$nm and inner radius of $R_2 = 11.2$nm. The scattering length density contrast the shell is set to 1 and the one of the core to -1, -0.5, and 2.

3.1.3. Spherical Shell ii.

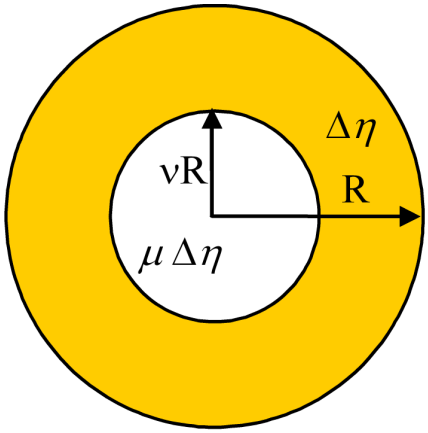

FIGURE 3.5. `Spherical Shell ii`

This implementation of a spherical shell is parametrised with an outer radius R and an inner radius νR. The scattering contrast relative to the matrix of the core is $\mu\Delta\eta$ and the one of the shell $\Delta\eta$.

$$I_{\text{Shell2}}(Q,R,\nu,\Delta\eta,\mu) = \left(K(Q,R,\Delta\eta) - K(Q,\nu R,\Delta\eta(1-\mu))\right)^2 \tag{3.4}$$

with

$$K(Q,R,\Delta\eta) = \frac{4}{3}\pi R^3\Delta\eta\, 3\frac{\sin QR - QR\cos QR}{(QR)^3} \tag{3.5}$$

The forward scattering for $Q = 0$ is given by

$$\lim_{Q=0} I_{\text{Shell2}}(Q,R,R,\Delta\eta,\mu) = \left(\frac{4}{3}\pi\Delta\eta\left[R^3 - \nu^3R^3(1-\mu)\right]\right)^2$$

Input Parameters for model `Spherical Shell ii`:

`R:` overall radius of spherical shell R
`nu:` the radius of the core is only the fraction ν of the overall radius R
`eta:` scattering length density difference between shell and matrix $\Delta\eta$
`mu:` scattering length density difference between core and matrix relative to the shell contrast μ

Note:

None

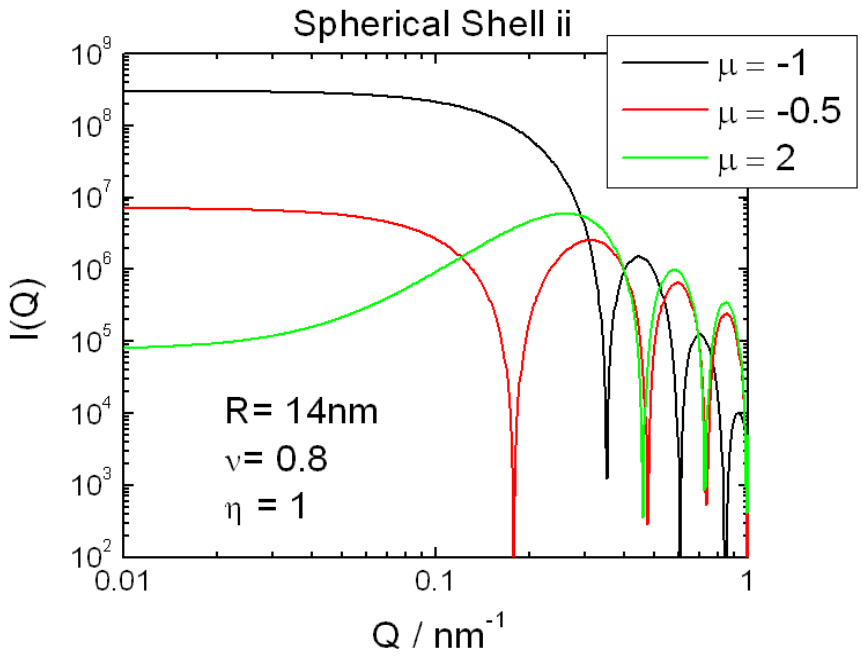

FIGURE 3.6. Scattering intensity of spherical shell with outer radius of $R = 14$nm and inner radius of $\nu R = 11.2$nm. The scattering length density contrast the shell is set to 1 and the one of the core to -1, -0.5, and 2.

3.1.4. Spherical Shell iii.

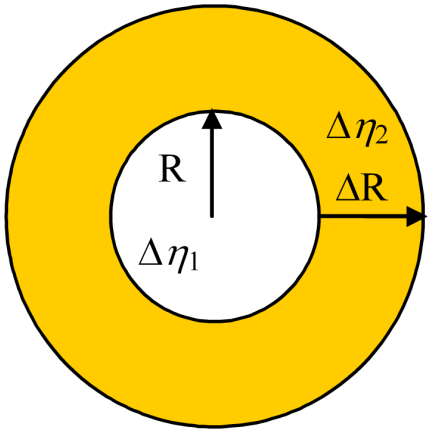

FIGURE 3.7. Spherical Shell iii

This implementation of a spherical shell is parametrised with an inner radius R and a shell thickness ΔR. The scattering contrast relative to the matrix of the core is $\Delta\eta_1$ and the one of the shell $\Delta\eta_2$.

$$I_{\text{Shell3}}(Q,R,\Delta R,\Delta\eta_1,\Delta\eta_2) = [K(Q,R+\Delta R,\Delta\eta_2) - K(Q,R,\Delta\eta_2-\Delta\eta_1)]^2 \tag{3.6}$$

with

$$K(Q,R,\Delta\eta) = \frac{4}{3}\pi R^3\Delta\eta\, 3\frac{\sin QR - QR\cos QR}{(QR)^3} \tag{3.7}$$

The forward scattering for $Q=0$ is given by

$$\lim_{Q=0} I_{\text{Shell3}}(Q,R,\Delta R,\Delta\eta_1,\Delta\eta_2) = \left(\frac{4}{3}\pi\left[(R+\Delta R)^3\Delta\eta_2 - R^3(\Delta\eta_2-\Delta\eta_1)\right]\right)^2$$

Input Parameters for model `Spherical Shell iii`:

`R:` radius of core R
`dR:` thickness of the shell ΔR
`eta1:` scattering length density difference between core and matrix $\Delta\eta_1$
`eta2:` scattering length density difference between shell and matrix $\Delta\eta_2$

Note:

None

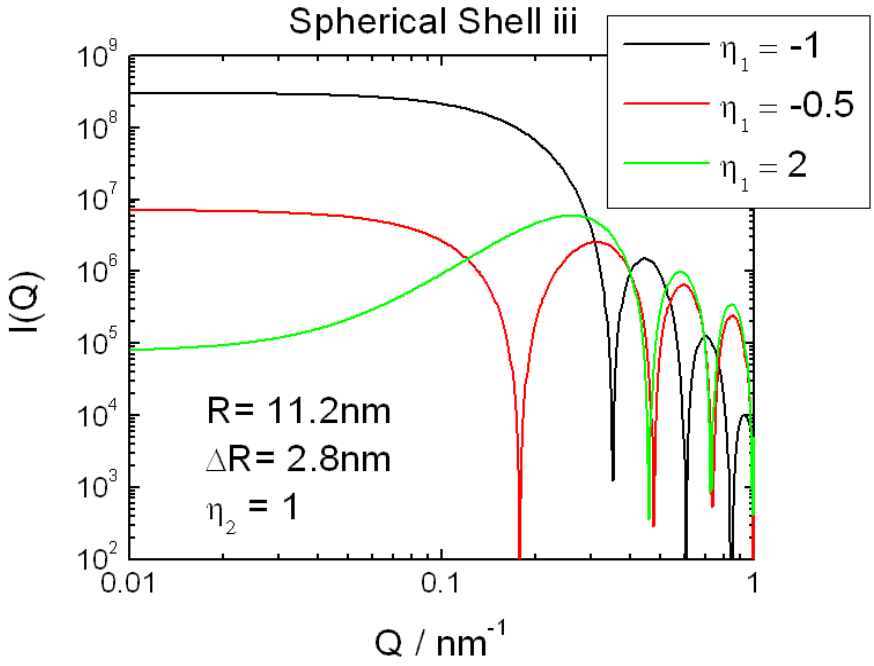

FIGURE 3.8. Scattering intensity of spherical shell with core radius of $R = 11.2$nm and shell thickness of $\Delta R = 2.8$nm. The scattering length density contrast the shell is set to 1 and the one of the core to -1, -0.5, and 2.

3.1.5. Bilayered Vesicle.

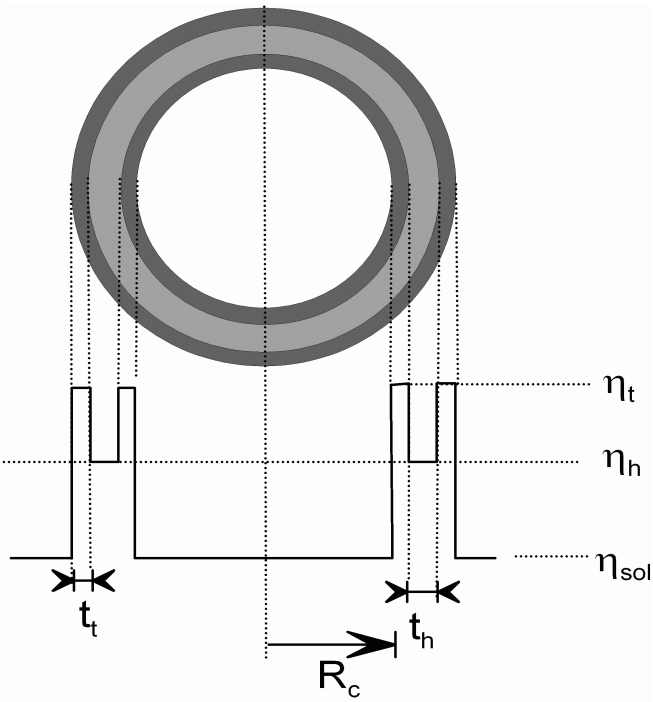

FIGURE 3.9. BiLayeredVesicle

$$I_{\mathrm{BLV}}(Q) = \Big(+ K(Q, R_c, \eta_{sol} - \eta_t) + K(Q, R_c + t_t, \eta_t - \eta_h) \tag{3.8}$$
$$+ K(Q, R_c + t_t + t_h, \eta_h - \eta_t) + K(Q, R_c + 2t_t + t_h, \eta_t - \eta_{sol}) \Big)^2$$

with

$$K(Q, R, \Delta\eta) = \frac{4}{3}\pi R^3 \Delta\eta \, 3\frac{\sin QR - QR\cos QR}{(QR)^3} \tag{3.9}$$

Input Parameters for model `BilayeredVesicle`:

`R_c`: radius of core R_c which consists of solvent
`t_h`: thickness of outer part of bilayer (in contact with solvent, head group) t_h
`t_t`: thickness of inner part of bilayer (tail group) t_t
`eta_sol`: scattering length density of solvent η_sol
`eta_h`: scattering length density of outer part of bilayer η_h
`eta_t`: scattering length density of inner part of bilayer η_t

Note:

None

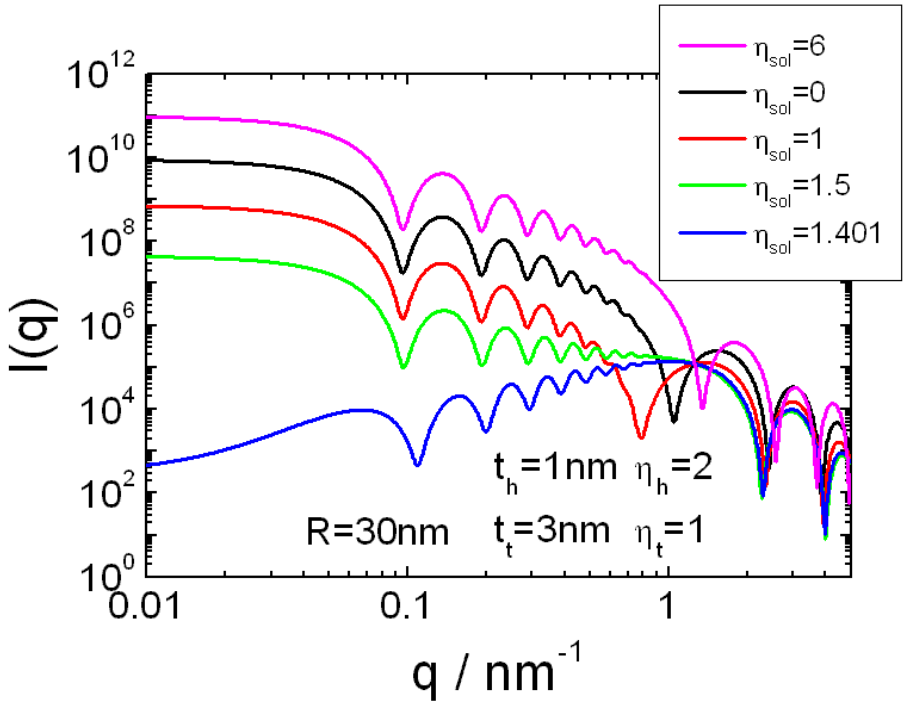

FIGURE 3.10. Scattering intensity of a bilayered vesicle. The scattering intensity has been calculated with a lognormal [LogNorm($N=1, \sigma=0.05, p=1, R=30$)] size distribution for the vesicle radius R_c.

3.1.6. Multi Lamellar Vesicle.

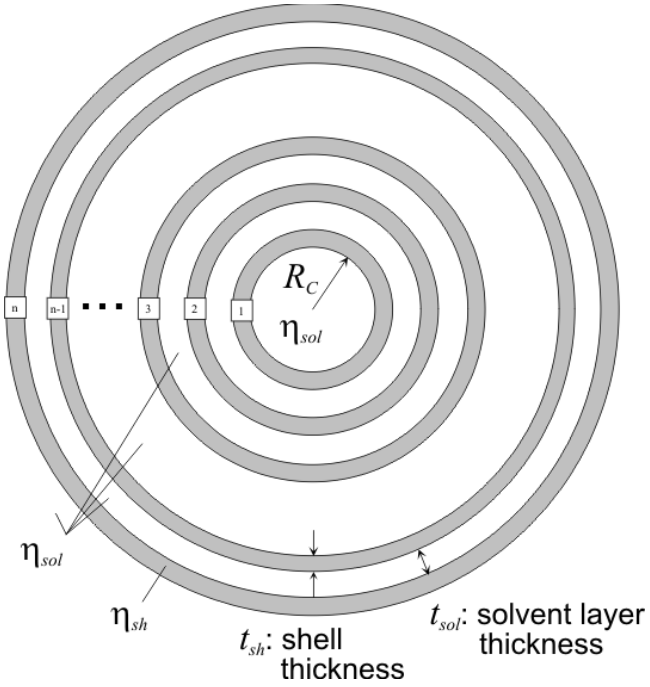

FIGURE 3.11. MultiLamellarVesicle

$$I_{\mathrm{MLV}}(Q) = \left(\sum_{i=0}^{n-1} \Big[K(Q, R_c + it_{sh} + it_{sol}, \eta_{sol} - \eta_{sh}) + K(Q, R_c + (i+1)t_{sh} + it_{sol}, \eta_{sh} - \eta_{sol}) \Big] \right)^2 \tag{3.10}$$

with

$$K(Q, R, \Delta\eta) = \frac{4}{3}\pi R^3 \Delta\eta \, 3\frac{\sin QR - QR\cos QR}{(QR)^3} \tag{3.11}$$

Input Parameters for model `MultiLamellarVesicle`:

`R_c`: radius of core R_c which consists of solvent
`t_sh`: surfactant layer thickness t_{sh}
`t_sol`: thickness of solvent layer t_{sol}
`eta_sh`: scattering length density of surfactant layer η_{sh}
`eta_sol`: scattering length density of solvent η_{sol}
`n`: total number of surfactant layers n

Note:

None

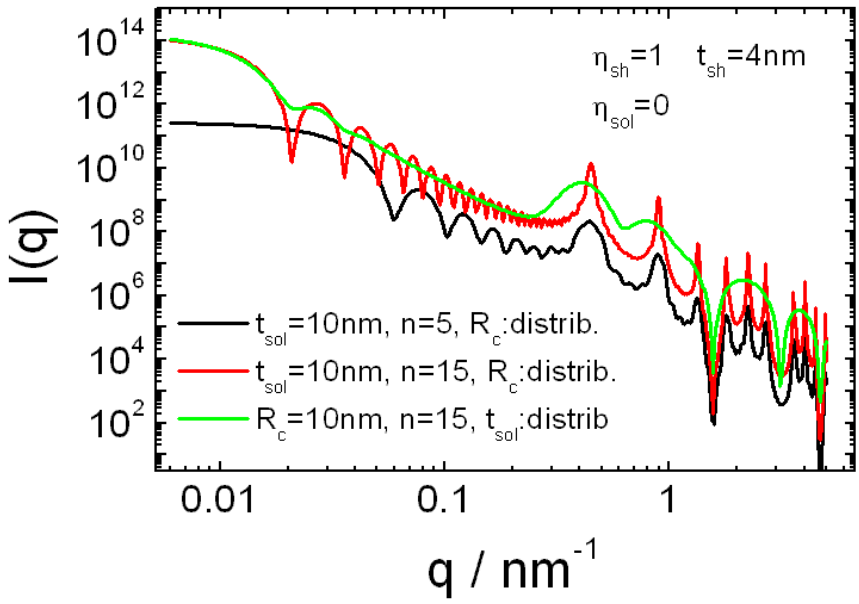

FIGURE 3.12. Scattering intensity of a multilamellar vesicle. The scattering intensities has been calculated for a&b) a distribution of the core radius R_c by $\int \mathrm{LogNorm}(R_c; N=1, \sigma=0.3, p=1, R=10) I(q, R_c)\, \mathrm{d}R_c$ and c) for a distribution of the distances between the lamellars $\int \mathrm{LogNorm}(t_{\mathrm{sol}}; N=1, \sigma=0.3, p=1, R=10) I(q, t_{\mathrm{sol}})\, \mathrm{d}t_{\mathrm{sol}}$.

3.1.7. RNDMultiLamellarVesicle.

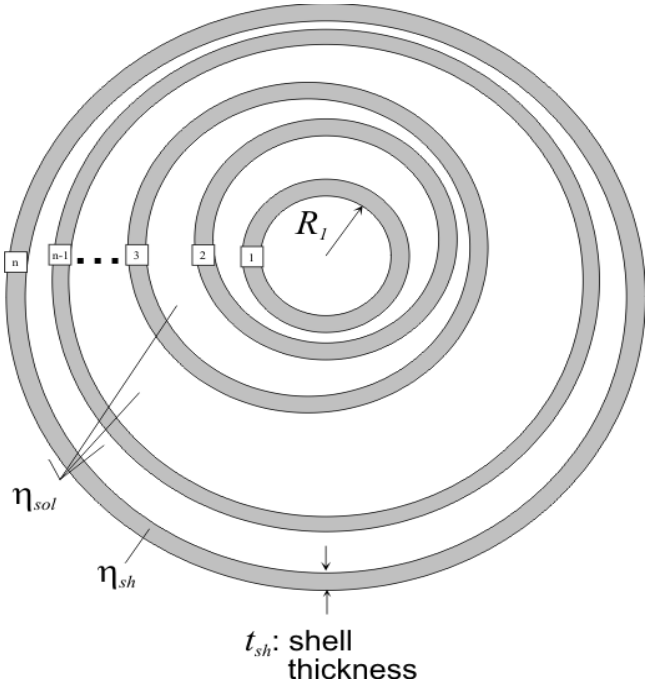

FIGURE 3.13. randomMultiLamellarVesicle

$$I_{\mathrm{RndMLV}}(Q) = \Delta\eta^2 \sum_{i=1}^{N} F_i^2(q, R_i, t_{sh,i}) + \Delta\eta^2 \sum_{i<j}^{N} 2F_i(q, R_i, t_{sh,i}) F_j(q, R_j, t_{sh,j}) \frac{\sin qr_{ij}}{qr_{ij}} \tag{3.12}$$

with

$$r_{ij} = |\mathbf{R}_i - \mathbf{R}_j| \tag{3.13a}$$

$$F_i(q, R_i, t_{sol,i}) = K(q, R_i + t_{sol,i}, \Delta\eta) - K(q, R_i, \Delta\eta) \tag{3.13b}$$

$$K(q, R, \Delta\eta) = \frac{4}{3}\pi R^3 \Delta\eta \, 3\frac{\sin qR - qR\cos qR}{(qR)^3} \tag{3.13c}$$

$$R_1 = \mathrm{ran}_{lognormal}\left(\log(R_c), \sigma_{R_c}\right) \tag{3.14a}$$

$$\Delta R_i = \mathrm{ran}_{gaussian}\left(\sigma_{t_{sol}}\right) \tag{3.14b}$$

$$R_i = R_{i-1} + t_{sh,i-1} + \Delta R_i \tag{3.14c}$$

$$\mathbf{R}_i = R_i \, \mathbf{ran}_{dir,3D} \mathrm{ran}_{uniform} \, \Delta t_{sol} \tag{3.14d}$$

Input Parameters for model `RNDMultiLamellarVesicle`:

`t_sh`: average surfactant layer thickness t_{sh}
`s_sh`: Gaussian thickness distribution of surfactant layer with a width of σ_{sh}
`R_c`: average radius of core R_c which consists of solvent
`s_c`: lognormal size distribution of core radius R_c with a width of σ_c
`n`: average number of surfactant layers n
`s_n`: lognormal distribution of the number of surfactant layers with a width of σ_n
`t_sol`: average thickness of solvent layer t_{sol}
`s_sol`: lognormal thickness distribution of solvent layer with a width of σ_{sol}
`Deta_sh`: scattering length density contrast $\Delta\eta$ between surfactant layer and solvent

Note:

The number of Monte Carlo iterations can be set via the menu `[Options|Customize...]`

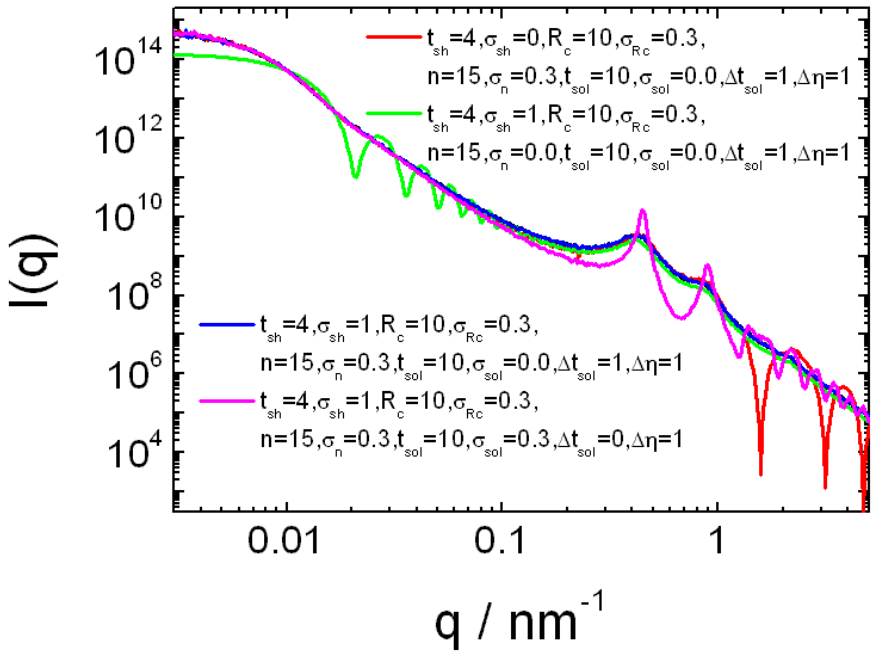

FIGURE 3.14. Scattering intensity of a multilamellar vesicle where several distribution of parameters within a single vesicle are calculated via a Monte Carlo algorithm. .

3.1.8. Vesicle with aligned flat capped ends [52, 53].

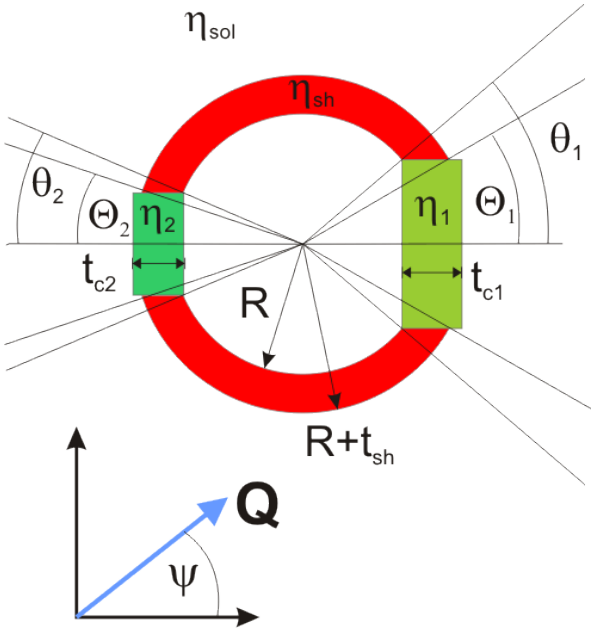

FIGURE 3.15. Sketch of a vesicle with horizontally aligned flat capped ends perpendicular to the incoming neutron beam

The shape of this form factor consist of spherical vesicle containing to flat domains. The flat thought to be aligned in a horizontal magnetic field perpendicular to the incoming neutron beam. The size of the domains are characterized by the angles θ_1 and $theta_2$. The thicknesses t_{c1} and t_{c2} can be different than the thickness t_{sh} of the spherical part of the vesicles. The same hold for the scattering length densities η_{c1}, η_{c2} and η_{sh}. The form factor $F_{\mathrm{cv}}(Q)$ of this object can be calculated by performing the Fourier transformation of the scattering length density in separate steps. First one calculates the Fourier transformation of a sphere F_{cSph} with flat capped ends on each side in cylinder coordinates.

$$F_{\mathrm{cSph}}(Q,R,\psi,\theta_1,\theta_2,\Delta\eta) = \Delta\eta \int_{-R\cos\theta_2}^{R\cos\theta_1} \mathrm{d}z \int_0^{\sqrt{R^2-z^2}} \mathrm{d}\rho \int_0^{2\pi} \mathrm{d}\phi \;\; e^{\imath\mathbf{Q}\cdot\mathbf{r}}\,\rho \tag{3.15a}$$

$$\text{with} \quad \mathbf{Q} = Q\begin{pmatrix} 0 \\ \sin\psi \\ \cos\psi \end{pmatrix} \quad \text{and} \quad \mathbf{r} = \begin{pmatrix} \rho\cos\phi \\ \rho\sin\phi \\ z \end{pmatrix} \tag{3.15b}$$

The form factor of vesicle $F_{\mathrm{cv}}(Q)$ with a layer thickness of t_{sh} can than be calculated by

$$\begin{aligned} F_{\mathrm{cv}}(Q,R,t_{\mathrm{sh}},\theta_1,\theta_2,\Delta\eta_{\mathrm{sh}}) = &+ F_{\mathrm{cSph}}(Q,R+t_{\mathrm{sh}},\Theta_1,\Theta_2,\Delta\eta_{\mathrm{sh}}) \\ &- F_{\mathrm{cSph}}(Q,R,\theta_1,\theta_2,\Delta\eta_{\mathrm{sh}}) \end{aligned} \tag{3.16a}$$

with

$$\Theta_1 = \arcsin\left(\frac{R_{c1}}{R+t_{\mathrm{sh}}}\right), \quad R_{c1} = R\sin(\theta_1), \tag{3.16b}$$

$$\Theta_2 = \arcsin\left(\frac{R_{c2}}{R+t_{\mathrm{sh}}}\right), \quad R_{c2} = R\sin(\theta_2). \tag{3.16c}$$

As the flat capped ends are allowed to have independent thicknesses t_{c1}, t_{c2} and scattering length densities η_1, η_2 the scattering amplitude contribution of the flat capped ends, which have the shape of a disc, need to be corrected. Their contribution can be calculated by

$$\begin{aligned} F_{\mathrm{c}}(Q,R,\theta_1,\theta_2,\dots) = \quad & F_{\mathrm{c1}}(Q,R,\theta_1,\Delta\eta_{\mathrm{c1}}) - F_{\mathrm{d1}}(Q,R,t_{\mathrm{d1}},\Delta\eta_{\mathrm{sh}}) \\ & + F_{c2}(Q,R,\theta_2,\Delta\eta_{\mathrm{c2}}) - F_{\mathrm{d2}}(Q,R,t_{\mathrm{d2}},\Delta\eta_{\mathrm{sh}}) \\ = \quad & \Delta\eta_{\mathrm{c1}} \int_{l_{\mathrm{c1}}}^{l_{\mathrm{c1}}+t_{\mathrm{c1}}} \mathrm{d}z \int_0^{R_{\mathrm{c1}}} \mathrm{d}\rho \int_0^{2\pi} \mathrm{d}\phi \; e^{\imath\mathbf{Q}\cdot\mathbf{r}}\,\rho - \Delta\eta_{\mathrm{sh}} \int_{l_{\mathrm{c1}}}^{l_{\mathrm{c1}}+t_{\mathrm{d1}}} \mathrm{d}z \int_0^{R_{\mathrm{c1}}} \mathrm{d}\rho \int_0^{2\pi} \mathrm{d}\phi \; e^{\imath\mathbf{Q}\cdot\mathbf{r}}\,\rho \\ & + \Delta\eta_{\mathrm{c2}} \int_{-(l_{\mathrm{c2}}+t_{\mathrm{c2}})}^{-l_{\mathrm{c2}}} \mathrm{d}z \int_0^{R_{\mathrm{c2}}} \mathrm{d}\rho \int_0^{2\pi} \mathrm{d}\phi \; e^{\imath\mathbf{Q}\cdot\mathbf{r}}\,\rho - \Delta\eta_{\mathrm{sh}} \int_{-(l_{\mathrm{c2}}+t_{\mathrm{d2}})}^{-l_{\mathrm{c2}}} \mathrm{d}z \int_0^{R_{\mathrm{c2}}} \mathrm{d}\rho \int_0^{2\pi} \mathrm{d}\phi \; e^{\imath\mathbf{Q}\cdot\mathbf{r}}\,\rho \end{aligned} \tag{3.17}$$

with

$$\Delta\eta_{\mathrm{sh}} = \eta_{\mathrm{sh}} - \eta_{\mathrm{sol}},\ \Delta\eta_{\mathrm{c1}} = \eta_1 - \eta_{\mathrm{sol}},\ \Delta\eta_{\mathrm{c2}} = \eta_2 - \eta_{\mathrm{sol}} \tag{3.18a}$$

$$l_{\mathrm{c1}} = R\cos\theta_1,\ l_{\mathrm{c2}} = R\cos\theta_2 \tag{3.18b}$$

$$R_{\mathrm{c1}} = R\sin\theta_1,\ R_{\mathrm{c2}} = R\sin\theta_2 \tag{3.18c}$$

$$t_{\mathrm{d1}} = \sqrt{(R+t_{\mathrm{sh}})^2 - R_{\mathrm{c1}}^2} - \sqrt{R^2 - R_{\mathrm{c1}}^2} \tag{3.18d}$$

$$t_{\mathrm{d2}} = \sqrt{(R+t_{\mathrm{sh}})^2 - R_{\mathrm{c2}}^2} - \sqrt{R^2 - R_{\mathrm{c2}}^2} \tag{3.18e}$$

$$\tag{3.18f}$$

The solution of the integrals in eq. 3.15a and 3.17 are

$$\begin{aligned} F_{\mathrm{cSph}}(Q,R,\psi,\theta_1,\theta_2,\Delta\eta) = \Delta\eta & \int_{-R\cos\theta_2}^{R\cos\theta_1} \mathrm{d}z \int_0^{\sqrt{R^2-z^2}} \mathrm{d}\rho \int_0^{2\pi} \mathrm{d}\phi \;\; e^{\imath\mathbf{Q}\cdot\mathbf{r}}\,\rho \\ \Delta\eta & \int_{-R\cos\theta_2}^{R\cos\theta_1} \mathrm{d}z \;\; \exp(\imath Qz\cos\psi)\, 2\pi\left(R^2-z^2\right) \frac{J_1\left(Q\sqrt{R^2-z^2}\sin\psi\right)}{Q\sqrt{R^2-z^2}\sin\psi} \end{aligned} \tag{3.19a}$$

and

$$F_{\mathrm{c}_i,\mathrm{d}_i}(Q,R_{\mathrm{c}_i,\mathrm{d}_i},\psi,\Delta\eta) = \Delta\eta \int_a^b \mathrm{d}z \int_0^{R_{\mathrm{c}_i}} \mathrm{d}\rho \int_0^{2\pi} \mathrm{d}\phi \;\; e^{\imath\mathbf{Q}\cdot\mathbf{r}}\,\rho$$

$$= 4\pi R \frac{\imath\left(\exp\left(\imath aQ\cos\psi\right) - \exp\left(\imath bQ\cos\psi\right)\right) J_1\left(QR\sin\psi\right)}{\sin\left(2\psi\right)Q^2} \tag{3.19b}$$

whereby J_1 the regular cylindrical Bessel function of first order. The overall scattering intensity $I_{\mathrm{alignedVes}}(Q,\psi,\dots)$ is finally given by

$$I_{\mathrm{alignedVes}}(Q,\psi,\dots) = \left|F_{\mathrm{cv}}(Q,R,\psi,t_{\mathrm{sh}},\theta_1,\theta_2,\Delta\eta_{\mathrm{sh}}) + F_{\mathrm{c}}(Q,R,\psi,\theta_1,\theta_2,\dots)\right|^2 \tag{3.20}$$

Input Parameters for the models of `MagneticFieldAlignedVesicle`:

`Rsh`: radius of spherical vesicle shell
`theta1`: angle to describe size of first capped side
`theta2`: angle to describe size of second capped side
`t_sh`: thickness of spherical vesicle shell
`t_c1`: thickness of first flat capped side
`t_c2`: thickness of second flat capped side
`eta_sh`: scattering length density of spherical vesicle shell
`eta_1`: scattering length density of first capped side
`eta_2`: scattering length density of second capped side
`eta_sol`: scattering length density of solvent

Note:

None

3.2. Ellipsoidal Objects

3.2.1. Ellipsoid with two equal semi-axis R and semi-principal axes νR.

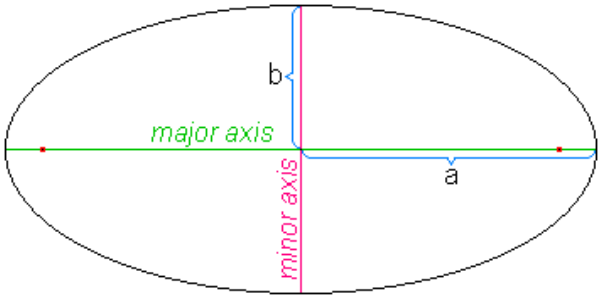

FIGURE 3.16. Ellipse, showing major and minor axes and parameters a and b

An ellipsoid is a quadric surface in three dimensions obtained by rotating an ellipse about one of its principal axes. Three particular cases of an ellipsoid are:

- If the ellipse is rotated about its major axis, the surface is a prolate spheroid.
- If the ellipse is rotated about its minor axis, the surface is an oblate spheroid.
- If the generating ellipse is a circle, the surface is a sphere.

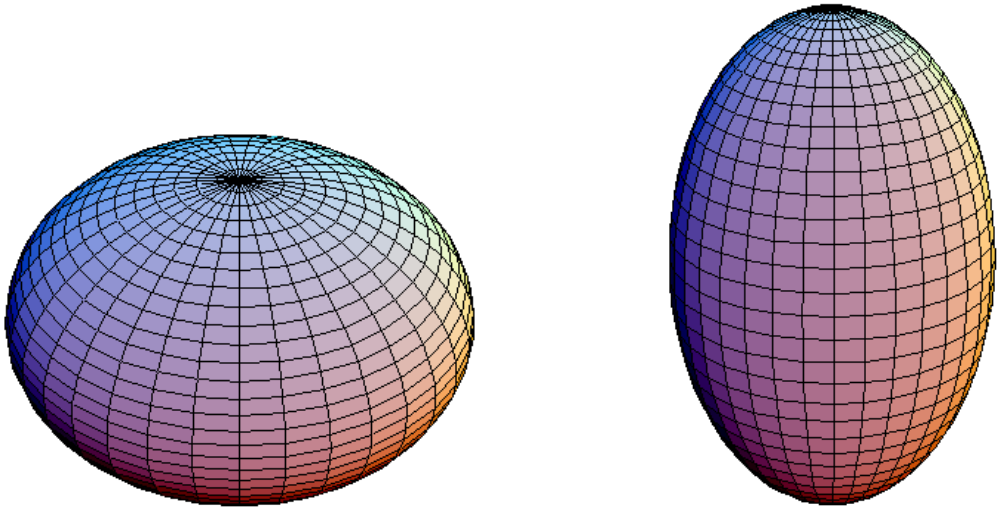

(a) oblate spheroid ($\nu < 1$) (b) prolate spheroid ($\nu > 1$)

FIGURE 3.17. A spheroid is an ellipsoid having two equal equatorial semi-axes. If the equatorial semi-axis are larger than the principal axis the spheroid becomes oblate (a), if they are smaller it becomes prolate (b) and if they are equal the spheroid becomes a perfect sphere

$$I_{\text{ii}}(Q,R,\nu) = \left(\frac{4}{3}\pi R^3\Delta\eta\right)^2 \int_0^{\frac{\pi}{2}} K^2\left(Q, R\sqrt{\nu^2\cos^2\Theta + \sin^2\Theta}\right)\sin\Theta\, d\Theta \qquad (3.21)$$

with $\lim_{Q=0} I_{\text{ii}}(Q,R,\nu) = \left(\frac{4}{3}\pi\nu R^3\Delta\eta\right)^2$

Input Parameters for model `Ellipsoid ii`:

`R:` radius of the rotational axes

`nu:` ratio between radius of the semi-principle axes and equatorial axis. Values of $\nu < 1$ describe a oblate ellipsoid, a value of $\nu = 1$ a sphere, and $\nu > 1$ a prolate ellipsoid.

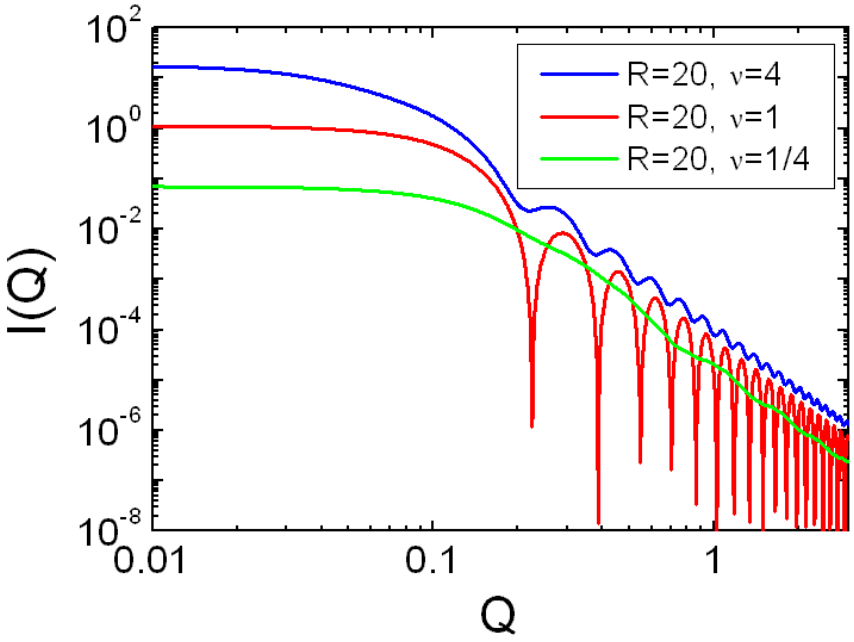

FIGURE 3.18. form factor of an ellipsoid with axis R, R and νR.

3.2.2. Ellipsoid with two equal equatorial semi-axis R and volume V.

$$I_{\mathrm{i}}(Q,R,\nu) = (V\Delta\eta)^2 \int_0^{\frac{\pi}{2}} K^2\left(Q, R\sqrt{\nu^2\cos^2\Theta + \sin^2\Theta}\right)\sin\Theta\, d\Theta \tag{3.22}$$

with

$$\nu = \frac{V}{R^3}\frac{3}{4\pi} \quad \text{so that} \quad V = \frac{4}{3}\pi\nu R^3$$

and $\lim_{Q=0} I_{\mathrm{i}}(Q,R,\nu) = (V\Delta\eta)^2$

Input Parameters for model `Ellipsoid i`:

`R:` radius of the rotational axes
`V:` total volume of the ellipsoid.

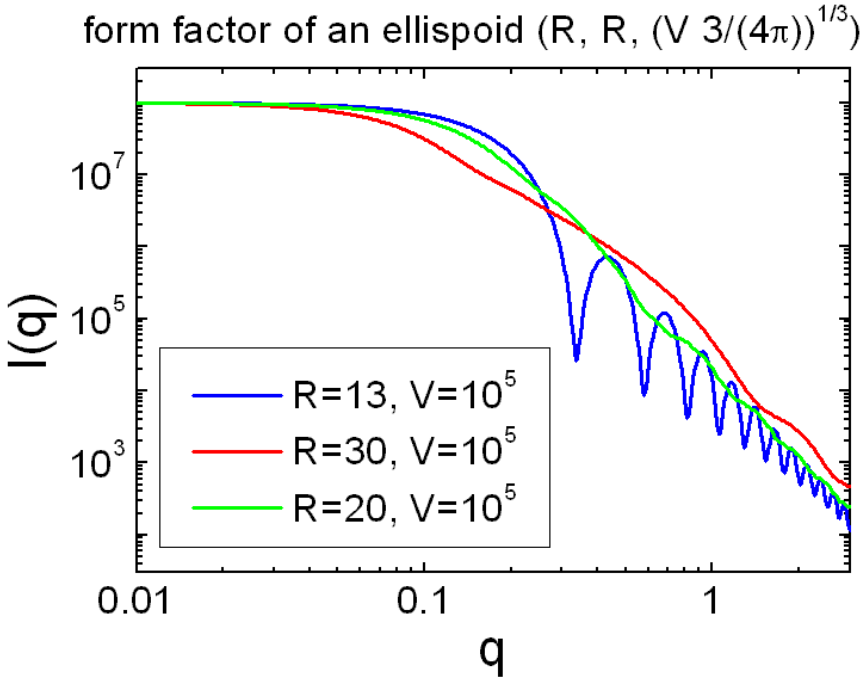

FIGURE 3.19. form factor of an ellipsoid with axis R, R and $\sqrt[3]{V\frac{3}{4\pi}}$.

3.2.3. Ellipsoidal core shell structure.

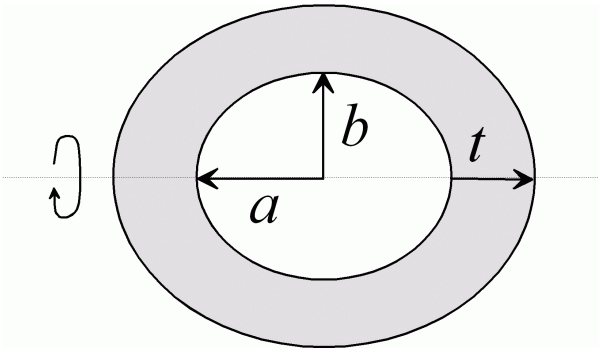

FIGURE 3.20.

$$I_{\mathrm{ECSh}}(Q) = \left\langle F^2(Q,\mu)\right\rangle = \int_0^1 \left[F(Q,\mu)\right]^2 d\mu \tag{3.23}$$

$$\left\langle F(Q,\mu)\right\rangle^2 = \left[\int_0^1 F(Q,\mu)d\mu\right]^2 \tag{3.24}$$

$$F(Q,\mu) = (\eta_{\mathrm{c}} - \eta_{\mathrm{sh}})\, V_c \left[\frac{3j_1(x_c)}{x_c}\right] + (\eta_{\mathrm{sh}} - \eta_{\mathrm{sol}})\, V_t \left[\frac{3j_1(x_t)}{x_t}\right]$$

$$j_1(x) = \frac{\sin(x) - x\cos(x)}{x^2}$$

$$x_c = Q\sqrt{a^2\mu^2 + b^2(1-\mu^2)}$$

$$x_c = Q\sqrt{(a+t)^2\mu^2 + (b+t)^2(1-\mu^2)}$$

$$V_c = \frac{4}{3}\pi ab^2$$

$$V_t = \frac{4}{3}\pi(a+t)(b+t)^2$$

η_{c} : scattering length density of core
η_{sh} : scattering length density of shell
η_{sol} : scattering length density of solvent
a : semi-principal axes of elliptical core
b : equatorial semi-axis of elliptical core
t : thickness of shell
V_c : volume of core
V_t : total volume of core along with shell

Input Parameters for model `EllipsoidalCoreShell`:

- `a`: semi-principal axes of elliptical core a
- `b`: equatorial semi-axis axes of elliptical core b
- `t`: thickness of shell t
- `eta_c`: scattering length density of core η_{c}
- `eta_sh`: scattering length density of shell η_{sh}
- `eta_sol`: scattering length density of solvent η_{sol}

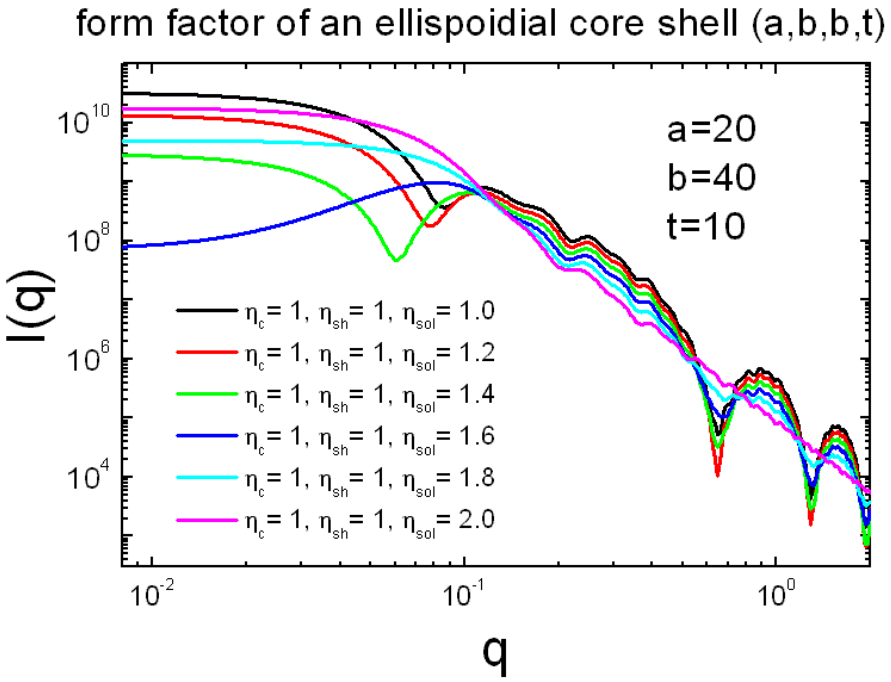

FIGURE 3.21. form factor of an ellipsoidal core shell a, b, b and t.

3.2.4. triaxial ellipsoidal core shell structure.

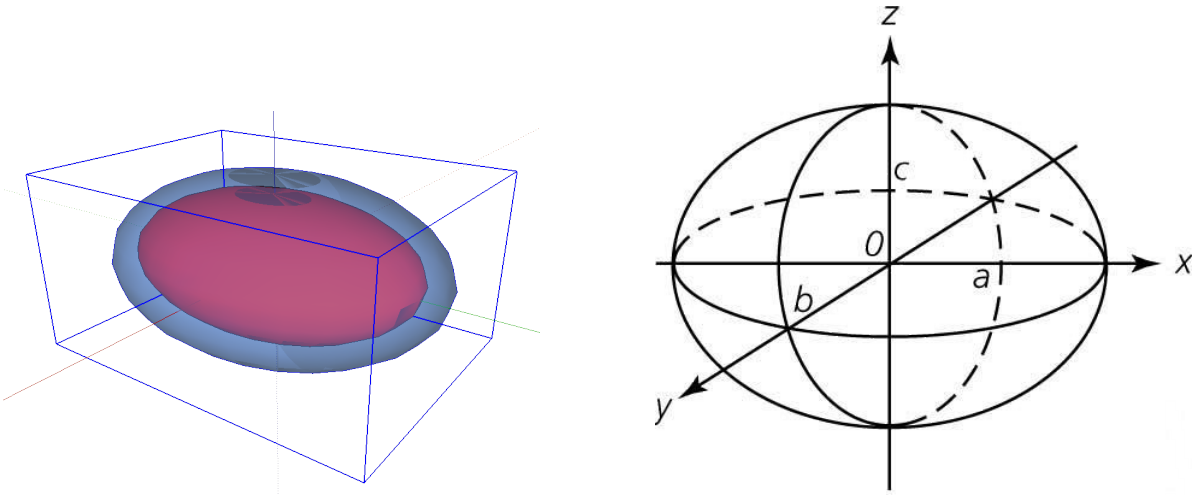

FIGURE 3.22. triaxial ellipsoidal core shell structure

$$I_{\text{triaxEllSh}}(Q) = \int_0^1 \int_0^1 dx\, dy\, K_{\text{sh}}^2(Q, R, R_t) \tag{3.25}$$

$$K(QR) = 3\frac{\sin QR - QR\cos QR}{(QR)^3} \tag{3.26}$$

$$K_{\text{sh}}(Q, R, R_t) = (\eta_{\text{c}} - \eta_{\text{sh}})\, K(QR) + (\eta_{\text{sh}} - \eta_{\text{sol}})\, K(QR_t) \tag{3.27}$$

$$R^2 = \left[a^2\cos^2(\pi x/2) + b^2\sin^2(\pi x/2)\right](1-y^2) + c^2y^2$$

$$R_t^2 = \left[(a+t)^2\cos^2(\pi x/2) + (b+t)^2\sin^2(\pi x/2)\right](1-y^2) + (c+t)^2y^2$$

$$V_c = \frac{4}{3}\pi abc$$

$$V_t = \frac{4}{3}\pi(a+t)(b+t)(c+t)$$

η_{c} : scattering length density of core
η_{sh} : scattering length density of shell
η_{sol} : scattering length density of solvent
a : semi-axes of elliptical core
b : semi-axes of elliptical core
c : semi-axes of elliptical core
t : thickness of shell
V_c : volume of core
V_t : total volume of core along with shell

Input Parameters for model `triaxEllShell1`:

`a`: semi-axes of elliptical core a
`b`: semi-axes of elliptical core b
`c`: semi-axes of elliptical core c
`t`: thickness of shell t
`eta_c`: scattering length density of core η_c
`eta_sh`: scattering length density of shell η_{sh}
`eta_sol`: scattering length density of solvent η_{sol}

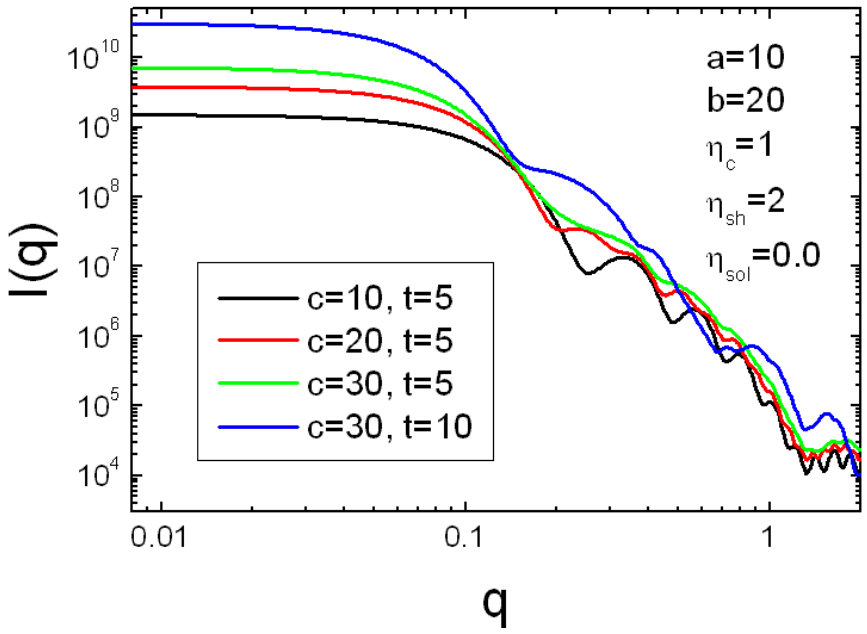

FIGURE 3.23. Form factor of an triaxial ellipsoidal core shell with semi axis a, b and c and a shell thickness t.

3.3. Polymers and Micelles

3.3.1. Gaussian chain.

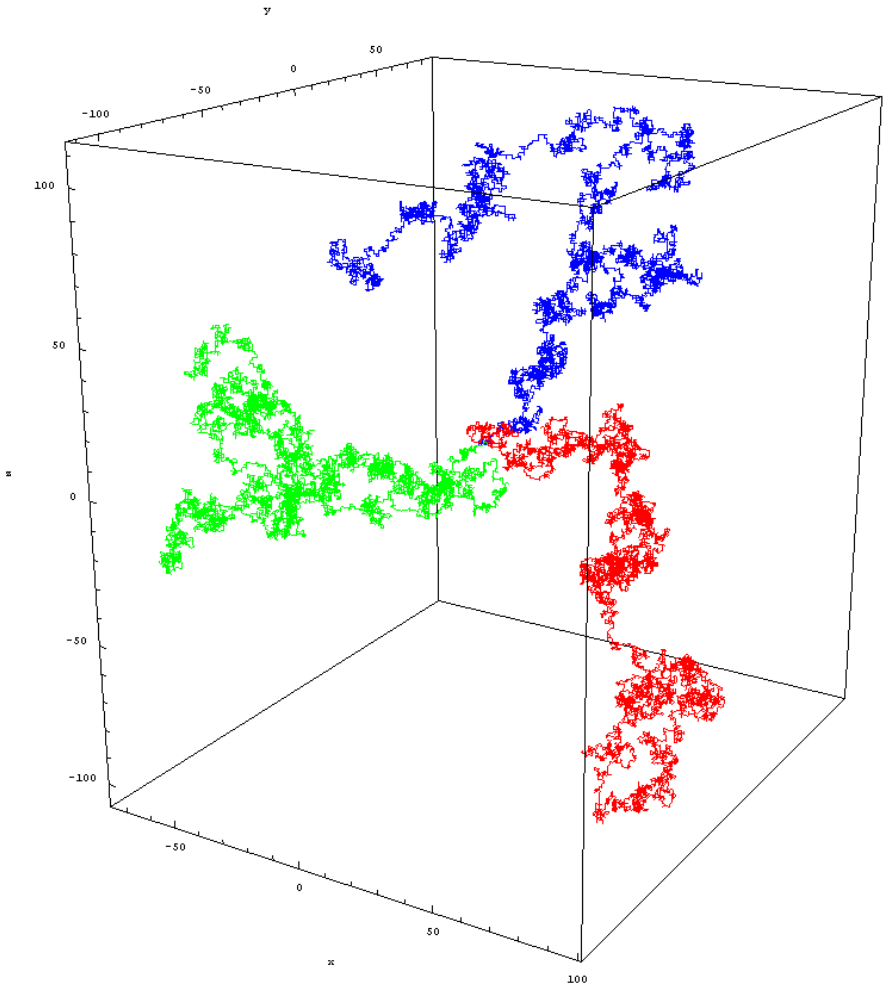

FIGURE 3.24. The underlying model for a polymer chain is an isotropic random walk on the euclidean lattice $\mathbb{Z}^3$. This picture shows three different walks after 10 000 unit steps, all three starting from the origin.

Consider a flexible polymer coil where each monomer located at a distance $\mathbf{R}_m$ its scattering field amplitude is given by

$$F(\mathbf{q},t)=\sum_{m=1}^{N} e^{-\imath\mathbf{q}\cdot\mathbf{R}_m(t)}. \tag{3.28}$$

The scattering intensity averaged over all molecule configurations reads

$$\left\langle |F(\mathbf{q})|^2 \right\rangle = \sum_{m,n} \left\langle e^{-\imath\mathbf{q}\cdot(\mathbf{R}_m-\mathbf{R}_n)} \right\rangle \tag{3.29}$$

As the monomer segments $\mathbf{R}_m - \mathbf{R}_n$ are Gaussian distributed the averages $\langle \cdots \rangle$ can be written as

$$\left\langle e^{-\imath \mathbf{q}\cdot(\mathbf{R}_m - \mathbf{R}_n)} \right\rangle = e^{\frac{q^2}{6}\left\langle (\mathbf{R}_m - \mathbf{R}_n)^2 \right\rangle} \tag{3.30a}$$

$$= e^{-\frac{q^2 b^2}{6}|m-n|^{2\nu}} \tag{3.30b}$$

Here b is the statistical segment length and the contour length L equals $L = Nb$. The average of the segment inter-distances squares is kept in the general form

$$\left\langle (\mathbf{R}_m - \mathbf{R}_n)^2 \right\rangle = b^2 |m-n|^{2\nu}. \tag{3.31}$$

ν is the excluded volume parameter from the Flory mean field theory[12] of polymer solutions. The radius of gyration R_G is given by

$$R_G^2 = \frac{1}{2N^2} \sum_{m,n}^{N} \left\langle (\mathbf{R}_m - \mathbf{R}_n)^2 \right\rangle \tag{3.32a}$$

$$= \frac{1}{2N^2} \sum_{m,n}^{N} b^2 |m-n|^{2\nu} \tag{3.32b}$$

$$= \frac{b^2}{N} \sum_{k}^{N} \left(1 - \frac{k}{N}\right) k^{2\nu} \tag{3.32c}$$

$$= \frac{b^2}{(2\nu+1)(2\nu+2)} N^{2\nu} \tag{3.32d}$$

Three cases are relevant:

(1) Self-avoiding walk corresponds to swollen chains with $\nu = 3/5$, for which $R_G^2 = \frac{25}{176} b^2 N^{6/5}$.
(2) Pure random walk corresponds to chains in Θ-conditions (where solvent-solvent, monomer-monomer and solvent-monomer interactions are equivalent) with $\nu = 1/2$, for which $R_G^2 = \frac{1}{6} b^2 N$.
(3) Self attracting walk corresponds to collapsed chains with $\nu = 1/3$, for which $R_G^2 = \frac{9}{40} b^2 N^{2/3}$.

Using the general identity

$$\sum_{i,j}^{N} y(|i-j|) = N + 2 \sum_{k=1}^{N} (N-k) y(k) \tag{3.33}$$

the form factor reads

$$P(q) = \frac{1}{N^2} |F(q)|^2 = \frac{1}{N^2} \left\{ N + 2 \sum_{k=1}^{N} (N-k) e^{-\frac{q^2 b^2}{6} k^{2\nu}} \right\} \tag{3.34}$$

[1] P.J. Flory, "Statistical Mechanics of Chain Molecules", Interscience Publishers (1969)
[2] Boualem Hammouda, `the_SANS_toolbox.pdf`

Going to the continuous limit ($N \gg 1$), one obtains:

$$P(q) = 2\int_0^1 \mathrm{d}x\ (1-x)e^{-\frac{q^2b^2}{6}N^{2\nu}x^{2\nu}} \tag{3.35a}$$

$$= \frac{U^{\frac{1}{2\nu}}\Gamma\left(\frac{1}{2\nu}\right) - \Gamma\left(\frac{1}{\nu}\right) - U^{\frac{1}{2\nu}}\Gamma\left(\frac{1}{2\nu}, U\right) + \Gamma\left(\frac{1}{\nu}, U\right)}{\nu U^{1/\nu}} \tag{3.35b}$$

with the modified variable

$$U = \frac{q^2b^2N^{2\nu}}{6} = (2\nu+1)\,(2\nu+2)\,\frac{q^2R_G^2}{6} \tag{3.36}$$

and the unnormalized incomplete Gamma Function $\Gamma(a,x) = \int_x^\infty \mathrm{d}t\ t^{a-1}\exp(-t)$ for a real and $x \geq 0$ and the Gamma function $\Gamma(a) = \Gamma(a,0) = \int_0^\infty \mathrm{d}t\ t^{a-1}\exp(-t)$. Polymer chains follow Gaussian statistics in polymer solutions: they are swollen in good solvents $\nu = 3/5$, are thermally relaxed in "theta"-solvents $\nu = 1/2$ and partially precipitate in poor solvents $\nu = 1/3$. The familiar Debye function is recovered when $\nu = 1/2$. The asymptotic limit at large q-values of the generalized Gaussian chain is dominated by the $\frac{1}{\nu U^{\frac{1}{2\nu}}}\Gamma\left(\frac{1}{2\nu}\right)$ term which varies like $U^{-1/(2\nu)} \sim q^{-1/\nu}$. For $\nu = 1$ we get the limit of an infinitesimal thin rod and for $\nu = 1/4$ a compact object with a Porod law of q^{-4}.

`SASfit` has implemented the generalized form of a Gaussian (`generalized Gaussian coil`) coil and the standard Debye formula `Gauss`. In both cases three version are implemented which only differ in their parametrization of the forward scattering. In case of the the Debye-formula also the polydisperse `GaussPoly` is implemented.

3.3.1.1. *Gauss* [**23**].
Flexible polymer chains which are not selfavoiding and obey Gaussian statistics. Debye (1947) has calculated the form factor of such chains:

$$I_{\mathrm{Gauss}}(q) = I_0 2\frac{\exp(-u) + u - 1}{u^2} \tag{3.37}$$

$$u = q^2R_g^2 \tag{3.38}$$

Input Parameters for model `Gauss`:

`Rg`: radius of gyration R_g
`I0`: forward scattering I_0 for $q = 0$

3.3.1.2. *Gauss2* [**23**].
This form factor differs only by the parametrization for the forward scattering $I_0 =$

$(b_p - V\eta_s)^2$ from the Debye formula in eq. 3.37

$$I_{\text{Gauss2}}(q) = \beta^2 2\frac{\exp(-u) + u - 1}{u^2} \tag{3.39}$$
$$u = q^2 R_g^2$$
$$\beta = b_p - V\eta_s,$$

where b_p is the scattering length of a polymer molecule of molecular volume V dissolved in a solvent of scattering length density η_s from which the excess scattering length of a polymer molecule β can be calculated. Combining this form factor with a `Delta` size distribution 5.1 is needed to scale the scattering intensity. With proper values for the form factor the parameter N of the `Delta`-distribution yields the particle number density.

Input Parameters for model `Gauss2`:

`Rg`: radius of gyration R_g
`b_p`: scattering length of polymer b_p in [cm]
`V`: molecular volume of a single polymer molecule V in [cm^3]
`eta_s`: scattering length density of solvent η_s in [cm^{-1}]

3.3.1.3. *Gauss3* [**23**].
This form factor differs only by the parametrization for the forward scattering $I_0 = (b_p - \frac{M_w}{N_a\rho_p}\eta_s)^2$ from the Debye formula in eq. 3.37

$$I_{\text{Gauss3}}(q) = \beta^2 2\frac{\exp(-u) + u - 1}{u^2} \tag{3.40}$$

with

$$u = q^2 R_g^2$$
$$\beta = b_p - V\eta_s$$
$$V = \frac{M_w}{N_a\rho_p}$$
$$N_a = \text{Avogadro number}$$

Input Parameters for model `Gauss3`:

`Rg`: radius of gyration R_g
`b_p`: scattering length of polymer b_p in [cm]
`M_w`: molecular weight of polymer M_w in [g/mol]
`rho_p`: mass density of polymer ρ_p in [g cm^{-3}]
`eta_s`: scattering length density of solvent η_s in [cm^{-1}]

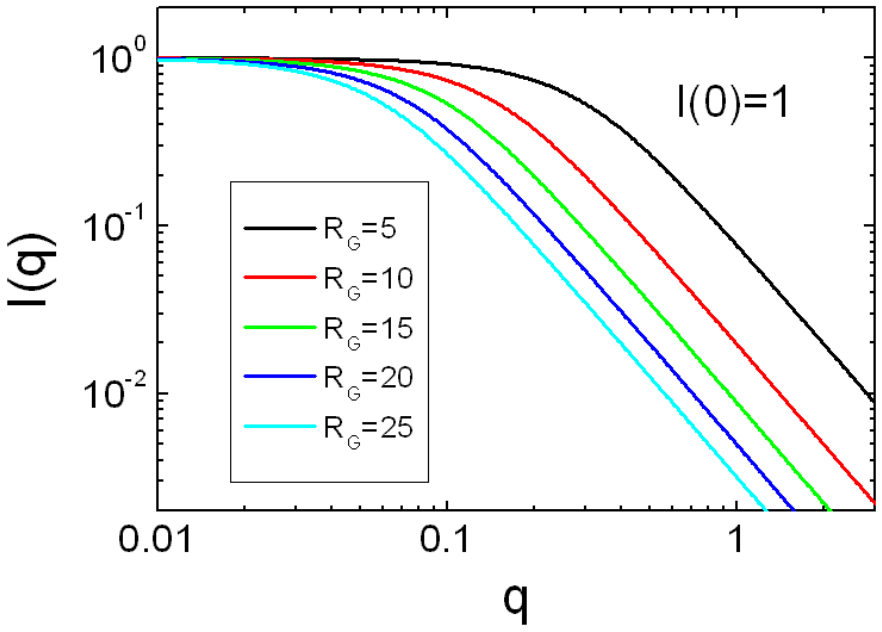

FIGURE 3.25. Scattering function of Gaussian coils plotted for several radii of gyration.

3.3.1.4. *Polydisperse flexible polymers with Gaussian statistics* [**74**].
Polydispersity has been included in terms of a SchulzZimm mass distribution by Zimm (1948) [**109**] and Greschner (1973) [**35**]

$$I_{\text{GaussPoly}}(q) = I_0 2\frac{(1+Ux)^{-1/U} + x - 1}{(1+U)x^2} \tag{3.41}$$
$$x = q^2 R_g^2/(1+2U)$$
$$U = \frac{M_w}{M_n} - 1$$

Input Parameters for model `GaussPoly`:

`Rg`: radius of gyration R_g
`M_w`: weight averaged molecular weight M_w
`M_n`: number averaged molecular weight M_n
`I0`: forward scattering I_0 for $q = 0$

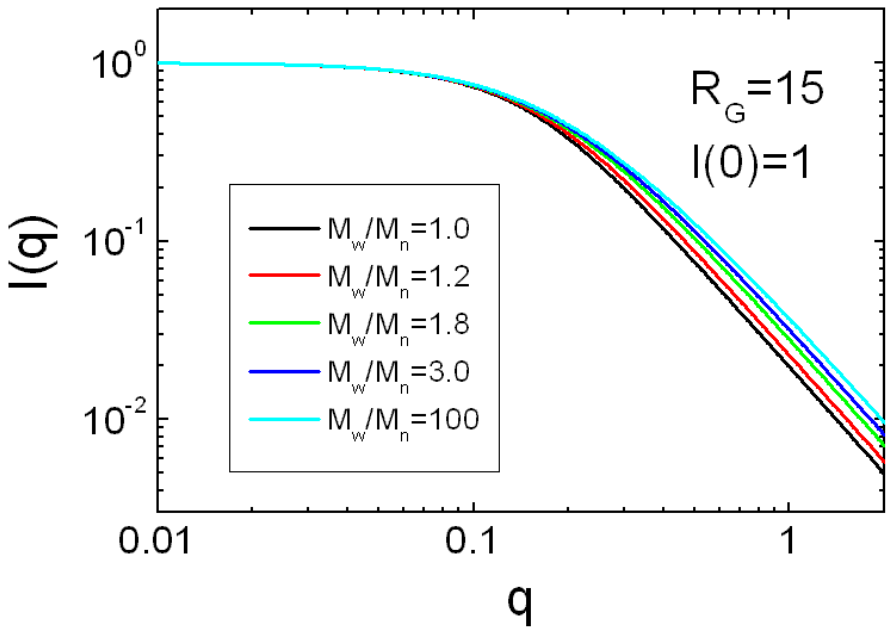

FIGURE 3.26. Scattering function of polydisperse Gaussian coil plotted for several ratios of M_w/M_n.

3.3.1.5. *generalalized Gaussian coil* [**39**].
The scattering function for the generalized Gaussian coil is according to eq. 3.35b

$$I_{\mathrm{gGc}}(q) = I_0 \frac{U^{\frac{1}{2\nu}}\Gamma\left(\frac{1}{2\nu}\right) - \Gamma\left(\frac{1}{\nu}\right) - U^{\frac{1}{2\nu}}\Gamma\left(\frac{1}{2\nu}, U\right) + \Gamma\left(\frac{1}{\nu}, U\right)}{\nu U^{1/\nu}} \tag{3.42}$$

with the modified variable

$$U = (2\nu+1)(2\nu+2)\frac{q^2 R_G^2}{6} \tag{3.43}$$

and the unnormalized incomplete Gamma Function $\Gamma(a,x) = \int_x^\infty \mathrm{d}t\ t^{a-1}\exp(-t)$ and the Gamma function $\Gamma(a) = \Gamma(a,0) = \int_0^\infty \mathrm{d}t\ t^{a-1}\exp(-t)$. ν is the excluded volume parameter from the Flory mean field theory and typical values for them are

$\nu = 1/3$**:** partially precipitate in poor solvents
$\nu = 1/2$**:** thermally relaxed in "theta"-solvents
$\nu = 3/5$**:** swollen in good solvents

Input Parameters for model `generalized Gaussian coil`:

`Rg`**:** radius of gyration R_g
`nu`**:** excluded volume parameter $\nu \in [1/2; 1]$
`I0`**:** forward scattering I_0 for $q = 0$

3.3.1.6. *generalized Gaussian coil 2* [**39**].
The scattering function for the generalized Gaussian coil is according to eq. 3.35b and differs only by the parametrization for the forward scattering $I_0 = (b_p - V\eta_\mathrm{s})^2$ from the formula in eq. 3.44

$$I_{\mathrm{gGc2}}(q) = (b_p - V\eta_\mathrm{s})^2 \, \frac{U^{\frac{1}{2\nu}}\Gamma\left(\frac{1}{2\nu}\right) - \Gamma\left(\frac{1}{\nu}\right) - U^{\frac{1}{2\nu}}\Gamma\left(\frac{1}{2\nu}, U\right) + \Gamma\left(\frac{1}{\nu}, U\right)}{\nu U^{1/\nu}} \tag{3.44}$$

with the modified variable

$$U = (2\nu + 1)\,(2\nu + 2)\,\frac{q^2 R_G^2}{6} \tag{3.45}$$

Input Parameters for model `generalized Gaussian coil 2`:

`Rg`: radius of gyration R_g
`b_p`: scattering length of polymer b_p in [cm]
`V`: molecular volume of a single polymer molecule V in [cm^3]
`eta_s`: scattering length density of solvent η_s in [cm^{-1}]

3.3.1.7. *generalized Gaussian coil 3* [**39**].
The scattering function for the generalized Gaussian coil is according to eq. 3.35b and differs only by the parametrization for the forward scattering $I_0 = (b_p - \frac{M_w}{N_a\rho_p}\eta_\mathrm{s})^2$ from the formula in eq. 3.44

$$I_{\mathrm{gGc3}}(q) = \left(b_p - \frac{M_w}{N_a\rho_p}\eta_\mathrm{s}\right)^2 \, \frac{U^{\frac{1}{2\nu}}\Gamma\left(\frac{1}{2\nu}\right) - \Gamma\left(\frac{1}{\nu}\right) - U^{\frac{1}{2\nu}}\Gamma\left(\frac{1}{2\nu}, U\right) + \Gamma\left(\frac{1}{\nu}, U\right)}{\nu U^{1/\nu}} \tag{3.46}$$

with the modified variable

$$U = (2\nu + 1)\,(2\nu + 2)\,\frac{q^2 R_G^2}{6} \tag{3.47}$$

Input Parameters for model `generalized Gaussian coil 3`:

`Rg`: radius of gyration R_g
`b_p`: scattering length of polymer b_p in [cm]
`M_w`: molecular weight of polymer M_w in [g/mol]
`rho_p`: mass density of polymer ρ_p in [g cm^{-3}]
`eta_s`: scattering length density of solvent η_s in [cm^{-1}]

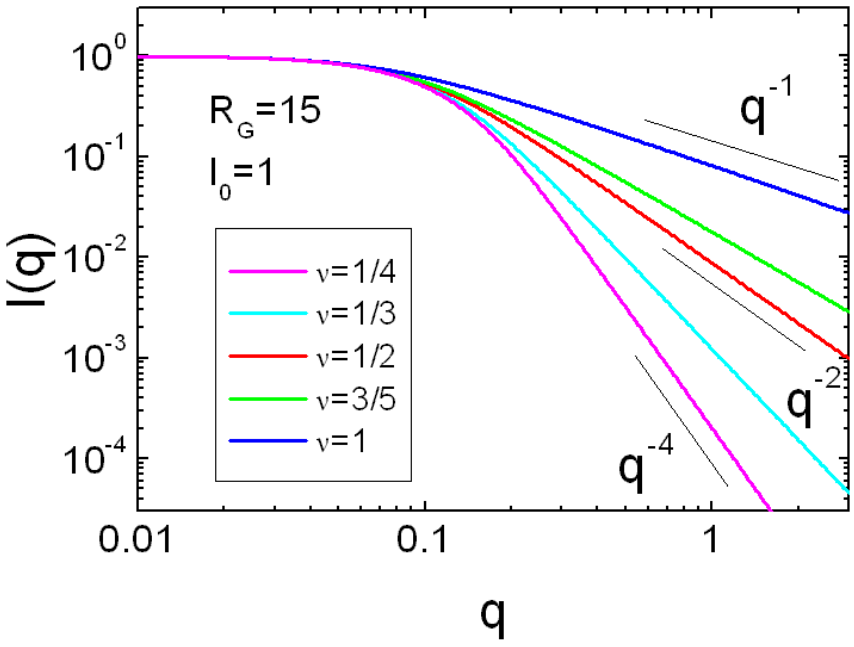

FIGURE 3.27. Scattering function of the generalized Gaussian coil plotted for several excluded volume parameters.

3.3.2. Star polymer with Gaussian statistic according to Benoit [6].

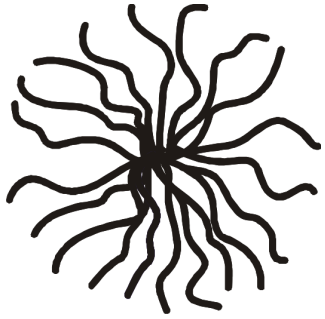

FIGURE 3.28. Sketch of a branched or star polymers with f number of arms

Benoit [**6**] derived an expression for the scattering from branched or star polymers with a number of arms f, which can be expressed in the following way:

$$I_{\text{Star}}(Q, R_G, f) = I_0 \frac{2}{f\nu^2}\left(\nu - \left[1 - e^{-\nu}\right] + \frac{f-1}{2}\left[1 - e^{-\nu}\right]^2\right) \tag{3.48}$$

with $u = R_G^2 Q^2$, $\nu = \dfrac{uf}{3f-2}$ and $\lim\limits_{Q=0} I_{\text{Star}}(Q, R_G, f) = I_0$. f denotes the number of arms and R_G the Guinier radius of a single arm.

Input Parameters for model `Benoit`:

`RG:` radius of gyration of the star polymer R_g
`f:` number of arms f
`I0:` forward scattering I_0 for $q = 0$

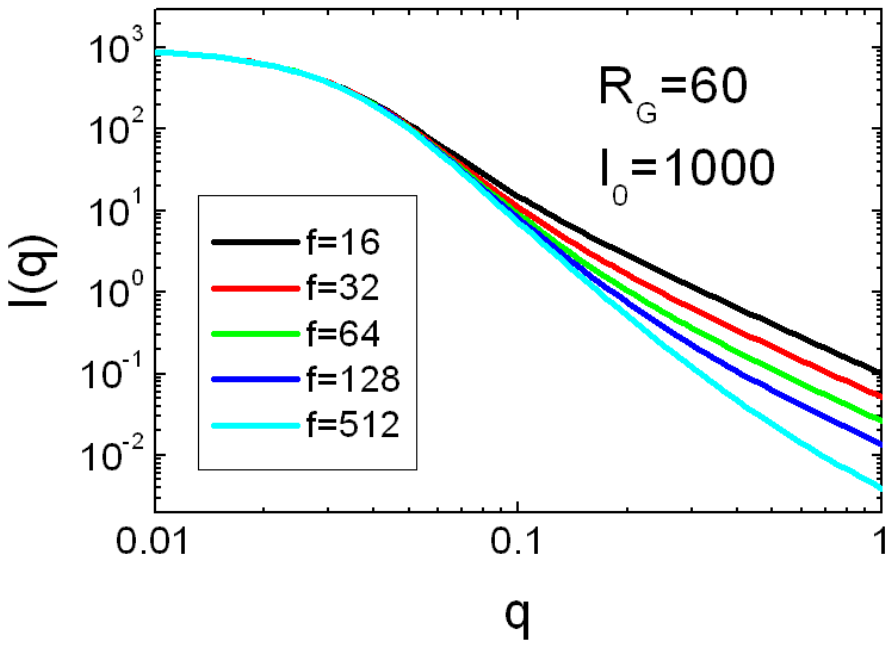

FIGURE 3.29. Scattering function of a star polymer according to Benoit.

3.3.3. Polydisperse star polymer with Gaussian statistics [14].

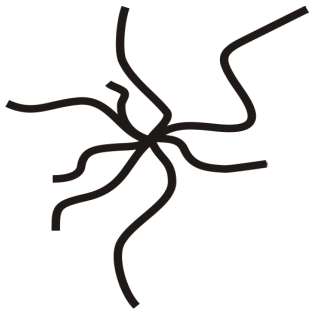

FIGURE 3.30. Polydisperse star polymer with Gaussian statistics

For a SchulzFlory (most probable) distribution (SchulzZimm distribution with $z = 1$) for the mass distribution of the arms, Burchard [**14**] has given the form factor:

$$I_{\text{PolydisperseStar}}(Q) = I_0 \frac{1 + \frac{u^2}{3f}}{\left(1 + \frac{u^2(f+1)}{6f}\right)^2} \tag{3.49}$$

where f is the number of arms and $u^2 = \langle R_g^2 \rangle_z \, Q^2$, where $\langle R_g^2 \rangle_z$ is the z-average radius of gyration squared of an arm.

Input Parameters for model `PolydisperseStar`:

`R_G`: radius of gyration R_G
`f`: number of arms f
`I0`: forward scattering I_0

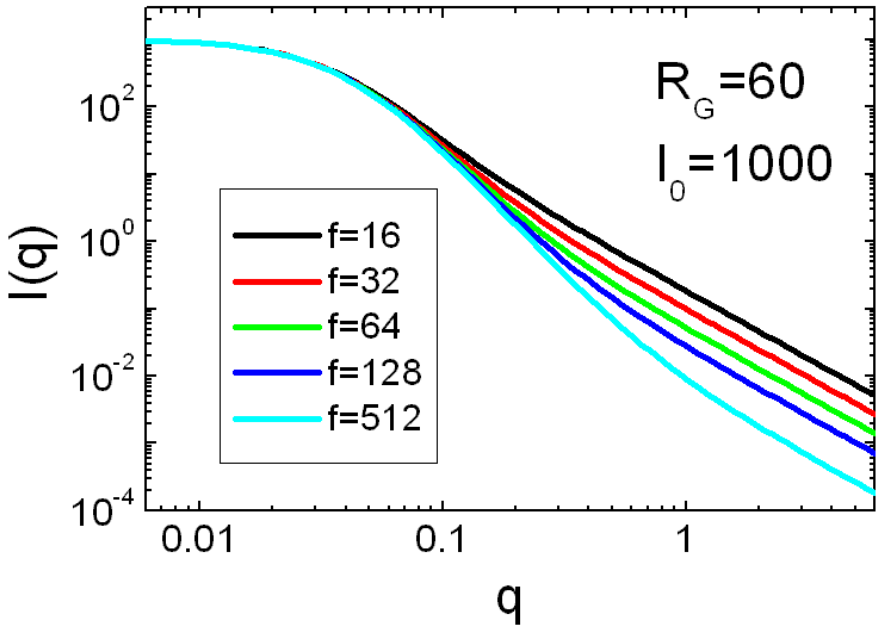

FIGURE 3.31. Scattering function of a polydisperse star polymer with Gaussian statistics.

3.3.4. Star polymer according to Dozier [26].

3.3.4.1. *Dozier.*
Branched polymers having all branches emanating from the center of the macromolecule

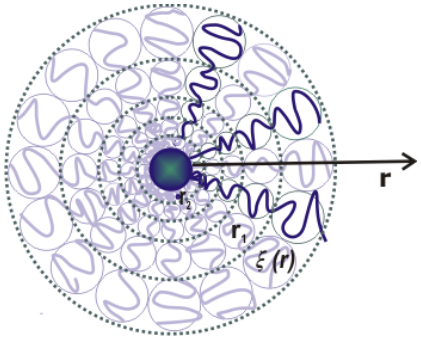

FIGURE 3.32. Star polymer according to Dozier

are commonly called star polymers. For a star polymer Dozier [**26**] has developed a scattering function which reads:

$$I_{\text{DozierStar}}(Q, I_0, R_G, \alpha, \nu, \xi) = I_0 \exp\left(-\frac{Q^2 R_G^2}{3}\right) + \frac{4\pi\alpha}{Q\xi}\Gamma(\mu)\frac{\sin(\mu \arctan(Q\xi))}{(1+Q^2\xi^2)^{\mu/2}} \tag{3.50}$$

with $\mu = 1/\nu - 1$

R_G : radius of gyration
I_0 : scale parameter
α : scale parameter for fractal term
ξ : exponential damping length in mass fractal
ν : Flory exponent, 3/5 in good solvent, 1/2 in theta solvent (i.e. $\mu = 2/3$ to 1)

Input Parameters for model `Dozier`:

`R_G`: radius of gyration R_G
`I_0`: scale parameter I_0
`alpha`: scale parameter for fractal term α
`xi`: exponential damping length in mass fractal ξ
`nu`: excluded volume parameter or Flory exponent ν

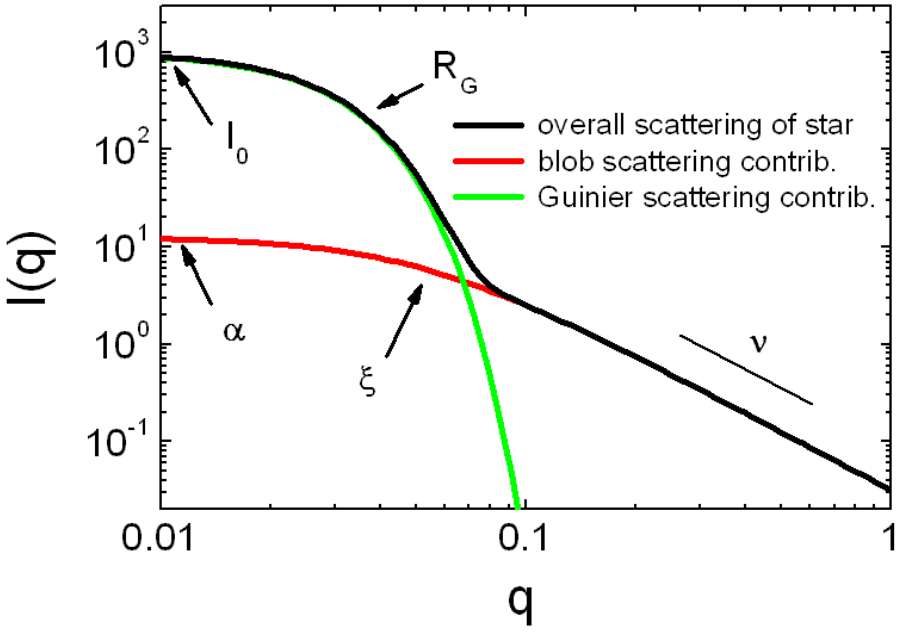

FIGURE 3.33. Scattering function of a star polymer according to Dozier: $I0 = 10^3$, $R_g = 60$, $alpha = 1$ $\xi = 20$, $\nu = 1/2$

3.3.4.2. *Dozier2.*

This is a re-parametrization of the `Dozier` form factor to scale the scattering of the overall star to the local scattering of the individual arms.

$$I_{\text{DozierStar2}}(Q, I_0, R_G, N_{\text{agg}}, \nu, \xi) = \frac{I_0}{N_{\text{agg}}}\left((N_{\text{agg}} - 1)\exp\left(-\frac{Q^2 R_G^2}{3}\right) + \frac{\Gamma(\mu)}{Q\xi}\frac{\sin(\mu \arctan(Q\xi))}{(1+Q^2\xi^2)^{\mu/2}}\right) \tag{3.51}$$

with $\mu = 1/\nu - 1$

R_G : radius of gyration of the star

I_0 : scale parameter

N_{agg} : number of arms in the star

ξ : exponential damping length in mass fractal

ν : Flory exponent, 3/5 in good solvent, 1/2 in theta solvent (i.e. $\mu = 2/3$ to 1)

Input Parameters for model `Dozier2`:

`R_G`: radius of gyration of the star R_G

`I_0`: scale parameter I_0

`Nagg`: number of arms N_{agg} in the star from which the scale parameter for fractal term is calculated

`xi`: exponential damping length in mass fractal ξ

`nu`: Flory exponent, $\nu = 3/5$ in good solvent, $\nu = 1/2$ in theta solvent (i.e. $\mu = 2/3$ to 1)

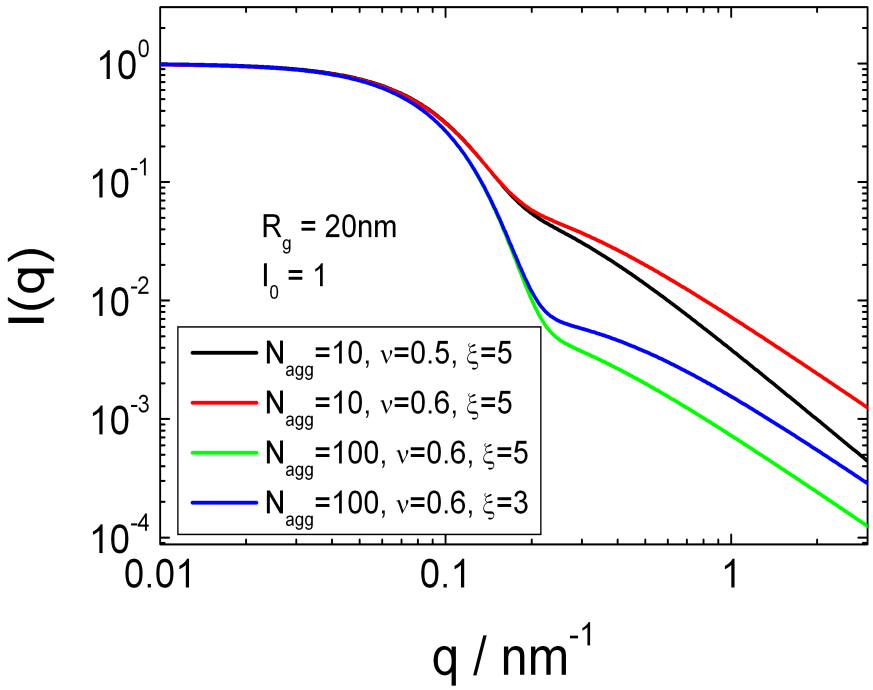

FIGURE 3.34. Scattering function of a star polymer according to Dozier but modified to scale the scattering of the overall star to the local scattering of the individual arms by the number of arms

3.3.5. Flexible Ring Polymer [15].

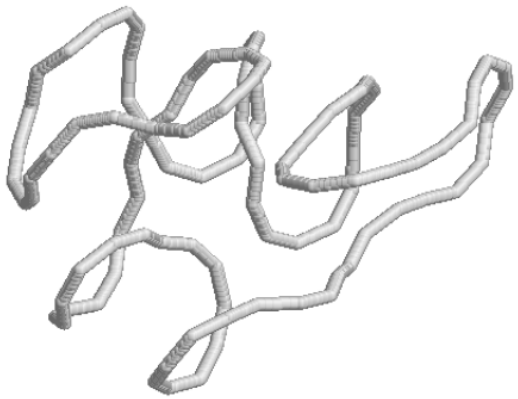

FIGURE 3.35. Sketch of a flexible ring polymer.

$$P_{1r}(q) = \sqrt{\frac{2}{u_{1r}^2}}\, D\left[\sqrt{\frac{u_{1r}^2}{2}}\right] \tag{3.52}$$

$$u_{1r}^2 = q^2 R_{g,1r}^2 \tag{3.53}$$

$$R_{g,1r}^2 = \sqrt{\frac{b^2 N}{12}} \tag{3.54}$$

$$D(X) = \exp\left(X^2\right) \int_0^X \exp(t^2)\, \mathrm{d}t \tag{3.55}$$

Input Parameters for model `FlexibleRingPolymer`:

`Rg`: radius of gyration R_G
`I0`: forward scattering I_0

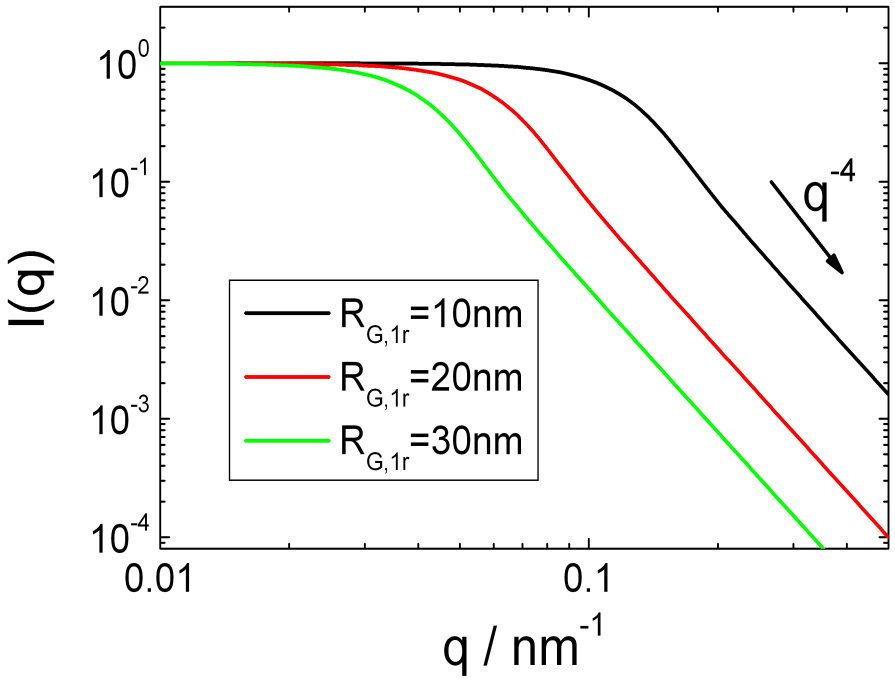

FIGURE 3.36. Scattering intensity of ring polymers of different radius of gyration.

3.3.6. m-membered twisted ring [15].

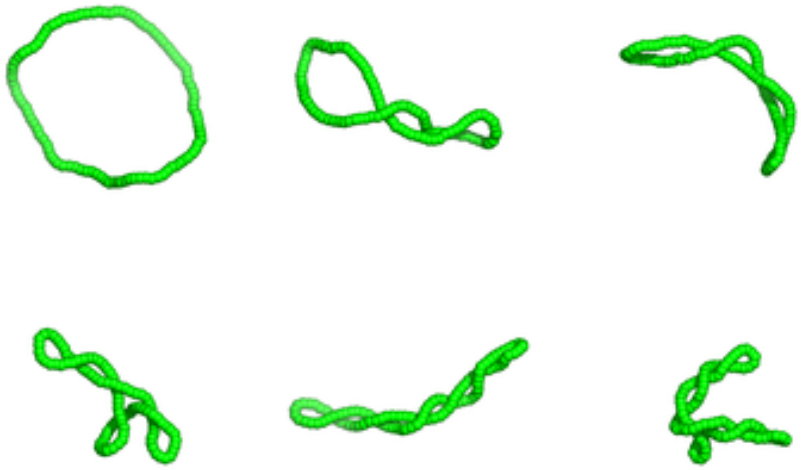

FIGURE 3.37. Sketch of ing polymers which different degree of twisting

$$P_{mr}(q) = I_0 \left(\frac{P_{1r}(q)}{m} + \frac{2}{m^2} P_{1r}^2(q) \sum_{j=1}^{m-1} (m-j) \exp\left(-\frac{q^2 R_{g,1r}^2}{2} (j-1) \right) \right) \tag{3.56}$$

$$P_{1r}(q) = \sqrt{\frac{2}{u_{1r}^2}}\, D\left[\sqrt{\frac{u_{1r}^2}{2}} \right] \tag{3.57}$$

$$u_{1r}^2 = q^2 R_{g,1r}^2 \tag{3.58}$$

$$R_{g,1r}^2 = \sqrt{\frac{b^2 N}{12}} \tag{3.59}$$

$$D(X) = \exp\left(X^2\right) \int_0^X \exp(t^2)\, \mathrm{d}t \tag{3.60}$$

Input Parameters for model `mMemberedTwistedRing`:

`R_G,1r`: radius of gyration $R_{G,1r}$ of one of m loop
`m`: number of twists m
`I0`: forward scattering I_0

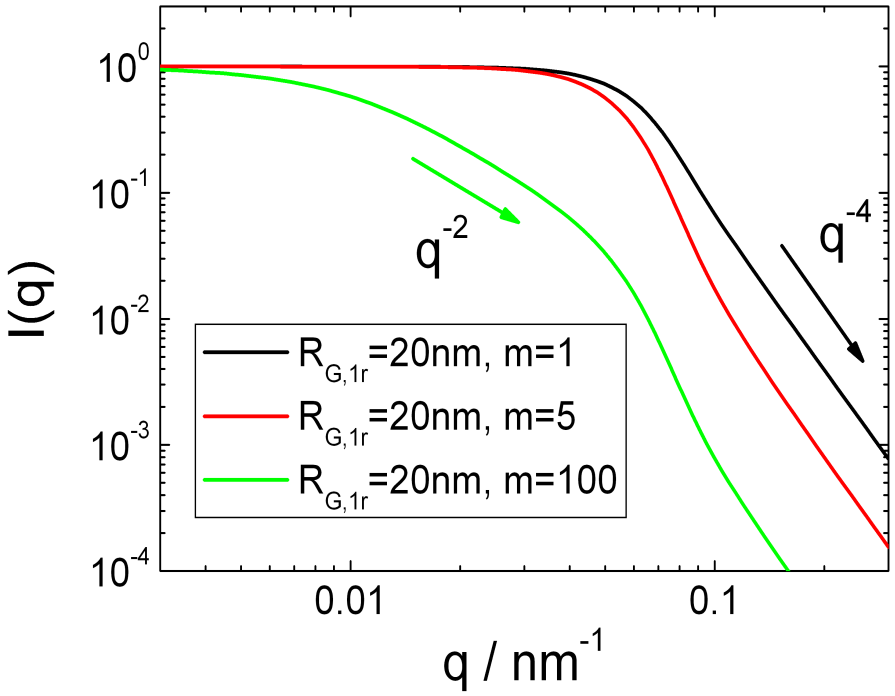

FIGURE 3.38. Scattering intensity of an m-membered twisted ring polymers with different values for m.

3.3.7. Daisy-like Ring [15].

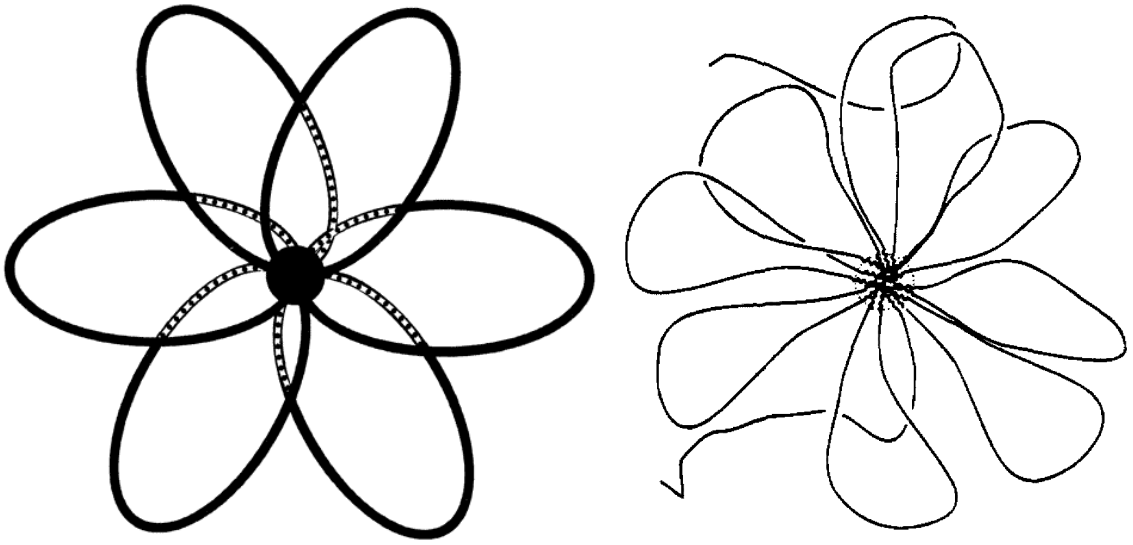

FIGURE 3.39. Sketch of a Daisy-like polymer.

$$P_{mr}(q) = \frac{I_0}{m}\left(P_{1r}(q) + (m-1)P_{1r}^2(q)\right) \tag{3.61}$$

$$P_{1r}(q) = \sqrt{\frac{2}{u_{1r}^2}}\, D\left[\sqrt{\frac{u_{1r}^2}{2}}\right] \tag{3.62}$$

$$u_{1r}^2 = q^2 R_{g,1r}^2 \tag{3.63}$$

$$R_{g,1r}^2 = \sqrt{\frac{b^2 N}{12}} \tag{3.64}$$

$$D(X) = exp(X^2) \int_0^X exp(t^2)\,\mathrm{d}t \tag{3.65}$$

Input Parameters for model `DaisyLikeRing`:

`R_G,1r:` radius of gyration $R_{G,1r}$ of one of m loop
`m:` number of loops m
`I0:` forward scattering I_0

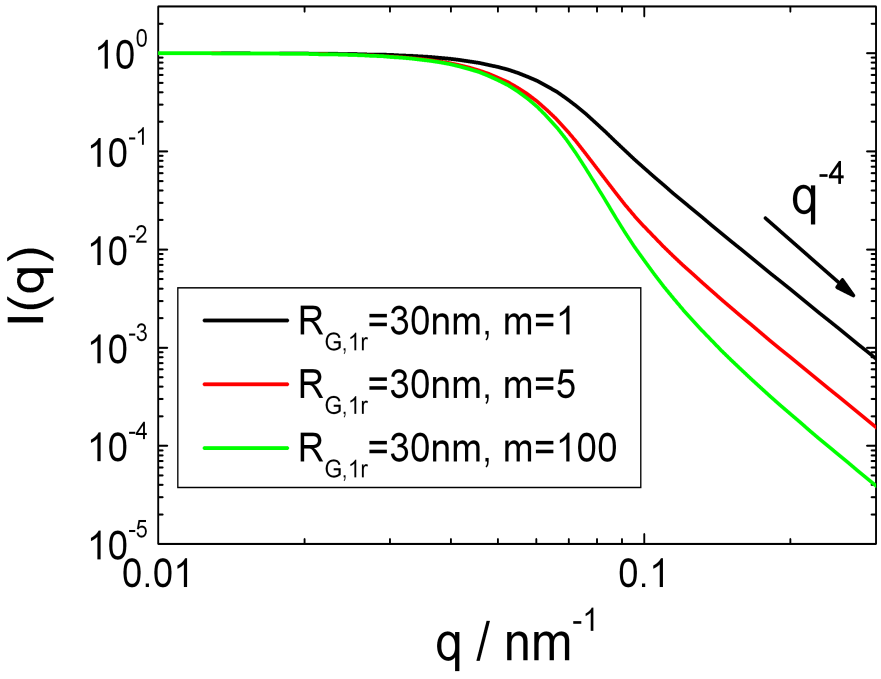

FIGURE 3.40. Scattering intensity of a Daisy-like ring polymers with different number of loops.

3.3.8. Unified Exponential Power Law according to Beaucage [4, 5].

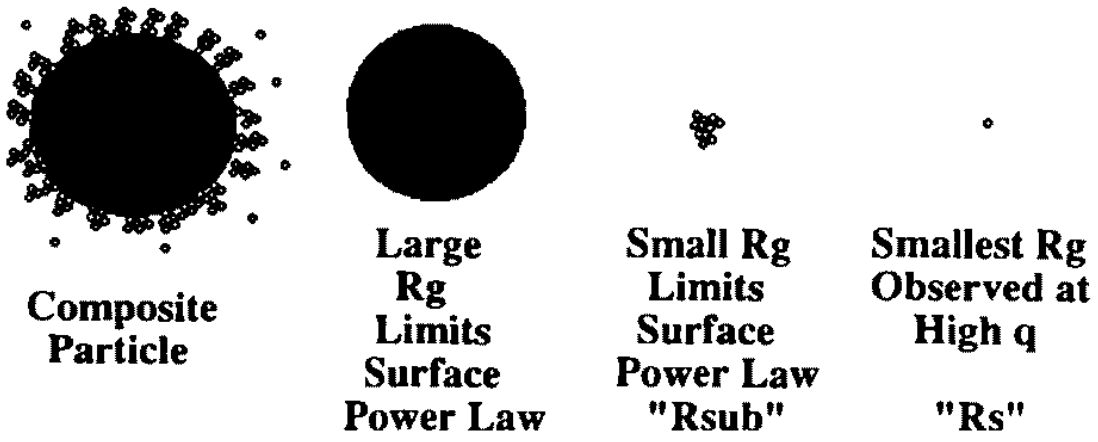

FIGURE 3.41. A typical case in which two R_g's are observed. Particles composed of sub-particles where a radius of gyration for the entire particle, R_g, and a radius of gyration for the sub-particles, R_s, are observed. The surface-fractal cut-off radius of gyration, R_{sub}, differs from the high-Q radius of gyration, R_s, in this case. Generally, $R_s = R_{sub}$

3.3.8.1. *Beaucage.*

$$\begin{aligned} I_{\text{Beaucage}}(Q) \simeq\ & G \exp\left(-\frac{Q^2 R_g^2}{3}\right) \\ & + B \exp\left(-\frac{Q^2 R_{sub}^2}{3}\right) \left(\frac{\left[\text{erf}\left(Qk R_g/\sqrt{6}\right)\right]^3}{Q}\right)^P \\ & + G_s \exp\left(-\frac{Q^2 R_s^2}{3}\right) \\ & + B_s \left(\frac{\left[\text{erf}\left(Qk_s R_s/\sqrt{6}\right)\right]^3}{Q}\right)^{P_s} \end{aligned} \tag{3.66}$$

The first term in eq. 3.66 describes the large-scale structure of size R_g composed of small subunits of size R_s, captured in the third term. The second term describes the mass-fractal regime with two structural limits. The low-Q limit is at R_g and is described by the error function. The high-Q limit is at R_{sub} and is described by the exponential pre-factor [**4**] . The final two terms are for the sub-structural mer unit. Using eq. 3.66, scattering from a system with multiple-size-scale features is parameterized. Generally, the high-Q cutoff for the intermediate power law, R_{sub}, is identical to the sub-structural radius of gyration, R_s. The assumption that $R_{sub} = R_s$ should always be true for typical

mass fractals. It should be noted that, although eq. 3.66 appears cumbersome, no new parameters have been introduced over local fits using exponentials and power laws.

G is the Guinier pre-factor defined above and B is a pre-factor specific to the type of power-law scattering: B is defined according to the regime in which the exponent P falls. Generally, for surface fractals $4 > P > 3$, for mass fractals $P < 3$ and for diffuse interfaces $P > 4$. For Porod's law, $P = 4$ and $B = N_p 2\pi\rho_c^2 p S_p$, where S_p, is the particulate surface area. For a Gaussian polymer, $P = 2$, and B is given by $2G/R_g^2$, through a comparison with the Debye form factor 3.3.1 at the high-Q limit as discussed below. The constant, k in 3.66, accounts for an approximation involved in the description of the low-Q power-law limit [**4**]. This is an empirical constant that has a value of 1 for steep power-law decays, $P > 3$. For weak power-law decays, k deviates slightly from 1. For polymeric mass fractals of fractal dimension d_f close to 2 (1.5 to 3), k is empirically found to be close to 1.06. Weak deviations are observed between the scattered intensity as calculated using 3.66 and exact calculations for values of Q between $2\pi/R_g$ and π/R_g in these cases when $k = 1$. These deviations are reduced to less than 3% of the calculated intensity using $k = 1.06$.

Input Parameters for model `Beaucage`:

`G:` G is the Guinier pre-factor of the larger structure
`B:` B is a pre-factor specific to the type of power-law scattering: B is defined according to the regime in which the exponent P falls.
`Gs:` G_s is the Guinier pre-factor of the smaller structure
`Bs:` B_s is a pre-factor specific to the type of power-law scattering: B_s is defined according to the regime in which the exponent P_s falls.
`Rg:` large-scale structure
`Rsub:` surface-fractal cut-off radius of gyration, R_{sub} defines the high-Q cutoff for the intermediate power law
`Rs:` size R_s of small subunits
`P:` scaling exponent of the power law assigned to the larger structure R_g
`Ps:` scaling exponent of the power law assigned to the smaller structure R_s

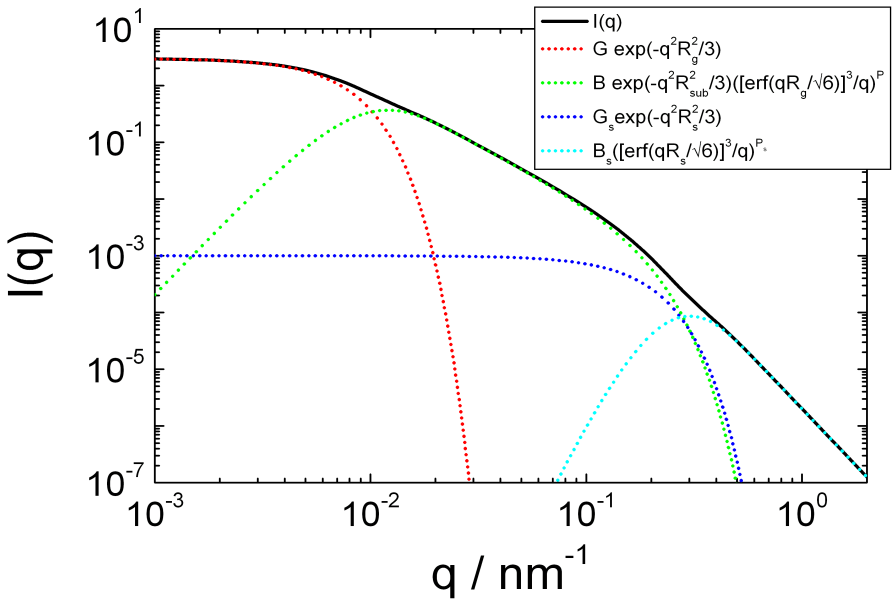
I(q)
G exp(-q²R_g²/3)
B exp(-q²R_sub²/3)([erf(qR_g/√6)]³/q)^P
G_s exp(-q²R_s²/3)
B_s([erf(qR_s/√6)]³/q)^P,
I(q)
q / nm⁻¹
10¹
10⁻¹
10⁻³
10⁻⁵
10⁻⁷
10⁻³
10⁻²
10⁻¹
10⁰

FIGURE 3.42.

3.3.8.2. *Beaucage2.*

Equation 3.66 can be extended to describe an arbitrary number of interrelated structural levels under the generally applicable assumption that $R_{\text{sub}} = R_s$,

$$I_{\text{Beaucage}}(Q) \simeq \sum_{i=1}^{n} G_i \exp\left(-\frac{Q^2 R_{g,i}^2}{3}\right) + B_i \exp\left(-\frac{Q^2 R_{g,i+1}^2}{3}\right) \left(\frac{\left[\text{erf}\left(Qk_i R_{g,i}/\sqrt{6}\right)\right]^3}{Q}\right)^{P_i} \tag{3.67}$$

In 3.67, $i = 1$ refers to the largest-size structural level. Extensions, such as eq. 3.67, can only be justified when data extend over many decades in Q. Eq. 3.67 introduces no new parameters over local Guinier and power-law fits.

Input Parameters for model `Beaucage2`:

`G_i`: G_i is the Guinier pre-factor
`B_i`: B_i is a pre-factor specific to the type of power-law scattering: B_i is defined according to the regime in which the exponent P_i falls.
`Rg_i`: large-scale structure $R_{g,i}$
`Rg_i+1`: size $R_{g,i+1}$ of smaller subunits
`k_i`: This is an empirical constant that has a value of 1 for steep power-law decays, $P > 3$. For weak power-law decays, k deviates slightly from 1
`k_i+1`: This is an empirical constant that has a value of 1 for steep power-law decays, $P_s > 3$. For weak power-law decays, k_s deviates slightly from 1
`P_i`: scaling exponent of the power law assigned to the larger structure $R_{g,i}$
`P_i+1`: scaling exponent of the power law assigned to the smaller structure $R_{g,i+1}$

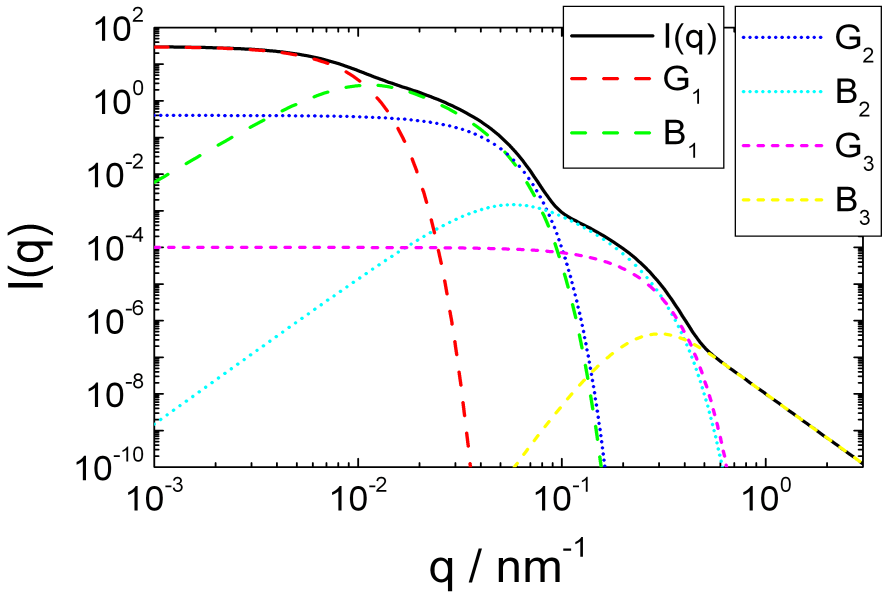
I(q)
G1
B1
G2
B2
G3
B3
I(q)
q / nm-1
10^2
10^0
10^-2
10^-4
10^-6
10^-8
10^-10
10^-3
10^-2
10^-1
10^0

FIGURE 3.43.

3.3.9. WormLikeChainEXV [73].

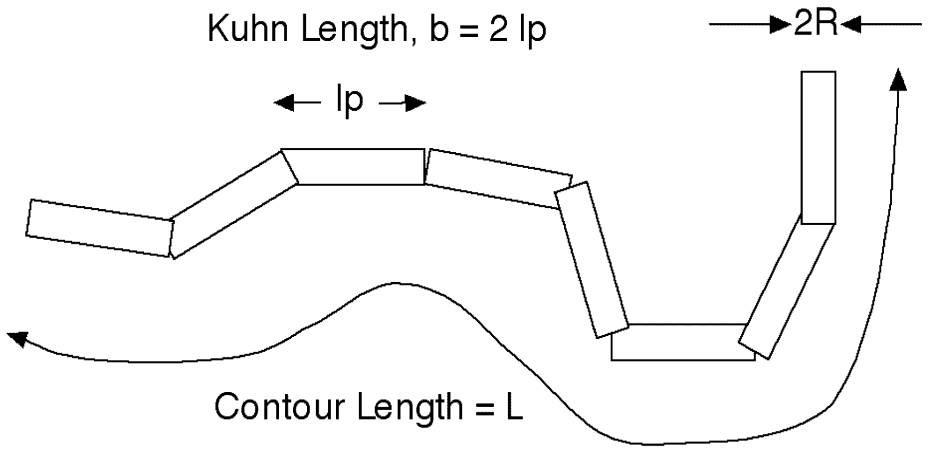

FIGURE 3.44. The chain of contour length, L, (the total length) can be described a chain of some number of locally stiff segments of length l_p. The persistence length,l_p, is the length along the cylinder over which the flexible cylinder can be considered a rigid rod. The Kuhn length (b) used in the model is also used to describe the stiffness of a chain, and is simply $b = 2l_p$.

This form factor calculates the form factor for a flexible cylinder with a circular cross section and a uniform scattering length density. The non-negligible diameter of the cylinder is included by accounting for excluded volume interactions within the walk of a single cylinder. Inter-cylinder interactions are NOT included. The function calculated has been given by Pedersen et al. [**73**]. The model "Method 3 With Excluded Volume" is used, which is a parametrization of simulations of a discrete representation of the worm-like chain model of Kratky and Porod applied in the pseudo-continuous limit.

Input Parameters for model `WormLikeChainEXV`:

`R:` radius R of cylindrical core with uniform scattering length density
`l:` Kuhn length[3] l of semi-flexible worm-like structure
`L:` contour length L of semi-flexible worm-like structure

[3]The Kuhn length l is related to the length a of locally stiff segment simply via $l = 2a$

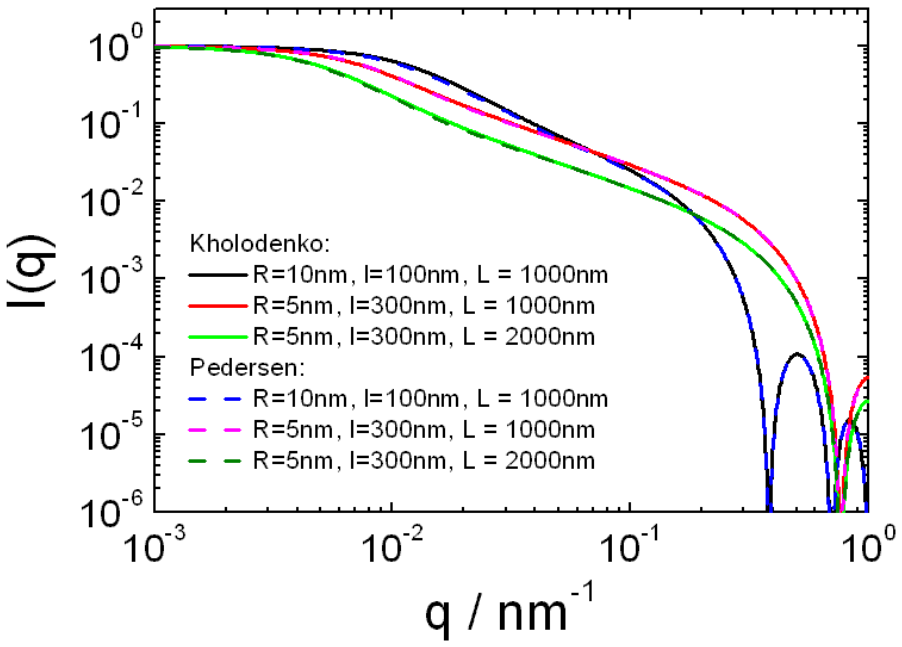

FIGURE 3.45. Comparison of wormlike micelles according to Pedersen [**73**] and Kholodenko [**54**]

3.3.10. KholodenkoWorm.

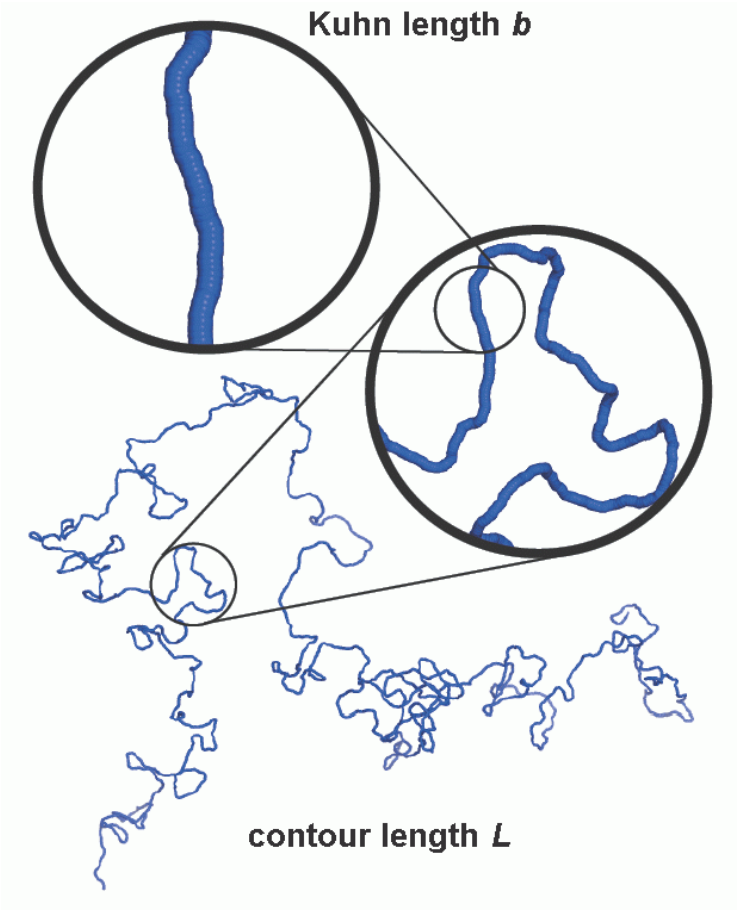

FIGURE 3.46.

Kholodenko [**54**] presented a new approach using the analogy between Diracs fermions and semi-flexible polymers. The form factor $P_0(Q)$ resulting from Kholodenkos approach is designed to reproduce correctly the rigid-rod limit and the random-coil limit. Defining $x = 3L/l$ (L: contour length, l: Kuhn length), it is given by

$$P_0(Q, L, l) = \frac{2}{x}\left[I_{(1)} - \frac{1}{x} I_{(2)}\right] \tag{3.68}$$

where

$$I_{(n)}(x) = \int_0^x f(z)\, z^{n-1}\, dz \tag{3.69}$$

together with

$$f(z)) = \begin{cases} \dfrac{1}{E}\dfrac{\sinh(Ez)}{\sinh(z)} & \text{for} \quad Q \leq \dfrac{3}{l} \\ \\ \dfrac{1}{F}\dfrac{\sin(Fz)}{\sinh(z)} & \text{for} \quad Q > \dfrac{3}{l} \end{cases} \tag{3.70}$$

and

$$E = \sqrt{1 - \left(\frac{lQ}{3}\right)^2} \quad \text{and} \quad F = \sqrt{\left(\frac{lQ}{3}\right)^2 - 1} \tag{3.71}$$

For flexible cylinders with a circular cross section and a uniform scattering length density the cross section form factor is given by

$$P_{cs} = \left(2\frac{J_1(QR)}{QR}\right)^2 \tag{3.72}$$

so that the overall form factor is given by

$$P(Q, L, l, R) = P_0(Q, L, l)\, P_{cs}(Q, R) \tag{3.73}$$

Input Parameters for model `KholodenkoWorm`:

- `R:` radius R of cylindrical core with uniform scattering length density
- `l:` Kuhn length[4] l of semi-flexible worm-like structure
- `L:` contour length L of semi-flexible worm-like structure

[4]The Kuhn length l is related to the length a of locally stiff segment simply via $l = 2a$

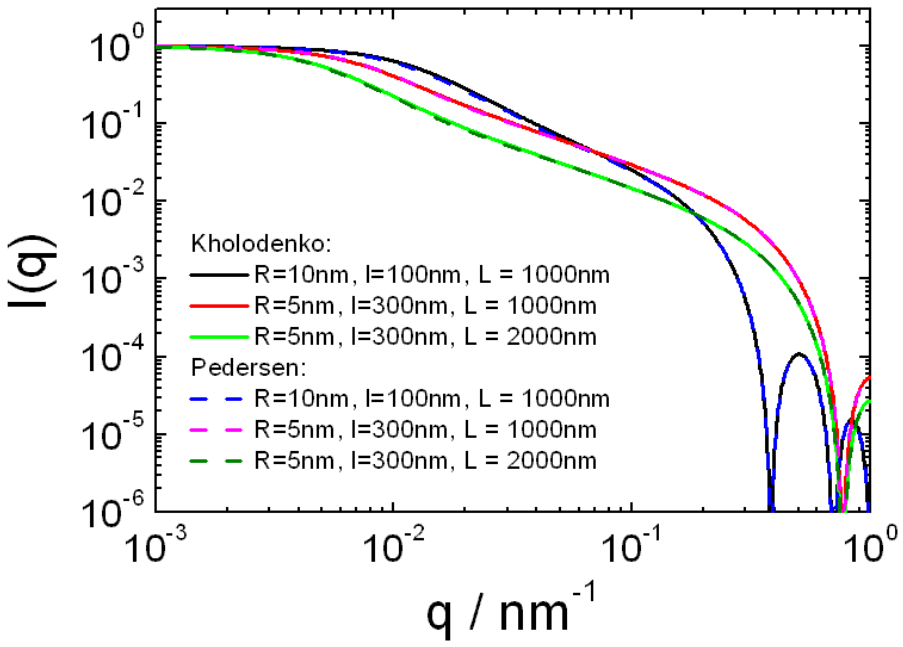

FIGURE 3.47. Comparison of wormlike micelles according to Pedersen [**73**] and Kholodenko [**54**].

3.3.11. Diblock copolymer micelles.

(a) spherical micelle (b) ellipsoidal micelle (c) cylindrical micelle

FIGURE 3.48. Block copolymer forming micelles of different shapes

For block copolymers, which form micelles, several form factor have been implemented [**75, 76, 95**] for spherical, ellipsoidal, and cylindrical shapes. It has been assumed that one unit is forming the core of the micelles and the other the corona. The core is assumed to have a homogeneous scattering length density, but may contain some amount of solvent. For the polymer chains in the corona either a model where Gaussian chains are attached to the core or a corona model of semi-flexible interacting self-avoiding chains (only for spherical core) or a continuous model, where a radial profile of the form $\Phi(r) \propto r^{-\alpha}$ has been assumed. The form factors have been parameterized such, that the excess scattering of the corona and the core are consistent with the composition and density of the two separate block units of the copolymer.

3.3.11.1. *Micelles with a homogeneous core and Gaussian chains on the surface.*

It is assumed that the diblock copolymer consist of a block unit for which the solvent is poor and a block unit with is good. The insoluble blocks form a relatively compact core whereas the soluble blocks form a diffuse corona surrounding the core. The form factor of a micelle contains four different terms: the self-correlation term of the core $N_{\text{agg}}^2 \beta_{\text{core}}^2 P_{\text{core}}(q)$, the self-correlation term of the chains $N_{\text{agg}} \beta_{\text{brush}}^2 P_{\text{brush}}(q)$, the cross-term between the core and chains $2N_{\text{agg}}^2 \beta_{\text{core}} \beta_{\text{brush}} S_{\text{brush-core}}(q)$, and the cross term between different chains $N_{\text{agg}}(N_{\text{agg}} - 1) \beta_{\text{brush}}^2 S_{\text{brush-brush}}(q)$. It can be written (Pedersen & Gerstenberg, 1996)

$$\begin{aligned} I_{\text{mic}} &= N_{\text{agg}}^2 \beta_{\text{core}}^2 P_{\text{core}}(q) + N_{\text{agg}} \beta_{\text{brush}}^2 P_{\text{brush}}(q) \\ &\quad + 2N_{\text{agg}}^2 \beta_{\text{core}} \beta_{\text{brush}} S_{\text{brush-core}}(q) + N_{\text{agg}}(N_{\text{agg}} - 1) \beta_{\text{brush}}^2 S_{\text{brush-brush}}(q) \end{aligned} \tag{3.74}$$

N_{agg} is the aggregation number of diblock polymers forming the micelle and $\beta_{\text{brush}} = V_{\text{brush}}(\eta_{\text{brush}} - \eta_{\text{solv}})$ and $\beta_{\text{core}} = V_{\text{core}}(\eta_{\text{core}} - \eta_{\text{solv}})$ the excess scattering length of a block in the corona and in the core, respectively. V_{brush} and V_{core} are the total volume of a block in the corona and in the core. η_{brush} and η_{core} are the corresponding scattering length densities and η_{solv} is the scattering length density of the surrounding solvent. The functions $P_{\text{core}}(q)$, $P_{\text{brush}}(q)$, $S_{\text{brush-core}}(q)$, and $S_{\text{brush-brush}}(q)$ are all 1 for $q = 0$. The definitions of these four functions depend on the shape of the core and are given below.

3.3.11.2. **Spherical core:**

$$P_{\text{core}}(q, R_{\text{core}}) = \Phi^2(qR_{\text{core}}) \tag{3.75}$$

$$\Phi(qR) = 3\frac{\sin(qR) - qR\cos(qR)}{(qR)^3} \tag{3.76}$$

$$P_{\text{brush}}(q, R_g) = 2\frac{\exp(-x) - 1 + x}{x^2} \text{ with } x = R_g^2 q^2 \tag{3.77}$$

$$S_{\text{brush-core}}(q, R_{\text{core}}, Rg, d) = \Phi(qR_{\text{core}})\psi(qR_g)\frac{\sin(q[R_{\text{core}} + dR_g])}{q[R_{\text{core}} + dR_g]} \tag{3.78}$$

$$\psi(qRg) = \frac{1 - \exp(-x)}{x} \text{ (form factor amplitude of the chain)}$$

$$S_{\text{brush-brush}}(q, R_{\text{core}}, d, R_g) = \psi^2(qR_g)\left[\frac{\sin(q[R_{\text{core}} + dR_g])}{q[R_{\text{core}} + dR_g]}\right]^2 \tag{3.79}$$

For micelles with a spherical core a few different parameterizations have been implemented `SPHERE+Chains(RW)`, `SPHERE+Chains(RW)_Rc` and `SPHERE+Chains(RW)_Nagg`. The parameters they all have in common are:

V_{brush}: molecular volume the diblock copolymer part forming the corona
η_{core}: scattering length density of the diblock copolymer part forming the core
η_{brush}: scattering length density of the diblock copolymer part forming the corona
η_{solv}: scattering length density of the solvent
$x_{\text{solv,core}}$: volume fraction of solvent in the micellar core
R_g: radius of gyration of the block unit in the corona
d: non-penetration of the chains into the core is mimicked by $d \sim 1$ for $R_{\text{core}} \gg R_g$

For the model `SPHERE+Chains(RW)` the other parameters are

R_{core}: radius of the micellar core
n_{agg}: grafting density (number of copolymer molecules N_{agg} per surface are S, $n_{\text{agg}} = N_{\text{agg}}/S$)

In contrast to the form factor `SPHERE+Chains(RW)_Rc` and `SPHERE+Chains(RW)_Nagg` this one does not necessary consist of copolymers. The excess scattering lengths and

aggregation number needed in eq. 3.74 are than given by

$$N_{\text{agg}} = n_{\text{agg}} S \tag{3.80}$$

where the surface of the core is given by $S = 4\pi R_{\text{core}}^2$. Together with the core volume $V = \frac{4}{3}\pi R_{\text{core}}^3$ one gets for the excess scattering lengths

$$\beta_{\text{core}} = \frac{V(1 - x_{\text{solv,core}})}{N_{\text{agg}}}(\eta_{\text{core}} - \eta_{\text{solv}}) \tag{3.81}$$

$$\beta_{\text{brush}} = V_{\text{brush}}(\eta_{\text{brush}} - \eta_{\text{solv}}) \tag{3.82}$$

Input Parameters for model `SPHERE+Chains(RW)`:

`R_core`: core radius
`n_agg`: specific aggregation number (number of chains per surface area)
`V_brush`: molecular volume of a block unit in the micellar corona
`eta_core`: scattering length density of spherical core
`eta_brush`: scattering length density of the block unit in the corona
`eta_solv`: scattering length density of solvent
`xsolv_core`: amount of solvent in core
`Rg`: gyration radius of polymer chains in the corona
`d`: This value should be around 1. Non-penetration of the chains into the core is mimicked by $d \sim 1$ for $R_{\text{core}} \gg R_g$

For the model `SPHERE+Chains(RW)_Rc` the other parameters are

$R_{\mathbf{core}}$: core radius
$V_{\mathbf{core}}$: molecular volume of single block unit in the micellar core

The excess scattering lengths and aggregation number in eq. 3.74 are given by

$$\beta_{\text{core}} = V_{\text{core}}(\eta_{\text{core}} - \eta_{\text{solv}}) \tag{3.83}$$

$$\beta_{\text{brush}} = V_{\text{brush}}(\eta_{\text{brush}} - \eta_{\text{solv}}) \tag{3.84}$$

$$N_{\text{agg}} = (1 - x_{\text{solv,core}})\frac{4}{3}\pi R_{\text{core}}^3 / V_{\text{core}} \tag{3.85}$$

Input Parameters for model `SPHERE+Chains(RW)_Rc`:

`R_core`: core radius
`V_core`: molecular volume of single block unit in the micellar core
`V_brush`: molecular volume of single block unit in the micellar corona
`eta_core`: scattering length density of spherical core
`eta_brush`: scattering length density of the block unit in the corona
`eta_solv`: scattering length density of solvent
`xsolv_core`: amount of solvent in core
`Rg`: gyration radius of polymer chains in the corona

`d`: This value should be around 1. Non-penetration of the chains into the core is mimicked by $d \sim 1$ for $R_{\text{core}} \gg R_g$

For the model `SPHERE+Chains(RW)_Nagg` the other parameters are

$N_{\mathbf{agg}}$: aggregation number
$V_{\mathbf{core}}$: molecular volume of single block unit in the micellar core

The excess scattering lengths and the core radius R_{core} needed in eq. 3.74 are given by

$$\beta_{\text{core}} = V_{\text{core}}(\eta_{\text{core}} - \eta_{\text{solv}}) \tag{3.86}$$

$$\beta_{\text{brush}} = V_{\text{brush}}(\eta_{\text{brush}} - \eta_{\text{solv}}) \tag{3.87}$$

$$R_{\text{core}} = \left(\frac{N_{\text{agg}} V_{\text{core}}}{1 - x_{\text{solv,core}}} \frac{3}{4\pi} \right)^{1/3} \tag{3.88}$$

Input Parameters for model `SPHERE+Chains(RW)_Nagg`:

`N_agg`: aggregation number
`V_core`: molecular volume of single block unit in the micellar core
`V_brush`: molecular volume of single block unit in the micellar corona
`eta_core`: scattering length density of spherical core
`eta_brush`: scattering length density of the block unit in the corona
`eta_solv`: scattering length density of solvent
`xsolv_core`: amount of solvent in core
`Rg`: gyration radius of polymer chains in the corona
`d`: This value should be around 1. Non-penetration of the chains into the core is mimicked by $d \sim 1$ for $R_{\text{core}} \gg R_g$

3.3.11.3. **ellipsoidal core with semi-axis** $(R, R, \epsilon R)$**:**

$$P_{\text{core}}(q, R_{\text{core}}, \epsilon) = \int_0^{\pi/2} \Phi^2[qr(R_{\text{core}}, \epsilon, \alpha)] \, \sin\alpha \, d\alpha \tag{3.89}$$

$$\text{with } \; r(R_{\text{core}}, \epsilon, \alpha) = R_{\text{core}} \sqrt{\sin^2\alpha + \epsilon^2 \cos^2\alpha}$$

$$P_{\text{brush}}(q, R_g) = 2\frac{\exp(-x) - 1 + x}{x^2} \text{ with } x = R_g^2 q^2 \tag{3.90}$$

$$S_{\text{brush-core}}(q, R_{\text{core}}, \epsilon, Rg, d) = \psi(qR_g) \int_0^{\pi/2} \Phi(qr(\dots)) \frac{\sin(q[r(\dots) + dR_g])}{q[r(\dots) + dR_g]} \, \sin\alpha \, d\alpha \tag{3.91}$$

$$S_{\text{brush-brush}}(q, R_{\text{core}}, d, R_g) = \psi^2(qR_g) \int_0^{\pi/2} \left[\frac{\sin(q[r(\dots) + dR_g])}{q[r(\dots) + dR_g]}\right]^2 \, \sin\alpha \, d\alpha \tag{3.92}$$

As for micelles with spherical core also for those with an ellipsoidal core several parameterizations have been implemented `ELL+Chains(RW)`, `ELL+Chains(RW)_Rc` and `ELL+Chains(RW)_Nagg`. The parameters they all have in common are:

$V_{\mathbf{brush}}$**:** molecular volume the diblock copolymer part forming the corona
$\eta_{\mathbf{core}}$**:** scattering length density of the diblock copolymer part forming the core
$\eta_{\mathbf{brush}}$**:** scattering length density of the diblock copolymer part forming the corona
$\eta_{\mathbf{solv}}$**:** scattering length density of the solvent
$x_{\mathbf{solv,core}}$**:** volume fraction of solvent in the micellar core
R_g**:** radius of gyration of the block unit in the corona
d**:** non-penetration of the chains into the core is mimicked by $d \sim 1$ for $R_{\text{core}} \gg R_g$
ϵ**:** eccentricity of the ellipsoidal micelle $(R_{\text{core}}, R_{\text{core}}, \epsilon R_{\text{core}})$

For the model `ELL+Chains(RW)` the other parameters are

$R_{\mathbf{core}}$**:** radius of the micellar core $(R_{\text{core}}, R_{\text{core}}, \epsilon R_{\text{core}})$
$n_{\mathbf{agg}}$**:** grafting density (number of copolymer molecules N_{agg} per surface are S, $n_{\text{agg}} = N_{\text{agg}}/S$)

In contrast to the form factor `ELL+Chains(RW)_Rc` and `ELL+Chains(RW)_Nagg` this one does not necessary consist of copolymers. The excess scattering lengths and aggregation number needed in eq. 3.74 are given by

$$N_{\text{agg}} = n_{\text{agg}} S \tag{3.93}$$

where the surface of the core is given by

$$S = \begin{cases} 2\pi R_{\text{core}}^2 \left(1 + \frac{\text{arctanh}(\sin(æ))}{\sin(æ)}\right) & \text{for } \epsilon < 1 \\ 2\pi R_{\text{core}}^2 \left(1 + \frac{æ}{\tan(æ)}\right) & \text{for } \epsilon \geq 1 \end{cases} \tag{3.94}$$

$$æ = \begin{cases} \arccos(\epsilon) & \text{for } \epsilon < 1 \\ \arccos(1/\epsilon) & \text{for } \epsilon \geq 1 \end{cases}$$

Together with the core volume $V = \frac{4}{3}\pi\epsilon R_{\text{core}}^3$ one gets for the excess scattering lengths

$$\beta_{\text{core}} = \frac{V(1 - x_{\text{solv,core}})}{N_{\text{agg}}}(\eta_{\text{core}} - \eta_{\text{solv}}) \tag{3.95}$$

$$\beta_{\text{brush}} = V_{\text{brush}}(\eta_{\text{brush}} - \eta_{\text{solv}}) \tag{3.96}$$

Input Parameters for model `ELL+Chains(RW)`:

`R_core`: core radius
`n_agg`: specific aggregation number (number of chains per surface area)
`V_brush`: molecular volume of a block unit in the micellar corona
`eta_core`: scattering length density of spherical core
`eta_brush`: scattering length density of the block unit in the corona
`eta_solv`: scattering length density of solvent
`xsolv_core`: amount of solvent in core
`Rg`: gyration radius of polymer chains in the corona
`d`: This value should be around 1. Non-penetration of the chains into the core is mimicked by $d \sim 1$ for $R_{\text{core}} \gg R_g$
`epsilon`: eccentricity of the ellipsoidal micelle $(R_{\text{core}}, R_{\text{core}}, \epsilon R_{\text{core}})$

For the model `ELL+Chains(RW)_Rc` the other parameters are

$R_{\mathbf{core}}$: core radius
$V_{\mathbf{core}}$: molecular volume of single block unit in the micellar core

The excess scattering lengths and aggregation number in eq. 3.74 are given by

$$\beta_{\text{core}} = V_{\text{core}}(\eta_{\text{core}} - \eta_{\text{solv}}) \tag{3.97}$$

$$\beta_{\text{brush}} = V_{\text{brush}}(\eta_{\text{brush}} - \eta_{\text{solv}}) \tag{3.98}$$

$$N_{\text{agg}} = (1 - x_{\text{solv,core}})\frac{4}{3}\pi\epsilon R_{\text{core}}^3 / V_{\text{core}} \tag{3.99}$$

Input Parameters for model `ELL+Chains(RW)_Rc`:

`R_core`: core radius
`V_core`: molecular volume of single block unit in the micellar core
`V_brush`: molecular volume of single block unit in the micellar corona
`eta_core`: scattering length density of spherical core
`eta_brush`: scattering length density of the block unit in the corona

`eta_solv`: scattering length density of solvent
`xsolv_core`: amount of solvent in core
`Rg`: gyration radius of polymer chains in the corona
`d`: This value should be around 1. Non-penetration of the chains into the core is mimicked by $d \sim 1$ for $R_{\text{core}} \gg R_g$
`epsilon`: eccentricity of the ellipsoidal micelle $(R_{\text{core}}, R_{\text{core}}, \epsilon R_{\text{core}})$

For the model `ELL+Chains(RW)_Nagg` the other parameters are

$N_{\mathbf{agg}}$: aggregation number
$V_{\mathbf{core}}$: molecular volume of single block unit in the micellar core

The excess scattering lengths and the core radius R_{core} needed in eq. 3.74 are given by

$$\beta_{\text{core}} = V_{\text{core}}(\eta_{\text{core}} - \eta_{\text{solv}}) \tag{3.100}$$

$$\beta_{\text{brush}} = V_{\text{brush}}(\eta_{\text{brush}} - \eta_{\text{solv}}) \tag{3.101}$$

$$R_{\text{core}} = \left(\frac{N_{\text{agg}} V_{\text{core}}}{1 - x_{\text{solv,core}}} \frac{3}{4\pi\epsilon} \right)^{1/3} \tag{3.102}$$

Input Parameters for model `ELL+Chains(RW)_Nagg`:

`N_agg`: aggregation number
`V_core`: molecular volume of single block unit in the micellar core
`V_brush`: molecular volume of single block unit in the micellar corona
`eta_core`: scattering length density of spherical core
`eta_brush`: scattering length density of the block unit in the corona
`eta_solv`: scattering length density of solvent
`xsolv_core`: amount of solvent in core
`Rg`: gyration radius of polymer chains in the corona
`d`: This value should be around 1. Non-penetration of the chains into the core is mimicked by $d \sim 1$ for $R_{\text{core}} \gg R_g$
`epsilon`: eccentricity of the ellipsoidal micelle $(R_{\text{core}}, R_{\text{core}}, \epsilon R_{\text{core}})$

3.3.11.4. **cylindrical core with radius $R_{\mathbf{core}}$ and height H:**

$$P_{\text{core}}(q, R_{\text{core}}, H) = \int_0^{\pi/2} \Psi^2(q, R_{\text{core}}, H, \alpha)\, \sin\alpha\, d\alpha \tag{3.103}$$

$$\text{with } \Psi(q, R_{\text{core}}, H, \alpha) = \frac{2J_1(qR_{\text{core}} \sin\alpha)}{qR_{\text{core}} \sin\alpha} \frac{\sin(qH/2\, \cos\alpha)}{qH/2\, \cos\alpha} \tag{3.104}$$

and $J_1(x)$ is the first order Bessel function of the first kind.

$$P_{\text{brush}}(q, R_g) = 2\frac{\exp(-x) - 1 + x}{x^2} \text{ with } x = R_g^2 q^2 \tag{3.105}$$

$$S_{\text{brush-core}}(q, R_{\text{core}}, H, Rg, d) = \psi(qR_g) \quad \times \tag{3.106}$$
$$\int_0^{\pi/2} \Psi(q, R_{\text{core}}, H, \alpha)\Xi(q, R + dR_g, H + 2dR_g, \alpha)\, \sin\alpha\, d\alpha$$

where $\Xi(q, R_{\text{core}}, H, \alpha)$ is the form factor amplitude of the shell:

$$\Xi(q, R_{\text{core}}H, \alpha) = \left[\frac{R}{R_{\text{core}} + H} \frac{2J_1(qR_{\text{core}} \sin\alpha)}{qR_{\text{core}} \sin\alpha} \cos(qH/2\, \cos\alpha)\right. \tag{3.107}$$
$$\left. + \frac{H}{R_{\text{core}} + H} J_0(qR_{\text{core}} \sin\alpha) \frac{\sin(qH/2\, \cos\alpha)}{qH/2\, \cos\alpha}\right]$$

where $J_0(x)$ is the zeroth order Bessel function of the first kind.

$$S_{\text{brush-brush}}(q, R_{\text{core}}, H, d, R_g) = \psi^2(qR_g) \quad \times \tag{3.108}$$
$$\int_0^{\pi/2} \Xi^2(q, R_{\text{core}} + dR_g, H + 2dR_g, \alpha)\, \sin\alpha\, d\alpha$$

As for micelles with spherical core also for those with a cylindrical core several parameterizations have been implemented `CYL+Chains(RW)`, `CYL+Chains(RW)_Rc` and `CYL+Chains(RW)_Nagg`. The parameters they all have in common are:

$V_{\mathbf{brush}}$**:** molecular volume the diblock copolymer part forming the corona
$\eta_{\mathbf{core}}$**:** scattering length density of the diblock copolymer part forming the core
$\eta_{\mathbf{brush}}$**:** scattering length density of the diblock copolymer part forming the corona
$\eta_{\mathbf{solv}}$**:** scattering length density of the solvent
$x_{\mathbf{solv,core}}$**:** volume fraction of solvent in the micellar core
R_g**:** radius of gyration of the block unit in the corona
d**:** non-penetration of the chains into the core is mimicked by $d \sim 1$ for $R_{\text{core}} \gg R_g$
H**:** height of the cylindrical core of the micelle

For the model `CYL+Chains(RW)` the other parameters are

$R_{\mathbf{core}}$**:** radius of the micellar core $(R_{\text{core}}, R_{\text{core}}, \epsilon R_{\text{core}})$

$n_{\mathbf{agg}}$**:** grafting density (number of copolymer molecules N_{agg} per surface are S, $n_{\text{agg}} = N_{\text{agg}}/S$)

In contrast to the form factor `CYL+Chains(RW)_Rc` and `CYL+Chains(RW)_Nagg` this one does not necessary consist of copolymers. The excess scattering lengths and aggregation number needed in eq. 3.74 are than given by

$$N_{\text{agg}} = n_{\text{agg}} S \tag{3.109}$$

where the surface of the core is given by

$$S = 2\pi R_{\text{core}} H \tag{3.110}$$

Together with the core volume $V = \pi R_{\text{core}}^2 H$ one can calculate the excess scattering lengths by

$$\beta_{\text{core}} = \frac{V(1 - x_{\text{solv,core}})}{N_{\text{agg}}}(\eta_{\text{core}} - \eta_{\text{solv}}) \tag{3.111}$$

$$\beta_{\text{brush}} = V_{\text{brush}}(\eta_{\text{brush}} - \eta_{\text{solv}}) \tag{3.112}$$

Input Parameters for model `CYL+Chains(RW)`:

`R_core`**:** core radius
`n_agg`**:** specific aggregation number (number of chains per surface area)
`V_brush`**:** molecular volume of a block unit in the micellar corona
`eta_core`**:** scattering length density of spherical core
`eta_brush`**:** scattering length density of the block unit in the corona
`eta_solv`**:** scattering length density of solvent
`xsolv_core`**:** amount of solvent in core
`Rg`**:** gyration radius of polymer chains in the corona
`d`**:** This value should be around 1. Non-penetration of the chains into the core is mimicked by $d \sim 1$ for $R_{\text{core}} \gg R_g$
`H`**:** height of the cylindrical core of the micelle

For the model `CYL+Chains(RW)_Rc` the other parameters are

$R_{\mathbf{core}}$**:** core radius
$V_{\mathbf{core}}$**:** molecular volume of single block unit in the micellar core

The excess scattering lengths and aggregation number in eq. 3.74 are than given by

$$\beta_{\text{core}} = V_{\text{core}}(\eta_{\text{core}} - \eta_{\text{solv}}) \tag{3.113}$$

$$\beta_{\text{brush}} = V_{\text{brush}}(\eta_{\text{brush}} - \eta_{\text{solv}}) \tag{3.114}$$

$$N_{\text{agg}} = (1 - x_{\text{solv,core}})\pi R_{\text{core}}^2 H / V_{\text{core}} \tag{3.115}$$

Input Parameters for model `CYL+Chains(RW)_Rc`:

`R_core`**:** core radius
`V_core`**:** molecular volume of single block unit in the micellar core
`V_brush`**:** molecular volume of single block unit in the micellar corona
`eta_core`**:** scattering length density of spherical core

`eta_brush`: scattering length density of the block unit in the corona
`eta_solv`: scattering length density of solvent
`xsolv_core`: amount of solvent in core
`Rg`: gyration radius of polymer chains in the corona
`d`: This value should be around 1. Non-penetration of the chains into the core is mimicked by $d \sim 1$ for $R_{\text{core}} \gg R_g$
`H`: height of the cylindrical core of the micelle

For the model `CYL+Chains(RW)_Nagg` the other parameters are

$N_{\mathbf{agg}}$: aggregation number
$V_{\mathbf{core}}$: molecular volume of single block unit in the micellar core

The excess scattering lengths and the core radius R_{core} are given by

$$\beta_{\text{core}} = V_{\text{core}}(\eta_{\text{core}} - \eta_{\text{solv}}) \tag{3.116}$$

$$\beta_{\text{brush}} = V_{\text{brush}}(\eta_{\text{brush}} - \eta_{\text{solv}}) \tag{3.117}$$

$$R_{\text{core}} = \sqrt{\frac{N_{\text{agg}} V_{\text{core}}}{1 - x_{\text{solv,core}}} \frac{1}{\pi H}} \tag{3.118}$$

Input Parameters for model `CYL+Chains(RW)_Nagg`:

`N_agg`: aggregation number
`V_core`: molecular volume of single block unit in the micellar core
`V_brush`: molecular volume of single block unit in the micellar corona
`eta_core`: scattering length density of spherical core
`eta_brush`: scattering length density of the block unit in the corona
`eta_solv`: scattering length density of solvent
`xsolv_core`: amount of solvent in core
`Rg`: gyration radius of polymer chains in the corona
`d`: This value should be around 1. Non-penetration of the chains into the core is mimicked by $d \sim 1$ for $R_{\text{core}} \gg R_g$
`H`: height of the cylindrical core of the micelle

3.3.11.5. **wormlike micelles with cylindrical cross-section with radius $R_{\mathbf{core}}$, Kuhn-length l and contour length L:**
The form factors for a worm-like micelles are approximated by the form factor of the Kholodenko-worm according to section 3.3.10 where the scattering length density profile across the worm segments are described by those of a rod-like micelle 3.3.11.6. The corresponding function in eq. 3.74 are given by

$$P_{\text{core}}(q, R_{\text{core}}, l, L) = P_{\text{worm}}(q, l, L) P_{\text{cs}}(q, R_{\text{core}}, d, R_g) \tag{3.119}$$

the contributiion of the worm-like conformation of the micelle $P_{\text{worm}}(q, l, L)$ is described by the formula of Kholodenko for worm-like structures given in eq. 3.68. The contribution of the cross-section P_{cs} is the same as for rod-like micelles and given by

$$P_{\text{cs}}(q, R_{\text{core}}, d, R_g) = \left[\frac{2J_1(qR_{\text{core}})}{qR_{\text{core}}}\right]^2 \tag{3.120}$$

$$\text{Si}(x) = \int_0^x t^{-1} \sin t \, dt \tag{3.121}$$

$$P_{\text{brush}}(q, R_g) = 2\frac{\exp(-x) - 1 + x}{x^2} \text{ with } x = R_g^2 q^2 \tag{3.122}$$

$$S_{\text{brush-core}}(q, R_{\text{core}}, l, L, Rg, d) = \psi(qR_g) \quad \times \tag{3.123}$$
$$\frac{2J_1(qR_{\text{core}})}{qR_{\text{core}}} J_0[q(r_{\text{core}} + dR_g)] P_{\text{worm}}(q, l, L)$$

$$S_{\text{brush-brush}}(q, R_{\text{core}}, l, L, d, R_g) = \psi^2(qR_g) J_0^2[q(r_{\text{core}} + dR_g)] P_{\text{worm}}(q, l, L) \tag{3.124}$$

As for micelles with spherical core also for those worm-like micelles several parameterizations have been implemented `WORM+Chains(RW)`, `WORM+Chains(RW)_Rc` and `WORM+Chains(RW)_nagg`. The parameters they all have in common are:

$V_{\mathbf{brush}}$**:** molecular volume the diblock copolymer part forming the corona
$\eta_{\mathbf{core}}$**:** scattering length density of the diblock copolymer part forming the core
$\eta_{\mathbf{brush}}$**:** scattering length density of the diblock copolymer part forming the corona
$\eta_{\mathbf{solv}}$**:** scattering length density of the solvent
$x_{\mathbf{solv,core}}$**:** volume fraction of solvent in the micellar core
R_g**:** radius of gyration of the block unit in the corona
l**:** contour length of the worm-like of the micelle
L**:** contour length of the worm-like of the micelle

For the model `WORM+Chains(RW)` the other parameters are

$R_{\mathbf{core}}$**:** radius of the micellar core
$n_{\mathbf{agg}}$**:** grafting density (number of copolymer molecules N_{agg} per surface are S, $n_{\text{agg}} = N_{\text{agg}}/S$)

In contrast to the form factor `WORM+Chains(RW)_Rc` and `WORM+Chains(RW)_nagg` this one does not necessary consist of copolymers. The excess scattering lengths and aggregation number needed in eq. 3.74 are than given by

$$N_{\text{agg}} = n_{\text{agg}} S \tag{3.125}$$

where the surface of the core is given by

$$S = 2\pi R_{\text{core}} L \tag{3.126}$$

Together with the core volume $V = \pi R_{\text{core}}^2 L$ one can calculate the excess scattering lengths by

$$\beta_{\text{core}} = \frac{V(1 - x_{\text{solv,core}})}{N_{\text{agg}}}(\eta_{\text{core}} - \eta_{\text{solv}}) \tag{3.127}$$

$$\beta_{\text{brush}} = V_{\text{brush}}(\eta_{\text{brush}} - \eta_{\text{solv}}) \tag{3.128}$$

Input Parameters for model `WORM+Chains(RW)`:

`R_core`: core radius
`n_agg`: specific aggregation number (number of chains per surface area)
`V_brush`: molecular volume of a block unit in the micellar corona
`eta_core`: scattering length density of spherical core
`eta_brush`: scattering length density of the block unit in the corona
`eta_solv`: scattering length density of solvent
`xsolv_core`: amount of solvent in core
`Rg`: gyration radius of polymer chains in the corona
`l`: contour length of the worm-like of the micelle
`L`: contour length of the worm-like of the micelle

For the model `WORM+Chains(RW)_Rc` the other parameters are

$R_{\mathbf{core}}$: core radius
$V_{\mathbf{core}}$: molecular volume of single block unit in the micellar core

The excess scattering lengths and aggregation number in eq. 3.74 are than given by

$$\beta_{\text{core}} = V_{\text{core}}(\eta_{\text{core}} - \eta_{\text{solv}}) \tag{3.129}$$

$$\beta_{\text{brush}} = V_{\text{brush}}(\eta_{\text{brush}} - \eta_{\text{solv}}) \tag{3.130}$$

$$N_{\text{agg}} = (1 - x_{\text{solv,core}})\pi R_{\text{core}}^2 L / V_{\text{core}} \tag{3.131}$$

Input Parameters for model `CYL+Chains(RW)_Rc`:

`R_core`: core radius
`V_core`: molecular volume of single block unit in the micellar core
`V_brush`: molecular volume of single block unit in the micellar corona
`eta_core`: scattering length density of spherical core
`eta_brush`: scattering length density of the block unit in the corona
`eta_solv`: scattering length density of solvent
`xsolv_core`: amount of solvent in core

`Rg`: gyration radius of polymer chains in the corona
`l`: contour length of the worm-like of the micelle
`L`: contour length of the worm-like of the micelle

For the model `WORM+Chains(RW)_Nagg` the other parameters are

$N_{\mathbf{agg}}$: aggregation number
$V_{\mathbf{core}}$: molecular volume of single block unit in the micellar core

The excess scattering lengths and the core radius R_{core} are given by

$$\beta_{\text{core}} = V_{\text{core}}(\eta_{\text{core}} - \eta_{\text{solv}}) \tag{3.132}$$

$$\beta_{\text{brush}} = V_{\text{brush}}(\eta_{\text{brush}} - \eta_{\text{solv}}) \tag{3.133}$$

$$R_{\text{core}} = \sqrt{\frac{N_{\text{agg}} V_{\text{core}}}{1 - x_{\text{solv,core}}} \frac{1}{\pi L}} \tag{3.134}$$

Input Parameters for model `CYL+Chains(RW)_Nagg`:

`N_agg`: aggregation number
`V_core`: molecular volume of single block unit in the micellar core
`V_brush`: molecular volume of single block unit in the micellar corona
`eta_core`: scattering length density of spherical core
`eta_brush`: scattering length density of the block unit in the corona
`eta_solv`: scattering length density of solvent
`xsolv_core`: amount of solvent in core
`Rg`: gyration radius of polymer chains in the corona
`l`: contour length of the worm-like of the micelle
`L`: contour length of the worm-like of the micelle

3.3.11.6. **micelles with rod-like core:**
The form factors for micelles with a rod-like core are an approximations of the form factors of micelles with a cylindrical core where $H \gg R_{\text{core}} + dR_g$. The corresponding function in eq. 3.74 are given by

$$P_{\text{core}}(q, R_{\text{core}}, H) = P_H(q, H) P_{\text{cs}}(q, R_{\text{core}}, d, R_g) \tag{3.135}$$

with

$$P_H(q, H) = 2\text{Si}(qH)/(qH) - 4\sin^2(qH/2)/(q^2H^2) \tag{3.136}$$

$$P_{\text{cs}}(q, R_{\text{core}}, d, R_g) = \left[\frac{2J_1(qR_{\text{core}})}{qR_{\text{core}}}\right]^2 \tag{3.137}$$

$$\text{Si}(x) = \int_0^x t^{-1} \sin t \, dt \tag{3.138}$$

$$P_{\text{brush}}(q, R_g) = 2\frac{\exp(-x) - 1 + x}{x^2} \text{ with } x = R_g^2 q^2 \tag{3.139}$$

$$S_{\text{brush-core}}(q, R_{\text{core}}, H, Rg, d) = \psi(qR_g) \quad \times \tag{3.140}$$
$$\frac{2J_1(qR_{\text{core}})}{qR_{\text{core}}} J_0[q(r_{\text{core}} + dR_g)] P_H(q, H)$$

$$S_{\text{brush-brush}}(q, R_{\text{core}}, H, d, R_g) = \psi^2(qR_g) J_0^2[q(r_{\text{core}} + dR_g)] P_H(q, H) \tag{3.141}$$

As otherwise the definitions of the geometry for rod-like micelles are mainly the same than for cylindrical micelles only the list of input parameters are given here. There is only one difference in the model `ROD+Chains(RW)_Nagg` compared to the model `CYL+Chains(RW)_Nagg` and that is that for rod-like structures always the grafting density of polymer chains on the surface of the core is used, i.e. $n_{\text{agg}} = N_{\text{agg}}/S$ instead of N_{agg}. For the model `ROD+Chains(RW)_nagg` this means that the core radius has to be calculated by $R_{\text{core}} = 2n_{\text{agg}} V_{\text{core}}/(1 - x_{\text{solv,core}})$

Input Parameters for model `ROD+Chains(RW)`:

`R_core`: core radius
`n_agg`: specific aggregation number (number of chains per surface area)
`V_brush`: molecular volume of a block unit in the micellar corona
`eta_core`: scattering length density of spherical core
`eta_brush`: scattering length density of the block unit in the corona
`eta_solv`: scattering length density of solvent
`xsolv_core`: amount of solvent in core
`Rg`: gyration radius of polymer chains in the corona
`d`: This value should be around 1. Non-penetration of the chains into the core is mimicked by $d \sim 1$ for $R_{\text{core}} \gg R_g$
`H`: height of the rod-like core of the micelle

Input Parameters for model `ROD+Chains(RW)_Rc`:

`R_core`: core radius
`V_core`: molecular volume of single block unit in the micellar core
`V_brush`: molecular volume of single block unit in the micellar corona
`eta_core`: scattering length density of spherical core
`eta_brush`: scattering length density of the block unit in the corona
`eta_solv`: scattering length density of solvent
`xsolv_core`: amount of solvent in core
`Rg`: gyration radius of polymer chains in the corona
`d`: This value should be around 1. Non-penetration of the chains into the core is mimicked by $d \sim 1$ for $R_{\text{core}} \gg R_g$
`H`: height of the rod-like core of the micelle

Input Parameters for model `ROD+Chains(RW)_nagg`:

`n_agg`: specific aggregation number (number of chains per surface area)
`V_core`: molecular volume of single block unit in the micellar core
`V_brush`: molecular volume of single block unit in the micellar corona
`eta_core`: scattering length density of spherical core
`eta_brush`: scattering length density of the block unit in the corona
`eta_solv`: scattering length density of solvent
`xsolv_core`: amount of solvent in core
`Rg`: gyration radius of polymer chains in the corona
`d`: This value should be around 1. Non-penetration of the chains into the core is mimicked by $d \sim 1$ for $R_{\text{core}} \gg R_g$
`H`: height of the rod-like core of the micelle

3.3.11.7. *Micelles with a homogeneous core and a corona with decaying density profile . of the form* $\varphi(r) \propto r^{-\alpha}$.

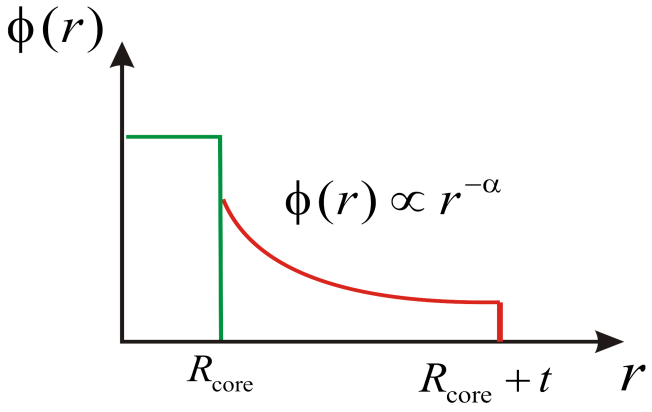

FIGURE 3.49. radial profile.

The structure of block copolymer micelles may be described in terms of the model of starlike polymer as proposed by Daoud and Cotton [**19**]. Starlike polymers consist of a homogeneous, dense polymer core surrounded by a polymer layer. As a consequence of the spherical or cylindrical geometry, the density profile $\phi(r)$ in the polymer layer decreases according to Wijmans & Zhulina [**103**] as

$$\phi(r) \begin{cases} \phi_{\text{core}} & \text{for } r < R_{\text{core}} \\ \phi_{\text{brush}} \left(\frac{r}{R_{\text{core}}} \right)^{-\alpha} & \text{for } R_{\text{core}} \leq r \leq R_{\text{core}} + t \\ 0 & \text{for } r > R_{\text{core}} + t \end{cases} \tag{3.142}$$

with $\alpha = (D-1)(3\nu - 1)/(2\nu)$. D is determined by the dimension of the curvature of the grafted surface (spherical $D = 3$, cylindrical $D = 2$, planar $D = 1$). ν is the Flory exponent, which has characteristic values as given in Table 1. The corresponding density profile is schematically shown in Figure 3.49. Micelles consist of a well-defined micellar core with a radius R_{core} and a micellar shell or corona extending to the outer micellar radius $R_m = R_{\text{core}} + t$, where t is the thickness of the corona.

TABLE 1. Flory exponent ν and exponent α of the radial density profile for different thermodynamic states of the polymer chains

ν	α_{sphere} $D = 3$	α_{cylinder} $D = 2$	α_{planar} $D = 1$	remarks
1/3	0	0	0	collapsed polymer
1/2	1	1/2	0	polymer in Θ-solvent, semi-dilute solution
3/5	4/3	2/3	0	polymer in good solvent
1	2	1	0	polymer in stretched conformation, e.g. polyelectrolyte

For a given radial profile according to eq. 3.142 the form factor of spherical micelle can be calculated by

$$F_{\text{SPHERE}} = \int_0^\infty 2\pi r^2 \phi(r) \frac{\sin(qr)}{qr}\, dr \tag{3.143}$$

In case of a rod-like micelle the form factor can be separated in two terms $I(q) = P_H(q)P_{\text{cs}}(q)$ as already in shown in eq. 3.135. The cross-term contribution to the scattering intensity is given by

$$\begin{aligned} P_{\text{cs}}(q) &= F_{\text{cs}}^2(q) \\ F_{\text{cs}}(q) &= \int_0^\infty 2\pi r \phi(r) J_0(q)\, dr \end{aligned} \tag{3.144}$$

However, as it is more convenient here to formulate the scattering intensity in terms of excess scattering length of the block units in the core β_{core} and the corona β_{brush} like in eq. 3.74 the form factor is split into two parts, the form factor of the homogeneous core $F_{\text{core}}(q)$ and the form factor of the corona $F_{\text{brush}}(q)$. The overall scattering intensity $I(q)$ is than given by

$$\begin{aligned} I(q) = {} & N_{\text{agg}}^2 \beta_{\text{core}}^2 F_{\text{core}}^2(q) + 2N_{\text{agg}}^2 \beta_{\text{core}} \beta_{\text{corona}} F_{\text{core}}(q) F_{\text{corona}}(q) \\ & + N_{\text{agg}}(N_{\text{agg}} - 1)\beta_{\text{corona}}^2 F_{\text{corona}}^2(q) + N_{\text{agg}} P_{\text{brush}}(q) \end{aligned} \tag{3.145}$$

The excess scattering length of a block in the corona and in the core, respectively, $\beta_{\text{brush}} = V_{\text{brush}}(\eta_{\text{brush}} - \eta_{\text{solv}})$ and $\beta_{\text{core}} = V_{\text{core}}(\eta_{\text{core}} - \eta_{\text{solv}})$ are defined in the same way than in eq. 3.74. V_{brush} and V_{core} are the total volume of a block in the corona and in the core. η_{brush} and η_{core} are the corresponding scattering length densities and η_{solv} is the scattering length density of the surrounding solvent. $F_{\text{core}}(q)$ is the form factor of the core and normalized to 1 for $q = 0$. Also the form factor of the corona $F_{\text{corona}}(q)$ and the form factor of the local fluctuations in the corona originating from the individual chains $P_{\text{brush}}(q)$ are normalized to 1 for $q = 0$. Similar to section 3.3.11.1 models for spherical and rod-like shapes have been implemented which are described in the following paragraphs.

3.3.11.8. **spherical core:**

$$F_{\text{core}}(q, R) = 3\frac{\sin(qR) - qR\cos(qR)}{(qR)^3} \tag{3.146}$$

$$F_{\text{brush}}(q, R, t) = \frac{1}{C_{norm}} \int_{R_{\text{core}}}^{R_{\text{core}}+t} 2\pi r^2 r^{-\alpha} \frac{\sin(qr)}{qr}\, dr \tag{3.147}$$

with

$$C_{norm} = \begin{cases} \frac{4}{3-\alpha}\pi\left((R_{\text{core}}+t)^{3-\alpha} - R_{\text{core}}^{3-\alpha}\right) & \text{for } \alpha \neq 2 \\ 4\pi \ln\left(\frac{R_{\text{core}}+t}{R_{\text{core}}}\right) & \text{for } \alpha = 2 \end{cases}$$

For the scattering contribution of the individual chains in the corona P_{brush} the scattering function for worm-like chains with excluded volume and negligible cross-section, contour length L and Kuhn-length b according to section 3.3.9 has been implemented.

For micelles with a spherical core a few different parameterizations have been implemented `SPHERE+R^-a`, `SPHERE+R^-a_Rc` and `SPHERE+R^-a_Nagg`.

The parameters they all have in common are:

$V_{\mathbf{brush}}$**:** molecular volume the diblock copolymer part forming the corona
$\eta_{\mathbf{core}}$**:** scattering length density of the diblock copolymer part forming the core
$\eta_{\mathbf{brush}}$**:** scattering length density of the diblock copolymer part forming the corona
$\eta_{\mathbf{solv}}$**:** scattering length density of the solvent
α**:** exponent of the radial scattering length density profile ($r^{-\alpha}$)
t**:** corona thickness
L**:** contour length of the chain in the corona
b**:** Kuhn-length of the chain in the corona

For the model `SPHERE+R^-a` the other parameters are

$R_{\mathbf{core}}$**:** radius of the micellar core
$n_{\mathbf{agg}}$**:** grafting density (number of copolymer molecules N_{agg} per surface are S, $n_{\text{agg}} = N_{\text{agg}}/S$)

In contrast to the form factor `SPHERE+R^-a_Rc` and `SPHERE+R^-a_Nagg` this one does not necessary consist of copolymers. The excess scattering lengths and aggregation number are given by

$$N_{\text{agg}} = n_{\text{agg}} S \tag{3.148}$$

where the surface of the core is given by $S = 4\pi R_{\text{core}}^2$. Together with the core volume $V = \frac{4}{3}\pi R_{\text{core}}^3$ one gets for the excess scattering lengths

$$\beta_{\text{core}} = \frac{V(1 - x_{\text{solv,core}})}{N_{\text{agg}}}(\eta_{\text{core}} - \eta_{\text{solv}}) \tag{3.149}$$

$$\beta_{\text{brush}} = V_{\text{brush}}(\eta_{\text{brush}} - \eta_{\text{solv}}) \tag{3.150}$$

Input Parameters for model `SPHERE+R^-a`:

`R_core`**:** core radius
`n_agg`**:** specific aggregation number (number of chains per surface area)
`V_brush`**:** molecular volume of a block unit in the micellar corona
`eta_core`**:** scattering length density of spherical core
`eta_brush`**:** scattering length density of the block unit in the corona
`eta_solv`**:** scattering length density of solvent
`alpha`**:** exponent of the radial scattering length density profile ($r^{-\alpha}$)
`t`**:** corona thickness

`L:` contour length of the chain in the corona
`b:` Kuhn-length of the chain in the corona

For the model `SPHERE+R^-a_Rc` the other parameters are

$R_{\mathbf{core}}$**:** core radius
$V_{\mathbf{core}}$**:** molecular volume of single block unit in the micellar core

The excess scattering lengths and aggregation number for eq. 3.74 are given by

$$\beta_{\text{core}} = V_{\text{core}}(\eta_{\text{core}} - \eta_{\text{solv}}) \tag{3.151}$$

$$\beta_{\text{brush}} = V_{\text{brush}}(\eta_{\text{brush}} - \eta_{\text{solv}}) \tag{3.152}$$

$$N_{\text{agg}} = (1 - x_{\text{solv,core}})\frac{4}{3}\pi R_{\text{core}}^3/V_{\text{core}} \tag{3.153}$$

Input Parameters for model `SPHERE+R^-a_Rc`:

`R_core`**:** core radius
`V_core`**:** molecular volume of single block unit in the micellar core
`V_brush`**:** molecular volume of single block unit in the micellar corona
`eta_core`**:** scattering length density of spherical core
`eta_brush`**:** scattering length density of the block unit in the corona
`eta_solv`**:** scattering length density of solvent
`alpha`**:** exponent of the radial scattering length density profile ($r^{-\alpha}$)
`t`**:** corona thickness
`L`**:** contour length of the chain in the corona
`b`**:** Kuhn-length of the chain in the corona

For the model `SPHERE+R^-a_Nagg` the other parameters are

$N_{\mathbf{agg}}$**:** aggregation number
$V_{\mathbf{core}}$**:** molecular volume of single block unit in the micellar core

The excess scattering lengths and the core radius R_{core} needed for eq. 3.74 are given by

$$\beta_{\text{core}} = V_{\text{core}}(\eta_{\text{core}} - \eta_{\text{solv}}) \tag{3.154}$$

$$\beta_{\text{brush}} = V_{\text{brush}}(\eta_{\text{brush}} - \eta_{\text{solv}}) \tag{3.155}$$

$$R_{\text{core}} = \left(\frac{N_{\text{agg}}V_{\text{core}}}{1 - x_{\text{solv,core}}}\,\frac{3}{4\pi}\right)^{1/3} \tag{3.156}$$

Input Parameters for model `SPHERE+R^-a_Nagg`:

`N_agg`**:** aggregation number
`V_core`**:** molecular volume of single block unit in the micellar core
`V_brush`**:** molecular volume of single block unit in the micellar corona
`eta_core`**:** scattering length density of spherical core
`eta_brush`**:** scattering length density of the block unit in the corona
`eta_solv`**:** scattering length density of solvent
`alpha`**:** exponent of the radial scattering length density profile ($r^{-\alpha}$)
`t`**:** corona thickness
`L`**:** contour length of the chain in the corona
`b`**:** Kuhn-length of the chain in the corona

3.3.11.9. **rodlike core:**
In case of a rod-like micelle the form factor can be separated in two terms $I(q) = P_H(q)P_{\text{cs}}(q)$ as already in shown in eq. 3.135. The cross-term contribution to the scattering intensity is given by

$$\begin{aligned} P_{\text{cs}}(q) &= F_{\text{cs}}^2(q) \\ F_{\text{cs}}(q) &= \int_0^\infty 2\pi r\phi(r)J_0(qr)\,dr = F_{\text{cs,core}}(q) + F_{\text{cs,brush}}(q) \end{aligned} \tag{3.157}$$

The contribution of the homogeneous core is given by

$$F_{\text{cs,core}}(q) = \frac{2J_1(qR_c)}{qR_c} \tag{3.158}$$

and for the corona by

$$F_{\text{cs,brush}}(q) = \frac{1}{c_\alpha}\int_{R_c}^{R_c+t} 2\pi r\, r^{-\alpha} J_0(qr)\,dr \tag{3.159}$$

$$\begin{aligned} c_\alpha &= \int_{R_c}^{R_c+t} 2\pi r\, r^{-\alpha}\,dr \\ &= \begin{cases} 2\pi \ln\left(\frac{R_c+t}{R_c}\right) & \text{for } \alpha = 2 \\ \frac{2}{2-\alpha}\pi\left((R_c+t)^{2-\alpha} - R_c^{2-\alpha}\right) & \text{for } \alpha \neq 2 \end{cases} \end{aligned} \tag{3.160}$$

For the scattering contribution of the individual chains in the corona P_{local} normally can be neglected for rod-like micelles in contrast to spherical structures as for structures with a lower dimension than spheres, this contribution becomes more and more negligible. To account for the scattering of the individual chains at least in first approximation and without introducing new parameters a form factor similar to the one of star polymers has been implemented.

$$\begin{aligned} P_{\text{local}}(q) &= \frac{\Gamma(\mu)}{qt}\frac{\sin\left(\mu \arctan(qt)\right)}{(1+q^2t^2)^{\mu/2}} \\ \mu &= \frac{1}{\nu} - 1, \quad \alpha = \frac{3\nu-1}{2\nu} \quad \Leftrightarrow \quad \mu = 2(1-\alpha) \end{aligned} \tag{3.161}$$

The form factor to describe the scattering of the individual chains is identical to the blob scattering contribution in star-like polymers according to Dozier (3.3.4). The exponential damping length ξ in the definition of the star polymer has been set to the shell thickness t. In the original paper of Pedersen the P_{local} was described by the scattering of a semi-flexible chain with excluded volume according to section 3.3.9, which however would require to define two more parameters.

For micelles with a rod-like core a few different parameterizations have been implemented `ROD+R^-a`, `ROD+R^-a_Rc` and `ROD+R^-a_Nagg`.

The parameters they all have in common are:

$V_{\mathbf{brush}}$**:** molecular volume the diblock copolymer part forming the corona
$\eta_{\mathbf{core}}$**:** scattering length density of the diblock copolymer part forming the core
$\eta_{\mathbf{brush}}$**:** scattering length density of the diblock copolymer part forming the corona
$\eta_{\mathbf{solv}}$**:** scattering length density of the solvent
$x_{\mathbf{solv,core}}$**:** amount of solvent in the core
α**:** exponent of the radial scattering length density profile ($r^{-\alpha}$)
t**:** corona thickness
H**:** height of the cylinder

For the model `ROD+R^-a` the other parameters are

$R_{\mathbf{core}}$**:** radius of the micellar core
$n_{\mathbf{agg}}$**:** grafting density (number of copolymer molecules N_{agg} per surface are S, $n_{\text{agg}} = N_{\text{agg}}/S$)

In contrast to the form factor `ROD+R^-a_Rc` and `ROD+R^-a_Nagg` this one does not necessary consist of copolymers. The excess scattering lengths and aggregation number are given by

$$N_{\text{agg}} = n_{\text{agg}} S \tag{3.162}$$

where the surface of the core is given by $S = 2\pi R_{\text{core}} H$. Together with the core volume $V = \pi R_{\text{core}}^2 H$ one gets for the excess scattering lengths

$$\beta_{\text{core}} = \frac{V_{\text{core}}(1 - x_{\text{solv,core}})}{N_{\text{agg}}}(\eta_{\text{core}} - \eta_{\text{solv}}) \tag{3.163}$$

$$\beta_{\text{brush}} = V_{\text{brush}}(\eta_{\text{brush}} - \eta_{\text{solv}}) \tag{3.164}$$

Input Parameters for model `ROD+R^-a`:

`R_core`**:** core radius
`n_agg`**:** specific aggregation number (number of chains per surface area)
`V_brush`**:** molecular volume of a block unit in the micellar corona
`eta_core`**:** scattering length density of spherical core
`eta_brush`**:** scattering length density of the block unit in the corona
`eta_solv`**:** scattering length density of solvent
`xsolv_core`**:** amount of solvent in the core
`alpha`**:** exponent of the radial scattering length density profile ($r^{-\alpha}$)
`t`**:** corona thickness
`H`**:** rod height

For the model `ROD+R^-a_Rc` the other parameters are

$R_{\mathbf{core}}$**:** core radius
$V_{\mathbf{core}}$**:** molecular volume of single block unit in the micellar core

The excess scattering lengths and aggregation number for eq. 3.74 are given by

$$\beta_{\text{core}} = V_{\text{core}}(\eta_{\text{core}} - \eta_{\text{solv}}) \tag{3.165}$$

$$\beta_{\text{brush}} = V_{\text{brush}}(\eta_{\text{brush}} - \eta_{\text{solv}}) \tag{3.166}$$

$$N_{\text{agg}} = 2\pi R_{\text{core}}^2 H \frac{1 - x_{\text{solv,core}}}{V_{\text{core}}} \tag{3.167}$$

Input Parameters for model `ROD+Rˆ-a_Rc`:

`R_core`: core radius
`V_core`: molecular volume of single block unit in the micellar core
`V_brush`: molecular volume of single block unit in the micellar corona
`eta_core`: scattering length density of spherical core
`eta_brush`: scattering length density of the block unit in the corona
`eta_solv`: scattering length density of solvent
`xsolv_core`: amount of solvent in the core
`alpha`: exponent of the radial scattering length density profile ($r^{-\alpha}$)
`t`: corona thickness
`H`: rod height

For the model `ROD+Rˆ-a_Nagg` the other parameters are

$n_{\mathbf{agg}}$: specific aggregation number, aggregation number per surface area
$V_{\mathbf{core}}$: molecular volume of single block unit in the micellar core

The excess scattering lengths and the core radius R_{core} needed for eq. 3.74 are given by

$$\beta_{\text{core}} = V_{\text{core}}(\eta_{\text{core}} - \eta_{\text{solv}}) \tag{3.168}$$

$$\beta_{\text{brush}} = V_{\text{brush}}(\eta_{\text{brush}} - \eta_{\text{solv}}) \tag{3.169}$$

$$R_{\text{core}} = \frac{2 n_{\text{agg}} V_{\text{core}}}{1 - x_{\text{solv,core}}} \tag{3.170}$$

Input Parameters for model `ROD+Rˆ-a_nagg`:

`n_agg`: specific aggregation number (number of chains per surface area)
`V_core`: molecular volume of single block unit in the micellar core
`V_brush`: molecular volume of single block unit in the micellar corona
`eta_core`: scattering length density of spherical core
`eta_brush`: scattering length density of the block unit in the corona
`eta_solv`: scattering length density of solvent
`xsolv_core`: amount of solvent in the core
`alpha`: exponent of the radial scattering length density profile ($r^{-\alpha}$)
`t`: corona thickness
`H`: rod height

REFERENCES:
[**19, 28, 67, 103**]

3.3.11.10. *spherical Micelles with a homogeneous core and a corona of semi-flexible interacting self-avoiding chains.*

3.3.12. Sphere with Gaussian chains attached.

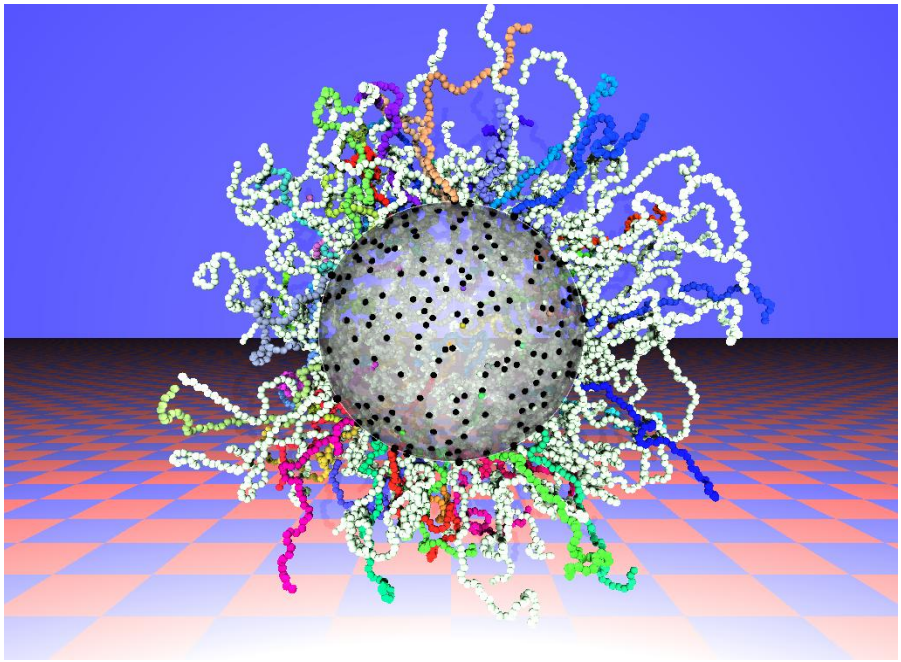

FIGURE 3.50. Block copolymer micelles.

The expressions have been derived by Pedersen and Gerstenberg [**75, 76**]. For a sphere with radius R and total excess scattering length ρ_s with $N_{\rm agg}$ attached chains

$$\begin{aligned} P_{mic}(Q) &= N_{\rm agg}^2\rho_s^2 P_s(Q,R) + N_{agg}\rho_c^2 P_c(Q,R_g) \\ &\quad + N_{\rm agg}(N_{agg}-1)\rho_c^2 S_{cc}(Q) + 2N_{\rm agg}^2\rho_s\rho_c S_{sc}(Q) \end{aligned} \tag{3.171}$$

with:

$$P_s = \Phi^2(Q, R) \tag{3.172}$$

$$\Phi(Q, R) = 3\frac{\sin(QR) - QR\cos(QR)}{(QR)^3} \tag{3.173}$$

$$P_c(Q, R_g) = 2\frac{\exp(-x) - 1 + x}{x^2} \tag{3.174}$$

$$x = R_g^2 Q^2 \tag{3.175}$$

$$\Psi(Q, R_g) = \frac{1 - \exp(-x)}{x} \tag{3.176}$$

$$S_{\rm cc}(Q) = \Psi^2(Q, R_g)\left(\frac{\sin(Q(R + d\ R_g))}{Q(R + d\, R_g)}\right)^2 \tag{3.177}$$

$$S_{\rm sc}(Q) = \Psi(Q, R_g)\Phi(QR_g)\frac{\sin(Q(R + d\, R_g))}{Q(R + d\, R_g)} \tag{3.178}$$

where R_g is the root-mean-square radius of gyration of a chain. ρ_c is the total excess scattering length of a single chain. Non-penetrating of the chains into the core region is mimicked by $d \approx 1$ for $R \gg R_g$.

Input Parameters for model `SphereWithGaussChains`:

`R:` radius of core R
`Rg:` gyration radius of chain R_g
`d:` for non-penetration of the chains into the core region $d \approx 1$.
`Nagg:` aggregation number $N_{\rm agg}$
`rc:` excess scattering length of a block in the chains ρ_c
`rs:` excess scattering length of a block in the core ρ_s

3.3.13. Sphere with Gaussian chains attached (block copolymer micelle).

This form factor is the same than for `SphereWithGaussChains`. It has only been slightly re-parametrised. Instead of the core radius R and excess scattering lengths ρ_s and ρ_c the volumes $V_{\text{polym,c}}$ and $V_{\text{polym,sh}}$ of the block units building the core and the shell are required together with the corresponding scattering length densities $\eta_{\text{poly,c}}$, $\eta_{\text{poly,sh}}$ and that one of the solvent η_{solv}. Furthermore $x_{\text{solv,c}}$ is the amount of solvent in the core which takes account for a possible swelling of the core. These parameters allow one to calculate the core radius and excess scattering lengths by

$$R = \left(\left| \frac{N_{\text{agg}} V_{\text{polym,c}}}{1 - x_{\text{solv,c}}} \right| \frac{3}{4\pi} \right)^{1/3} \tag{3.179}$$

$$\rho_s = V_{\text{polym,c}} \left(\eta_{\text{poly,c}} - \eta_{\text{solv}} \right) \tag{3.180}$$

$$\rho_c = V_{\text{polym,sh}} \left(\eta_{\text{poly,sh}} - \eta_{\text{solv}} \right) \tag{3.181}$$

The volumes $V_{\text{polym,c}}$ and $V_{\text{polym,sh}}$ can be calculated by knowing the molecular weights[5] of the block units of the polymer in the core $M_{\text{polym,c}}$ and in the shell $M_{\text{polym,sh}}$ together with their bulk mass densities $\rho_{\text{polym,c}}$ and $\rho_{\text{polym,sh}}$. The volumes are then given by

$$V_{\text{polym,c}} = \frac{M_{\text{polym,c}}}{N_a \, \rho_{\text{polym,c}}} \quad \text{and} \quad V_{\text{polym,sh}} = \frac{M_{\text{polym,sh}}}{N_a \, \rho_{\text{polym,sh}}} \tag{3.182}$$

whereby N_a is Avogadro's constant[6]. The units of the block units has to be supplied in units corresponding to the scattering vector Q, i.e. in nm^3 in case Q is given in nm^{-1} or in Å^3 in case Q is given in Å^{-1}.

Input Parameters for model `BlockCopolymerMicelle`:

`Vpolym_c`: volume of a single block unit of the chains in the core $V_{\text{polym,c}}$, it should be given in units of nm^3 in case Q is given in nm^{-1} and in units of Å^3 in case Q is given in Å^{-1}.

`xsolv_c`: amount of solvent in the core ($x_{\text{solv,c}} \neq 1$)

`Vpolym_sh`: volume of a single block unit of the chains in the shell $V_{\text{polym,sh}}$, it should be given in units of nm^3 in case Q is given in nm^{-1} and in units of Å^3 in case Q is given in Å^{-1}.

`eta_poly_c`: scattering length density of the block units in the core η_{c}

`eta_poly_sh`: scattering length density of the block units in the chains η_{sh}

`eta_solv`: scattering length density of the solvent η_{solv}

`Nagg`: aggregation number N_{agg}

`Rg`: gyration radius of chain R_g

`d`: for non-penetration of the chains into the core region $d \approx 1$.

[5] $u = 1.66053886 \times 10^{-27}$ kg

[6] $N_a = 6.0221415 \times 10^{23} \text{mol}^{-1}$

3.4. Bi-continuous and non-particular structures

3.4.1. TeubnerStrey.

The Teubner and Strey [**96, 87**] phenomenological model often accurately describes scattering from bi-continuous micro-emulsions. The scattered intensity for this model is

$$I(q) = \frac{8\pi\langle\eta^2\rangle/\xi}{a^2 - 2bq^2 + q^4} \tag{3.183}$$

where $a^2 = (k^2 + 1/\xi^2)^2$ is a positive quantity, and $b = k^2 - 1/\xi^2$ can be a positive or negative depending on the relative magnitude of $d = 2\pi/k$ and ξ. A positive b, i.e. $\xi > d/2\pi$, leads to a peak at $q_{\max} = \sqrt{b}$ whereby for $\xi < d/2\pi$, hence negative b, no distinct peak appears. The length scale d represents a quasi-periodic repeat distance between water and oil regions within the solution, while the correlation length, ξ , corresponds to a characteristic length for positional correlation. k is defined as $2\pi/d$. The corresponding isotropic real space correlation function, $\gamma(r)$, that incorporates alternating regions of the two phases in the bi-continuous system (e.g. water and oil), is given by

$$\gamma(r) = \frac{\sin(kr)}{kr} \exp\left(-\frac{r}{\xi}\right) \tag{3.184}$$

Input Parameters for model `TeubnerStrey`:

`xi:` correlation length ξ
`d:` characteristic domain size d
`eta2:` squared scattering length density contrast η^2

Note:

- None

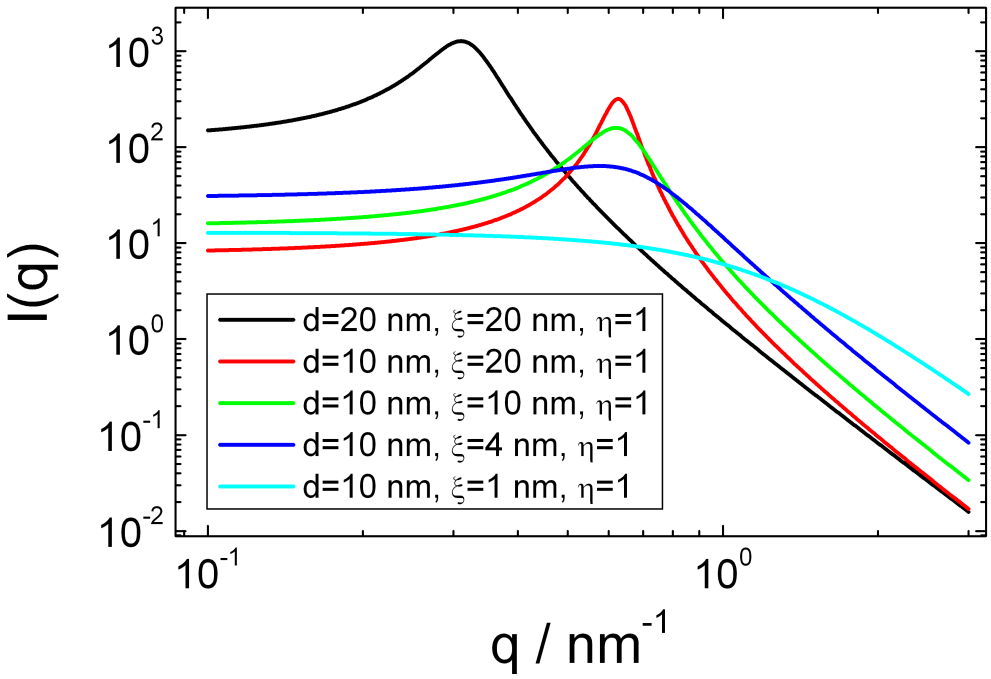
I(q)
q / nm^{-1}
10^{3}
10^{2}
10^{1}
10^{0}
10^{-1}
10^{-2}
10^{-1}
10^{0}
d=20 nm, ξ=20 nm, η=1
d=10 nm, ξ=20 nm, η=1
d=10 nm, ξ=10 nm, η=1
d=10 nm, ξ=4 nm, η=1
d=10 nm, ξ=1 nm, η=1

FIGURE 3.51.

3.4.2. Debye Anderson Brumberger(DAB).

This form factor calculates the scattering from a randomly distributed (i.e. non-particulate), two-phase system based on the Debye-Anderson-Brumberger (DAB) [**24, 25**] model for such systems. The two-phase system is characterized by a single length scale, the correlation length ξ, which is a measure of the average spacing between regions of phase 1 and phase 2. The model also assumes smooth interfaces between the phases and hence exhibits Porod behavior ($I \propto q^{-4}$) at large q ($q\xi \gg 1$). The pair correlation function is give by [**25**]

$$\gamma(r) = \exp(-r/\xi) \tag{3.185}$$

The macroscopic scattering cross-section in the DBA model is given by

$$I(q) = I_0 \frac{1}{[1 + (q\xi)^2]^2} \tag{3.186}$$

Input Parameters for model `DAB`:

`xi`: correlation length ξ
`I0`: forward scattering I_0

Note:

- None

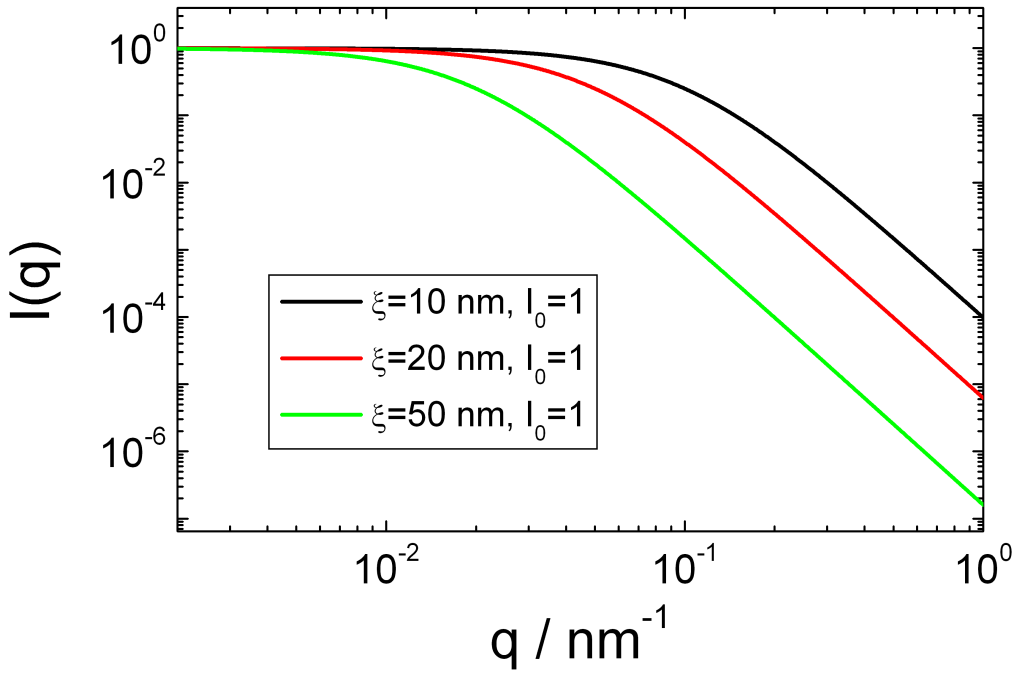

FIGURE 3.52.

3.4.3. Spinodal.

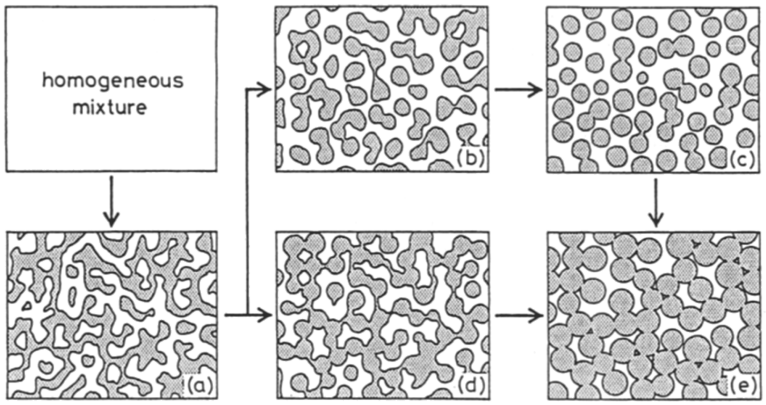

FIGURE 3.53. Schematic representation of a phase separation scheme resulting in a connected globule structure.

Spinodal decomposing systems show a characteristic small angle scattering signal with a correlation peak at some scattering value $q_{\max}$. The scattering curve $I(q)$ can be approximated by

$$I(q) = I_{\max}\frac{(1+\gamma/2)x^2}{\gamma/2 + x^{2+\gamma}} \tag{3.187}$$

according to Furukawa [**32**], where $x = q/q_{\max}$. The position of the correlation peak at $q_{\max}$ contain information about the size of the structures, which scatter. The exponent γ is equal to $\gamma = D + 1$ for off-critical mixtures and $\gamma = 2D$ for critical concentration mixtures, whereby D is the dimensionality of the system.

Input Parameters for model `Spinodal`:

`Qmax`: peak maximum $q_{\max}$
`gamma`: exponent γ
`Imax`: scattering intensity at peak position $I_{\max}$

Note:

- None

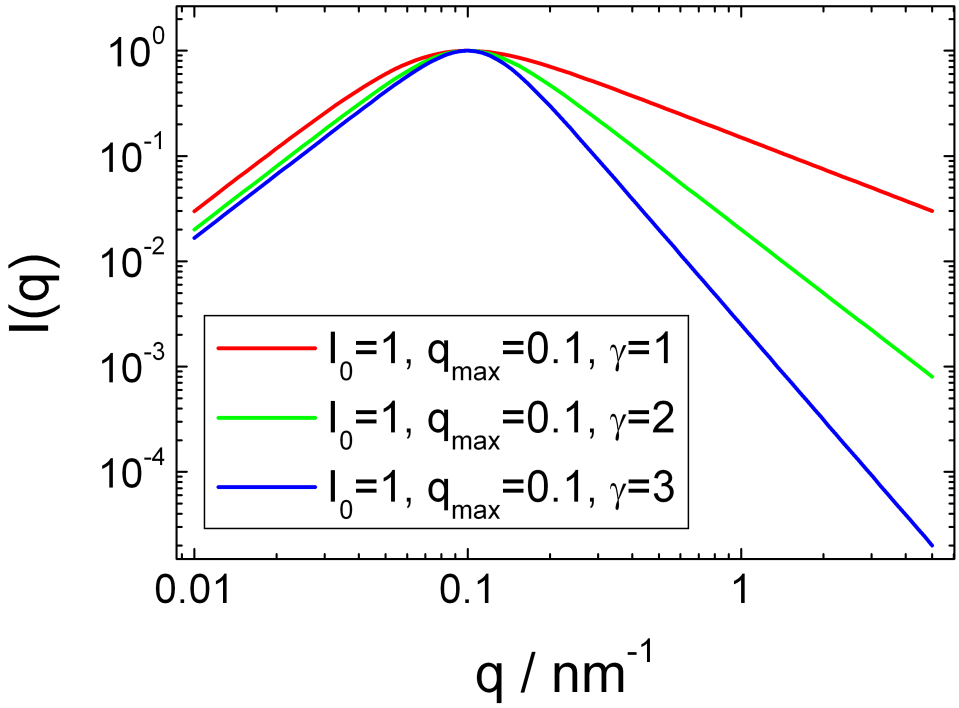
I(q)
10^0
10^-1
10^-2
10^-3
10^-4
0.01
0.1
1
q / nm^-1
I0=1, qmax=0.1, γ=1
I0=1, qmax=0.1, γ=2
I0=1, qmax=0.1, γ=3

FIGURE 3.54.

3.4.4. OrnsteinZernike.

The low-angle scattering of thermal composition fluctuations can be described according to the Ornstein-Zernike formulation by a Lorentzian profile

$$I(q) = \frac{I_0}{1 + q^2\xi^2} \tag{3.188}$$

characterizing the exponential decay of the composition fluctuations correlation function, with correlation length ξ. The Fourier transform of a Lorentzian function corresponds to correlations dying out as $\gamma(r) \simeq \frac{1}{r} exp(-r/\xi)$. Note that the low-$Q$ limit of this empirical form reproduces the Guinier law.

Input Parameters for model `OrnsteinZernike`:

`I0`: forward scattering I_0 at $q = 0$.
`xi`: correlation length ξ

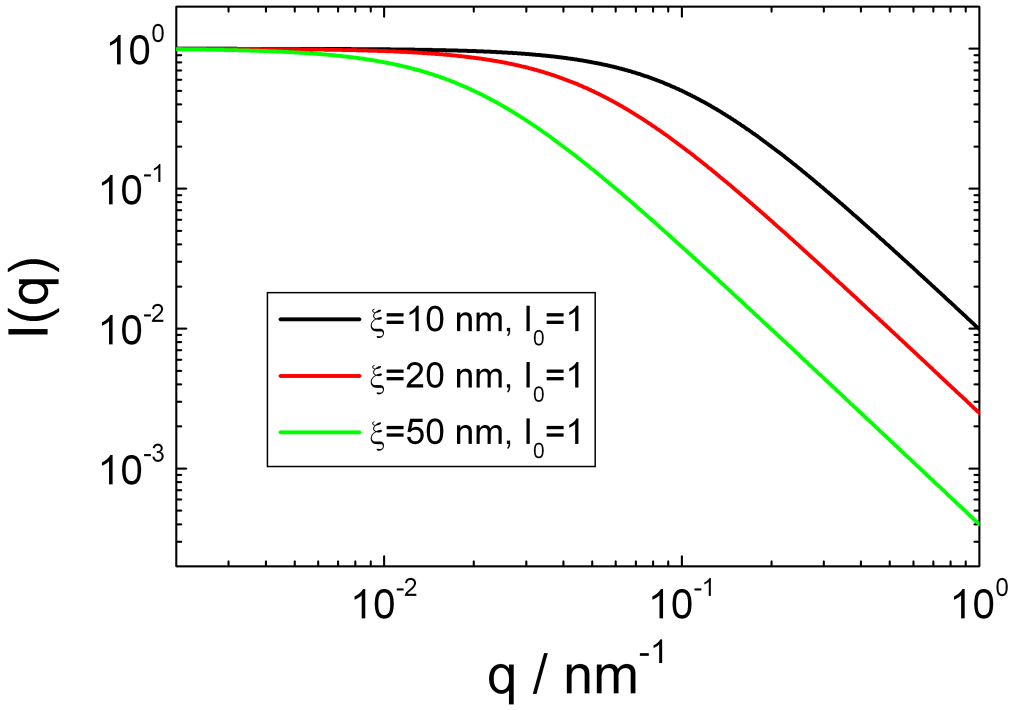

FIGURE 3.55. Ornstein-Zernike Scattering intensity $I(q)$ for different correlation lengths ξ

3.4.5. BroadPeak.

Many SANS spectra are characterized by a broad peak even though they are from amorphous soft materials. The d-spacing corresponding to the broad peak is a characteristic distance between the scattering inhomogeneities (such as in lamellar, cylindrical, or spherical morphologies or for bicontinuous structures). The following simple functional form reproduces the broad peak feature:

$$I(q) = \frac{I_0}{1 + (|q - q_0|\xi)^m} \tag{3.189}$$

Here the peak position is related to the d-spacing as $q_0 = 2\pi/d$. Soft systems that show a SANS peak include copolymers, polyelectrolytes, multiphase systems, layered structures, etc.

3.4.6. Generalized Guinier approximation [30, 47, 45, 46].

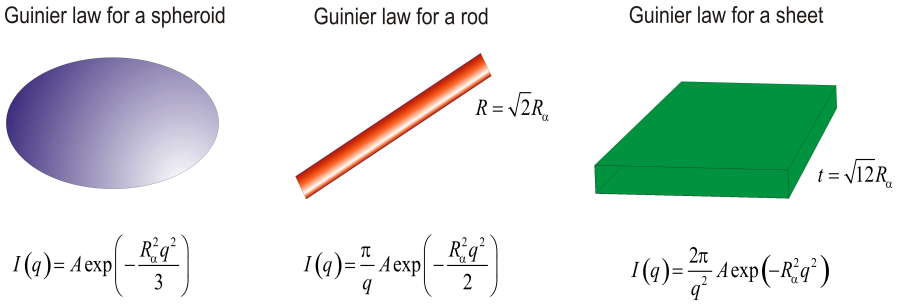

FIGURE 3.56. generalized Guinier approximation

Quantitative analysis of particle size and shape starts with the Guinier approximations. For three-dimensional objects the Guinier approximation is given by $I(q) = \exp(-Rg^2q^2/3)$ This approximation can be extended also to rod-like and plane objects by

$$I(q) = \left\{ \begin{array}{ll} 1 & \text{for} \quad \alpha = 0 \\ \alpha\pi q^{-\alpha} & \text{for} \quad \alpha = 1, 2 \end{array} \right\} A \ \exp\left(-\frac{R_\alpha^2 q^2}{3-\alpha}\right) \tag{3.190}$$

$\alpha = 0$**:** spheroid
$\alpha = 1$**:** rod-like
$\alpha = 2$**:** plane

The apparent particle shape (also called the dimensionality) is represented in eq. 3.190 by α, which has integer values of 0, 1, and 2 for a point, a line, and a plane, respectively. Equation 3.190 states that there are q ranges, corresponding to length scales as q^{-1}, from which the particle dimension or shape, α, the radius of gyration, R_α, and the pre-factor, A, characteristic of α can be inferred. α has a value of 0 for a q range such that $qR_g < 1 - 1.3$ (the larger applies when the particle is known to be a spheroid), where R_g is the particle radius of gyration (computed about the particle centroid). In this case, the pre-factor A describes the excess differential cross-section per unit mass (cm^2 g^{-1}) of a particle. If the particle has one dimension of length L, that is, much larger than the others (i.e., elongated, rod-like, or worm-like), then there is a q range such that $qR_c < 1 \ll qL$, where $\alpha = 1$. Here, R_c is the radius of gyration (computed about a line centered along L) of the cross-section perpendicular to L. If these conditions apply, the pre-factor A describes the excess differential cross section per unit length per unit mass (cm^2 Å^{-1} g^{-1}). Finally, for planar shapes, including single bilayer vesicles, with two locally large dimensions, D, and planar cross-sectional radius of gyration (computed about a central plain),R_d, there may be a region of q such that $qR_d < 1 \ll qD$, where $\alpha = 2$. For such planar structures, the pre-factor is the excess differential cross-section per unit area per unit mass (cm^2 Å^{-2} g^{-1}) of a sheet.

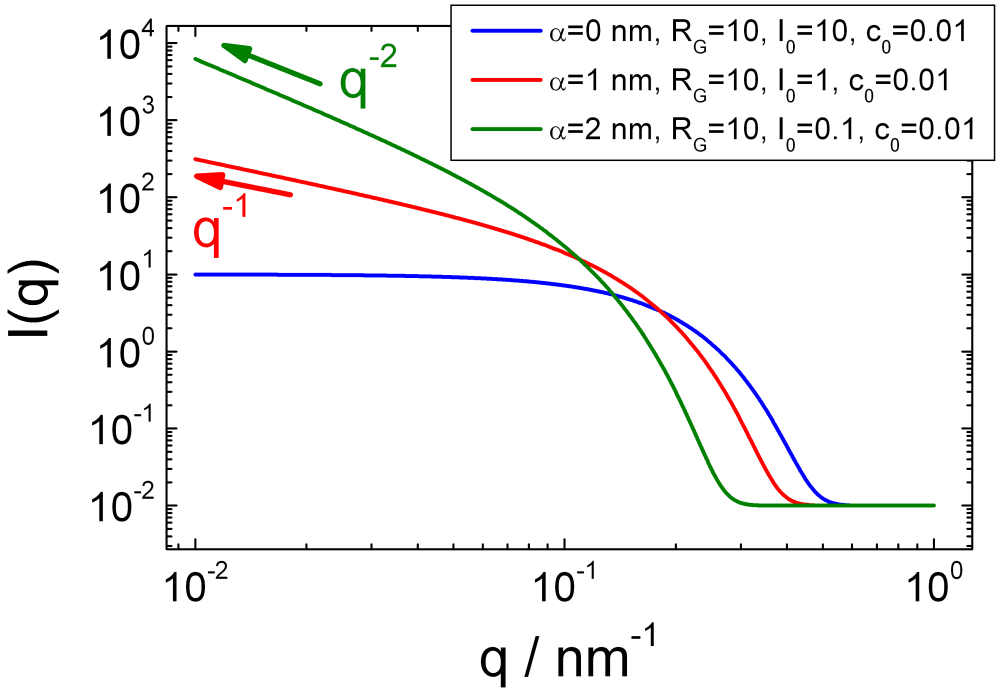

FIGURE 3.57. generalized Guinier law

3.5. Clustered Objects

3.5.1. Mass Fractal [92, 91, 49, 57, 59, 58].

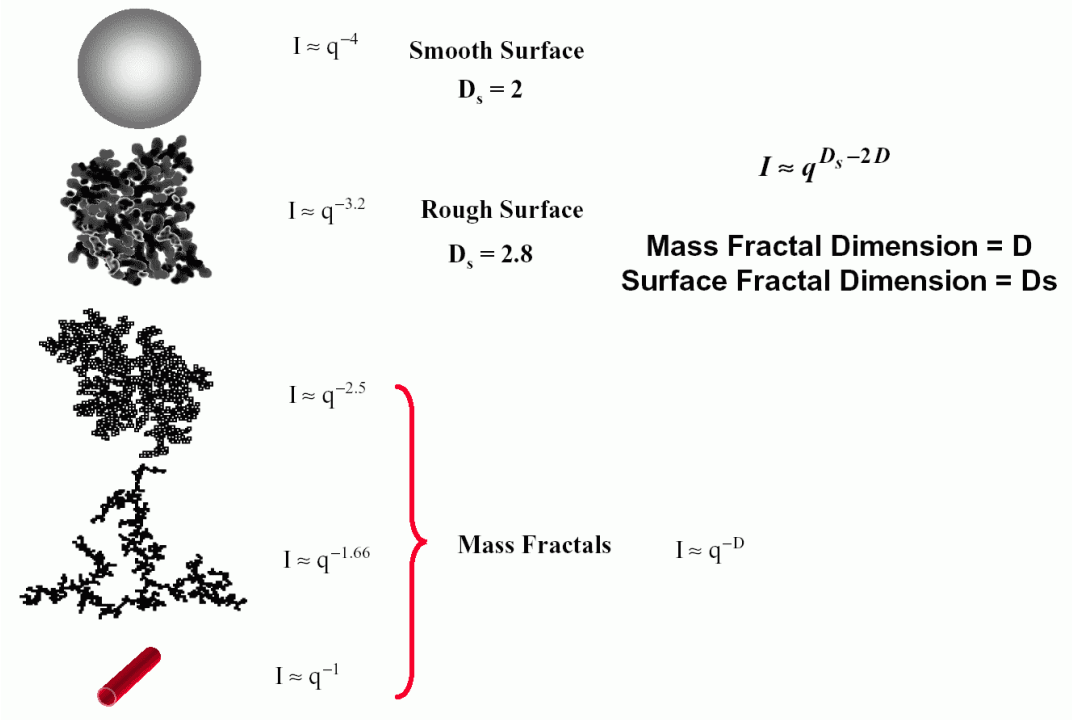

FIGURE 3.58.

Aggregates and clusters often have a fractal morphology. These self-similar clusters are well described by

$$N = k_0 (R_g / r_0)^D \tag{3.191}$$

where N is the number of primary particles or monomers in the aggregate, k_0 is a constant of order unity, R_g is the radius of gyration of the aggregate, r_0 is the monomer radius, and D is the fractal dimension.

The scattering function and the density autocorrelation function of the aggregate are Fourier transform pairs; thus

$$I(q) = 4\pi \int_0^\infty g(r)\, r^2\, \frac{\sin(qr)}{qr}\, dr \tag{3.192}$$

For a fractal aggregate the autocorrelation function has the form

$$g(r) \sim r^{D-d} h(r, \xi) \tag{3.193}$$

Here D is the fractal dimension, d the spatial dimension, and ξ a measure of the linear size of the aggregate proportional to the radius of gyration R_g. The function $h(r, \xi)$ is the cutoff function describing the perimeter of the aggregate. Its properties are that $h(r, \xi) \simeq 1$ for $r/\xi \lesssim 1$, but for large r/ξ it falls off faster than any power law.

TABLE 2. Scattering functions $I(q)$ for different cutoff functions $h(r,\xi)$.

SASfit-name	$h(r,\xi)$	ξ^2	$I(q)$	Ref.
Fischer-Burford	ca. $\exp\left[-\frac{r}{\xi}\right]$	$R_g^2/3$	$\left(1+\frac{2}{3D}q^2R_g^2\right)^{-D/2}$	
MassFractExp	$\exp\left[-\frac{r}{\xi}\right]$	$\frac{2R_g^2}{D(D+1)}$	$\frac{\sin[(D-1)\arctan(q\xi)]}{(D-1)q\xi(1+q^2\xi^2)^{(D-1)/2}}$	
MassFractGauss	$\exp\left[-\left(\frac{r}{\xi}\right)^2\right]$	$\frac{4R_g^2}{D}$	$e^{-\frac{q^2R_g^2}{D}}\,{}_1F_1\left[\frac{3-D}{2},\frac{3}{2},\frac{q^2R_g^2}{D}\right]$	
Aggregate (Exp(-x^a) Cut-Off)	$\exp\left[-\left(\frac{r}{\xi}\right)^\alpha\right]$	—	numerical	
Aggregate (OverlapSph Cut-Off)	$\begin{cases}\left(1+\frac{r}{4\xi}\right)\left(1-\frac{r}{2\xi}\right)^2, & r<2\xi \\ 0, & r\geq 2\xi\end{cases}$	$\frac{(D+2)(D+5)}{2D(D+1)}R_g^2$	numerical	
DLCAggregate	—	—	$\left[1+\sum_{s=1}^{4}C_s(qR_g)^{2s}\right]^{-D/8}$ $C_1=\frac{8}{3}D, C_2=2.5$ $C_3=-1.52, C_4=1.02$	
RLCAggregate	—	—	$C_1=\frac{8}{3}D, C_2=3.13$ $C_3=-2.58, C_4=0.95$	

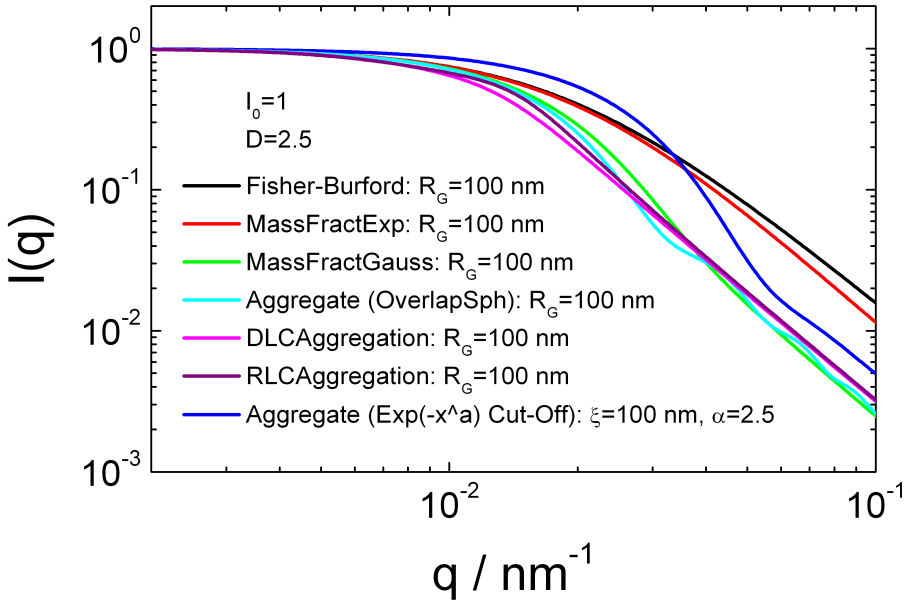

FIGURE 3.59. Form factor for the different types of mass fractals listed in 2.

3.5.2. Stacked Discs [56, 40].

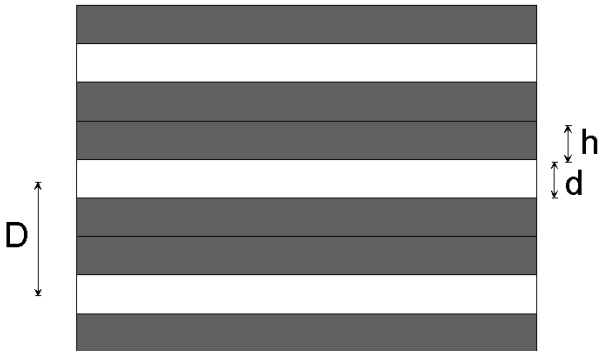

FIGURE 3.60. Sketch for a stack of discs with an additional surface layer

$$I_{\text{StackedDiscs}}(Q,R) = \int_0^{\pi/2} \left(\Delta\eta_l \left(V_t f_t - V_c f_c\right) + \Delta\eta_c V_c f_c\right)^2 S(Q,\Theta)\sin(\Theta)\, d\Theta \tag{3.194}$$

Here it is assume that the nearest neighbor distance between the platelets obeys a Gaussian distribution and consider an internal structure factor, $S(Q,\Theta)$, first proposed by Kratky and Porod in 1949 [**56**]

$$S(Q,\Theta) = 1 + \frac{2}{n}\sum_{k=1}^{n-1}(n-k)\cos(kDQ\cos(\Theta))\exp\left(-\frac{k}{2}\left(Q\cos(\Theta)\sigma_D\right)^2\right) \tag{3.195}$$

$$f_t = f_t = \frac{\sin\left(Q(\frac{d}{2}+h)\cos(\Theta)\right)}{Q(\frac{d}{2}+h)\cos(\Theta)} \quad 2\frac{J_1(QR\sin(\Theta))}{QR\sin(\Theta)} \tag{3.196}$$

$$f_c = f_c = \frac{\sin\left(Q\frac{d}{2}\cos(\Theta)\right)}{Q\frac{d}{2}\cos(\Theta)} \quad 2\frac{J_1(QR\sin(\Theta))}{QR\sin(\Theta)} \tag{3.197}$$

$$V_t = \pi R^2(d+2h) \tag{3.198}$$

$$V_c = \pi R^2 d \tag{3.199}$$

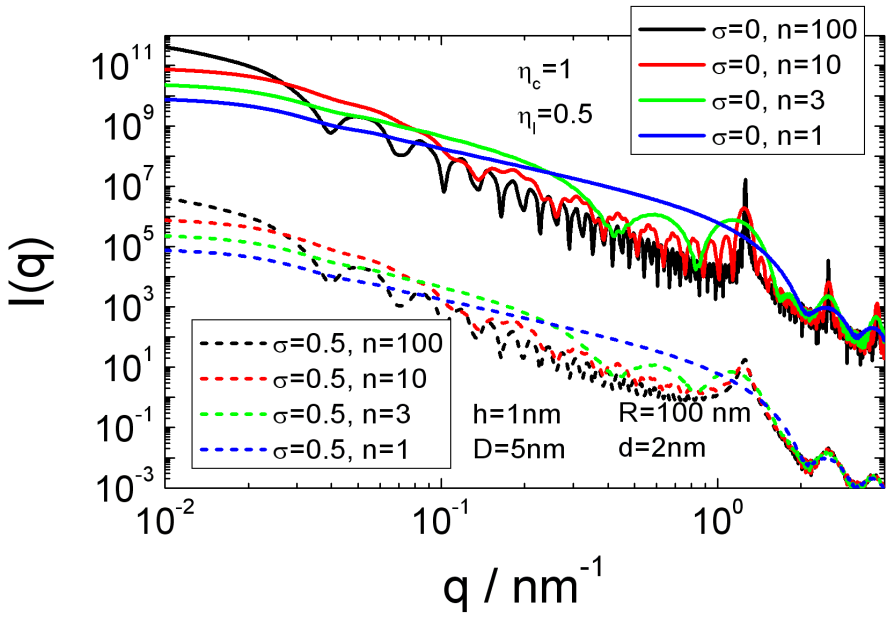

FIGURE 3.61. Scattering Intensity for a stack of discs with a layer.

3.5.3. DumbbellShell.

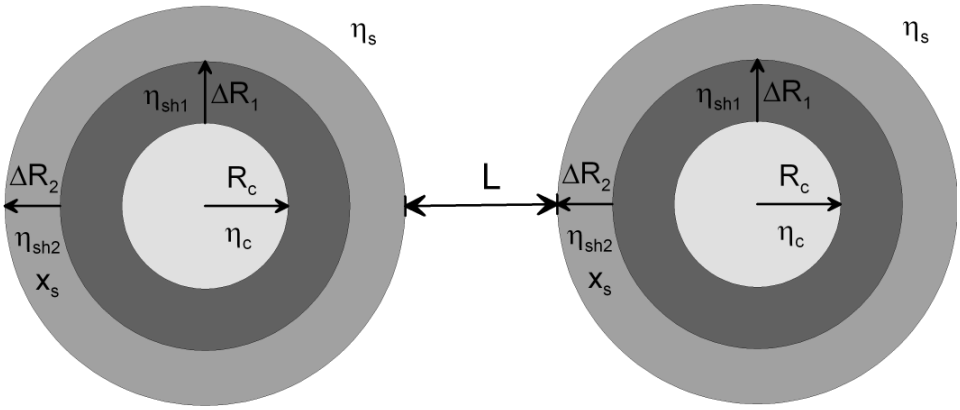

FIGURE 3.62.

3.5.4. DoubleShellChain.

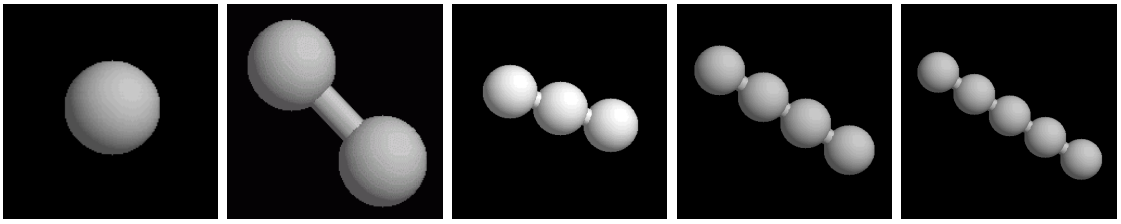

FIGURE 3.63.

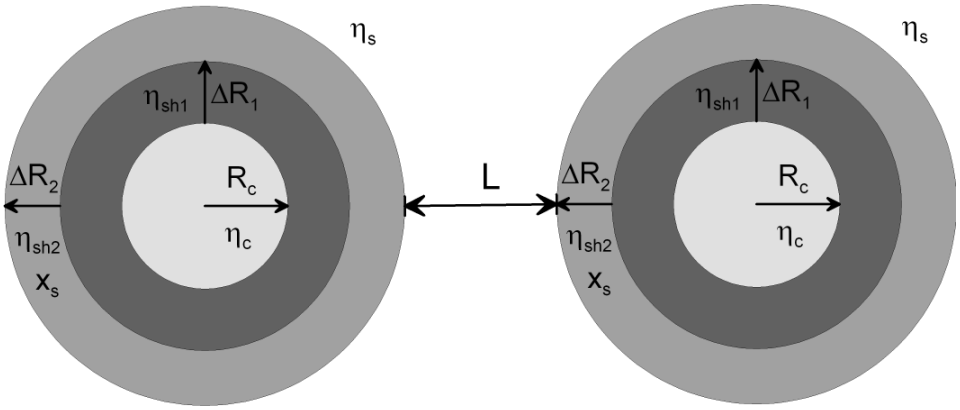

FIGURE 3.64.

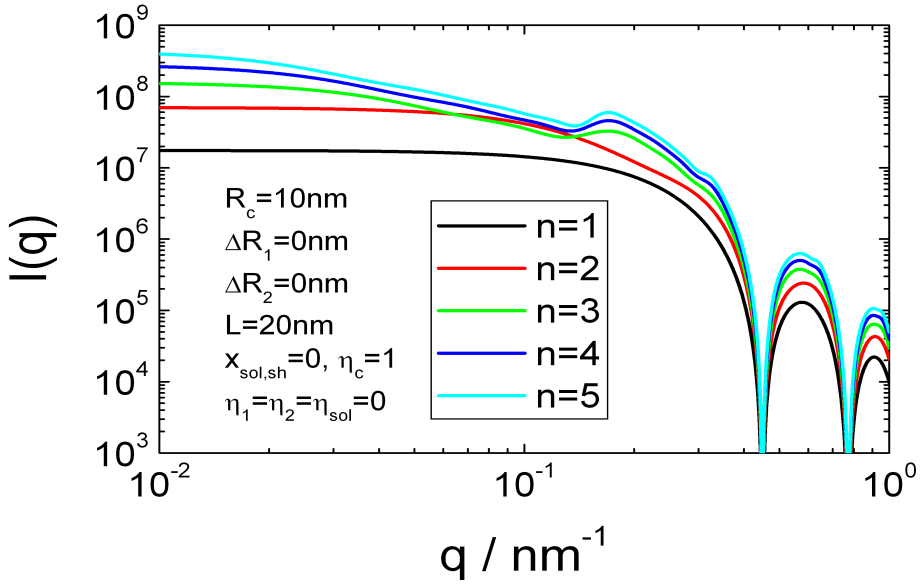

FIGURE 3.65.

3.5.5. TetrahedronDoubleShell.

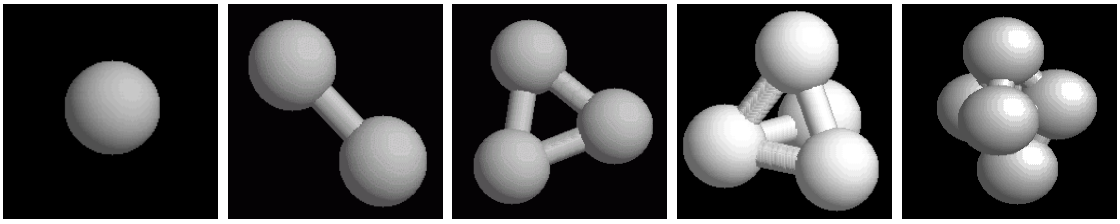

FIGURE 3.66.

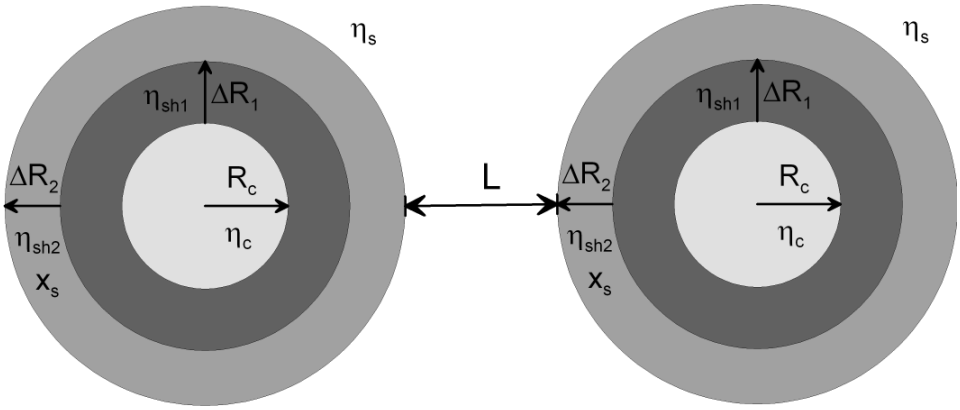

FIGURE 3.67.

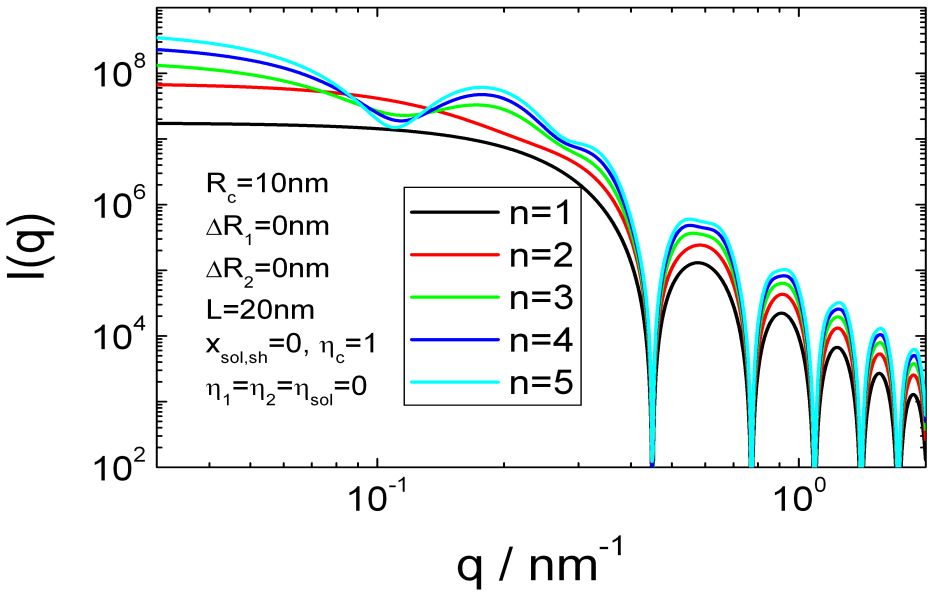

FIGURE 3.68.

3.6. Cylindrical Objects

3.6.1. Disc.

FIGURE 3.69.

$$I_{\text{Disc}}(q,R) = \pi^2 R^4 \Delta\eta^2 \frac{2}{(qR)^2}\left(1 - \frac{1}{qR}\mathrm{J}_1(2qR)\right) \tag{3.200}$$

with $\lim_{q=0} I_{\text{Disc}}(q,R) = \pi^2 R^4 \Delta\eta^2$

Input Parameters for model `Disc`:

`R:` radius of disc R

`eta:` scattering contrast $\Delta\eta$

Note:

- none

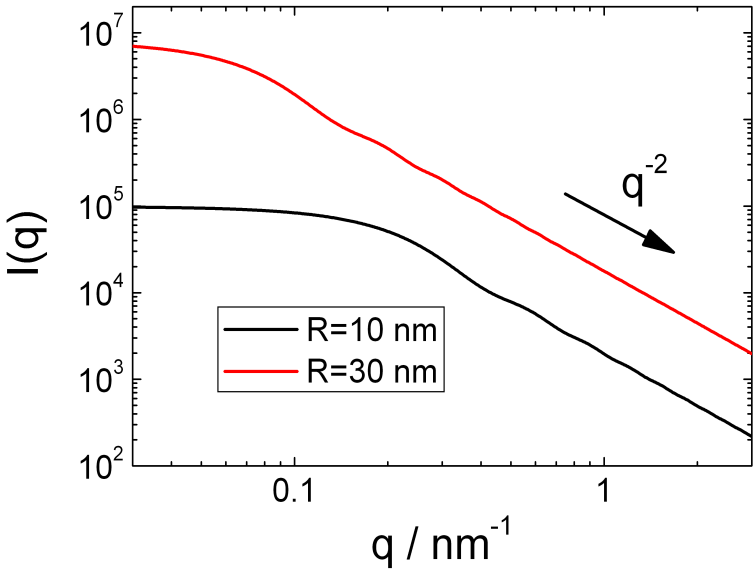

FIGURE 3.70. Scattering intensity of a disc with radii $R = 10$ nm and $R = 30$ nm. The scattering length density contrast is set to 1.

3.6.2. Rod.

FIGURE 3.71.

$$I_{\text{Rod}}(q,L) = \Delta\eta^2 L^2 \left(\frac{2}{qL}\text{Si}(qL) - \frac{\sin(qL/2)}{qL/2} \right) \tag{3.201}$$

with $\text{Si}(x) = \int_0^x \frac{\sin t}{t}\, dt$ and $\lim_{q=0} I_{\text{Rod}}(q,L) = \Delta\eta^2 L^2$

Input Parameters for model `Rod`:

`L`: length of rod L

`eta`: scattering contrast $\Delta\eta$

Note:

- none

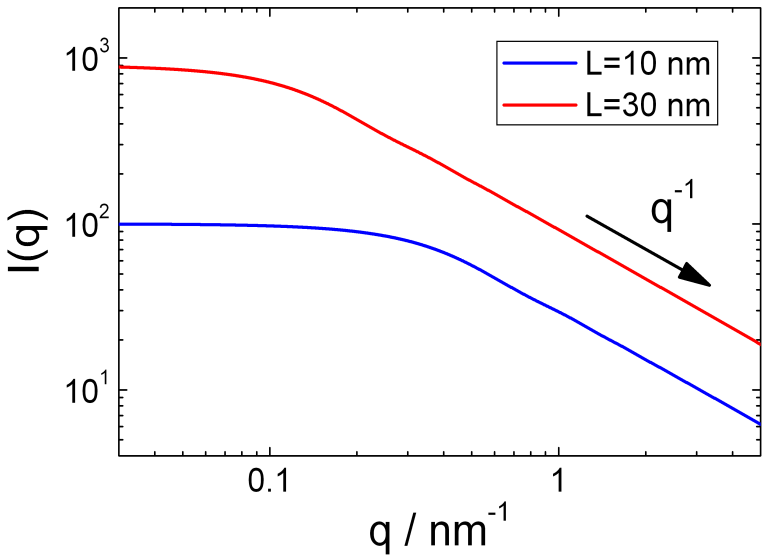

FIGURE 3.72. Scattering intensity of a rod of length $L = 10$ nm and $L = 30$ nm. The scattering length density contrast is set to 1.

3.6.3. Porod's approximation for a long cylinder [80].

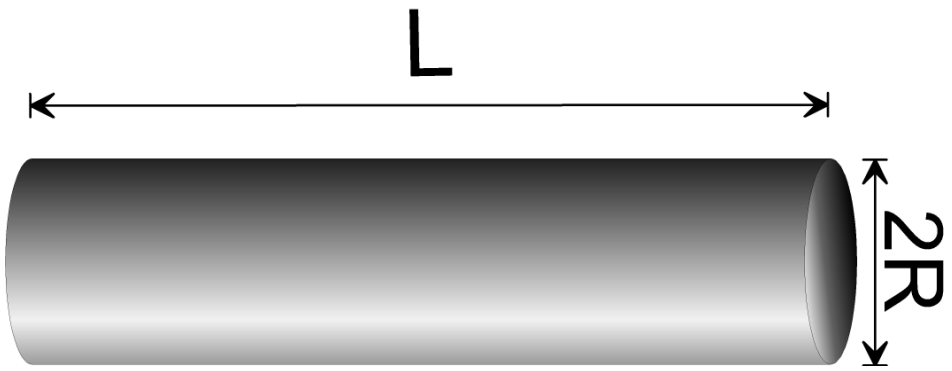

FIGURE 3.73.

$$\mathrm{Si}_{\frac{\pi}{2}}(x) = \left(\mathrm{Si}(x) + \frac{\cos x}{x} + \frac{\sin x}{x^2}\right) \quad \xrightarrow{x\to\infty} \quad \frac{\pi}{2} \tag{3.202}$$

$$\Lambda_1(x) = \frac{2}{x} J_1(x) \tag{3.203}$$

$$\Lambda_2(x) = \frac{8}{x^2} J_2(x) \tag{3.204}$$

$$\Phi_{\mathrm{disc}}(x) = \frac{2}{x^2}\left[1 - \Lambda_1(x)\right] \tag{3.205}$$

$$\Phi_{\mathrm{long}}(q, R, L) = \left(\Delta\eta\pi R^2 L\right)^2 \frac{2}{QL} \times \left\{\mathrm{Si}_{\frac{\pi}{2}}(QL)\Lambda_1^2(QR) - \frac{2\Lambda_2(2QR) - \Phi_{\mathrm{disc}}(2QR)}{QL} - \frac{\sin(QL)}{(QL)^2}\right\} \tag{3.206}$$

Input Parameters for model `LongCylinder`:

- `R:` radius of cylinder R
- `L:` length of cylinder L
- `eta:` scattering contrast $\Delta\eta$

Note:

- The approximation is valid for $L > 2R$

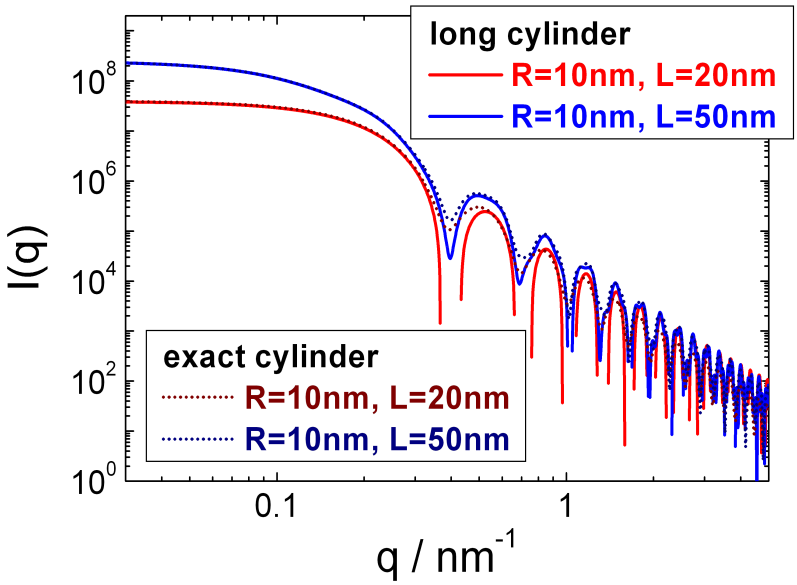

FIGURE 3.74. Scattering intensity of a cylinder with radius $R = 10$ nm and lengths of $L = 20$ nm and $L = 50$ nm. Next to Porod's axproximation for long cylinders also the exact integral solution is shown for comparison. The scattering length density contrast is set to 1.

3.6.4. Porod's approximation for a flat cylinder [80].

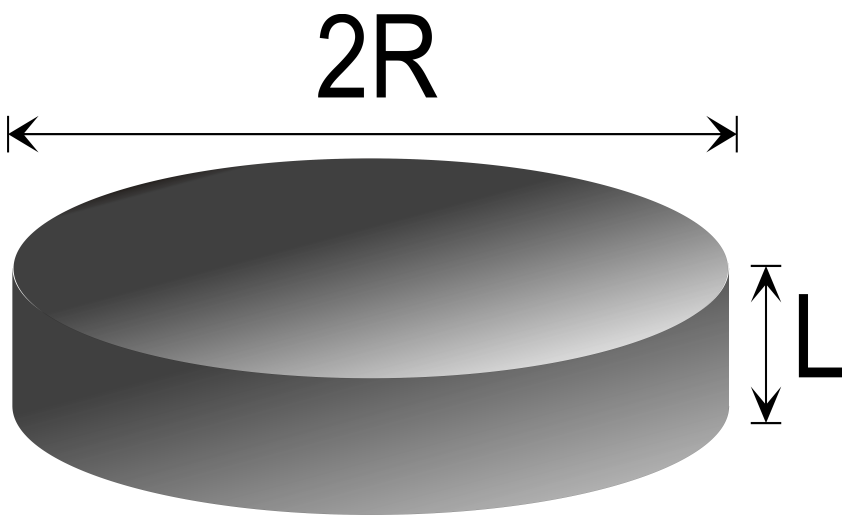

FIGURE 3.75.

$$\Lambda_1(x) = \frac{2}{x} J_1(x) \tag{3.207}$$

$$I_1(x) = \int_0^x \Lambda_1(x')dx' = \pi x \left[J_0(x) H_{\text{Struve}}(1,x) - J_1(x) H_{\text{Struve}}(0,x) \right] \tag{3.208}$$

$$I_0(x) = \frac{I_1(x) + x\Lambda_1(x)}{2} \tag{3.209}$$

$$\Omega(x) = \frac{2}{x} \left[I_0(x) - 2J_1(x) \right] \tag{3.210}$$

$$\chi(x) = \left(\frac{\sin(x/2)}{x/2} \right)^2 \tag{3.211}$$

$$\Phi_{\text{flat}}(q,R,L) = \left(\Delta\eta\pi R^2 L\right)^2 \frac{8}{(2qR)^2} \times \left\{ \chi(qL) + \frac{I_1(2QR)\,\Omega(qL)}{2qR} - \Lambda_1(2qR) \right\} \tag{3.212}$$

Input Parameters for model `FlatCylinder`:

`R:` radius of cylinder R
`L:` length of cylinder L
`eta:` scattering contrast $\Delta\eta$

Note:

- The approximation is valid for $L < 2R$

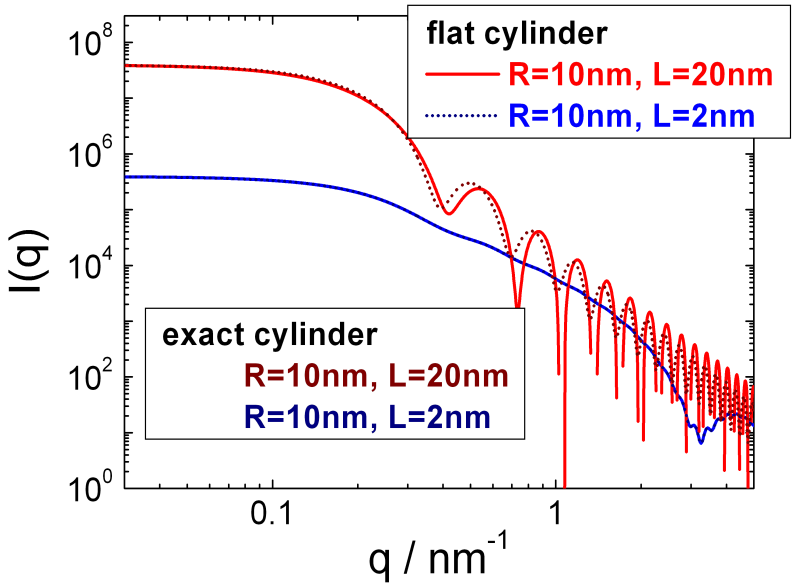

FIGURE 3.76. Scattering intensity of a cylinder with radius $R = 10$ nm and lengths of $L = 2$ nm and $L = 20$ nm. Next to Porod's axproximation for flat cylinders also the exact integral solution is shown for comparison. The scattering length density contrast is set to 1.

3.6.5. Porod's approximations for cylinder [80].

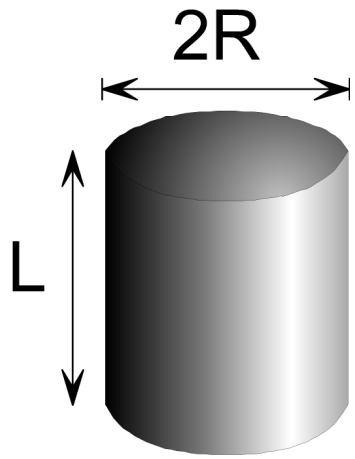

FIGURE 3.77.

This form factor combines the two solutions of Porod for a long $\Phi_{\text{long}}(q, R, L)$ (3.206) and a flat $\Phi_{\text{flat}}(q, R, L)$ (3.212) cylinder by a linear combination of both. A simple linear transition at $L = 2R$ is assumed.

$$\Phi_{\text{Porod}}(q, R, L) = p\left(\frac{2R}{L}\right)\Phi_{\text{flat}}(q, R, L) + \left(1 - p\left(\frac{2R}{L}\right)\right)\Phi_{\text{long}}(q, R, L) \tag{3.213}$$

$$p(x) = \begin{cases} 1 & \text{for } x > \frac{5}{4} \\ 2\left(x - \frac{3}{4}\right) & \text{for } \frac{3}{4} \le x \le \frac{5}{4} \\ 0 & \text{for } x < \frac{3}{4} \end{cases} \tag{3.214}$$

Input Parameters for model `PorodCylinder`:

`R:` radius of cylinder R
`L:` length of cylinder L
`eta:` scattering contrast $\Delta\eta$

Note:

- less good approximation for $L \sim 2R$

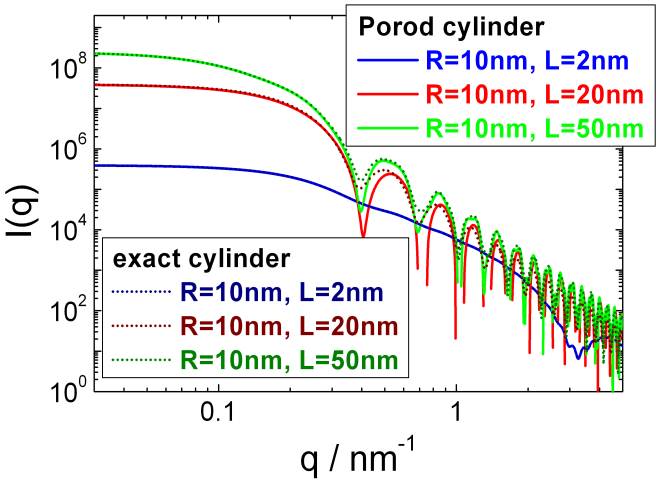

FIGURE 3.78. Scattering intensity of a cylinder with radius $R = 10$ nm and lengths of $L = 2$ nm, $L = 20$ nm, and $L = 50$ nm. Next to Porod's axproximation for a cylinders also the exact integral solution is shown for comparison. The scattering length density contrast is set to 1.

3.6.6. Cylinder of length L, radius R and scattering contrast $\Delta\eta$.

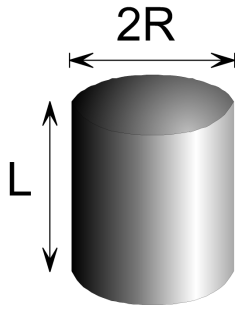

FIGURE 3.79.

$$I_{\rm cyl} = 16(\pi R^2 L)^2 \Delta\eta^2 \int_0^1 \left(\frac{J_1\left(QR\sqrt{1-x^2}\right)\sin(QLx/2)}{Q^2 R\sqrt{1-x^2}\,Lx} \right)^2 dx \tag{3.215}$$

Input Parameters for model `Cylinder`:

`R:` radius of cylinder R
`L:` length of cylinder L
`eta:` scattering contrast $\Delta\eta$

Note:

- None

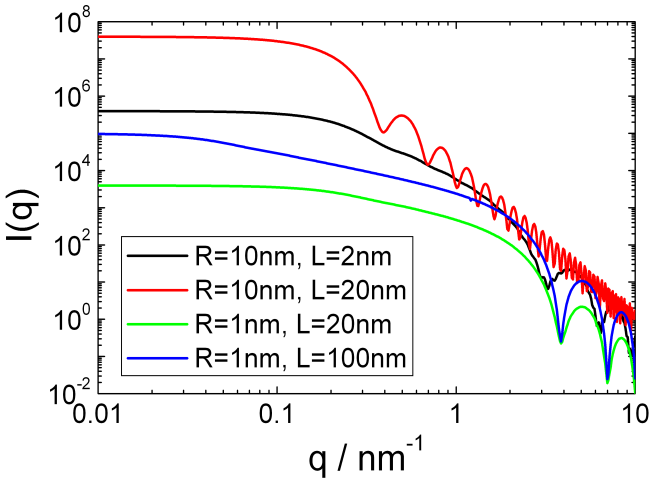

FIGURE 3.80. Scattering intensity of a cylinder for different radii radius R nm and lengths L. The scattering length density contrast is set to 1.

3.6.7. Random oriented cylindrical shell with circular cross-section.

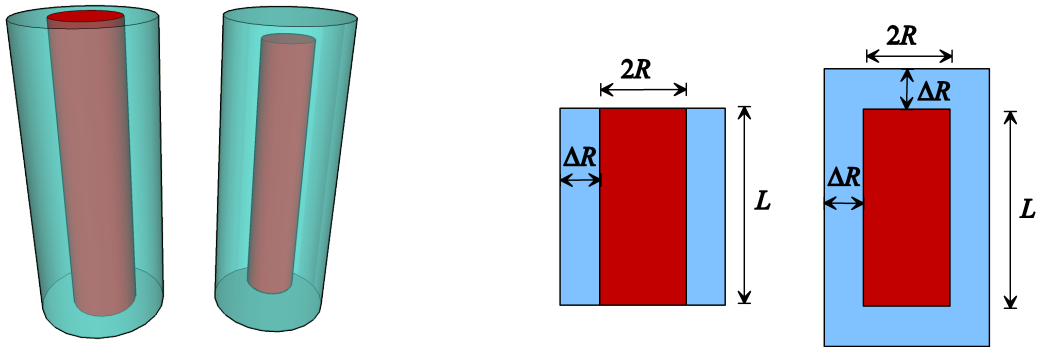

FIGURE 3.81. cylindrical shell with circular cross-section

To different versions for a random oriented cylindrical shell with a circular cross-section has been implemented. One without `CylShell1` and one with `CylShell2` capped ends. For very long cylinders a faster approximation for the uncapped version can be used `LongCylShell`

$$K_{\mathrm{Cyl}}(Q,\Delta\eta,R,L,x) = 2\pi R^2 L\Delta\eta \frac{J_1\left(QR\sqrt{1-x^2}\right)}{QR\sqrt{1-x^2}} \frac{\sin(QLx/2)}{QLx/2} \tag{3.216}$$

$$I_{\mathrm{CylShell1}} = \int_0^1 \Big(K_{\mathrm{Cyl}}\left(Q,\eta_{\mathrm{core}}-\eta_{\mathrm{shell}},R,L,x\right) + K_{\mathrm{Cyl}}\left(Q,\eta_{\mathrm{shell}}-\eta_{\mathrm{solv}},R+\Delta R,L,x\right)\Big)^2 dx \tag{3.217}$$

$$I_{\mathrm{CylShell2}} = \int_0^1 \Big(K_{\mathrm{Cyl}}\left(Q,\eta_{\mathrm{core}}-\eta_{\mathrm{shell}},R,L,x\right) + K_{\mathrm{Cyl}}\left(Q,\eta_{\mathrm{shell}}-\eta_{\mathrm{solv}},R+\Delta R,L+2\Delta R,x\right)\Big)^2 dx \tag{3.218}$$

$$I_{\text{LongCylShell}}(Q) = P'(Q)P_{\text{cs}}(Q) \tag{3.219}$$

$$P'(Q) = 2\frac{\text{Si}(QL)}{QL} - \left(\frac{\sin(QL/2)}{QL/2}\right) \tag{3.220}$$

$$\text{Si}(x) = \int_0^x \frac{\sin t}{t}\, dt \tag{3.221}$$

$$P_{\text{cs}}(Q) = \left(2\frac{J_1(QR)}{QR}\left(\eta_{\text{core}} - \eta_{\text{shell}}\right) R^2 L\pi + 2\frac{J_1(Q(R+\Delta R))}{Q(R+\Delta R)}\left(\eta_{\text{shell}} - \eta_{\text{solv}}\right)(R+\Delta R)^2 L\pi\right)^2 \tag{3.222}$$

Input Parameters for models `CylShell1`, `CylShell2` and `LongCylShell`:

`R:` core radius R
`DR:` shell thickness ΔR
`L:` cylinder length L
`eta_core:` scattering length density η_{core} of cylinder core
`eta_shell:` scattering length density η_{shell} of cylinder shell
`eta_solv:` scattering length density η_{solv} of solvent

Note:

- The approximation for a long cylindrical shell (`LongCylShell`) only holds for $L \gg 2R$.

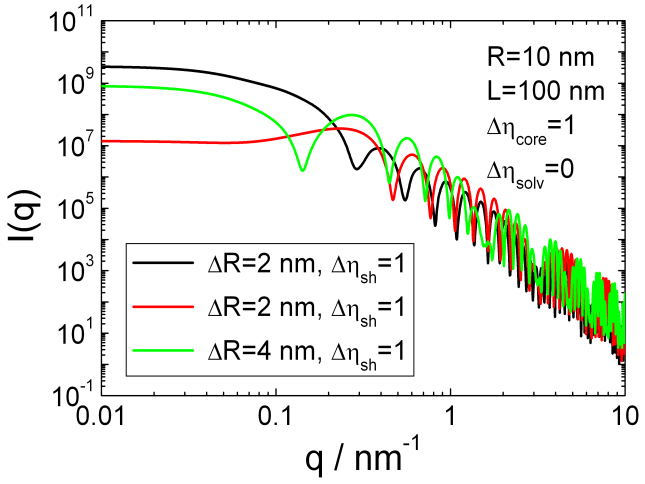

FIGURE 3.82. Scattering intensity of a cylinder shell `CylShell1`.

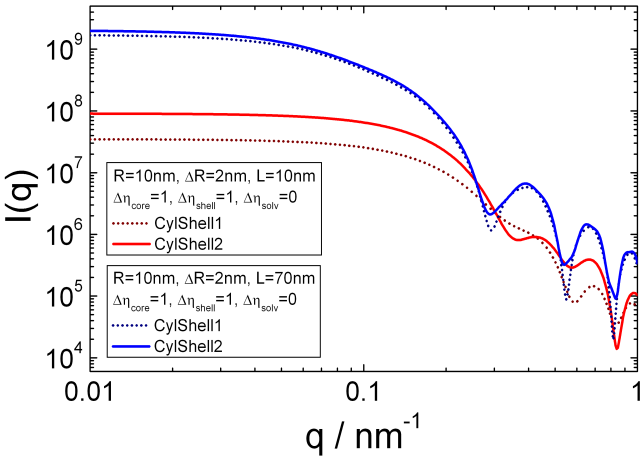

FIGURE 3.83. Scattering intensity of a cylinder shell `CylShell2`.

3.6.8. Random oriented cylindrical shell with elliptical cross-section.

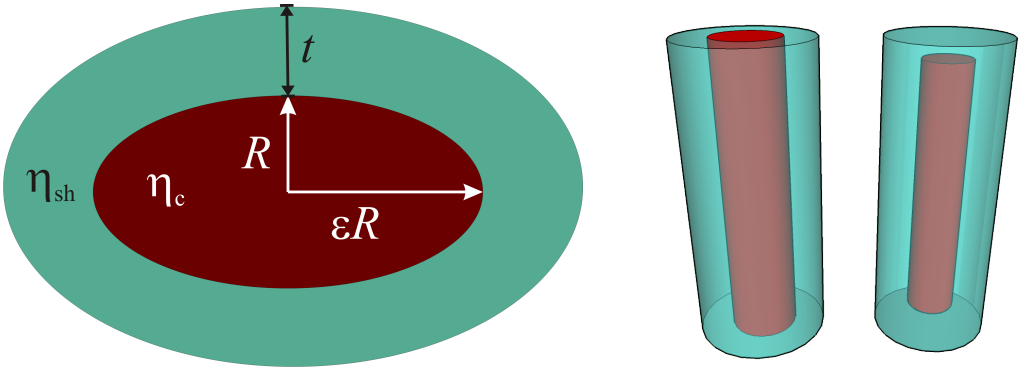

FIGURE 3.84. cylindrical shell with elliptical cross-section

To different versions for a random oriented cylindrical shell with an elliptical cross-section has been implemented. One without `ellCylShell1` and one with `ellCylShell2` capped ends.

$$K_{\text{ellCyl}}(q,\Delta\eta,R,\epsilon,L,t,\phi,\alpha) = \pi\epsilon R(\epsilon R+t)L\Delta\eta \times \frac{2J_1\left(qr(R,\epsilon,\phi,\alpha)\right)}{qr(R,\epsilon,\phi,\alpha)} \frac{\sin(q\frac{L}{2}\cos(\alpha))}{q\frac{L}{2}\cos(\alpha)} \tag{3.223}$$

$$r(R,\epsilon,t,\phi,\alpha) = \sqrt{R^2\sin^2(\phi)+(\epsilon R+t)^2\cos^2(\phi)}\,\sin(\alpha) \tag{3.224}$$

$$I_{\text{ellCylShell1}}(q) = \frac{2}{\pi}\int_0^{\frac{\pi}{2}}\int_0^{\frac{\pi}{2}}\Big(K_{\text{ellCyl}}\left(q,\eta_{\text{core}}-\eta_{\text{shell}},R,\epsilon,L,0,\phi,\alpha\right) + K_{\text{ellCyl}}\left(q,\eta_{\text{shell}}-\eta_{\text{sol}},R,\epsilon,L,t,\phi,\alpha\right)\Big)^2 \sin(\alpha)\,d\alpha\,d\phi \tag{3.225}$$

$$I_{\text{ellCylShell2}}(q) = \frac{2}{\pi}\int_0^{\frac{\pi}{2}}\int_0^{\frac{\pi}{2}}\Big(K_{\text{ellCyl}}\left(q,\eta_{\text{core}}-\eta_{\text{shell}},R,\epsilon,L,0,\phi,\alpha\right) + K_{\text{ellCyl}}\left(q,\eta_{\text{shell}}-\eta_{\text{sol}},R,\epsilon,L+2t,t,\phi,\alpha\right)\Big)^2 \sin(\alpha)\,d\alpha\,d\phi \tag{3.226}$$

Input Parameters for models `ellCylShell1` and `ellCylShell2`:

`R`: core radius R
`epsilon`: eccentricity ϵ of cross-section
`L`: cylinder length L

`t`: shell thickness t
`eta_core`: scattering length density η_{core} of cylinder core
`eta_shell`: scattering length density η_{shell} of cylinder shell
`eta_sol`: scattering length density η_{sol} of solvent

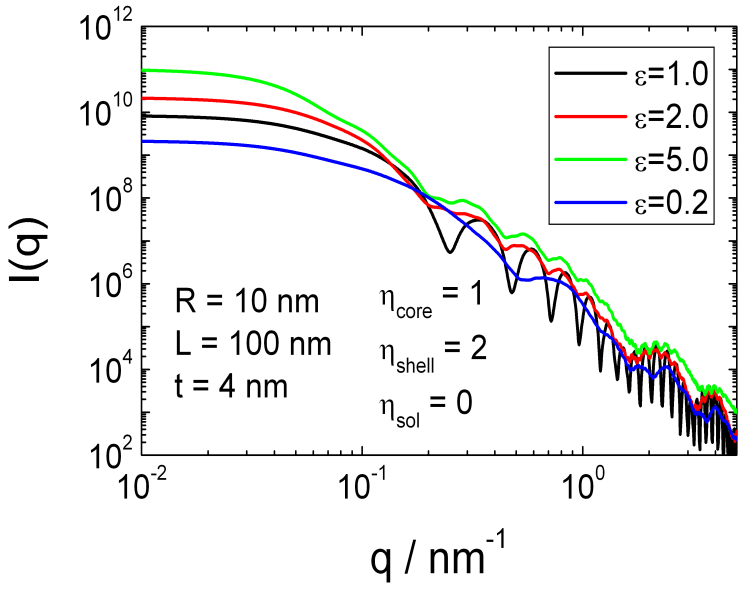

FIGURE 3.85. Scattering intensity of a cylinder with elliptical cross-section.

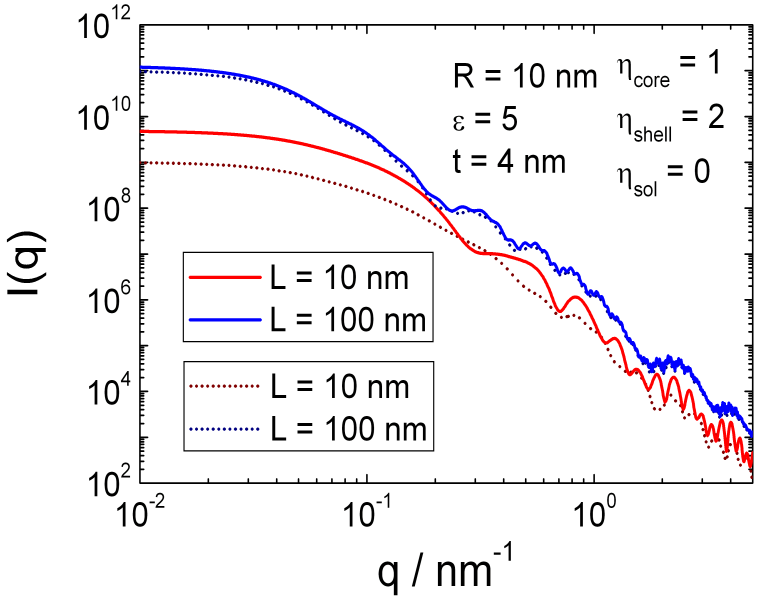

FIGURE 3.86. Scattering intensity of a cylinder with elliptical cross-section with and without capped ends.

For very long cylinders a faster approximation for the uncapped version can be used `Pcs:ellCylSh` combined with the structure factor `P'(Q):Rod`. The implemented approximation is the following

$$I_{\text{Long\_ellCylShell}}(q) = P'(q)P_{\text{cs}}(q) \tag{3.227}$$

$$P'(q) = 2\frac{\text{Si}(qL)}{qL} - \left(\frac{\sin(qL/2)}{qL/2}\right) \tag{3.228}$$

$$\text{Si}(x) = \int_0^x \frac{\sin t}{t}\, dt \tag{3.229}$$

$$r(R,\epsilon,\phi) = \sqrt{R^2\sin^2(\phi) + (\epsilon R + t)^2\cos^2(\phi)} \tag{3.230}$$

$$P_{\text{cs}}(q) = \frac{2}{\pi}\int_0^{\frac{\pi}{2}} \left(\frac{2J_1(qr(R,\epsilon,\phi))}{qr(R,\epsilon,\phi)} (\eta_{\text{core}} - \eta_{\text{shell}})\, \epsilon R^2 L\pi + \right. \tag{3.231}$$

$$\left. \frac{2J_1(q(r(R,\epsilon,\phi)+t))}{Q(r(R,\epsilon,\phi)+t)} (\eta_{\text{shell}} - \eta_{\text{sol}})\, (R+t)(\epsilon R + t)L\pi \right)^2 d\phi$$

Input Parameters for model `Pcs:ellCylSh`:

`R:` core radius R
`epsilon:` eccentricity ϵ of cross-section
`t:` shell thickness t
`eta_core:` scattering length density η_{core} of cylinder core
`eta_shell:` scattering length density η_{shell} of cylinder shell
`eta_sol:` scattering length density η_{sol} of solvent

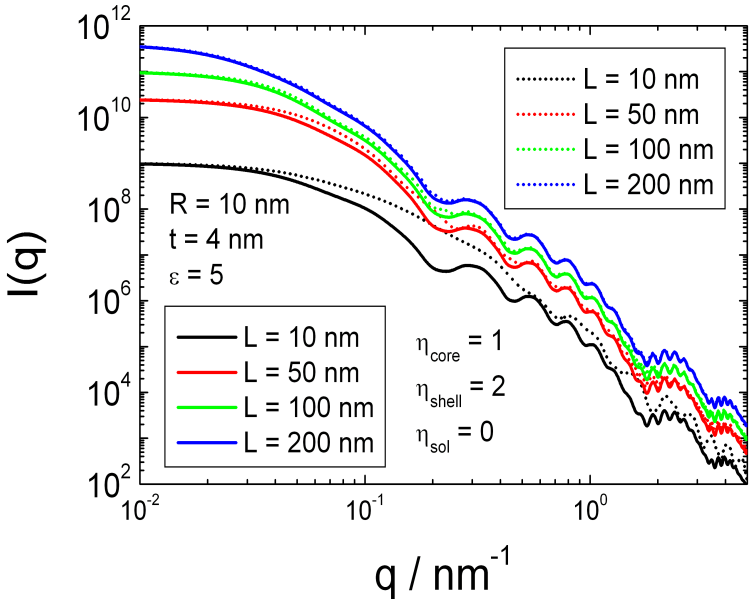

FIGURE 3.87. Scattering intensity of a cylinder with elliptical cross-section. The exact solutions `ellCylShell1` (dotted lines) are compared with `Pcs:ellCylSh` (solid lines), which is only valid for very long cylinders $L \gg 2R$.

3.6.9. partly aligned cylindrical shell [42].

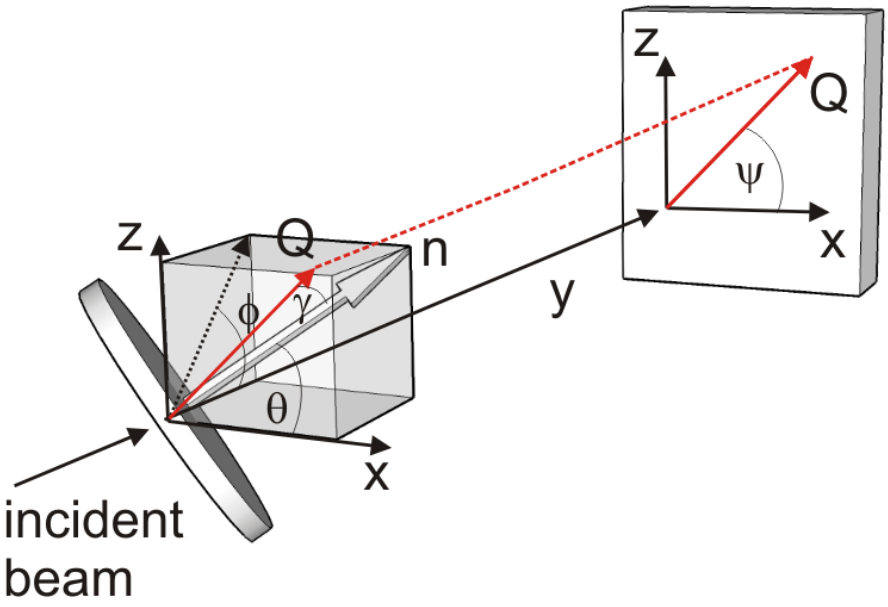

FIGURE 3.88. Sketch of relative orientation **n** of partly aligned cylinders or discs to the scattering vector **Q**.

The scattering amplitude of a cylindrical shell is given by

$$K_{\text{CylShell}}(Q,\ldots,\gamma) = K_{\text{Cyl}}(Q,\eta_{\text{core}}-\eta_{\text{shell}},R,L,\gamma) \tag{3.232}$$

$$+ K_{\text{Cyl}}(Q,\eta_{\text{shell}}-\eta_{\text{solv}},R+\Delta R,L,\gamma) \tag{3.233}$$

with

$$K_{\text{Cyl}}(Q,\Delta\eta,R,L,\gamma) = 2\pi R^2 L\Delta\eta \frac{J_1(QR\sin\gamma)}{QR\sin\gamma}\frac{\sin\left(\frac{QL}{2}\cos\gamma\right)}{\frac{QL}{2}\cos\gamma} \tag{3.234}$$

where γ is the angle between **Q** and the cylinder axis **n**. L is the length of the cylinder, R its radius, $\Delta\eta$ the scattering length density contrast relative to the solvent and $J_1(x)$ is the first order Bessel function of the first kind. γ can be calculated from the orientation (θ, ϕ) of the cylinder and the direction of the scattering vector ψ in the plane of the detector by

$$\frac{\mathbf{Q}}{|\mathbf{Q}|} = \begin{pmatrix}\cos\psi\\0\\\sin\psi\end{pmatrix} \qquad \frac{\mathbf{n}}{|\mathbf{n}|} = \begin{pmatrix}\cos\theta\\\sin\theta\sin\phi\\\sin\theta\cos\phi\end{pmatrix} \tag{3.235}$$

$$\cos\measuredangle(\mathbf{Q},\mathbf{n}) = \cos\gamma = \frac{\mathbf{Q}\cdot\mathbf{n}}{|\mathbf{Q}||\mathbf{n}|} = \cos\psi\cos\theta + \sin\psi\sin\theta\cos\phi \tag{3.236}$$

If the orientation distribution of the orientation vector $\mathbf{n}$ is described by $p(\theta, \phi)$ so that the scattering intensity is given by

$$I_{\text{p.a.CylShell}}(Q) = \int_0^{\pi} d\theta \int_0^{2\pi} d\phi \; K_{\text{CylShell}}\left(Q, \ldots, \gamma\right) \; p(\theta, \phi) \; \sin(\theta) \tag{3.237}$$

For this form factor it is assumed that the orientation distribution is independent of ϕ, i.e. $p(\theta, \phi) = p(\theta)$ and that $p(\theta) = p(\pi - \theta)$, which means that turning the cylinder by 180° results in the same scattering intensity. Instead of assuming a special parametrization of $p(\theta)$ the orientation distribution was expanded in terms of Legendre polynomials $P_l(\cos(\theta))$

$$p(\theta) = \sum_{l=0,even}^{\infty} \frac{2l+1}{2} \langle P_l \rangle \; P_l(\cos(\theta)) \tag{3.238}$$

Due to the symmetrie $p(\theta) = p(\pi - \theta)$ all terms with odd values for l are zero and only the even terms needs to be considered. For this form factor the first three terms up to $l = 6$ are implemented. As $\int_0^{\pi} p(\theta) \sin\theta \, d\theta = 1$ the zero order parameter is one $\langle P_0 \rangle = 1$.

Input Parameters for model `partly aligned CylShell`:

`R`: core radius R
`DR`: shell thickness ΔR
`L`: cylinder length L
`eta_core`: scattering length density η_{core} of cylinder core
`eta_shell`: scattering length density η_{shell} of cylinder shell
`eta_solv`: scattering length density η_{solv} of solvent
`psi`: direction ψ of the scattering vector in the plane of the detector
`P2`: order parameter $\langle P_2 \rangle$
`P4`: order parameter $\langle P_4 \rangle$
`P6`: order parameter $\langle P_6 \rangle$

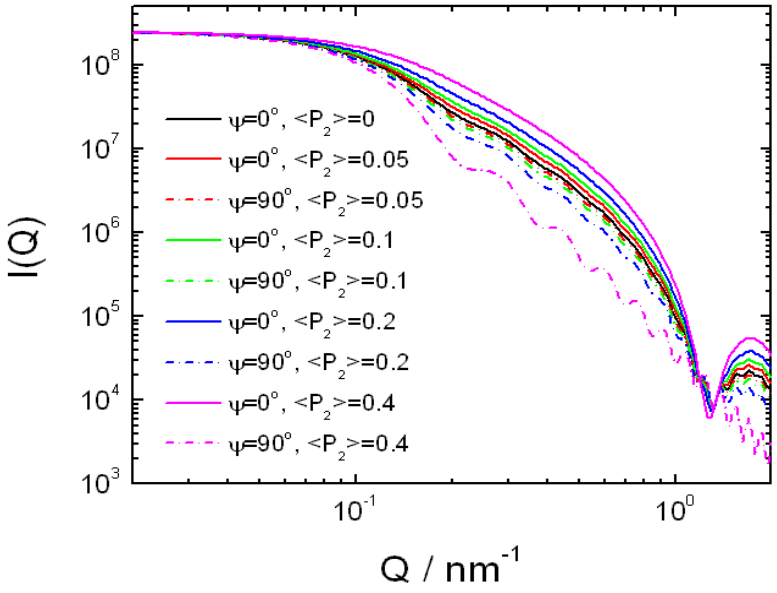

FIGURE 3.89. Scattering curve for partly aligned discs with radius $R =$ 20nm, $L = 5$nm, $\Delta R = 0$nm, and $\langle P_2 \rangle$ =0, 0.05, 0.1, 0.2, and 0.4. Higher order parameters are set zero. $I(Q)$ is calculated for $\psi = 0°$ and $\psi = 90°$.

3.6.10. aligned cylindrical shell [?].

3.6.11. Torus with elliptical shell cross-section [51, 29].

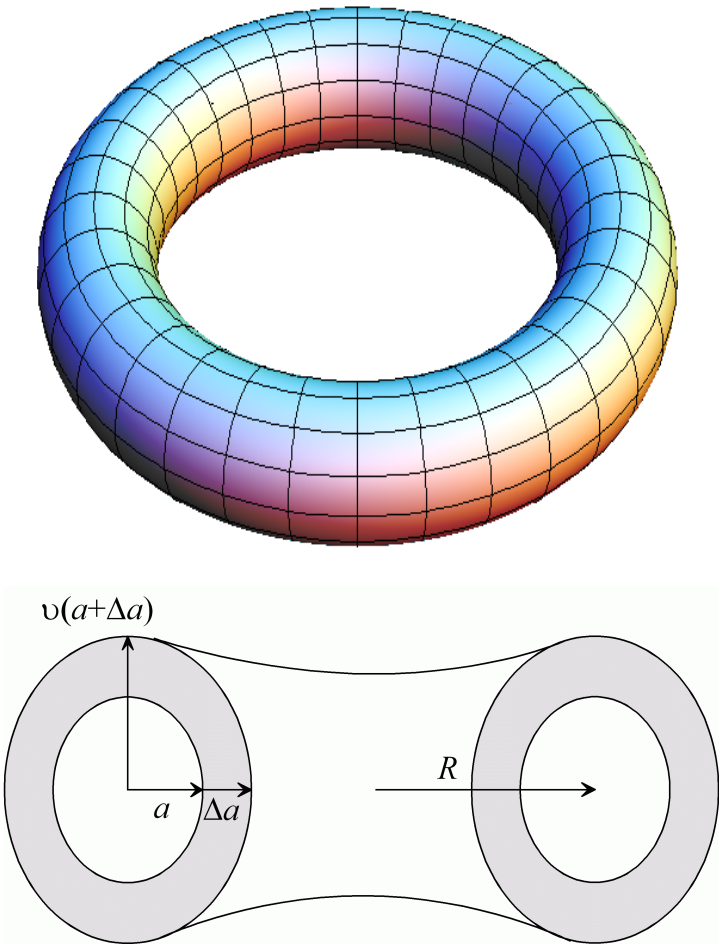

FIGURE 3.90.

$$F_{\text{torus}}(Q,\Theta,R,x,\nu,\Delta\eta)=\int_{R-x}^{R+x}4\pi r\Delta\eta\frac{J_0(Qr\sin\Theta)\sin(Q\gamma(r)\cos\Theta)}{Q\cos(\Theta)}\,dr \tag{3.239}$$

$$\text{with } \gamma(r)=\nu\sqrt{x^2-(r-R)^2} \tag{3.240}$$

$$I_{\text{torus}}(Q,R,a,\nu,\Delta\eta)=\int_0^{\pi/2}\left|F_{\text{torus}}(Q,\Theta,R,a,\nu,\Delta\eta)\right|^2\sin\Theta\,d\Theta \tag{3.241}$$

$$I_{\text{torus,sh}}(Q,R,a,\Delta a,\nu,\Delta\eta_{sh},\Delta\eta_c) = \int_0^{\pi/2} \Big| F_{\text{torus}}(Q,\Theta,R,a+\Delta a,\nu,\Delta\eta_{sh}) - F_{\text{torus}}(Q,\Theta,R,a,\nu,\Delta\eta_c)\Big|^2 \sin\Theta\, d\Theta \quad (3.242)$$

An alternative form factor for F_{torus} following [**29**] is

$$F_{\text{torus}}(Q,\Theta,R,x,\nu,\Delta\eta) = 2\pi \int_{-x}^{x} \Big[R_{(+)} J_1(QR_{(+)}\sin\theta) - R_{(-)} J_1(QR_{(-)}\sin\theta)\Big] \frac{\cos(Qz\cos\theta)}{Q\sin\theta}\, dz \quad (3.243)$$

with $R_{(\pm)} = R \pm \nu\sqrt{x^2 - z^2}$

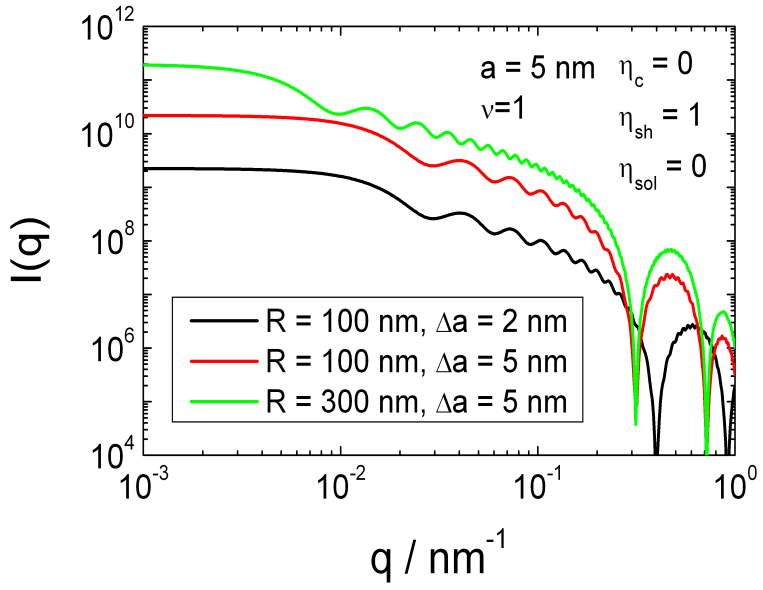

FIGURE 3.91. Scattering intensity of a torus.

3.6.12. stacked tori with elliptical shell cross-section.

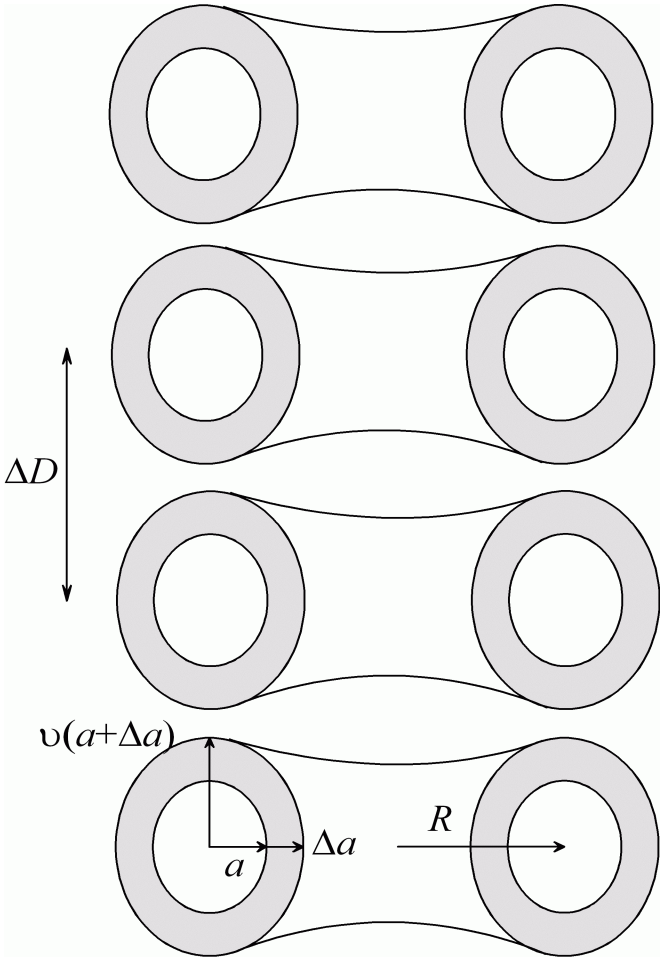

FIGURE 3.92.

$$F_{\text{stackedtori}}(Q,\Theta,R,x,\nu,\Delta\eta,\Delta D,N) = \tag{3.244}$$
$$\sum_{n=1}^{N}\int_{R-x}^{R+x} 4\pi r\Delta\eta\frac{J_0(Qr\sin\Theta)\sin(Q(\gamma(r)+\frac{2(n-1)-(N-1)}{4}\Delta D)\cos\Theta)}{Q\cos(\Theta)}\,dr$$

The scattering intensity is than calculated in the same way as for a single torus with an elliptical shell cross-section.

3.7. Local Planar Objects

The form factor of very anisotropic particles with local planar geometry can be shown to factorize (see, e.g. [**80**]) into a cross-section form factor $P_{\text{cs}}(Q)$ for the shorter dimensions and a shape factor $P'(Q)$ for the larger dimension:

$$P_{\text{planar}}(Q) = P'(Q)P_{\text{cs}}(Q) \tag{3.245}$$

The factorization in the cross-section factor $P_{\text{cs}}(Q)$, which only depends on parameters describing the inner structure of the layer with short dimensions and the shape factor $P'(Q)$, describing the overall shape in the larger dimension has the big advantage when both the shorter dimension as well as the larger dimensions have a polydispersity. In this case we do not end up with a double integral but rather a product of two integrals when both a short and a large dimension have a polydispersity. This speeds up the numerical computation significantly. Therefore the following form factors already have a polydispersity parameter included.

3.7.1. Shape factors $P'(Q)$.

The shape form factor $P'(Q)$ are normalized for $Q \to 0$ on the squared surface area S ($\lim_{Q\to 0} P'(Q) = S^2$) and can be that of an infinitely thin disc, spherical shell, elliptical shell, or cylindrical shell: The shape factors are accessible as a structure factor under `[anisotropic obj.|P'(Q):local planar geometry|P'(Q) xxx]` and using the monodisperse approximation. Actually these shape factors are foreseen to be used with the cross-section factors available as form factors under `[anisotropic obj.|Pcs(Q) for planar obj.|Pcs(Q) xxx]`. The shape factors are also available in combination with some cross-section factors as form factors under `[planar obj.]`.

3.7.1.1. *Polydisperse infinitesimal thin discs.*

$$P'_{\text{disc}}(Q,R) = \frac{2\pi^2 R^4}{(QR)^2}\left(1 - \frac{\mathrm{J}_1(2QR)}{QR}\right) \tag{3.246}$$

The polydispersity is included as a `LogNormal`-distribution from section 5.4 by

$$P'_{\text{ThinDiscs}}(Q,R,\sigma) = \int_0^\infty \text{LogNorm}(R',R,\sigma,1)P'_{\text{disc}}(Q,R')\,\mathrm{d}R' \tag{3.247}$$

3.7.1.2. *Infinitesimal thin spherical shell.*

$$P'_{\text{sph. shell}}(Q,R) = \left(4\pi R^2 \frac{\sin QR}{QR}\right)^2 \tag{3.248}$$

$$\tag{3.249}$$

3.7.1.3. *Infinitesimal thin elliptical shell.*

$$P'_{\text{ell. shell}}(Q,R,\epsilon) = S^2 \int_0^{\pi/2} \left(\frac{\sin\left(QR\sqrt{\sin^2\alpha + \epsilon^2\cos^2\alpha}\right)}{QR\sqrt{\sin^2\alpha + \epsilon^2\cos^2\alpha}} \right)^2 \sin(\alpha)\,\mathrm{d}\alpha \quad (3.250)$$

$$\text{with} \quad S = \begin{cases} 4\pi R^2 & \text{for } \epsilon = 1 \\ 2\pi R^2 \left(1 + \epsilon \frac{\arccos(1/\epsilon)}{\tan(\arccos(1/\epsilon))}\right) & \text{for } \epsilon > 1 \\ 2\pi R^2 \left(1 + \epsilon \frac{\operatorname{arctanh}(\sin(\arccos(\epsilon)))}{\sin(\arccos(\epsilon))}\right) & \text{for } \epsilon < 1 \end{cases} \quad (3.251)$$

3.7.1.4. *Infinitesimal thin cylindrical shell.*

$$P'_{\text{closed cyl. sh.}}(Q,R,H) = \int_0^{\pi/2} \left(2\pi R^2 + 2\pi RH\right)^2 \left(\frac{R}{R+H} \frac{2\mathrm{J}_1\left(QR\sin(\alpha)\right)}{QR\sin(\alpha)} \cos(QH\cos(\alpha)/2) + \frac{H}{R+H} \mathrm{J}_0(QR\sin\alpha) \frac{\sin(QH\cos(\alpha)/2)}{QH\cos(\alpha)/2} \right)^2 \sin(\alpha)\,\mathrm{d}\alpha \quad (3.252)$$

3.7.2. Cross-section form factors $P_{\mathbf{cs}}(Q)$.

3.7.2.1. *homogeneousXS.*

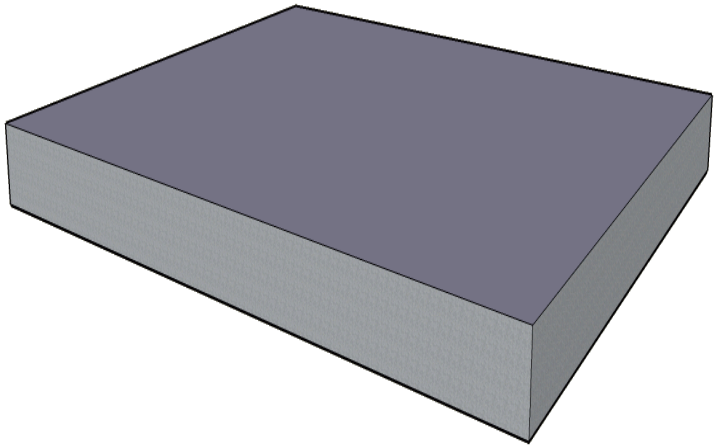

FIGURE 3.93. Planar object with homogeneous cross-section.

$$P_{\mathrm{cs}}(Q,\eta,L)=\left(\eta L\frac{\sin(QL/2)}{QL/2}\right)^2 \tag{3.253}$$

3.7.3. TwoInfinitelyThinPlates.

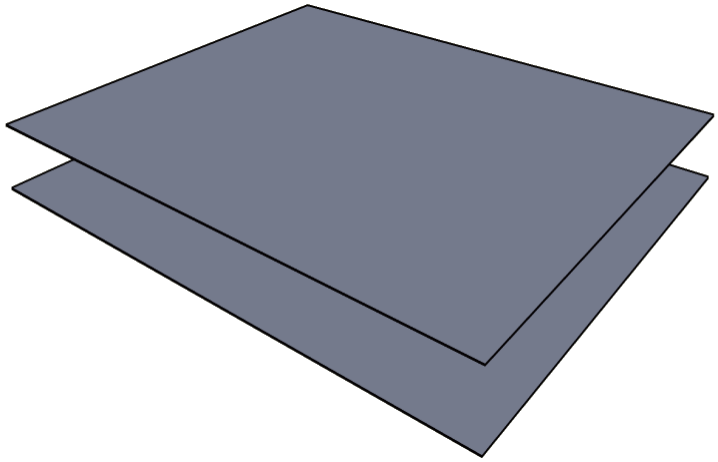

FIGURE 3.94. planar2thin.

$$P_{\rm cs}(Q,\eta,L) = \eta^2 \cos^2(QL/2) \tag{3.254}$$

3.7.4. LayeredCentroSymmetricXS.

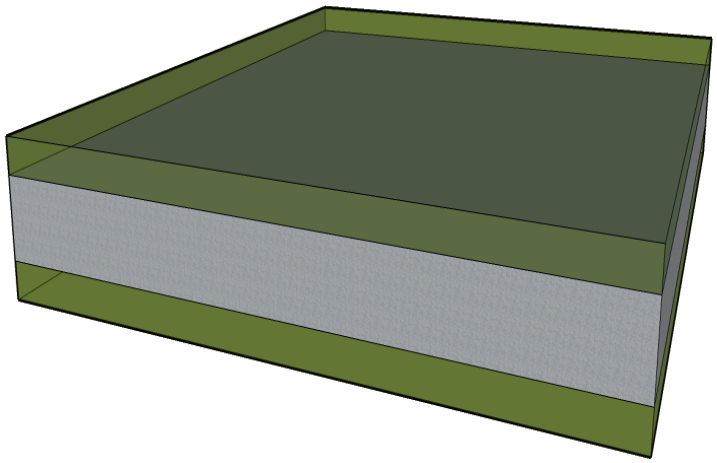

FIGURE 3.95. planar2centrosymHomo.

A layered centro symmetric cross-section structure with outer thickness L_{out} and a core of thickness L_c, where the core and the outer part have the scattering lengths density η_{out} and η_c, respectively, has

$$P_{\text{cs}}(Q, \eta_{\text{out}}, L_{\text{out}}, \eta_c, L_c) = \left(\frac{\eta_{\text{out}} L_{\text{out}} \sin\left(\frac{QL_{\text{out}}}{2}\right)}{QL_{\text{out}}/2} - \frac{(\eta_{\text{out}} - \eta_c) L_c \sin\left(\frac{QL_c}{2}\right)}{QL_c/2} \right)^2 \tag{3.255}$$

3.7.5. BiLayerGauss.

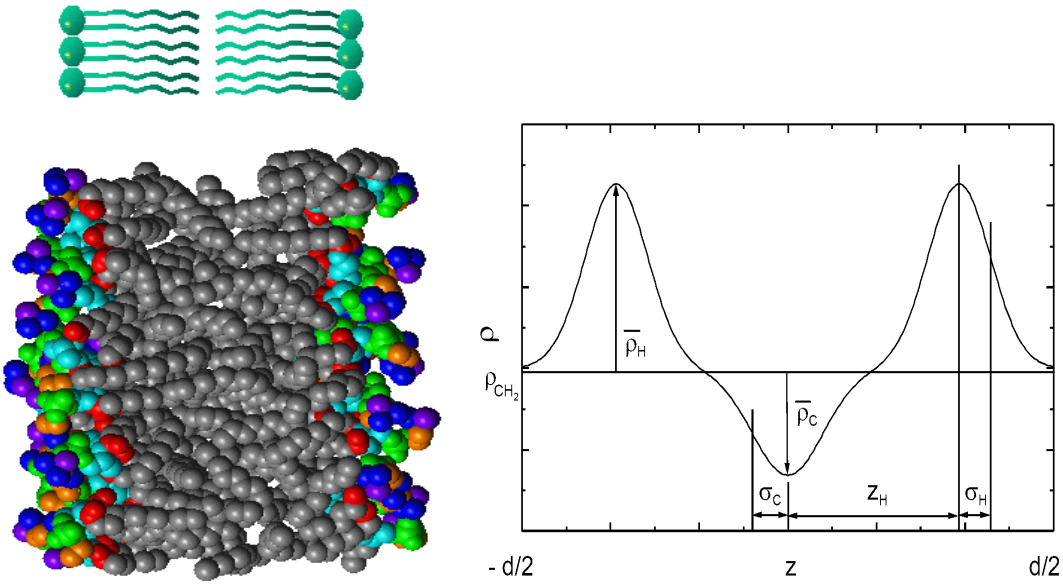

FIGURE 3.96. bilayerprof.

$$u_{\text{out}} = Q\sigma_{\text{out}} \tag{3.256}$$

$$u_{\text{core}} = Q\sigma_{\text{core}} \tag{3.257}$$

$$F_{\text{out}} = \sqrt{2\pi}\,\sigma_{\text{out}} b_{\text{out}} \exp(-u_{\text{out}}^2/2)\cos(Qt/2) \tag{3.258}$$

$$F_{\text{core}} = \sqrt{2\pi}\,\sigma_{\text{core}} b_{\text{core}} \exp(-u_{\text{core}}^2/2) \tag{3.259}$$

$$P_{\text{cs}} = (F_{\text{core}} + 2F_{\text{out}})^2 \tag{3.260}$$

3.8. Sheared Objects

3.8.1. ShearedCylinderHayterPenfold [42].

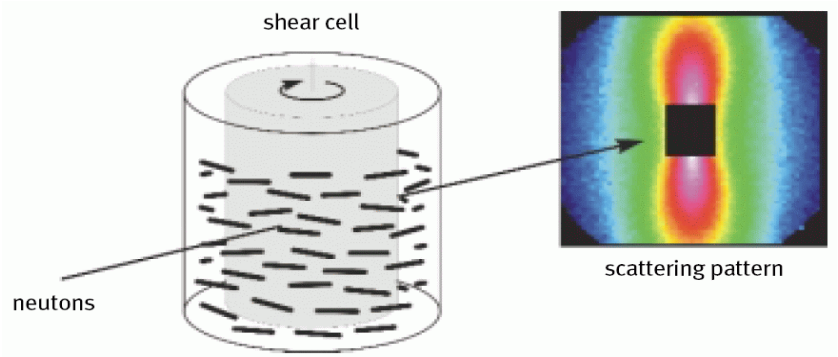

FIGURE 3.97. Shear orientation of micelles in a shear cell with the corresponding SANS-pattern.

The scattering from monodisperse dilute (non-interacting) isotropic solution of anisotropic micelles is given by

$$I(Q) = \left\langle |F(Q)|^2 \right\rangle_Q \tag{3.261}$$

where $F(Q)$ is the form factor for a micelle at a given orientation relative to the momentum transfer Q and $\langle\rangle_Q$ denotes an average over all such orientations.

For a uniform cylinder of length L and diameter $2R$ the form factor is given by:

$$F(Q) = F(Q,\gamma) = 2\Delta\eta V \frac{\sin\left(QL/2\cos\gamma\right)}{QL/2\cos\gamma} \frac{J_1(QR\sin\gamma)}{QR\sin\gamma} \tag{3.262}$$

where γ is the angle between Q and the cylinder axis, V is the volume, $\Delta\eta$ the scattering length density contrast relative to the solvent, $J_1(x)$ is the first order Bessel function of the first kind.

The scattering geometry for shear alignment is shown in Fig. 3.98. In general perfect alignment will not be achieved, and an orientation distribution must be employed such that the resultant scattering will be given by

$$I(Q,\psi) = \int_0^{2\pi} d\Phi \int_0^{\pi} p(\theta,\Phi;\Gamma)\ \left(F^2(Q,\gamma^+) + F^2(Q,\gamma^-)\right) \sin\theta d\theta \tag{3.263}$$

where

$$\cos\gamma^{\pm} = \sin\theta\cos\phi\cos\psi \pm \cos\theta\sin\psi \tag{3.264}$$

$$p(\theta,\phi;\Gamma) = \frac{(1-\cos 2\Phi_0)(1+\sin^2\theta\cos 2\Phi_0)^{3/2}}{4\pi\left[1-\sin^2\theta\cos 2\Phi_0\cos 2(\phi-\Phi_0)\right]^2} \tag{3.265}$$

and

$$2\Phi_0 = \arctan(8/\Gamma) \tag{3.266}$$

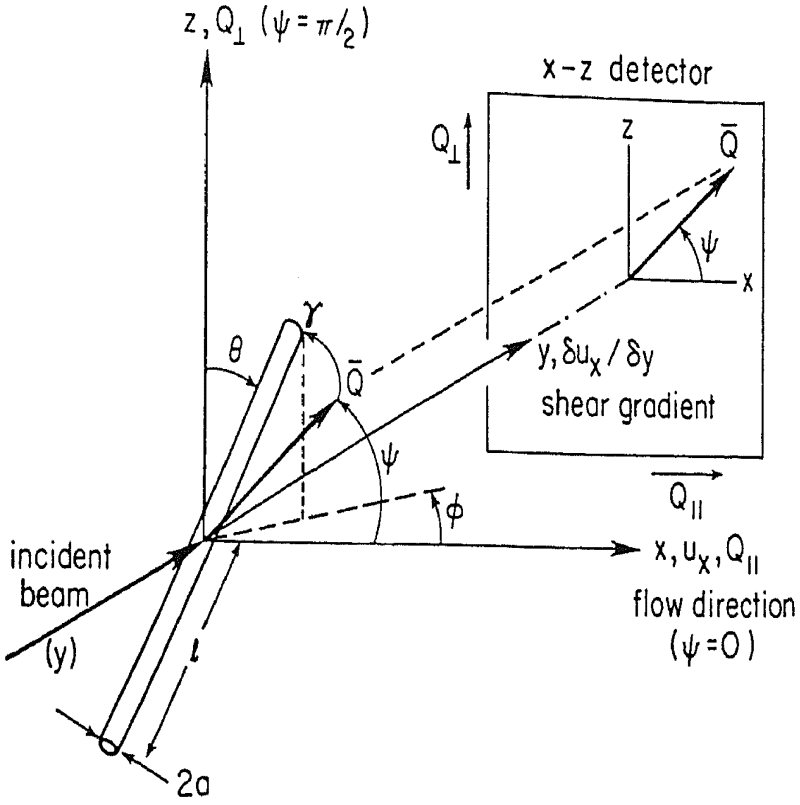

FIGURE 3.98. Cartesian and angular coordinates referred to the center of a cylindrical micelle at origin. The relationship to the spectrometer geometry is shown schematically. The momentum transfer, Q, lies in the $z - x$ plane.

$$\frac{\mathbf{Q}}{|\mathbf{Q}|} = \begin{pmatrix} \cos\psi \\ 0 \\ \sin\psi \end{pmatrix} \qquad \frac{\mathbf{n}}{|\mathbf{n}|} = \begin{pmatrix} \sin\theta\cos\phi \\ \sin\theta\sin\phi \\ \cos\theta \end{pmatrix} \tag{3.267}$$

$$\cos\angle(\mathbf{Q},\mathbf{n}) = \cos\gamma = \frac{\mathbf{Q}\cdot\mathbf{n}}{|\mathbf{Q}||\mathbf{n}|} = \cos\psi\sin\theta\cos\phi + \sin\psi\cos\theta \tag{3.268}$$

3.8.2. ShearedCylinderBoltzmann.

$$p(\theta, \phi; \bar{\theta}) = \exp(-\theta/\bar{\theta}) \tag{3.269}$$

$$\cos\gamma^{\pm} = \sin\theta\cos\phi\cos\psi \pm \cos\theta\sin\psi \tag{3.270}$$

3.8.3. ShearedCylinderGaussian.

$$p(\theta, \phi; \bar{\theta}) = \exp(-(\theta/\bar{\theta})^2) \tag{3.271}$$

$$\cos\gamma^{\pm} = \sin\theta\cos\phi\cos\psi \pm \cos\theta\sin\psi \tag{3.272}$$

3.8.4. ShearedCylinderHeaviside.

$$p(\theta, \phi; \bar{\theta}) = \Theta[\theta - \bar{\theta}] \tag{3.273}$$

$$\cos \gamma^{\pm} = \sin\theta \cos\phi \cos\psi \pm \cos\theta \sin\psi \tag{3.274}$$

3.9. Magnetic Scattering

In the case of magnetic moments in the sample, the neutron undergoes a magnetic interaction in addition to the nuclear interaction. The corresponding interaction potential is given by

$$V(\boldsymbol{r}) = -\boldsymbol{\mu}_N \cdot \boldsymbol{B}(\boldsymbol{r}) \quad \text{with} \quad \boldsymbol{\mu}_N = \gamma \frac{e\hbar}{2m_N c}\boldsymbol{\sigma}$$

where $\boldsymbol{\mu}_N = \gamma \frac{e\hbar}{2m_N c}\boldsymbol{\sigma}$ is the magnetic dipole moment of the neutron, $\boldsymbol{\sigma}$ the Pauli spin operator, $\gamma = -1.913$ the gyromagnetic ratio and $\boldsymbol{B}(\boldsymbol{r})$ the magnetic field induced by an atom at the position of the neutron. The latter has two components, one induced by the magnetic dipole moment $\boldsymbol{\mu}_S$ of the electrons, denoted $\boldsymbol{B}_S(\boldsymbol{r})$, and one by their orbital moment $\boldsymbol{\mu}_L$, denoted $\boldsymbol{B}_L(\boldsymbol{r})$. The (weak) magnetic interaction $V(\boldsymbol{r}) = -\boldsymbol{\mu}_N \cdot (\boldsymbol{B}_S(\boldsymbol{r}) + \boldsymbol{B}_L(\boldsymbol{r}))$ can as well be treated in first Born approximation, resulting in the magnetic scattering amplitude, in analogy to the nuclear scattering amplitude, given by the Fourier transform of the magnetic interaction potential $\mathcal{F}[V(\boldsymbol{r})]$:

$$b_M = -\frac{m_N}{2\pi\hbar^2}\,\boldsymbol{\mu}_N \cdot \int d^3r\, e^{\imath \boldsymbol{Q}\boldsymbol{r}}\,(\boldsymbol{B}_S(\boldsymbol{r}) + \boldsymbol{B}_L(\boldsymbol{r})). \tag{3.275}$$

An additional static magnetic field $\boldsymbol{H}(\boldsymbol{r})$ at the point of local magnetization $\boldsymbol{H}(\boldsymbol{r})$ (stemming from $\boldsymbol{B}_S(\boldsymbol{r}) + \boldsymbol{B}_L(\boldsymbol{r})$) induces a total local magnetic induction of

$$\boldsymbol{B}(\boldsymbol{r}) = \mu_0(\boldsymbol{H}(\boldsymbol{r}) + \boldsymbol{M}(\boldsymbol{r}))$$

and the Fourier transform of yields

$$\boldsymbol{B}(\boldsymbol{Q}) = \mu_0\,\frac{\boldsymbol{Q} \times [\boldsymbol{M}(\boldsymbol{Q}) \times \boldsymbol{Q}]}{Q^2} = \mu_0\,\boldsymbol{M}_\perp(\boldsymbol{Q}) = \mu_0\,\boldsymbol{M}(\boldsymbol{Q})\sin(\angle(\boldsymbol{Q},\boldsymbol{M})) \tag{3.276}$$

where $\boldsymbol{M}(\boldsymbol{Q}) = \int d^3r \exp(\imath \boldsymbol{Q}\cdot\boldsymbol{r})\boldsymbol{M}(\boldsymbol{r})$, with $\boldsymbol{M}(\boldsymbol{r})$ given in units of Am. $\boldsymbol{M}_\perp(\boldsymbol{Q}) = \boldsymbol{Q} \times [\boldsymbol{M}(\boldsymbol{Q}) \times \boldsymbol{Q}]/Q^2$ is the magnetization component perpendicular to the scattering vector Q. The magnetic scattering length then is

$$b_M = D_M\,\mu_0\,\boldsymbol{\sigma}\cdot\boldsymbol{M}_\perp(\boldsymbol{Q}) \text{ with } D_M = \frac{m_N}{2\pi\hbar^2}\,\mu_N = 2.3161 \times 10^{14}\,\frac{1}{\mathrm{Vs}}. \tag{3.277}$$

For the differential scattering cross section one finally obtains

$$\frac{d\sigma_M}{d\Omega}(\boldsymbol{Q}) = \frac{D_M^2}{N}|\mu_0 \boldsymbol{M}_\perp(\boldsymbol{Q})|^2 \tag{3.278}$$

In the presence of a preferred direction, for example induced by an external magnetic field, the magnetic scattering depends on the spin state of the neutrons. Let the z-axis be the preferred direction, and let $(+)$ and $(-)$ denote the neutron spin polarizations parallel and antiparallel to the z-axis, then the scattering is described by four scattering processes: two processes where the incident states $(+)$ and $(-)$ remain unchanged $(++$ and $--)$, the so-called 'non-spin-flip' processes, and two processes where the spin is flipped $(+-$ and $-+)$, the 'spin-flip' processes. Keeping in mind that the nuclear scattering does not flip the neutron spin, the four related scattering lengths are

$$b_{\pm\pm} = b_N \mp D_M \, \mu_0 \, M_{\perp x} \tag{3.279}$$

$$b_{\pm\mp} = -D_M \, \mu_0 \, (M_{\perp z} \pm \imath \, M_{\perp y}). \tag{3.280}$$

Hereby b_N is the nuclear scattering length. For an unpolarized neutron beam (which may be taken as composed of 50% (+) and 50% (−) polarization) the square of the modulus of the scattering length is

$$(b_{++}^2 + b_{--}^2 + b_{+-}^2 + b_{-+}^2)/2 = b_N^2 + D_M^2 \mu_0^2 M_\perp^2. \tag{3.281}$$

The differential cross section of the unpolarized neutron beam can therefore be described by the sum of the nuclear and the magnetic cross section, without any cross terms.

3.9.1. Magnetic Saturation.

3.9.1.1. *MagneticShellAniso.*

$$K(Q,R,\Delta\eta) = \frac{4}{3}\pi R^3 \Delta\eta\, 3\frac{\sin QR - QR\cos QR}{(QR)^3} \tag{3.282}$$

$$K_{\mathrm{sh}}(Q,R,\Delta R,\Delta\eta_{\mathrm{sh}},\Delta\eta_{\mathrm{c}}) = K(Q,R+\Delta R,\Delta\eta_{\mathrm{sh}}) - K(Q,R,\Delta\eta_{\mathrm{c}}) \tag{3.283}$$

$$K_{\mathrm{NUC}}(Q) = K_{\mathrm{sh}}(Q,R,\Delta R,\eta_{\mathrm{sh\ NUC}} - \eta_{\mathrm{m\ NUC}},\eta_{\mathrm{c\ NUC}} - \eta_{\mathrm{m\ NUC}}) \tag{3.284}$$

$$K_{\mathrm{MAG}}(Q) = K_{\mathrm{sh}}(Q,R,\Delta R,\eta_{\mathrm{sh\ MAG}} - \eta_{\mathrm{m\ MAG}},\eta_{\mathrm{c\ MAG}} - \eta_{\mathrm{m\ MAG}}) \tag{3.285}$$

$$\begin{aligned} I(Q) &= \frac{1-p}{2}\left(K^2_{\mathrm{MAG}}(Q) + 2K_{\mathrm{NUC}}(Q)K_{\mathrm{MAG}}(Q)\right) \\ &\quad + \frac{1+p}{2}\left(K^2_{\mathrm{MAG}}(Q) - 2K_{\mathrm{NUC}}(Q)K_{\mathrm{MAG}}(Q)\right) \qquad (3.286) \\ &= K^2_{\mathrm{MAG}}(Q) - 2pK_{\mathrm{NUC}}(Q)K_{\mathrm{MAG}}(Q) \qquad (3.287) \end{aligned}$$

p : neutron polarization, $p \in [-1:1]$

R : radius of particle core

ΔR : thickness of particle shell

$\eta_{\mathrm{sh\ NUC}}$: nuclear scattering length density of particle shell

$\eta_{\mathrm{m\ NUC}}$: nuclear scattering length density of matrix

$\eta_{\mathrm{c\ NUC}}$: nuclear scattering length density of particle core

$\eta_{\mathrm{sh\ MAG}}$: magnetic scattering length density of particle shell

$\eta_{\mathrm{m\ MAG}}$: magnetic scattering length density of matrix

$\eta_{\mathrm{c\ MAG}}$: magnetic scattering length density of particle core

3.9.1.2. *MagneticShellCrossTerm.*

$$K(Q,R,\Delta\eta) = \frac{4}{3}\pi R^3 \Delta\eta\, 3\frac{\sin QR - QR\cos QR}{(QR)^3} \tag{3.288}$$

$$K_{\rm sh}(Q,R,\Delta R,\Delta\eta_{\rm sh},\Delta\eta_{\rm c}) = K(Q,R+\Delta R,\Delta\eta_{\rm sh}) - K(Q,R,\Delta\eta_{\rm c}) \tag{3.289}$$

$$K_{\rm NUC}(Q) = K_{\rm sh}(Q,R,\Delta R,\eta_{\rm sh\ NUC}-\eta_{\rm m\ NUC},\eta_{\rm c\ NUC}-\eta_{\rm m\ NUC}) \tag{3.290}$$

$$K_{\rm MAG}(Q) = K_{\rm sh}(Q,R,\Delta R,\eta_{\rm sh\ MAG}-\eta_{\rm m\ MAG},\eta_{\rm c\ MAG}-\eta_{\rm m\ MAG}) \tag{3.291}$$

$$I(Q) = 4pK_{\rm NUC}(Q)K_{\rm MAG}(Q) \tag{3.292}$$

p : neutron polarization, $p \in [-1:1]$

R : radius of particle core

ΔR : thickness of particle shell

$\eta_{\rm sh\ NUC}$: nuclear scattering length density of particle shell

$\eta_{\rm m\ NUC}$: nuclear scattering length density of matrix

$\eta_{\rm c\ NUC}$: nuclear scattering length density of particle core

$\eta_{\rm sh\ MAG}$: magnetic scattering length density of particle shell

$\eta_{\rm m\ MAG}$: magnetic scattering length density of matrix

$\eta_{\rm c\ MAG}$: magnetic scattering length density of particle core

3.9.1.3. *MagneticShellPsi.*

$$K(Q,R,\Delta\eta) = \frac{4}{3}\pi R^3 \Delta\eta\, 3\frac{\sin QR - QR\cos QR}{(QR)^3} \tag{3.293}$$

$$K_{\mathrm{sh}}(Q,R,\Delta R,\Delta\eta_{\mathrm{sh}},\Delta\eta_{\mathrm{c}}) = K(Q,R+\Delta R,\Delta\eta_{\mathrm{sh}}) - K(Q,R,\Delta\eta_{\mathrm{c}}) \tag{3.294}$$

$$K_{\mathrm{NUC}}(Q) = K_{\mathrm{sh}}(Q,R,\Delta R,\eta_{\mathrm{sh\ NUC}} - \eta_{\mathrm{m\ NUC}},\eta_{\mathrm{c\ NUC}} - \eta_{\mathrm{m\ NUC}}) \tag{3.295}$$

$$K_{\mathrm{MAG}}(Q) = K_{\mathrm{sh}}(Q,R,\Delta R,\eta_{\mathrm{sh\ MAG}} - \eta_{\mathrm{m\ MAG}},\eta_{\mathrm{c\ MAG}} - \eta_{\mathrm{m\ MAG}}) \tag{3.296}$$

$$I(Q) = K^2_{\mathrm{NUC}}(Q) + \left(K^2_{\mathrm{MAG}}(Q) - 2pK_{\mathrm{NUC}}(Q)K_{\mathrm{MAG}}(Q)\right)\sin^2\Psi \tag{3.297}$$

p : neutron polarization, $p \in [-1:1]$

R : radius of particle core

Ψ : angle between $\boldsymbol{Q}$ and $\boldsymbol{H}$

ΔR : thickness of particle shell

$\eta_{\mathrm{sh\ NUC}}$: nuclear scattering length density of particle shell

$\eta_{\mathrm{m\ NUC}}$: nuclear scattering length density of matrix

$\eta_{\mathrm{c\ NUC}}$: nuclear scattering length density of particle core

$\eta_{\mathrm{sh\ MAG}}$: magnetic scattering length density of particle shell

$\eta_{\mathrm{m\ MAG}}$: magnetic scattering length density of matrix

$\eta_{\mathrm{c\ MAG}}$: magnetic scattering length density of particle core

3.9.2. Superparamagnetic Particles (like ferrofluids).

$$\frac{I_{\pm\pm}(\boldsymbol{Q})}{N} = \left|F_N(\boldsymbol{Q}) \mp \tilde{F}_M(\boldsymbol{Q})\,[L(\alpha)-\gamma]\,\sin^2\epsilon\right|^2 + \left|\tilde{F}_M(\boldsymbol{Q})\right|^2 \left(\frac{L(\alpha)}{\alpha}\,\sin^2\epsilon - \mathcal{L}(\alpha)\,\sin^4\epsilon\right) \tag{3.298}$$

$$\frac{I_{\mp\pm}(\boldsymbol{Q})}{N} = \left(\sin^2\epsilon - \sin^4\epsilon\right)[L(\alpha)-\gamma]^2\left|\tilde{F}_M(\boldsymbol{Q})\right|^2 + \left|\tilde{F}_M(\boldsymbol{Q})\right|^2 \left(\left(\sin^4\epsilon - \sin^2\epsilon\right)\mathcal{L}(\alpha) + (2-\sin^2\epsilon)\,\frac{L(\alpha)}{\alpha}\right) \tag{3.299}$$

$$\begin{aligned} I_{\text{unp}}(\boldsymbol{Q}) &= \frac{1}{2}\left(I_{++}(\boldsymbol{Q}) + I_{+-}(\boldsymbol{Q}) + I_{--}(\boldsymbol{Q}) + I_{-+}(\boldsymbol{Q})\right) \\ &= N\left(\left|\tilde{F}_M(\boldsymbol{Q})\right|^2 [L(\alpha)-\gamma]^2\,\sin^2\epsilon + |F_N(\boldsymbol{Q})|^2\right) \\ &\quad + N\left|\tilde{F}_M(\boldsymbol{Q})\right|^2\left(2\,\frac{L(\alpha)}{\alpha} - \mathcal{L}(\alpha)\,\sin^2\epsilon\right) \end{aligned} \tag{3.300}$$

Hereby $L(\alpha) = \coth\alpha - \frac{1}{\alpha}$ is the classical Langevin function with
$\alpha = \mu_0(H + M_{\text{eff}})M_s^{cr}V_P/kT$.
Furthermore the following functions are defined as:
$\mathcal{L}(\alpha) = L^2(\alpha) - 1 + 3\,\frac{L(\alpha)}{\alpha}$,
$F_N(\boldsymbol{Q}) = \Delta\eta\,V_N\,f_N(\boldsymbol{Q})$,
$\tilde{F}_M(\boldsymbol{Q}) = D_M\,M_s^{cr}\,V_M\,f_M(\boldsymbol{Q})$ and
$\gamma = M_s^{am}/M_s^{cr}$.
ϵ describes the angle between $\boldsymbol{Q}$ and the applied magnetic field $\boldsymbol{B}$. If the magnetic field lies in the plane of the detector, i.e. perpendicular to the incoming beam direction, ϵ is in practice identical to Ψ so that $\cos\epsilon = \sin\delta\,\cos\Psi \simeq \cos\Psi$ for $\delta \simeq \pi/2$ ($\boldsymbol{Q}$ in plane of detector for SANS, only for large scattering angle this will change).

3.9.2.1. *SuperparamagneticFFpsi.*
3.9.2.2. *SuperparamagneticFFAniso.*
3.9.2.3. *SuperparamagneticFFIso.*
3.9.2.4. *SuperparamagneticFFCrossTerm.*

3.10. Lorenz-Mie Form Factors for Static Light Scattering

Mie theory, also called Lorenz-Mie theory [**64, 99, 12**], is a complete mathematical-physical theory of the scattering of electromagnetic radiation by spherical particles. Mie theory is named after its developer German physicist Gustav Mie (1868 Rostock - 1957 Freiburg im Breisgau) and Danish physicist Ludvig Lorenz (1829-1891) who independently developed the theory of electromagnetic plane wave scattering by a dielectric sphere in 1908.

Mie scattering describes the scattering of electromagnetic radiation by spherical particles of any size r, relative to the wavelength, λ. Since the cases $r \ll \lambda$ and $r \gg \lambda$ are covered by Rayleigh (dipole) scattering and geometric scattering theories, respectively, Mie scattering often refers to the case of $r \sim \lambda$.

3.10.1. MieSphere.

The Mie scattering formulae are given in several books (Van de Hulst, 1957; Kerker, 1969; Deirmendjian, 1969) and by Dave (1968a, 1969a), although not always in the forms most suited to computation. The algorithm used here is based on the MIEV0 package described in [**105, 106**]. The following input values are used:

$\Theta = 2\arcsin(Q\lambda/(4\pi))$ with $Q < Q_{\max} = 4\pi/\lambda$

$R =$ radius of scattering sphere

$\lambda =$ wavelength of incident plane wave inside the solvent

$m =$ complex refractive index of sphere relative to surrounding medium

$= m_{\text{re}} - im_{\text{im}}$

$|m| \geq 1$ and $m_{\text{im}} \geq 0$

or

$|m| < 1$ and $m_{\text{im}} = 0$

$\text{pol} = 0$ unpolarized light

$\text{pol} = 1$ parallel to scattering plane polarized light

$\text{pol} = -1$ perpendicular to scattering plane polarized light

$|m| < 1$ would, for example, include visible light scattering from air bubbles in water.

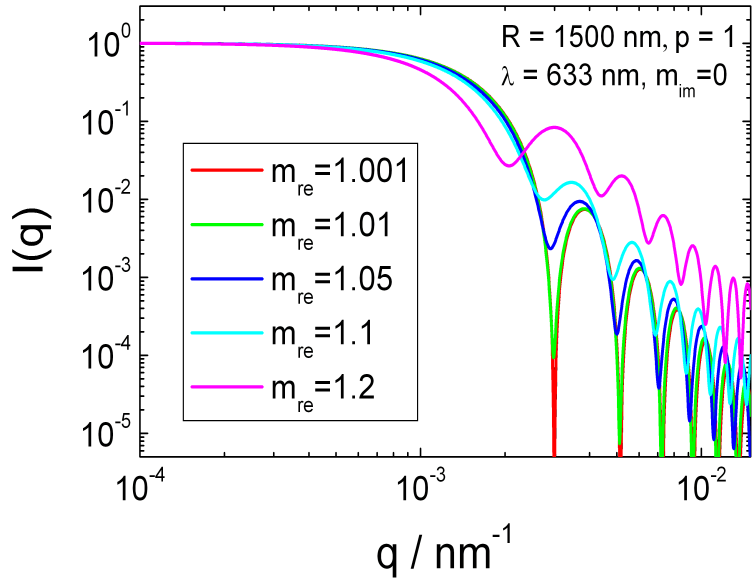

FIGURE 3.99. Scattering intensity of a sphere using the formalism for Mie scattering. The data are normalized to one for $q = 0$.

3.10.2. MieShell.

This form factor is basing on the version of MieLay, which computes electromagnetic scattering by a stratified sphere, i.e. a particle consisting of a spherical core surrounded by a spherical shell. The surrounding medium is assumed to have refractive index unity. The formulas, manipulated to avoid the ill-conditioning that plagued earlier formulations, were published in [**97**]. Further documentation, including definitons of input and output arguments, is inside the single precision version of this program (`SUBROUTINE MieLay`, available by anonymous ftp from `climate.gsfc.nasa.gov` in directory `pub/wiscombe`). The following input values are used:

$$\begin{aligned}
\Theta &= 2\arcsin(Q\lambda/(4\pi)) \text{ with } Q < Q_{\max} = 4\pi/\lambda \\
R_{\mathrm{c}} &= \text{radius of the core of scattering sphere} \\
R_{\mathrm{sh}} &= \text{thickness of the shell of scattering sphere} \\
\lambda &= \text{wavelength of incident plane wave inside the solvent} \\
m_{\mathrm{c}} &= \text{complex refractive index of core relative to surrounding medium} \\
&= m_{\mathrm{c,re}} - i m_{\mathrm{c,im}} \\
&|m_{\mathrm{c}}| \geq 1 \text{ and } m_{\mathrm{c,im}} \geq 0 \\
&\text{or} \\
&|m_{\mathrm{c}}| < 1 \text{ and } m_{\mathrm{c,im}} = 0 \\
m_{\mathrm{s}} &= \text{complex refractive index of core relative to surrounding medium} \\
&= m_{\mathrm{s,re}} - i m_{\mathrm{s,im}} \\
\mathrm{pol} &= 0 \text{ unpolarized light} \\
\mathrm{pol} &= 1 \text{ parallel to scattering plane polarized light} \\
\mathrm{pol} &= -1 \text{ perpendicular to scattering plane polarized light}
\end{aligned}$$

$|m| < 1$ would, for example, include visible light scattering from air bubbles in water.

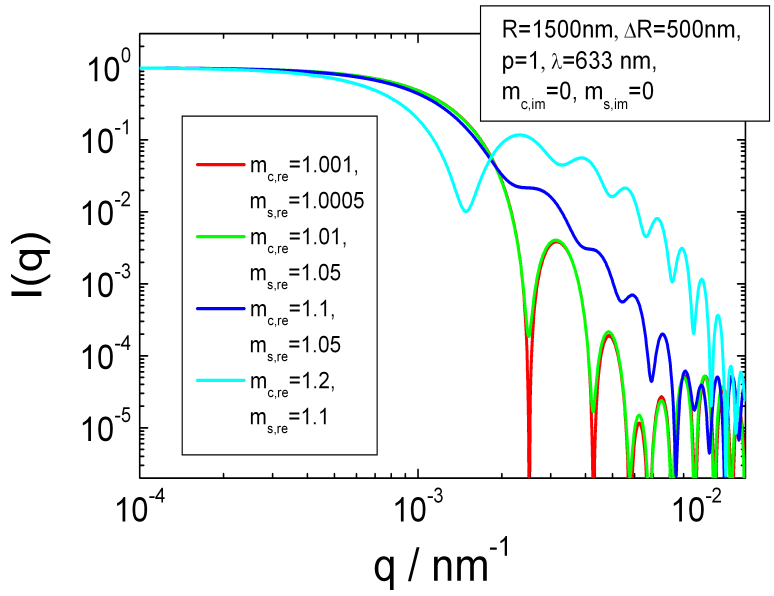

FIGURE 3.100. Scattering intensity of a spherical shell using the formalism for Mie scattering. The data are normalized to one for $q = 0$.

3.11. Other functions

3.11.1. DLS_Sphere_RDG.

This function has been implemented to simulate the relaxation signal $g_2(t)-1 = g_1^2(t)$ of a DLS (dynamic light scattering) measurement. The Q dependent contribution to the relaxation signal by particles of different radius R is considered by weighting $g_2(t) - 1$ with the form factor of sperical particles in Raylay-Debye-Gans approximation:

$$I_{\text{DLS\_Sphere\_RDG}}(t, \eta, T, Q) = \int_0^\infty N(R)\ K_{\text{sp}}^2(Q, R)\, e^{-DQ^2 t}\, dR \tag{3.301}$$

with

$$D = \frac{k_B T}{6\pi\eta R}$$

$$K_{\text{sp}}(Q, R) = \frac{4}{3}\pi R^3\, 3\frac{\sin QR - QR\cos QR}{(QR)^3}$$

R : radius

T : temperature

η : viscosity

Q : scattering vector

3.11.2. Langevin.

This function has been implemented to simulate the magnetisation curve $M(B)$ of superparamagnetic particles following the Langevin statistics with a size distribution $N(R)$: Magnetization curve of superparamagnetic particles with magnetization a M_s at temperature T

$$M(B) = \frac{\int_0^\infty N(R)\,\frac{4}{3}\pi R^3\,M_p(B,R)\,dR}{\int_0^\infty N(R)\frac{4}{3}\pi R^3\,dR} \tag{3.302}$$

$$M_p(B,R) = M_\infty\left(\coth(\alpha) - \tfrac{1}{\alpha}\right)$$

$$\alpha = \frac{BM_s\frac{4}{3}\pi R^3}{k_B T}$$

3.11.3. SuperParStroboPsi.

In the following the scattering of polarized incident neutrons with polarization analysis (POLARIS) is described. Experimental measured scattering signal are always a mixture of the spin dependent scattering cross-sections $I^{\pm\pm}(\boldsymbol{Q})$ and $I^{\pm\mp}(\boldsymbol{Q})$. The relative contribution of these cross-sections to the measured cross-section depend on the polarisation of the polarizer P_{pol} the efficiency of the spin flipper ϵ and the transmission values $T_{\pm}$ of the polarization analyzer, which is assumed to be an opaque He-filter. If the neutron polarization of the polarizer is $P_{pol} \in [-1;1]$ and the spin flipper is off the incident polarisation on the sample P_{in} is given by

$$P_{in} = P_{pol} = \frac{N_+ - N_-}{N_+ + N_-} = n_+ - n_- \tag{3.303a}$$

with

$$n_+ = \frac{N_+}{N_+ + N_-} \text{ and } n_- = \frac{N_-}{N_+ + N_-} \tag{3.303b}$$

$$\Rightarrow n_+ = \frac{1 + P_{pol}}{2} \text{ and } n_- = \frac{1 - P_{pol}}{2} \tag{3.303c}$$

$N_{\pm}$ are the number of incident neutrons with spin polarizations up $(+)$ and down $(-)$. After switching on the spin flipper, which works with an efficiency of $\epsilon \in [0;1]$ ($\epsilon = 0$: flipper off, $\epsilon \lessapprox 1$: flipper on), one gets

$$\begin{aligned} n_+(P_{pol},\epsilon) &= \epsilon\,\frac{1 - P_{pol}}{2} + (1-\epsilon)\,\frac{1 + P_{pol}}{2} \quad \text{and} \\ n_-(P_{pol},\epsilon) &= \epsilon\,\frac{1 + P_{pol}}{2} + (1-\epsilon)\,\frac{1 - P_{pol}}{2} \end{aligned} \tag{3.304}$$

The efficiency of the analyzer to filter spin up $(+)$ or spin down $(-)$ neutrons is given in case of an opaque spin filter by its transmission $T_{\pm}(t) \in [0;1]$, which can be a function of time, so that the measured scattering cross section $I_{\mathrm{m}}(\boldsymbol{Q})$ is given by

$$\begin{aligned} I_{\mathrm{m}}(\boldsymbol{Q}) = \quad & n_+(P_{pol},\epsilon)T_+(t)I_{++}(\boldsymbol{Q}) + n_+(P_{pol},\epsilon)T_-(t)I_{+-}(\boldsymbol{Q}) \\ & + n_-(P_{pol},\epsilon)T_-(t)I_{--}(\boldsymbol{Q}) + n_-(P_{pol},\epsilon)T_+(t)I_{-+}(\boldsymbol{Q}) \end{aligned} \tag{3.305}$$

The spin dependent scattering intensities of magnetic particles with an orientation distribution $f(\theta,\phi)$ of its magnetic moment can easily be calculated in terms of order parameters S_l if one assumes that the particle are spherical symmetric or the orientation of the magnetic moment of a particle is not correlated to the particle orientation. Furthermore it will be assumed that an external magnetic field is applied perpendicular to the incident neutron beam and that all orientations ϕ for a given angle θ, which is defined as the angle between the magnetisation vector of the particle and the direction of the external field $\boldsymbol{B}$ have the same probability, i.e. the orientation distribution only depends on θ so that $f(\theta,\phi) = f(\theta)$. The orientation probability distribution function can be expanded in terms of a complete set of orthogonal functions. Expanding it in

terms of Legendre polynomials $P_l(\cos\theta)$ gives

$$f(\theta) = \sum_l c_l P_l(\cos\theta) = \sum_l \frac{2l+1}{2} S_l P_l(\cos\theta) \tag{3.306}$$

The expansion coefficients can be calculated by

$$c_l = \frac{2l+1}{2} \int_0^\pi f(\theta)\, P_l(\cos\theta) \sin\theta \, \mathrm{d}\theta$$

or (3.307)

$$S_l = \int_0^\pi f(\theta)\, P_l(\cos\theta) \sin\theta \, \mathrm{d}\theta$$

The first three Legendre polynomials are defined by

$$P_0(\cos\theta) = 1 \tag{3.308a}$$

$$P_1(\cos\theta) = \cos\theta \tag{3.308b}$$

$$P_2(\cos\theta) = \frac{1}{2}\left(3\cos^2\theta - 1\right) \tag{3.308c}$$

For superparamagnetic particle the orientation probability distribution is given by

$$f(\theta) = \frac{\alpha}{4\pi \sinh\alpha} \exp(\alpha\cos\theta) \tag{3.309}$$

with $\alpha = BM_pV_p/(k_BT)$ being the Langevin parameter. For this orientation probability distribution the first order parameters can be calculates as

$$S_0 = 1 \tag{3.310a}$$

$$S_1 = L(\alpha) = \coth\alpha - \frac{1}{\alpha} \tag{3.310b}$$

$$S_2 = 1 - 3\frac{L(\alpha)}{\alpha} \tag{3.310c}$$

The scattering from a system of many particles is obtained by summing up the scattering amplitudes of all precipitates weighted by the phase shift at each particle position. In the decoupling approach scattering intensity is given by

$$\frac{\mathrm{d}\sigma^{\pm\pm}_{\pm\mp}}{\mathrm{d}\Omega}(\boldsymbol{Q}) = N\left\{\left\langle\left|F^{\pm\pm}_{\pm\mp}(\boldsymbol{Q})\right|^2\right\rangle + \left|\left\langle F^{\pm\pm}_{\pm\mp}(\boldsymbol{Q})\right\rangle\right|^2 (S(\boldsymbol{Q})-1)\right\} \tag{3.311}$$

which consists of two terms. The first one depends only on the particle structure and corresponds to the independent scattering of N particles, while the second one is also a function of their statistical distribution and reflects the interparticle interference, which is described by $S(\boldsymbol{Q})$. The $\langle\rangle$ indicates an average over all possible configurations, sizes and orientations of the magnetic moments of the particles. The spin dependent scattering amplitudes $F^{\pm\pm}_{\pm\mp}(\boldsymbol{Q})$ can be calculated from the nuclear and magnetic amplitudes

$$F_{\pm\pm}(\boldsymbol{Q}) = F_N(\boldsymbol{Q}) \mp F_{M_\perp x}(\boldsymbol{Q}) \tag{3.312}$$

$$F_{\pm\mp}(\boldsymbol{Q}) = -\left(F_{M_\perp y}(\boldsymbol{Q}) \pm \imath F_{M_\perp z}(\boldsymbol{Q})\right) \tag{3.313}$$

The nuclear scattering amplitude is proportional to the nuclear excess scattering $\beta_N = F_N(Q=0)$ and the nuclear form factor $f_N(\boldsymbol{Q})$

$$F_N(\boldsymbol{Q}) = \beta_N f_N(\boldsymbol{Q}) \tag{3.314}$$

The magnetic scattering amplitude $\boldsymbol{F}_{M_\perp}(\boldsymbol{Q})$ can be described as a vector, with

$$\boldsymbol{F}_{M_\perp}(\boldsymbol{Q}) = \hat{\boldsymbol{\mu}}_\perp D_M \mu f_M(\boldsymbol{Q}) = \hat{\boldsymbol{\mu}}_\perp F_M(\boldsymbol{Q}) \tag{3.315}$$

where $f_M(Q)$ is the magnetic form factor, $\boldsymbol{\mu} = \boldsymbol{M}_p V_p$ the magnetic moment of the particle, $D_M = \frac{\gamma e}{2\pi\hbar}$, and $\hat{\boldsymbol{\mu}}_\perp$ the Halpern-Johnson vector defined as

$$\hat{\boldsymbol{\mu}}_\perp = \frac{\boldsymbol{Q}}{Q} \times \left(\frac{\boldsymbol{\mu}}{\mu} \times \frac{\boldsymbol{Q}}{Q} \right) \tag{3.316}$$

It is assumed here that the neutron spin polarization is parallel or antiparallel to the axes $\boldsymbol{e}_x$ which is the direction perpendicular to the incoming neutron beam. If only the Halpern-Johnson vector $\hat{\boldsymbol{\mu}}_\perp$ depends on the orientation distribution $f(\theta)$ of the magnetic moments $\boldsymbol{\mu}$ of the particles but not the form factor $f_M(\boldsymbol{Q})$, which is valid for spherical symmetric particles or anisotropic shaped particles where the particle shape is not correlated to the direction of the magnetic moment, the averages in 3.311 can be written in terms of the order parameters S_1 and S_2

$$\langle F_{\pm\pm}(\boldsymbol{Q}) \rangle = F_N(\boldsymbol{Q}) + F_M(\boldsymbol{Q}) S_1 \sin^2\psi \tag{3.317a}$$

$$\langle F_{\pm\mp}(\boldsymbol{Q}) \rangle = F_M(\boldsymbol{Q}) S_1 \sin\psi\cos\psi \tag{3.317b}$$

$$\begin{aligned} \left\langle |F_{\pm\pm}(\boldsymbol{Q})|^2 \right\rangle = {} & |F_N(\boldsymbol{Q})|^2 + |F_M(\boldsymbol{Q})|^2 \left[S_2 \sin^4\psi + \frac{1-S_2}{3} \sin^2\psi \right] \\ & \mp \left[F_M(\boldsymbol{Q}) F_N^*(\boldsymbol{Q}) + F_M^*(\boldsymbol{Q}) F_N(\boldsymbol{Q}) \right] S_1 \sin^2\psi \end{aligned} \tag{3.317c}$$

$$\left\langle |F_{\pm\mp}(\boldsymbol{Q})|^2 \right\rangle = |F_M(\boldsymbol{Q})|^2 \left[2\,\frac{1-S_2}{3} - S_2 \sin^4\psi + \frac{4S_2-1}{3} \sin^2\psi \right] \tag{3.317d}$$

The spin-flip and spin-nonflip cross-section $\frac{\mathrm{d}\sigma^{\pm\pm}_{\pm\mp}}{\mathrm{d}\Omega}(\boldsymbol{Q})$ can be obtained by combining 3.311 and 3.317. The cross-sections without polarization analysis $I_\pm(\boldsymbol{Q})$ and for unpolarized

neutrons $I_{unp}(\boldsymbol{Q})$ are given by

$$\begin{aligned} I_{\pm}(\boldsymbol{Q}) &= I_{\pm\pm}(\boldsymbol{Q}) + I_{\pm\mp}(\boldsymbol{Q}) \\ &= \Big[|F_N(\boldsymbol{Q})|^2 + |F_M(\boldsymbol{Q})|^2 S_1^2 \sin^2\psi \\ &\quad \mp \left[F_M(\boldsymbol{Q}) F_N^*(\boldsymbol{Q}) + F_M^*(\boldsymbol{Q}) F_N(\boldsymbol{Q}) \right] S_1 \sin^2\psi \Big] S(\boldsymbol{Q}) \\ &\quad |F_M(\boldsymbol{Q})|^2 \left(\frac{2}{3}(1 - S_2) + \left(S_2 - S_1^2\right) \sin^2\psi \right) \end{aligned} \tag{3.318a}$$

$$\begin{aligned} I_{unp}(\boldsymbol{Q}) &= \frac{1}{2}\left(I_+(\boldsymbol{Q}) + I_-(\boldsymbol{Q})\right) \\ &= \left(|F_N(\boldsymbol{Q})|^2 + |F_M(\boldsymbol{Q})|^2 S_1^2 \sin^2\psi \right) S(\boldsymbol{Q}) \\ &\quad + |F_M(\boldsymbol{Q})|^2 \left(\frac{2}{3}(1 - S_2) + \left(S_2 - S_1^2\right) \sin^2\psi \right) \end{aligned} \tag{3.318b}$$

In the case of a Boltzmann orientation distribution $f(\theta) = \exp\left(\frac{\boldsymbol{B\mu}}{k_B T}\right) = \exp\left(\frac{B\mu\cos\theta}{k_B T}\right)$ the order parameter S_l already have been given in eq. 3.310 and the spin dependent intensities can be written as

$$\begin{aligned} \frac{I_{\pm\pm}(\boldsymbol{Q})}{N} &= \left| F_M(\boldsymbol{Q}) L(\alpha) \sin^2\psi \pm F_N(\boldsymbol{Q}) \right|^2 S(\boldsymbol{Q}) \\ &\quad + |F_M(\boldsymbol{Q})|^2 \left(\frac{L(\alpha)}{\alpha} \sin^2\psi - \left(L^2(\alpha) - 1 + 3\frac{L(\alpha)}{\alpha} \right) \sin^4\psi \right) \end{aligned} \tag{3.319a}$$

$$\begin{aligned} \frac{I_{\mp\pm}(\boldsymbol{Q})}{N} &= \left(\sin^2\psi - \sin^4\psi \right) L^2(\alpha) |F_M(\boldsymbol{Q})|^2 S(\boldsymbol{Q}) \\ &\quad + |F_M(\boldsymbol{Q})|^2 \left(\left(\sin^4\psi - \sin^2\psi \right) \left(L^2(\alpha) - 1 + 3\frac{L(\alpha)}{\alpha} \right) + (2 - \sin^2\psi) \frac{L(\alpha)}{\alpha} \right) \end{aligned} \tag{3.319b}$$

ψ is the angle between $\boldsymbol{Q}$ and the horizontal axis in the plane of the detector. $L(\alpha) = \coth(\alpha) - \frac{1}{\alpha}$ is the Langevin function. In the case of a static field the superparamagnetic particle are thermodynamic equilibrium and α is given by

$$\alpha = \frac{B M_P V_P}{k_B T}, \tag{3.320}$$

with M_P being the particle magnetization, V_P the particle volume, T the temperature in Kelvin and k_B the Boltzmann constant.

In our experiments we applied an oscillating magnetic field to the sample described by:

$$B(t, \nu; d_{\mathrm{SD}}, \lambda, \rho_0) = B_1 - B_0 \cos(\phi(t, \nu); \dots) \tag{3.321a}$$

$$\phi(t, \nu; d_{\mathrm{SD}}, \lambda, \rho_0) = 2\pi\nu(t - d_{\mathrm{SD}}\lambda/3956) + \rho_0 \tag{3.321b}$$

where t in [s] is the time between neutron detection and the trigger signal from the frequency generator, d_{SD} in [m] is the sample detector distance, λ in [Å] the neutron

wavelength, and ν in [Hz] the frequency of the oscillating magnetic field. As t is defined here as the time of the neutron detection one has therefore to correct the phase in the argument for the magnetic field with an additional phase term. The term $t_{\mathrm{SD}} = d_{\mathrm{SD}}\lambda/3956$ takes into account the flight time t_{SD} of the neutrons between the sample and the detector. The term ρ_0 accounts for any other additional constant phase shift between trigger signal and the magnetic field due to phase shifts in the amplifier. If the neutron polarization can follow adiabatically the varying magnetic field needs to be verified experimentally. Therefore we introduce here a parameter $a_{\mathrm{ad}} \in [0;1]$ which takes into account wether ($a_{\mathrm{ad}} = 1$) or not ($a_{\mathrm{ad}} = 0$) the neutron spin adiabatically follows the change of of magnetic field direction ($\mathrm{sgn}(B(t))$).

$$\boldsymbol{r}_{\mathrm{ad}} = \begin{pmatrix} a_{\mathrm{ad}} \\ (1 - a_{\mathrm{ad}}) \end{pmatrix} \text{ and } \boldsymbol{s}_{\mathrm{ad}} = \begin{pmatrix} \mathrm{sgn}(B(t)) \\ 1 \end{pmatrix} \tag{3.322}$$

The measured intensity than reads as

$$\begin{aligned} I_{\mathrm{m}}(\boldsymbol{Q},t) = \sum_{i=1,2} r_{ad,i} \Big[& && \text{(3.323a)} \\ & n_+\left(s_{ad,i}P_{pol},\epsilon\right) A_+ I_{++}(\boldsymbol{Q},t) + n_+\left(s_{ad,i}P_{pol},\epsilon\right) A_- I_{+-}(\boldsymbol{Q},t) \\ & + n_-\left(s_{ad,i}P_{pol},\epsilon\right) A_- I_{--}(\boldsymbol{Q},t) + n_-\left(s_{ad,i}P_{pol},\epsilon\right) A_+ I_{-+}(\boldsymbol{Q},t) \Big] \\ = \sum_{i=1,2} \sum_{k,l=+,-} & r_{ad,i}\; n_k\left(s_{ad,i}P_{pol},\epsilon\right)\; A_l\; I_{kl}(\boldsymbol{Q},t) && \text{(3.323b)} \end{aligned}$$

with

$$\begin{aligned} A_\pm = & \left(\frac{1+s_{ad,2}}{2} r_{ad,1} + \frac{1+s_{ad,1}}{2} r_{ad,2}\right) T_\pm(t) \\ & + \left(\frac{1-s_{ad,2}}{2} r_{ad,1} + \frac{1-s_{ad,1}}{2} r_{ad,2}\right) T_\mp(t) \end{aligned} \tag{3.323c}$$

To calculate the time dependent scattering cross section a model for the time evolution of the orientation distribution of the magnetic moments $f(\theta,t)$ is needed, from which the time dependent order parameter $S_1(t)$ and $S_2(t)$ can be obtained, as well as a model

for the time evolution of the structure factor $S(\boldsymbol{Q}, t)$.

$$\frac{\mathrm{d}M}{\mathrm{d}t} = -\frac{M(t) - M_\infty L(\alpha'(t))}{\tau} \tag{3.324a}$$

$$M(t=0) = M_0 \tag{3.324b}$$

$$\alpha'(t) = \alpha_0 \cos(\omega t + \phi_0) + \alpha_1 \tag{3.324c}$$

$$\alpha_0 = \frac{-B_0 \mu}{k_B T} \tag{3.324d}$$

$$\alpha_1 = \frac{B_1 \mu}{k_B T} \tag{3.324e}$$

$$\omega = 2\pi\nu \tag{3.324f}$$

$$\phi_0 = \varphi_0 - \frac{\omega d_{\mathrm{SD}} \lambda}{3956} \tag{3.324g}$$

In the limit of small values for the Langevin parameter α the Langevin function can be approximated by

$$L(\alpha) \to \frac{\alpha}{3} \tag{3.325}$$

for which the differential equation has an analytical solution

$$\begin{aligned} M(t) = e^{-\frac{t}{\tau}} &\left[M_0 - M_\infty \left(\frac{\alpha_0}{3} \, \frac{\cos(\phi_0) + \omega\tau \, \sin(\phi_0)}{1 + \omega^2\tau^2} + \frac{\alpha_1}{3} \right) \right] \\ &+ M_\infty \left(\frac{\alpha_0}{3} \, \frac{\cos(\omega\, t + \phi_0) + \omega\tau \, \sin(\omega\, t + \phi_0)}{1 + \omega^2\tau^2} + \frac{\alpha_1}{3} \right) \end{aligned} \tag{3.326}$$

$$\underset{t \gg \tau}{\simeq} M_\infty \left(\frac{\alpha_0}{3} \, \frac{\cos\left(\omega\, t + \phi_0 - \frac{\pi}{2} + \arcsin\left(\frac{1}{\sqrt{1+\omega^2\tau^2}}\right)\right)}{\sqrt{1 + \omega^2\tau^2}} + \frac{\alpha_1}{3} \right) \tag{3.327}$$

Assuming that the system is at any time in thermodynamic equilibrium with the actual magnetic field $B(t)$ than the time dependent oscillating SANS signal can be described by simply introducing a time dependent value for $\alpha(t)$:

$$\alpha(t, \lambda, d_{\mathrm{SD}}, \rho_0, \mu_{\mathrm{kT}}) = B(t, \lambda, d_{\mathrm{SD}}, \rho_0) \frac{M_P V_P}{k_B T} = B(\dots)\, \mu_{\mathrm{kT}} \tag{3.328}$$

with

$$\mu_{\mathrm{kT}} = \frac{M_P V_P}{k_B T} \tag{3.329}$$

In case that the magnetic moments can not follow the external magnetic field this could be described by an additional phase $\Delta\phi_\alpha$ between α and B and a damping factor d_α so that

$$\alpha(t, \lambda, d_{\mathrm{SD}}, \rho_0 - \Delta\phi_\alpha, \mu_{\mathrm{kT}}) = d_\alpha B(t, \lambda, d_{\mathrm{SD}}, \rho_0 - \Delta\phi_\alpha) \frac{M_P V_P}{k_B T}. \tag{3.330}$$

In such a case of such

$$\boldsymbol{r}_{\mathrm{ad}} = \begin{pmatrix} (1 - a_{\mathrm{ad}}) \, \mathrm{sgn}(B(t)) \\ a_{\mathrm{ad}} \, \mathrm{sign}(B(t)\alpha(t)) \end{pmatrix} \tag{3.331}$$

Furthermore we assume here that the size of the form factors of the magnetic and nuclear scattering are the same except the scattering contrast that means the ratio of magnetic to nuclear form factor is Q-independent and equal to the squared ratio of magnetic to nuclear scattering length density

$$\frac{F_N^2(Q)}{\tilde{F}_M^2(Q)} = const = \left(\frac{\Delta b_{\text{nuc}}}{\Delta b_{\text{mag}}}\right)^2 \tag{3.332}$$

Therefore the time dependent signal on the detector for a given direction ψ is given by

$$y(t,\dots) = \int_{\lambda_0-\Delta\lambda}^{\lambda_0+\Delta\lambda} p_{\triangle}(\lambda)\ \ I_m(t,\lambda,\psi,\dots)\ \ d\lambda \tag{3.333}$$

whereby $p_{\triangle}(\lambda)$ describes the triangular shaped wave length distribution of the neutron beam.

3.11.4. SuperParStroboPsiSQ.

The external applied field is given by:

$$B(t, d_{\mathrm{SD}}, \lambda, \rho_0) = B_1 - B_0 \cos(2\pi\nu(t - d_{\mathrm{SD}}\lambda/3956) + \rho_0) \tag{3.334}$$

where t in [s] is the time between neutron detection and the trigger signal from the frequency generator, d_{SD} in [m] is the sample detector distance, λ in [Å] the neutron wavelength, and ν in [Hz] the frequency of the oscillating magnetic field. As t is defined here as the time of the neutron detection one has therefore to correct the phase in the argument for the magnetic field with an addition phase term. The term $t_{\mathrm{SD}} = d_{\mathrm{SD}}\lambda/3956$ takes account for the flight time t_{SD} of the neutrons between the sample and the detector. The term ρ_0 takes account for any other additional constant phase shift between trigger signal and the magnetic field due to phase shifts in the amplifier.

The scattering intensity of superparamagnetic particles including a structure factor $S(Q)$is given by

$$\begin{aligned} I(Q) = & \underbrace{\tilde{F}_M^2(Q)\, 2\frac{L(\alpha)}{\alpha} + F_N^2(Q)S(Q)}_{A(Q)} \\ & + \underbrace{\tilde{F}_M^2(Q)\left[\left(1 - 3\frac{L(\alpha)}{\alpha} - L^2(\alpha)\right) + L^2(\alpha)S(Q)\right]}_{B(Q)} \sin^2\Psi \end{aligned} \tag{3.335}$$

Assuming that the system is in equilibrium faster than $1/\nu$ than the above equation can be used to describe the time dependent oscillating SANS signal simply by introducing a time dependent value for α:

$$\alpha(t, \lambda, d_{\mathrm{SD}}, \rho_0, \mu_{\mathrm{kT}}) = B(t, \lambda, d_{\mathrm{SD}}, \rho_0)\frac{M_P V_P}{k_B T} = B(\dots)\, \mu_{\mathrm{kT}} \tag{3.336}$$

with

$$\mu_{\mathrm{kT}} = \frac{M_P V_P}{k_B T} \tag{3.337}$$

Furthermore we assume here that the size of the form factors of the magnetic and nuclear scattering are the same except the scattering contrast that means the ratio of magnetic to nuclear form factor is Q-independent and equal to the squared ratio of magnetic to nuclear scattering length density

$$\frac{F_N^2(Q)}{\tilde{F}_M^2(Q)} = const = \left(\frac{\Delta b_{\mathrm{nuc}}}{\Delta b_{\mathrm{mag}}}\right)^2 \tag{3.338}$$

Therefore the time dependent signal on the detector for a given direction Ψ and integrated over Q in this direction is given by

$$\begin{aligned} i(t,\dots) &= \int_{Q_{\min}}^{Q_{\min}} I(Q,t,\lambda,\Psi,d_{\rm SD},\rho_0)dQ \qquad (3.339)\\ &= c\left[2\frac{L(\alpha)}{\alpha}+\frac{F_N^2(Q)}{\tilde{F}_M^2(Q)}S(Q)+\left[\left(1-3\frac{L(\alpha)}{\alpha}-L^2(\alpha)\right)+L^2(\alpha)S(Q)\right]\sin^2\Psi\right]\\ &= c\left[2\frac{L(\alpha)}{\alpha}+\left(\frac{\Delta b_{\rm nuc}}{\Delta b_{\rm mag}}\right)^2 S(Q)+\left[\left(1-3\frac{L(\alpha)}{\alpha}-L^2(\alpha)\right)+L^2(\alpha)S(Q)\right]\sin^2\Psi\right] \end{aligned}$$

$$y(t,\dots) = \int_{\lambda_0-\Delta\lambda}^{\lambda_0+\Delta\lambda} p_{\triangle}(\lambda)\ \ i(t,\lambda,\Psi,d_{\rm SD},\rho_0)\ \ d\lambda \qquad (3.340)$$

whereby $p_{\triangle}(\lambda)$ describes the triangular shaped wave length distribution of the neutron beam.

3.11.5. SuperParStroboPsiSQBt.
The same as `SuperParStroboPsiSQ` except that the structure factor $S(Q,t)$ becomes field dependent:

$$S(Q,t) = 1+[S(Q)-1]\left|\frac{B(t,d_{\rm SD},\lambda,\rho_0)}{|B_1|+\frac{2}{\pi}|B_0|}\right| \qquad (3.341)$$

3.11.6. SuperParStroboPsiSQLx.
The same as `SuperParStroboPsiSQ` except that the structure factor $S(Q,t)$ becomes field dependent:

$$S(Q,t) = 1+[S(Q)-1]\,|L(\alpha)| \qquad (3.342)$$

3.11.7. SuperParStroboPsiSQL2x.
The same as `SuperParStroboPsiSQ` except that the structure factor $S(Q,t)$ becomes field dependent:

$$S(Q,t) = 1+[S(Q)-1]\,L^2(\alpha) \qquad (3.343)$$

CHAPTER 4

Structure factors

The different types of structure factors can be selected in the different submenus. Below one finds how they are ordered. The definitions of the individual structure factors are defined below. Under the submenu `other` all structure factors under development and those functions, which are not structure factors at all but which have been implemented for some other purposes are listed.

- None
- Hard & Sticky Hard Sphere
  - Hard Sphere
  - Sticky Hard Sphere
  - Sticky Hard Sphere 2
  - Square Well Potential
  - Square Well Potential 2
- Multi Lamellar Structures
  - ThermalDisorder
  - Paracrystalline
  - ModifiedCaille
- anisotropic obj.
  - P'(Q): local planar geometry
    - P'(Q):ThinDisc
    - P'(Q):ThinSphericalShell
    - P'(Q):ThinEllipsoidalShell
    - P'(Q):ThinHollowShell
  - P'(Q): local cylindrical geometry
    - P'(Q):TinRod
    - P'(Q):SAW(withEXV)
    - P'(Q):SAW(withoutEXV)
- fractal obj.
  - Mass Fractal (Exp Cut-Off)
  - Mass Fractal (Gaussian Cut-Off)
  - Mass Fractal (Exp(-xˆa) Cut-Off)
  - Mass Fractal (OverlapSph Cut-Off)
- other
  - Mass Fractal
  - Cylinder (PRISM)
  - VoigtPeak
  - Correlation Hole
  - Critical Scattering

– Macro Ion (HP)
– Local Order
– RandomDistribution

4.1. Methods to include structure factors

For each scattering object i next to a size distribution $N_i(x;\underline{l}_i)$ also a structure factor $S_i(Q;\underline{s}_i)$ can be included. When a structure factor is included several theoretical ways to account for it have been implemented like the monodisperse approximation (4.1.1), decoupling approach (4.1.2), local monodisperse approximation (4.1.3), partial structure factor (4.1.4) and scaling approximation of partial structure factors (4.1.5). At the moment it is assumed that there are no interactions between different species of scatterers so that the total scattering is given by the sum of the scattering of the individual species

$$\frac{d\sigma}{d\Omega}(Q) = \sum_{i=1}^{N} \frac{d\sigma_i}{d\Omega}(Q) \tag{4.1}$$

whereby different approaches to include structure factor effects in the differential scattering cross-sections $\frac{d\sigma_i}{d\Omega}(Q)$ of the species i of scatterer are defined below.

4.1.1. Monodisperse approach.

The monodisperse approach is the simplest way to include a structure factor in the analysis. This approach simply multiplies the size averaged form factor with the structure factor. Here it is assumed that the interaction potential between particles are spherical symmetric and independent of the particle size.

$$\frac{d\sigma_i}{d\Omega}(Q) = \left[\int_0^\infty N_i(x;\underline{l}_i) F_i^2(Q;\underline{a}_i,x)dx\right] S_i(Q;\underline{s}_i) \tag{4.2}$$

4.1.2. Decoupling approximation.

For systems with small polydispersities and small anisotropies leads to a decoupling approach of Kotlarchyk and Chen [**55**]. It is assumed that interactions are independent of particle size and orientation.

$$\frac{d\sigma_i}{d\Omega}(Q) = \int_0^\infty N_i(x;\underline{l}_i) F_i^2(Q;\underline{a}_i,x)dx + \frac{1}{n_i}\left[\int_0^\infty N_i(x;\underline{l}_i) F_i(Q;\underline{a}_i,x)dx\right]^2 \times [S_i(Q;\underline{s}_i) - 1] \tag{4.3}$$

with

$$n_i = \int_0^\infty N_i(x;\underline{l}_i)dx. \tag{4.4}$$

The decoupling approximation can only be combined with those form factor, for which the scattering amplitude $F_i(Q;\underline{a}_i,x)$ has been implemented. However, for many form factors only the scattering intensity $F_i^2(Q;\underline{a}_i,x)$ is available. The combination of those form factors with the decoupling approach produces an error message in `SASfit` .

4.1.3. Local monodisperse approximation.

The opposite limit of the approximations as used for the decoupling approximation is used in the local monodisperse approximation [**77**]. In this approach it is assumed that a particle of a certain size is always surrounded by particles with the same size. Following this the scattering is approximated by that of monodisperse sub-systems weighted by the size distribution:

$$\frac{d\sigma_i}{d\Omega}(Q) = \int_0^\infty N_i(x;\underline{l}_i)F_i^2(Q;\underline{a}_i,x)S_i(Q;\underline{s}_i,R_i(\underline{a}_i,x))dx \tag{4.5}$$

in which it has been indicated that the structure factor is for particles of size $R_i(\underline{a}_i,x)$. As the distribution $N_i(x;\underline{l}_i)$ does not necessarily describe the distribution of the overall size. `SASfit` assumes, that the radius of a particle with the form factor $F_i(Q;\underline{a}_i,x)$ used in the structure factor is given by the radius of a sphere with the same volume $V_i(\underline{a}_i,x)$

$$R_i(\underline{a}_i,x) = \sqrt[3]{\frac{3}{4\pi}V_i(\underline{a}_i,x)}. \tag{4.6}$$

This local monodisperse approximation works better than the decoupling approximation for systems with larger polydispersities and higher concentrations. As compared to the decoupling approximation and the scaling approximation described below, it has the advantage that the cross section is linear in the size distribution.

4.1.4. partial structure factors.

For polydisperse systems it is also not possible to write the scattering cross section as a product of a form factor and a structure factor. The scattering cross section has the form

$$\begin{aligned}\frac{d\sigma_i}{d\Omega}(Q) = &\int_0^\infty N_i(x;\underline{l}_i)F_i^2(Q;\underline{a}_i,x)dx \\ &+\frac{1}{n_i}\int_0^\infty\int_0^\infty N_i(x;\underline{l}_i)N_i(x';\underline{l}_i)F_i(Q;\underline{a}_i,x)F_i(Q;\underline{a}_i,x') \\ &\times\left[S_i(Q;\underline{s}_i,R_i(\underline{a}_i,x),R_i(\underline{a}_i,x'))-1\right]dxdx'\end{aligned} \tag{4.7}$$

where monodisperse structure factor $S_i(Q;\underline{s}_i,\dots)$ is evaluated for the radius $(R_i(\underline{a}_i,x)+R_i(\underline{a}_i,x'))/2$. n_i and $R_i(\underline{a}_i,x)$ have the same definition as those in eq. 4.4 and 4.6.

4.1.5. Scaling approximation.

A scaling approximation has recently been introduced by Gazzillo et al. [**33**]. It is assumed that the pair correlation functions are identical except for a scaling constant. This leads to the following expression:

$$\begin{aligned}\frac{d\sigma_i}{d\Omega}(Q) = &\int_0^\infty N_i(x;\underline{l}_i)F_i^2(Q;\underline{a}_i,x)dx \\ &+\frac{1}{n_i}\int_0^\infty\int_0^\infty N_i(x;\underline{l}_i)N_i(x';\underline{l}_i)F_i(Q;\underline{a}_i,x)F_i(Q;\underline{a}_i,x') \\ &\times\frac{\overline{V}_i(\underline{a}_i,x,x')}{V_{i,av}}\left[S_i(Q;\underline{s}_i,R_i(\underline{a}_i,x),R_i(\underline{a}_i,x'))-1\right]\,dxdx'\end{aligned} \tag{4.8}$$

where $V_{i,av}$ is given by

$$V_{i,av} = \frac{\int_0^\infty N_i(x;\underline{l}_i)V_i(\underline{a}_i,x)dx}{\int_0^\infty N_i(x;\underline{l}_i)dx} \tag{4.9}$$

and $V_i(\underline{a}_i,x,x')$ by

$$\overline{V}_i(\underline{a}_i,x,x') = \frac{4}{3}\pi\left(\frac{1}{2}\left(\sqrt[3]{\frac{3}{4\pi}V_i(\underline{a}_i,x)}+\sqrt[3]{\frac{3}{4\pi}V_i(\underline{a}_i,x')}\right)\right)^3 \tag{4.10}$$

and the monodisperse structure factor is evaluated for the radius $(R_i(\underline{a}_i,x)+R_i(\underline{a}_i,x'))/2$. n_i and $R_i(\underline{a}_i,x)$ have the same definition as those in eq. 4.4 and 4.6.

Note that the expression is not linear in the size distribution and that it involves double integrations, which makes least-square fitting with this expression relatively slow.

4.1.6. van der Waals one-fluid approximation.

This approximation is similar to the scaling approximation introduced by Gazzillo et al. [**33**]. The exact formular is given by

$$\begin{aligned}\frac{d\sigma_i}{d\Omega}(Q) = &\int_0^\infty N_i(x;\underline{l}_i)F_i^2(Q;\underline{a}_i,x)dx \\ &+\frac{1}{n_i}\int_0^\infty\int_0^\infty N_i(x;\underline{l}_i)N_i(x';\underline{l}_i)F_i(Q;\underline{a}_i,x)F_i(Q;\underline{a}_i,x') \\ &\times\frac{\overline{V}_i(\underline{a}_i,x,x')}{V_{i,x}}\left[S_i(Q;\underline{s}_i,R_i(\underline{a}_i,x),R_i(\underline{a}_i,x'))-1\right]\,dxdx'\end{aligned} \tag{4.11}$$

where $V_{i,x}$ is given by

$$V_{i,av} = \frac{\int_0^\infty N_i(x;\underline{l}_i)V_i(\underline{a}_i,x)dx}{\int_0^\infty N_i(x;\underline{l}_i)dx} \tag{4.12}$$

and $V_i(\underline{a}_i, x, x')$ by

$$\overline{V}_i(\underline{a}_i, x, x') = \frac{4}{3}\pi \left(\frac{1}{2} \left(\sqrt[3]{\frac{3}{4\pi} V_i(\underline{a}_i, x)} + \sqrt[3]{\frac{3}{4\pi} V_i(\underline{a}_i, x')} \right) \right)^3 \tag{4.13}$$

and the monodisperse structure factor is evaluated for the radius $(R_i(\underline{a}_i, x)+R_i(\underline{a}_i, x'))/2$. n_i and $R_i(\underline{a}_i, x)$ have the same definition as those in eq. 4.4 and 4.6.

Note that the expression is not linear in the size distribution and that it involves double integrations, which makes least-square fitting with this expression relatively slow.

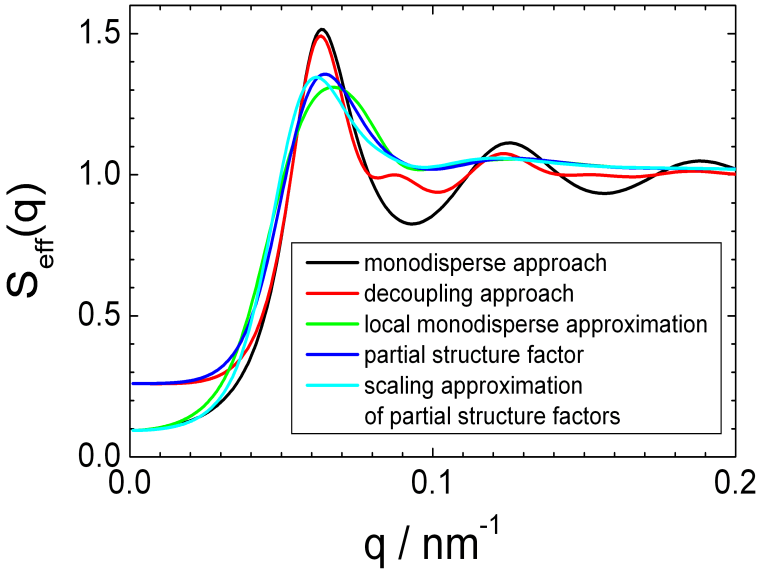

FIGURE 4.1. Effective structure factor $S_{\text{eff}}(q)$ for Spheres with Hard Sphere interaction potential. The fraction is assumed to be $\eta = 0.3$. A LogNormal distribution with $\sigma = 0.15$ and $R_0 = 50nm$ is assumed.

4.2. Hard & Sticky Hard Sphere

4.2.1. Hard Sphere [78, 101].

$$U(r) = \begin{cases} \infty & \text{for} \quad 0 < r < \sigma \\ 0 & \text{for} \quad r > \sigma \end{cases} \tag{4.14}$$

$$\alpha = \frac{(1+2f_p)^2}{(1-f_p)^4} \tag{4.15a}$$

$$\beta = -6f_p \frac{(1+f_p/2)^2}{(1-f_p)^4} \tag{4.15b}$$

$$\gamma = \frac{f_p \alpha}{2} \tag{4.15c}$$

$$A = 2R_{\mathrm{HS}}q \tag{4.15d}$$

$$G(q) = \alpha \frac{\sin A - A\cos A}{A^2} + \beta \frac{2A\sin A + (2-A^2)\cos A - 2}{A^3} + \gamma \frac{-A^4\cos A + 4\left[(3A^2-6)\cos A + (A^3-6A)\sin A + 6\right]}{A^5} \tag{4.15e}$$

$$S_{\mathrm{HS}}(q, R_{\mathrm{HS}}, f_p) = \frac{1}{1 + 24 f_p \dfrac{G(f_p, R_{\mathrm{HS}}q)}{R_{\mathrm{HS}}q}} \tag{4.15f}$$

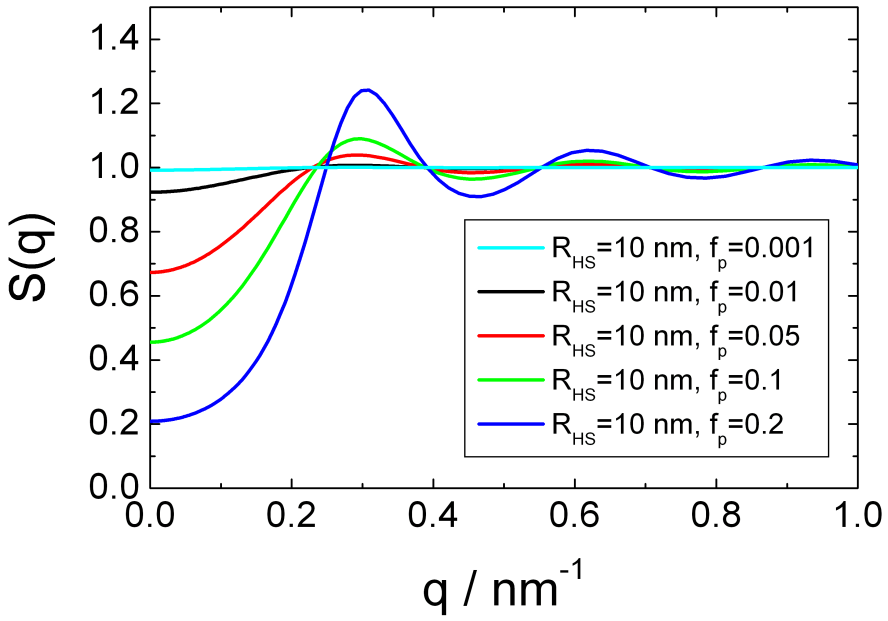

FIGURE 4.2. Structure factor $S(q)$ for a hard sphere interaction potential for the different volume fractions f_p.

4.2.2. Sticky Hard Sphere.

In Baxter's model [**3, 85, 21, 2, 62, 63**] of adhesive hard spheres the pair interaction potential $U(r)$ is replaces by

$$\frac{U(r)}{k_BT} = \begin{cases} \infty & \text{for} \quad 0 < r < \sigma \\ \ln \frac{12\tau\Delta}{\sigma+\Delta} & \text{for} \quad \sigma < r < \sigma + \Delta \\ 0 & \text{for} \quad r > \sigma + \Delta \end{cases} \tag{4.16}$$

after which, when applied, the limit $\Delta \to 0$ is taken. Thus, only a single parameter, the so-called stickiness parameter τ, characterizes the adhesive strength.

$$\kappa = 2qR_{\text{HS}} \tag{4.17a}$$

$$\eta = f_p \left(\frac{2R_{\text{HS}} + \Delta}{2R_{\text{HS}}} \right)^3 \tag{4.17b}$$

$$\epsilon = \tau + \frac{\eta}{1-\eta} \tag{4.17c}$$

$$\gamma = f_p \frac{1 + \eta/2}{3\left(1-\eta\right)^2} \tag{4.17d}$$

$$\lambda = \frac{6}{\eta} \left(\epsilon - \sqrt{\epsilon^2 - \gamma} \right) \tag{4.17e}$$

$$\mu = \lambda\eta(1-\eta) \tag{4.17f}$$

$$\beta = -\frac{3\eta\left(2+\eta\right)^2 - 2\mu\left(1 + 7\eta + \eta^2\right) + \mu^2(2+\eta)}{2\left(1-\eta\right)^4} \tag{4.17g}$$

$$\alpha = \frac{\left(1 + 2\eta - \mu\right)^2}{\left(1-\eta\right)^4} \tag{4.17h}$$

$$\begin{aligned} C(q) =& 2\frac{\eta\lambda}{\kappa}\sin\kappa - 2\frac{\eta^2\lambda^2}{\kappa^2}\left(1-\cos\kappa\right) - \\ & \Big\{ \alpha\kappa^3(\sin\kappa - \kappa\cos\kappa) + \beta\kappa^2(2\kappa\sin\kappa - (\kappa^2-2)\cos\kappa - 2) \\ & + \frac{\eta\alpha}{2}\left((4\kappa^3 - 24\kappa)\sin\kappa - (\kappa^4 - 12\kappa^2 + 24)\cos\kappa + 24\right) \Big\} \times 24\frac{\eta}{\kappa^6} \end{aligned} \tag{4.17i}$$

$$S_{\text{sHS}}(q, R_{\text{HS}}, f_p, \tau) = \frac{1}{1 - C(q)} \tag{4.17j}$$

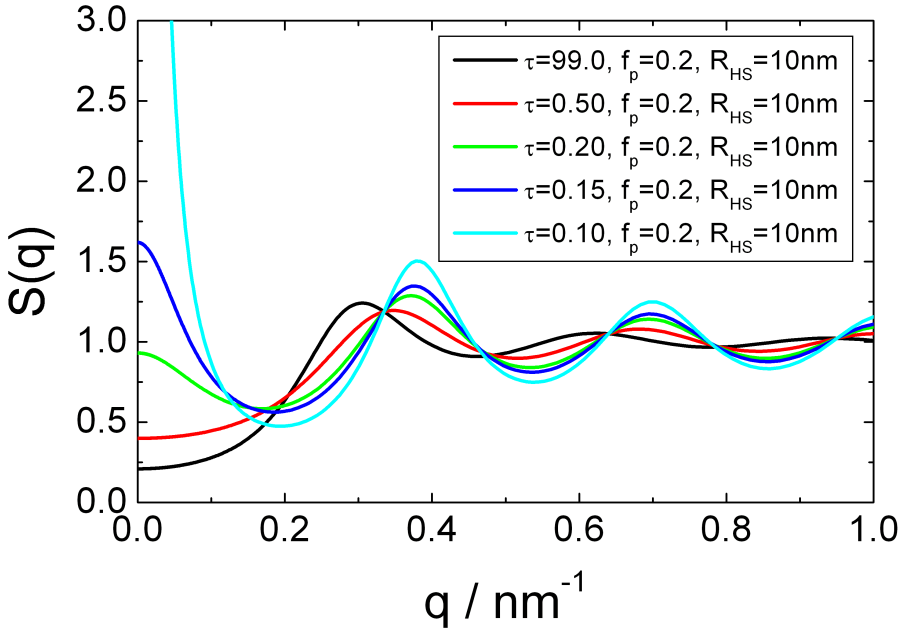

FIGURE 4.3. Structure factor $S(q)$ for a sticky hard sphere interaction potential for the different stickiness parameters τ.

4.2.3. Sticky Hard Sphere (2^{nd} version [83, 84]).

In Baxter's model of adhesive hard spheres the pair interaction potential $U(r)$ is replaces by

$$\frac{U(r)}{k_B T} = \begin{cases} \infty & \text{for} \quad 0 < r < \sigma \\ \ln \frac{12\tau\Delta}{\sigma+\Delta} & \text{for} \quad \sigma < r < \sigma + \Delta \\ 0 & \text{for} \quad r > \sigma + \Delta \end{cases} \tag{4.18}$$

$$\sigma = 2R_{\text{HS}} + \Delta \tag{4.19}$$

$$\kappa = q\sigma \tag{4.20}$$

$$\phi = f_p \left(\frac{\sigma}{2R_{\text{HS}}} \right)^3 \tag{4.21}$$

$$\lambda_{\pm} = 6 \left(\frac{\tau}{\phi} + \frac{1}{1-\phi} \right) \pm \sqrt{36 \left[\frac{\tau}{\phi} + \frac{1}{1-\phi} \right]^2 - \frac{12}{\phi} \frac{1 + \frac{\phi}{2}}{(1-\phi)^2}} \tag{4.22}$$

$$\lambda = \begin{cases} \lambda_+ & \text{for } \lambda_+ < |\lambda_-| \\ \lambda_- & \text{otherwise} \end{cases} \tag{4.23}$$

$$\mu = \lambda\phi(1-\phi) \tag{4.24}$$

$$A = \frac{1}{2} \frac{1 + 2\phi - \mu}{(1-\phi)^2} \tag{4.25}$$

$$B = \frac{\sigma}{2} \frac{\mu - 3\phi}{2(1-\phi)^2} \tag{4.26}$$

$$C = -A\sigma^2 - B\sigma + \lambda\sigma^2/12 \tag{4.27}$$

$$I_n(\kappa) = \int_0^1 x^n \cos(\kappa x)\, dx \tag{4.28}$$

$$J_n(\kappa) = \int_0^1 x^n \sin(\kappa x)\, dx \tag{4.29}$$

$$\alpha = 1 - 12 f_p \left(C\sigma^{-2} I_0(\kappa) + B\sigma^{-1} I_1(\kappa) + A I_2(\kappa) \right) \tag{4.30}$$

$$\beta = 12 f_p \left(C\sigma^{-2} J_0(\kappa) + B\sigma^{-1} J_1(\kappa) + A J_2(\kappa) \right) \tag{4.31}$$

$$S(Q) = \frac{1}{\alpha^2 + \beta^2} \tag{4.32}$$

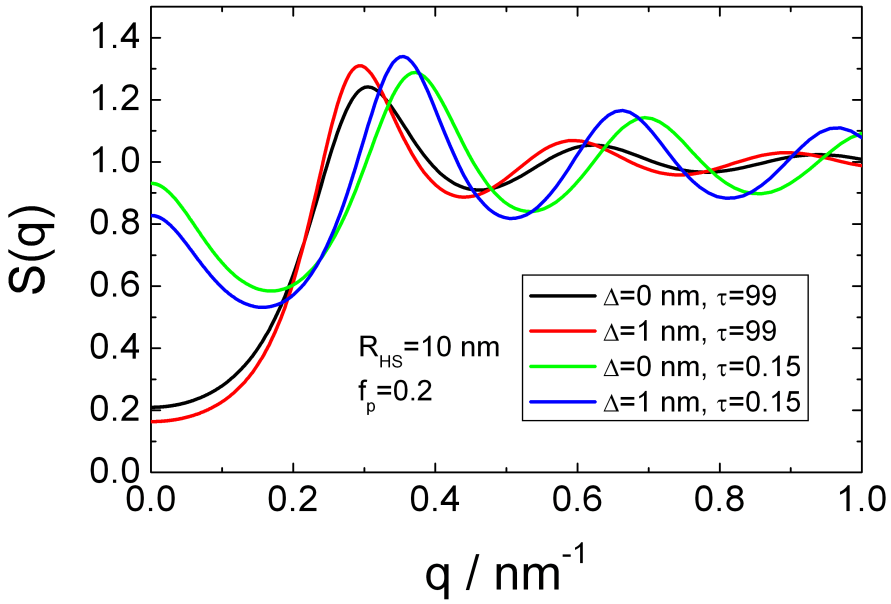

FIGURE 4.4. Structure factor $S(q)$ for a sticky hard sphere interaction potential for the different stickiness parameters τ.

4.2.4. Square Well Potential [89].

The Square well potential can be written as

$$U(r) = \begin{cases} \infty & \text{for} \quad 0 < r < \sigma \\ -\epsilon & \text{for} \quad \sigma < r < \lambda\sigma \\ 0 & \text{for} \quad r > \lambda\sigma \end{cases} \tag{4.33}$$

where λ and ϵ correspond to the breadth and the depth of the square well potential. The structure factor $S(Q)$ is than given by the following relations:

$$S(Q) = \frac{1}{1 - C(Q)} \tag{4.34a}$$

$$\begin{aligned} C(Q) = &- \frac{24\eta}{(Q\sigma)^6}\Big\{\alpha(Q\sigma)^3\left[\sin(Q\sigma) - Q\sigma\cos(Q\sigma)\right] \\ &+ \beta(Q\sigma)^2\left[2Q\sigma\sin(Q\sigma) - (Q^2\sigma^2 - 2)\cos(Q\sigma) - 2\right] \\ &+ \gamma\left[(4Q^3\sigma^3 - 24Q\sigma)\sin(Q\sigma) - (Q^4\sigma^4 - 12Q^2\sigma^2 + 24)\cos(Q\sigma) + 24\right] \\ &- \frac{\epsilon}{k_BT}(Q\sigma)^3\left[\sin(\lambda Q\sigma) - \lambda Q\sigma\cos(\lambda Q\sigma) + Q\sigma\cos(Q\sigma) - \sin(Q\sigma)\right]\Big\} \end{aligned} \tag{4.34b}$$

where α, β and γ are given by

$$\alpha = \frac{(1+2\eta)^2 + \eta^3(\eta - 4)}{(1-\eta)^4} \tag{4.34c}$$

$$\beta = -\frac{1}{3}\eta\frac{18 + 20\eta - 12\eta^2 + \eta^4}{(1-\eta)^4} \tag{4.34d}$$

$$\gamma = \frac{1}{2}\eta\frac{(1+2\eta)^2 + \eta^3(\eta - 4)}{(1-\eta)^4} \tag{4.34e}$$

NOTE:
Values for the depth of $\epsilon > 1.5k_BT$ and for the volume fraction of $\eta > 0.08$ may give unphysical results when compared to Monte Carlo simulations according to [**89**].

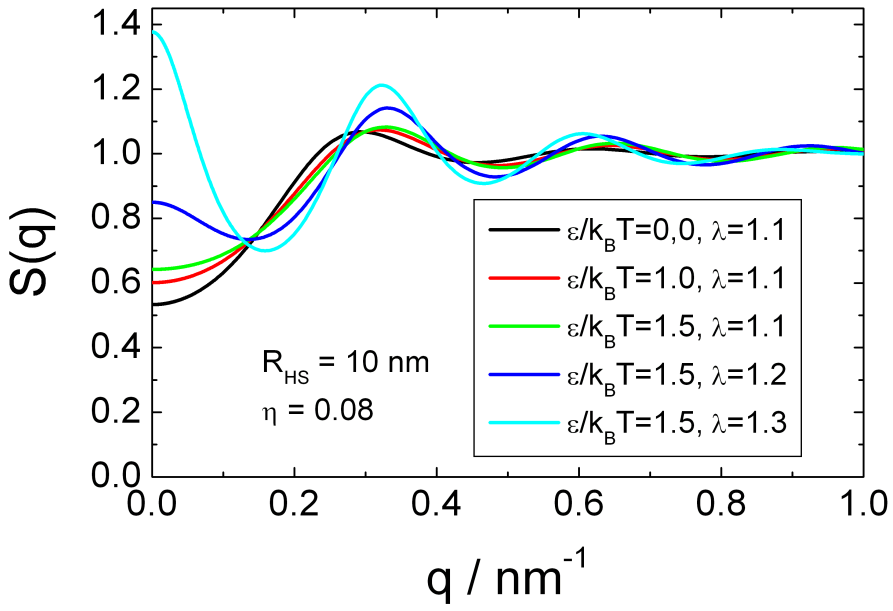

FIGURE 4.5. Structure factor $S(q)$ for a square well interaction potential.

4.2.5. Square Well Potential 2.

The Square well potential can be written as

$$U(r) = \begin{cases} \infty & \text{for} \quad 0 < r < \sigma \\ -\epsilon & \text{for} \quad \sigma < r < \sigma + \Delta \\ 0 & \text{for} \quad r > \sigma + \Delta \end{cases} \tag{4.35}$$

where Δ and ϵ correspond to the width and the depth of the square well potential. The structure factor $S(Q)$ is than given by the following relations:

$$S(Q) = 1 - 4\pi\rho\sigma^3 \frac{\sin(Q\sigma) - Q\sigma\cos(Q\sigma)}{Q^3\sigma^3} + 4\pi\rho\sigma^2 \left[e^{\frac{\epsilon}{k_B T}} - 1\right] \frac{\sin(Q\sigma)}{Q\sigma}\Delta \tag{4.36}$$

where σ is the particle diameter ($R_{HS} = \sigma/2$: hard sphere radius is requested by software as input parameter), Δ the width of the square well potential, ϵ (input value in software is ϵ/k_B, i.e. in Kelvin), T (in Kelvin) the sample temperature, the depth and ρ the colloid concentration, which is related to the colloid volume fraction η by $\eta = \pi\rho\sigma^3/6$.

4.3. Multi Lamellar Structures [70, 31]

4.3.1. Multi-Lamellar Structures, Thermal Disorder.

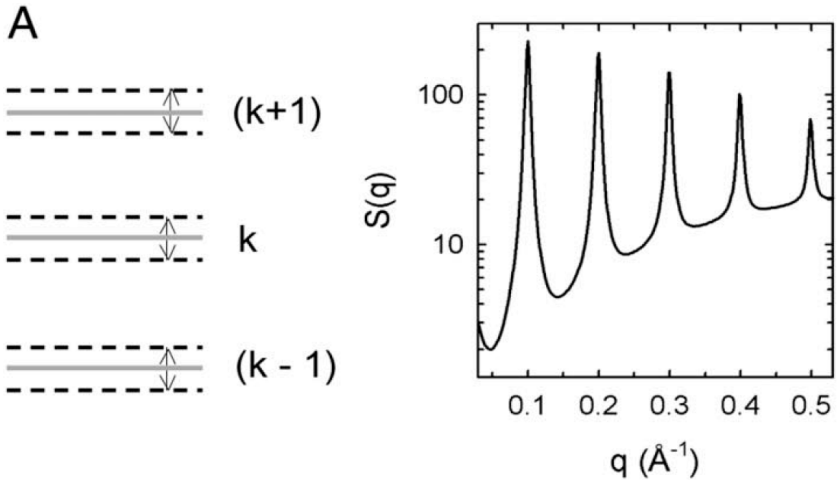

FIGURE 4.6. Thermal disorder, considering fluctuations of flat layers around well defined and evenly spaced equilibrium positions.

The first type describes thermal disorder (TD) caused by small fluctuations of the bilayers around well defined mean layer positions of equal separation (Fig. 4.6). In such a crystal lattice the long-range order is preserved and the structure factor for a single domain of size $L = Nd$ is identical to that of a perfect finite crystal multiplied by the well known Debye-Waller temperature factor, where $\Delta = \langle (d_k - d)^2 \rangle$ denotes the mean square fluctuations of the bilayers. As shown in Fig. 4.6, $S_{\mathrm{TD}}(Q)$ is characterized by a set of Bragg peaks of equal width, the diffraction order amplitudes of which decrease exponentially with the Debye-Waller factor. The lost intensity is found as a diffuse background scattering, which increases to the limit of N for large Q.

$$S_{\mathrm{TD}}(Q, N, d, \Delta, N_{\mathrm{diff}}) = N_{\mathrm{diff}} + \sum_{N_k = N-2\sigma}^{N+2\sigma} x_k S_{\mathrm{k,TD}} \tag{4.37}$$

with

$$S_{\mathrm{k,TD}} = \left(N_k + 2 \exp\left(-\frac{Q^2 \Delta^2}{2} \right) \sum_{m=1}^{N_k - 1} (N_k - m) \cos(mQd) \right) \tag{4.38}$$

N_{diff} accounts for an additional diffuse background, due to a number of uncorrelated scattering bilayers in $S_{\mathrm{TD}}(Q, N, d, \Delta, N_{\mathrm{diff}})$, which is not included in the TD theory. Its origin is attributed to bilayers with strong lattice defects or unilamellar vesicles, which display neither short-range nor (quasi-) long-range order.

The structure factors $S_{\mathrm{k,TD}}(Q)$ with low, but fixed stacking numbers N show oscillations at low Q (as can be seen in Fig. 4.6), but no such oscillations are found in experimental data. This can be understood as the consequence of polydispersity in the

size of the different stacks. In order to eliminate these artifacts from strictly monodisperse systems, we use a 'polydisperse' structure factor, i.e. we use an average of a series of structure factors with varying numbers of bilayers [**31**]. The analytical form of the distribution is not known a priori. We use a Gaussian distribution approximated by a discrete series The standard deviation σ for the Gaussian-weighted distribution is chosen as

$$\sigma = \begin{cases} \sqrt{N} & \text{for} N \geq 5, \\ 0.5(N-1) & \text{for} N < 5 \end{cases} \tag{4.39}$$

Therefore, N must be greater or equal to 2, which is a reasonable restriction for multilamellar stacks of bilayers. In the range of $N \pm 2\sigma$, structure factors weighted by

$$x_k = \frac{1}{\sigma\sqrt{2\pi}} \exp\left[-\frac{(N_k - N)^2}{2\sigma^2}\right] \tag{4.40}$$

are calculated, where N is the mean number of stacks and N_k is one of the bilayers in the range $N \pm 2\sigma$. This polydispersity model does not introduce new free parameters and is symmetrical around the mean N.

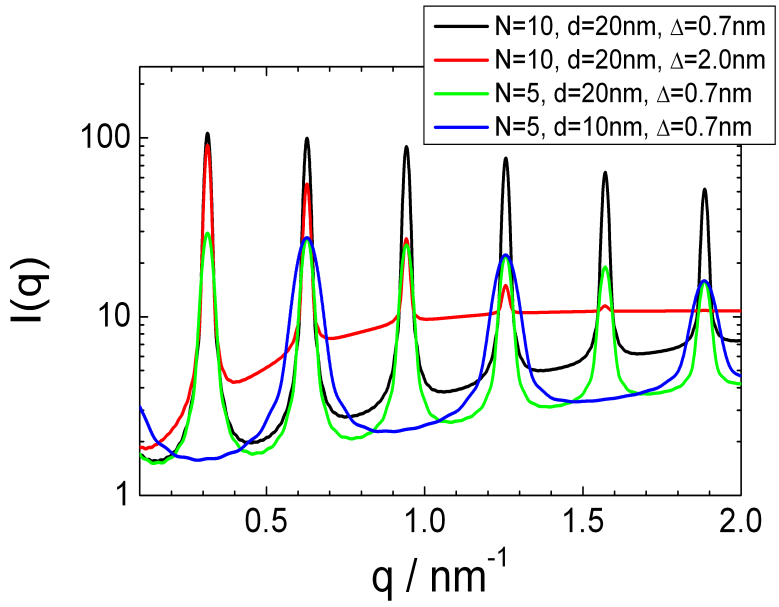

FIGURE 4.7. Structure factor of multi-lamellar structures with thermal disorder.

Input Parameters for model `ThermalDisorder`:

`N`: mean number of stacks N
`d`: stacking separation d
`Delta`: Debye-Waller disorder parameter Δ
`Nu`: number of uncorrelated scattering bilayers N_{diff}

Note:

- This structure factor is intended to be used with the `monodisperse approximation`.

4.3.2. Multi-Lamellar Structures, Paracrystalline Theory.

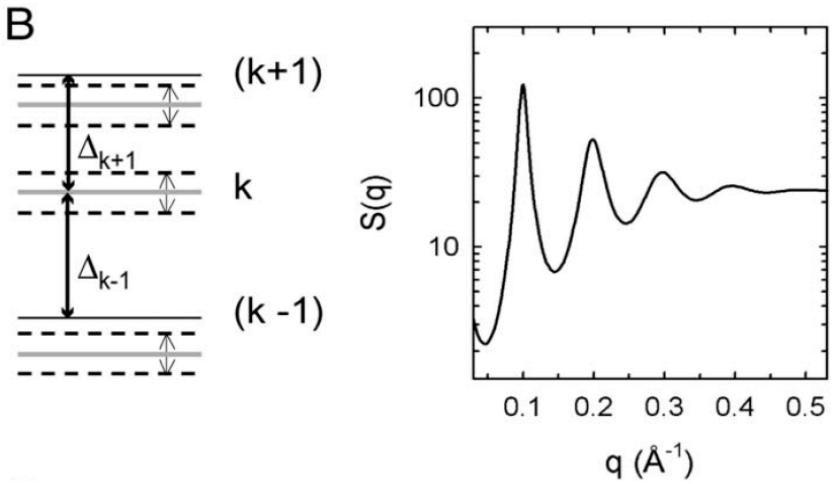

FIGURE 4.8. Stacking disorder as described within paracrystalline theory (PT) is due to displacements from the mean layer positions.

The second type of disorder accounts for the presence of small variations in the bilayer separations (Fig. 4.8), so-called stacking disorder, and is described within the paracrystalline theory (PT) [**48, 36, 11**]. As the position of an individual fluctuating layer in a paracrystal is determined solely by its nearestneighbour membranes, the crystalline long-range order is lost. Still, we are able to observe Bragg-peak scattering due to the fact that there is quasi long-range order. However, these quasi-Bragg peaks will display a typical line shape. In the case of disorder of the second kind, the structure factor derived from paracrystalline theory is given by [**36**]

$$S_{\mathrm{PT}}(Q, N, d, \Delta, N_{\mathrm{diff}}+) = N_{\mathrm{diff}} + \sum_{N_k=N-2\sigma}^{N+2\sigma} x_k S_{\mathrm{k,PT}} \tag{4.41}$$

with

$$S_{\mathrm{k,PT}} = \left(N_k + 2 \sum_{m=1}^{N_k-1} (N_k - m) \cos(mQd) \exp\left(-\frac{m^2 Q^2 \Delta^2}{2} \right) \right) \tag{4.42}$$

N_{diff} accounts for an additional diffuse background, due to a number of uncorrelated scattering bilayers in $S_{\mathrm{PT}}(Q, N, d, \Delta, N_{\mathrm{diff}})$, which is not included in the paracrystalline theory. Its origin is attributed to bilayers with strong lattice defects or unilamellar vesicles, which display neither short-range nor (quasi-) long-range order.

Fig. 4.8 shows that the quasi-Bragg peak intensity decreases for $S_{\mathrm{PT}}(Q)$, as in the previous case of thermal disorder. However, the decrease in peak height is also accompanied by a progressive broadening proportional to the square of the diffraction order h [**88**]. The line shape of the tails is essentially Lorentzian with

$$S_{\mathrm{k,PT}}(Q) \propto (Q - Q_h)^2,$$

where Q_h is the position of the h^{th} diffraction order in Q space. Again, the loss in intensity shows up as diffuse background scattering, which is stronger than from pure thermal disorder.

The structure factors $S_{\text{k,PT}}(Q)$ with low, but fixed stacking numbers N show oscillations at low Q (as can be seen in Fig. 4.8), but no such oscillations are found in experimental data. This can be understood as the consequence of polydispersity in the size of the different stacks. In order to eliminate these artifacts from strictly monodisperse systems, we use a 'polydisperse' structure factor, i.e. we use an average of a series of structure factors with varying numbers of bilayers [**31**]. The analytical form of the distribution is not known a priori. We use a Gaussian distribution approximated by a discrete series The standard deviation σ for the Gaussian-weighted distribution is chosen as

$$\sigma = \begin{cases} \sqrt{N} & \text{for} N \geq 5, \\ 0.5(N-1) & \text{for} N < 5 \end{cases} \tag{4.43}$$

Therefore, N must be greater or equal to 2, which is a reasonable restriction for multilamellar stacks of bilayers. In the range of $N \pm 2\sigma$, structure factors weighted by

$$x_k = \frac{1}{\sigma\sqrt{2\pi}} \exp\left[-\frac{(N_k - N)^2}{2\sigma^2}\right] \tag{4.44}$$

are calculated, where N is the mean number of stacks and N_k is one of the bilayers in the range $N \pm 2\sigma$. This polydispersity model does not introduce new free parameters and is symmetrical around the mean N.

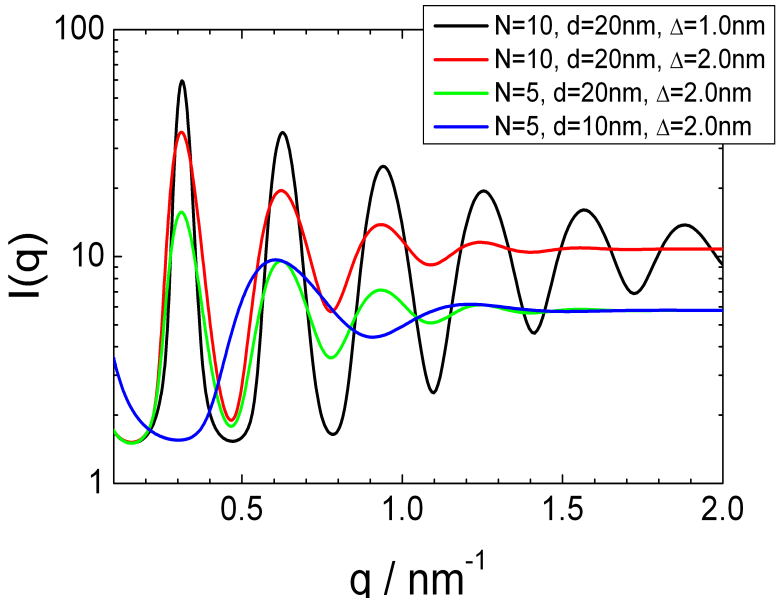

FIGURE 4.9. Structure factor of multi-lamellar structures with paracrystalline disorder.

Input Parameters for model `Paracrystalline`:

`N:` mean number of stacks N
`d:` stacking separation d
`Delta:` stacking disorder parameter Δ
`Nu:` number of uncorrelated scattering bilayers N_{diff}

Note:

- This structure factor is intended to be used with the `monodisperse approximation`.

4.3.3. Multi-Lamellar Structures, Modified Caillé Theory.

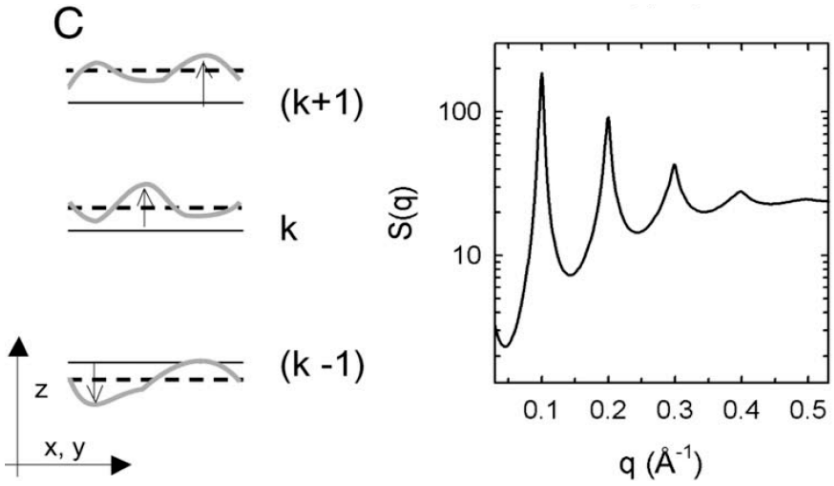

FIGURE 4.10. Bending fluctuation disorder is a particular feature of the L_α (smectic A) phase and is caused by bilayer undulations. The particular shape of the Bragg peaks is given by the modified Caillé theory (MCT).

There is another type of disorder when bilayer bending fluctuations are considered (Fig. 4.10). Such fluctuations are particularly pronounced in the fluid L_α phase (equivalent to smectic A). Caillé Bending fluctuation disorder is a particular feature of the L_α (smectic A) phase and is caused by bilayer undulations. The particular shape of the Bragg peaks is given by the modified Caillé theory (MCT). [**16**] realized the impact on the structure factor, which in a modified version [**108**] of the Caillé theory (MCT) is

$$S_{\mathrm{MC}}(Q, N, d, \eta_1, \gamma, N_{\mathrm{diff}}) = N_{\mathrm{diff}} + \sum_{N_k=N-2\sigma}^{N+2\sigma} x_k S_{\mathrm{k,MC}} \tag{4.45}$$

with

$$S_{\mathrm{k,MC}} = N_k + 2\sum_{m=1}^{N_k-1}(N_k - m)\cos(mQd)\; e^{-\left(\frac{d}{2\pi}\right)^2 Q^2\eta_1\gamma}\; (\pi m)^{-(d/2\pi)^2 Q^2\eta_1} \tag{4.46}$$

Here, γ is Euler's constant and

$$\eta = \pi k_B T/2d^2(BK_c)^{1/2}$$

is the Caillé parameter, which is a measure for the bilayer fluctuations and is inversely proportional to the square root of the bilayer bending rigidity K_c times the bulk modulus of compression B (De Gennes & Prost, 1993). Therefore, a lineshape analysis of the quasi-Bragg peaks opens an important experimental window on interbilayer interactions. Further, K_c and B can be decoupled as demonstrated recently by hydration studies [**79, 70**], or more elegantly by measuring multibilayers aligned on a solid substrate [**61**]. N_{diff} accounts for an additional diffuse background, due to a number of uncorrelated scattering bilayers in $S_{\mathrm{MC}}(Q, N, d, \eta_1, \gamma, N_{\mathrm{diff}})$, which is not included in the MCT. Its

origin is attributed to bilayers with strong lattice defects or unilamellar vesicles, which display neither short-range nor (quasi-) long-range order.

Fig. 4.10 shows a typical example of $S_{\mathrm{k,MCT}}(Q)$, which is similar to $S_{\mathrm{PT}}(Q)$ with respect to the progressive decrease in peak height and increase in peak width, but which differs significantly in line shape as

$$S_{\mathrm{k,MCT}} \propto (Q - Q_h)^{-1+\eta h^2}$$

for randomly oriented scattering domains [**86, 108**].

The structure factors $S_{\mathrm{k,MCT}}(Q)$ with low, but fixed stacking numbers N show oscillations at low Q (as can be seen in Fig. 4.10), but no such oscillations are found in experimental data. This can be understood as the consequence of polydispersity in the size of the different stacks. In order to eliminate these artifacts from strictly monodisperse systems, we use a 'polydisperse' structure factor, i.e. we use an average of a series of structure factors with varying numbers of bilayers [**31**]. The analytical form of the distribution is not known a priori. We use a Gaussian distribution approximated by a discrete series The standard deviation σ for the Gaussian-weighted distribution is chosen as

$$\sigma = \begin{cases} \sqrt{N} & \text{for} N \geq 5, \\ 0.5(N-1) & \text{for} N < 5 \end{cases} \tag{4.47}$$

Therefore, N must be greater or equal to 2, which is a reasonable restriction for multilamellar stacks of bilayers. In the range of $N \pm 2\sigma$, structure factors weighted by

$$x_k = \frac{1}{\sigma\sqrt{2\pi}} \exp\left[-\frac{(N_k - N)^2}{2\sigma^2}\right] \tag{4.48}$$

are calculated, where N is the mean number of stacks and N_k is one of the bilayers in the range $N \pm 2\sigma$. This polydispersity model does not introduce new free parameters and is symmetrical around the mean N.

Input Parameters for model `ModifiedCaile`:

- `N:` mean number of stacks N
- `d:` stacking separation d
- `eta:` the Caillé parameter η is a measure for the bilayer fluctuations and inversely proportional to the square root of the bilayer bending rigidity
- `Nu:` number of uncorrelated scattering bilayers N_{diff}

Note:

- This structure factor is intended to be used with the `monodisperse approximation`.

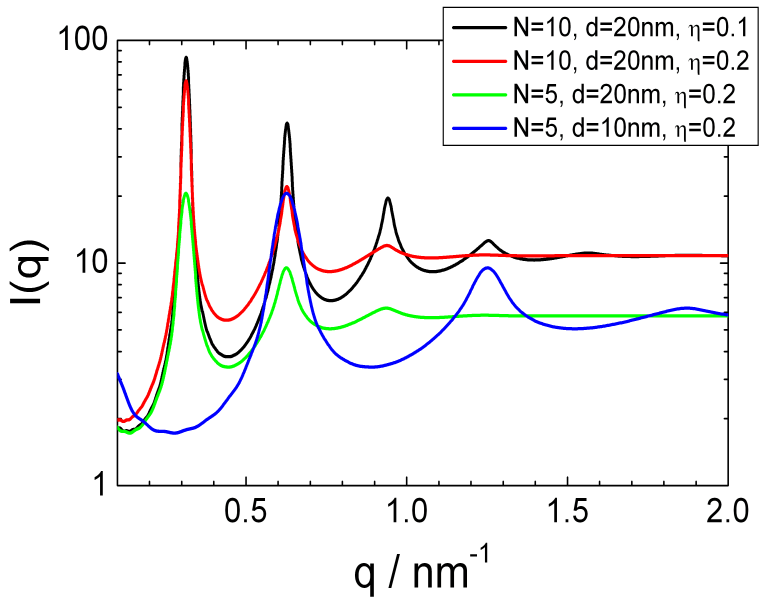

FIGURE 4.11. Structure factor of multi-lamellar structures according to the modified Caillé theory.

4.4. Mass Fractal

For a fractal object, the structure factor $S(q)$ can be calculated [**92, 91**] via the pair correlation function $g(r)$, which describes the total number of particles within a sphere of radius r centered in a central particle and is given (for dim = 3) by

$$N(r) = \Phi \int_0^r g(r)\, 4\pi r^2\, dr \tag{4.49}$$

or

$$\mathrm{d}N(r) = \Phi g(r)\, 4\pi r^2\, dr \tag{4.50}$$

On the other hand, a fractal object is characterized by a spatial distribution of the individual scatterers given by

$$N(r) = \left(\frac{r}{r_0}\right)^D \tag{4.51}$$

where r_0 is the gauge of the measurement, which has the magnitude of the characteristic dimension of each individual scatterer. Differentiation of 4.51 and identification with 4.50 gives

$$\Phi g(r) = \frac{D}{4\pi r_0^D} r^{D-3} \tag{4.52}$$

Because D is smaller than 3, $g(r)$ goes to zero at large r. This is clearly unphysical. At some large scale, the sample will show a macroscopic density. A good knowledge of the sample allows in general a reasonable assumption for the large-scale behavior of $g(r)$. Therefore a cut-off function $h(r, \xi)$ has to be introduced, where ξ is a cut-off distance, to describe the behavior of the pair correlation function at large distances. To derive the analytical form of $S(q)$ within this assumption, one can use the general theory of liquids, where the uniform density is subtracted to avoid a divergence in the evaluation of $S(q)$. We then write

$$4\pi\Phi[g(r) - 1] = \frac{D}{r_0^D}\, r^{D-3} h(r, \xi) \tag{4.53}$$

The meaning of ξ is only qualitative and has to be made precise in any particular situation. Generally speaking, it represents the characteristic distance above which the mass distribution in the sample is no longer described by the fractal law. In practice, it can represent the size of an aggregate or a correlation length in a disordered material. For isotropic systems

$$S(q) = 1 + 4\pi\Phi \int_0^\infty [g(r) - 1] \frac{\sin(qr)}{qr}\, r^2\, dr \tag{4.54}$$

Combined with 4.53 one gets

$$S(q) = 1 + \frac{D}{r_0^D} \int_0^\infty r^{D-3} h(r, \xi) \frac{\sin(qr)}{qr}\, r^2\, dr \tag{4.55}$$

Several cut-off functions $h(r,\xi)$ have been discussed in the literature and compared by Sorensen et al. [**92, 91**].

$$h_{\text{Exp}}(r,\xi) = \exp\left[-\frac{r}{\xi}\right] \tag{4.56}$$

$$h_{\text{Gauss}}(r,\xi) = \exp\left[-\left(\frac{r}{\xi}\right)^2\right] \tag{4.57}$$

$$h_{\text{Exp(-x^a)}}(r,\xi,\alpha,D) = \exp\left[-\left(\frac{r}{\xi}\right)^{\alpha}\right] \tag{4.58}$$

$$h_{\text{OverlapSph}}(r,\xi) = \begin{cases} \left(1+\frac{r}{4\xi}\right)\left(1-\frac{r}{2\xi}\right)^2 & \text{for } r \le 2\xi \\ 0 & \text{for } r > 2\xi \end{cases} \tag{4.59}$$

For the cut-off functions 4.56 and 4.57 the integral 4.55 can be solved analytically and the corresponding structure factors are given by

$$S_{\text{Exp}}(q,\xi,D,r_0) = 1 + \frac{D\Gamma(D-1)\sin\left([D-1]\arctan(q\xi)\right)}{(qr_0)^D\left[1+\frac{1}{q^2\xi^2}\right]^{(D-1)/2}} \tag{4.60}$$

$$S_{\text{Gauss}}(q,\xi,D,r_0) = 1 + \Gamma\left[\frac{D}{2}\right]\frac{D}{2}\left(\frac{\xi}{r_0}\right)^D {}_1F_1\left[\frac{D}{2},\frac{3}{2},-\frac{q^2\xi^2}{8}\right] \tag{4.61}$$

where D is the fractal dimension, ξ is a cut-off length for the fractal correlations, $\Gamma(x)$ is the gamma function. ${}_1F_1\,[]$ is the Kummer or hypergeometric function. For the cut-off functions 4.58 and 4.59 the integral 4.55 is solved numerically.

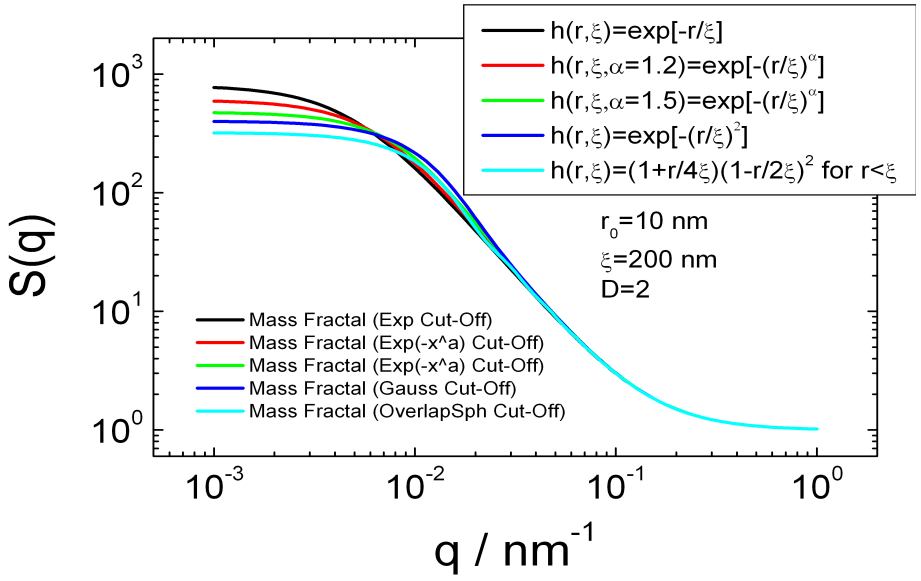

FIGURE 4.12. Comparison of the different structure factors for mass fractals.

4.4.1. Mass Fractal (Exp Cut-Off).

Input Parameters for model `Mass Fractal (Exp Cut-Off)`:

`r0`: characteristic dimension of individual scattering objects r_0
`xi`: cut-off length for the fractal correlations ξ
`D`: fractal dimension D

Note:

- D needs to be larger than 1 ($D > 1$). Physical values for D are between 1 and 3 ($1 < D < 3$).
- The fractal dimension needs to be large than the size of the individual scattering objects ($r_0 < \xi$).

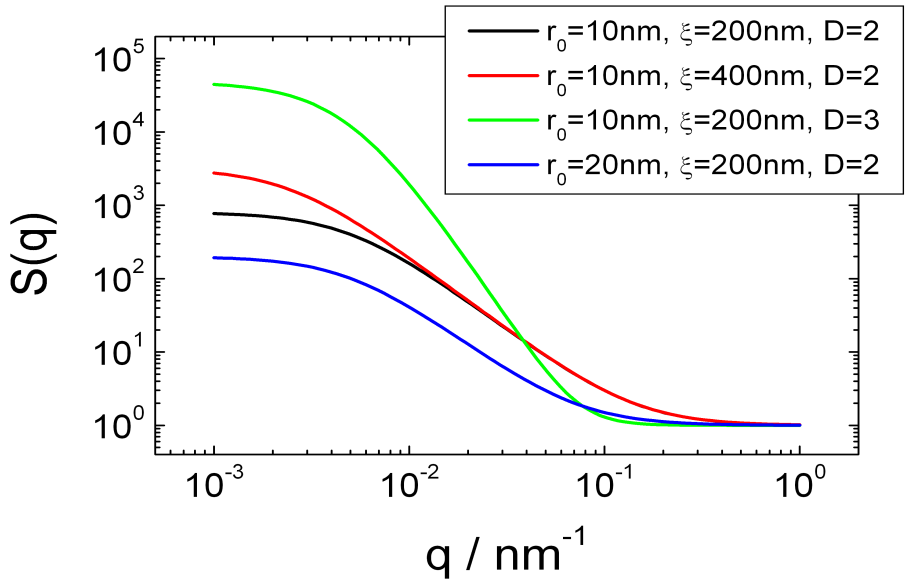

FIGURE 4.13. Structure factor of a mass fractal with an exponential cut-off function $h_{\text{Exp}}(r,\xi) = \exp\left[-\left(\frac{r}{\xi}\right)^{\alpha}\right]$.

4.4.2. Mass Fractal (Exp(-xˆa) Cut-Off).

Input Parameters for model `Mass Fractal (Exp(-xˆa) Cut-Off)`:

`r0`: characteristic dimension of individual scattering objects r_0
`xi`: cut-off length for the fractal correlations ξ
`D`: fractal dimension D

Note:

- D needs to be larger than 1 ($D > 1$). Physical values for D are between 1 and 3 ($1 < D < 3$).
- The fractal dimension needs to be large than the size of the individual scattering objects ($r_0 < \xi$).
- the exponents α should be larger than 1, as otherwise the integral 4.55 for $S(q)$ does not converges.

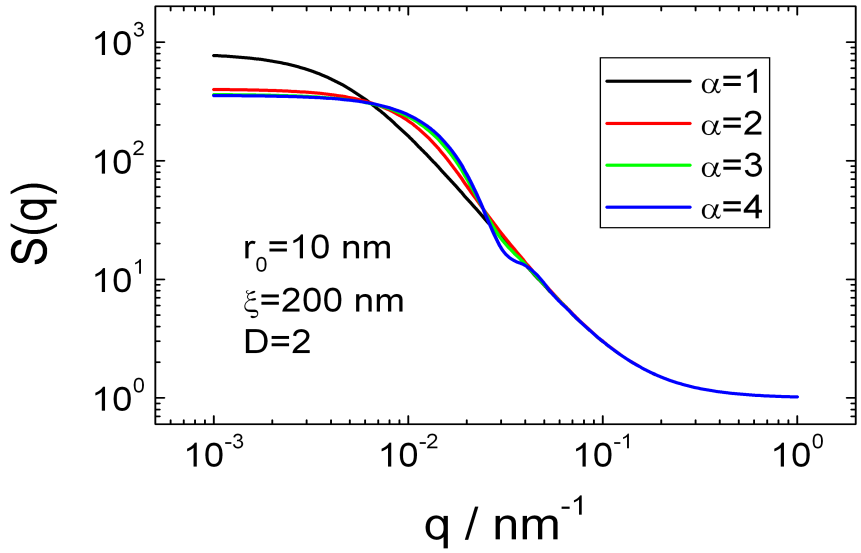

FIGURE 4.14. Structure factor of a mass fractal with a cut-off function $h_{\text{Exp(-xˆa)}}(r, \xi, \alpha) = \exp\left[-\left(\frac{r}{\xi}\right)^{\alpha}\right]$.

4.4.3. Mass Fractal (Gaussian Cut-Off).

Input Parameters for model `Mass Fractal (Gaussian Cut-Off)`:

`r0`: characteristic dimension of individual scattering objects r_0
`xi`: cut-off length for the fractal correlations ξ
`D`: fractal dimension D

Note:

- D needs to be larger than 1 ($D > 1$). Physical values for D are between 1 and 3 ($1 < D < 3$).
- The fractal dimension needs to be large than the size of the individual scattering objects ($r_0 < \xi$).

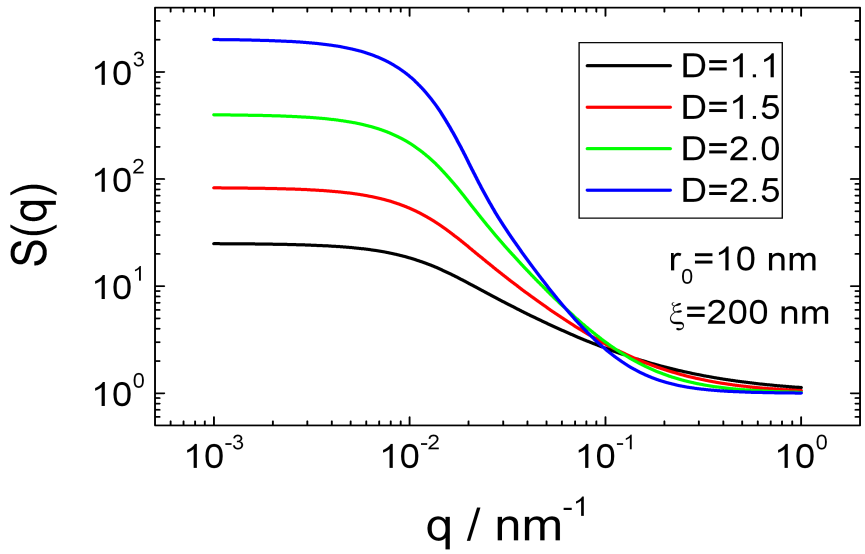

FIGURE 4.15. Structure factor of a mass fractal with an Gaussian cut-off function $h_{\text{Gauss}}(r,\xi) = \exp\left[-\left(\frac{r}{\xi}\right)^2\right]$.

4.4.4. Mass Fractal (OverlapSph Cut-Off).

Input Parameters for model `Mass Fractal (OverlapSph Cut-Off)`:

`r0`: characteristic dimension of individual scattering objects r_0
`xi`: cut-off length for the fractal correlations ξ
`D`: fractal dimension D

Note:

- D needs to be between 1 and 3 ($1 < D < 3$).
- The fractal dimension needs to be large than the size of the individual scattering objects ($r_0 < \xi$).

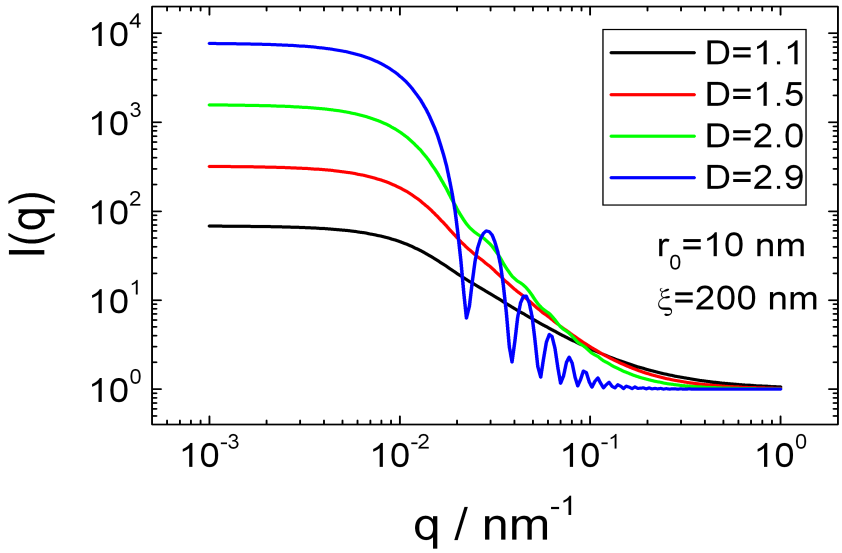

FIGURE 4.16. Structure factor of a mass fractal with a cut-off function $h_{\text{OverlapSph}}(r,\xi) = \left(1+\frac{r}{4\xi}\right)\left(1-\frac{r}{2\xi}\right)^2$ for $r \leq 2\xi$.

4.5. Other Structure Factors

4.5.1. Hayter-Penfold RMSA [43, 41]. This is the structure factor for a system of charged, spheroidal objects in a dielectric medium. When combined with an appropriate form factor (such as sphere, core+shell, ellipsoid etc.), this allows for inclusion of the interparticle interference effects due to screened coulomb repulsion between charged particles. The salt concentration, is used to compute the ionic strength of the solution which in turn is used to compute the Debye screening length. At present there is no provision for entering the ionic strength directly nor for use of any multivalent salts. The counterions are also assumed to be monovalent.

Input Parameters for model `Hayter Penfold RMSA`:

`RHS:` hard sphere radius R_{HS} of particles in [nm].
`Z:` charge of particle in units of the charge of an electron e =?$1.60217653 \times 10^{?19}$C
`eta:` volume fraction η of particles
`T:` sample temperature T in Kelvin
`salt:` monovalent salt concentration in [M]
`eps_r:` dielectric constant ϵ_r of solvent

4.5.2. MacroIon.

$$ETA = \text{volume fraction} \tag{4.62a}$$

$$AK = \kappa\sigma = \text{inv. screening length times diameter} \tag{4.62b}$$

$$\kappa = \sqrt{e^2/(\epsilon\epsilon_0 k_B T) * (\rho_c + 2\rho_s)} \tag{4.62c}$$

$$\rho_c = \text{density of counterions} = \rho_{\text{colloids}} Z \tag{4.62d}$$

$$\rho_s = \text{density of salt cations or anions} \tag{4.62e}$$

$$GEK = \text{charge}^2/(\pi k_B T \epsilon\epsilon_0 \sigma (2 + AK)^2) \tag{4.62f}$$

$$\text{charge} = \text{Ladung eines Kolloids} = eZ \tag{4.62g}$$

$$S = ETA^{1./3} = \text{scaling factor for rescaled MSA (RMSA)} \tag{4.62h}$$

$$GAMK = 2 * S * GEK * \exp(AK - AK/S). \tag{4.62i}$$

4.5.3. Critical Scattering.

$$S_{\text{crit}}(Q) = 1 + \frac{\kappa}{1 + \zeta^2 Q^2} \tag{4.63}$$

ζ: correlation length, κ: scaling factor

4.5.4. Correlation Hole.

$$S_{\text{corr. hole}}(Q, h, \eta) = 1 + \eta\Phi(Qh) \tag{4.64}$$

$\Phi(x) = 3\frac{\sin(x) - x\cos(x)}{x^3}$ η: volume fraction, h: hole radius

4.5.5. Random Distribution Model.

$$S_{\text{RDM}}(Q) = \frac{1}{1 + 8\frac{V_{ca}/V_p}{\epsilon}\Phi(x)} \tag{4.65}$$

$x = 2QR_{ca}$
$V_{ca} = \frac{4}{3}\pi R_{ca}^3$
$V_p = \frac{4}{3}\pi R^3/f_p$
$\Phi(x) = 3\frac{\sin(x) - x\cos(x)}{x^3}$

4.5.6. Local Order Model.

$$S_{\text{LOM}}(Q) = 1 + 4\frac{\sin(QD)}{QD} - z\Phi(x); \tag{4.66}$$

$x = \alpha QD$
$\Phi(x) = 3\frac{\sin(x) - x\cos(x)}{x^3}$

4.5.7. Cylinder(PRISM).

$$S_{\text{Cyl,PRISM}} = \frac{1}{1 + \nu C_q P_{15}} \tag{4.67}$$

$x = 2QR$

$x_{P15} = Q(L - 2R)$

$$P_{15} = 2\frac{\text{Si}(x_{P15})}{x_{P15}} - 4\frac{\sin^2(x_{P15}/2)}{x_{P15}^2}$$

$$C_q = 3\frac{\sin(x) - x\cos(x)}{x^3}$$

4.5.8. Voigt Peak.

In spectroscopy, the Voigt profile is a spectral line profile named after Woldemar Voigt and found in all branches of spectroscopy in which a spectral line is broadened by two types of mechanisms, one of which alone would produce a Doppler profile, and the other of which would produce a Lorentzian profile. All normalized line profiles can be considered to be probability distributions. The Doppler profile is essentially a normal distribution and a Lorentzian profile is essentially a Cauchy distribution. Without loss of generality, we can consider only centered profiles which peak at zero. The Voigt profile is then the convolution of a Lorentzian profile and a Doppler profile:

$$V(x|\sigma,\gamma) = \int_{\infty}^{\infty} D(x'|\sigma)\, L(x-x'|\gamma)\, dx' \tag{4.68a}$$

where x is frequency from line center, $D(x|\sigma)$ is the centered Doppler profile:

$$D(x|\sigma) = \frac{e^{-x^2/2\sigma^2}}{\sigma\sqrt{2\pi}} \tag{4.68b}$$

and $L(x|\gamma)$ is the centered Lorentzian profile:

$$L(x|\gamma) = \frac{\gamma}{\pi(x^2+\gamma^2)}. \tag{4.68c}$$

The defining integral can be evaluated as:

$$V(x) = \frac{\Re[w(z)]}{\sigma\sqrt{2\pi}} \tag{4.68d}$$

where $\Re[w(z)]$ is the real part of the complex error function of z and

$$z = \frac{x+i\gamma}{\sigma\sqrt{2}} \tag{4.68e}$$

$$S_{\text{Voigt}}(Q, Q_m, A, \sigma, \gamma, c_0) = A\; V(Q-Q_m|\sigma,\gamma) + c_0 \tag{4.68f}$$

CHAPTER 5

Size Distributions

5.1. Delta

Choosing `Delta` as a size distribution simply scales the form factor with a constant value N

Input Parameters for size distribution `Delta`:

`N:` particle number density N

5.2. Uniform distribution

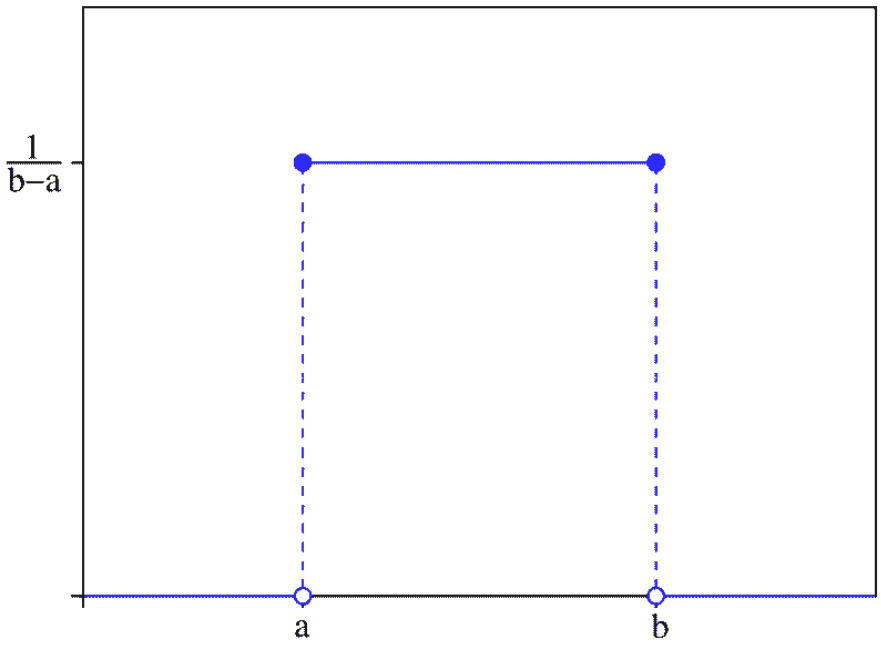

FIGURE 5.1. Uniform distribution function. $x_{\min}, x_{\max} \in (-\infty, \infty)$, $x_{\max} > x_{\min}$, $x_{\min} \leq x \leq x_{\max}$

The uniform distribution defines equal probability over a given range for a continuous distribution. The support is defined by the two parameters, $x_{\min}$ and $x_{\max}$, which are its minimum and maximum values.

$$\text{Uniform}(x|N, x_{\min}, x_{\max}) = \begin{cases} \dfrac{N}{x_{\max} - x_{\min}} & \text{for} \quad x_{\min} \leq x \leq x_{\max}, \\ 0 & \text{for} \quad x < x_{\min} \text{ or } x > x_{\max} \end{cases} \tag{5.1a}$$

Input Parameters for size distribution `Uniform`:

`N:` particle number density N
`Xmin:` minimum value of the distribution ($x_{\min}$)
`Xmax:` maximum value of the distribution ($x_{\max}$)

5.3. Triangular distribution

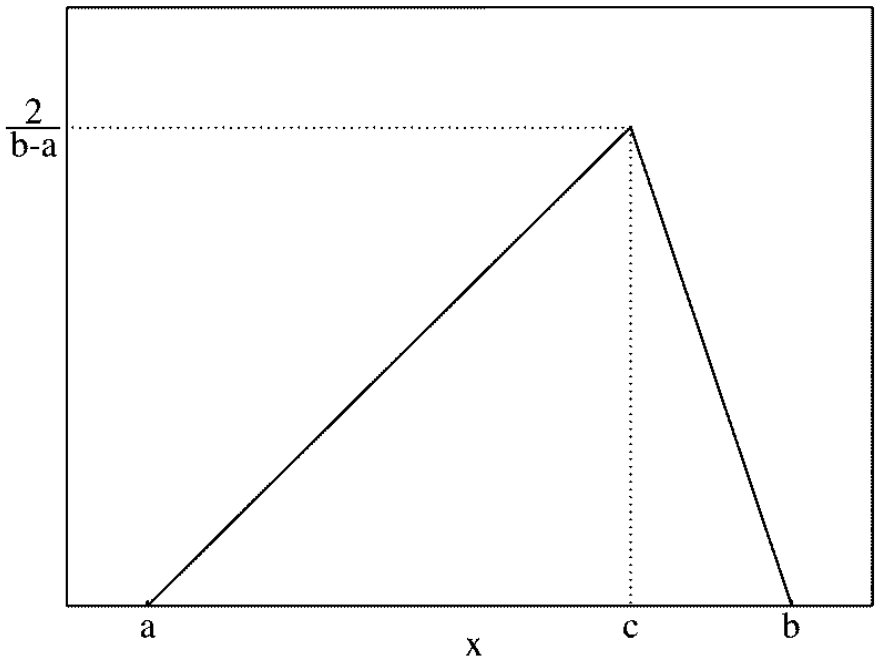

FIGURE 5.2. Triangular distribution function. $x_{\min}, x_{\mode}, x_{\max} \in (-\infty, \infty)$, $x_{\max} > x_{\min}$, $x_{\min} \leq x_{\mode} \leq x_{\max}$, $x_{\min} \leq x \leq x_{\max}$

$$\text{Triangular}(x|x_{\min}, x_{\max}, x_{\mode}) = \begin{cases} \dfrac{2(x - x_{\min})}{(x_{\max} - x_{\min})(x_{\mode} - x_{\min})} & \text{for} \quad x_{\min} < x \leq x_{\mode} \\ \dfrac{2(x_{\max} - x)}{(x_{\max} - x_{\min})(x_{\max} - x_{\mode})} & \text{for} \quad x_{\mode} < x \leq x_{\max} \end{cases} \tag{5.2a}$$

5.4. Log-Normal distribution

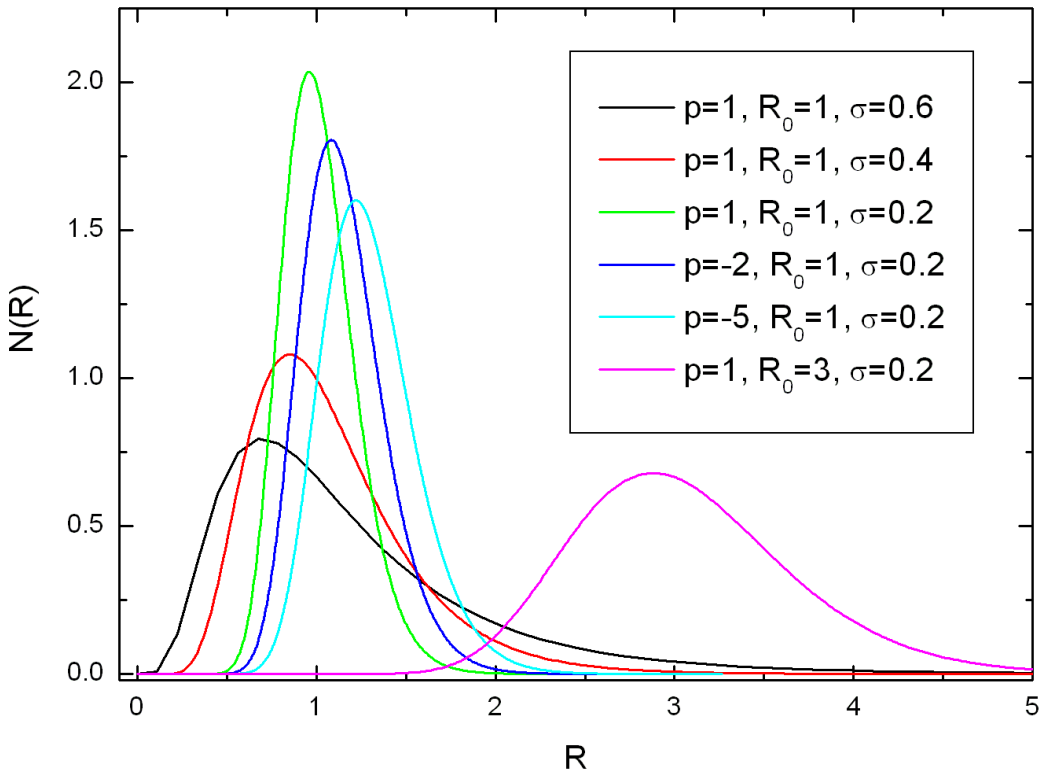

FIGURE 5.3. LogNormal distribution function ($R_0 = 1$ and $p = 1$ has been been set both to one here). Valid parameter ranges: $R \in (0, \infty)$, $R_0 \in (0, \infty)$, $\sigma \geq 0$, $p \in (-\infty, \infty)$

The `LogNorm` distribution is a continuous distribution in which the logarithm of a variable has a normal distribution.

$$\mathrm{LogNorm}(X, \mu, \sigma, p) = \frac{N}{c_{\mathrm{LN}}} \frac{1}{X^p} \exp\left(-\frac{\ln(X/\mu)^2}{2\sigma^2}\right) \tag{5.3a}$$

$$c_{\mathrm{LN}} = \sqrt{2\pi}\, \sigma\, \mu^{1-p} \exp\left((1-p)^2 \frac{\sigma^2}{2}\right) \tag{5.3b}$$

where σ is the width parameter, p a shape parameter, μ is the location parameter. c_{LN} is choosen so that $\int_0^\infty \mathrm{LogNorm}(X, \mu, \sigma, p)\, dX = N$ The mode of the distribution X_{mode} and the variance $\mathrm{Var}(X)$ are defined as

$$X_{\mathrm{mode}} = \mu e^{-p\sigma^2} \tag{5.4}$$

$$\mathrm{Var}(X) = \mu^2 \left(e^{\sigma^2} - 1\right) e^{(3-2p)\sigma^2} \tag{5.5}$$

and the m^{th} moment $\langle X^m \rangle$ of the `LogNorm` distribution as

$$\langle X^m \rangle = \frac{\int X^m\, \mathrm{LogNorm}(X)\, dX}{\int \mathrm{LogNorm}(X)\, dX} = \mu^m\, e^{\frac{1}{2}\sigma^2 m(2-2p+m)}. \tag{5.6}$$

5.5. Schulz-Zimm (Flory) distribution

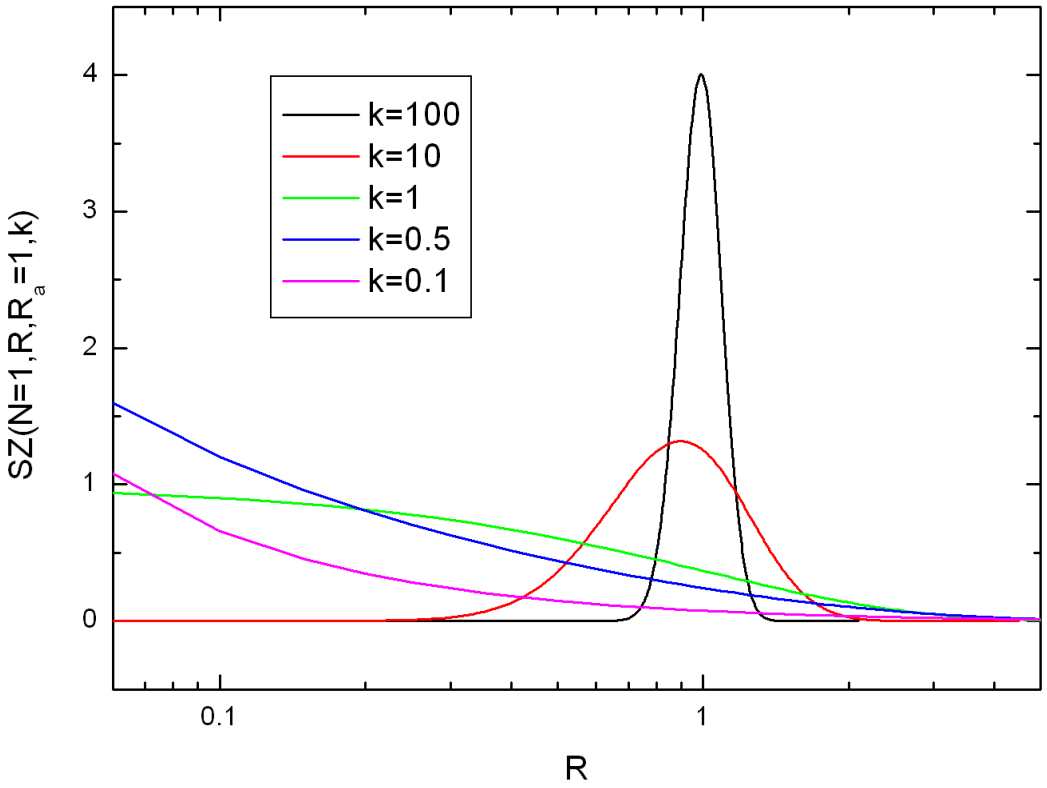

FIGURE 5.4. The $\mathrm{SZ}(X, N, X_a, k)$ distribution function. Valid parameter ranges: $X \in [0, \infty)$, $X_a \in (0, \infty)$, $k = X_a^2/\sigma^2 > 0$

A function commonly used to present polymer molecular weight distributions is the Schulz-Zimm function

$$\mathrm{SZ}_n(X, N, X_a, k) = \frac{N}{X_a}\left(\frac{X}{X_a}\right)^{k-1} \frac{k^k \exp(-kX/X_a)}{\Gamma(k)} \tag{5.7}$$

$\mathrm{SZ}_n(X, N, X_a, k)$ is normalized so that $\int_0^\infty \mathrm{SZ}_n(X, N, X_a, k)\, dX = N$. In polymer science X would be the molecular weight M, $\overline{M}_n = X_a$, and $\overline{M}_w = \overline{M}_n \frac{k+1}{k}$, and $\Gamma(k)$ is the gamma function. The above form (5.7) gives the number distribution. Its mode, mean, variance and m^{th}-moment are given by

$$X_{\text{mode}} = X_a\left(1 - \frac{1}{k}\right) \tag{5.8a}$$

$$X_{\text{mean}} = X_a \tag{5.8b}$$

$$\mathrm{Var}\,(X) = \sigma^2 = \frac{X_a^2}{k} \tag{5.8c}$$

$$\langle X^m \rangle = \left(\frac{X_a}{k}\right)^m \frac{\Gamma\,(k+m)}{\Gamma(k)} \tag{5.8d}$$

The corresponding weight distribution is

$$\mathrm{SZ}_w(X, N, X_a, k) = \frac{X}{X_a}\mathrm{SZ}_n(X, N, X_a, k) = \frac{NX^k \left(\frac{k}{X_a}\right)^{k+1} e^{-\frac{kX}{X_a}}}{\Gamma(k+1)} \tag{5.9}$$

Also $\mathrm{SZ}_w(X, N, X_a, k)$ is normalized so that $\int_0^\infty \mathrm{SZ}_w(X, N, X_a, k)\, dX = N$. The mode, mean, variance and m^{th}-moment of the weight distribution are given by

$$X_{\text{mode}} = X_a \tag{5.10a}$$

$$X_{\text{mean}} = X_a \frac{1+k}{k} \tag{5.10b}$$

$$\mathrm{Var}\,(X) = \sigma^2 = X_a^2 \frac{1+k}{k^2} \tag{5.10c}$$

$$\langle X^m \rangle = \left(\frac{X_a}{k}\right)^m \frac{\Gamma\,(k+m+1)}{\Gamma\,(k+1)} \tag{5.10d}$$

5.6. Gamma distribution

The Gamma distribution is a two parameter continuous distribution with a scale parameter θ and a shape parameter k.

$$\text{gammaSD}(x, N, x_{\text{mode}}, \sigma) = \frac{N}{\theta}\left(\frac{x}{\theta}\right)^{k-1}\frac{\exp(-x/\theta)}{\Gamma(k)} \tag{5.11}$$

The mean x_{mean}, mode x_{mode} and variane σ^2 of the distribution are given by

$$x_{\text{mean}} = k\theta \tag{5.12}$$

$$x_{\text{mode}} = (k-1)\theta \text{ for } k \geq 1 \tag{5.13}$$

$$\sigma^2 = k\theta^2 \tag{5.14}$$

The gamma distribution is more flexible than the exponential or ξ^2 distribution function which are special cases of the gamma distribution function. When k is large, the gamma distribution closely approximates a normal distribution with the advantage that the gamma distribution has density only for positive real numbers. For small values of k the distribution becomes a right tailed distribution.

The m^{th} moment $\langle X^m \rangle$ of the size distribution is given by

$$\langle X^m \rangle = \theta^m \frac{\Gamma(k+m)}{\Gamma(k)}. \tag{5.15}$$

In the present version the Gamma distribution is parametrised as a function of the mode and variance, i.e. with

$$k = \frac{x_{\text{mode}}\sqrt{x_{\text{mode}}^2 + 4\sigma^2} + x_{\text{mode}}^2 + 2\sigma^2}{2\sigma^2} \tag{5.16}$$

and

$$\theta = \frac{1}{2}\left(\sqrt{x_{\text{mode}}^2 + 4\sigma^2} - x_{\text{mode}}\right) \tag{5.17}$$

$\text{gammaSD}(R, N, R_m, \sigma)$ is normalized so that $\int_0^\infty \text{gammaSD}(R, N, R_m, \sigma)\, dR = N$.

Input Parameters for model `Sphere`:

`N:` N

`mode:` mod of the distribution (maximum, most probable size) $x_{\text{mode}} > 0$

`sigma:` width parameter $\sigma > 0$. The variance of the distribution is σ^2.

Note:

- The parameters `mode` and `sigma` needs to be positive.

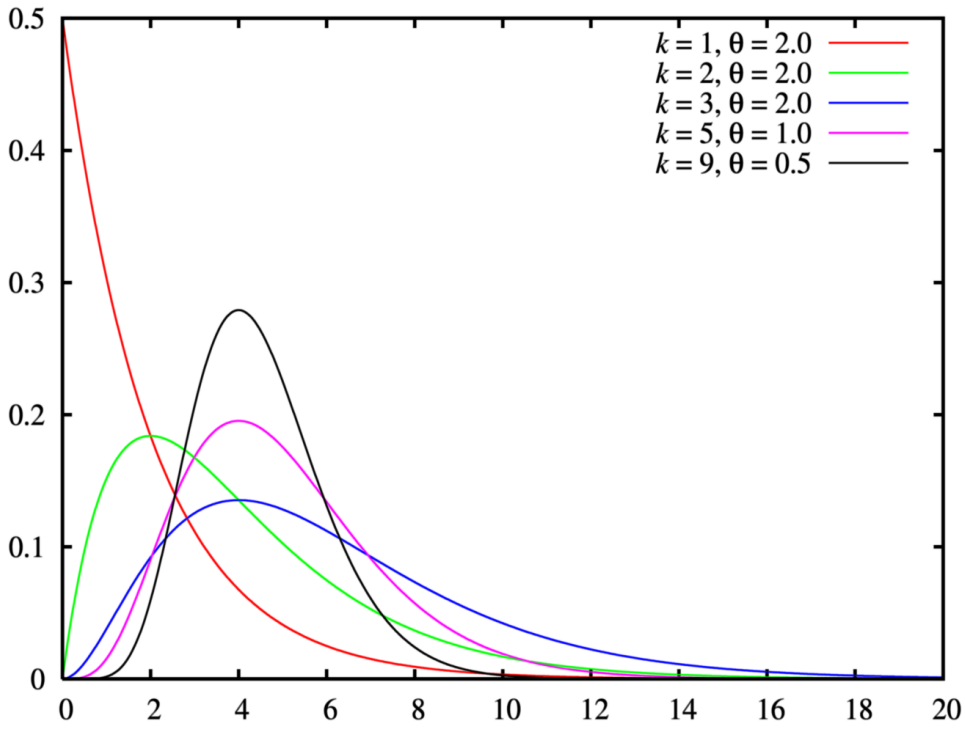

FIGURE 5.5. The gammaSD(R, N, x_{mode}, σ) distribution function. Valid parameter ranges: $x \in [0, \infty)$, $x_{\text{mode}} \in (0, \infty)$, $\sigma > 0$

5.7. PearsonIII distribution

The Pearson distribution is a family of probability distributions that are a generalisation of the normal distribution. The Pearson Type III distribution is given by the probability density function

$$f(x) = \frac{1}{\beta\,\Gamma(p)} \left(\frac{x-\alpha}{\beta} \right)^{p-1} e^{-(x-\alpha)/\beta}, \tag{5.18}$$

where $x \in [\alpha, \infty)$ and α, β and p are parameters of the distribution with $\beta > 0$ and $p > 0$ (Abramowitz and Stegun 1954, p. 930). Here, $\Gamma()$ denotes the Gamma function.

- Mean:
$$\alpha + p\beta$$
- Variance:
$$p\beta^2$$
- Skewness:
$$\frac{2}{\sqrt{p}}$$
- Kurtosis:
$$\frac{6}{p}$$

The Pearson Type III distribution is identical to the Gamma distribution (5.11). When $\alpha = 0$, $\beta = 2$, and p is half-integer, the Pearson Type III distribution becomes the χ^2 distribution of $2p$ degrees of freedom.

5.8. Gauss distribution

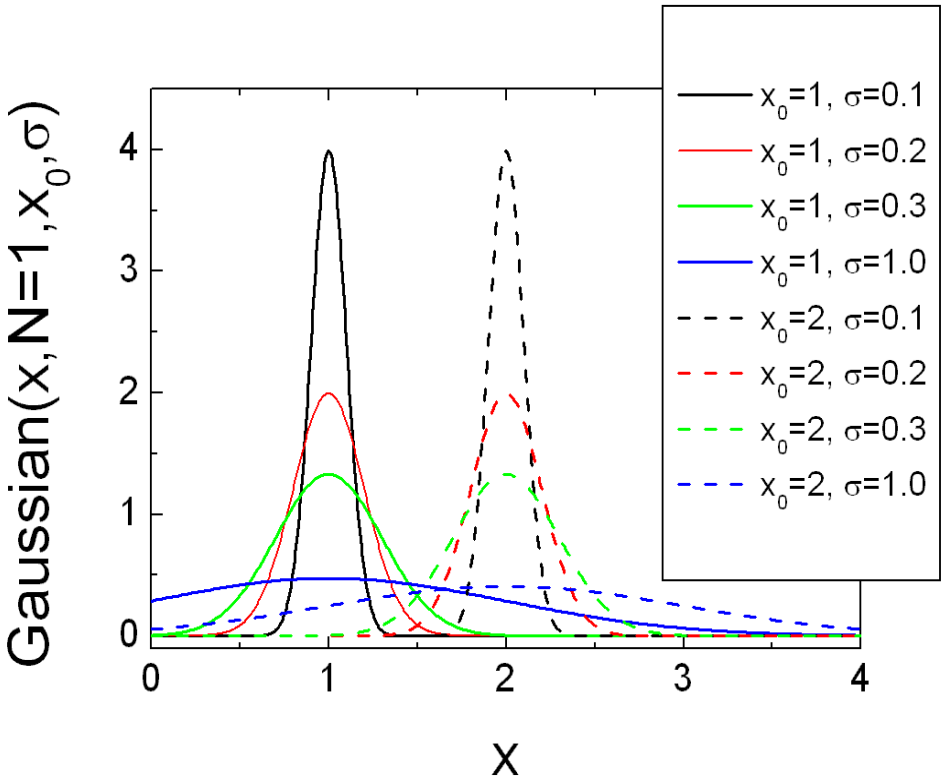

FIGURE 5.6. Normal or Gauss distribution function ($R_0 = \mu = 0$ has been chosen in the plot). Valid parameter ranges: $R \in (0, \infty)$, $R_0 \in (-\infty, \infty)$, $\sigma > 0$

$$\text{Gauss}(R, N, \sigma, R_0) = \frac{N}{c_{\text{Gauss}}} e^{-\frac{(R-R_0)^2}{2\sigma^2}} \tag{5.19a}$$

$$c_{\text{Gauss}} = \sqrt{\frac{\pi}{2}}\,\sigma \left(1 + \text{erf}\left(\frac{R_0}{\sqrt{2}\,\sigma}\right)\right) \tag{5.19b}$$

c_{Gauss} is choosen so that $\int_0^\infty \text{Gauss}(R, \sigma, R_0)\, dR = N$

5.9. Generalized exponential distribution (GEX)

$$\mathrm{GEX}(R,\beta,\lambda,\gamma)) = N\frac{\beta}{\gamma}\left(\frac{x}{\gamma}\right)^{\lambda+1}\frac{e^{-(x/\gamma)^{\beta}}}{\Gamma\left(\frac{\lambda+2}{\beta}\right)} \tag{5.20a}$$

5.10. Generalized extreme value distribution (GEV)

FIGURE 5.7. The shape parameter governs the tail behaviour of the distribution, the sub-families defined by $\xi \to 0$, $\xi > 0$ and $\xi < 0$ correspond, respectively, to the Gumbel, Fréchet and Weibull families, whose cumulative distribution functions are reminded below. Gumbel or type I extreme value distribution

$$\mathrm{GEV}(R, \mu, \sigma, \xi) = \frac{N}{c_1} \frac{e^{-\left(1+\frac{\xi\,(R-\mu)}{\sigma}\right)^{-1/\xi}}}{\sigma\left(1+\frac{\xi\,(R-\mu)}{\sigma}\right)^{1+1/\xi}} \tag{5.21}$$

with

$$c_1 = \begin{cases} 1 & \text{for } \xi > 0 \\ 1 - \exp\left(-\left(1-\frac{\xi\mu}{\sigma}\right)^{-\frac{1}{\xi}}\right) & \text{for } \xi < 0 \end{cases} \tag{5.22}$$

The shape parameter ξ governs the tail behaviour of the distribution, the sub-families defined by $\xi \to 0$, $\xi > 0$ and $\xi < 0$ correspond, respectively, to the Gumbel, Fréchet and Weibull families, whose cumulative distribution functions are reminded below.

- Gumbel or type I extreme value distribution

$$F(x; \mu, \sigma) = e^{-e^{-(x-\mu)/\sigma}} \quad for \;\; x \in \mathbb{R}$$

- Fréchet or type II extreme value distribution

$$F(x; \mu, \sigma, \alpha) = \begin{cases} 0 & x \le \mu \\ e^{-((x-\mu)/\sigma)^{-\alpha}} & x > \mu \end{cases}$$

- Weibull or type III extreme value distribution

$$F(x; \mu, \sigma, \alpha) = \begin{cases} e^{-(-(x-\mu)/\sigma)^{-\alpha}} & x < \mu \\ 1 & x \ge \mu \end{cases}$$

where $\xi > 0$ and $\xi > 0$

Remark I: For reliability issues the Weibull dist ribution is used with the variable $t = \mu - x$, the time, which is strictly positive. Thus the support is positive - in contrast to the use in extreme value theory.

Remark II: Be aware of an important distinctive feature of the three extreme value distributions: The support is either unlimited, or it has an upper or lower limit.

- Parameters
$\mu \in [-\infty, \infty]$ location (real)
$\sigma \in (0, \infty]$ scale (real)
$\xi \in [-\infty, \infty]$ shape (real)

- Support
  $x > \mu - \sigma/\xi \ \ (\xi > 0)$
  $x < \mu - \sigma/\xi \ \ (\xi < 0)$
  $x \in [-\infty, \infty] \ \ (\xi = 0)$

[1] http://en.wikipedia.org/wiki/Generalized_extreme_value_distribution

5.11. Maxwell distribution

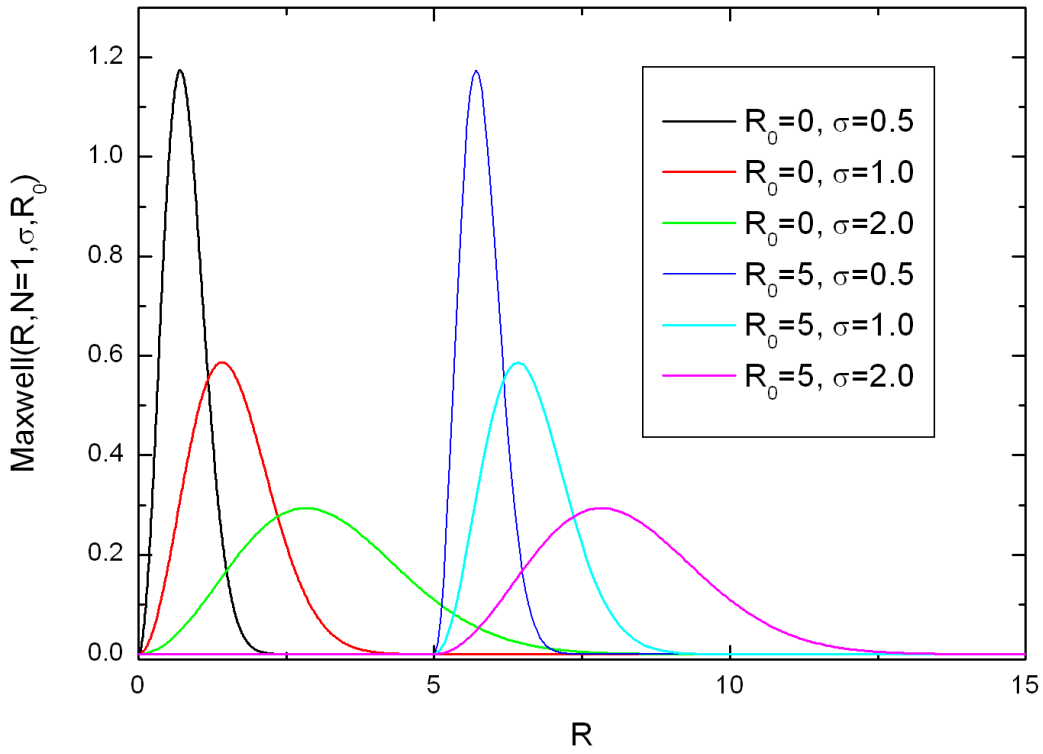

FIGURE 5.8. Maxwell distribution function. Valid parameter ranges: $R \in [0, \infty)$, $R_0 \in (-\infty, \infty)$, $\sigma > 0$

$$\text{Maxwell}(R, R_0, \sigma) = \begin{cases} \text{if } R \geq R_0\text{:} & N \frac{c}{c_{\text{mw}}} (R - R_0)^2 \, e^{-(R-R_0)^2/(2\sigma^2)} \\ \text{else:} & 0 \end{cases} \tag{5.23a}$$

$$c = \frac{4}{\sqrt{\pi}} \left(2\sigma^2\right)^{-3/2} \tag{5.23b}$$

$$c_{\text{mw}} = \begin{cases} \text{if } R_0 < 0\text{:} & 1 - \frac{1}{\sigma}\sqrt{\frac{2}{\pi}} \frac{R_0}{\sqrt{\exp\left(R_0^2/\sigma^2\right)}} + \text{erf}\left(\frac{R_0}{\sqrt{2}\,\sigma}\right) \\ \text{else:} & 1 \end{cases} \tag{5.23c}$$

5.12. Weibull distribution

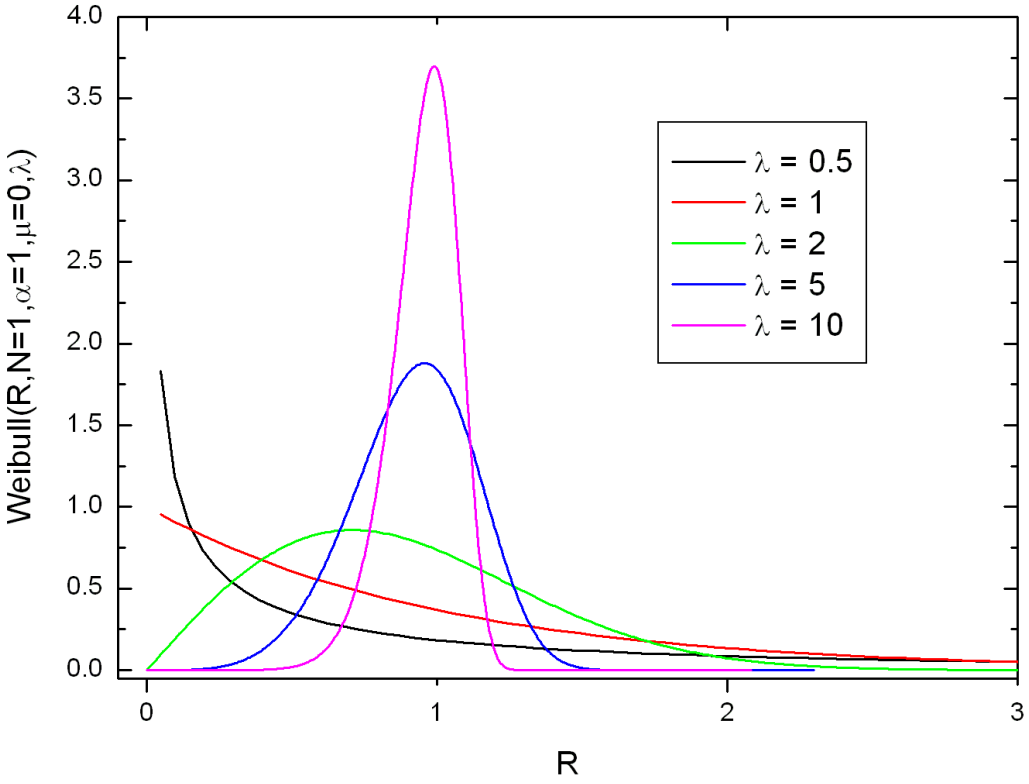

FIGURE 5.9. Weibull distribution function ($\mu = 0$, $\alpha = 1$ has been chosen in the plot). Valid parameter ranges: $R \in [0, \infty)$, $\mu \in [0, \infty)$, $\alpha > 0$, $\lambda > 0$

$$\text{Weibull}(R, \alpha, \lambda, \mu) = \frac{N\lambda}{\alpha}\left(\frac{R-\mu}{\alpha}\right)^{\lambda-1} e^{-\left(\frac{R-\mu}{\alpha}\right)^{\lambda}} e^{-\left(\frac{\mu}{\alpha}\right)^{\lambda}} \tag{5.24}$$

where λ is the shape parameter, μ is the location parameter and α is the scale parameter.

5.13. fractal size distribution

FIGURE 5.10. fractal size distribution function. Valid parameter ranges: $R \in [R_{\min}, R_{\max}]$, $f_D \in (-1, \infty)$, $R_{\max} > R_{\min} > 0$

$$\text{fractalSD}(R, N, R_{\min}, R_{\max}, f_D) = \frac{N f_D}{R_{\min}^{-f_D} - R_{\max}^{-f_D}} \; R^{-(1+f_D)} \tag{5.25}$$

CHAPTER 6

Peak functions

6.1. Beta

The Beta distribution is a very versatile function which can be used to model several different shapes of probability density curves. In probability theory and statistics, the beta distribution is a family of continuous probability distributions defined on the interval $[0, 1]$ parameterized by two positive shape parameters, typically denoted by α and β.

$$p_{\text{Beta}}(x;\alpha,\beta) = \begin{cases} \frac{1}{\text{B}(\alpha,\beta)}\, x^{\alpha-1}(1-x)^{\beta-1} & \text{for } 0 < x < 1 \\ 0 & \text{otherwise} \end{cases} \tag{6.1}$$

The beta function, B, appears as a normalization constant to ensure that the total probability integrates to unity. α and β are positive numbers that define the shape parameters. The mode of the beta distribution for shape parameters $\alpha > 1$ and $\beta > 1$ is given by

$$\text{mode}\left(p_{\text{Beta}}\right) = \frac{\alpha - 1}{\alpha + \beta - 2} \tag{6.2}$$

6.1.1. Beta (Amplitude).

$$y_{\text{Beta(ampl)}}\left(x; A, x_{\min}, x_{\max}, \alpha, \beta, c_0\right) = A\, \frac{p_{\text{Beta}}\left(\frac{x - x_{\min}}{x_{\max} - x_{\min}}; \alpha, \beta\right)}{p_{\text{Beta}}\left(\frac{\alpha-1}{\alpha+\beta-2}; \alpha, \beta\right)} + c_0 \tag{6.3}$$

Required parameters:

ampl.: amplitude A of the Beta peak
xmin: continuous lower boundary parameters $x_{\min}$
xmax: continuous upper boundary parameters $x_{\max}$
alpha: first shape parameter $\alpha > 1$
beta: second shape parameter $\beta > 1$
backgr: offset c_0

Note

- Both shape parameter needs to be larger than one ($\alpha, \beta > 1$), as only than the distribution has a peak shape.
- where the Beta distribution is not defined the offset value is returned: $\forall x \notin (x_{\min}, x_{\max}) \quad y_{\text{Beta(ampl)}}(x) = c_0$
- Default (size) distribution: Monodisperse

6.1.2. Beta (Area).

$$y_{\text{Beta(area)}}\left(x; A, x_{\min}, x_{\max}, \alpha, \beta, c_0\right) = A\, \frac{p_{\text{Beta}}\left(\frac{x - x_{\min}}{x_{\max} - x_{\min}}; \alpha, \beta\right)}{x_{\max} - x_{\min}} + c_0 \tag{6.4}$$

Required parameters:

area: area A of the beta distribution

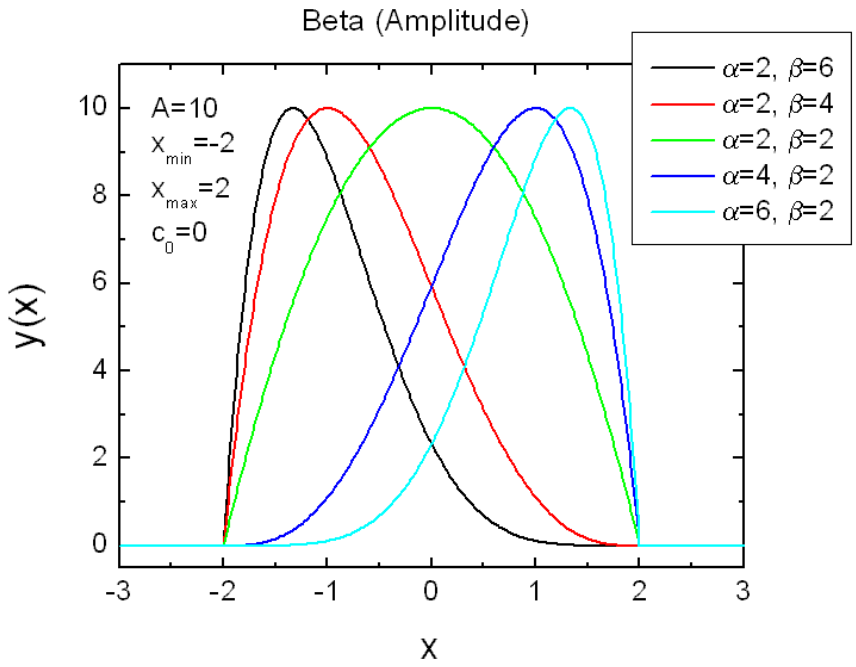

FIGURE 6.1. Plot of `Beta (Amplitude)` distribution.

xmin: continuous lower boundary parameters $x_{\min}$
xmax: continuous upper boundary parameters $x_{\max}$
alpha: first shape parameter $\alpha > 0$
beta: second shape parameter $\beta > 0$
backgr: offset c_0

Note

- Both shape parameter needs to be larger than zero $(\alpha, \beta > 0)$
- where the Beta distribution is not defined the offset value is returned: $\forall x \notin (x_{\min}, x_{\max}) \quad y_{\text{Beta(area)}}(x) = c_0$
- Default (size) distribution: Monodisperse

6.2. Chi-Squared

[1]In probability theory and statistics, the chi-square distribution (also chi-squared or ξ^2 distribution) is one of the most widely used theoretical probability distributions in inferential statistics, e.g., in statistical significance tests. It is useful because, under reasonable assumptions, easily calculated quantities can be proven to have distributions that approximate to the chi-square distribution if the null hypothesis is true.

The best-known situations in which the chi-square distribution are used are the common chi-square tests for goodness of fit of an observed distribution to a theoretical one, and of the independence of two criteria of classification of qualitative data. Many other statistical tests also lead to a use of this distribution, like Friedman's analysis of variance by ranks.

A probability density function of the chi-square distribution is

$$f(x;k) = \begin{cases} \dfrac{1}{2^{k/2}\Gamma(k/2)}\, x^{(k/2)-1} e^{-x/2} & \text{for } x > 0 \\ 0 & \text{for } x \leq 0 \end{cases} \tag{6.5}$$

where Γ denotes the Gamma function, which has closed-form values at the half-integers. The mode of the distribution is

$$\text{mode} = k - 2 \text{ if } k \geq 2. \tag{6.6}$$

The χ^2 distribution is a special case of the gamma distribution 6.8 where $\theta = 2$ in the equation 6.31.

6.2.1. Chi-Squared (Amplitude).

$$\chi^2(x; A, x_c, \sigma, k, c_0) = \begin{cases} c_0 + A_0 \left(z+u\right)^v \exp\left(-\frac{z+u}{2}\right) & \text{for } z+u \geq 0 \\ c_0 & \text{otherwise} \end{cases} \tag{6.7}$$

with

$$z = \frac{x - x_x}{\sigma} \tag{6.8}$$

$$u = k - 2 \tag{6.9}$$

$$v = \frac{k}{2} - 1 \tag{6.10}$$

$$A_0 = \frac{A \exp(v)}{u^v} \tag{6.11}$$

The standard statistical form has been reparameterized. The parameter x_c has been added to enable variable x positioning, and σ to enable scaling. The mode is x_c. The function returns 0 for those x where it is undefined ($z + u < 0$).

Required parameters:

amplitude: amplitude a of the Gamma peak
center: location parameter (mode) x_c

[1]Description taken partly from Wikipedia, the free encyclopedia

width: scaling parameter $\sigma > 0$
shape: shape parameter $k > 2$
backgr: offset c_0

Note

- The width parameter needs to be larger than zero ($\sigma > 0$).
- The shape parameter needs to be larger than two ($k > 2$)
- Default (size) distribution: Monodisperse

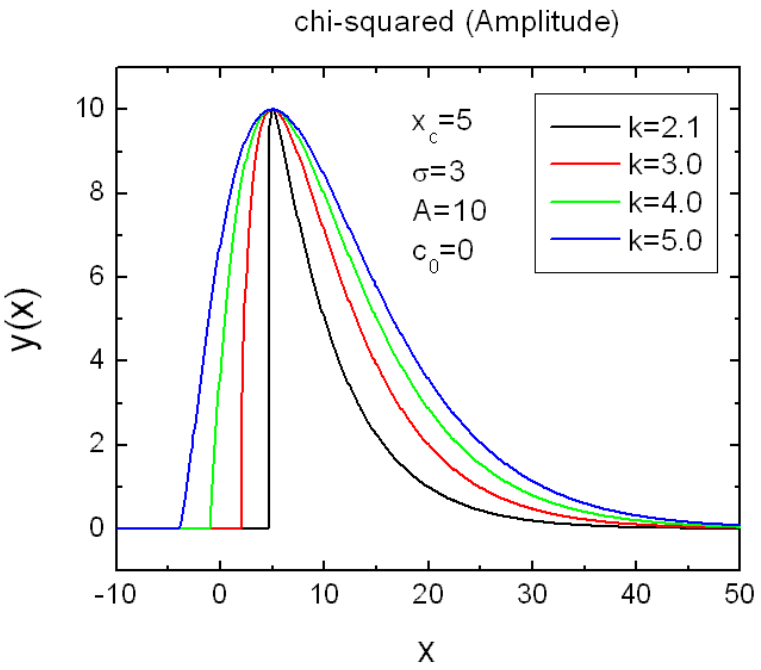

FIGURE 6.2. Plot of `Chi-Squared (Amplitude)` distribution.

6.2.2. Chi-Squared (Area).

$$\chi^2(x; A, x_c, \sigma, k, c_0) = \begin{cases} c_0 + A_0 \left(z+u\right)^v \exp\left(-\frac{z+u}{2}\right) & \text{for } z+u \geq 0 \\ c_0 & \text{otherwise} \end{cases} \tag{6.12}$$

with

$$z = \frac{x - x_x}{\sigma} \tag{6.13}$$

$$u = k - 2 \tag{6.14}$$

$$v = \frac{k}{2} - 1 \tag{6.15}$$

$$A_0 = \frac{A}{2^{\frac{k}{2}} \sigma \Gamma\left(\frac{k}{2}\right)} \tag{6.16}$$

The standard statistical form has been reparameterized. The parameter x_c has been added to enable variable x positioning, and σ to enable scaling. The mode is x_c. The function returns 0 for those x where it is undefined ($z + u < 0$).

Required parameters:

area: area a of the Gamma peak
center: location parameter (mode) x_c
width: scaling parameter $\sigma > 0$
shape: shape parameter $k > 2$
backgr: offset c_0

Note

- The width parameter needs to be larger than zero ($\sigma > 0$).
- The shape parameter needs to be larger than two ($k > 2$)
- Default (size) distribution: Monodisperse

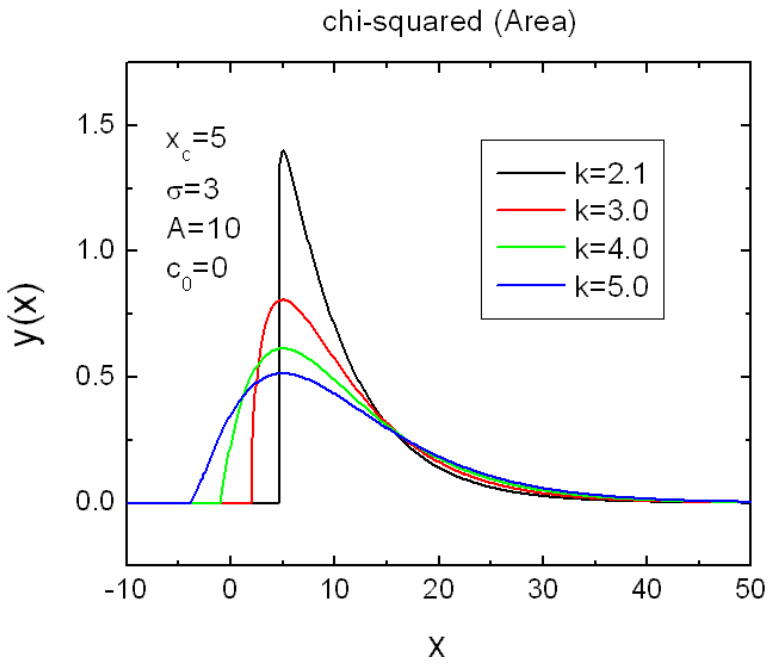

FIGURE 6.3. Plot of `Chi-Squared (Area)` distribution.

6.3. Erfc peak

6.3.1. Erfc (Amplitude).

$$y(x; a, x_c, \sigma, c_0) = a\,\mathrm{erfc}\left(\left(\frac{x - x_c}{\sigma}\right)^2\right) + c_0 \tag{6.17}$$

Required parameters:

ampl.: amplitude a of the erfc peak
center: location parameter (mode) x_c
width: scaling parameter $\sigma > 0$
backgr: offset c_0

Note

- The width parameter needs to be non-zero ($\sigma \neq 0$).
- Default (size) distribution: Monodisperse

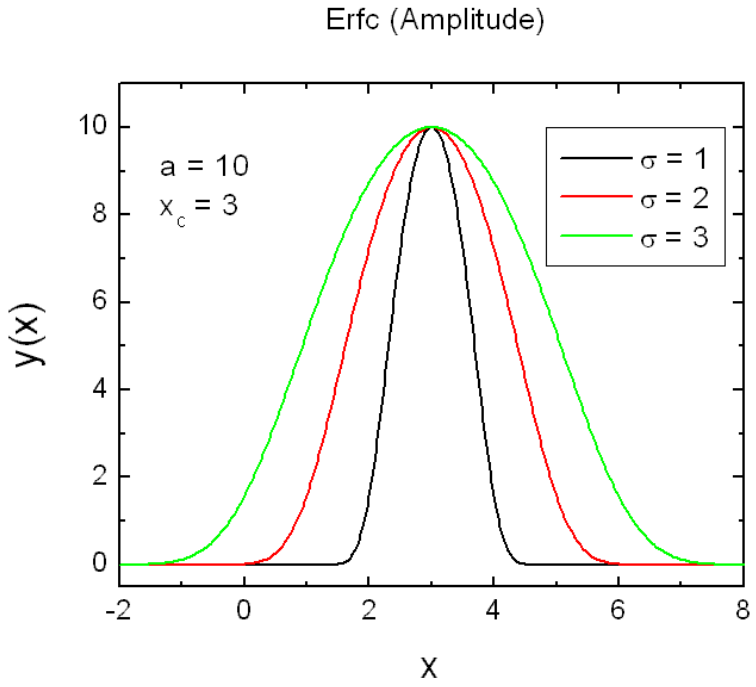

FIGURE 6.4. Plot of `Erfc (Amplitude)` distribution.

6.3.2. Erfc (Area).

$$y(x; a, x_c, \sigma, c_0) = a \frac{\operatorname{erfc}\left(\left(\frac{x-x_c}{\sigma}\right)^2\right)}{\int_{-\infty}^{\infty} \operatorname{erfc}\left(\left(\frac{x-x_c}{\sigma}\right)^2\right) dx} + c_0 \tag{6.18}$$

Required parameters:

area: area a below the erfc peak
center: location parameter (mode) x_c
width: scaling parameter $\sigma > 0$
backgr: offset c_0

Note

- The width parameter needs to be non-zero ($\sigma \neq 0$).
- Default (size) distribution: Monodisperse

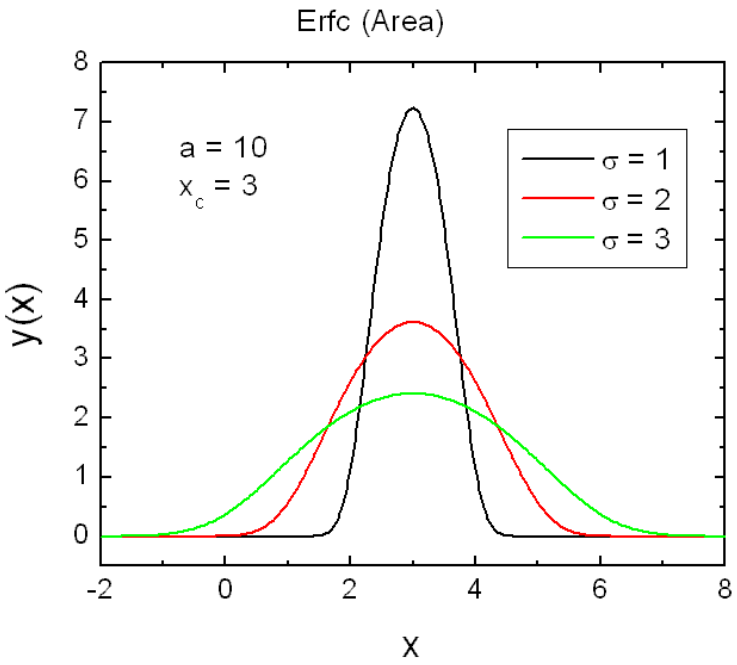

FIGURE 6.5. Plot of `Erfc (Area)` distribution.

6.4. Error peak

6.4.1. Error (Amplitude).

$$y(x; a, x_c, \sigma, k, c_0) = a \exp\left(-\frac{1}{2}\frac{|x - x_c|^{\frac{2}{k}}}{|\sigma|}\right) + c_0 \tag{6.19}$$

Required parameters:

ampl.: amplitude a of the error distribution
center: location parameter (mode) x_c
width: scaling parameter $\sigma \neq 0$
shape: shape parameter $k > 0$
backgr: offset c_0

Note

- The width parameter needs to be non-zero ($\sigma \neq 0$).
- The shape parameter needs to be larger than zero ($k > 0$).
- Default (size) distribution: Monodisperse

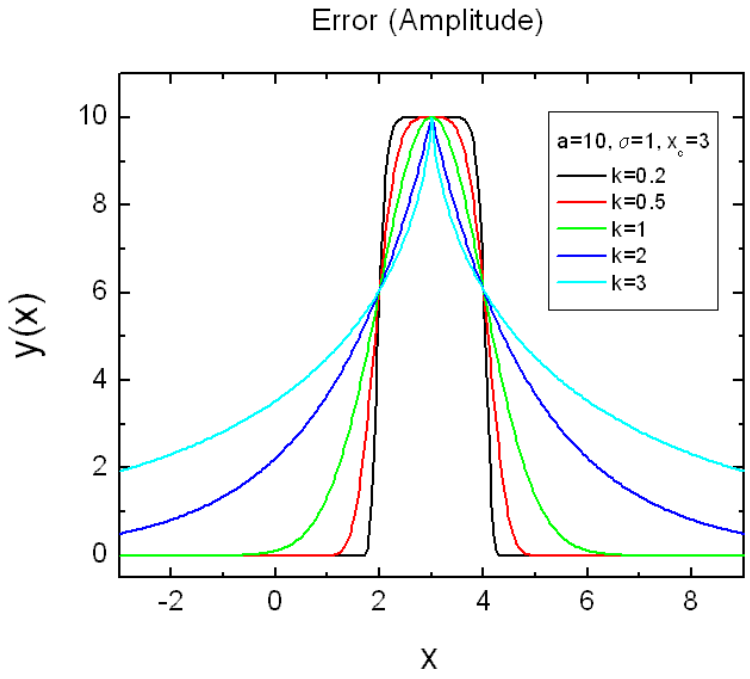

FIGURE 6.6. Plot of `Error (Amplitude)` distribution.

6.4.2. Error (Area).

$$y(x; a, x_c, \sigma, k, c_0) = \frac{a}{|\sigma|^{\frac{k}{2}}\, 2^{\frac{k}{2}+1}\Gamma\left(\frac{k}{2}+1\right)} \exp\left(-\frac{1}{2}\frac{|x-x_c|^{\frac{2}{k}}}{|\sigma|}\right) + c_0 \tag{6.20}$$

Required parameters:

area: area a below the error distribution
center: location parameter (mode) x_c
width: scaling parameter $\sigma \neq 0$
shape: shape parameter $k > 0$
backgr: offset c_0

Note

- The width parameter needs to be non-zero ($\sigma \neq 0$).
- The shape parameter needs to be larger than zero ($k > 0$).
- Default (size) distribution: Monodisperse

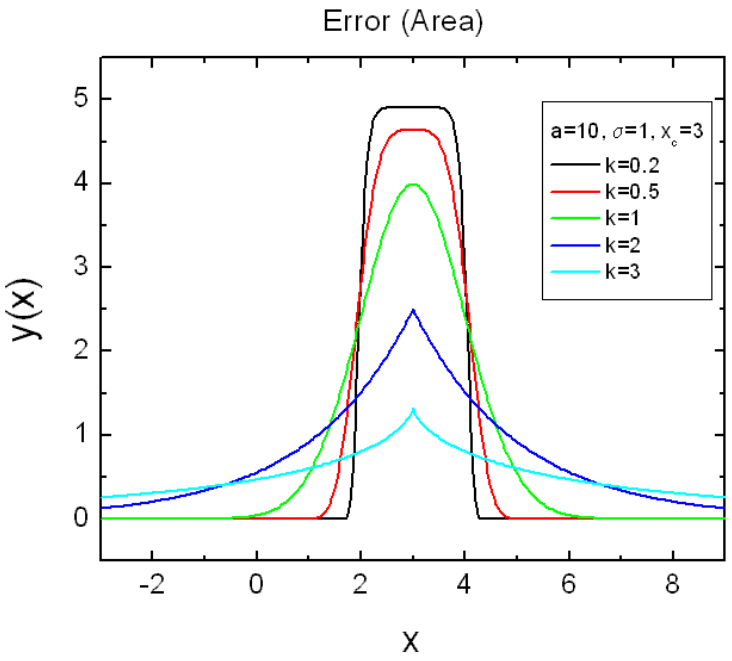

FIGURE 6.7. Plot of `Error (Area)` distribution.

6.5. Exponentially Modified Gaussian

6.5.1. Exponentially Modified Gaussian (Amplitude).

$$y(x; a, x_c, \sigma, \gamma, c_0) = \frac{a}{\text{const}} \exp\left(\frac{\sigma^2}{2\gamma^2} + \frac{x_c - x}{\gamma}\right) \left[\text{erf}\left(\frac{x - x_c}{\sqrt{2}\sigma} - \frac{\sigma}{\sqrt{2}\gamma}\right) + \frac{\gamma}{|\gamma|}\right] + c_0 \quad (6.21)$$

const is calculated numerically so that "a" represents the amplitude of the distribution.

Required parameters:

ampl.: amplitude a of the distribution
center: location parameter x_c
width: scaling parameter $\sigma > 0$
distortion: distortion parameter $\gamma \neq 0$
backgr: offset c_0

Note

- The width parameter needs to be non-zero ($\sigma \neq 0$).
- The distortion parameter needs to be non-zero ($\gamma \neq 0$).
- Default (size) distribution: Monodisperse

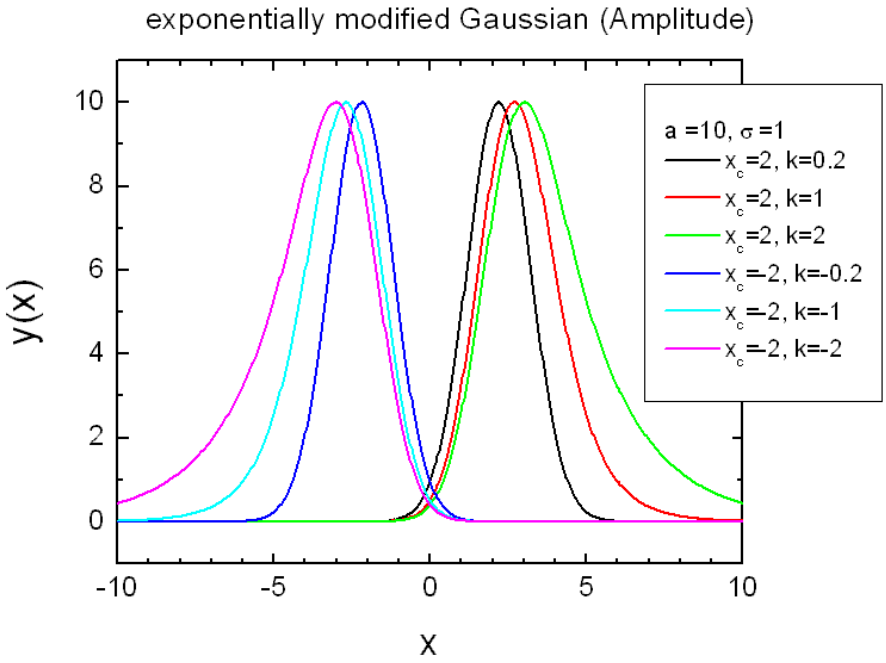

FIGURE 6.8. Plot of `Exponentially Modified Gaussian (Amplitude)` distribution.

6.5.2. Exponentially Modified Gaussian (Area).

$$y(x; a, x_c, \sigma, \gamma, c_0) = \frac{a}{2\gamma} \exp\left(\frac{\sigma^2}{2\gamma^2} + \frac{x_c - x}{\gamma}\right) \left[\operatorname{erf}\left(\frac{x - x_c}{\sqrt{2}\sigma} - \frac{\sigma}{\sqrt{2}\gamma}\right) + \frac{\gamma}{|\gamma|}\right] + c_0 \tag{6.22}$$

Required parameters:

area: area a below the distribution
center: location parameter x_c
width: scaling parameter $\sigma > 0$
distortion: distortion parameter $\gamma \neq 0$
backgr: offset c_0

Note

- The width parameter needs to be non-zero ($\sigma > 0$).
- The distortion parameter needs to be non-zero ($\gamma \neq 0$).
- Default (size) distribution: Monodisperse

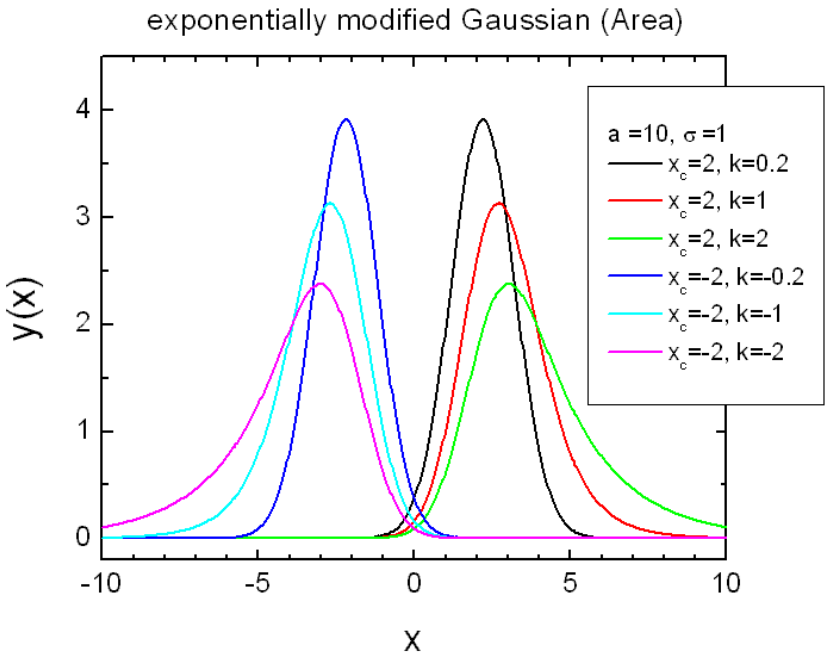

FIGURE 6.9. Plot of `Exponentially Modified Gaussian (Area)` distribution.

6.6. Extreme Value

6.6.1. Extreme Value (Amplitude).

$$y(x; a, x_c, \sigma, c_0) = a \exp\left[-\exp\left(-\frac{x - x_c}{|\sigma|}\right) - \frac{x - x_c}{|\sigma|} + 1\right] + c_0 \tag{6.23}$$

Required parameters:

ampl.: amplitude a of the peak
center: location parameter (mode) x_c
width: scaling parameter $\sigma \neq 0$
backgr: offset c_0

Note

- The width parameter needs to be non-zero ($\sigma \neq 0$).
- Default (size) distribution: Monodisperse

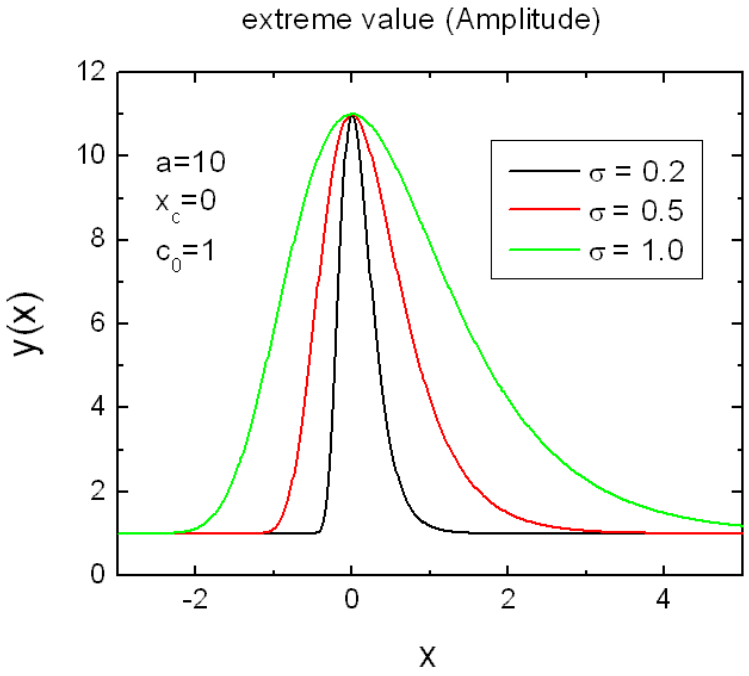

FIGURE 6.10. Plot of `extreme value (Amplitude)` distribution.

6.6.2. Extreme Value (Area).

$$y(x; a, x_c, \sigma, c_0) = \frac{a}{|\sigma|} \exp\left[-\exp\left(-\frac{x - x_c}{|\sigma|}\right) - \frac{x - x_c}{|\sigma|}\right] + c_0 \tag{6.24}$$

Required parameters:

area: area a below the peak
center: location parameter (mode) x_c
width: scaling parameter $\sigma \neq 0$
backgr: offset c_0

Note

- The width parameter needs to be non-zero ($\sigma \neq 0$).
- Default (size) distribution: Monodisperse

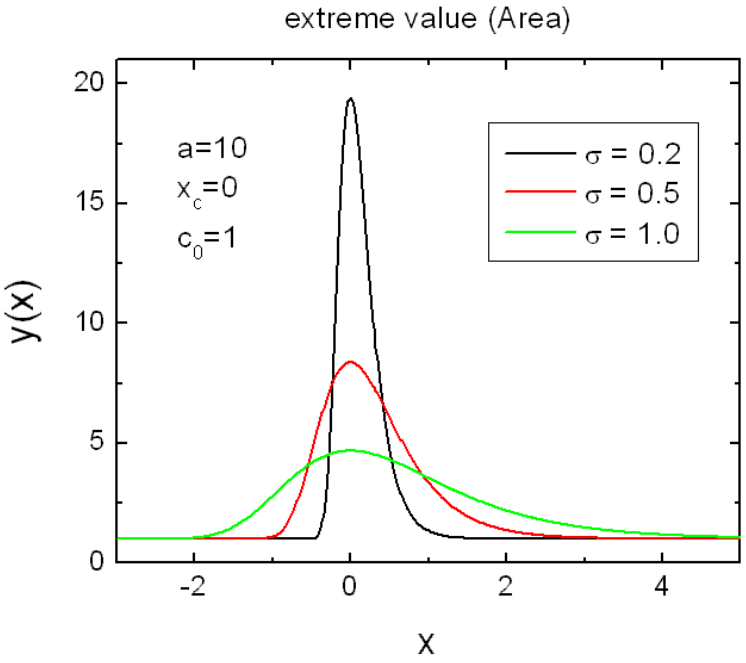

FIGURE 6.11. Plot of `extreme value (Area)` distribution.

6.7. F-Variance

In probability theory and statistics, the F-distribution is a continuous probability distribution. It is also known as Snedecor's F distribution or the Fisher-Snedecor distribution. The probability density is given by

$$p_{\mathrm{F-var}}(x,\nu_1,\nu_2) = \frac{\sqrt{\dfrac{(\nu_1 x)^{\nu_1}\,\nu_2^{\nu_2}}{(\nu_1 x+\nu_2)^{\nu_1+\nu_2}}}}{x\,\mathrm{B}\left(\frac{\nu_1}{2},\frac{\nu_2}{2}\right)} \tag{6.25}$$

for real $x \geq 0$, where $\nu > 1$ and ν_2 are positive, and B() is the beta function. For $\nu_1 > 2$ the mode of the distribution is defined by

$$\mathrm{mode}_F(\nu_1,\nu_2) = \frac{\nu_1-2}{\nu_1}\frac{\nu_2}{\nu_2+2} \tag{6.26}$$

6.7.1. F-Variance (Amplitude).

The amplitude version represents a re-parametrization of the standard statistical form.

$$\begin{aligned} y(x;a,x_c,\sigma,\nu_1,\nu_2) &= \begin{cases} c_0 + a\,\frac{p_{\mathrm{F-var}}(z,\nu_1,\nu_2)}{p_{\mathrm{F-var}}(\mathrm{mode}_F(\nu_1,\nu_2),\nu_1,\nu_2)} & \text{for } z>0 \\ c_0 & \text{otherwise} \end{cases} \\ &= \begin{cases} c_0 + a\,\dfrac{z^{\frac{\nu_1}{2}-1}\left(1+\frac{\nu_1-2}{\nu_2+2}\right)^{\frac{\nu_1+\nu_2}{2}}}{\left(1+\frac{\nu_1}{\nu_2}z\right)^{\frac{\nu_1+\nu_2}{2}}\left(\frac{\nu_2}{\nu_1}\frac{\nu_1-2}{\nu_2+2}\right)^{\frac{\nu_1}{2}-1}} & \text{for } z>0 \\ c_0 & \text{otherwise} \end{cases} \end{aligned} \tag{6.27}$$

with

$$z = \frac{x-x_c}{\sigma} + \frac{\nu_1-2}{\nu_1}\frac{\nu_2}{\nu_2+2} \tag{6.28}$$

The location parameter x_c has been added to enable variable x positioning, and σ to enable scaling. The mode of the distribution function is x_c due to the additional term $\frac{\nu_1-2}{\nu_1}\frac{\nu_2}{\nu_2+2}$ in the definition of z. The distribution function returns the offset c_0 for values $z \leq 0$.

Required parameters:

ampl.: amplitude a of the F-distribution
center: location parameter (mode) x_c
width: scaling parameter $\sigma > 0$
shape1: shape parameter $\nu_1 > 2$
shape2: shape parameter $\nu_2 > 2$
backgr: offset c_0

Note

- The scale parameter needs to be larger than zero $\sigma > 0$
- The first shape parameter needs to be larger than zero $\nu_1 > 2$

- The second shape parameter needs to be larger than zero $\nu_2 > 2$
- Default (Size) distribution: Monodisperse

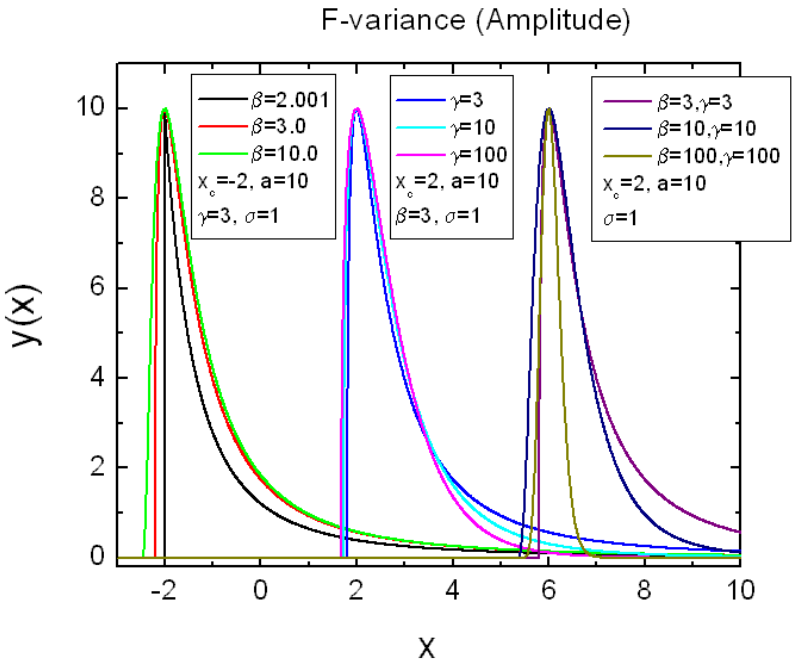

FIGURE 6.12. Plot of `F-variance (Amplitude)` distribution.

6.7.2. F-Variance (Area).

The area version represents a re-parametrization of the standard statistical form.

$$y(x; a, x_c, \sigma, \nu_1, \nu_2) = \begin{cases} c_0 + \frac{a}{\sigma}\, p_{\mathrm{F-var}}(z, \nu_1, \nu_2) & \text{for } z > 0 \\ c_0 & \text{otherwise} \end{cases} \tag{6.29}$$

with

$$z = \frac{x - x_c}{\sigma} + \frac{\nu_1 - 2}{\nu_1}\frac{\nu_2}{\nu_2 + 2} \tag{6.30}$$

The location parameter x_c has been added to enable variable x positioning, and σ to enable scaling. The mode of the distribution function is x_c due to the additional term $\frac{\nu_1-2}{\nu_1}\frac{\nu_2}{\nu_2+2}$ in the definition of z. The distribution function returns the offset c_0 for values $z \leq 0$.

Required parameters:

area: area a of the F-distribution
center: location parameter (mode) x_c
width: scaling parameter $\sigma > 0$
shape1: shape parameter $\nu_1 > 2$
shape2: shape parameter $\nu_2 > 2$

backgr: offset c_0

Note

- The scale parameter needs to be larger than zero $\sigma > 0$
- The first shape parameter needs to be larger than zero $\nu_1 > 2$
- The second shape parameter needs to be larger than zero $\nu_2 > 2$
- Default (Size) distribution: Monodisperse

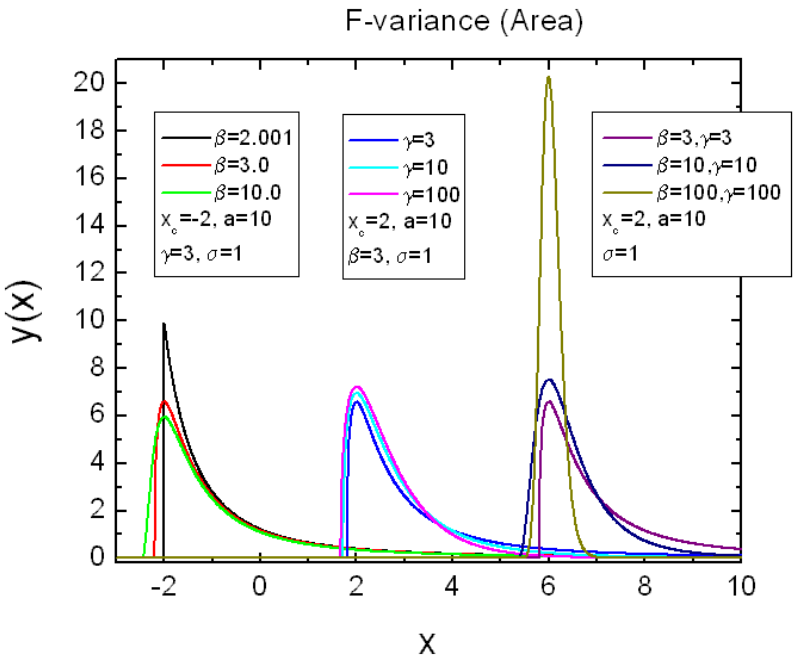

FIGURE 6.13. Plot of `F-variance (Area)` distribution.

6.8. Gamma

The gamma distribution models sums of exponentially distributed random variables.

The gamma distribution family is based on two parameters. The chi-square and exponential distributions, which are children of the gamma distribution, are one-parameter distributions that fix one of the two gamma parameters. The standard form is given by

$$p(x;k,\theta) = x^{k-1}\frac{e^{-x/\theta}}{\theta^k\,\Gamma(k)} \text{ for } x>0 \text{ and } k,\theta>0. \tag{6.31}$$

When k is large, the gamma distribution closely approximates a normal distribution with the advantage that the gamma distribution has density only for positive real numbers. In probability theory and statistics, the gamma distribution is a two-parameter family of continuous probability distributions. It has a scale parameter θ and a shape parameter k. If k is an integer then the distribution represents the sum of k independent exponentially distributed random variables, each of which has a mean of θ (which is equivalent to a rate parameter of θ^{-1}).

Alternatively, the gamma distribution can be parameterized in terms of a shape parameter $\alpha = k$ and an inverse scale parameter $\beta = 1/\theta$, called a rate parameter:

$$p(x;\alpha,\beta) = x^{\alpha-1}\frac{\beta^\alpha\, e^{-\beta\, x}}{\Gamma(\alpha)} \text{ for } x>0. \tag{6.32}$$

6.8.1. Gamma (Amplitude).

The parameter x_c has been added to enable variable x positioning, whereas the $+\theta(k-1)$ adjusts x_c so that it represents the mode. c_0 is the offset value. The function returns the offset c_0 for those x where it is undefined

$$y(x) = \begin{cases} c_0 + a\exp(-z)\left(\frac{z+k-1}{k-1}\right)^{k-1} & \text{for } (z+k-1)>0 \\ c_0 & \text{otherwise} \end{cases} \tag{6.33}$$

with $z = \frac{x-x_c}{\theta}$

Required parameters:

ampl.: amplitude a of the Gamma peak
center: location parameter (mode) x_c
width: scaling parameter $\theta > 0$
backgr: offset c_0

Note

- The shape parameter needs to be larger than one $k > 1$.
- The scale parameter needs to be larger than zero $\theta > 0$
- Default (Size) distribution: Monodisperse

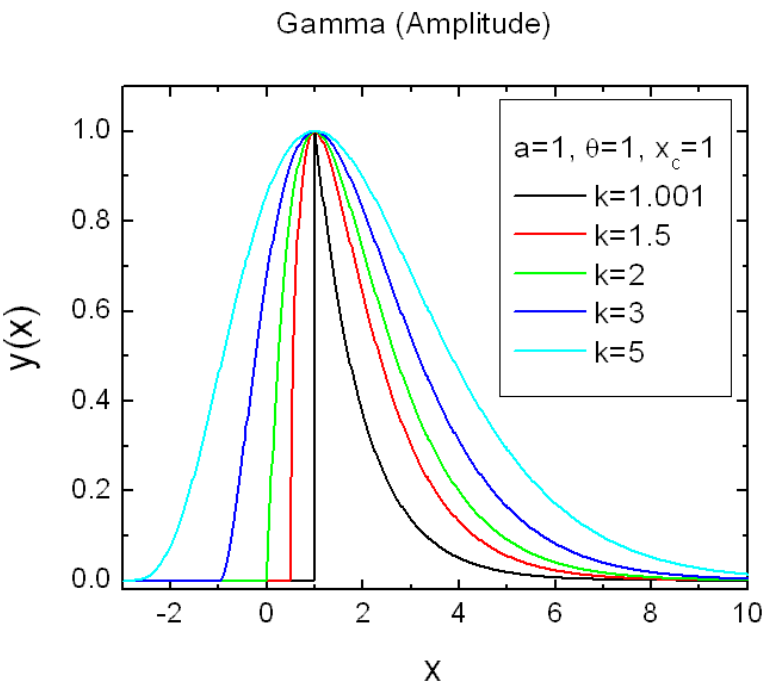

FIGURE 6.14. Plot of `Gamma (Amplitude)` distribution.

6.8.2. Gamma (Area).

The parameter x_c has been added to enable variable x positioning, whereas the $+\theta(k-1)$ adjusts x_c so that it represents the mode. c_0 is the offset value. The function returns the offset c_0 for those x where it is undefined

$$y(x) = \begin{cases} c_0 + \frac{a}{\theta\Gamma(k)} \exp(-z) z^{k-1} & \text{for } z > 0 \\ c_0 & \text{otherwise} \end{cases} \tag{6.34}$$

with $z = \frac{x-x_c}{\theta} + k - 1$

Required parameters:

area: area a of the Gamma peak
center: location parameter (mode) x_c
width: scaling parameter $\theta > 0$
backgr: offset c_0

Note

- The shape parameter needs to be larger than one $k > 1$.
- The scale parameter needs to be larger than zero $\theta > 0$
- Default (Size) distribution: Monodisperse

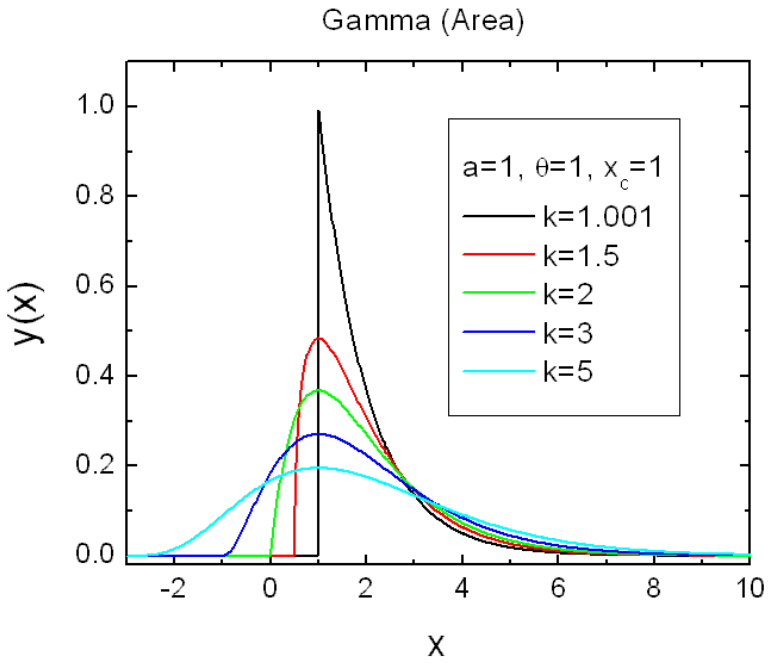

FIGURE 6.15. Plot of `Gamma (Area)` distribution.

6.9. Gaussian or Normal distribution

6.9.1. Gaussian (Amplitude).

$$y(x; a, x_c, \sigma, c_0) = a \exp\left[-\frac{1}{2}\left(\frac{x - x_c}{|\sigma|}\right)^2\right] + c_0 \tag{6.35}$$

Required parameters:

ampl.: amplitude a of the peak
center: location parameter (mode) x_c
width: scaling parameter $\sigma \neq 0$
backgr: offset c_0

Note

- The width parameter needs to be non-zero ($\sigma \neq 0$).
- Default (size) distribution: Monodisperse

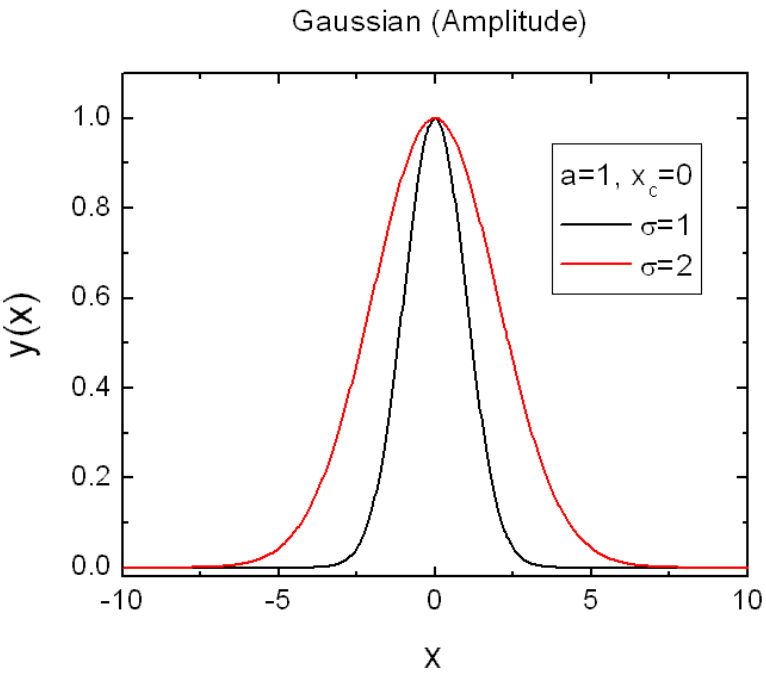

FIGURE 6.16. Plot of `Gaussian (Amplitude)` distribution.

6.9.2. Gaussian (Area).

$$y(x; a, x_c, \sigma, c_0) = \frac{a}{|\sigma|\sqrt{2\pi}} \exp\left[-\frac{1}{2}\left(\frac{x - x_c}{|\sigma|}\right)^2\right] + c_0 \tag{6.36}$$

Required parameters:

area: area a below the peak
center: location parameter (mode) x_c
width: scaling parameter $\sigma \neq 0$
backgr: offset c_0

Note

- The width parameter needs to be non-zero ($\sigma \neq 0$).
- Default (size) distribution: Monodisperse

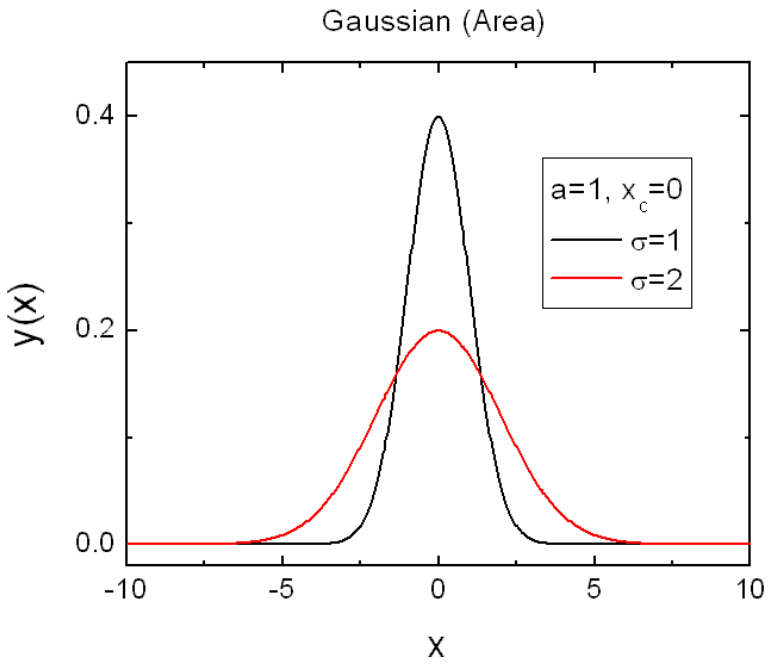

FIGURE 6.17. Plot of `Gaussian (Area)` distribution.

6.10. Gaussian-Lorentzian cross product

This distribution function is a Voigt approximation. It combines a Gaussian and Lorentzian in a multiplicative form. The shape parameter ν varies from 0 to 1. The pure Lorentzian occurs with $\nu = 1$ and the pure Gaussian with $\nu = 0$ but the transition from Lorentzian to Gaussian shape in not a linear function of ν

6.10.1. Gaussian-Lorentzian cross product (Amplitude).

$$y(x, a, x_c, \sigma, \nu, c_0) = a \frac{\exp\left(-\frac{1-\nu}{2}\left(\frac{x-x_c}{|\sigma|}\right)^2\right)}{1+\nu\left(\frac{x-x_c}{|\sigma|}\right)^2} + c_0 \tag{6.37}$$

Required parameters:

amplitude: amplitude a of the peak
center: location parameter (mode) x_c
shape: shape parameter $\nu \in [0, 1]$
width: scaling parameter $\sigma \neq 0$
backgr: offset c_0

Note

- The width parameter needs to be non-zero ($\sigma \neq 0$).
- The shape parameter need to be between 0 and 1 ($\nu \in [0, 1]$)
- Default (size) distribution: Monodisperse

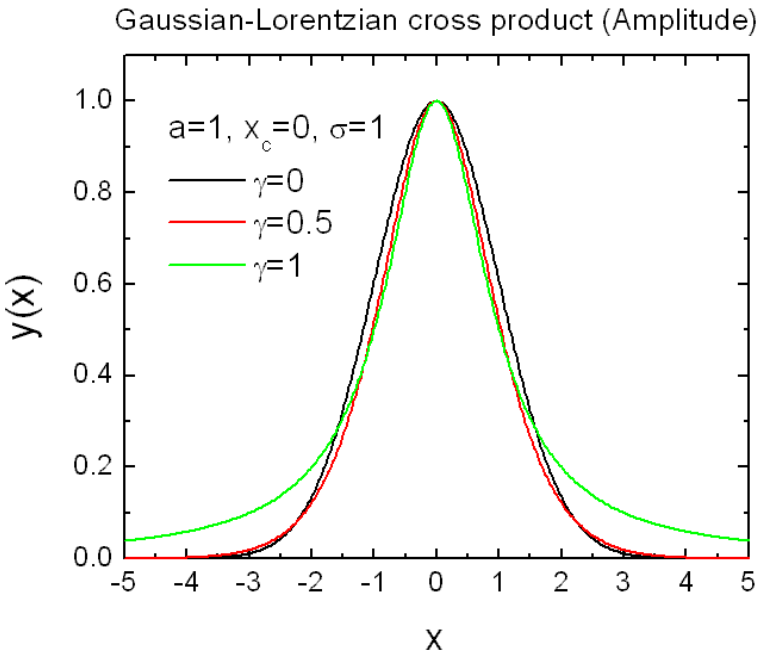

FIGURE 6.18. Plot of `Gaussian-Lorentzian cross product (Amplitude)` distribution.

6.10.2. Gaussian-Lorentzian cross product (Area).

$$y(x, a, x_c, \sigma, \nu, c_0) = a\,\frac{\sqrt{\nu}}{|\sigma|\pi}\,\frac{\exp\left(-\frac{1-\nu}{2\nu}\right)}{\operatorname{erfc}\left(\sqrt{\frac{1-\nu}{2\nu}}\right)}\,\frac{\exp\left(-\frac{1-\nu}{2}\left(\frac{x-x_c}{|\sigma|}\right)^2\right)}{1+\nu\left(\frac{x-x_c}{|\sigma|}\right)^2} + c_0 \tag{6.38}$$

Required parameters:

area: area a below the peak
center: location parameter (mode) x_c
shape: shape parameter $\nu \in [0, 1]$
width: scaling parameter $\sigma \neq 0$
backgr: offset c_0

Note

- The width parameter needs to be non-zero ($\sigma \neq 0$).
- The shape parameter need to be between 0 and 1 ($\nu \in [0, 1]$)
- Default (size) distribution: Monodisperse

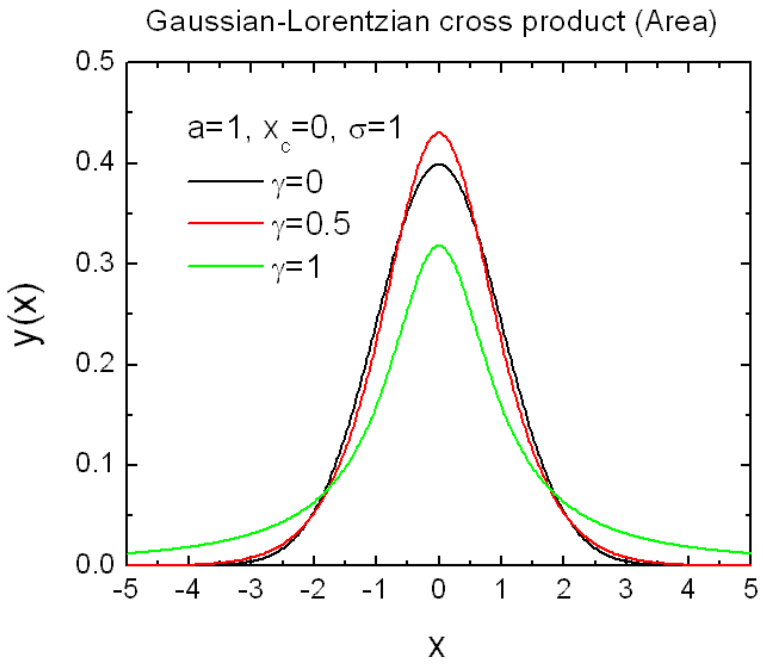

FIGURE 6.19. Plot of `Gaussian-Lorentzian cross product (Area)` distribution.

6.11. Gaussian-Lorentzian sum

This distribution function is another Voigt approximation, which is simply a sum of Lorentzian and Gaussian with equal FWHM. The shape parameter ν varies from 0 to 1. The pure Lorentzian occurs with $\nu = 1$ and the pure Gaussian with $\nu = 0$. The width parameter σ directly computes the full-width at half-maximum (FWHM).

6.11.1. Gaussian-Lorentzian sum (Amplitude).

$$y(x, a, x_c, \sigma, \nu, c_0) = a \frac{\frac{\nu}{|\sigma|}\sqrt{\frac{\ln 2}{\pi}} \exp\left(-4\ln 2\left(\frac{x-x_c}{|\sigma|}\right)^2\right) + \frac{1-\nu}{\pi|\sigma|\left[1+4\left(\frac{x-x_c}{|\sigma|}\right)^2\right]}}{\frac{\nu}{|\sigma|}\sqrt{\frac{\ln 2}{\pi}} + \frac{1-\nu}{\pi|\sigma|}} + c_0 \quad (6.39)$$

Required parameters:

amplitude: amplitude a of the peak
center: location parameter (mode) x_c
shape: shape parameter $\nu \in [0, 1]$
width: scaling parameter $\sigma \neq 0$
backgr: offset c_0

Note

- The width parameter needs to be non-zero ($\sigma \neq 0$).
- The shape parameter need to be between 0 and 1 ($\nu \in [0, 1]$)
- Default (size) distribution: Monodisperse

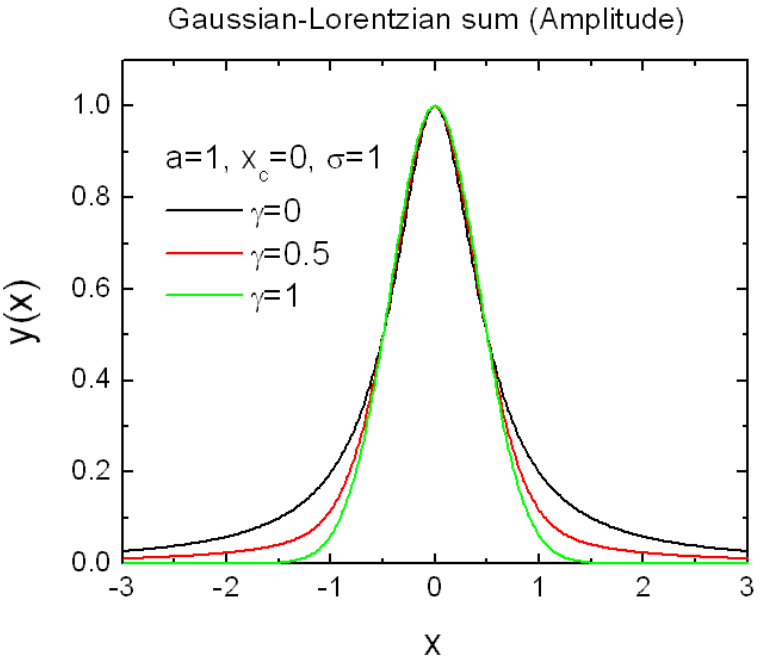

FIGURE 6.20. Plot of `Gaussian-Lorentzian sum (Amplitude)` distribution.

6.11.2. Gaussian-Lorentzian sum (Area).

$$y(x, a, x_c, \sigma, \nu, c_0) =$$
$$2a \left[\frac{\nu}{|\sigma|}\sqrt{\frac{\ln 2}{\pi}} \exp\left(-4\ln 2\left(\frac{x-x_c}{|\sigma|}\right)^2\right) + \frac{1-\nu}{\pi|\sigma|\left[1+4\left(\frac{x-x_c}{|\sigma|}\right)^2\right]} \right] + c_0 \quad (6.40)$$

Required parameters:

area: area a below the peak
center: location parameter (mode) x_c
shape: shape parameter $\nu \in [0, 1]$
width: scaling parameter $\sigma \neq 0$
backgr: offset c_0

Note

- The width parameter needs to be non-zero ($\sigma \neq 0$).
- The shape parameter need to be between 0 and 1 ($\nu \in [0, 1]$)
- Default (size) distribution: Monodisperse

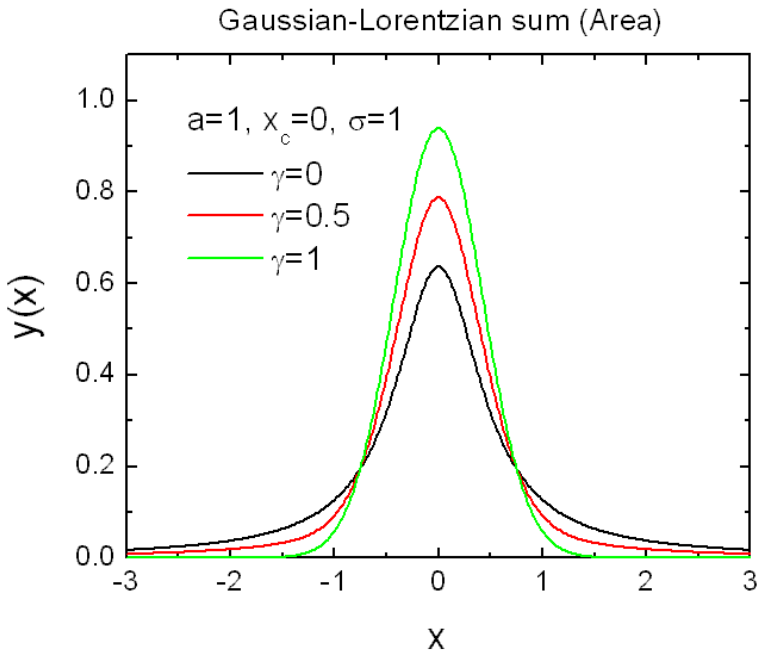

FIGURE 6.21. Plot of `Gaussian-Lorentzian sum (Area)` distribution.

6.12. generalized Gaussian 1

The generalized Gaussian distribution is one of two families of continuous probability distributions, which has an additional shape parameter to the normal distribution. Known also as the exponential power distribution, or the generalized error distribution, this is a parametric family of symmetric distributions. It includes all normal and Laplace distributions, and as limiting cases it includes all continuous uniform distributions on bounded intervals of the real line.

This family includes the normal distribution when $\beta = 2$ (with mean μ and variance $\frac{\alpha^2}{2}$) and it includes the Laplace distribution when $\beta = 1$. As $\beta \to \infty$, the density converges pointwise to a uniform density on $(\mu - \alpha, \mu + \alpha)$.

6.12.1. generalized Gaussian 1 (Amplitude).

$$y(x, a, \mu, \alpha, \beta) = ae^{-\left|\frac{x-\mu}{\alpha}\right|^{\beta}} \tag{6.41}$$

Required parameters:

amplitude: amplitude a of the peak
center: location parameter (mode) μ
width: scaling parameter $\alpha \neq 0$
shape: shape parameter β
backgr: offset c_0

Note

- The width parameter needs to be non-zero ($\alpha \neq 0$).
- The area parameter needs to be positive ($\beta > 0$).
- Default (size) distribution: Monodisperse

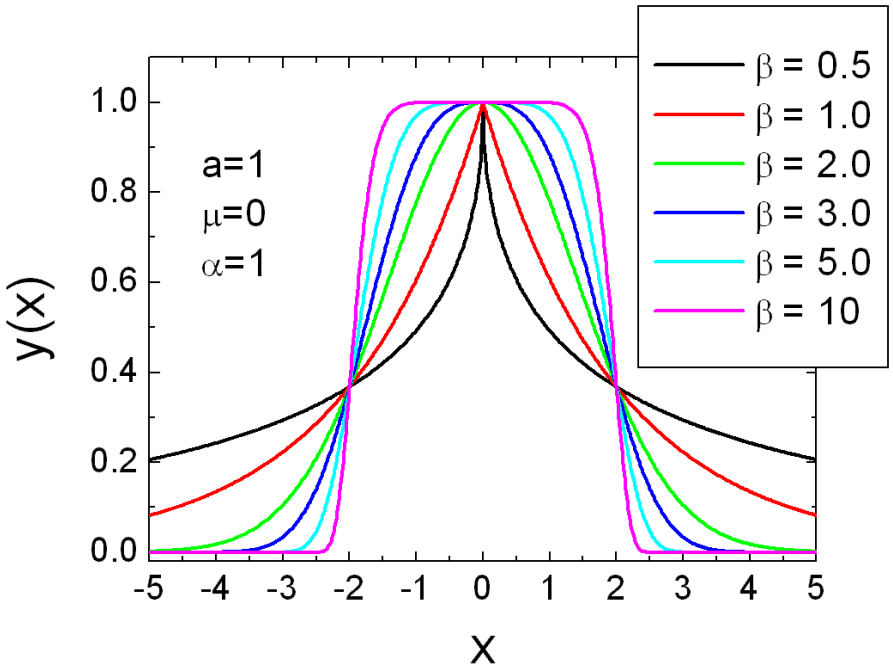

FIGURE 6.22. Plot of `generalized Gaussian 1 (Amplitude)` distribution.

6.12.2. generalized Gaussian 1 (Area).

$$y(x, a, \mu, \alpha, \beta) = a \frac{\beta}{2\alpha\Gamma(1/\beta)} e^{-\left|\frac{x-\mu}{\alpha}\right|^{\beta}} \tag{6.42}$$

Required parameters:

area: area a below the peak
center: location parameter (mode) μ
width: scaling parameter $\alpha \neq 0$
shape: shape parameter β
backgr: offset c_0

Note

- The scaling parameter needs to be positive ($\alpha > 0$).
- Default (size) distribution: Monodisperse

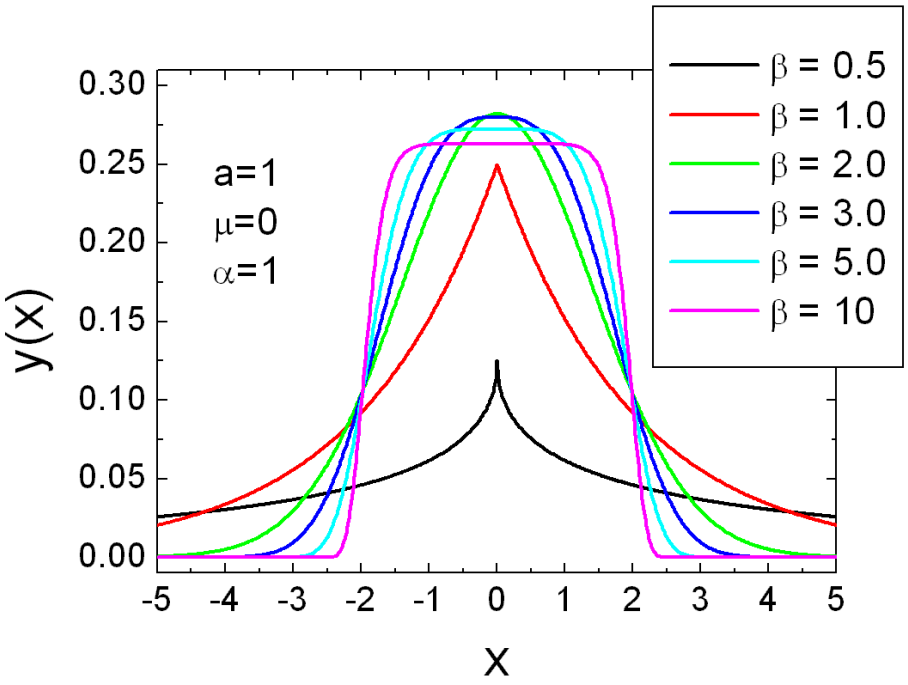

FIGURE 6.23. Plot of `generalized Gaussian 1 (Area)` distribution.

6.13. generalized Gaussian 2

$$x_{\text{mode}} = \begin{cases} \frac{\alpha}{\kappa} - \frac{\alpha}{\kappa} e^{-\kappa^2/2} + \xi & \text{if } \kappa \neq 0 \\ \xi & \text{if } \kappa = 0 \end{cases} \tag{6.43}$$

6.13.1. generalized Gaussian 2 (Amplitude).

$$y(x) = A\,\alpha\sqrt{2\pi}\,\exp\left(-\frac{\kappa^2}{2}\right)\frac{\phi(u)}{\alpha-\kappa(x-\xi)} + c_0 \tag{6.44}$$

where

$$u = \begin{cases} -\frac{1}{\kappa}\log\left[1-\frac{\kappa(x-\xi)}{\alpha}\right] & \text{if } \kappa \neq 0 \\ \frac{x-\xi}{\alpha} & \text{if } \kappa = 0 \end{cases} \tag{6.45}$$

where

$$\phi(x) = \frac{1}{\sqrt{2\pi}}\exp\left(-\frac{x^2}{2}\right) \tag{6.46}$$

Required parameters:

amplitude: amplitude A of the peak
location: location parameter ξ
width: scaling parameter $\alpha > 0$
shape: shape parameter κ
backgr: offset c_0

Note

- The scaling parameter needs to be positive ($\alpha > 0$).
- Default (size) distribution: Monodisperse

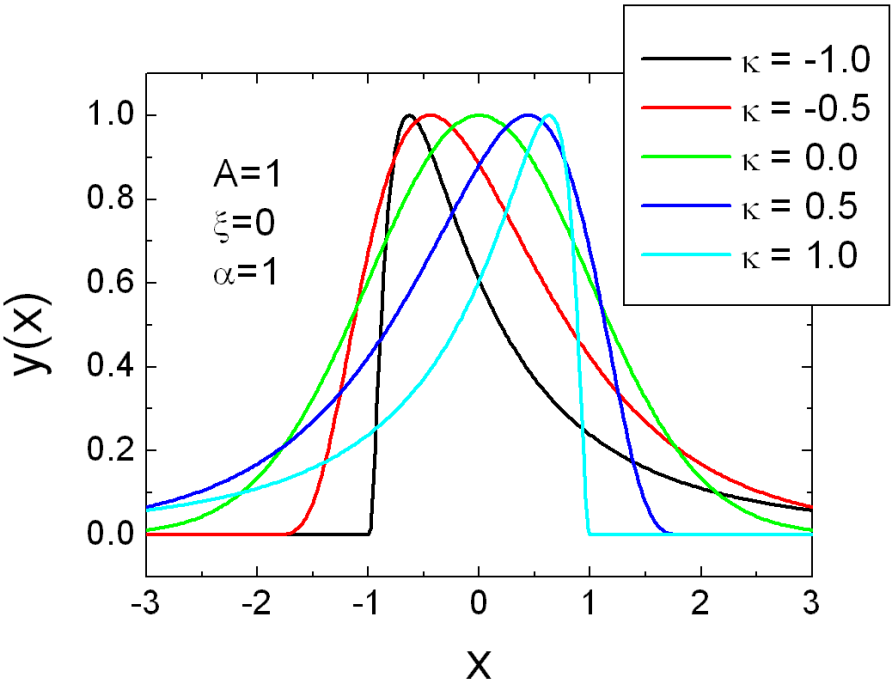

FIGURE 6.24. Plot of `generalized Gaussian 2(Amplitude)` distribution.

6.13.2. generalized Gaussian 2 (Area).

$$y(x) = A\,\frac{\phi(u)}{\alpha - \kappa(x-\xi)} + c_0 \tag{6.47a}$$

where

$$u = \begin{cases} -\frac{1}{\kappa}\log\left[1 - \frac{\kappa(x-\xi)}{\alpha}\right] & \text{if } \kappa \neq 0 \\ \frac{x-\xi}{\alpha} & \text{if } \kappa = 0 \end{cases} \tag{6.47b}$$

and

$$\phi(u) = \frac{1}{\sqrt{2\pi}}\exp\left(-\frac{u^2}{2}\right) \tag{6.47c}$$

Required parameters:

area: area A below the peak
location: location parameter ξ
width: scaling parameter $\alpha > 0$
shape: shape parameter κ
backgr: offset c_0

Note

- The scaling parameter needs to be positive ($\alpha > 0$).
- Default (size) distribution: Monodisperse

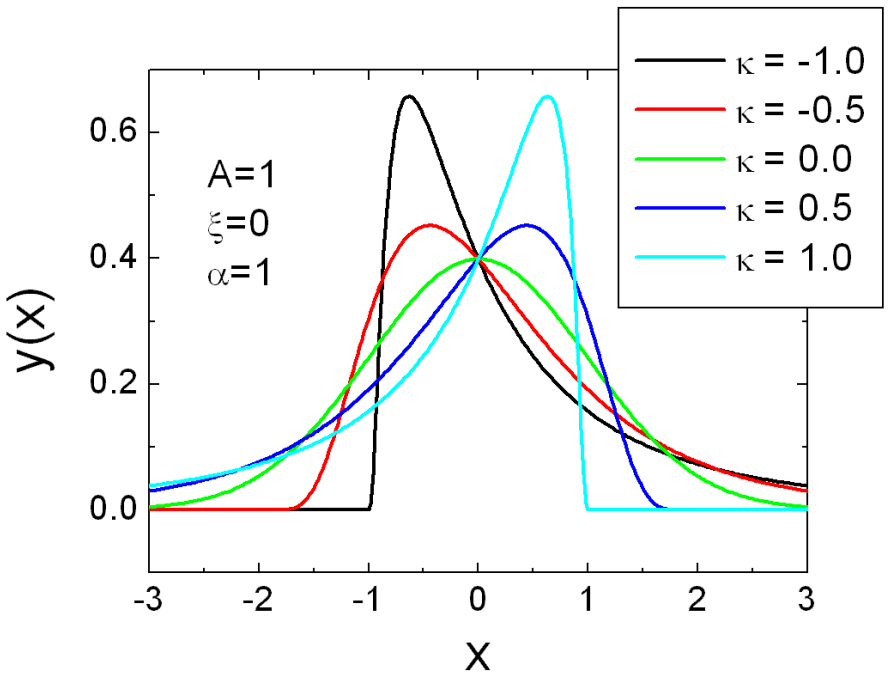

FIGURE 6.25. Plot of `generalized Gaussian 2 (Area)` distribution.

6.14. Giddings

The Giddings equation was derived by J. C. Giddings (Dynamics of Chromatography, Part I, Marcel Decker, New York, 1965). The equation provides a theoretical description for chromatographic peaks. The used formulae have been taken from the Manual of the Peakfit Software package (SeaSolve Software Inc.), which contains an expression for the for the `Giddings (Area)`. As the mode x_{mode} of the peak can not be calculated analytical the amplitude version of this peaks `Giddings (Amplitude)` calculates first numerically the mode of the peak and than normalizes the value at x_{mode} to be $y(x_{\text{mode}}) = A$.

6.14.1. Giddings (Amplitude).

As the mode x_{mode} of this peak can not be calculated analytical this version of the Giddings peak calculates first numerically the mode of the peak and than normalizes the value at x_{mode} to be $y(x_{\text{mode}}) = A$.

$$y(x) = \frac{A}{c}\sqrt{\frac{\beta}{x}}\,\mathrm{I}_1\left(\frac{2\sqrt{\beta x}}{\sigma}\right)\exp\left(-\frac{x+\beta}{\sigma}\right) \tag{6.48a}$$

with

$$c = \sqrt{\frac{\beta}{x_{\text{mode}}}}\,\mathrm{I}_1\left(\frac{2\sqrt{\beta x_{\text{mode}}}}{\sigma}\right)\exp\left(-\frac{x_{\text{mode}}+\beta}{\sigma}\right) \tag{6.48b}$$

Required parameters:

amplitude: amplitude A of the peak
location: location parameter β
width: scaling parameter $\sigma > 0$
backgr: offset c_0

Note

- The scaling parameter needs to be positive ($\sigma > 0$).
- Default (size) distribution: Monodisperse

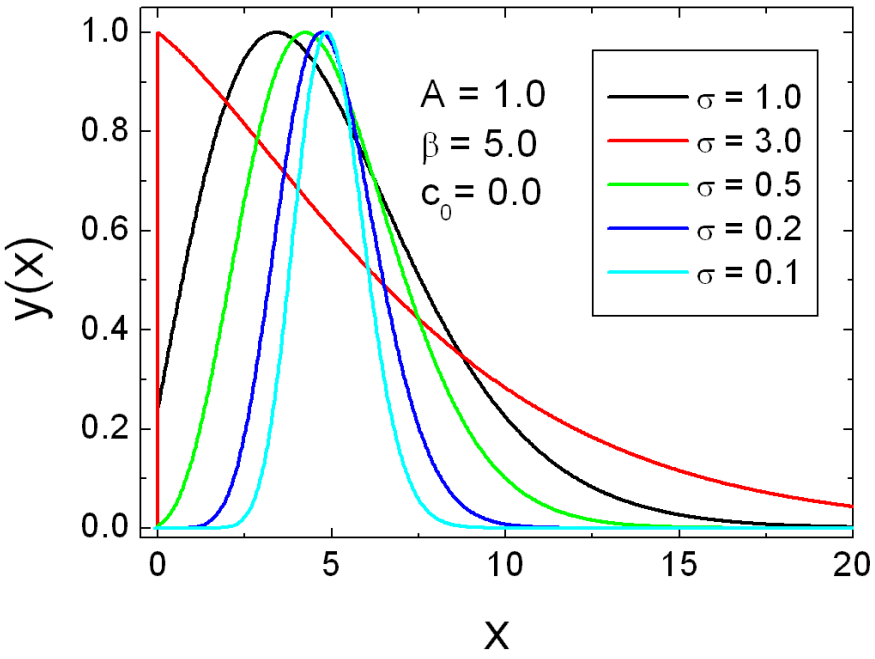

FIGURE 6.26. Plot of `Giddings (Amplitude)` distribution.

6.14.2. Giddings (Area).

$$y(x) = \frac{A}{1-\exp\left(-\frac{\beta}{\sigma}\right)}\,\frac{1}{\sigma}\sqrt{\frac{\beta}{x}}\,\mathrm{I}_1\left(\frac{2\sqrt{\beta x}}{\sigma}\right)\exp\left(-\frac{x+\beta}{\sigma}\right) \tag{6.49}$$

Required parameters:

area: area A below the peak
location: location parameter β
width: scaling parameter $\sigma > 0$
backgr: offset c_0

Note

- The scaling parameter needs to be positive ($\sigma > 0$).
- Default (size) distribution: Monodisperse

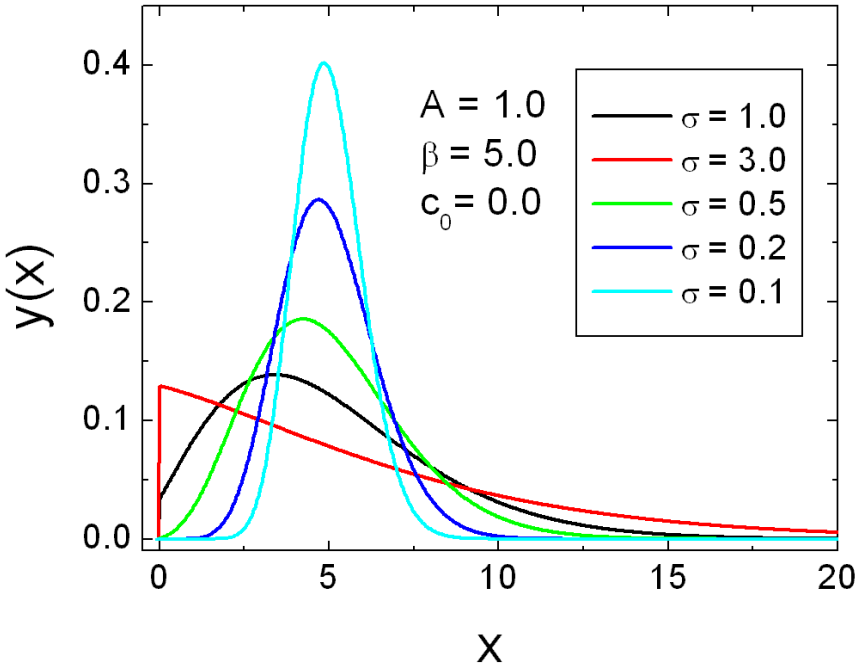

FIGURE 6.27. Plot of `Giddings (Area)` distribution.

6.15. Haarhoff - Van der Linde (Area)

Required parameters:

$$y(x) = \frac{\frac{A\sigma}{\mu\delta\sqrt{2\pi}} \exp\left[-\frac{1}{2}\left(\frac{x-\mu}{\sigma}\right)^2\right]}{\exp\left(1-\frac{\mu\delta}{\sigma^2}\right) + \frac{1}{2}\left[1+\operatorname{erf}\left(\frac{x-\mu}{\sqrt{2}\,\sigma}\right)\right]} \tag{6.50}$$

Required parameters:

area: area A below the peak
location: location parameter $\mu > 0$
width: scaling parameter $\sigma > 0$
delta: distortion parameter $\delta \neq 0$
backgr: offset c_0

Note

- The location parameter needs to be positive ($\mu > 0$).
- The scaling parameter needs to be positive ($\sigma > 0$).
- The distortion parameter needs to be nonzero ($\delta \neq 0$).
- Default (size) distribution: Monodisperse

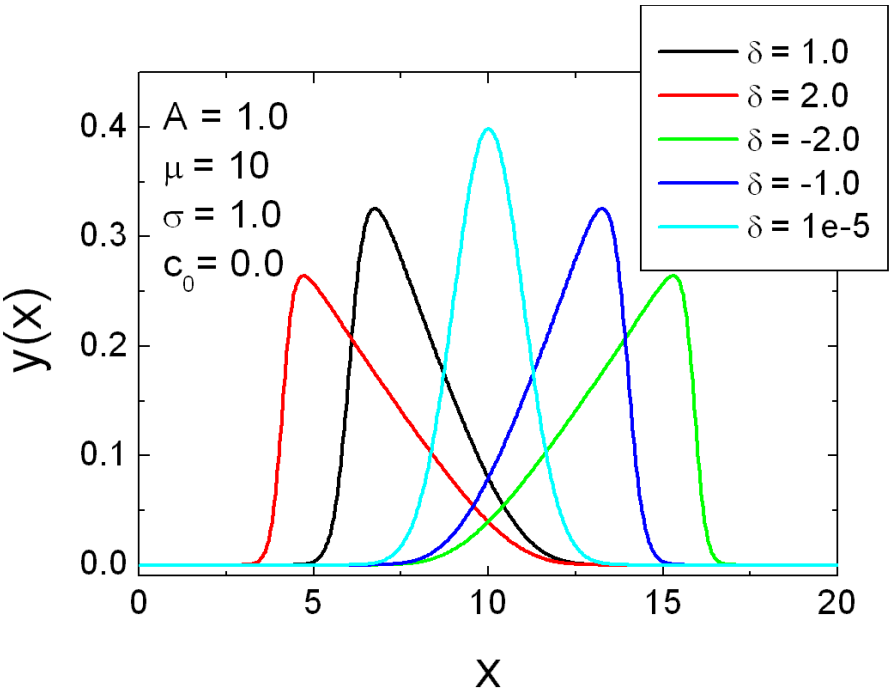

FIGURE 6.28. Plot of `HaarhoffVanderLinde (Area)` distribution.

6.16. Half Gaussian Modified Gaussian (Area)

The `Half Gaussian Modified Gaussian (Area)` is the mathematical convolution of a Gaussian with a half-Gaussian response function. There are only two components to this model, a primary Gaussian, and a response function which convolves or smears the Gaussian as in the profiles above. As the width of the half-Gaussian response increases, peaks become more asymmetric or tailed. This function directly fit both tailed and fronted peaks. The transition from tailed to smooth is continuous and occurs at $\delta = 0$. The formula has been taken from the Manual of the Peakfit Software package (SeaSolve Software Inc.).

$$y(x) = A\frac{\exp\left(-\frac{1}{2}\frac{(x-\mu)^2}{\sigma^2+\delta^2}\right)\left[1+\operatorname{erf}\left(\frac{\delta(x-\mu)}{\sqrt{2}\sigma\sqrt{\sigma^2+\delta^2}}\right)\right]}{\sqrt{2\pi}\sqrt{\sigma^2+\delta^2}} \tag{6.51}$$

Required parameters:

area: area A below the peak
location: location parameter μ
width: scaling parameter $\sigma > 0$
distortion: distortion parameter $\delta \neq 0$
backgr: offset c_0

Note

- The scaling parameter needs to be positive ($\sigma > 0$).
- The distortion parameter needs to be nonzero ($\delta \neq 0$).
- Default (size) distribution: Monodisperse

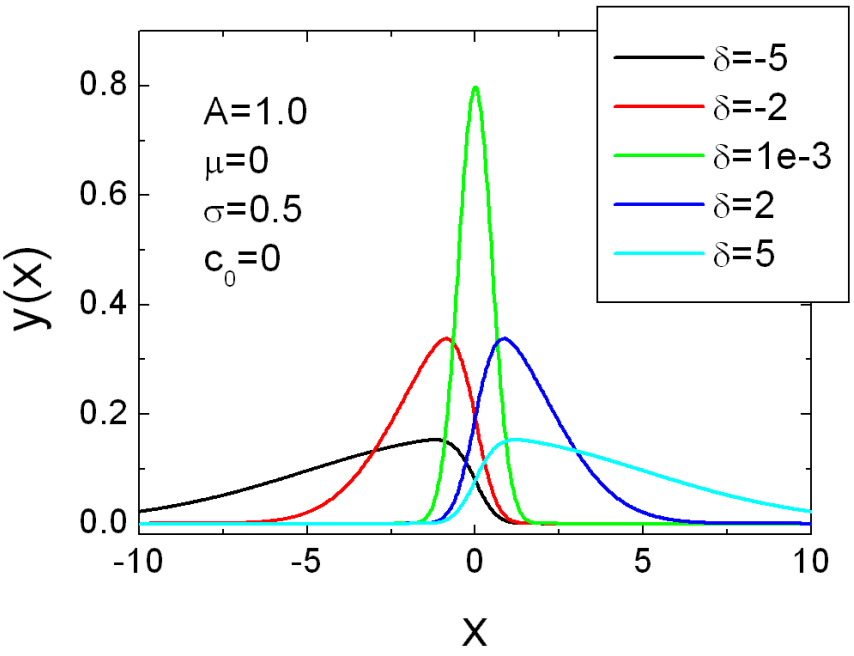

FIGURE 6.29. Plot of `Half Gaussian Modified Gaussian (Area)` distribution.

6.17. Inverted Gamma

The inverse gamma distribution is a two-parameter family of continuous probability distributions on the positive real line, which is the distribution of the reciprocal of a variable distributed according to the gamma distribution. The inverse gamma distribution's probability density function is defined over the support $x > 0$. The probability density function is given by

$$p(x) = \frac{\beta^{\alpha}}{\Gamma(\alpha)} x^{-\alpha-1} \exp\left(\frac{-\beta}{x}\right) \tag{6.52}$$

the mode x_{mode} of the probabilty function is given by $x_{\text{mode}} = \frac{\beta}{\alpha+1}$. The shape parameter α needs to be positive and non-zero as well as the scale parameter β ($\alpha > 0$, $\beta > 0$). The `SASfit` version represents a reparametrization of the standard statistical form. The parameter μ has been added to enable variable x positioning. Adjustment terms have been added so that μ is the mode x_{mode}. The function returns c_0 for those x where it is undefined. Note that the amplitude form is much faster.

6.17.1. Inverted Gamma (Amplitude).

$$y(x) = A\frac{\beta \exp\left(\frac{(x-\mu)(\alpha+1)^2}{x(\alpha+1)+\beta-\mu(\alpha+1)}\right)\left(\frac{x(\alpha+1)-\mu(\alpha+1)}{\beta}+1\right)^{-\alpha}}{x(\alpha+1)+\beta-\mu(\alpha+1)} + c_0 \tag{6.53}$$

Required parameters:

amplitude: amplitude A of the peak
location: location parameter μ
width: scaling parameter $\beta > 0$
shape: shape parameter $\alpha > 0$
backgr: offset c_0

Note

- The scaling parameter needs to be positive ($\beta > 0$).
- The shape parameter needs to be positive ($\alpha > 0$).
- Default (size) distribution: Monodisperse

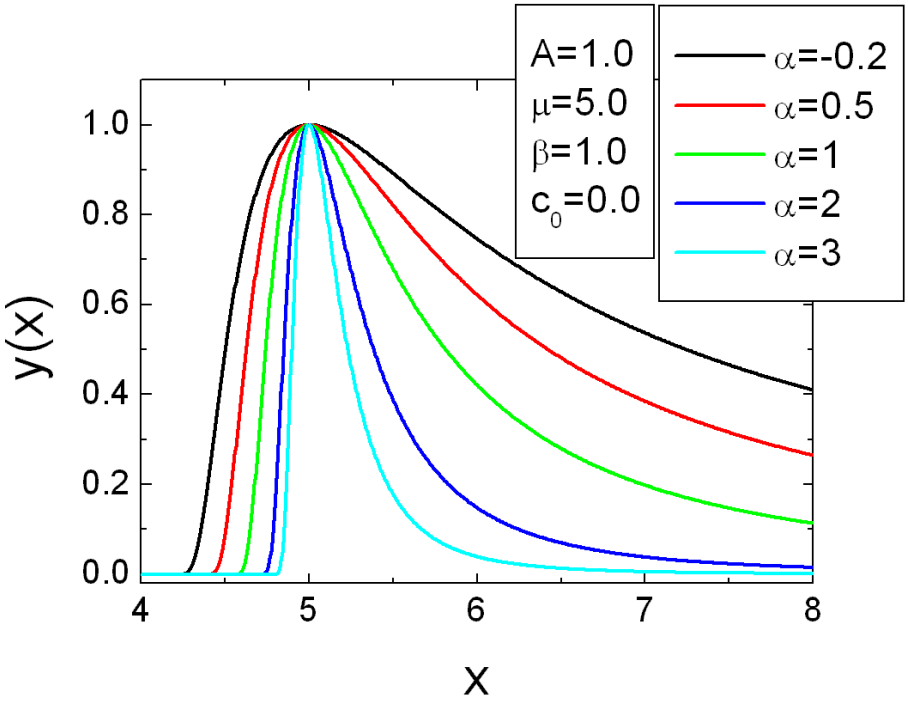

FIGURE 6.30. Plot of `inverted Gamma (Amplitude)` distribution.

6.17.2. Inverted Gamma (Area).

$$y(x) = A\frac{(\alpha+1)\exp\left(\frac{\beta(\alpha+1)}{x(\alpha+1)+\beta-\mu(\alpha+1)}\right)\left(\frac{\beta(\alpha+1)}{x(\alpha+1)+\beta-\mu(\alpha+1)}\right)^{\alpha}}{(x(\alpha+1)+\beta-\mu(\alpha+1))\,\Gamma(\alpha)} + c_0 \tag{6.54}$$

Required parameters:

area: area A below the peak
location: location parameter μ
width: scaling parameter $\beta > 0$
shape: shape parameter $\alpha > 0$
backgr: offset c_0

Note

- The scaling parameter needs to be positive ($\beta > 0$).
- The shape parameter needs to be positive ($\alpha > 0$).
- Default (size) distribution: Monodisperse

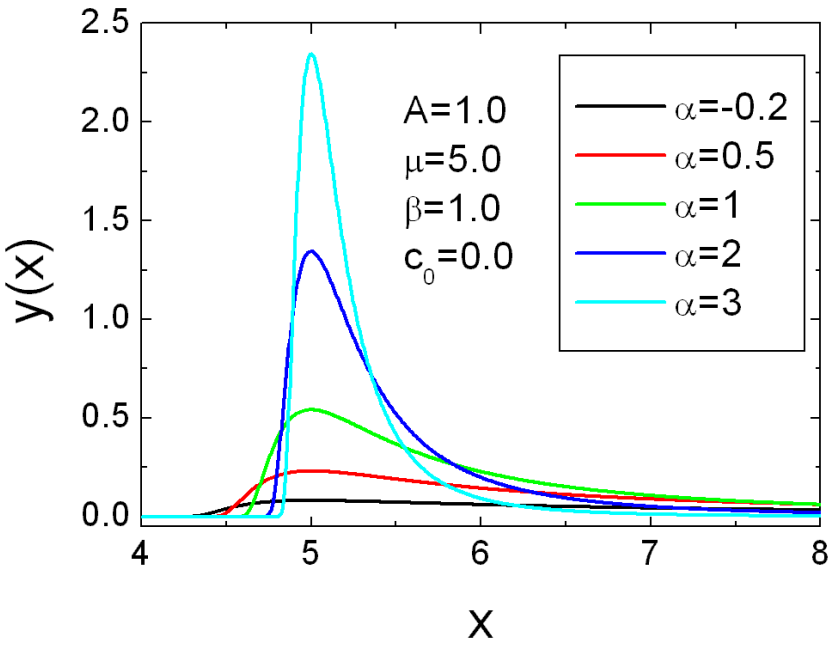

FIGURE 6.31. Plot of `inverted Gamma (Area)` distribution.

6.18. Kumaraswamy

The Kumaraswamy's double bounded distribution is a family of continuous probability distributions defined on the interval $[0, 1]$ differing in the values of their two non-negative shape parameters, a and b. It is similar to the Beta distribution, but much simpler to use especially in simulation studies due to the simple closed form of both its probability density function and cumulative distribution function. The probability density function of the Kumaraswamy distribution is

$$p(x; \alpha, \beta) = \alpha\beta x^{\alpha-1}(1 - x^{\alpha})^{\beta-1}. \tag{6.55}$$

For $\alpha > 1$ and $\beta > 1$ the mode of the distribution reads as

$$x_{\text{mode}} = \left(\frac{\alpha - 1}{\alpha\beta - 1}\right)^{1/\alpha} \tag{6.56}$$

6.18.1. Kumaraswamy (Amplitude).

$$y(x) = \begin{cases} \frac{A\alpha\beta\left(\frac{x+x_{\min}}{x_{\max}-x_{\min}}\right)^{\alpha-1}\left(1-\left(\frac{x+x_{\min}}{x_{\max}-x_{\min}}\right)^{\alpha}\right)^{\beta-1}}{\alpha\beta x_{\text{mode}}^{\alpha-1}(1-x_{\text{mode}}^{\alpha})^{\beta-1}} + c_0 & \text{for } x \in [x_{\min}, x_{\max}] \\ c_0 & \text{for } x \notin [x_{\min}, x_{\max}] \end{cases} \tag{6.57}$$

Required parameters:

ampl.: amplitude A of the Kumaraswamy peak
xmin: continuous lower boundary parameters $x_{\min}$
xmax: continuous upper boundary parameters $x_{\max}$
alpha: first shape parameter $\alpha > 1$
beta: second shape parameter $\beta > 1$
backgr: offset c_0

Note

- Both shape parameter needs to be larger than one ($\alpha, \beta > 1$), as only than the distribution has a peak shape.
- where the Kumaraswamy distribution is not defined the offset value is returned: $\forall x \notin (x_{\min}, x_{\max}) \quad y_{\text{Beta(ampl)}}(x) = c_0$
- Default (size) distribution: Monodisperse

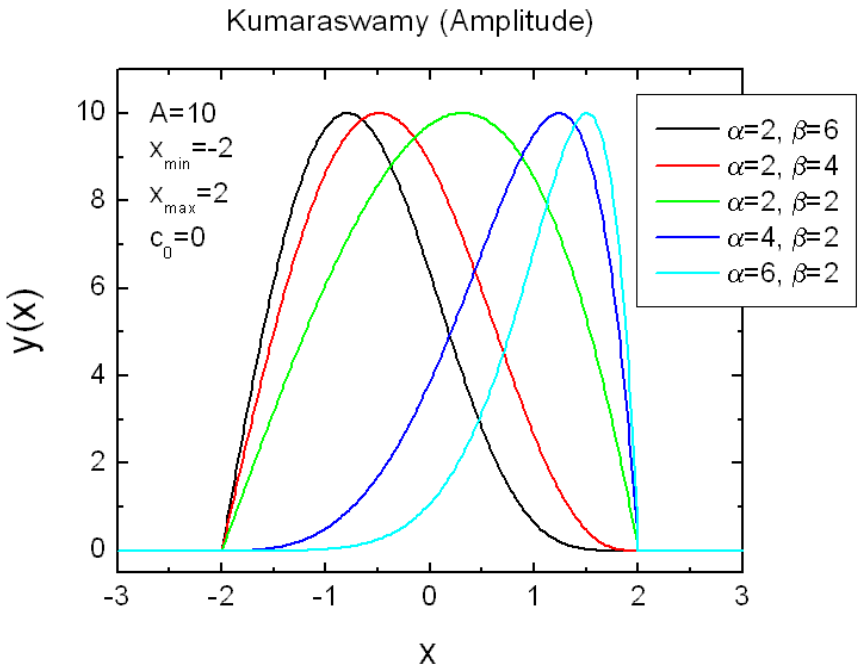

FIGURE 6.32. Plot of `Kumaraswamy (Amplitude)` distribution.

6.19. Kumaraswamy (Area)

$$y(x) = \begin{cases} \frac{A\alpha\beta\left(\frac{x+x_{\min}}{x_{\max}-x_{\min}}\right)^{\alpha-1}\left(1-\left(\frac{x+x_{\min}}{x_{\max}-x_{\min}}\right)^{\alpha}\right)^{\beta-1}}{x_{\max}-x_{\min}} + c_0 & \text{for } x \in [x_{\min}, x_{\max}] \\ c_0 & \text{for } x \notin [x_{\min}, x_{\max}] \end{cases} \quad (6.58)$$

Required parameters:

area: area A of the Kumaraswamy distribution
xmin: continuous lower boundary parameters $x_{\min}$
xmax: continuous upper boundary parameters $x_{\max}$
alpha: first shape parameter $\alpha > 0$
beta: second shape parameter $\beta > 0$
backgr: offset c_0

Note

- Both shape parameter needs to be larger than zero $(\alpha, \beta > 0)$
- where the Kumaraswamy distribution is not defined the offset value is returned: $\forall x \notin (x_{\min}, x_{\max}) \quad y_{\text{Beta(area)}}(x) = c_0$
- Default (size) distribution: Monodisperse

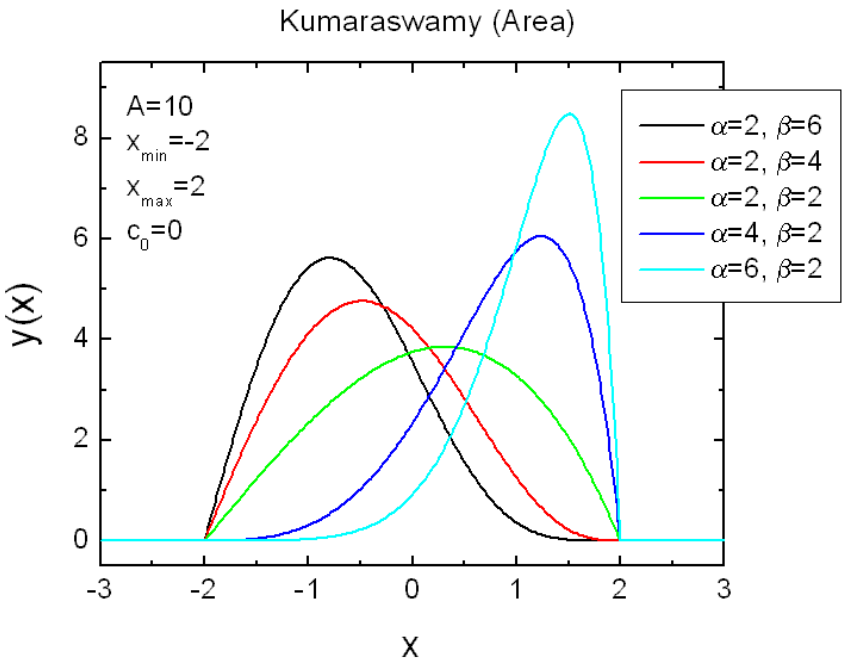

FIGURE 6.33. Plot of `Kumaraswamy (Area)` distribution.

6.20. Laplace

A random variable has a Laplace distribution if its probability density function is

$$p(x; x_0, \sigma) = \frac{1}{2\sigma} \exp\left(-\frac{|x - x_0|}{\sigma}\right) \tag{6.59}$$

Here, x_0 is a location parameter and $\sigma > 0$ is a scale parameter. The Laplace distribution is also sometimes called the double exponential distribution, because it can be thought of as two exponential distributions (with an additional location parameter) spliced together back-to-back, but the term double exponential distribution is also sometimes used to refer to the Gumbel distribution.

6.20.1. Laplace (Amplitude).

$$y(x; x_0, \sigma) = A \exp\left(-\frac{|x - x_0|}{\sigma}\right) + c_0 \tag{6.60}$$

Required parameters:

amplitude: amplitude A of the Laplace distribution
center: peak center (mode) x_0 of the Laplace distribution
width: width parameter $\sigma > 0$
backgr: offset c_0

Note

- Width parameter needs to be larger than zero ($\sigma > 0$)
- Default (size) distribution: Monodisperse

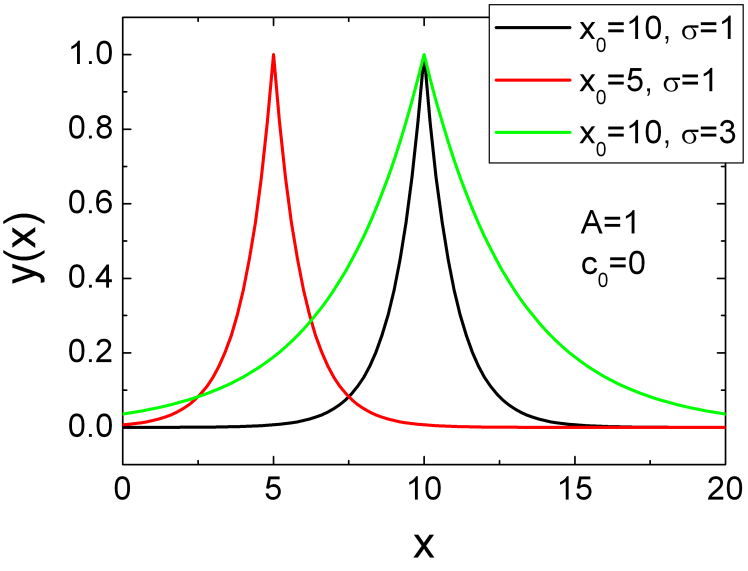

FIGURE 6.34. Plot of `Laplace (Amplitude)` distribution.

6.20.2. Laplace (Area).

$$y(x; x_0, \sigma) = \frac{A}{2\sigma} \exp\left(-\frac{|x - x_0|}{\sigma}\right) + c_0 \tag{6.61}$$

Required parameters:

area: area A of the Laplace distribution
center: peak center (mode) x_0 of the Laplace distribution
width: width parameter $\sigma > 0$
backgr: offset c_0

Note

- Width parameter needs to be larger than zero ($\sigma > 0$)
- Default (size) distribution: Monodisperse

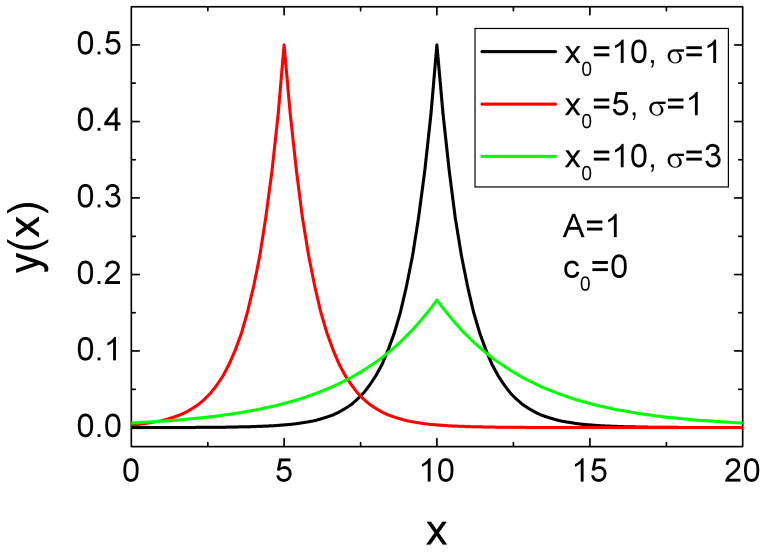

FIGURE 6.35. Plot of `Laplace (Area)` distribution.

6.21. Logistic

The logistic distribution is a continuous probability distribution. It resembles the normal distribution in shape but has heavier tails (higher kurtosis). The probability density function (pdf) of the logistic distribution is given by:

$$p(x; x_0, \sigma) = \frac{\exp\left(-\frac{x-x_0}{\sigma}\right)}{\sigma\left(1+\exp\left(-\frac{x-x_0}{\sigma}\right)\right)^2} = \frac{1}{4\,\sigma}\ \operatorname{sech}^2\left(\frac{x-x_0}{2\,\sigma}\right). \tag{6.62}$$

Because the pdf can be expressed in terms of the square of the hyperbolic secant function sech, it is sometimes referred to as the sech-squared distribution. The mode, mean and median values are x_0.

6.21.1. Logistic (Amplitude).

$$y(x; x_0, \sigma) = 4A\frac{\exp\left(-\frac{x-x_0}{\sigma}\right)}{\left(1+\exp\left(-\frac{x-x_0}{\sigma}\right)\right)^2} \tag{6.63}$$

Required parameters:

amplitude: amplitude A of the Logistic distribution
x0: location parameter (mode) x_0
sigma: width parameters σ
backgr: offset c_0

Note

- the width parameter needs to be larger than zero $\sigma > 0$
- Default (size) distribution: Monodisperse

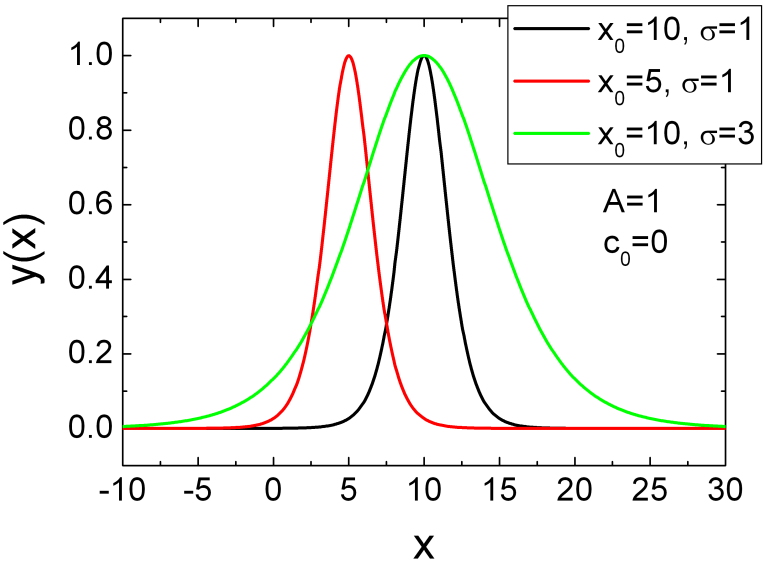

FIGURE 6.36. Plot of `Logistic (Amplitude)` distribution.

6.21.2. Logistic (Area).

$$y(x;x_0,\sigma) = A\,\frac{\exp\left(-\frac{x-x_0}{\sigma}\right)}{\sigma\left(1+\exp\left(-\frac{x-x_0}{\sigma}\right)\right)^2} \tag{6.64}$$

Required parameters:

area: area A of the Logistic distribution
x0: location parameter (mode) x_0
sigma: width parameters σ
backgr: offset c_0

Note

- the width parameter needs to be larger than zero $\sigma > 0$
- Default (size) distribution: Monodisperse

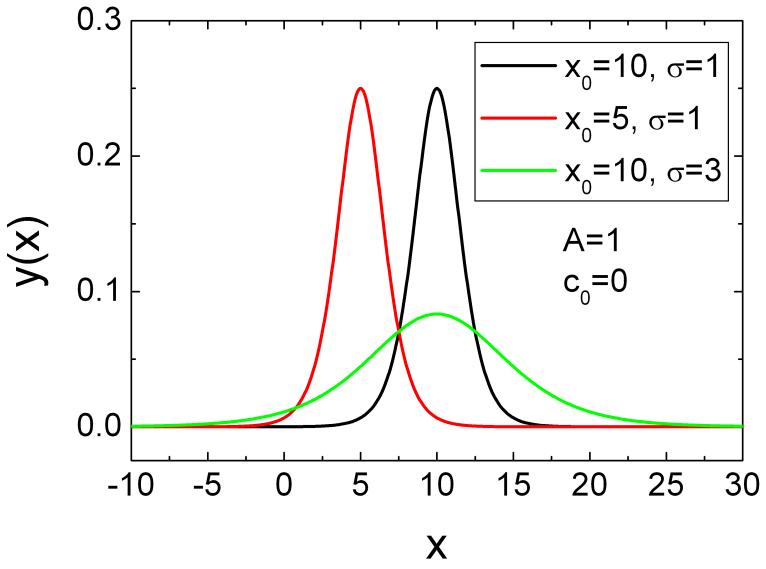

FIGURE 6.37. Plot of `Logistic (Area)` distribution

.

6.22. LogLogistic

As may be indicated by the name, the loglogistic (known as the Fisk distribution in economics) distribution has certain similarities to the logistic distribution. A random variable is loglogistically distributed if the logarithm of the random variable is logistically distributed. The `LogLogistic` distribution is a two-parameter distribution with parameters σ and x_0. It is similar in shape to the log-normal distribution but has heavier tails.

The pdf for this distribution is given by:

$$p(x;\mu,\sigma) = \frac{\exp\left(-\frac{\log(x)-\log(\mu)}{\sigma}\right)}{\sigma\,(x)\left(1+\exp\left(-\frac{\log(x)-\log(\mu)}{\sigma}\right)\right)^2} = \frac{\left(\frac{x}{\mu}\right)^{-1/\sigma}}{x\sigma\left[1+\left(\frac{x}{\mu}\right)^{-1/\sigma}\right]^2}. \tag{6.65}$$

where $0 < x < \infty$, $-\infty < x_0 < \infty$ and $0 < \sigma < \infty$. The mode of the `LogLogistic` distribution, if $\sigma < 1$, is given by:

$$\text{mode} = \mu\left(\frac{1-\sigma}{1+\sigma}\right)^{\sigma} \tag{6.66}$$

6.22.1. LogLogistic (Amplitude).

$$y(x) = \begin{cases} A\frac{\left(\frac{x-x_0}{\mu}\right)^{-1/\sigma}}{(x-x_0)\sigma\left[1+\left(\frac{x-x_0}{\mu}\right)^{-1/\sigma}\right]^2} + c_0 & \text{for } x \geq x_0 \\ c_0 & \text{for } x < x_0 \end{cases} \tag{6.67}$$

Required parameters:

amplitude: amplitude A of the LogLogistic distribution
x0: location parameter x_0
mu: scale parameter μ
sigma: shape parameters σ
backgr: offset c_0

Note

- the width parameter needs to be larger than zero $0 < \sigma < 1$
- Default (size) distribution: Monodisperse

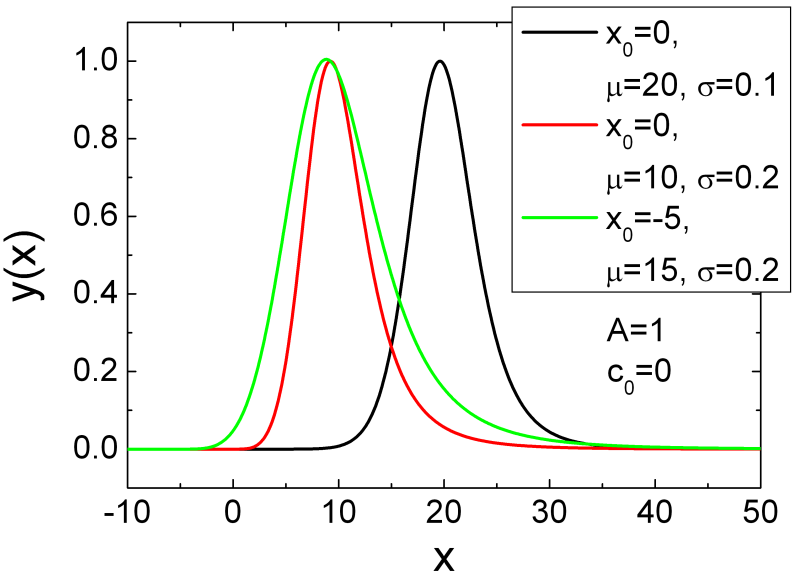

FIGURE 6.38. Plot of `LogLogistic (Amplitude)` distribution.

6.22.2. LogLogistic (Area).

$$y(x) = A\frac{\left(\frac{x}{x_0}\right)^{-1/\sigma}}{x\sigma\left[1+\left(\frac{x}{x_0}\right)^{-1/\sigma}\right]^2}. \tag{6.68}$$

Required parameters:

area: area A of the LogLogistic distribution
x0: location parameter x_0
mu: scale parameter μ
sigma: shape parameters $0 < \sigma < 1$
backgr: offset c_0

Note

- the width parameter needs to be larger than zero $\sigma > 0$
- Default (size) distribution: Monodisperse

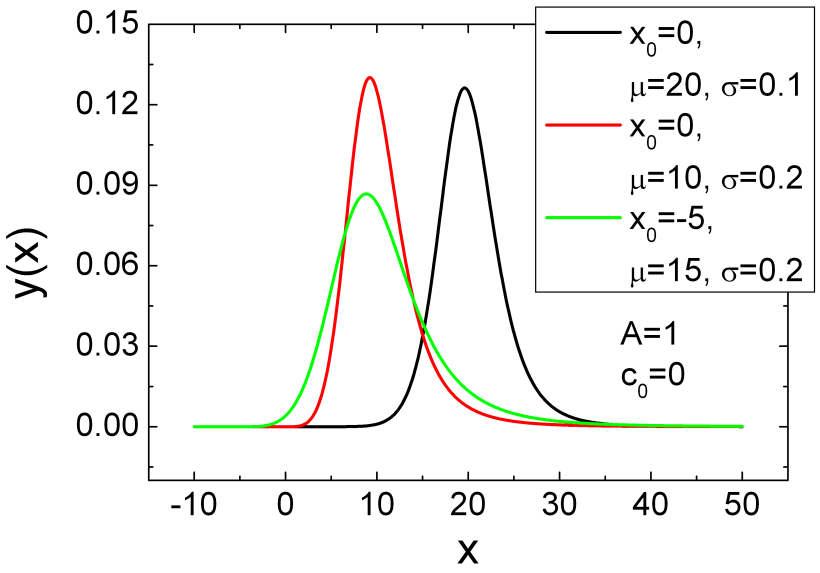

FIGURE 6.39. Plot of `LogLogistic (Area)` distribution.

6.23. Lognormal 4-Parameter

6.23.1. Lognormal 4-Parameter (Amplitude).

$$y(x) = \begin{cases} c_0 + A \exp\left[-\frac{\ln(2) \ln\left(\frac{(x-x_0)(\gamma^2-1)}{\sigma\gamma} + 1 \right)^2}{\ln(\gamma)} \right] & \text{for } \gamma \neq 1, \gamma > 0 \\ c_0 + A 2^{-4\left(\frac{x-x_0}{\sigma}\right)^2} & \text{for } \gamma = 1 \end{cases} \tag{6.69}$$

For $\left(x \geq x_0 - \frac{\sigma\gamma}{\gamma^2-1} \wedge \gamma < 1 \right) \vee \left(x \leq x_0 - \frac{\sigma\gamma}{\gamma^2-1} \wedge \gamma > 1 \right)$ the function returns c_0.

Required parameters:

amplitude: amplitude A of the LogLogistic distribution
x0: location parameter x_0
sigma: width parameter $\sigma > 0$
gamma: shape parameters $\gamma > 0$
backgr: offset c_0

Note

- the width parameter needs to be larger than zero $\sigma > 0$
- the shape parameter needs to be larger than zero $\gamma > 0$
- Default (size) distribution: Monodisperse

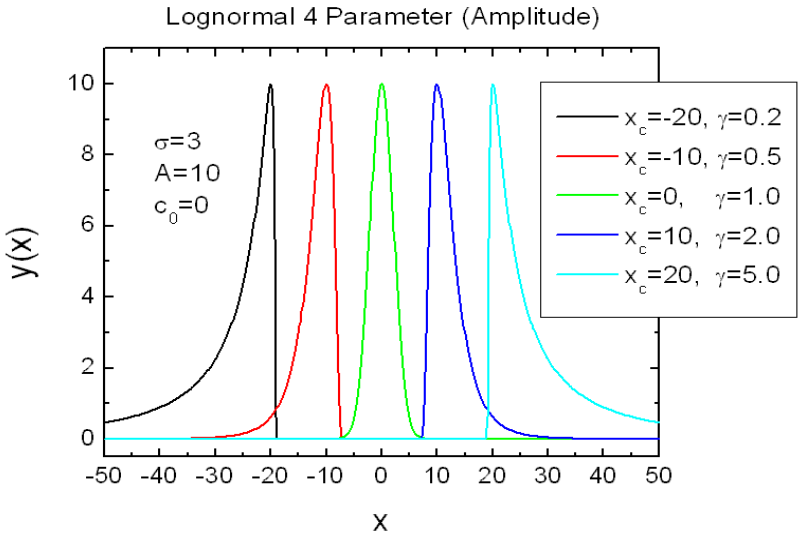

FIGURE 6.40. Plot of `Lognormal 4-Parameter (Amplitude)` distribution.

6.23.2. Lognormal 4-Parameter (Area).

$$y(x) = \begin{cases} c_0 + A\frac{\sqrt{\ln 2}(\gamma^2-1)}{\sigma\gamma\ln(\gamma)\sqrt{\pi}\exp\left(\frac{\ln(\gamma^2)}{4\ln 2}\right)}\exp\left[-\frac{\ln(2)\ln\left(\frac{(x-x_0)(\gamma^2-1)}{\sigma\gamma}+1\right)^2}{\ln(\gamma)}\right] & \text{for } \gamma \neq 1, \gamma > 0 \\ c_0 + A\frac{\sqrt{\ln 2}}{\sigma\sqrt{\pi}}2^{-4\left(\frac{x-x_0}{\sigma}\right)^2} & \text{for } \gamma = 1 \end{cases} \tag{6.70}$$

For $\left(x \geq x_0 - \frac{\sigma\gamma}{\gamma^2-1} \wedge \gamma < 1\right) \vee \left(x \leq x_0 - \frac{\sigma\gamma}{\gamma^2-1} \wedge \gamma > 1\right)$ the function returns c_0.

Required parameters:

area: area A of the LogLogistic distribution
x0: location parameter x_0
sigma: width parameter $\sigma > 0$
gamma: shape parameters $\gamma > 0$
backgr: offset c_0

Note

- the width parameter needs to be larger than zero $\sigma > 0$
- the shape parameter needs to be larger than zero $\gamma > 0$
- Default (size) distribution: Monodisperse

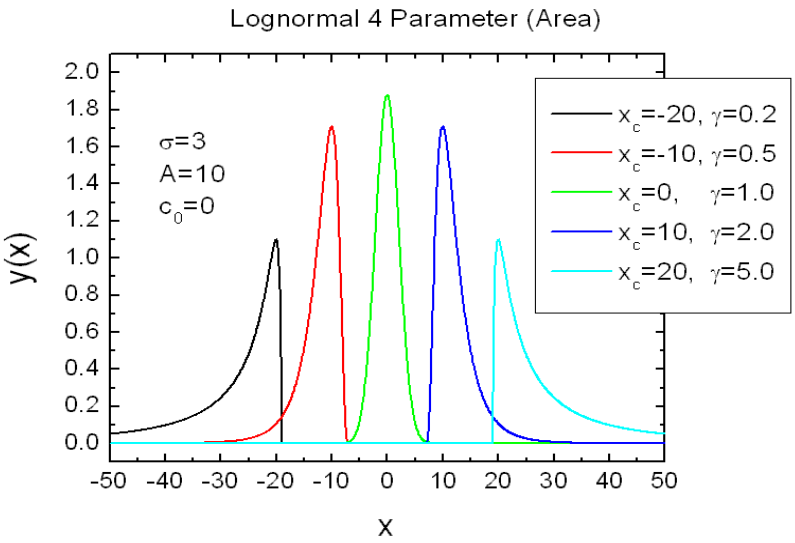

FIGURE 6.41. Plot of `Lognormal 4-Parameter (Area)` distribution.

6.24. LogNormal

The LogNormal distribution is defined with reference to the normal distribution. A random variable is Lognormally distributed if the logarithm of the random variable is normally distributed.

The LogNormal distribution is commonly used for general reliability analysis, cycles-to-failure in fatigue, material strengths and loading variables in probabilistic design. Another advantage of the LogNormal distribution is that it is positive-definite, so it is often useful for representing quantities that cannot have negative values. LogNormal distributions have proven useful as distributions for rainfall amounts, for the size distributions of aerosol particles or droplets, and for many other cases. The log-normal distribution has the probability density function

$$f(x') = \frac{1}{\sigma\sqrt{2\pi}} \exp\left(-\frac{1}{2}\left(\frac{x'-\mu'}{\sigma}\right)^2\right) \tag{6.71}$$

where $\mu' = \ln(\mu)$ and $x' = \ln(x)$. The lognormal pdf can be obtained, realizing that for equal probabilities under the normal and lognormal pdfs, incremental areas should also be equal, or:

$$f(x;\mu,\sigma)dx = f(x';\mu,\sigma)dx' \tag{6.72}$$

Taking the derivative yields:

$$dx' = \frac{dx}{x} \tag{6.73}$$

Substitution yields:

$$f(x;\mu,\sigma) = \frac{f(x';\mu,\sigma)}{x} \tag{6.74}$$

where:

$$f(x;\mu,\sigma) = \frac{1}{x\sigma\sqrt{2\pi}} \exp\left(-\frac{1}{2}\left(\frac{\ln(x)-\ln(\mu)}{\sigma}\right)^2\right) \tag{6.75}$$

for $x \in (0,\infty]$, where $\mu > 0$ and $\sigma \neq 0$ are the location and scale parameter. The mode of the distribution is

$$\text{mode} = \mu \exp\left(-\sigma^2\right) \tag{6.76}$$

6.24.1. LogNormal (Amplitude).

$$y(x) = \begin{cases} \frac{A\exp\left(-\frac{1}{2}\sigma^2\right)\mu}{x-x_0}\exp\left(-\frac{1}{2}\left(\frac{\ln(x-x_0)-\ln(\mu)}{\sigma}\right)^2\right)+c_0 & \text{for } x > x_0 \\ c_0 & \text{for } x \leq x_0 \end{cases} \tag{6.77}$$

Required parameters:

amplitude: amplitude A of the LogNormal distribution
mu: location parameter μ
sigma: width parameter $\sigma > 0$
x0: shift parameters x_0
backgr: offset c_0

Note

- the width parameter needs to be larger than zero $\sigma > 0$
- the location parameter needs to be larger than the shift parameter $\mu > x_0$
- Default (size) distribution: Monodisperse

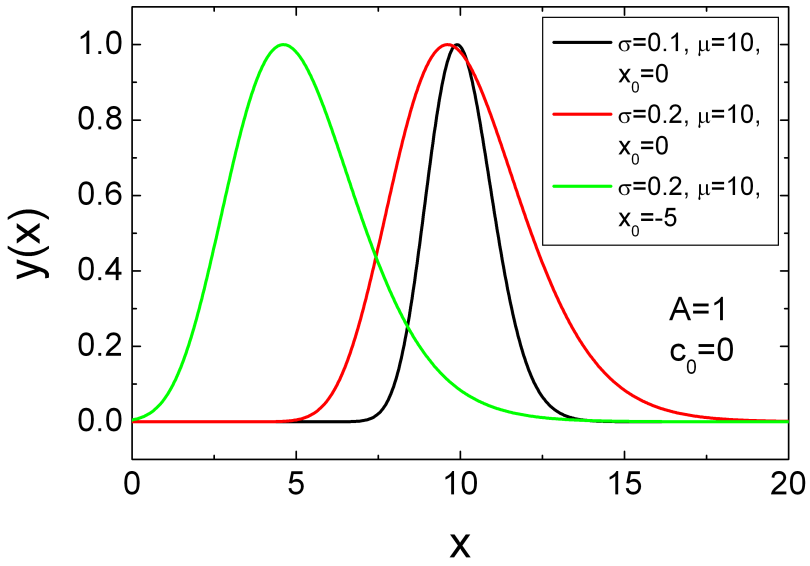

FIGURE 6.42. Plot of `LogNormal (Amplitude)` distribution.

6.24.2. LogNormal (Area).

$$y(x) = \begin{cases} \frac{A}{(x-x_0)\sigma\sqrt{2\pi}} \exp\left(-\frac{1}{2}\left(\frac{\ln(x-x_0)-\ln(\mu)}{\sigma}\right)^2\right) + c0 & \text{for } x > x0 \\ c_0 & \text{for } x \leq x0 \end{cases} \tag{6.78}$$

Required parameters:

area: area A of the LogNormal distribution
mu: location parameter μ
sigma: width parameter $\sigma > 0$
x0: shift parameters x_0
backgr: offset c_0

Note

- the width parameter needs to be larger than zero $\sigma > 0$
- the location parameter needs to be larger than the shift parameter $\mu > x_0$
- Default (size) distribution: Monodisperse

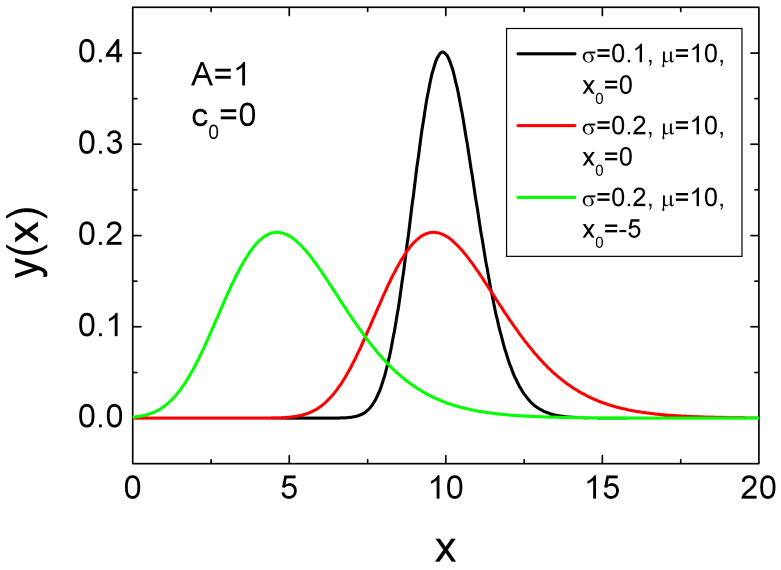

FIGURE 6.43. Plot of `LogNormal (Area)` distribution.

6.25. Lorentzian or Cauchy distribution

The CauchyLorentz Distribution, named after Augustin Cauchy and Hendrik Lorentz, is a continuous probability distribution. As a probability distribution, it is known as the Cauchy distribution, while among physicists, it is known as a Lorentz distribution, or a Lorentz(ian) function or the BreitWigner distribution. Its importance in physics is due to it being the solution to the differential equation describing forced resonance. The Lorntzian distribution has the probability density function

$$\begin{aligned} f(x; x_0, \sigma) &= \frac{1}{\pi\sigma\left[1 + \left(\frac{x-x_0}{\sigma}\right)^2\right]} \\ &= \frac{1}{\pi}\left[\frac{\sigma}{(x-x_0)^2 + \sigma^2}\right] \end{aligned} \tag{6.79}$$

where x_0 is the location parameter, specifying the location of the peak of the distribution, and σ is the scale parameter which specifies the half-width at half-maximum (HWHM).

6.25.1. Lorentzian (Amplitude).

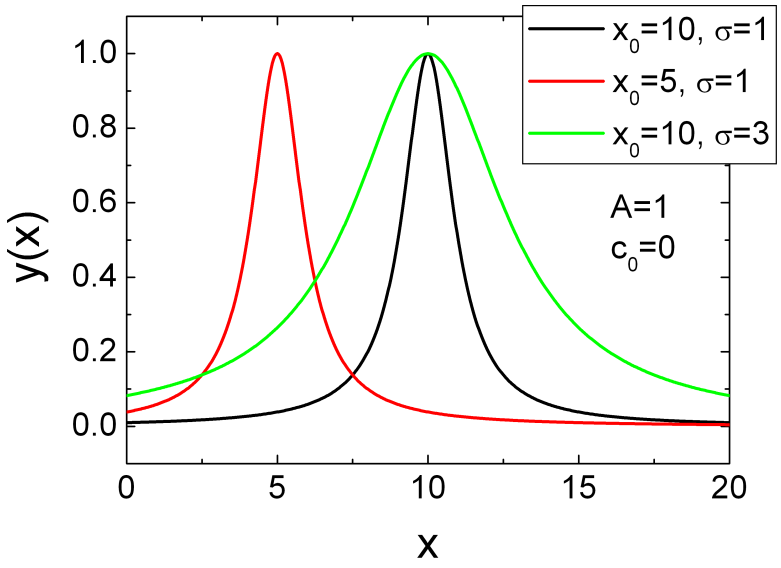

FIGURE 6.44. Plot of `Lorentzian (Amplitude)` distribution.

6.25.2. Lorentzian (Area).

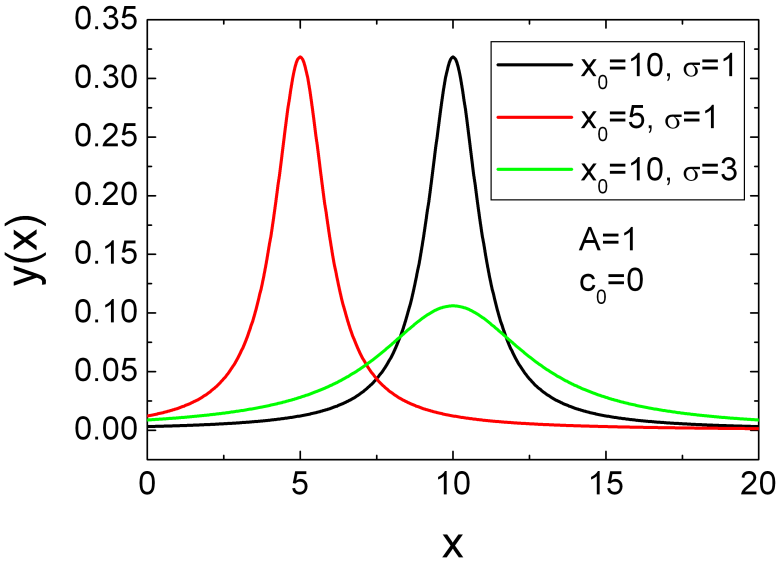

FIGURE 6.45. Plot of `Lorentzian (Area)` distribution.

6.26. Maxwell-Boltzmann distribution

The Maxwell-Boltzmann distribution describes particle speeds in gases, where the particles do not constantly interact with each other but move freely between short collisions. It describes the probability of a particle's speed (the magnitude of its velocity vector) being near a given value as a function of the temperature of the system, the mass of the particle, and that speed value. This probability distribution is named after James Clerk Maxwell and Ludwig Boltzmann.

The Maxwell-Boltzmann distribution is usually thought of as the distribution for molecular speeds, but it can also refer to the distribution for velocities, momenta, and magnitude of the momenta of the molecules, each of which will have a different probability distribution function, all of which are related. Two Maxwell distributions have been implemented, one distribution for speed and a generalized Maxwell distribution, which includes also the energy distribution.

The generalized Maxwell distribution is here defined as

$$p(x;x_0,\sigma,n,m)=\begin{cases}0 & \text{for } x<x_0\\ \frac{(x-x_0)^m\exp\left(-\frac{1}{2}\left(\frac{x-x_0}{|\sigma|}\right)^n\right)}{2^{(1+m)/n}|\sigma|^{1+m}\frac{1}{|n|}\Gamma\left(\frac{1+m}{n}\right)} & \text{for } x\geq x_0.\end{cases} \tag{6.80}$$

where x_0 is the location parameter, specifying the location of the peak of the distribution, and σ is the scale parameter which specifies the width. The mode of the distribution is given by

$$x_{\text{mode}}=\left(\frac{2m}{n}\right)^{1/n}|\sigma|+x_0. \tag{6.81}$$

For the case $m=n=2$ one gets the "Maxwell-Boltzmann distribution" to refers to the distribution of speed. To get the distribution for the energy one has to set $m=1/2$ and $n=1$. In case of the width parameter σ always the modulus is used in the calculation of the distribution function to avoid negative values for which the function is not always well defined. For $\sigma=0$ the distribution function is not defined.

6.26.1. Maxwell (Amplitude).

$$y(x;A,\sigma,x_0,y_0) = \begin{cases} y_0 & \text{for } x < x_0 \\ y_0 + A\,\frac{(x-x_0)^2}{(x_{\text{mode}}-x_0)^2}\,\frac{\exp\left(-\frac{1}{2}\left(\frac{x-x_0}{\sigma}\right)^2\right)}{\exp\left(-\frac{1}{2}\left(\frac{x_{\text{mode}}-x_0}{\sigma}\right)^2\right)} & \text{for } x \geq x_0 \end{cases} \tag{6.82}$$

with $x_{\text{mode}} = \sqrt{2}\,|\sigma| + x_0$.

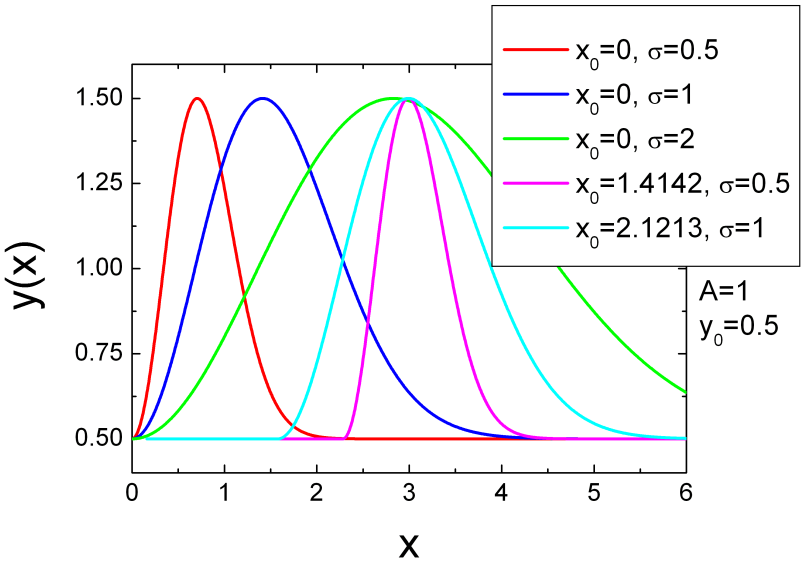

FIGURE 6.46. Plot of `Maxwell (Amplitude)` distribution.

6.26.2. Maxwell (Area).

$$y(x; A, \sigma, x_0, y_0) = \begin{cases} y_0 & \text{for } x < x_0 \\ y_0 + \sqrt{\frac{2}{\pi}} \frac{A(x-x_0)^2}{\sigma^3} \exp\left(-\frac{1}{2}\left(\frac{x-x_0}{\sigma}\right)^2\right) & \text{for } x \geq x_0 \end{cases} \tag{6.83}$$

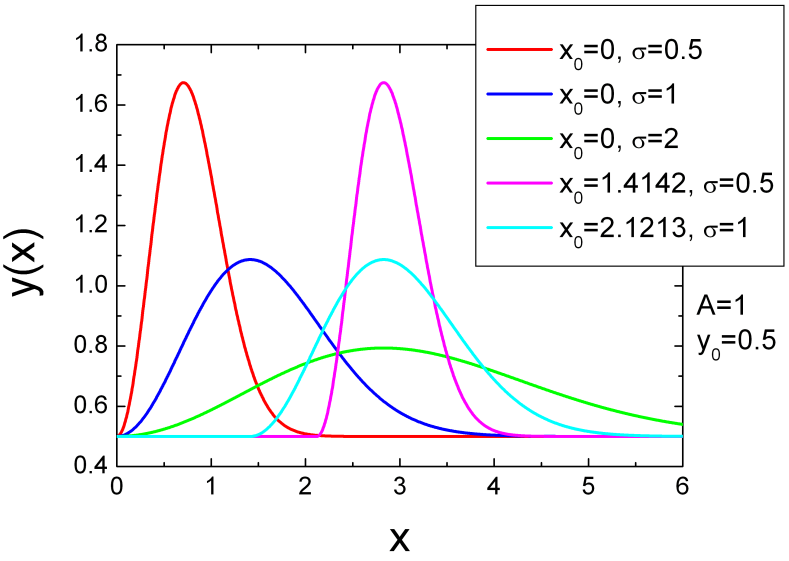

FIGURE 6.47. Plot of `Maxwell (Area)` distribution.

6.26.3. generalized Maxwell (Amplitude).

$$y(x;x_0,\sigma,n,m) = \begin{cases} y_0 & \text{for } x < x_0 \\ y_0 + A\,\frac{(x-x_0)^m \exp\left(-\frac{1}{2}\left(\frac{x-x_0}{|\sigma|}\right)^n\right)}{(x_{\text{mode}}-x_0)^m \exp\left(-\frac{1}{2}\left(\frac{x_{\text{mode}}-x_0}{|\sigma|}\right)^n\right)} & \text{for } x \geq x_0 \end{cases} \tag{6.84}$$

with $x_{\text{mode}} = \left(\frac{2m}{n}\right)^{1/n} |\sigma| + x_0$.

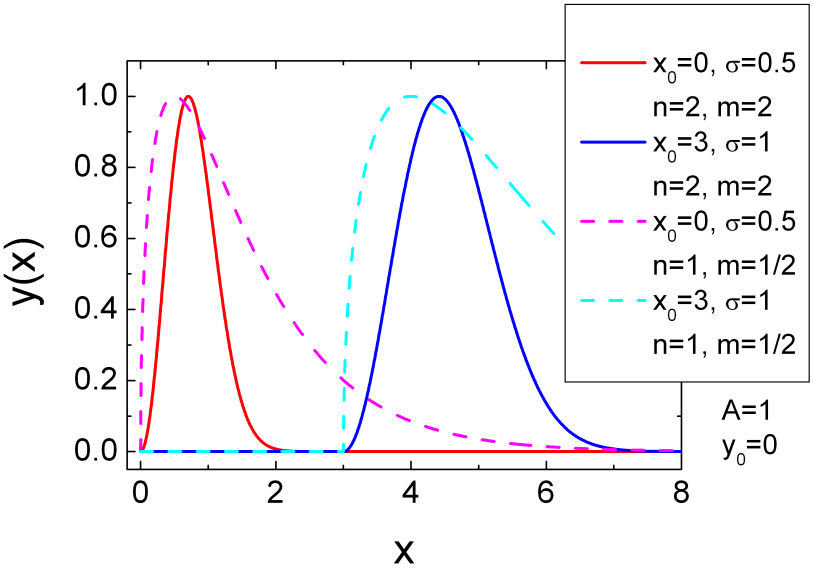

FIGURE 6.48. Plot of `generalized Maxwell (Amplitude)` distribution.

6.26.4. generalized Maxwell (Area).

$$y(x;x_0,\sigma,n,m) = \begin{cases} 0 & \text{for } x < x_0 \\ A\,\frac{(x-x_0)^m \exp\left(-\frac{1}{2}\left(\frac{x-x_0}{|\sigma|}\right)^n\right)}{2^{(1+m)/n}|\sigma|^{1+m}\frac{1}{|n|}\Gamma\left(\frac{1+m}{n}\right)} & \text{for } x \geq x_0. \end{cases} \tag{6.85}$$

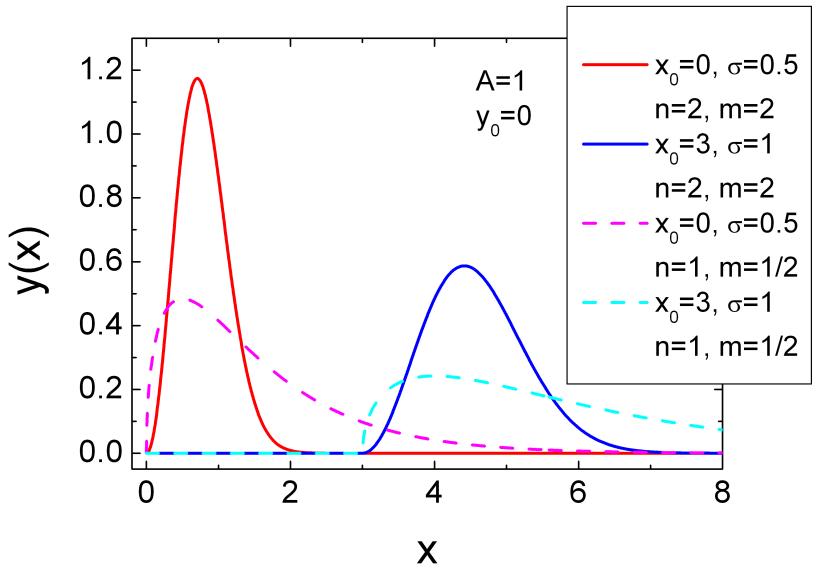

FIGURE 6.49. Plot of `generalized Maxwell (Area)` distribution.

6.27. Pearson-IV

Pearson type IV distribution:

$$p(x) = \frac{\left|\frac{\Gamma\left(m+\frac{\nu}{2}i\right)}{\Gamma(m)}\right|^2}{\alpha\,\mathrm{B}\left(m-\frac{1}{2},\frac{1}{2}\right)}\left[1+\left(\frac{x-\lambda}{\alpha}\right)^2\right]^{-m}\exp\left[-\nu\arctan\left(\frac{x-\lambda}{\alpha}\right)\right]. \quad (6.86)$$

The normalizing constant involves the complex Gamma function (Γ) and the Beta function (B).

6.27.1. Pearson-IV (Amplitude).

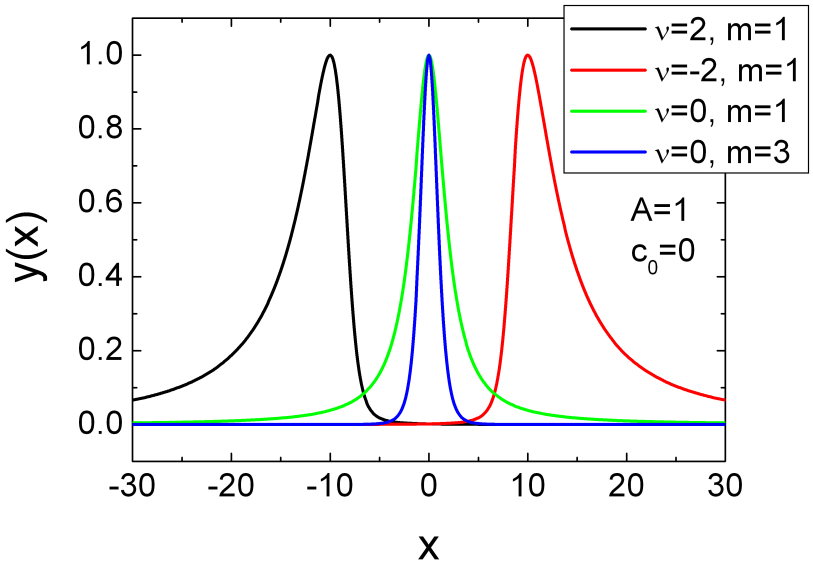

FIGURE 6.50. Plot of `Pearson-IV (Amplitude)` distribution.

6.27.2. Pearson-IV (Area).

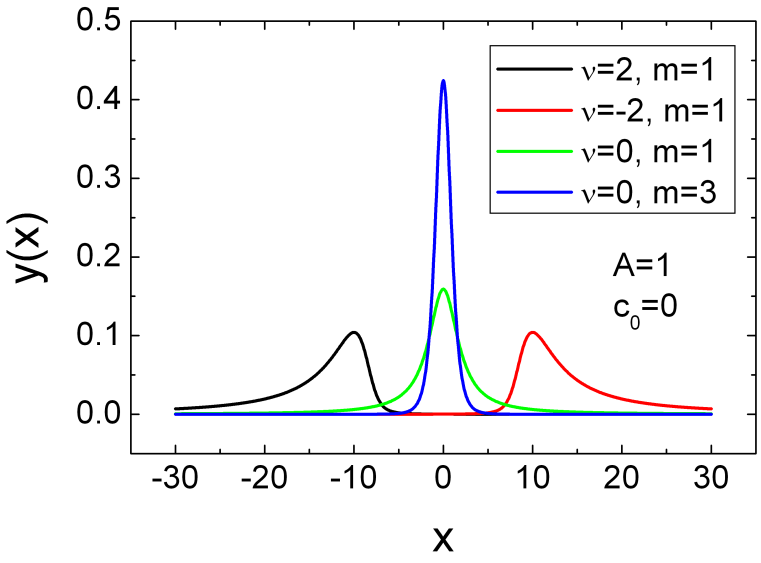

FIGURE 6.51. Plot of `Pearson-IV (Area)` distribution.

6.28. Pearson-VII

The `Pearson-VII` model has been used as an approximation for the `Voigt` function. The parameter σ is the FWHM (full-width at half-maxima). When m is 1.0, the function is an exact Lorentzian. As the m-power term increases, the function tends toward the Gaussian. For $m \sim 50$, the function is essentially Gaussian. The `Pearson VII` function is a different parametrization of the Student-t distribution function and reads as

$$p(x) = \frac{1}{\alpha\,\mathrm{B}\left(m-\frac{1}{2},\frac{1}{2}\right)}\left[1+\left(\frac{x-\lambda}{\alpha}\right)^2\right]^{-m} \tag{6.87}$$

with $\alpha = \frac{1}{2}\sigma/\sqrt{2^{1/m}-1}$ we get

$$p(x) = \frac{2\sqrt{2^{1/m}-1}}{\sigma\,\mathrm{B}\left(m-\frac{1}{2},\frac{1}{2}\right)}\left[1+4\left(\frac{x-x_0}{\sigma}\right)^2\left(2^{1/m}-1\right)\right]^{-m} \tag{6.88}$$

where B is the Beta function.

6.28.1. Pearson-VII (Amplitude).

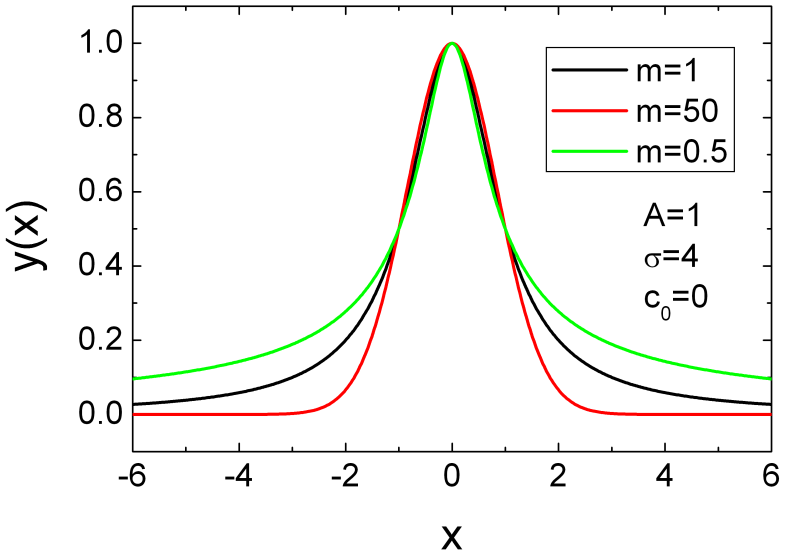

FIGURE 6.52. Plot of `Pearson-VII (Amplitude)` distribution.

6.28.2. Pearson-VII (Area).

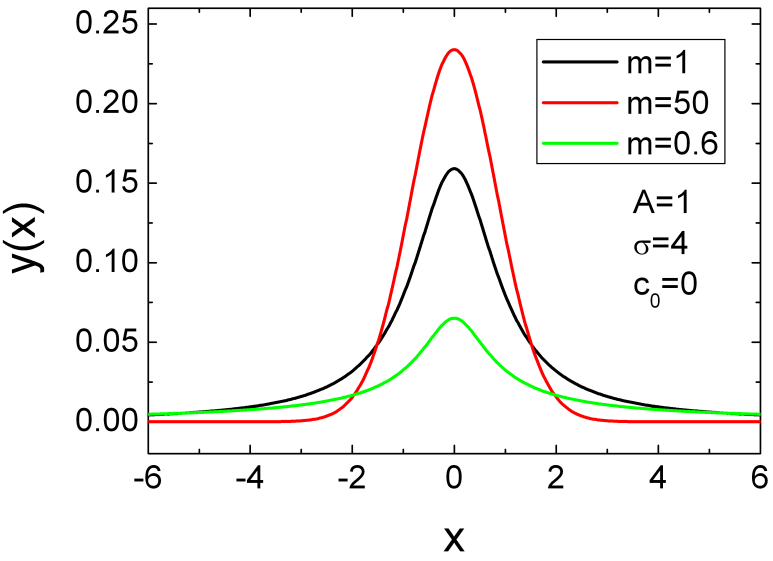

FIGURE 6.53. Plot of `Pearson-VII (Area)` distribution.

6.29. Pulse Peak

$$p(x) = \frac{2}{\sigma} \exp\left(\frac{x - x_0}{\sigma}\right)\left(1 - \exp\left(\frac{x - x_0}{\sigma}\right)\right) \tag{6.89}$$

$$\text{mode} = x_0 - \sigma \ln\left(\frac{1}{2}\right) \tag{6.90}$$

6.29.1. Pulse Peak (Amplitude).

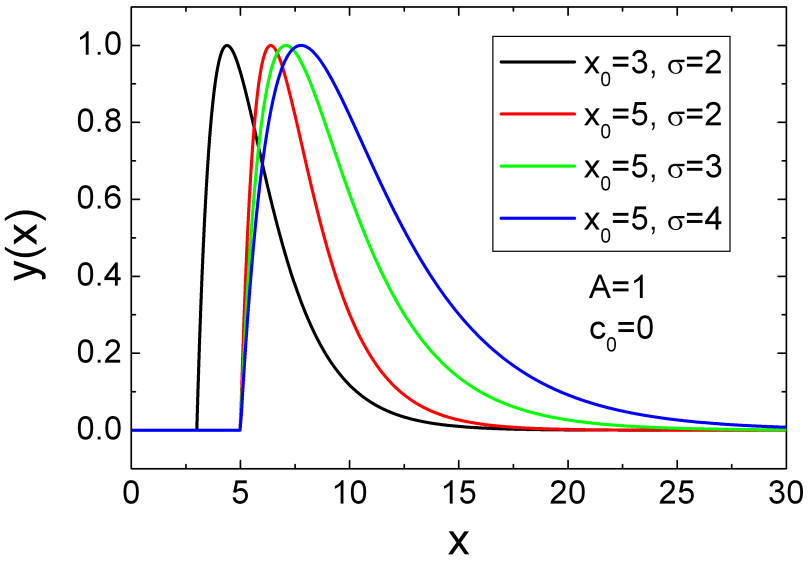

FIGURE 6.54. Plot of `Pulse Peak (Amplitude)` distribution.

6.29.2. Pulse Peak (Area).

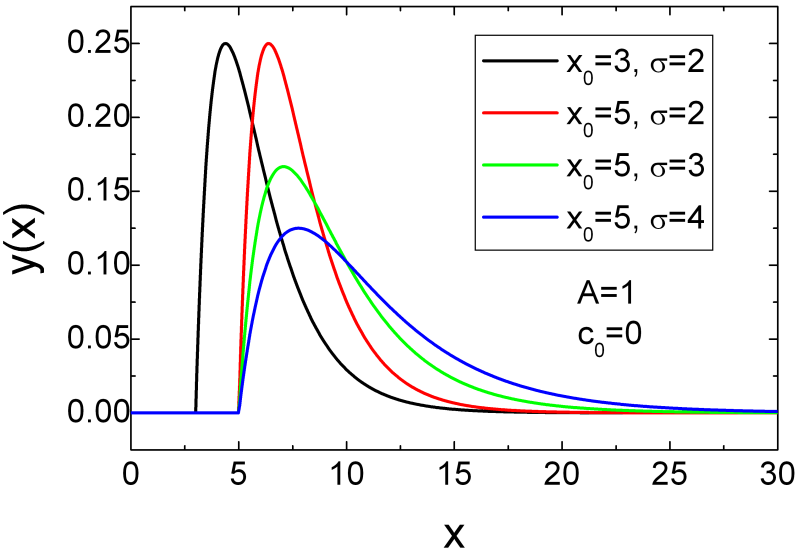

FIGURE 6.55. Plot of `Pulse Peak (Area)` distribution.

6.30. Pulse Peak with 2nd Width Term

$$p(x) = \frac{\sigma_1 + \sigma_2}{\sigma_2^2}\left(1 - \exp\left(\frac{x - x_0}{\sigma_1}\right)\right)\exp\left(\frac{x - x_0}{\sigma_2}\right) \tag{6.91}$$

$$\text{mode} = x_0 - \sigma_1 \ln\left(\frac{\sigma_1}{\sigma_2 + \sigma_1}\right) \tag{6.92}$$

6.30.1. Pulse Peak with 2nd Width Term (Amplitude).

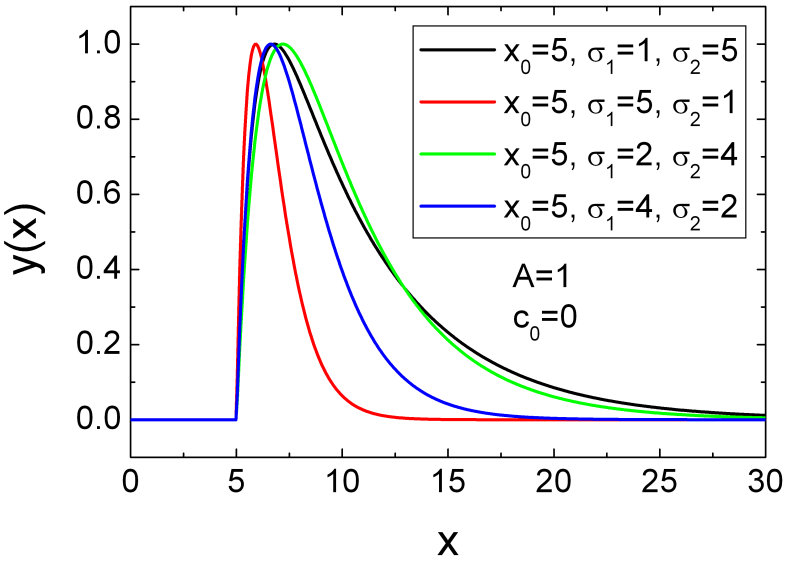

FIGURE 6.56. Plot of `pulse with 2nd width (Amplitude)` distribution.

6.30.2. Pulse Peak with 2nd Width Term (Area).

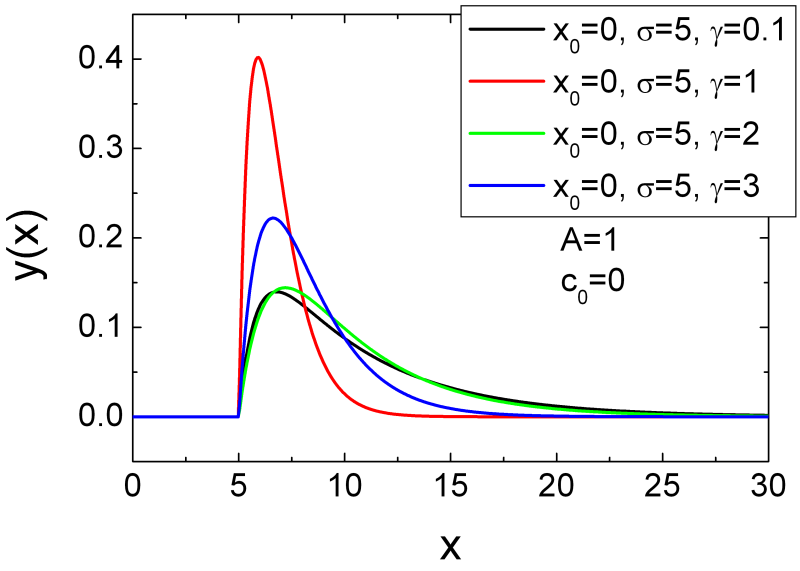

FIGURE 6.57. Plot of `pulse with 2nd width (Area)` distribution.

6.31. Pulse Peak with Power Term

$$p(x) = \frac{\gamma+1}{\sigma}\left(1-\exp\left(\frac{x-x_0}{\sigma}\right)\right)^{\gamma}\exp\left(\frac{x-x_0}{\sigma}\right) \tag{6.93}$$

$$\text{mode} = x_0 - \sigma\ln\left(\frac{1}{\gamma+1}\right) \tag{6.94}$$

6.31.1. Pulse Peak with Power Term (Amplitude).

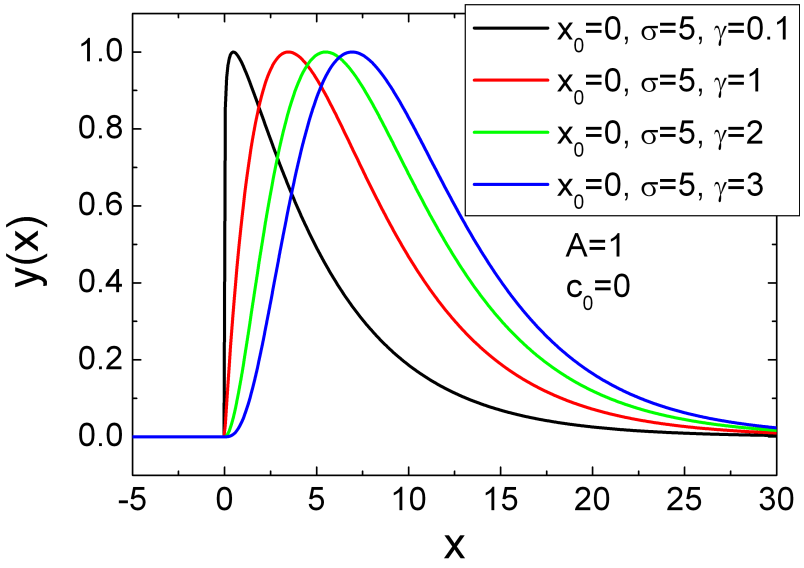

FIGURE 6.58. Plot of `pulse with power term (Amplitude)` distribution.

6.31.2. Pulse Peak with Power Term (Area).

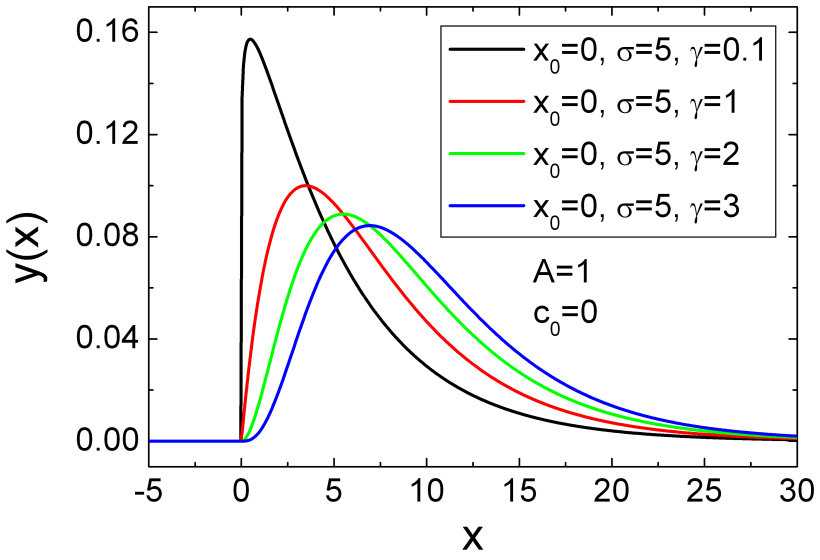

FIGURE 6.59. Plot of `pulse with power term (Area)` distribution.

6.32. Student-t

$$p(x) = \frac{\Gamma(\frac{\nu+1}{2})}{\sqrt{\nu\pi}\,\Gamma(\frac{\nu}{2})}\left(1+\frac{x^2}{\nu}\right)^{-(\frac{\nu+1}{2})} \tag{6.95}$$

6.32.1. Student-t (Amplitude).

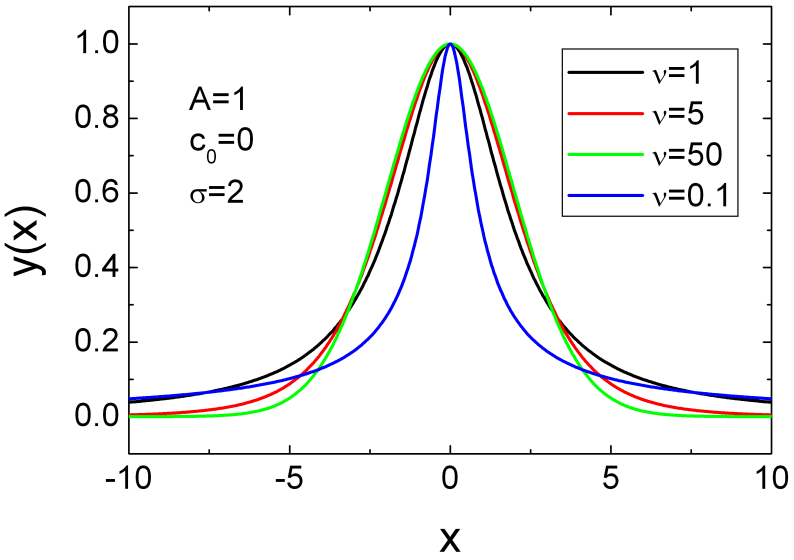

FIGURE 6.60. Plot of `Student-t (Amplitude)` distribution.

6.32.2. Student-t (Area).

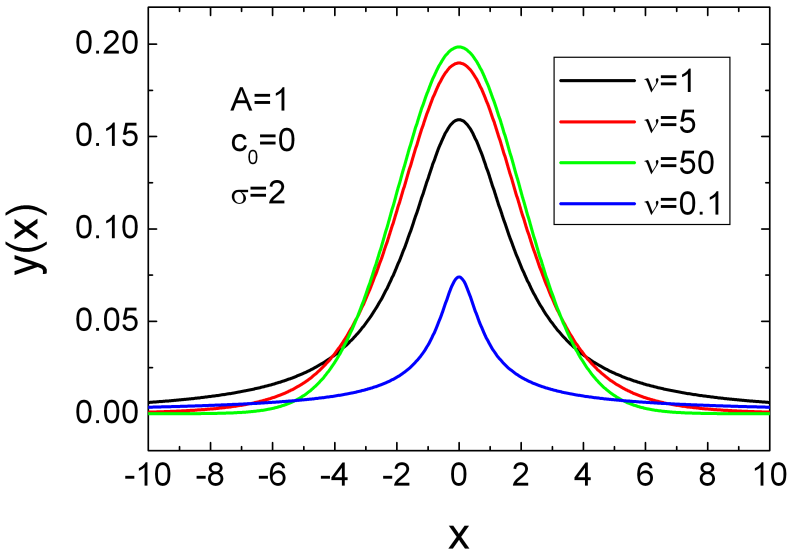

FIGURE 6.61. Plot of `Student-t (Area)` distribution.

6.33. Voigt

The Voigt profile is a spectral line profile found in all branches of spectroscopy in which a spectral line is broadened by two types of mechanisms, one of which alone would produce a Gaussian profile (usually, as a result of the Doppler broadening), and the other would produce a Lorentzian profile. The Voigt profile is then a convolution of a Lorentz profile and a Gaussian profile:

$$V(x, x_c|\sigma, \gamma) = \int_{\infty}^{\infty} D(x'|\sigma)\, L(x - x_c - x'|\gamma)\, dx' \tag{6.96a}$$

where $x - x_c$ is distance from line center x_c, $D(x|\sigma)$ is the centered Doppler profile:

$$D(x|\sigma) = \frac{e^{-x^2/2\sigma^2}}{\sigma\sqrt{2\pi}} \tag{6.96b}$$

and $L(x - x_c|\gamma)$ is the centered Lorentzian profile:

$$L(x - x_c|\gamma) = \frac{\gamma}{\pi((x - x_c)^2 + \gamma^2)}. \tag{6.96c}$$

The defining integral can be evaluated as [**20, 50**]:

$$V(x, x_c) = \frac{\Re[w(z)]}{\sigma\sqrt{2\pi}} \tag{6.96d}$$

where $\Re[w(z)]$ is the real part of the complex error function of z and

$$z = \frac{x - x_c + i\gamma}{\sigma\sqrt{2}} \tag{6.96e}$$

The full width at half maximum (FWHM) of the Voigt profile can be found from the widths of the associated Gaussian and Lorentzian widths. The FWHM of the Gaussian profile is $f_G = 2\sigma\sqrt{2\ln(2)}$. The FWHM of the Lorentzian profile is just $f_L = 2\gamma$. Define $\phi = f_{\mathrm{L}}/f_{\mathrm{G}}$. Then the FWHM of the Voigt profile (f_{V}) can be estimated as:

$$f_{\mathrm{V}} \approx f_{\mathrm{G}} \left(1 - c_0 c_1 + \sqrt{\phi^2 + 2c_1\phi + c_0^2 c_1^2}\right) \tag{6.97}$$

where $c_0 = 2.0056$ and $c_1 = 1.0593$. This estimate will have a standard deviation of error of about 2.4 percent for values of ϕ between 0 and 10. Note that the above equation will have the proper behavior in the limit of $\phi = 0$ and $\phi = \infty$. A different approximation was given by [**69, 60**]

$$f_{\mathrm{V}} \approx 0.5346 f_{\mathrm{L}} + \sqrt{0.2166 f_{\mathrm{L}}^2 + f_{\mathrm{G}}^2} \tag{6.98}$$

with an accuracy of 0.02

6.33.1. Voigt (Amplitude).

The amplitude version of the Voigt peak is parameterized as

$$V_{\text{Amplitude}}(x|A,\sigma,\gamma) = A\,\frac{\displaystyle\int_{-\infty}^{\infty}\frac{\exp(-u^2)}{\frac{\gamma^2}{2\sigma^2}+\left(\frac{x-x_c}{\sqrt{2}\sigma}-u\right)^2}\,du}{\displaystyle\int_{-\infty}^{\infty}\frac{\exp(-u^2)}{\frac{\gamma^2}{2\sigma^2}+u^2}\,du} = A\,\frac{V(x,x_c|\sigma,\gamma)}{V(x_c,x_c|\sigma,\gamma)} \tag{6.99}$$

Required parameters:

ampl.: amplitude A of the Voigt peak
center: location parameter (mode) x_c
sigma: width of Doppler (Gaussian) contribution $\sigma > 0$
gamma: width of Lorentzian contribution $\gamma > 0$
backgr: offset c_0

Note

- The Doppler (Gaussian) width parameter needs to be larger than 0 $\sigma > 0$.
- The Lorentzian width parameter needs to be larger than 0 $\gamma > 0$.
- Default (Size) distribution: Monodisperse

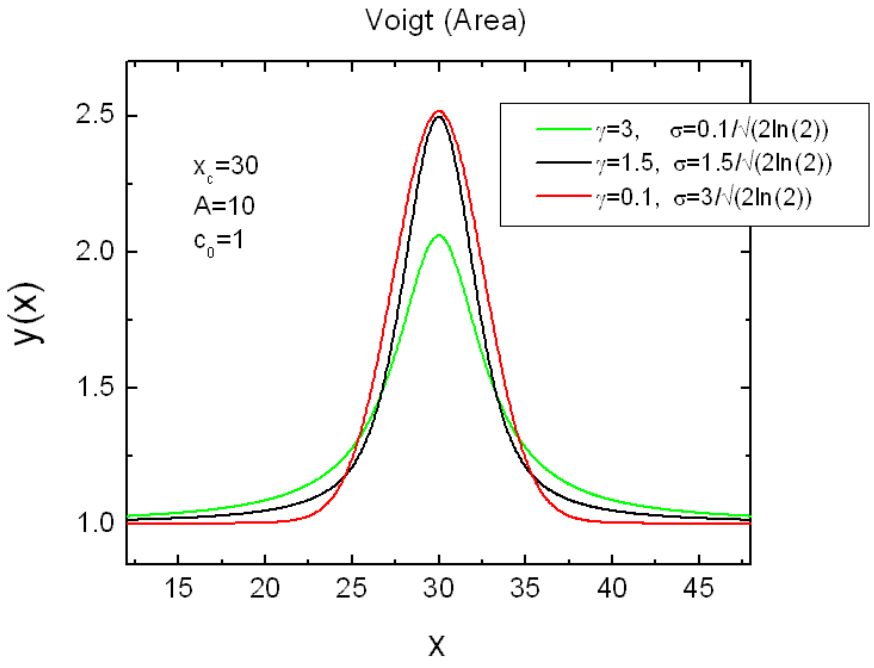

FIGURE 6.62. Plot of `Voigt (Area)` distribution.

6.33.2. Voigt (Area).

The area version of the Voigt peak is parameterized as

$$V_{\text{Area}}(x|A,\sigma,\gamma) = A\,\frac{\gamma}{2\pi\sqrt{\pi}\,\sigma^2}\int_{-\infty}^{\infty}\frac{\exp(-u^2)}{\frac{\gamma^2}{2\sigma^2}+\left(\frac{x-x_c}{\sqrt{2}\,\sigma}-u\right)^2}\,du = A\,V(x,x_c|\sigma,\gamma) \tag{6.100}$$

Required parameters:

area: area A of the Voigt peak
center: location parameter (mode) x_c
sigma: width of Doppler (Gaussian) contribution $\sigma > 0$
gamma: width of Lorentzian contribution $\gamma > 0$
backgr: offset c_0

Note

- The Doppler (Gaussian) width parameter needs to be larger than 0 $\sigma > 0$.
- The Lorentzian width parameter needs to be larger than 0 $\gamma > 0$.
- Default (Size) distribution: Monodisperse

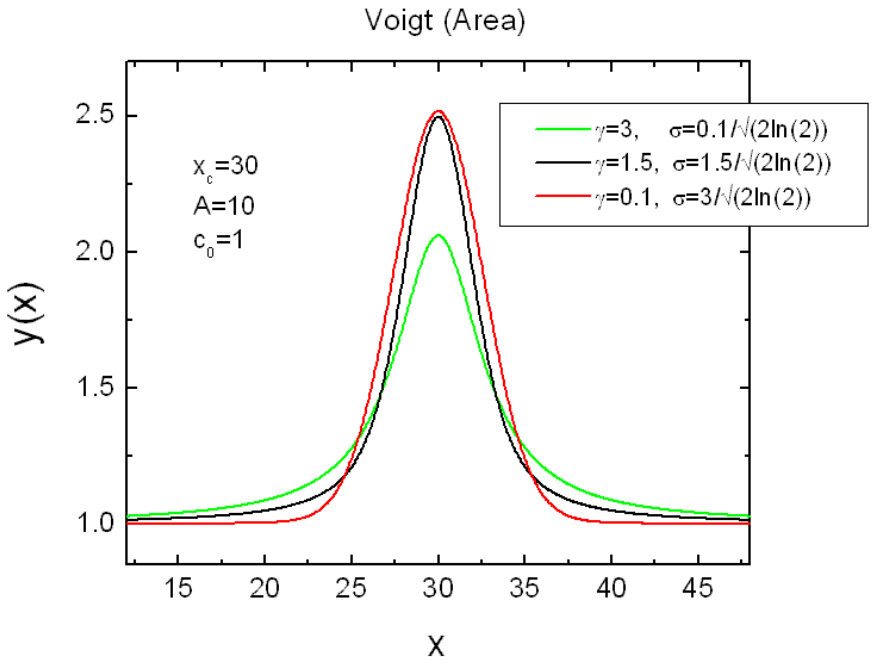

FIGURE 6.63. Plot of `Voigt (Area)` distribution.

6.33.3. Weibull.

The Weibull distribution is a continuous probability distribution. It is named after Waloddi Weibull who described it in detail in 1951, although it was first identified by Fréchet (1927) and first applied by Rosin & Rammler (1933) to describe the size distribution of particles. The probability density function of a Weibull random variable x is:

$$p(x;\lambda,k) = \begin{cases} \frac{k}{\lambda}\left(\frac{x}{\lambda}\right)^{k-1} e^{-(x/\lambda)^k} & x \geq 0 \\ 0 & x < 0 \end{cases} \tag{6.101}$$

where $k > 0$ is the shape parameter and $\lambda > 0$ is the scale parameter of the distribution. For $k > 1$ the mode is given by

$$\text{mode} = \lambda\left(\frac{k-1}{k}\right)^{\frac{1}{k}} \text{ if } k > 1. \tag{6.102}$$

6.33.4. Weibull (Amplitude).

The amplitude version represents a reparametrization of the standard statistical form. The parameter x_0 has been added to enable variable x positioning. An additional adjustment term has been added so that x_0 represents the mode. The function returns c_0 for those x where it is undefined.

$$u = \frac{k-1}{k}$$

$$z = \frac{x - x_0}{\lambda} + u^{1/k}$$

$$y(x;x_0,k,\lambda,c_0,A) = \begin{cases} c_0 + Au^{-u}z^{k-1}\exp\left(-z^k\right) & z >= 0 \\ c_0 & z < 0 \end{cases} \tag{6.103}$$

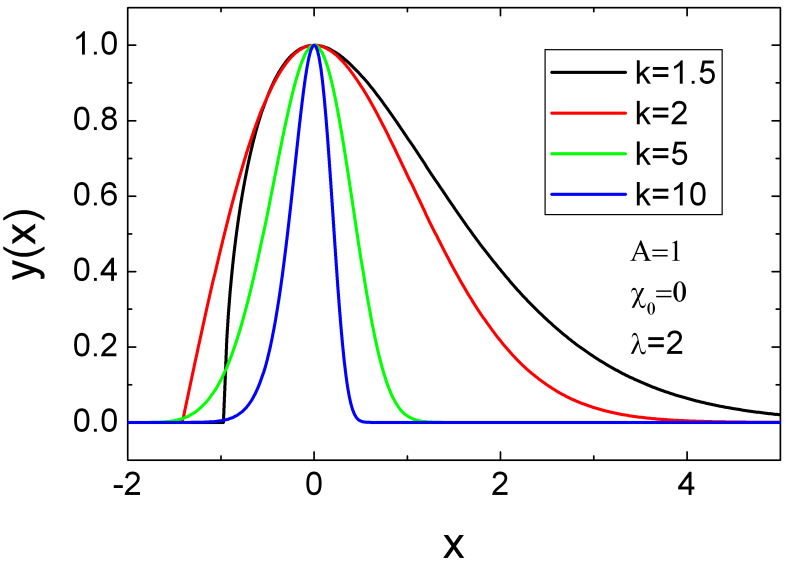

FIGURE 6.64. Plot of `Weibull (Amplitude)` distribution.

6.33.5. Weibull (Area).

The area version represents a reparametrization of the standard statistical form. The parameter x_0 has been added to enable variable x positioning. An additional adjustment term has been added so that x_0 represents the mode. The function returns c_0 for those x where it is undefined.

$$z = \frac{x - x_0}{\lambda} + \left(\frac{k-1}{k}\right)^{1/k}$$

$$y(x; x_0, k, \lambda, c_0, A) = \begin{cases} c_0 + A\frac{k}{\lambda} z^{k-1} \exp\left(-z^k\right) & z >= 0 \\ c_0 & z < 0 \end{cases} \tag{6.104}$$

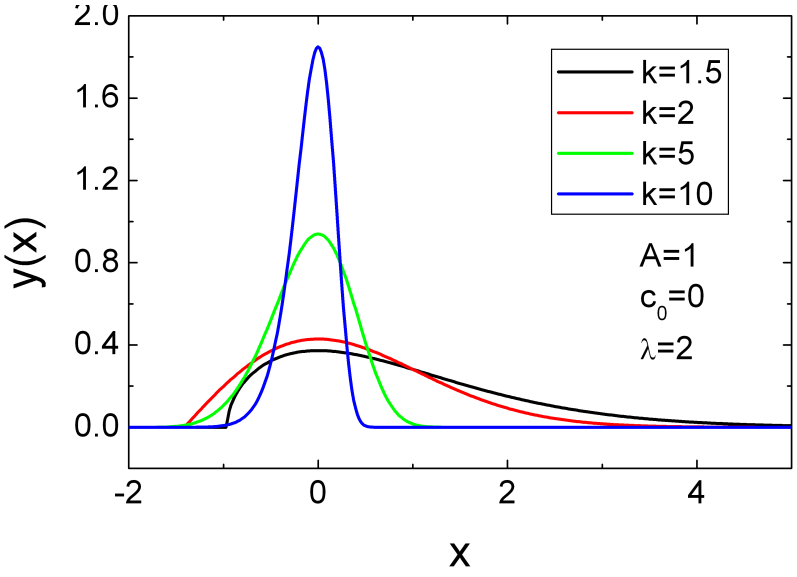

FIGURE 6.65. Plot of `Weibull (Area)` distribution.

CHAPTER 7

Plugin functions

7.1. Very anisotropic particles (local planar & local cylindrical objects)

For very anisotropic random orientated particles the form factor can be factorize according to Porod [**80**] in a cross section term $P_{\rm cs}(Q)$ for the shorter dimension and a shape factor $P'(Q)$ for the long dimension.

$$I(Q) = P'(Q)P_{cs}(Q). \tag{7.1}$$

In this plugin the form factors of two types of anisotropic particles are collected, those with a local cylindrical and with a local planar geometry. In case of local planar objects the cross section term $P_{\rm cs}(Q)$ can be homogeneous, a centro-symmetric bilayer, a gaussian bilayer, etc. . This cross section factor can than be combined with the overall shape factor $P'(Q)$ of for examples a thin spherical shell of elliptical shell, a then cylindrical shell or a thin disc. As the total form factor is the product of the cross-section form factor and a shape form factor one can either programm all combination of cross-section and shape factors into individual form factor functions or one can programm the cross-section factors as form factor and the shape factor as a structure factors. Using the monodisperse approximation yields than the same result.

In this plugin the product of the cross-section and shape term have been implemented as form factor under "`by plugin|anisotropic obj.|local planar obj.`" and "`by plugin|anisotropic obj.|local cylindrical obj.`". The cross-section terms alone are also implemented as form factors under "`by plugin|anisotropic obj.|Pcs(Q) for planar obj.`" and "`by plugin|anisotropic obj.|Pcs(Q) for cylindrical obj.`". The shape factors are also available as structure factors under "`by plugin|anisotropic obj.|P'Q): local planar obj.`" and "`by plugin|anisotropic obj.|P'(Q): local cylindrical obj.`".

The cross-section form factors can be easily calculated if the scattering length density contrast profile $\Delta\eta_{\rm cs}(r)$ is known. For structures with a local planar geometry and a symmetric cross-section the form factor is given by

$$P_{\rm cs}^{\rm planar}(Q) = \left[2\int_0^\infty \Delta\eta_{\rm cs}(r)\cos(Qr)\,{\rm d}r\right]^2 \tag{7.2}$$

In case of local cylindrical particles with a centro-symmetric scattering length density distribution the form factor is given by

$$P_{\rm cs}^{\rm cylindrical}(Q) = \left[2\pi\int_0^\infty \Delta\eta_{\rm cs}(r){\rm J}_0(Qr)r\,{\rm d}r\right]^2 \tag{7.3}$$

7.1.1. Pcs(Q) for planar obj.

The cross-section form factors with local planar geometry are valid when the cross-section dimension is much smaller the radius of curvature of the locally planar structure.

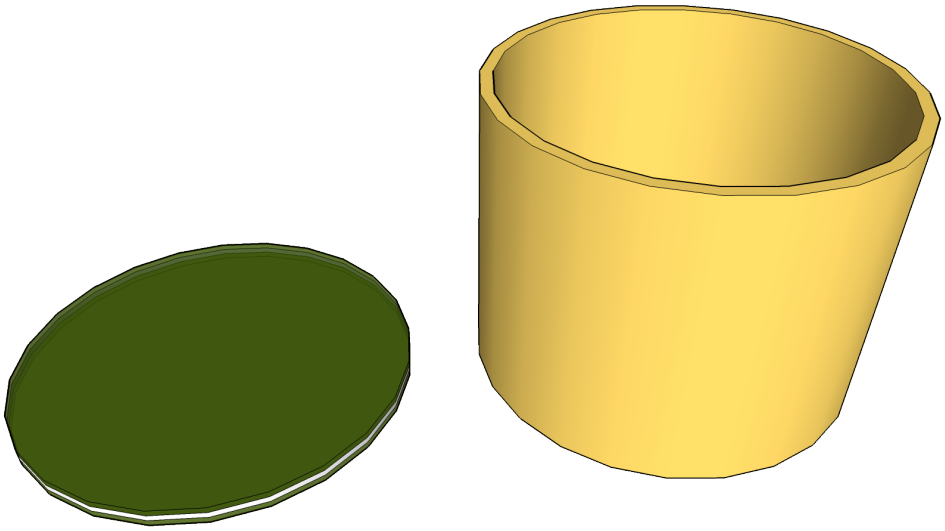

FIGURE 7.1. for local planar particles the cross section dimension is much smaller then the radius of curvature of the particle

Several cross-section profiles for local planar objects have been implemented, like a homogeneous cross-section, cross-section with two infinitely thin plates, layered centro-symmetric cross-section, bilayer with a Gaussian scattering length density profile, layer with Gaussian chains attached to the surface. These form factors are supposed to be combined with a shape factor for local planar objects which are implemented as structure plugins under "`by plugin|anisotropic obj.|P'Q): local planar obj.`".

7.1.1.1. *Pcs(Q) for a homogeneous cross-section.*

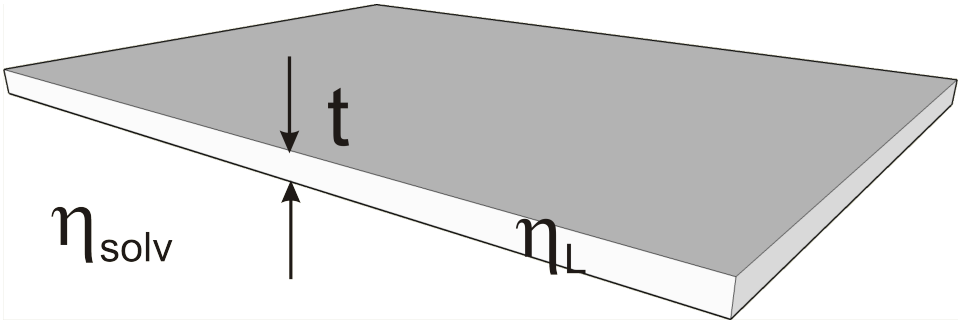

FIGURE 7.2. Plane with a homogeneous cross-section of thickness t.

This cross-section form factor describes the scattering of a layer with homogeneous scattering length density η_L in a matrix of a scattering length density η_{solv}. The thickness can have a distribution described by a log-normal distribution according to eq. 5.3b.

$$P_{\rm cs}(Q,\sigma_t,t) = \int_0^\infty \mathrm{LogNorm}(x,1,\sigma_t,1,t)\left[(\eta_L-\eta_{\rm solv})\,x\frac{\sin(Qx/2)}{Qx/2}\right]^2 \mathrm{d}x \qquad (7.4)$$

Input parameters for `Pcs:homogeneousPlate`**:**

`t`: most probable layer thickness t
`sigm_t`: width σ_t of thickness distribution (LogNorm)
`dummy`: unused disabled parameter
`dummy`: unused disabled parameter
`eta_l`: scattering length density of layer η_L
`eta_solv`: scattering length density of solvent η_{solv}

Note

- This form factor is supposed to be combined with a shape factor for local planar objects which are implemented as structure plugins under "`by plugin|anisotropic obj.|P'Q): local planar obj.`".
- As the form factor already have the width distribution included one normally uses in `SASfit` as a size distribution the `Delta`-distribution.

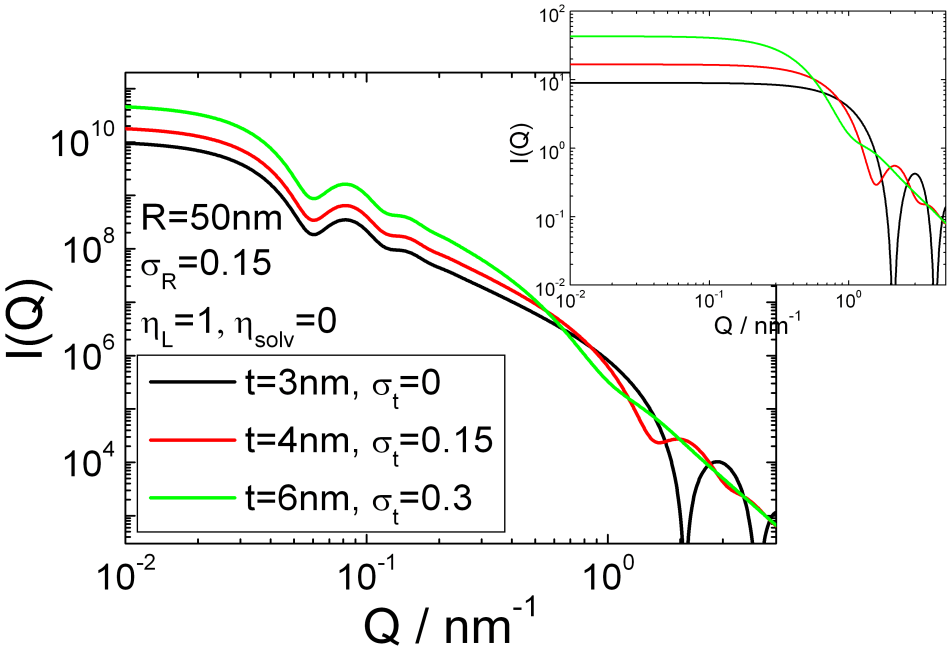

FIGURE 7.3. Scattering curve for the form factor "`Pcs:homogeneousPlate`" only (insert) and in combination with a structure factor "`P'(Q): Thin Spherical Shell`".

7.1.1.2. *Pcs(Q) for two infinitely thin parallel layers.*

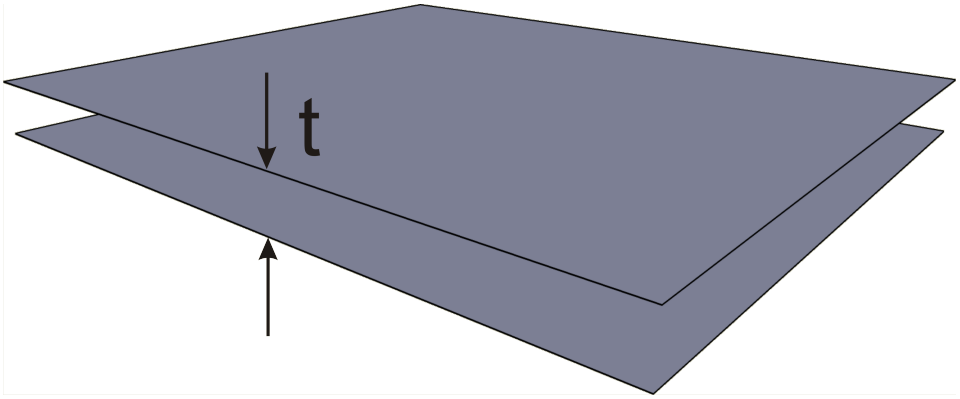

FIGURE 7.4. Two infinitely thin parallel layers separated by a distance t.

This cross-section form factor describes the scattering of two infinitely thin parallel layers. The separation distance can have a distribution described by a log-normal distribution according to eq. 5.3b.

$$P_{\mathrm{cs}}(Q,\sigma_T,T) = \int_0^\infty \mathrm{LogNorm}(x,1,\sigma_T,1,T)\cos^2(Qx/2)\,\mathrm{d}x \tag{7.5}$$

Input parameters for `Pcs:TwoInfinitelyThinLayers`:

`t:` most probable layer separation t
`sigm_t:` width σ_t of separation distribution (LogNorm)

Note

- This form factor is supposed to be combined with a shape factor for local planar objects which are implemented as structure plugins under "`by plugin|anisotropic obj.|P'Q): local planar obj.`".
- As the form factor already have the width distribution included one normally uses in `SASfit` as a size distribution the `Delta`-distribution.

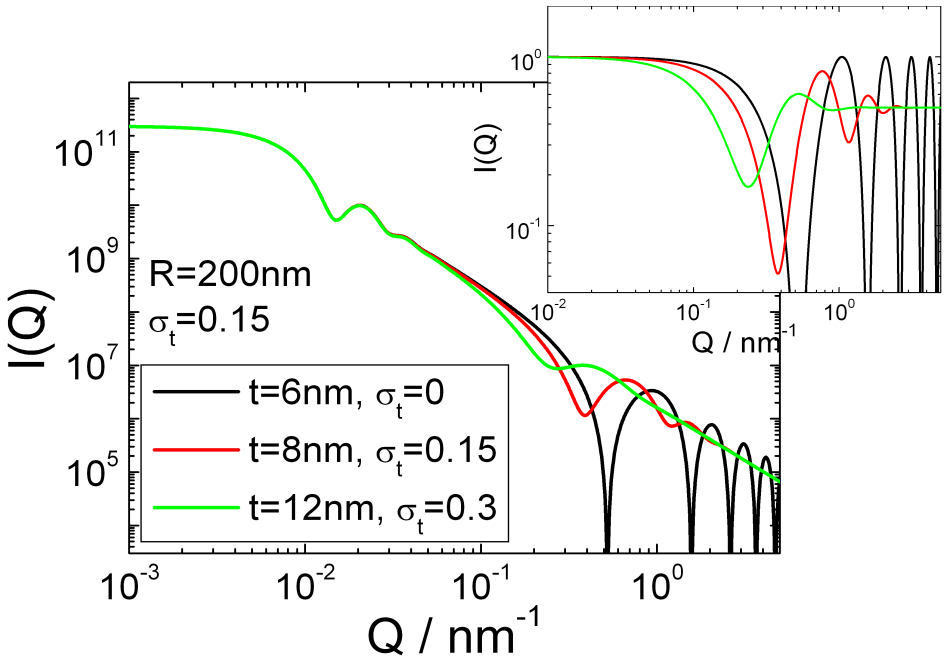

FIGURE 7.5. Scattering curve for the form factor "`Pcs:TwoInfinitelyThinLayers`" only (insert) and in combination with a structure factor "`P'(Q): Thin Spherical Shell`".

7.1.1.3. *Pcs(Q) for a layered centro symmetric cross-section structure.*

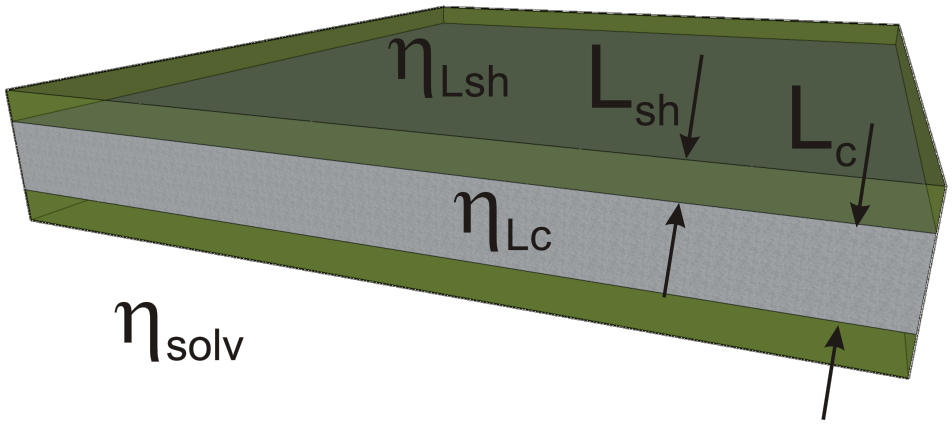

FIGURE 7.6. Two layered centro symmetric structure with a core thickness of L_{c} and an outer layer thickness $L_{L_{\mathrm{sh}}}$. The corresponding scattering length densities of the core, the shell layer and the solvent are $L_{L_{\mathrm{c}}}$, $L_{L_{\mathrm{sh}}}$, and $L_{L_{\mathrm{solv}}}$.

This cross-section form factor describes the scattering of a layered centro symmetric cross-section structure. Both the core thickness as well as the shell thickness can have a distribution described by a log-normal distribution as defined in eq. 5.3b.

$$P_{\mathrm{cs}}(Q, \sigma_{L_{\mathrm{c}}}, L_{\mathrm{c}}, \sigma_{L_{\mathrm{sh}}}, L_{\mathrm{sh}}, \eta_{L_{\mathrm{c}}}, \eta_{L_{\mathrm{sh}}}, \eta_{\mathrm{sol}}) =$$
$$\int_0^\infty \mathrm{LogNorm}(v, 1, \sigma_{L_{\mathrm{c}}}, 1, L_{\mathrm{c}}) \int_0^\infty \mathrm{LogNorm}(u, 1, \sigma_{L_{\mathrm{sh}}}, 1, L_{\mathrm{sh}})$$
$$\left[\frac{(\eta_{L_{\mathrm{sh}}} - \eta_{\mathrm{solv}})(v+2u) \sin\left(Q\frac{v+2u}{2}\right)}{Q\frac{v+2u}{2}} - \frac{(\eta_{L_{\mathrm{sh}}} - \eta_{L_{\mathrm{c}}}) v \sin\left(Q\frac{v}{2}\right)}{Q\frac{v}{2}} \right]^2 \mathrm{d}u\,\mathrm{d}v \quad (7.6)$$

Input parameters for `Pcs:LayeredCentroSymmetricXS`:

`L_c`: most probable layer separation L_{c}
`sigm_Lc`: width $\sigma_{L_{\mathrm{c}}}$ of core thickness distribution (LogNorm)
`L_sh`: most probable shell thickness L_{sh}
`sigm_Lsh`: width $\sigma_{L_{\mathrm{c}}}$ of shell thickness distribution (LogNorm)
`eta_Lc`: scattering length density of core layer $\eta_{L_{\mathrm{c}}}$
`eta_Lsh`: scattering length density of shell layer $\eta_{L_{\mathrm{sh}}}$
`eta_solv`: scattering length density of solvent η_{solv}

Note

- This form factor is supposed to be combined with a shape factor for local planar objects which are implemented as structure plugins under "`by plugin|anisotropic obj.|P'Q): local planar obj.`".

- As the form factor already have the width distribution included one normally uses in `SASfit` as a size distribution the `Delta`-distribution.

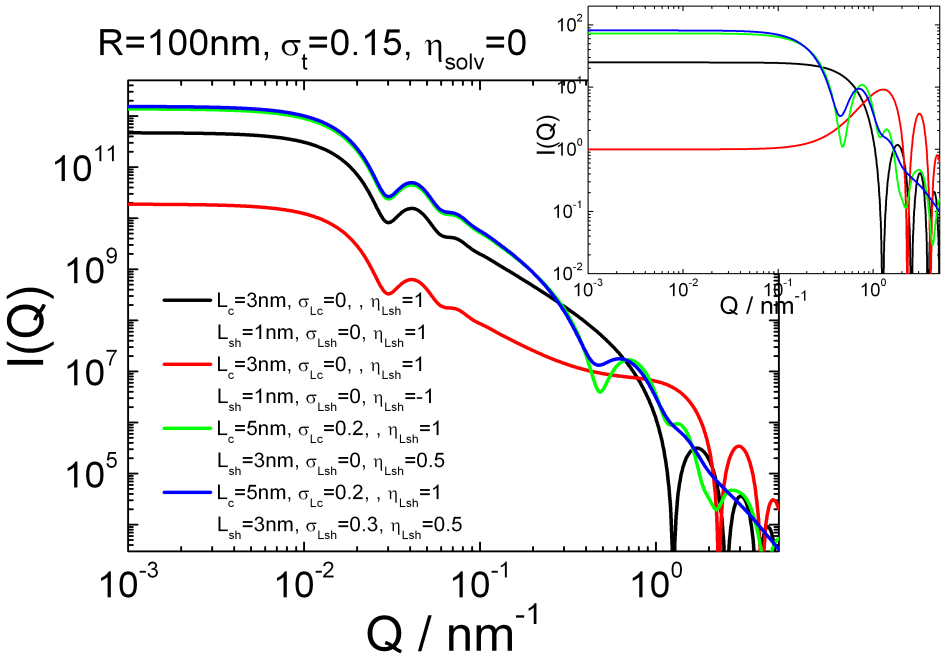

FIGURE 7.7. Scattering curve for the form factor "`Pcs:LayeredCentroSymmetricXS`" only (insert) and in combination with a structure factor "`P'(Q): Thin Spherical Shell`".

7.1.1.4. *Pcs(Q) for a bilayer with a Gaussian electron density profile* [**71, 70**].

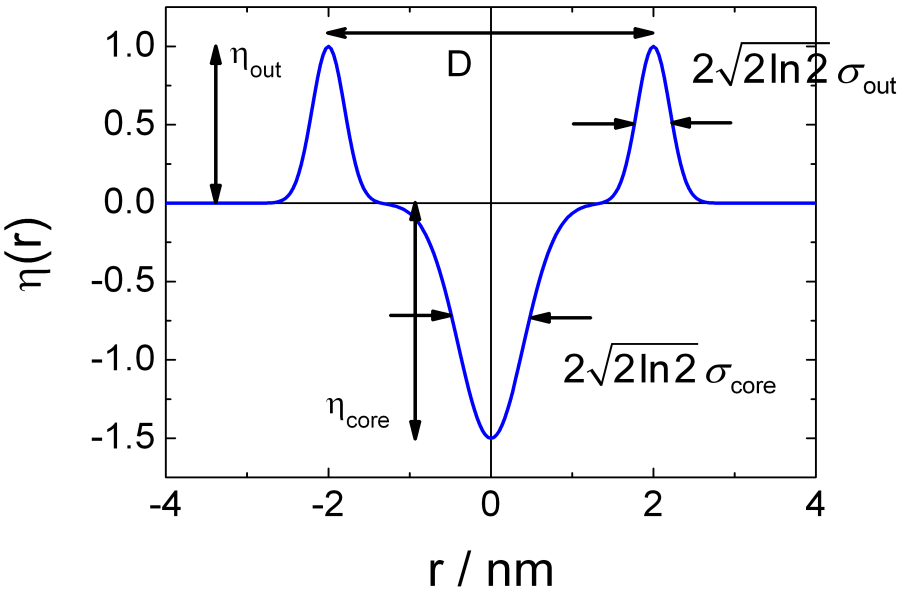

FIGURE 7.8. The plot shows a model for the Gaussian description of the bilayer electron density profile according to eq. 7.7. The origin of the profile is set to the bilayer centre. The model encountering a single Gaussian for the head group at $\pm t/2$. η_{out} is the amplitude of the headgroup Gaussian and η_{core} that of the hydrocarbon chains with respect to the average electron density of water. The FWHM of the Gaussian profiles are $2\sqrt{2\ln 2}\sigma_{\text{out}}$ and $2\sqrt{2\ln 2}\sigma_{\text{core}}$.

This model for a bilayer is using a real-space representation of the electron density profile using a Gaussian description [**71, 70**]. In comparison to other models it is simpler and requiring the adjustment of only four parameters. The electron density profile (Fig. 7.8) is described by

$$\begin{aligned}\eta(r) = \eta_{\text{out}} &\left[\exp\left(-\frac{\left(r-\frac{t}{2}\right)^2}{2\sigma_{\text{out}}^2}\right) + \exp\left(-\frac{\left(r+\frac{t}{2}\right)^2}{2\sigma_{\text{out}}^2}\right)\right] \\ &+ \eta_{\text{core}} \exp\left(-\frac{r^2}{2\sigma_{\text{core}}^2}\right)\end{aligned} \tag{7.7}$$

The scattering intensity of this cross section profile of a planar object can be calculated by eq. 7.2 and computes as

$$F_{\text{out}}\left(Q, D, \sigma_{\text{out}}, \eta_{\text{out}}\right) = \sqrt{2\pi}\,\sigma_{\text{out}}\eta_{\text{out}} \exp\left(-\frac{1}{2}\left(Q\sigma_{\text{out}}\right)^2\right) \cos\left(Q\frac{t}{2}\right) \tag{7.8}$$

$$F_{\text{core}}\left(Q, \sigma_{\text{core}}, \eta_{\text{core}}\right) = \sqrt{2\pi}\,\sigma_{\text{core}}\eta_{\text{core}} \exp\left(-\frac{1}{2}\left(Q\sigma_{\text{core}}\right)^2\right) \tag{7.9}$$

so that

$$P_{\mathrm{cs}}(Q) = \left[F_{\mathrm{core}}(Q, \sigma_{\mathrm{core}}, \eta_{\mathrm{core}}) + 2F_{\mathrm{out}}(Q, D, \sigma_{\mathrm{out}}, \eta_{\mathrm{out}})\right]^2 \tag{7.10}$$

Input parameters for `Pcs:BilayerGauss`:

`sigma_core`: width σ_{out} of the central Gaussian profile
`eta_core`: scattering length density contrast of the central Gaussian profile
`sigma_out`: width σ_{out} of the two outer Gaussian profiles
`eta_out`: scattering length density contrast of the two outer Gaussian profiles
`t`: distance between the centers of the outer Gaussian profiles

Note

- This form factor is supposed to be combined with a shape factor for local planar objects which are implemented as structure plugins under "`by plugin|anisotropic obj.|P'Q): local planar obj.`".

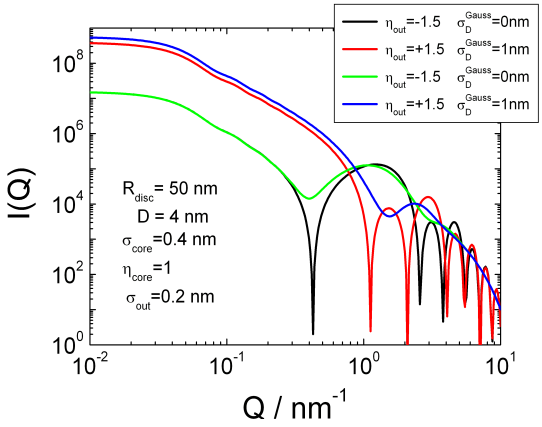

(a) Plot of the cross section form factor P_{cs} in combination with a structure factor "`P'(Q): Thin Disc`" as the shape factor $P'(Q)$.

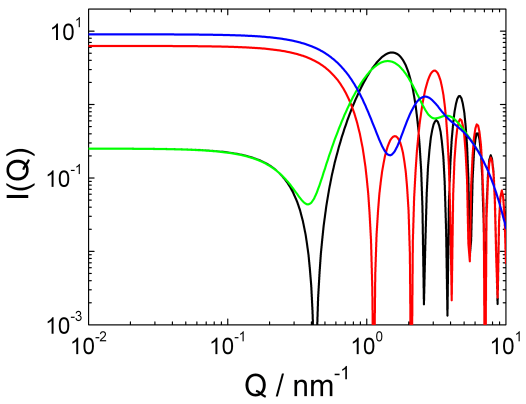

(b) Plot of the cross section form factor P_{cs} only according to eq. 7.10. The parameters for the profile are the same than in Fig. 7.9a

FIGURE 7.9. Scattering curve for the cross-section form factor "`Pcs:BilayerGaussian`". For some of the curves a distance distribution of the heads groups are assumed being Gaussian (see eq. 5.19a), i.e. calculating $\int_0^\infty \mathrm{Gauss}(D, 1, \sigma_D^{\mathrm{Gauss}}, D_0) P_{\mathrm{cs}}(Q, D)\, \mathrm{d}D$.

7.1.2. Pcs(Q) for cylindrical obj.

The cross-section form factors with cylindrical geometry are valid when the cross-section dimension is much smaller than the segment length or Kuhn length of the local cylindrical structure.

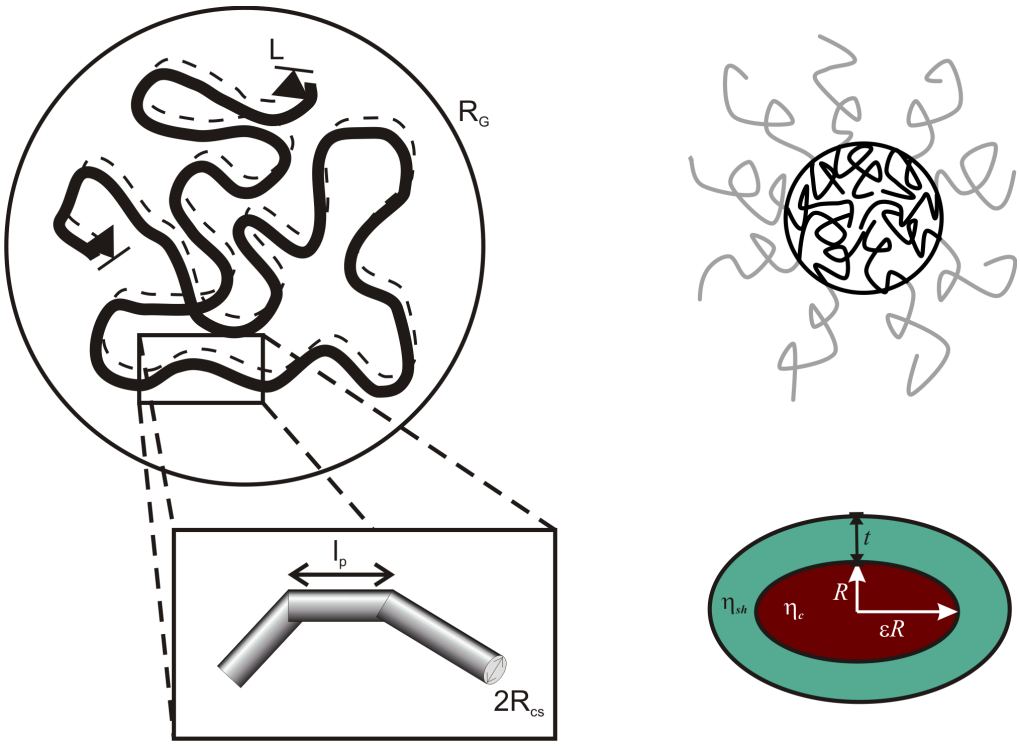

FIGURE 7.10. Sketch of wormlike structures which represent local cylindrical structures. The cross-section $2R_{\rm cs}$ is much smaller than the Kuhn length l_p, which is a typical length scale where a freely jointed chain can randomly orient in any direction without the influence of any forces, independent of the directions taken by other segments. For the cross-section term several profiles have been implemented, like homogeneous round profile or elliptical shell profile

7.1.2.1. *Pcs(Q) for homogeneous cross-section of a cylinder.*

This cross-section form factor describes the scattering of circular and homogeneous cross section. The cross-section radius R can have a distribution described by a log-normal distribution according to eq. 5.3b.

$$P_{\mathrm{cs}}(Q,\sigma_R,R) = \int_0^\infty \mathrm{LogNorm}(x,1,\sigma_R,1,R)\left((\eta_{\mathrm{core}}-\eta_{\mathrm{solv}})\,\pi x^2\frac{2\mathrm{J}_1(Qx)}{Qx}\right)^2 \mathrm{d}x \tag{7.11}$$

Input parameters for `Pcs:homogeneousCyl`**:**

`R`**:** most probable radius R
`sigm_R`**:** width σ_R of radius distribution (LogNorm)
`dummy`**:** not used
`dummy`**:** not used
`dummy`**:** not used
`dummy`**:** not used
`dummy`**:** not used
`eta_core`**:** scattering length density of the core η_{core}
`dummy`**:** not used
`eta_solv`**:** scattering length density of the solvent η_{solv}

Note

- This form factor is supposed to be combined with a shape factor for local cylindrical objects which are implemented as structure plugins under "`by plugin|anisotropic obj.|P'Q): local cylindrical obj.`".
- As the form factor already have the width distribution included one normally uses in `SASfit` as a size distribution the `Delta`-distribution.

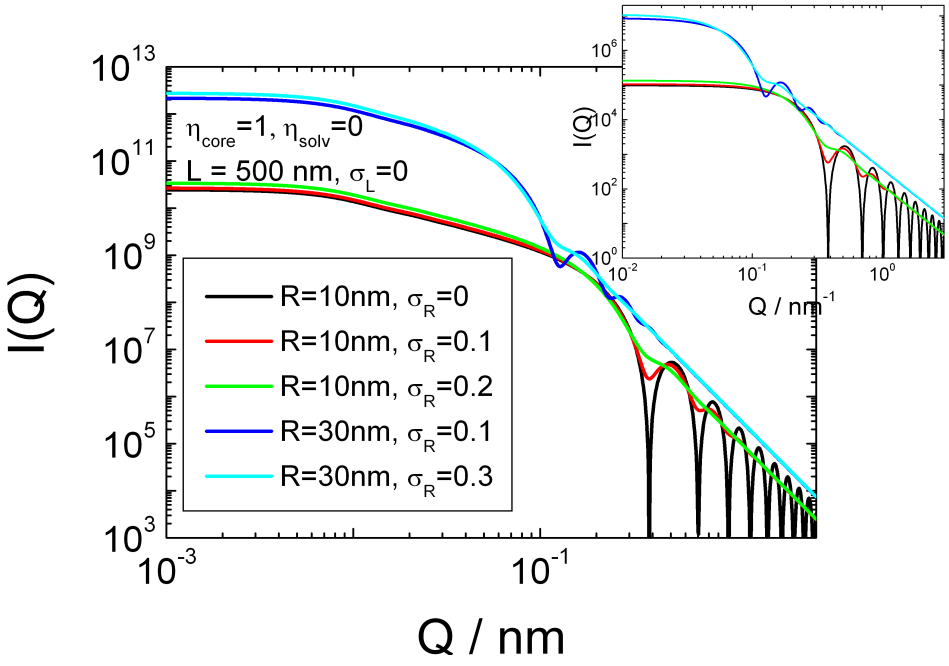

FIGURE 7.11. Scattering curve for the form factor "`Pcs:homogeneousCyl`" only (insert) and in combination with a structure factor "`P'(Q): Thin Rod`".

7.1.2.2. *Pcs(Q) for cross-section of a cylindrical shell with elliptical cross section.*

This cross-section form factor describes the scattering of an elliptical core-shell cross-section. The cross-section radius R can have a distribution with a width of *sigma* as described by a log-normal distribution according to eq. 5.3b.

$$\begin{aligned} P_{\mathrm{cs}}(Q) = & \int_0^\infty \mathrm{LogNorm}(x, 1, \sigma_R, 1, R) \quad \times \\ & \int_0^{\pi/2} \Big[(\eta_{\mathrm{shell}} - \eta_{\mathrm{solv}})\, F_{\mathrm{cs,ell}}(Q, R + t, \epsilon, \phi) \\ & \quad + (\eta_{\mathrm{core}} - \eta_{\mathrm{shell}})\, F_{\mathrm{cs,ell}}(Q, R, \epsilon, \phi) \Big]^2 \, \mathrm{d}\phi \end{aligned} \tag{7.12}$$

with

$$F_{\mathrm{cs,ell}}\,(Q, R, \epsilon, \Delta\eta\phi) = \frac{2\mathrm{J}_1(Qr(R, \epsilon, \phi))}{Qr(R, \epsilon, \phi)} \tag{7.13a}$$

$$r(R, \epsilon, \phi) = R\sqrt{\sin^2\phi + \epsilon^2 \cos^2\phi} \tag{7.13b}$$

Input parameters for `Pcs:homogeneousCyl`**:**

`R`**:** most probable radius R
`sigm_R`**:** width σ_R of radius distribution (LogNorm)
`epsilon`**:** eccentricity ϵ of ellipyical cross-section
`t`**:** shell thickness t
`dummy`**:** not used
`dummy`**:** not used
`dummy`**:** not used
`eta_core`**:** scattering length density of the core η_{core}
`eta_shell`**:** scattering length density of the shell η_{shell}
`eta_solv`**:** scattering length density of the solvent η_{solv}

Note

- This form factor is supposed to be combined with a shape factor for local cylindrical objects which are implemented as structure plugins under "`by plugin|anisotropic obj.|P'Q): local cylindrical obj.`".
- As the form factor already have the width distribution included one normally uses in `SASfit` as a size distribution the `Delta`-distribution.

7.1.3. P'(Q) for local planar obj.

7.1.4. P'(Q) for local cylindrical obj.

7.1.5. local planar obj.

7.1.6. local cylindrical obj.

7.2. JuelichCoreShell

This model considers a dense core and original two shells [**104**]. Besides, it considers two different density profiles: a parabolic and a star-like profile for the second shell.

$$\eta_{\text{shell}}(r) \propto r^{-x} \quad \text{for starlike profile } x = 4/3 \tag{7.14}$$

$$\eta_{\text{shell}}(r) \propto 1 - \left(\frac{r}{L_p}\right)^2 \quad \text{for parabolic profile of thickness } L_p \tag{7.15}$$

Model parameters:

$b_{\mathbf{solv}}$**:** scattering length density of the solvent
I_0**:** forward scattering
$M_{\mathbf{core}}$**:** molecular weight of core (g/mol)
$M_{\mathbf{brush}}$**:** molecular weight brush (g/mol)
$\rho_{\mathbf{core}}$**:** mass density of core matter (g/cm^3)
$\rho_{\mathbf{brush}}$**:** mass density of brush matter (g/cm^3)
$b_{\mathbf{core}}$**:** scattering length density of core material (cm^{-2})
$b_{\mathbf{brush}}$**:** scattering length density of brush material (cm^{-2})
$N_{\mathbf{agg}}$**:** aggregation number (real number)
d_c^+**:** extra radius of core (compared to compact)
p_{12}**:** relative distribution of shell amount in (1$^{\text{st}}$shell:2$^{\text{nd}}$shell) $(0 \ldots \infty)$
d_1^+**:** extra radius of first shell (compared to compact)
d_2^+**:** extra radius of second shell (compared to compact)
σ_c**:** core smearing
σ_1**:** smearing of 1$^{\text{st}}$ shell
σ_2**:** smearing of 2$^{\text{nd}}$ shell
$x_{\mathbf{star}}$**:** relative distribution of parbolic:starlike profile in 2$^{\text{nd}}$ shell, one has to put a very high value in order to consider only a star-like profile.
γ**:** for star-like profile the exponent is 4/3 and for a constant profile chose 0
L_p**:** thickness of parabolic brush (must fit in 2$^{\text{nd}}$ shell!)

$$I(Q) = \left[\Delta b_c F_c + \Delta b_b (F_1 + F_2)\right]^2 \tag{7.16}$$

$$\Delta b_c = b_{\text{core}} - b_{\text{solv}}(1 - f_{\text{core}}) \tag{7.17}$$

$$\Delta b_b = b_{\text{brush}} - b_{\text{solv}}(1 - f_{\text{brush}}) \tag{7.18}$$

V_c and V_b are the core and shell bulk volumes respectively.

Mass Conservation:
From the given values of the molecular weights of the two blocks and their densities, and an assumed aggregation number N_{agg}, the bulk volumes of the core and the shell, V_c and V_b, can be calculated.

Core:

$$\text{bulk core volume:} \quad V_c = \frac{N_{\text{agg}} M_{\text{core}}}{\rho_{\text{core}} N_a} \tag{7.19}$$

$$\text{minimal radius of core:} \quad R_c^0 = \left(\frac{3}{4\pi} V_c \right)^{1/3} \tag{7.20}$$

$$\text{effective core radius:} \quad R_c = R_c^0 + d_c^+ \tag{7.21}$$

$$\text{swollen core volume:} \quad V_{sc} = \frac{4}{3}\pi R_c^3 \tag{7.22}$$

$$\text{swelling factor:} \quad s_c = \frac{V_{sc}}{V_c} \tag{7.23}$$

Shell:

$$\text{bulk shell volume:} \quad V_b = \frac{N_{\text{agg}} M_{\text{shell}}}{\rho_{\text{shell}} N_a} \tag{7.24}$$

The relative amount of shell material in the first shell f_{shell1} is controlled by the parameter p_{12}, so that the portion of the second shell f_{shell2} can be obtained through:

$$f_{\text{shell1}} = \frac{p_{12}}{1 + p_{12}} \tag{7.25}$$

$$f_{\text{shell2}} = 1 - f_{\text{shell1}} \tag{7.26}$$

Shell 1:

$$\text{portion of the total shell volume in first shell:} \quad V_{s1} = f_{\text{shell1}} V_b \tag{7.27}$$

$$\text{minimal radius of shell:} \quad R_{c1} = \left(\frac{3}{4\pi} (V_{sc} + V_{s1}) \right)^{1/3} \tag{7.28}$$

$$\text{effective core radius:} \quad R_1 = R_{c1} + d_1^+ \tag{7.29}$$

$$\text{swollen volume of first shell:} \quad V_{s1s} = \frac{4}{3}\pi R_1^3 \tag{7.30}$$

$$\text{swelling factor:} \quad s_{s1} = \frac{V_{s1s} - V_{sc}}{V_{s1}} \tag{7.31}$$

Shell 2:

$$\text{portion of the total shell volume in second shell:} \quad V_{s2} = f_{\text{shell2}} V_b \tag{7.32}$$

$$\text{minimal radius of shell:} \quad R_{c2} = \left(\frac{3}{4\pi} (V_{s1s} + V_{s2}) \right)^{1/3} \tag{7.33}$$

$$\text{effective core radius:} \quad R_2 = R_{c2} + d_2^+ \tag{7.34}$$

$$\text{swollen volume of second shell:} \quad V_{s2s} = \frac{4}{3}\pi R_2^3 \tag{7.35}$$

$$\text{swelling factor:} \quad s_{s2} = \frac{V_{s2s} - V_{s1s}}{V_{s2}} \tag{7.36}$$

$$\text{fraction of star-like density profile in } 2^{\text{nd}} \text{ shell:} \quad f_{\text{star}} = 2\frac{\arctan(|p_{\text{star}}|)}{\pi} \tag{7.37}$$

Together with the profile functions $\Phi_c(r, R_c)$, $\Phi_1(r, R_1, R_2)$, $\Phi_2(r, R_1, R_2, f_{\text{star}})$ and

$$f_{\text{Fermi}}(x) = \frac{1}{1 + \exp(x)} \tag{7.38}$$

the volumes of the core and two shells and the corresponding form factor are determined by numerical integration.

Profiles:

$$\Phi_c(r, R_c) = f_{\text{Fermi}}(r - R_c)\, dr \tag{7.39}$$

$$\Phi_1(r, R_1, R_2) = (1 - f_{\text{Fermi}}(r - R_1))\ f_{\text{Fermi}}(r - R_2)\, dr \tag{7.40}$$

for $r < R_1$

$$\begin{aligned}\Phi_2(r, R_1, R_2, f_{\text{star}}, \gamma) =&(1 - f_{\text{Fermi}}(r - R_1))\ f_{\text{Fermi}}(r - R_2) \\ &\times \left[(1 - f_{\text{star}}) + \frac{f_{\text{star}}}{R_1^{\gamma}}\right]\end{aligned} \tag{7.41}$$

for $r > R_1$

$$\begin{aligned}\Phi_2(r, R_1, R_2, f_{\text{star}}, \gamma, L_p) =&(1 - f_{\text{Fermi}}(r - R_1))\ f_{\text{Fermi}}(r - R_2) \\ &\times \left[(1 - f_{\text{star}}) \left(1 - \left(\frac{r - R_1}{L_p}\right)^2\right) + \frac{f_{\text{star}}}{r^{\gamma}}\right]\end{aligned} \tag{7.42}$$

Input Parameters for model `JuelichCoreShell`:

`C`: scaling constant C
`Mcore`: molecular weight core (g/mol) M_{core}
`Mbrush`: molecular weight brush (g/mol) M_{brush}
`rho_core`: mass density core matter (g/cm^3) ρ_{core}
`rho_brush`: mass density brush matter (g/cm^3) ρ_{brush}
`b_core`: scattering length density of core material (cm^{-2}) b_{core}
`b_brush`: scattering length density of brush material (cm^{-2}) b_{brush}
`Nagg`: aggregation number N_{agg}
`d1_plus`: extra radius of shell1=core (compared to compact) d_c^+
`part23`: relative distribution of shell amount in (1^{st}shell:2^{nd}shell) $(0 \ldots \infty)$ p_{12}
`d2_plus`: extra radius of first shell2 (compared to compact) d_1^+
`d3_plus`: extra radius of second shell3 (compared to compact) d_2^+
`sigma1`: core smearing σ_c
`sigma2`: smearing of 1^{st} shell2 σ_1
`sigma3`: smearing of 2^{nd} shell3 σ_2
`partstar`: relative distribution of parbolic:starlike profile in shell3 x_{star}; one usually puts a very high value in order to consider only a star-like profile.
`gamma`: for star-like profile the exponent is $\gamma = 4/3$ and for a constant profile $\gamma = 0$
`lparabol`: thickness of parabolic brush L_p (must fit in shell3!)
`f_brush`: scattering length density correction factor brush
`f_core`: scattering length density correction factor core
`rhosolv`: scattering length density of solvent b_{solv}

7.3. Spherical core-shell structures with smooth or fuzzy interfaces

This plugin contains a collection of form factor for spherical core-shell structure with a smooth interface. The smooth interfaces are described by radial profiles of a form which are analytical integrable, i.e. for which the following integral for calculating the scattering amplitude $A_i(Q)$ of the i^{th} shell has an analytical solution.

$$A_i(Q) = \int_{R_i}^{R_i+t_i} \eta_i(r)\, 4\pi r^2\, \frac{\sin(Qr)}{Qr}\, \mathrm{d}r \tag{7.43}$$

Radial profiles for which the this integral can be solved are

$$\eta_{a,i}(r) = (\eta_{out,i} - \eta_{in,i})\, \frac{r-R}{t} + \eta_{in,i} \tag{7.44a}$$

$$\eta_{b,i}(r) = (\eta_{out,i} - \eta_{in,i}) \left(\frac{r-R}{t}\right)^2 + \eta_{in,i} \tag{7.44b}$$

$$\eta_{c,i}(r) = (\eta_{out,i} - \eta_{in,i}) \exp\left(\frac{r-R}{t}\right) + \eta_{in,i} \tag{7.44c}$$

$$\eta_{d,i}(r) = \tag{7.44d}$$

$$\eta_{e,i}(r) = \tag{7.44e}$$

$$\eta_{f,i}(r) = \tag{7.44f}$$

(7.44g)

7.3.1. Fuzzy Sphere.

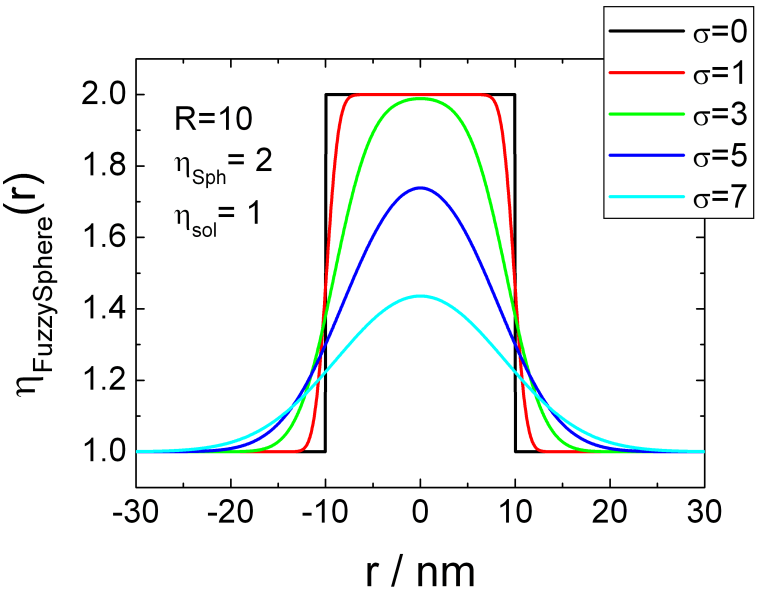

FIGURE 7.12. radial profile of a fuzzy sphere model

This model can be used to calculate the scattering from spherical particles with a "fuzzy" interface [**94**]. The fuzzy interface is obtained by convoluting the radial profile of a hard sphere with a Gaussian function.

$$\begin{aligned}\eta_{\text{FuzzySph}}\left(|\mathbf{r}|\right) &= \left(\eta_{\text{HS}} \star \eta_{\text{Gauss}}\right)(\mathbf{r}) \\ &= \int_{\mathbb{R}^3} \eta_{\text{HS}}(\boldsymbol{\tau})\eta_{\text{Gauss}}(\mathbf{r}-\boldsymbol{\tau})d\boldsymbol{\tau} \end{aligned} \tag{7.45}$$

with

$$\eta_{\text{HS}}\left(|\mathbf{r}|\right) = \begin{cases} (\eta_{\text{sph}} - \eta_{\text{sol}}) & \text{for } |\mathbf{r}| \leq R \\ 0 & \text{for } |\mathbf{r}| > R \end{cases} \tag{7.46a}$$

$$\eta_{\text{Gauss}}\left(|\mathbf{r}|\right) = \frac{1}{2\sqrt{2}\,\pi^{3/2}|\sigma|^3} \exp\left[-\frac{|\mathbf{r}|^2}{2|\sigma|^2}\right] \tag{7.46b}$$

The convolution has to be done in $\mathbb{R}^3$. As the hard sphere and Gaussian functions are radial symmetric also the profile of the fuzzy sphere only depends on $|\mathbf{r}|$. By defining the interface via a convolution the form factor can be easily calculated because the Fourier transform of a convolution is the pointwise product of the Fourier transforms according

to the convolution theorem, i.e.

$$\begin{aligned} F(Q) &= \mathcal{F}\left[\eta_{\text{FuzzySph}}(r)\right] \\ &= \mathcal{F}\left[\left(\eta_{\text{HS}} \star \eta_{\text{Gauss}}\right)(r)\right] = \mathcal{F}\left[\eta_{\text{HS}}(r)\right]\mathcal{F}\left[\eta_{\text{Gauss}}(r)\right] \\ &= \int_0^\infty \eta_{\text{HS}}(r)\; 4\pi r^2 \frac{\sin(Qr)}{Qr}\; dr \int_0^\infty \eta_{\text{Gauss}}(r)\; 4\pi r^2 \frac{\sin(Qr)}{Qr}\; dr \\ &= \left(\eta_{\text{sph}} - \eta_{\text{sol}}\right) 4\pi R^3 \frac{\sin(QR) - QR\cos(QR)}{(QR)^3} \quad e^{\left[-\frac{1}{2}\sigma^2 Q^2\right]} \end{aligned} \tag{7.47}$$

Instead of calculating the convolution integral one also can get the radial profile of the fuzzy interface by the inverse Fourier transformation of the scattering amplitude

$$\eta_{\text{FuzzySph}}(r) = \int_0^\infty \frac{1}{(2\pi)^3} F(Q) 4\pi Q^2 \frac{\sin(Qr)}{Qr} \mathrm{d}Q \tag{7.48}$$

$$\begin{aligned} \eta_{\text{FuzzySph}}(r) &= \left(\eta_{\text{sph}} - \eta_{\text{sol}}\right) \\ &\left(\frac{\left(e^{-\frac{(r+R)^2}{2\sigma^2}} - e^{-\frac{(r-R)^2}{2\sigma^2}}\right)\sigma}{\sqrt{2\pi}\, r} + \frac{1}{2}\mathrm{erf}\left[\frac{r+R}{\sqrt{2}|\sigma|}\right] - \frac{1}{2}\mathrm{erf}\left[\frac{r-R}{\sqrt{2}|\sigma|}\right] \right) \end{aligned} \tag{7.49}$$

Finally the scattering intensity is given by

$$\begin{aligned} I_{\text{FuzzySph}}(Q) &= F^2(Q) = \\ &\left[\left(\eta_{\text{sph}} - \eta_{\text{sol}}\right) 4\pi R^3 \frac{\sin(QR) - QR\cos(QR)}{(QR)^3} \quad e^{\left[-\frac{1}{2}\sigma^2 Q^2\right]}\right]^2 \end{aligned} \tag{7.50}$$

The intensity $I_{\text{FuzzySph}}(Q)$ and also the scattering length profile $\eta_{\text{FuzzySph}}(r)$ are normalized so that

$$\begin{aligned} \lim_{Q\to\infty} I_{\text{FuzzySph}}(Q) &= \left(\frac{4}{3}\pi R^3\right)^2 \\ \int_0^\infty 4\pi r^2\, \eta_{\text{FuzzySph}}(r)\, \mathrm{d}r &= \frac{4}{3}\pi R^3 \end{aligned}$$

$$\begin{aligned} R &= \text{radius of the fuzzy sphere} \\ \sigma &= \text{thickness of the fuzzy shell} \\ \eta_{\text{sph}} &: \text{scattering length density of sphere} \\ \eta_{\text{sol}} &: \text{scattering length density of the solvent} \end{aligned} \tag{7.51}$$

Input Parameters for model `FuzzySphere` and `radial profile of FuzzySphere`:

`R:` radius of the fuzzy sphere R
`sigma:` thickness of the fuzzy shell σ
`eta_sph:` scattering length density of sphere η_{sph}
`eta_sol:` scattering length density of solvent η_{sol}

Note:

- This form factor is only defined for positive radii $R > 0$.
- For $\sigma = 0$ the limiting case of a simple hard sphere form factor is used.
- In addition, scattering contributions arising from fluctuations of the microgel network are often included in this model expression as a Lorentzian function

$$I_{\text{fluct}}(Q) = \frac{I_{\text{fluct}}(0)}{1 + \xi^2 Q^2} \tag{7.52}$$

so that

$$I(Q) = I_{\text{FuzzySph}}(Q) + I_{\text{fluct}}(Q) \tag{7.53}$$

where $I_{\text{fluct}}(0)$ is the $Q = 0$ limiting intensity and ξ represents the correlation length of the fluctuations, which can be considered to be related to the blob or mesh size. It should be noted that the Lorentzian describes the ensemble average correlations in the polymer network.

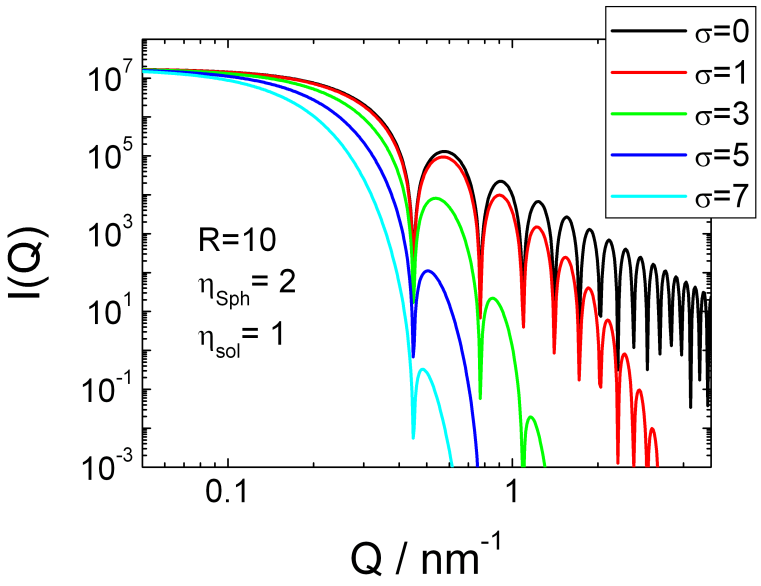

FIGURE 7.13. Scattering intensity of a fuzzy sphere. The scattering intensity has been calculated for a core radius $R = 10$, a scattering length density of the FuzzySphere of $\eta_{\text{Sph}} = 1$, a scattering length density of the solvent $\eta_{\text{sol}} = 1$, and several widths of the "fuzzy" shell

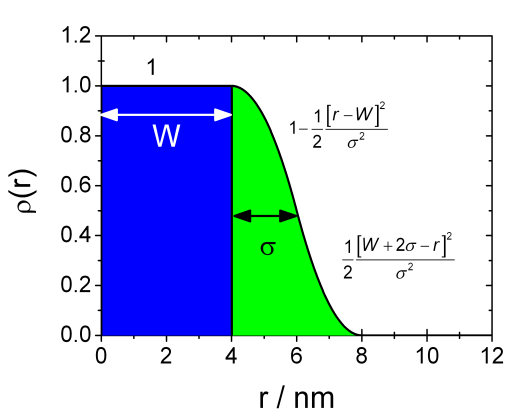

(a) radial profile of a sphere with a parabolic interface

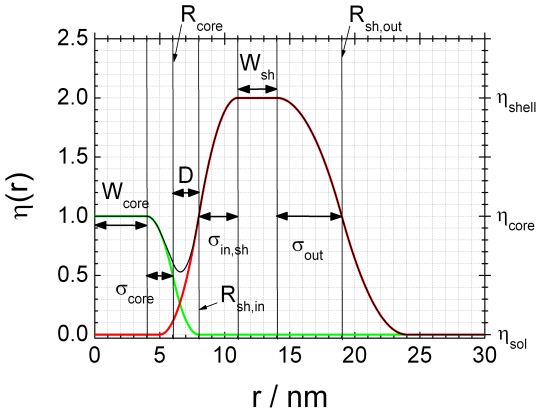

(b) radial profile of a spherical shell with parabolic interfaces

FIGURE 7.14. .....

7.3.2. CoreShellMicrogel. This model can be used to calculate the scattering from spherical particles with a parabolic "fuzzy" interface [**8, 7, 9**]. The radial profile is given by

$$\rho(r,R,\sigma) = \begin{cases} 1 & \text{for } r \leq R-\sigma \\ 1-\frac{1}{2}\frac{((r-R)+\sigma)^2}{\sigma^2} & \text{for } R-\sigma < r \leq R \\ \frac{1}{2}\frac{((R-r)+\sigma)^2}{\sigma^2} & \text{for } R < r \leq R+\sigma \\ 0 & \text{for } r >\leq R+\sigma \end{cases} \tag{7.54}$$

where $R = W+\sigma$. For such a radial profile the Fourier-transformation can be calculated analytically as

$$\begin{aligned} F(Q,R,\sigma) &= \mathcal{F}[\rho(r,R,\sigma)] = \\ 4\pi\Bigg(&\left(\frac{R}{\sigma^2}+\frac{1}{\sigma}\right)\frac{\cos(q(R+\sigma))}{q^4} + \left(\frac{R}{\sigma^2}-\frac{1}{\sigma}\right)\frac{\cos(q(R-\sigma))}{q^4} \\ &- 3\frac{\sin(q(R+\sigma))}{q^5\sigma^2} - 3\frac{\sin(q(R-\sigma))}{q^5\sigma^2} - 6\frac{\sin(qR)}{q^5\sigma^2} - 2R\frac{\cos(qR)}{q^4\sigma^2}\Bigg) \end{aligned} \tag{7.55}$$

The last term in the brackets needed to be corrected compared to the papers mentioned above due to a typo in the original papers. The radial scattering length density profile of a fuzzy core shell like in Fig. 7.14b can be obtained by

$$\begin{aligned} \eta_{core,sh}(r,W_{\text{core}},\sigma_{\text{core}},D,\sigma_{\text{sh,in}},W_{\text{sh}},\sigma_{\text{sh,out}}) &= \eta_{\text{sol}} + (\eta_{\text{shell}}-\eta_{\text{sol}})\rho(r,R_{\text{out}},\sigma_{\text{out}}) \\ &+ (\eta_{\text{shell}}-\eta_{\text{sol}})\rho(r,R_{\text{sh,in}},\sigma_{\text{sh,in}}) + (\eta_{\text{core}}-\eta_{\text{sol}})\rho(r,R_{\text{core}},\sigma_{\text{core}}) \end{aligned} \tag{7.56}$$

with

$$R_{\text{core}} = W_{\text{core}} + \sigma_{\text{core}} \tag{7.57a}$$

$$R_{\text{sh,in}} = R_{\text{core}} + D \tag{7.57b}$$

$$R_{\text{out}} = R_{\text{sh,in}} + \sigma_{\text{sh,in}} + W_{\text{sh}} + \sigma_{\text{sh,out}} \tag{7.57c}$$

In the same way also the scattering amplitude $F_{\text{core,sh}}(Q, \cdots)$ and the scattering intensity $I_{\text{core,sh}}(Q, \cdots) = |F_{\text{core,sh}}(Q, \cdots)|^2$ can be calculated

$$\begin{aligned} F_{\text{core,sh}}(Q, W_{\text{core}}, \sigma_{\text{core}}, D, \sigma_{\text{sh,in}}, W_{\text{sh}}, \sigma_{\text{sh,out}}) &= (\eta_{\text{shell}} - \eta_{\text{sol}}) F(Q, R_{\text{out}}, \sigma_{\text{out}}) \\ &+ (\eta_{\text{shell}} - \eta_{\text{sol}}) F(Q, R_{\text{sh,in}}, \sigma_{\text{sh,in}}) + (\eta_{\text{core}} - \eta_{\text{sol}}) F(Q, R_{\text{core}}, \sigma_{\text{core}}) \end{aligned} \tag{7.58a}$$

$$I_{\text{core,sh}}(Q, W_{\text{core}}, \sigma_{\text{core}}, D, \sigma_{\text{sh,in}}, W_{\text{sh}}, \sigma_{\text{sh,out}}) = |F_{\text{core,sh}}(Q, \cdots)|^2 \tag{7.58b}$$

Input parameters for "`CoreShellMicrogel`" and "`radial profile of CoreShellMicrogel`":

`W_core`: radius of center parts of core W_{core} with homogeneous scattering length density

`sigma_core`: interface half width of the core σ_{core}

`W_shell`: width of center parts of shell W_{sh} with homogeneous scattering length density

`sigma_sh,in`: half width of the inner interface of shell $\sigma_{\text{sh,in}}$

`D`: distance D between interface of core and in interface of shell

`sigma_out`: half width of the outer surface profile σ_{out}

`eta_core`: scattering length density of homogeneous core part η_{core}

`eta_shell`: scattering length density of homogeneous shell part η_{shell}

`eta_sol`: scattering length density of solvent η_{sol}

Note

- If one like to simulate a simple step profile one should set $D = 0$ and $\sigma_{\text{core}} = \sigma_{\text{sh,in}}$. The last equality in case of fitting this parameter can be simply obtained by a global parameter under fitting multiple data sets.
- Instead of using the radii in eq. 7.57 as input parameters the thickness of the homogeneous parts of the core and the shell have been used to avoid a problems (negative dimensions) by applying an integration over a size distribution starting from 0 on the radii.

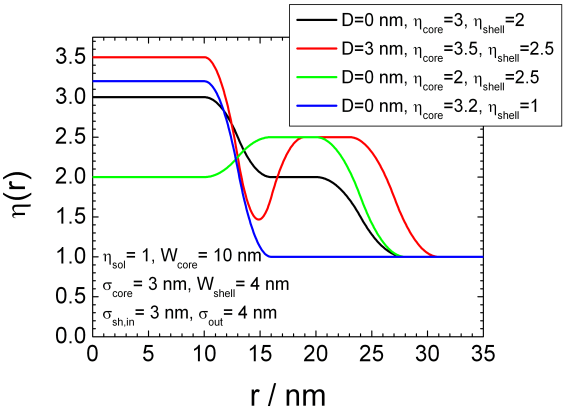

(a) Some radial profiles of spheres with a parabolic interfaces which have been used to calculate the scattering curve in Fig. (b).

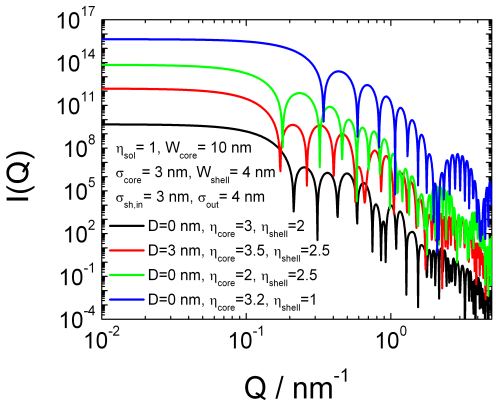

(b) Scattering curves of the radial profiles shown in Fig. (a).

FIGURE 7.15. The profiles and scattering curves hve been calculated with the plugin functions "`CoreShellMicrogel`" and "`Radial Profile of CoreShellMicrogel`".

7.3.2.1. *Spherical shell with linear varying contrast profile (LinShell).*

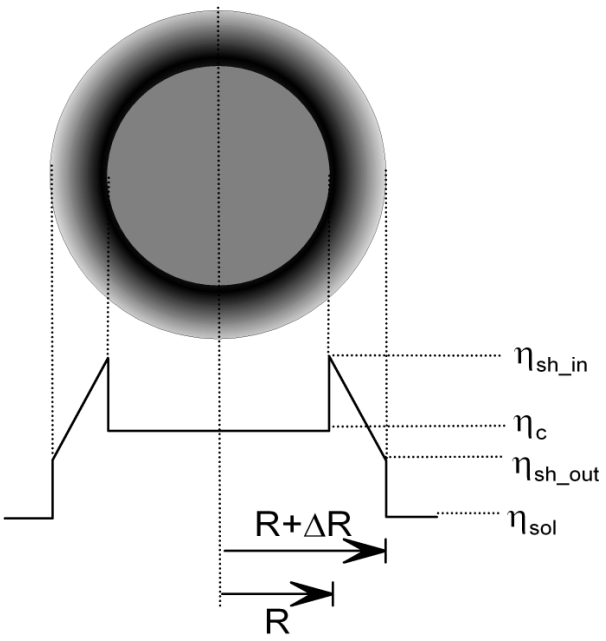

FIGURE 7.16. Radial profile for calculating the form factor of a spherical shell with a core radius R and a shell thickness of ΔR and a linear varying contrast profile.

Form factor of a spherical shell with a core radius R and a shell thickness of ΔR. Here a linear contrast profile within the shell has been assumed.

$$\Delta\eta(r) = \begin{cases} \eta_{\mathrm{c}} & \text{for } r < R \\ mr + b & \text{for } r \in [R, R + \Delta R] \\ \eta_{\mathrm{sol}} & \text{for } r > R + \Delta R \end{cases} \tag{7.59}$$

$$m = (\eta_{\mathrm{sh\_out}} - \eta_{\mathrm{sh\_in}})/\Delta R \tag{7.60}$$

$$b = -mR + \eta_{\mathrm{sh\_in}} \tag{7.61}$$

$$\eta_{\mathrm{sh\_in}} = (1 - x_{\mathrm{in,sol}})\,\eta_{\mathrm{sh}} + x_{\mathrm{in,sol}}\,\eta_{\mathrm{sol}} - \eta_{\mathrm{sol}} \tag{7.62}$$

: scattering length density at R

$$\eta_{\mathrm{sh\_out}} = (1 - x_{\mathrm{out,sol}})\,\eta_{\mathrm{sh}} + x_{\mathrm{out,sol}}\,\eta_{\mathrm{sol}} - \eta_{\mathrm{sol}} \tag{7.63}$$

: scattering length density at $R + \Delta R$

η_{sh} : scattering length density of pure shell material

η_{c} : scattering length density of core

$$F_{\text{sph}}(A,x) = \frac{4}{3}\pi x^3\ 3\frac{\sin(A) - A\cos(A)}{A^3} \tag{7.64}$$

$$F_{\text{shlin}}(A,x) = 4\pi x^4 \frac{2\cos(A) + 2A\sin(A) - A^2\cos(A)}{A^4} \tag{7.65}$$

$$\begin{aligned} I_{\text{LinShell}} = \big[\ & (\eta_{\text{c}} - \eta_{\text{sol}} - b)F_{\text{sph}}(QR, R) \\ & - mF_{\text{shlin}}(QR, R) \\ & + mF_{\text{shlin}}\left(Q(R+\Delta R), R+\Delta R\right) \\ & + bF_{\text{sph}}\left(Q(R+\Delta R), R+\Delta R\right)\big]^2 \end{aligned} \tag{7.66}$$

Input Parameters for model `LinShell` and `radial profile of LinShell`:

`R:` radius of core R
`dR:` thickness of the shell ΔR
`eta_c:` scattering length density η_{c}
`eta_sh:` scattering length density of non-swollen shell η_{sh}
`x_in:` amount of solvent $x_{\text{in,sol}}$ on core-shell interface at R
`x_out:` amount of solvent $x_{\text{out,sol}}$ on shell-solvent interface at $R + \Delta R$
`eta_sol:` scattering length density of solvent η_{sol}

Note:

- $x_{\text{in,sol}}$ and $x_{\text{out,sol}}$ are only physical for values between 0 and 1.

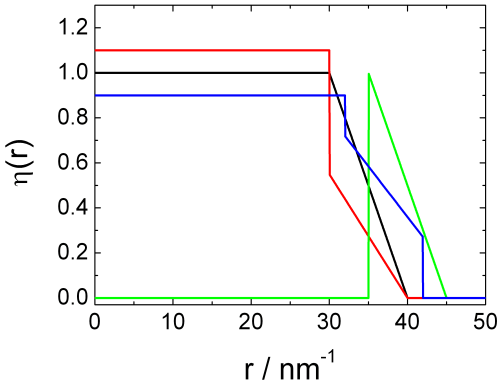

(a) Some radial profiles of spheres with a linear interface profiles due to penetration of solvent into the shell which have been used to calculate the scattering curve in Fig. (b).

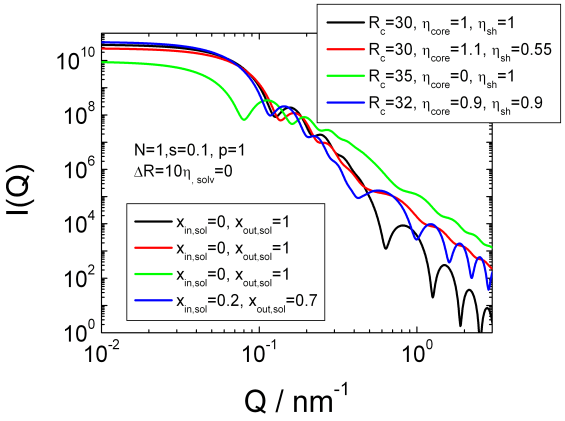

(b) Scattering curves of the radial profiles shown in Fig. (a).

FIGURE 7.17. Scattering intensity of a spherical shell with an linear shell profile. The scattering intensity has been calculated with a lognormal size distribution for the core radius R_c.

7.3.2.2. *LinShell2.*

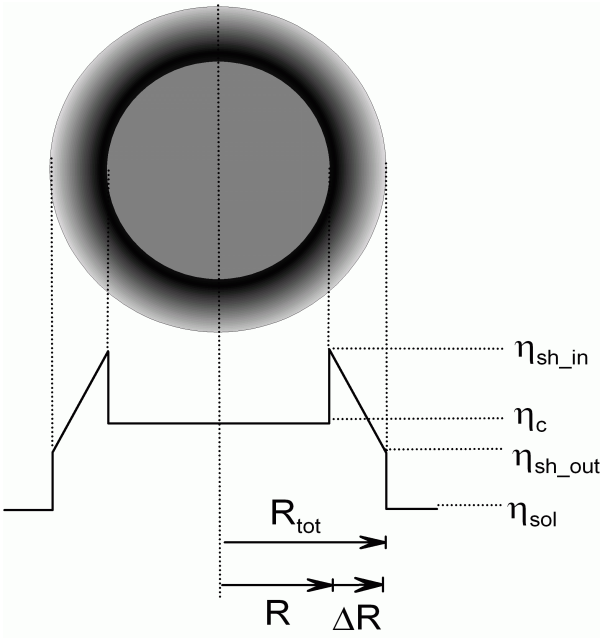

FIGURE 7.18. Radial profile for calculating the form factor of a spherical shell with a total radius R_{tot}, a shell thickness of ΔR, and a linear varying contrast profile.

Form factor of a spherical shell with a total radius R_{tot} and a shell thickness of ΔR. The definition are the same than for `LinShell` except that instead of the core radius R now the total radius R_{tot} is used to parameterize the form factor. The parameter definitions are the following:

$$R = \begin{cases} R_{\text{tot}} - \Delta R & \text{for } R_{\text{tot}} > \Delta R \\ 0 & \text{otherwise} \end{cases} \tag{7.67}$$

$$\Delta\eta(r) = \begin{cases} \eta_{\text{c}} & \text{for } r < R \\ mr + b & \text{for } r \in [R, R_{\text{tot}}] \\ \eta_{\text{sol}} & \text{for } r > R_{\text{tot}} \end{cases} \tag{7.68}$$

with

$$m = (\eta_{\text{sh\_out}} - \eta_{\text{sh\_in}})/\Delta R \tag{7.69}$$

$$b = -mR + \eta_{\text{sh\_in}} \tag{7.70}$$

and

$$\eta_{\text{sh\_in}} = (1 - x_{\text{in,sol}})\,\eta_{\text{sh}} + x_{\text{in,sol}}\,\eta_{\text{sol}} \tag{7.71}$$
: scattering length density at R

$$\eta_{\text{sh\_out}} = (1 - x_{\text{out,sol}})\,\eta_{\text{sh}} + x_{\text{out,sol}}\,\eta_{\text{sol}} \tag{7.72}$$
: scattering length density at $R_{\text{tot}} = R + \Delta R$

η_{sh} : scattering length density of pure shell material

η_{c} : scattering length density of core

$x_{\text{in,sol}}$: amount of solvent at R

$x_{\text{out,sol}}$: amount of solvent at $R_{\text{tot}} = R + \Delta R$

$$F_{\text{sph}}(A, x) = \frac{4}{3}\pi x^3\ 3\frac{\sin(A) - A\cos(A)}{A^3} \tag{7.73}$$

$$F_{\text{shlin}}(A, x) = 4\pi x^4 \frac{2\cos(A) + 2A\sin(A) - A^2\cos(A)}{A^4} \tag{7.74}$$

$$\begin{aligned} I_{\text{LinShell2}} = \big[\ & (\eta_{\text{c}} - \eta_{\text{sol}} - b)F_{\text{sph}}(QR, R) \\ & - mF_{\text{shlin}}(QR, R) \\ & + mF_{\text{shlin}}\left(QR_{\text{tot}}, R_{\text{tot}}\right) \\ & + bF_{\text{sph}}\left(QR_{\text{tot}}, R_{\text{tot}}\right)\big]^2 \end{aligned} \tag{7.75}$$

Input Parameters for model `LinShell2` and `radial profile of LinShell2`:

`Rtot`: total overall radius R_{tot}
`dR`: thickness of the shell ΔR
`eta_c`: scattering length density η_{c}
`eta_sh`: scattering length density of non-swollen shell η_{sh}
`x_in`: amount of solvent $x_{\text{in,sol}}$ on core-shell interface at R ($x_{\text{in,sol}} \in [0; 1]$)
`x_out`: amount of solvent $x_{\text{out,sol}}$ on shell-solvent interface at $R + \Delta R$ ($x_{\text{out,sol}} \in [0; 1]$).
`eta_s`: scattering length density of solvent η_{sol}

Note:

- $x_{\text{in,sol}}$ and $x_{\text{out,sol}}$ are only physical for values between 0 and 1.

7.3.2.3. *ExpShell.*

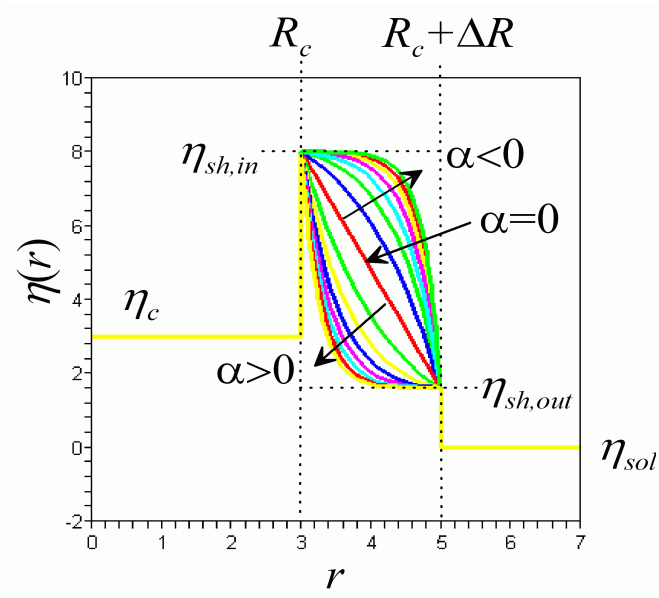

FIGURE 7.19. Radial profile for calculating the form factor of a spherical shell with a core radius R_c and a shell thickness of ΔR and a exponentially varying contrast profile. The profile shape can be varied by the parameter α describing the penetration of the solvent into the shell. A value of $\alpha = 0$ means linear profile and is equivalent to `LinShell` and `LinShell2`. For $\alpha > 0$ the solvent penetrates further into the shell and for $\alpha < 0$ less.

$$\eta_{\text{ExpShell}}(r, R_c, \Delta R, \alpha, \phi_{\text{in}}, \phi_{\text{out}}) = \begin{cases} \eta_c & r \leq R_c \\ \eta_{\text{exp}}(\frac{r-R_c}{\Delta R}) & R_c < r < R_c + \Delta R \\ \eta_{\text{sol}} & r > R_c + \Delta R \end{cases} \tag{7.76}$$

$$\eta_{\text{exp}}(x) = \begin{cases} \eta_{\text{sh,in}} + [\eta_{\text{sh,out}} - \eta_{\text{sh,in}}]\, x \exp\left([1-x]\,\alpha\right) & \alpha < 0 \\ [\eta_{\text{sh,in}} - \eta_{\text{sh,out}}]\,[1-x] \exp\left(-x\alpha\right) + \eta_{\text{sh,out}} & \alpha \geq 0 \end{cases} \tag{7.77}$$

$$\eta_{\text{sh,in}} = [\phi_{\text{in}}\, \eta_{\text{sol}} + (1-\phi_{\text{in}})\, \eta_{\text{sh}}] \tag{7.78}$$

$$\eta_{\text{sh,out}} = [\phi_{\text{out}}\, \eta_{\text{sol}} + (1-\phi_{\text{out}})\, \eta_{\text{sh}}] \tag{7.79}$$

The scattering intensity for the radial symmetric scattering length density profile $\eta_{\text{ExpShell}}(r)$ can be calculated analytical. The integral needed to be solved for that is

$$I_{\text{ExpShell}}(Q) = \int_0^\infty 4\pi r^2 \frac{\sin Qr}{Qr}\, \eta_{\text{ExpShell}}(r)\, dr \tag{7.80}$$

R_c = core radius

ΔR = shell thickness

$$\eta_{\text{sh,in}} = (1 - \phi_{\text{in,sol}})\,\eta_{\text{sh}} + \phi_{\text{in,sol}}\,\eta_{\text{sol}} \tag{7.81}$$

: scattering length density at R_c

$$\eta_{\text{sh,out}} = (1 - \phi_{\text{out,sol}})\,\eta_{\text{sh}} + \phi_{\text{out,sol}}\,\eta_{\text{sol}} \tag{7.82}$$

: scattering length density at $R_c + \Delta R$

η_{sh} : scattering length density of pure shell material

η_{c} : scattering length density of core

ϕ_{in} : amount of solvent at R_c

ϕ_{out} : amount of solvent at $R_c + \Delta R$

α : parameter for exponential diffuse profile of the shell (7.83)

Input Parameters for model `ExpShell`:

`R_core`: radius of core R_c
`DR`: thickness of the shell ΔR
`eta_core`: scattering length density η_{c}
`eta_shell`: scattering length density of non-swollen shell η_{sh}
`x_in_sol`: amount of solvent ϕ_{in} on core-shell interface at $r = R$
`x_out_sol`: amount of solvent ϕ_{out} on shell-solvent interface at $r = R + \Delta R$
`alpha`: a parameter (α) which describes the penetration profile of the solvent into the shell. A value of $\alpha = 0$ means linear profile and is equivalent to `LinShell` and `LinShell2`. For $\alpha > 0$ the solvent penetrates further into the shell and for $\alpha < 0$ less.
`eta_solvent`: scattering length density of solvent η_{sol}

Note:

- ϕ_{in} and ϕ_{out} are only physical for values between 0 and 1.

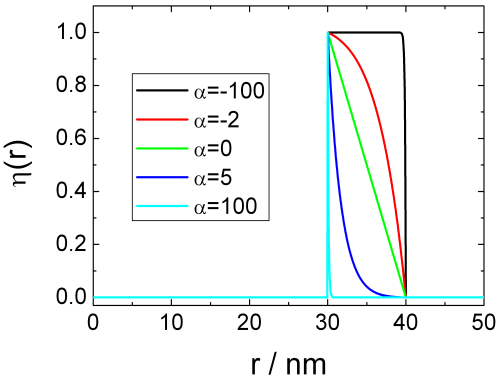

(a) Some radial profiles of spheres with a exponential interfaces which have been used to calculate the scattering curve in Fig. (b).

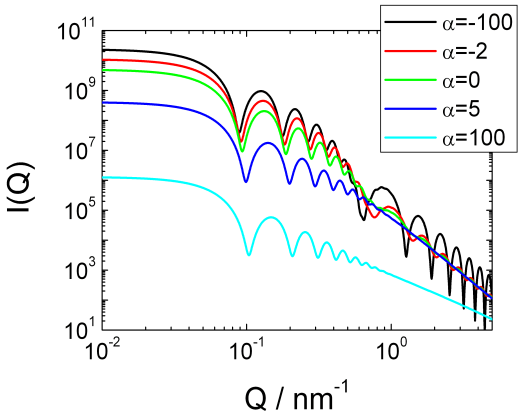

(b) Scattering curves of the radial profiles shown in Fig. (a).

FIGURE 7.20. Scattering intensity of a spherical shell with an exponential shell profile. The scattering intensity has been calculated with a lognormal [LogNorm($N = 1, \sigma = 0.05, p = 1, R = 30$)] size distribution for the core radius R_c. The scattering length density of the core η_c and the solvent η_{sol} are set to 0, $\eta_{sh} = 1$, $\phi_{in} = 0$, $\phi_{out} = 1$, and $\Delta R = 10$.

7.4. Ferrofluids

7.5. LogNorm_fp

The `LogNorm` distribution is a continuous distribuion in which the logarithm of a variable has a normal distribution.

$$\mathrm{LogNorm}(x, N, \sigma, p, \mu) = \frac{N}{c_{\mathrm{LN}}} \frac{1}{x^p} \exp\left(-\frac{\ln(x/\mu)^2}{2\sigma^2}\right) \tag{7.84a}$$

$$c_{\mathrm{LN}} = \sqrt{2\pi}\, \sigma\, \mu^{1-p} \exp\left((1-p)^2 \frac{\sigma^2}{2}\right) \tag{7.84b}$$

where σ is the width parameter, p a shape parameter, μ is the location parameter. c_{LN} is choosen so that $\int_0^\infty \mathrm{LogNorm}(x, \mu, \sigma, p)\, dR = N$ The mode of the distribution is defined as

$$x_{\mathrm{mode}} = \mu e^{-p\sigma^2} \tag{7.85}$$

and the n^{th} moment $\langle X^n \rangle$ of the `LogNorm` distribution as

$$\langle X^n \rangle = \frac{\int X^n \,\mathrm{LogNorm}(X)\, dX}{\int \mathrm{LogNorm}(X)\, dX} = \mu^n\, e^{\frac{1}{2}\sigma^2 n(2-2p+n)}. \tag{7.86}$$

Instead of using the parameter N (particle number density) another Log-Normal size distribution namely `LogNorm_fp` with the volume fraction f_p as a parameter has been implemented. Using the volume fraction as a scaling parameter requires that the intensity is given in units of cm^{-1} and the scattering vector in nm^{-1}. Furthermore the scattering contrast needs to be supplied in units of cm^{-2}. More details about absolute intensity can be found in chapter 8. The volume fraction f_p can be obtained from the `LogNorm`-distribution (eq. 7.84b) by integrating over the particle volume V_P. In case of spheres we get

$$f_p = 10^{21} \int_0^\infty \mathrm{LogNorm}(R, N, \sigma, p, \mu) V_P(R)\, dR \tag{7.87}$$

$$= 10^{21} \int_0^\infty \mathrm{LogNorm}(R, N, \sigma, p, \mu) \frac{4}{3}\pi R^3\, dR = 10^{21} N \frac{4}{3}\pi \langle X^3 \rangle. \tag{7.88}$$

The scaling factor 10^{21} depends on the actual units. More details are given in section 8.4.

For other shapes than spheres the corresponding volume of the object has to be used in eq. 7.89. In case of cylinders the volume is given by $V_{\mathrm{cyl}} = \pi R^2 L$. Depending whether the radius R or the cylinder length L has a size distribution the volume fraction f_p is

calculated differently namely in case for a radius distribution by

$$f_p = 10^{21} \int_0^\infty \text{LogNorm}(R) V_{\text{cyl}}(R, L)\, dR \tag{7.89}$$

$$= 10^{21} \int_0^\infty \text{LogNorm}(R) \pi R^2 L\, dR = 10^{21} N \pi L \langle X^2 \rangle \tag{7.90}$$

and in case of a length distribution by

$$f_p = 10^{21} \int_0^\infty \text{LogNorm}(L) \pi R^2 L\, dL = 10^{21} N \pi R^2 \langle X \rangle. \tag{7.91}$$

As the cylinder volume depends on R^2 and L either the second or the first moment of the distribution function is involved in calculating the volume fraction depending which parameter has a distribution. For a spherical shell a sum of different moments has to be used as listed in table 1.

shape	form factor	distrib. param.	length2	length3	volume	V	$N(f_p)$
1	Sphere	R	not used	not used	whole sph.	$\frac{4}{3}\pi R^3$	$\frac{f_p}{10^{21}}\frac{3}{4\pi}\frac{1}{\langle X^3\rangle}$
2	Cylinder	R	L	not used	whole cyl.	$\pi R^2 L$	$\frac{f_p}{10^{21}}\frac{1}{\pi}\frac{1}{\langle X^2\rangle L}$
3	Cylinder	L	R	not used	whole cyl.	$\pi R^2 L$	$\frac{f_p}{10^{21}}\frac{1}{\pi}\frac{1}{R^2\langle X^1\rangle}$
4	Sph.Sh.iii	R	ΔR	not used	core+shell	$4\pi\left(R^2\Delta R + R\Delta R^2 + \frac{1}{3}\Delta R^3 + \frac{1}{3}R^3\right)$	$\frac{f_p}{10^{21}}\frac{1}{4\pi}\frac{1}{\frac{1}{3}\langle X^3\rangle+\langle X^2\rangle\Delta R+\langle X^1\rangle\Delta R^2+\langle X^0\rangle\frac{\Delta R^3}{3}}$
5	Sph.Sh.iii	ΔR	R	not used	core+shell	$4\pi\left(R^2\Delta R + R\Delta R^2 + \frac{1}{3}\Delta R^3 + \frac{1}{3}R^3\right)$	$\frac{f_p}{10^{21}}\frac{1}{4\pi}\frac{1}{\frac{1}{3}R^3\langle X^0\rangle+R^2\langle X^1\rangle+R\langle X^2\rangle+\frac{1}{3}\langle X^3\rangle}$
6	Sph.Sh.iii	R	ΔR	not used	core	$\frac{4}{3}\pi R^3$	$\frac{f_p}{10^{21}}\frac{3}{4\pi}\frac{1}{\langle X^3\rangle}$
7	Sph.Sh.iii	ΔR	R	not used	core	$\frac{4}{3}\pi R^3$	$\frac{f_p}{10^{21}}\frac{3}{4\pi}\frac{1}{R^3\langle X^0\rangle}$
8	Sph.Sh.iii	R	ΔR	not used	shell	$4\pi\left(R^2\Delta R + R\Delta R^2 + \frac{1}{3}\Delta R^3\right)$	$\frac{f_p}{10^{21}}\frac{1}{4\pi}\frac{1}{\langle X^2\rangle\Delta R+\langle X^1\rangle\Delta R^2+\langle X^0\rangle\frac{\Delta R^3}{3}}$
9	Sph.Sh.iii	ΔR	R	not used	shell	$4\pi\left(R^2\Delta R + R\Delta R^2 + \frac{1}{3}\Delta R^3\right)$	$\frac{f_p}{10^{21}}\frac{1}{4\pi}\frac{1}{R^2\langle X^1\rangle+R\langle X^2\rangle+\frac{1}{3}\langle X^3\rangle}$
10	CylShell1	R	ΔR	L	core+shell	$\pi L\left(\Delta R^2 + 2R\Delta R + R^2\right)$	$\frac{f_p}{10^{21}}\frac{1}{\pi}\frac{1}{L\left(\Delta R^2\langle X^0\rangle+2\langle X^1\rangle\Delta R+\langle X^2\rangle\right)}$
11	CylShell1	ΔR	R	L	core+shell	$\pi L\left(\Delta R^2 + 2R\Delta R + R^2\right)$	$\frac{f_p}{10^{21}}\frac{1}{\pi}\frac{1}{L\left(\langle X^2\rangle+2R\langle X^1\rangle+R^2\langle X^0\rangle\right)}$
12	CylShell1	L	R	ΔR	core+shell	$\pi L\left(\Delta R^2 + 2R\Delta R + R^2\right)$	$\frac{f_p}{10^{21}}\frac{1}{\pi}\frac{1}{\langle X^1\rangle\left(\Delta R^2+2R\Delta R+R^2\right)}$
13	CylShell1	R	ΔR	L	core	$\pi L R^2$	$\frac{f_p}{10^{21}}\frac{1}{\pi}\frac{1}{\langle X^2\rangle L}$
14	CylShell1	ΔR	R	L	core	$\pi L R^2$	$\frac{f_p}{10^{21}}\frac{1}{\pi}\frac{1}{R^2 L\langle X^0\rangle}$
15	CylShell1	L	R	ΔR	core	$\pi L R^2$	$\frac{f_p}{10^{21}}\frac{1}{\pi}\frac{1}{R^2\langle X^1\rangle}$
16	CylShell1	R	ΔR	L	shell	$\pi L\left(\Delta R^2 + 2R\Delta R\right)$	$\frac{f_p}{10^{21}}\frac{1}{\pi}\frac{1}{L\left(\Delta R^2\langle X^0\rangle+2\langle X^1\rangle\Delta R\right)}$
17	CylShell1	ΔR	R	L	shell	$\pi L\left(\Delta R^2 + 2R\Delta R\right)$	$\frac{f_p}{10^{21}}\frac{1}{\pi}\frac{1}{L\left(\langle X^2\rangle+2R\langle X^1\rangle\right)}$
18	CylShell1	L	R	ΔR	shell	$\pi L\left(\Delta R^2 + 2R\Delta R\right)$	$\frac{f_p}{10^{21}}\frac{1}{\pi}\frac{1}{\langle X^1\rangle\left(\Delta R^2+2R\Delta R\right)}$

TABLE 1. The number density N expressed in terms of volume fraction f_p and moments $\langle X^n\rangle$ of the distribution function for some particle shapes and different parameters having a distribution. The factor 10^{21} is needed due to unit conversion. It is assumed that the radius is given in nm, the intensity in cm^{-1} and the scattering length densities in cm^{-2}.

CHAPTER 8

Absolute intensities, moments and volume fractions

8.1. Fitting absolute intensities

Absolute intensities in the simulation can be obtained by using proper units for the scattering vector **Q**, the size dimensions of the scatterer, the scattering length densities etc. In the following a few example are discussed for absolute calibrated data sets. One question which is asked quite frequently is "What is the meaning of N in the size distribution and what are its units?". The answer is normally "That depends on the units of your data you are fitting and the units of your scattering length densities". In the following a few explanations will be given to clarify this in some more detail.

Let us consider first the scattering intensity of a single sphere. The form factor of a sphere is given by eq. 3.1a as

$$I_{\text{Sphere}}(Q,R,\Delta\eta) = \left[\frac{4}{3}\pi R^3 \Delta\eta \, 3\frac{\sin QR - QR\cos QR}{(QR)^3}\right]^2 \tag{8.1}$$

The radius R and the scattering vector Q have reciprocal units, i.e. if Q is given in 1/nm the radius R has a unit of nm. The other variable in the form factor is the scattering length density contrast $\Delta\eta$ between sphere and surrounding matrix or solvent. The unit of the scattering length density is length/volume and has therefore a unit $1/\text{cm}^2$ or some other sites are using units of $1/\text{Å}^2$. The difference is only a constant factor of

$$\Delta\eta\frac{1}{\text{cm}} = 10^{16}\Delta\eta\,\frac{1}{\text{Å}}. \tag{8.2}$$

The overall unit of the scattering intensity (differential cross-section) of a single sphere is therefore

$$[I_{\text{Sphere}}(Q,R,\Delta\eta)] = [R]^6\,[\Delta\eta]^2 = \frac{\text{nm}^6}{\text{cm}^4} = 10^{-42}\text{cm}^2 \tag{8.3}$$

for the case that $[R] = \text{nm}$ and $[\Delta\eta] = \text{cm}^{-2}$. The unit for the scattering cross-section of a single sphere with $[R] = \text{Å}$ and $[\Delta\eta] = \text{Å}^{-2}$ is than

$$[I_{\text{Sphere}}(Q,R,\Delta\eta)] = [R]^6\,[\Delta\eta]^2 = \frac{\text{Å}^6}{\text{Å}^4} = \text{Å}^2 = 10^{-16}\text{cm}^2, \tag{8.4}$$

respectively. The scattering cross-section of a single scatterer is calculated by `SASfit` if one chooses in the tab for distribution functions the probability functions `Monodisperse`.

Differential cross-section have a unit of an area

$$\left[\frac{d\Sigma}{d\Omega}(Q)\right] = \text{cm}^2. \tag{8.5}$$

Many instruments deliver with their data reduction software a cross-section normalized by the sample volume so that the unit is in reciprocal length:

$$\left[\frac{d\sigma}{d\Omega}(Q)\right] = \frac{1}{[V]}\left[\frac{d\Sigma}{d\Omega}(Q)\right] = \frac{1}{\text{cm}}. \tag{8.6}$$

For fitting a form factor to experimental data one needs next to the size parameter also a scaling parameter. For the simplest case this is done by choosing as a distribution function `Delta`. `Delta` simply multiplies a constant value N to the form factor. The meaning and the unit of N now depends on the unit of the cross-section, wether it is normalized or not normalized on the sample volume. `SASfit` calculates in the case of a form factor of `Sphere` with `Delta` as a distribution function

$$I_{\texttt{SASfit}} = N \times I_{\text{Sphere}}(Q, R, \Delta\eta). \tag{8.7}$$

Fitting N to a data set, which is given in units of 1/cm and where $[Q] = \text{nm}^{-1}$, $[R] = \text{nm}$ and $[\Delta\eta] = \text{cm}^{-2}$ would mean that N has the unit

$$[N] = \frac{\left[\frac{d\sigma}{d\Omega}(Q)\right]}{[I_{\text{Sphere}}(Q, R, \Delta\eta)(Q)]} = \frac{\frac{1}{\text{cm}}}{10^{-42}\text{cm}^2} = 10^{42}\text{cm}^{-3}. \tag{8.8}$$

One therefore needs to multiply the value N obtained by `SASfit` with 10^{42} to get the number density of scatterers in units of cm^{-3}.

Let us now consider the simplest case of spheres with a size distribution and no structure factor, which are fitted to experimental data. All the size distribution have a scaling parameter N. The units of the parameter N in the size distribution is the same than for `Delta`. The size distribution $n(x)$ are implemented as distribution function $n(x) = Np(x)$ with $p(x)$ being a probability function. In case of polydisperse spheres `SASfit` calculates the integral

$$I_{\texttt{SASfit}}\,(Q) = \int_0^\infty n(R)\, I_{\text{Sphere}}(Q, R, \Delta\eta)\, dR \tag{8.9}$$

$$= N \int_0^\infty p(R)\, I_{\text{Sphere}}(Q, R, \Delta\eta)\, dR \tag{8.10}$$

The probability function $p(x)$ is normalized to

$$\int_0^\infty p(x)\, dx = 1, \tag{8.11}$$

so that the parameter N has like for the `Delta`-distribution the unit $[N] = 10^{42}\text{cm}^{-3}$ if the data set is given in units of 1/cm and $[Q] = \text{nm}^{-1}$, $[R] = \text{nm}$ and $[\Delta\eta] = \text{cm}^{-2}$.

Most of the form factor are implemented in a way that they return the scattering cross-section of a single object like the example of a sphere above, but a few are not, like for example the standard form of a gaussian chain `Gauss`. In this particular case two other versions `Gauss2` and `Gauss3` with different parameterizations of the forward scattering of a single gaussian chain are available. However, there are some form factors, which have been implemented according to the literature but which are normalized

differently. This has to be checked before the parameter N in the size distribution is interpreted in terms of number density of scatterers.

8.2. Contrast - Concentration - Forward Scattering - Particle Volume - Absolute Scale

A frequently asked question is if the scattering intensity is consistent with the concentration of material in the sample. Especially people working with micellar solution, star polymers, but also proteins, etc. want to cross-check the absolute intensity with the known concentration. In the dilute case the differential cross-section is simply N times the cross-section of an individual scatterer

$$\frac{d\sigma}{d\Omega}(Q) = \frac{N}{V_{\text{tot}}} P(Q) \tag{8.12}$$

N is number of particles/molecules/proteins in the illuminated volume, V_{tot} the illuminated sample volume, $n = N/V_{\text{tot}}$ the particle number density, and $P(Q)$ the scattering cross-section of a single particle. $P(Q)$ has the dimension cm^2, N/V_{tot} the dimension cm^{-3}, and $\frac{d\sigma}{d\Omega}(Q)$ the dimension cm^{-1}. Eq. 8.14 can also be expressed in terms of concentration c in units of g/cm^2

$$c = n\, m_{\text{mol}} = n\, M_r u = n \frac{M_r M_u}{N_A} = \frac{N}{V_{\text{tot}}} \frac{M_r M_u}{N_A} \tag{8.13}$$

so that

$$\frac{d\sigma}{d\Omega}(Q) = c \frac{N_A}{M_r M_u} P(Q) \tag{8.14}$$

M_r is the relative molar mass of the particle [1] (Molecular weight (M.W.) and formula weight (F.W.) are older terms) which is a dimensionless quantity (i.e., a pure number, without units). To get units in g/mol the relative molar mass needs to be multiplied by the molar mass constant M_u. The value of the molar mass constant M_u is defined to be 1 g/mol in SI units. The molar mass constant is important in writing dimensionally correct equations. It is common to see phrases such as "*The molar mass of an element is the atomic weight in grams per mole.*" However molecular or atomic weight are dimensionless quantities, and cannot take the units of grams per mole. Formally, the operation is the multiplication by a constant which has the value 1 g/mol, that is the molar mass constant[2]. The molecule mass m_{m} in units of g is $m_{\text{m}} = M_r M_u / N_A$.

---

[1] Definition of relative atomic mass and relative molecular mass can be found on the url-address http://physics.nist.gov/Pubs/SP811/sec08.html

Relative atomic mass (formerly atomic weight): ratio of the average mass per atom of an element to 1/12 of the mass of the atom of the nuclide ^{12}C.

Relative molecular mass (formerly molecular weight): ratio of the average mass per molecule or specified entity of a substance to 1/12 of the mass of an atom of the nuclide ^{12}C.

[2] Definition of unified atomic mass unit: $1\text{u} = m_{\text{u}} = m\left(^{12}\text{C}\right)/12 = 1 M_u/N_A = 1\,(\text{g/mol}) \,/\, \left(6.02214129 \times 10^{23}\text{mol}^{-1}\right) = 1.660538921 \times 10^{-}24\text{g}$

Now we need to look on the forward scattering $P(Q{=}0)$ of a single particle/protein/polymer chain. For a simple particle like a sphere, the forward scattering is given by

$$P(Q{=}0) = (\eta_{\mathrm{sol}} - \eta_{\mathrm{sp}})^2 \, V_{\mathrm{sp}}^2 \tag{8.15}$$

where $(\eta_{\mathrm{sol}} - \eta_{\mathrm{sp}})$ is the scattering contrast between spherical particle and solvent and V_{sp} the volume of a single sphere. In case of a spherical particle the boundary between particle and solvent is well defined and therefore also the volume of the particle as it has a sharp interface. The scattering contrast of a spherical particle can also be written in terms of the overall scattering length of the sphere b_{sp}, i.e. the sum of the scattering length of all atoms forming the sphere, the volume of the sphere and the scattering length density of the solvent. The volume of the sphere can be calculated from its mass m_{sp} or relative molar mass $M_{r,\mathrm{sp}}$ and its density ρ_{sp}.

$$(\eta_{\mathrm{sol}} - \eta_{\mathrm{sp}}) = \left(\eta_{\mathrm{sol}} - \frac{b_{\mathrm{sp}}}{V_{\mathrm{sp}}}\right) = \left(\eta_{\mathrm{sol}} - \frac{b_{\mathrm{sp}}\rho_{\mathrm{sp}}}{m_{\mathrm{sp}}}\right) = \left(\eta_{\mathrm{sol}} - \frac{b_{\mathrm{sp}}\rho_{\mathrm{sp}}N_A}{M_{r,\mathrm{sp}}M_u}\right) \tag{8.16}$$

But what about the forward scattering of a gaussian polymer coil? A polymer does not has a sharp boundary to the solvent. Polymer and solvent can penetrate each other. To determine the polymer volume one would need a detailed model for the polymer molecule and its interaction with solvent molecules. As a first approximation the volume of a polymer molecule can be obtained by $V_{\mathrm{polym}} = \frac{\rho_{\mathrm{polym}}}{m_{\mathrm{polym}}}$. For a polymer coil with a relative molar mass $M_{r,\mathrm{polym}}$ the forward scattering in a solvent is given by

$$P(Q{=}0) = \left(\frac{M_{r,\mathrm{polym}}M_u}{\rho_{\mathrm{polym}}N_A}\right)^2 \left(\eta_{\mathrm{sol}} - \frac{b_{\mathrm{polym}}\rho_{\mathrm{polym}}N_A}{M_{r,\mathrm{polym}}M_u}\right)^2 \tag{8.17}$$

The volume of a polymer molecule

$$V_{\mathrm{polym}} = \frac{M_{r,\mathrm{polym}}M_u}{\rho_{\mathrm{polym}}N_A}$$

is the volume occupied by single polymer chain in the solvent or in other word the amount of solvent volume displaced by one polymer chain. For the forward scattering it does not matter, if the coil is collapsed or swollen. As long as the scattering length density of the solvent inside the swollen polymer coil is the same than in the bulk and the molecular volume of the polymer chain does not change with the solvent quality the forward scattering does not depend on the conformation of the polymer. Sometimes the relative molar mass of a polymer is given in degree of polymerization p and relative molar mass of the monomer $M_{r,\mathrm{m}}$. In this case and assuming that the mass densities of polymer and monomer are the same the forward scattering is given by

$$\begin{aligned} P(Q{=}0) &= \left(\frac{p\ M_{r,\mathrm{m}}M_u}{\rho_{\mathrm{m}}N_A}\right)^2 \left(\eta_{\mathrm{sol}} - \frac{b_{\mathrm{m}}\rho_{\mathrm{m}}N_A}{M_{r,\mathrm{m}}M_u}\right)^2 \\ &= \left(\frac{p\ M_{r,\mathrm{m}}M_u}{\rho_{\mathrm{m}}N_A}\right)^2 \left(\eta_{\mathrm{sol}} - \frac{b_{\mathrm{m}}\rho_{\mathrm{m}}N_A}{M_{r,\mathrm{m}}M_u}\right)^2 \end{aligned} \tag{8.18}$$

Let us now come back to the measured differential cross-section $\frac{d\sigma}{d\Omega}(Q)$. For $Q = 0$ we get

$$\frac{d\sigma}{d\Omega}(Q{=}0) = \frac{N}{V_{\text{tot}}} P(Q{=}0) = c \frac{N_A}{M_{r,\text{Gauss}} M_u} P(Q{=}0) \tag{8.19}$$

$$= c \, \frac{N_A}{p \; M_{r,\text{m}} M_u} \left(\frac{p \; M_{r,\text{m}} M_u}{\rho_{\text{m}} N_A} \right)^2 \left(\eta_{\text{sol}} - \frac{b_{\text{m}} \rho_{\text{m}} N_A}{M_{r,\text{m}} M_u} \right)^2 \tag{8.20}$$

$$= c \, \frac{p \; M_{r,\text{m}} M_u}{N_A \rho_{\text{m}}^2} \left(\eta_{\text{sol}} - \frac{b_{\text{m}} \rho_{\text{m}} N_A}{M_{r,\text{m}} M_u} \right)^2 \tag{8.21}$$

The last equation says, that the forward scattering of a solution of dilute non-interacting polymer molecules consisting of p monomer units depends linearly on the number of monomer units p in the polymer. Even though the scattering of a single polymer molecule depends quadratically on on the number of monomer units. The reason is simply that the larger the degree of polymerization the lower the number density of molecules in the solution as we assume a constant concentration, i.e. $c \propto pn$ and therefore $\frac{d\sigma}{d\Omega}(Q{=}0) \propto p^2 n$.

8.3. Moments of scattering curves and size distribution

The relevance of moments both for scattering curves as well as size distributions has been discussed in several publications [**17, 90, 18, 102, 65, 37**].

Moments $\langle x^m \rangle$ of any order m of a function $f(x)$ are defined by integrating $f(x)$ with a suitable power of x over its domain $[a, b]$

$$\langle x^m \rangle = \int_a^b f(x) x^m dx \tag{8.22}$$

The different moments of the scattering curve together with the forward scattering $I(0)$ and the Porod constant can be used to calculate easily several structural parameters

of the scatterers.

$$\tilde{Q}_{\text{inv}} = \int_0^\infty Q^2 I(Q) \mathrm{d}Q \text{ (scattering invariant)} \tag{8.23a}$$

$$\frac{S}{V} = \frac{\pi}{\tilde{Q}_{\text{inv}}} \lim_{Q\to\infty} \left\{ Q^4 I(Q) \right\} \text{ (specific surface)} \tag{8.23b}$$

$$\langle R_G \rangle^2 = 3 \left(- \lim_{Q\to 0} \left\{ \frac{\mathrm{d}[\ln I(Q)]}{\mathrm{d}(Q^2)} \right\} \right) \text{ (squared Guinier radius)} \tag{8.23c}$$

$$l_i = \langle d \rangle = \frac{4}{\pi} \frac{\int_0^\infty Q^2 I(Q) \mathrm{d}Q}{\lim_{Q\to\infty} \left\{ Q^4 I(Q) \right\}} \text{ (average intersection length)} \tag{8.23d}$$

$$l_c = \langle l \rangle = \frac{\pi}{\tilde{Q}_{\text{inv}}} \int_0^\infty Q I(Q) \mathrm{d}Q \text{ (correlation length)} \tag{8.23e}$$

$$A_c = \langle A \rangle = \frac{2\pi}{\tilde{Q}_{\text{inv}}} \int_0^\infty I(Q) \mathrm{d}Q \text{ (correlation surface)} \tag{8.23f}$$

$$V_P = \langle V \rangle = \frac{2\pi^2}{\tilde{Q}_{\text{inv}}} I(0) \text{ (correlation volume, Porod volume)} \tag{8.23g}$$

These structural parameters are calculated by `SASfit` via the menu `[Calc|integral parameters...]`.

On the other side the structural parameters from above can depend on specific moments of the size distribution in the case the scattering objects are spheres. The m-th moment $\langle x^m \rangle$ of a size distribution $n(R)$ is given by

$$\langle R^m \rangle = \frac{\int_0^\infty n(R) R^m dR}{\int_0^\infty n(R) dR} \tag{8.24}$$

From these moments the following integral structural parameters in case of polydisperse spheres can be calculated and are listed together with a hypothetical radius of monodisperse spheres having the same structural parameter.

intersection length l_i:
$l_i = \dfrac{\langle R^3 \rangle}{\langle R^2 \rangle}$ and $R_{l_i} = \dfrac{3}{4} l_i$
correlation length l_c:
$l_c = \dfrac{\langle R^4 \rangle}{\langle R^3 \rangle}$ and $R_{l_c} = \dfrac{2}{3} l_c$

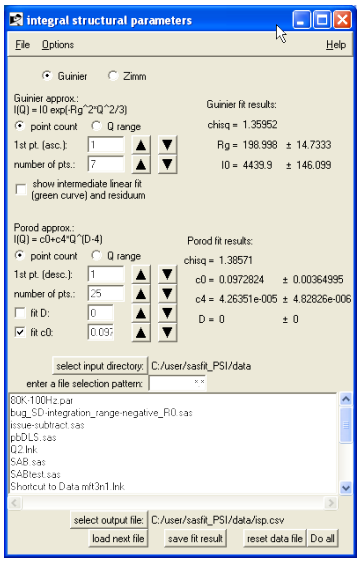

(a) GUI for defining fit ranges for Porod and Guinier approximations

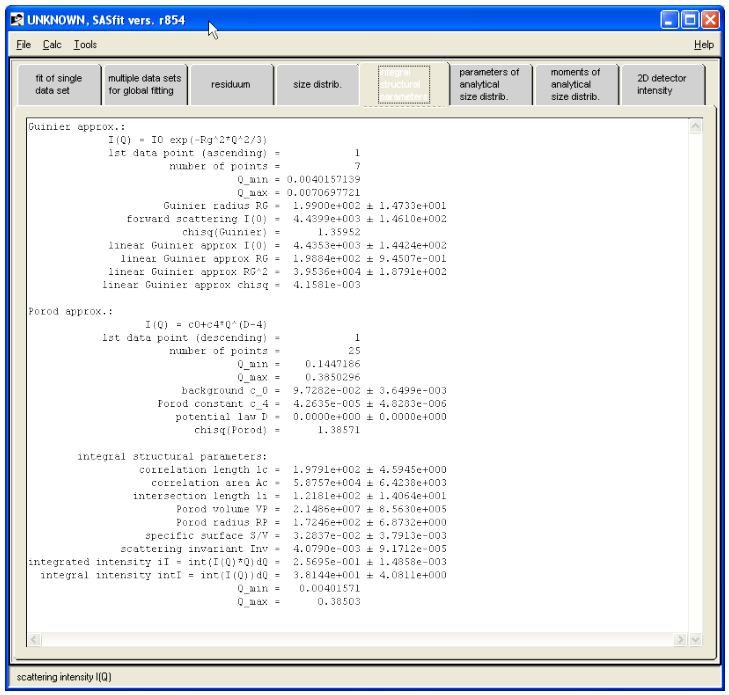

(b) Tabbed menu displaying the integral structural parameters calculated via the different moments of the scattering curve the Porod and Guinier extrapolations to $Q \to 0$ and $Q \to \infty$.

FIGURE 8.1. Menu and tabbed window for integral structural parameters. `SASfit` also supports analysis of series of data, whereby the structural parameters are stored in CSV format readable by many software packages in a separate file for further analysis.

Guinier radius R_G:

$$R_G = \sqrt{\frac{\langle R^8\rangle}{\langle R^6\rangle}} \text{ and } R_{R_G} = \sqrt{\frac{5}{3}}R_G$$

correlation cross section A_c:

$$A_c = \frac{4\pi}{5}\frac{\langle R^5\rangle}{\langle R^3\rangle} \text{ and } R_{A_c} = \sqrt{\frac{5}{4\pi}A_c}$$

Porod Radius R_{V_P}:

$$V_P = \frac{4\pi}{3}\frac{\langle R^6\rangle}{\langle R^3\rangle} \text{ and } R_{V_P} = \sqrt[3]{\frac{3}{4\pi}V_P}$$

Fig. 8.2 shows the `SASfit` menue displaying these values for each scattering contribution having a size distribution and also for the sum of all scattering contributions. Next to the integral structural parameters also the different moments of the size distribution up the the 8^{th} moment are supplied.

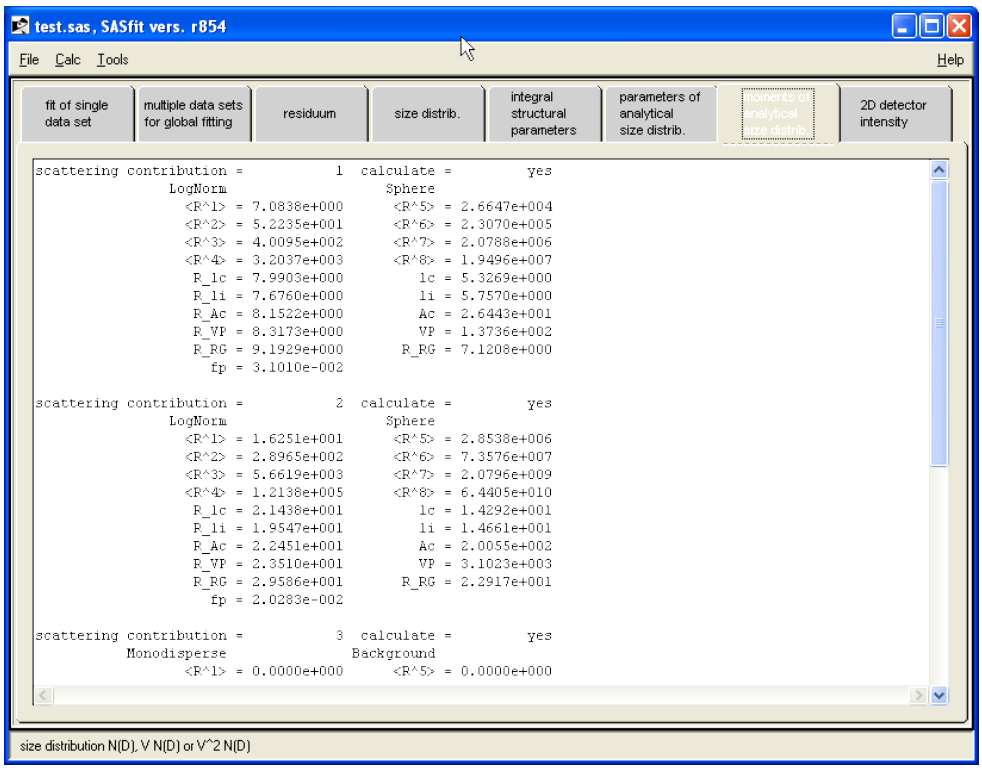

FIGURE 8.2. Menu displaying the different moments of a size distribution. At the moment these values are only calculated for single data sets but not yet for multiple data sets

8.4. Volume fractions

Having measured SAS-data versus $[Q] = nm^{-1}$ in absolute scale (1/cm) and knowing the scattering contrast also in absolute scale ($1/\text{cm}^2$) one can get the number density of particles. However, in general the volume fraction is known by other means but not the number density. The volume fraction can be calculated from the size distribution for some simple geometric shapes of the particles.

Let us first consider the case of simple spheres (`Sphere`) with a size distribution over there radii. The size distribution can be interpreted as a number density distribution function. The volume fraction f_p of the spheres can be easily calculated by

$$f_p = \int_0^\infty n(R)\frac{4}{3}\pi R^3\, dR = \int_0^\infty Np(R)\frac{4}{3}\pi R^3\, dR = N\frac{4}{3}\pi\langle R^3\rangle \tag{8.25}$$

where $\langle R^3\rangle$ is the third moment of the size distribution. The different moments of a size distribution can be calculated analytically for some special cases like the lognormal distribution. However, `SASfit` calculates the moments and displays them on the menu `[calc|single data single]`. Up to the 8^{th}-moment of a distribution function is displayed in the menu tab `moments of analytical size distrib.` like in Fig. 8.2 together with some other parameters defined in section 8.3. To compute the volume fraction f_p, which is a dimensionless parameter, one has to use the proper units for

N and $\langle R^3\rangle$. $\langle R^3\rangle$ has here units of $[\langle R^3\rangle] = \mathrm{nm}^3 = 10^{-21}\mathrm{cm}^3$ and N is in units of $[N] = 10^{42}\mathrm{cm}^{-3}$. The volume fraction f_p can as an example be computed for $N = 8.55241 \times 10^{-28}$ and $\langle R^3\rangle = 5.6619 \times 10^3$ as

$$f_p = 10^{42} \times 8.55241 \times 10^{-28} \frac{4}{3}\pi\, 5.6619 \times 10^3\, 10^{-21} = 0.020283. \tag{8.26}$$

The numbers for N and $\langle R^3\rangle$ can be directly taken from the `SASfit` gui.

Let us now consider the case of cylinders with a circular cross-section with radius R and length L. We will have a look on the two cases of having either a distribution in the radius R or a distribution in the length L. The volume of a cylinder V_{cyl} is given by

$$V_{\mathrm{cyl}}(R, L) = \pi R^2 L \tag{8.27}$$

To calculate the volume fraction from the size distribution we need to integrate over the particle volume. The integration is done either over the radius dR

$$f_p = \int_0^\infty n(R) V_{\mathrm{cyl}}(R, L)\, dR = \int_0^\infty N p(R) \pi R^2 L\, dR = NL\pi\langle R^2\rangle \tag{8.28}$$

or over the cylinder length dL

$$f_p = \int_0^\infty n(L) V_{\mathrm{cyl}}(R, L)\, dL = \int_0^\infty N p(R) \pi R^2 L\, dL = NR^2\pi\langle L\rangle \tag{8.29}$$

depending if we have a distribution over the radius R or the length L. In both cases the volume fraction can be expressed in terms of moments of the size distribution supplied by `SASfit`. In the first case it can be expresses by the second moment $\langle R^2\rangle$ of the cylinder radius and in the second case by the first moment $\langle L\rangle$ of the cylinder length, i.e. the mean cylinder length. The required moments are displayed in `SASfit` in the menu shown in Fig. 8.2. Also here one has to take care using proper units, but this is done equivalently to the first example of a sphere in eq. 8.26.

The three examples above show that the volume fraction f_p of scatterers can be calculated in many cases via the moments of the size distribution and for simple cases all necessary parameters are supplied in the `SASfit` menu interface. The volume fraction `fp` in Fig. 8.2 is numerically calculated from the size distribution. For some specific other form factor and the special case of a `LogNorm` distribution a plugin size distribution named `LogNorm_fp` described in section 7.5 has been implemented. Calculating volume fractions for any size distribution and for any form factor is not easy to implement. It would require quite some knowledge about the form factor and how exactly the volume fraction is defined. The plugin `LogNorm_fp` distinguish between volume fraction of a core only, a volume fraction of a core together with a shell and a volume fraction of a shell only. For the general case one also needs to know which size parameter of the form factor has a distribution. This already shows that the user has to supply additional information. For the calculation a volume function has to be associated to each form factor. If this is not the case the `SASfit` routine returns 0. For those function a volume function is associated to the form factor `SASfit` calculates numerically the volume fraction for any size distribution by integration. The plugin function `LogNorm_fp` on the other side has a lognormal distribution implemented and the information about the form factor and the

size parameter of the form factor having a distribution has to be given by the user via an input value called `shape`. Only a very limited number of form factor can be selected by this parameter. For other form factors the plugin needs to be extended or an routine calculating the volume for the specific form factor needs to be implemented.

CHAPTER 9

Basic Analysis of Dynamic Light Scattering Data

In a typical dynamic light scattering (DLS) or photo correlation scattering (PCS) experiment, the autocorrelation function $G^{(2)}(\tau)$ of the intensity scattered by dispersed particles is determined as a function of the delay τ. $G^{(2)}(\tau)$ is related to the modulus of the normalized field autocorrelation function $g_1(\tau)$ by a Siegert relationship

$$G^{(2)}(\tau) = Ag_1^2(\tau) + B. \tag{9.1}$$

Here B is a background term often designated as the baseline and A can be considered as another instrumental factor. The time dependence of $g_1(\tau)$ is related to the dynamics of the dispersed particles. For particles in Brownian motion, the time decay of $g_1(\tau)$ is determined by the diffusion coefficient of the dispersed particles. In particular, for monodisperse samples $g_1(\tau)$ is an exponentially decaying function:

$$g_1(\tau) = \exp(-\Gamma\tau) \tag{9.2}$$

or

$$G^{(2)}(\tau) = A\exp(-2\Gamma\tau) + B \tag{9.3}$$

where the decay rate Γ is linked to the particles' diffusion coefficient D by $\Gamma = DQ^2$, where Q is the modulus of the scattering vector

$$Q = \frac{4\pi m_1}{\lambda_0}\sin(\theta/2) \tag{9.4}$$

m_1 is the refraction index of the solution, λ_0 the wavelength in vacuo of the incident light and θ the scattering angle. At the end the Stokes-Einstein expression for the diffusion coefficient is used to get an average particle radius R_{DLS}

$$D = \frac{kT}{6\pi\eta R_{\mathrm{DLS}}} \tag{9.5}$$

where k is Boltzmann's constant, T the absolute temperature, η the viscosity of the dispersion medium and R_{DLS} the particle radius (only valid for noninteracting particles).

9.1. Cumulant Analysis

The formulas in eq. 9.2 to 9.5 are valid for monodisperse dispersions only. For polydisperse dispersions the cumulants method of Koppel (1972) is widely used, which assumes a multi-exponential behaviour so that $g_1(\tau)$ and $G^{(2)}(\tau)$ can be written in a series expansion as:

$$g_1(\tau) = \exp\left(-\Gamma_1\tau + \frac{\Gamma_2\tau^2}{2} - \frac{\Gamma_3\tau^3}{6} + \cdots\right) \tag{9.6}$$

$$G^{(2)}(\tau) = A\exp\left(-2\Gamma_1\tau + \Gamma_2\tau^2 - \frac{\Gamma_3\tau^3}{3} + \cdots\right) + B \tag{9.7}$$

`SASfit` assumes for the cumulant fit-routine that the function $G^{(2)}(\tau)$ is supplied. As normally no error bar is available from the correlator a robust least square procedure is implemented.

REFERENCE:

Dennis E. Koppel, Analysis of Macromolecular Polydispersity in Intensity Correlation Spectroscopy: The Method of Cumulants, The Journal of Chemical Physics, Vol.1, No. 11 (1972), 4815- 4820

9.2. Double Decay Cumulant Analysis

$$G^{(2)}(\tau) = A\left[p\, e^{-2\Gamma_{a,1}\,\tau+\Gamma_{a,2}\,\tau^2} + (1-p)\, e^{-2\Gamma_{b,1}\,\tau+\Gamma_{b,2}\,\tau^2}\right] + B \tag{9.8}$$

9.3. Fit of Double Stretched Exponentials

$$G^{(2)}(t) = A\left\{p\,\exp\left(\left[\frac{t}{\tau_1}\right]^{\gamma_1}\right) + (1-p)\,\exp\left(\left[\frac{t}{\tau_2}\right]^{\gamma_2}\right)\right\} + B \tag{9.9}$$

9.3.1. The least squares minimiser and the robust least squares procedure. The function to be minimised is

$$\chi^2 = \sum_i \left(\frac{r_i}{\Delta I_i} \right)^2$$

where the residual is defined as

$$r_i = I_i - I_{i,th}.$$

Here I_i is the intensity correlation function $G^{(2)}(t_i)$ at time t_i with already subtracted baseline as received from a correlator, $I_{i,th}$ is the value of the cumulant fit according to eq. 9.7 or a double exponential decay according to eq. 9.9. Normally no error values ΔI_i are supplied from the correlator so that all data points are weighted the same. A robust fitting with bisquare weights is implemented which uses an iteratively reweighted least squares algorithm, and follows the procedure:

(1) Fit the model by an unweighted least squares (that is, χ).
(2) Standardize the residuals via $u_i = r_i/(Ks)$. Here K is a tuning constant equal to 4.685, and s is the robust variance given by $MAD/0.6745$, where MAD is the median absolute deviation of the residuals

$$MAD = \sum_{i=1}^{N} \frac{1}{N} |I_{i,th} - I_i|$$

(3) Compute the robust weights w_i as a function of the standardized residuals u_i. The bisquare weights are given by

$$w_i = \begin{cases} (1 - u_i^2)^2 & |u_i| < 1 \\ 0 & |u_i| \geq 1 \end{cases}$$

(4) Re-do the fit using the weighted minimiser:

$$\chi^2 = \sum_i w_i \left(\frac{r_i}{\Delta I_i} \right)^2$$

(5) The fit converges when the MAD changes by no more than the fraction set by `residual_tolerance` (which has been chosen to be 10^{-8}). Otherwise, perform the next iteration of the fitting procedure by returning to the first step.

CHAPTER 10

Scattering Theory

10.1. Scattering Cross-Section

In a scattering experiment one is interested in a detailed analysis of the scattering pattern as a function of the characteristics of the incident beam. Monochromator and collimator specify direction and energy of the incident radiation. The radiation interacts with the sample and receives thereby a momentum transfer $\hbar\bar{\mathrm{Q}}$. By this process the radiation receives beside a direction change also an energy change. The result is described with the help of a cross-section.

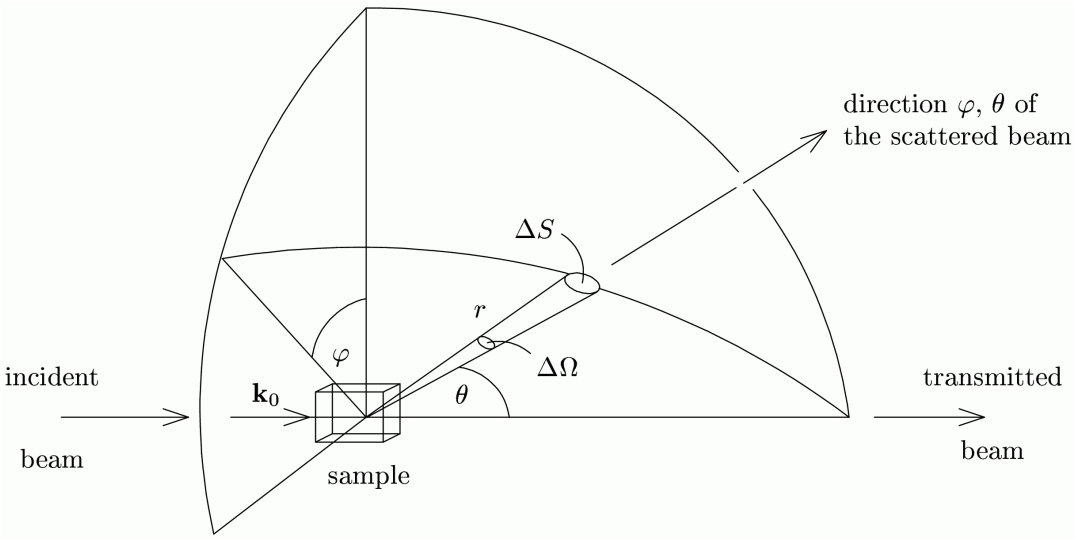

FIGURE 10.1. Schematic representation of a scattering process

A detector with an efficiency ϵ measures for this the number of the scattered neutrons or photons in a given direction $\mathbf{k}_0+\mathbf{Q}$. The distance between detector and sample should be large in comparison to the linear dimension of the detector, so that the solid angle included by the detector element $\Delta\Omega$ is small.

If the incident beam has a homogeneous, continuous flow density Φ_0 ($[\Phi_0]$ = neutron (photons -) per cm^2 and second) and if the beam contain N identical particles, then the counting rate C of the detector is proportional to all these quantities. The proportionality constant is called differential scattering cross-section $\frac{d\sigma}{d\Omega} = \frac{C}{\Phi_0\,\epsilon\,N\,\Delta\Omega}$. In the case of inelastic scattering the counting rate is in a certain interval δE of transferred energy in addition proportionally to δE. The appropriate proportionality constant is the partial

(or double) differential scattering cross-section

$$\frac{d^2\sigma}{d\Omega\, dE} = \frac{C}{\Phi_0\, \epsilon\, N\, \Delta\Omega\, \Delta E} = \frac{\text{Number of neutrons (photons), which are scattered per second into the solid angle } d\Omega \text{ toward } \phi, \theta \text{ with an energy between } E \text{ and } E + dE}{\mathrm{N}\Phi_0\, \mathrm{d}\Omega\, \mathrm{dE}}$$

The total differential cross-section is defined as

$$\sigma_t = (\text{total number of scattered neutrons (photons) per sec})/\Phi_0. \tag{10.1}$$

The three different cross-section are related to each other by

$$\sigma_t = \int d\Omega\, \frac{d\sigma}{d\Omega} \qquad \text{and} \qquad \frac{d\sigma}{d\Omega} = \int_0^\infty dE\, \frac{d^2\sigma}{d\Omega\, dE}. \tag{10.2}$$

10.1.1. Scattering of neutrons on atoms. The scattering of neutrons can be explained by two types of interactions between neutrons and matter; once the strong spin dependent nuclear forces between nuclei and neutron (interaction range $\sim 10^{-15}$m) and secondly the dipole-dipole interaction between the magnetic moment of the neutron and that of an unpaired electron, or nuclei accordingly. Both interactions have in common that their interaction potential $V(\underline{\mathrm{r}})$ for $r \to \infty$ decays faster than $1/r$. For this kind of interaction potential the quantum mechanical scattering theory [**44**] yields as an asymptotic approximation for the Schrödinger equation of the wave function

$$\psi_{\underline{\mathrm{k}}_0}(\underline{\mathrm{r}}) \xrightarrow[r\to\infty]{} \frac{1}{(2\pi)^{3/2}} \left[e^{\imath \underline{\mathrm{k}}_0 \underline{\mathrm{r}}} + f(\theta,\phi) \frac{e^{\imath k_0 r}}{r} \right] \quad . \tag{10.3}$$

For low energy particles and short range potential the partial waves methods yields for the scattering amplitude $f(\theta, \phi) = -b$, whereby the so called scattering length b can be determined experimentally. Via another Ansatz, the Born approximation, one gets a series expansion for $f(\theta, \phi)$. The first term of this series expansion is give by

$$f^{(0)}(\theta,\phi) = -\frac{m_N}{2\pi\hbar^2} \int d\underline{\mathrm{r}}\, e^{\imath \underline{\mathrm{Q}} r} V(\underline{\mathrm{r}}) \quad , \tag{10.4}$$

with $\underline{\mathrm{Q}} = \underline{\mathrm{k}} - k_0$. A comparison of this result with the partial wave method ($f(\theta, \phi) = -b$), shows that the pseudo potential $V(\underline{\mathrm{r}}) = \frac{2\pi\hbar^2}{m_N}\, b\, \delta(\underline{\mathrm{r}})$ (Fermi's pseudo potential) has an equivalent solution. For an ensemble of N atoms, e.g. a crystal, the total potential is in kinematic approximation the sum of the individual potentials

$$V(\underline{\mathrm{r}}) = \frac{2\pi\hbar^2}{m_N} \sum_{j=1}^{N} b_j \delta(\underline{\mathrm{r}} - r_j) \quad , \tag{10.5}$$

whereby $\underline{\mathrm{r}}_j$ describes the position of nuclei j with scattering the length b_j and N the number of scattering atoms. The scattering length b_j depends on the element or isotope which is the scattering center. Furthermore it can depend on the spin state of the neutron and the nuclei and on unpaired electrons in non fully occupied atomic electron shells. In the kinematic approximation it is assumed that the intensity of the incoming beam is identical at each scattering center, i.e. that the scattered intensity does not attenuate the incoming beam. Furthermore it is assumed that the incoming beam is only scattered once and multiple scattered can be neglected.

In the static approximation, i.e. for a scattering process which does not change the state of the scattering center and therefore is an elastic scattering process, the differential scattering cross-section can be described in terms of a scattering amplitude $f^{(0)}(\theta, \phi)$ by

$$\frac{d\sigma}{d\Omega}(\underline{\mathrm{Q}}) = \frac{1}{N} \left| f^{(0)}(\theta, \phi) \right|^2 = \frac{1}{N} \left(\frac{m_N}{2\pi\hbar^2} \right)^2 \left| \int d\underline{\mathrm{r}}\, e^{\imath \underline{\mathrm{Q}} r}\, V(\underline{\mathrm{r}}) \right|^2 \quad . \tag{10.6}$$

Using Fermi's pseudo potentials (eq. 10.5) leads to the expression

$$\frac{d\sigma}{d\Omega}(\underline{\mathrm{Q}}) = \frac{1}{N} \left| \sum_{j=1}^{N} b_j\, e^{\imath \underline{\mathrm{Q}} r_j} \right|^2 = \frac{1}{N} \sum_{i,j} b_i\, b_j\, e^{\imath \underline{\mathrm{Q}} r_i}\, e^{-\imath \underline{\mathrm{Q}} r_j} \tag{10.7}$$

Let us now consider a new system of scatterers, which are only different to those from eq. 10.7 that the scattering length of the nuclei are exchanged. Hereby both the position and fraction of the scattering length b_i are kept the same. For a large number of scattering centers the average over the cross-sections of all possible systems of scatterers which are identical to the one in 10.7 can be described by

$$\frac{d\sigma}{d\Omega}(\underline{\mathrm{Q}}) = \frac{1}{N} \sum_{i,j} \overline{b_i\, b_j}\, e^{\imath \underline{\mathrm{Q}} r_i}\, e^{-\imath \underline{\mathrm{Q}} r_j} \quad . \tag{10.8}$$

If the scattering length b_i occur in the same fraction x_i, whereby $\sum_i x_i = 1$, so that the averages $\overline{b}$ and $\overline{b^2}$ can be written as

$$\overline{b} = \sum_i x_i\, b_i \text{ and } \overline{b^2} = \sum_i x_i b_i^2 \quad . \tag{10.9}$$

Under the condition that there are no correlations between the scattering lengths of the individual nuclei one can write

$$\overline{b_i\, b_j} = \overline{b}^2 \text{ for } i \neq j \qquad \text{and} \qquad \overline{b_i\, b_j} = \overline{b^2} \text{ for } i = j \tag{10.10}$$

From this it follows for the differential cross-section

$$\frac{d\sigma}{d\Omega}(\underline{\mathrm{Q}}) = \frac{1}{N} \left(\overline{b^2} + \overline{b}^2 \sum_{\substack{i,j \\ i \neq j}} e^{\imath \underline{\mathrm{Q}} r_i}\, e^{-\imath \underline{\mathrm{Q}} r_j} \right) = \underbrace{\frac{1}{N} \left(\overline{b^2} - \overline{b}^2 \right)}_{\frac{d\sigma_{\mathrm{inc}}}{d\Omega}} + \underbrace{\frac{1}{N}\, \overline{b}^2 \left| \sum_i e^{\imath \underline{\mathrm{Q}} r_i} \right|^2}_{\frac{d\sigma_{\mathrm{coh}}}{d\Omega}} \tag{10.11}$$

10.1.1.1. *Nuclear scattering.* The simplest system of scatterers consist of only one isotope with nuclear spin I. As the spin of the neutron is $s = \pm 1/2$ only two orientations are possible: parallel spins of neutron and nuclei, i.e. a total spin of $J_{(+)} = I + 1/2$ or antiparallel spins, i.e $J_{(-)} = I - 1/2$. The corresponding scattering length are named $b_{(+)}$ and $b_{(-)}$.[1]

The number of possible states for the total spin $J_{(\pm)}$ are $2J_{(+)} + 1 = 2I + 2$ and $2J_{(-)} + 1 = 2I$. In case of unpolarized neutrons and/or random oriented nuclear spins

[1] For coherent scattering the spin of the neutrons keep constant in contrast to incoherent scattering where a part come along with a spin-flip. This can e.g. be used to change the ration between coherent and incoherent scattering.

parallel and antiparallel spin states have the same probability. The fraction $x_{(\pm)}$ of the scattering lengths $b_{(\pm)}$ is therefore proportional to the corresponding number of states

$$x_{(+)} = \frac{2J_{(+)}+1}{\left(2J_{(+)}+1\right)+\left(2J_{(-)}+1\right)} = \frac{I+1}{2I+1} \text{ and } x_{(-)} = \frac{I}{2I+1} \quad . \tag{10.12}$$

For the average scattering length $\overline{b}$ we therefore get

$$\overline{b} = \sum_{i=(+),(-)} x_i\, b_i = \frac{1}{2I+1}\left[(I+1)\, b_{(+)} + I\, b_{(-)}\right] \quad . \tag{10.13}$$

For a mixture of different elements and isotopes of type l with nuclear spin I_l and the fraction x_l (with $\sum_l x_l = 1$) the averages can be written as

$$\overline{b} = \sum_l \frac{x_l}{2I_l+1}\left[(I_l+1)\, b_{l(+)} + I_l\, b_{l(-)}\right] \tag{10.14}$$

$$\overline{b^2} = \sum_l \frac{x_l}{2I_l+1}\left[(I_l+1)\, \left(b_{l(+)}\right)^2 + I_l\, \left(b_{l(-)}\right)^2\right] \quad . \tag{10.15}$$

10.1.1.2. *Magnetic Scattering.* In magnetic materials the contribution of the interaction between neutrons and atomic magnetic dipole moments to the scattering length has the same order of magnitude than the nuclear scattering length. The magnetic scattering is based on the interaction of the magnetic moment of the neutron $\boldsymbol{\mu}_n$ with the magnetic moment of the scattering atom $\boldsymbol{\mu}_A$. The magnetic interaction potential $V(\underline{\mathrm{r}})$ is described by

$$V(\underline{\mathrm{r}}) = -\boldsymbol{\mu}_n \cdot \underline{\mathrm{B}}(\underline{\mathrm{r}}), \tag{10.16}$$

whereby $\boldsymbol{\mu}_n = \gamma \frac{e\hbar}{2m_p}\boldsymbol{\sigma} = \gamma \boldsymbol{\mu}_N$ is the magnetic dipole moment[2] of the neutron, $\boldsymbol{\sigma}$ Pauli's spin operator, γ the neutron magnetic moment to nuclear magneton ratio[3] and $\underline{\mathrm{B}}(\underline{\mathrm{r}})$ the magnetic field of an atom at the position of the neutron. An atom generates a magnetic field due to the magnetic dipole moment $\boldsymbol{\mu}_S$ of its electrons $\underline{\mathrm{B}}_S(\underline{\mathrm{r}})$

$$\underline{\mathrm{B}}_S(\underline{\mathrm{r}}) = \boldsymbol{\nabla} \times \underline{\mathrm{A}} \text{ with } \underline{\mathrm{A}} = \frac{\mu_0}{4\pi}\frac{\boldsymbol{\mu}_S \times \underline{\mathrm{r}}}{r^3} \tag{10.17}$$

and due to the orbital angular momentum of the electrons $\underline{\mathrm{l}} = -\underline{\mathrm{p}} \times \underline{\mathrm{r}}$ which generates a field of $\underline{\mathrm{B}}_L(\underline{\mathrm{r}})$

$$\underline{\mathrm{B}}_L(\underline{\mathrm{r}}) = -\frac{\mu_0}{4\pi}\frac{2\mu_B}{\hbar}\frac{\underline{\mathrm{p}} \times \underline{\mathrm{r}}}{r^3}. \tag{10.18}$$

The magnetic interaction potential $V(\underline{\mathrm{r}}) = -\boldsymbol{\mu}_n \cdot (\underline{\mathrm{B}}_S(\underline{\mathrm{r}}) + \underline{\mathrm{B}}_L(\underline{\mathrm{r}}))$ is a weak long range potential which also can be treated with Born's approximation. Compared to the nuclear

[2]neutron magnetic moment: $\mu_n = -0.96623645 \times 10^{-26}$ JT^{-1}, neutron magnetic moment to Bohr magneton ratio:$\mu_\mathrm{n}/\mu_\mathrm{B} = -1.04187563 \times 10^{-3}$, nuclear magneton: $\mu_\mathrm{n} = 5.05078343 \times 10^{-27}$ JT^{-1}, Bohr magneton: $\mu_\mathrm{B} = \frac{e\hbar}{2m_e} = 927.400949 \times 10^{-26}$ JT^{-1}, proton mass: $m_p = 1.67262171 \times 10^{-27}$ kg, neutron mass: m_n: $1.67492728 \times 10^{-27}$ kg, electron mass: $m_\mathrm{e}9.1093826 \times 10^{-31}$kg, elementary charge: $e = 1.60217653 \times 10^{-19}$ C, Planck constant over 2π: $\hbar = h/2\pi = 1.05457168 \times 10^{-34}$ J s

[3]neutron magnetic moment to nuclear magneton ratio $\gamma = \mu_\mathrm{n}/\mu_\mathrm{N} - 1.91304273$

scattering amplitude the corresponding magnetic scattering amplitude b_M is given by the Fourier transformation of the magnetic interaction potential $\mathcal{F}[V(\underline{\mathrm{r}})]$

$$b_M = -\frac{m_n}{2\pi\hbar^2}\,\boldsymbol{\mu}_n \cdot \int d^3r\, e^{\imath \underline{\mathrm{Q}} r}\,(\underline{\mathrm{B}}_S(\underline{\mathrm{r}}) + \underline{\mathrm{B}}_L(\underline{\mathrm{r}})). \tag{10.19}$$

The Fourier transformation of the magnetic field is related in case of a static magnetic field to the Fourier transformation of the local magnetization $\underline{\mathrm{M}}(\underline{\mathrm{Q}}) = \mathcal{F}[\underline{\mathrm{M}}(\underline{\mathrm{r}})]$ [**93**] by

$$\underline{\mathrm{B}}(\underline{\mathrm{Q}}) = \mu_0\,\frac{\underline{\mathrm{Q}} \times [\underline{\mathrm{M}}(\underline{\mathrm{Q}}) \times \underline{\mathrm{Q}}]}{Q^2} = \mu_0\,\underline{\mathrm{M}}_\perp(\underline{\mathrm{Q}}), \tag{10.20}$$

whereby $\underline{\mathrm{M}}_\perp(\underline{\mathrm{Q}})$ is the component of $\underline{\mathrm{M}}(\underline{\mathrm{Q}})$ perpendicular to $\underline{\mathrm{Q}}$ and $\mu_0 = 4\pi\,10^{-7}$ Vs/Am the magnetic constant. For the magnetic scattering amplitude[4] b_M we find than

$$b_M = D_M\,\mu_0\,\boldsymbol{\sigma} \cdot \underline{\mathrm{M}}_\perp(\underline{\mathrm{Q}}) \text{ with } D_M = -\gamma\,\frac{m_n}{2\pi\hbar^2}\,\mu_N = 2.31605 \times 10^{14}\,\frac{1}{\mathrm{m}^2\ \mathrm{Tesla}}. \tag{10.21}$$

For scattering on magnetic structures always two interactions have to be considered, nuclear scattering which is caused by fluctuations in the number density and composition and magnetic scattering caused by fluctuations in amplitude and/or orientation of the local magnetization. In case of a preferred orientation, e.g. the direction of an external applied magnetic field $\underline{\mathrm{H}}$, the magnetic scattering depends on the spin state $\boldsymbol{\sigma}$ of the neutron. If $\underline{\mathrm{e}}_x$ describes the direction of the preferred axis and $(+)$ and $(-)$ the neutron spin polarisation antiparallel and parallel to $\underline{\mathrm{e}}_x$ than the scattering can be described by four scattering processes; these are two spin non-flip $(++,--)$ and two spin flip $(+-,-+)$ processes. Moon, Riste und Koehler [**66**] have shown that for coherent scattering the four scattering length are given by

$$b_{\pm\pm} = b_N \mp D_M\,\mu_0\,M_{\perp x} \tag{10.22}$$

$$b_{\pm\mp} = -D_M\,\mu_0\,(M_{\perp z} \pm \imath\,M_{\perp y}). \tag{10.23}$$

whereby b_N is the nuclear scattering length. In case of unpolarized neutrons the differential scattering cross-section can be written as

$$\frac{d\sigma_{\mathrm{unp}}}{d\Omega}(\underline{\mathrm{Q}}) = \frac{d\sigma_{\mathrm{nuc}}}{d\Omega}(\underline{\mathrm{Q}}) + \frac{d\sigma_{\mathrm{mag}}}{d\Omega}(\underline{\mathrm{Q}}), \tag{10.24}$$

because $(b_{++}^2 + b_{--}^2 + b_{+-}^2 + b_{-+}^2)/2 = b_N^2 + D_M^2\mu_0^2 M_\perp^2$. For unpolarized neutrons the interference contribution only has an influence on the degree of polarization of the scattered neutrons but not on the scattering intensity.

[4]Frequently the magnetization is given in units of Bohr magnetons ($\mu_B = \frac{e\hbar}{2m_e} = 927.400949 \times 10^{-26}$ J/T, 1[J/T]=1[Am^2]) per atomic volume Ω so that the magnetic scattering length density can be written as $b_M = D_\mu \sum_i c_i M_i/\Omega_i$ with $D_\mu = 2.69914 \times 10^{-15}\mathrm{m}^2$. The two constants are related via $D_\mu = D_M \mu_0 \mu_B$.

10.1.2. Scattering of x-ray at atoms. The scattering of x-rays on matter practically exclusively depends on the interaction of the incoming radiation with electrons. The contribution on the nuclei is negligible small because the mass of the nuclei is more than 10^3 times larger than the mass of an electron and the energy of the nuclear scattering more than 10^6 smaller than the energy of the scattering on electrons.

The frequency $\nu_0 = c/\lambda$ of the incoming x-ray beam is in general large against the resonance frequency of the electrons. In this case the electrons can be considered to be free and the special properties of the chemical binding are of no importance. These are the conditions for Thomson-scattering. J.J. Thomson developed a simple classical model for this type of scattering. Under the influence of an electric field of x-rays electrons start to oscillate. For an incoming plane and monochromatic wave with an electric field $\underline{\mathrm{E}} = \underline{\mathrm{E}}_0 e^{\imath(\underline{\mathrm{k}}_0\underline{\mathrm{r}}-\omega t)}$ the amplitude E_s of a wave scattered on a free electron is

$$E_s = -E_0 \frac{e^2}{m_e c^2} \frac{1}{r} \sin\psi. \tag{10.25}$$

Hereby e and m_e are the charge[5] and mass[6] of the electron, respectively. c is the speed of light[7], r the distance between sample and detector and ψ the angle between the direction of the accelerated electrons by the incoming wave and the direction of the scattered wave.

Analogously to the neutron scattering length for an electron the x-ray scattering length (far field of a Hertz dipole) is defined as

$$b_{\mathrm{x-ray}} = \frac{e^2}{m_e c^2} \sin\psi = r_0 \sin\psi \tag{10.26}$$

whereby $r_0 = e^2/(m_e c^2) = 2.82\times10^{-13}$ cm is the classical electron radius. For small angle scattering $\psi \simeq \pi/2$ whereby the angle dependent polarization factor is approximately 1.

For calculating the scattering amplitude of an atom with Z electrons one has to sum up the scattered waves from the different electrons with the correct phase. To do this an electron density distribution $\rho_e(\underline{\mathrm{r}})$ can be introduced which describes the time average probability distribution of the electron in the atom. The scattering amplitude of an atom is than

$$f_a(\underline{\mathrm{Q}}) = r_0 \underbrace{L(Q)}_{\substack{\text{polarization}\\ \text{factor}}\sim 1} \int d\underline{\mathrm{r}}\, \rho_e(\underline{\mathrm{r}})\, e^{\imath \underline{\mathrm{Q}} r} \overset{Q\to 0}{=} r_0\, Z. \tag{10.27}$$

The charge distribution in an atom can be described in good approximation by a radial symmetric function so that

$$f_a(Q) = r_0 \int_0^\infty \frac{\sin Qr}{Qr}\, \rho_e(r)\, 4\pi r^2\, dr \overset{Q\to 0}{=} r_0 \int_0^\infty \rho_e(r)\, 4\pi r^2\, dr = r_0 Z. \tag{10.28}$$

In small angle scattering the scattering length of an atom is therefore $f_a = r_0 Z$ or in units of "electon units [e.u.]" $f = f_a/r_0 = Z$.

---

[5] $e = 1.60217653 \times 10^{-19}$ C

[6] $m_e = 9.1093826 \times 10^{-31}$ kg

[7] $c = 299792458$ m s^{-1}

10.1.2.1. *Anomalous scattering of x-rays.* The relation $f = Z$ for atomic scattering length is only valid as long as the energy of the incoming radiation is much larger than the energy of the K-, L-, etc. shells. In case that the absorption edge of an atom is close to the energy of the incoming beam the scattering length has to be corrected by a dispersion term. In general the scattering length of an atom depends on the energy of the x-rays and is a complex number

$$f(E) = Z + f'(E) + \imath f''(E) \quad . \tag{10.29}$$

The correction terms f' and f'' change the scattering length f near a K_α absorption edge typically up to 30%. Figure 10.2 shows the energy dependency of the scattering length of iron f'_{Fe} und f''_{Fe}. The dispersion terms are related via the Karamer-Kronig relation

$$f'(E) = \frac{2}{\pi} \int_0^\infty dE' \, \frac{E' \, f''(E')}{E'^2 - E^2}. \tag{10.30}$$

In general the imaginary part f'' can be determined experimentally by the mass ab-

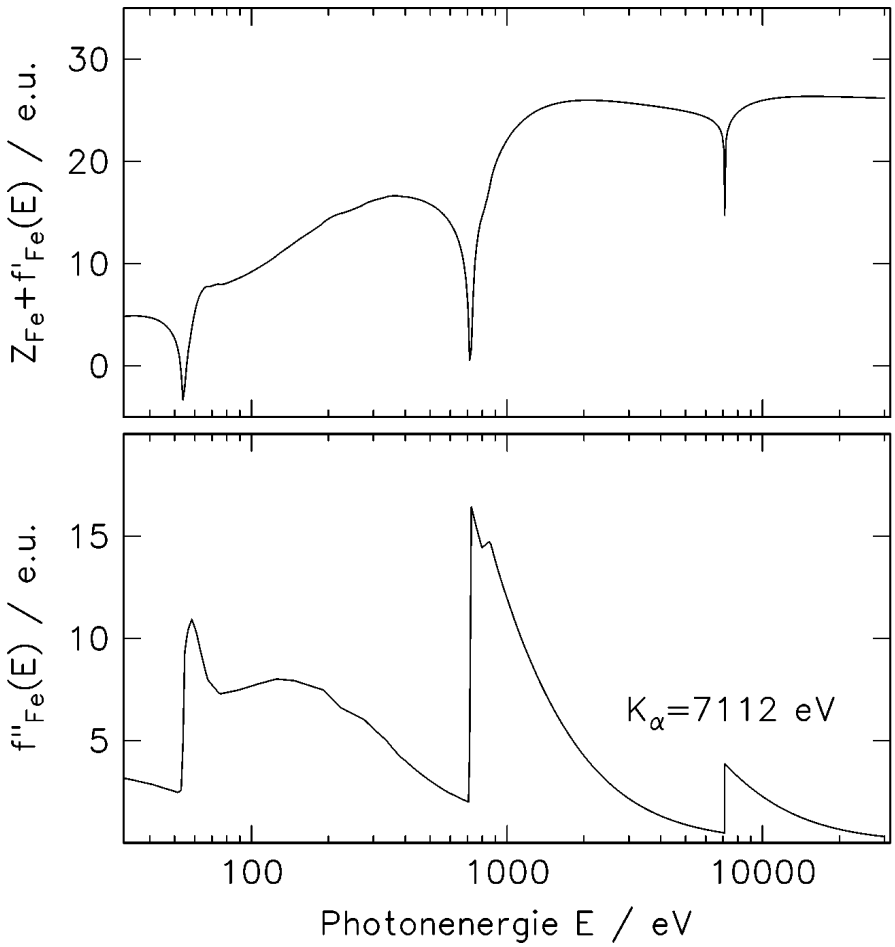

FIGURE 10.2. Energy dependence of the real and imaginary part of the scattering length of iron: $Z_{\mathrm{Fe}} + f'_{\mathrm{Fe}}(E)$ and $f''_{\mathrm{Fe}}(E)$ ($Z_{\mathrm{Fe}} = 26$)

sorption coefficient $\mu_m(E) = \frac{2N_A}{A}\,\lambda\, r_0\, f''(E)$ (N_a Avogadro number, A mass of atom in resonance) to calculate than with equation 10.30 the real part of the scattering length $f'(E)$.

10.2. Small angle scattering

In small angle scattering geometry the structural unit down to single atoms can not be resolved, only structures larger than several atomic layers can be seen by that method. Small angle scattering techniques measure the beam scattered close to forward direction whereby the beam divergence is in the order $\lambda/L \ll 1$. For a wavelength of $\lambda = 1$ nm and a characteristic dimension $L = V^{1/3}$ of the scatterer of about 10 nm the divergency of the beam is about $\lambda/L = 0.1$ rad $\simeq 6.3°$.

In principle with small angle scattering both information on size as well as shape of the scatterer and information on the relative arrangement of the scatterer can be obtained. In the following an overview of the theoretical basics to analyze small angle scattering data will be given.

In section 10.1 the scattering of an ensemble of atoms has been discussed. There interference terms between the waves scattered by the individual atoms were important for the differential scattering cross-section (eq. 10.7 ,10.28).

$$\frac{d\sigma}{d\Omega}(\underline{\mathrm{Q}}) = \frac{1}{N}\left|\sum_{j=1}^{N} b_j\, e^{\imath \underline{\mathrm{Q}} \underline{r}_j}\right|^2 \qquad \text{or} \qquad \frac{d\sigma}{d\Omega}(\underline{\mathrm{Q}}) = \frac{1}{N}\left|\sum_{j=1}^{N} f_{a,j}(\underline{\mathrm{Q}})\, e^{\imath \underline{\mathrm{Q}} \underline{r}}\right|^2 . \quad (10.31)$$

Small angle scattering normally does not resolve dimension down to atomic dimensions. Therefore the summation over the individual atoms can be replaced by an integration over the illuminated volume V:

$$\frac{d\sigma}{d\Omega}(\underline{\mathrm{Q}}) = \frac{1}{N}\left|\int_V d\underline{\mathrm{r}}\, \rho(\underline{\mathrm{r}})\, e^{\imath \underline{\mathrm{Q}} \underline{r}}\right|^2 = \frac{1}{N}\, I(\underline{\mathrm{Q}}) \quad , \quad (10.32)$$

whereby $\rho(\underline{\mathrm{r}})$ is the local scattering length density and $F(\underline{\mathrm{Q}})$ the scattering amplitude. The differential scattering cross-section is mathematically the square of the modulus of the Fourier transformation of the scattering length density. The scattering length density $\rho(\underline{\mathrm{r}})$ is proportional to the locally averaged scattering potential $\bar{V}(\underline{\mathrm{r}})$. Thats why equation 10.32 is except a constant identical to equation 10.6. The scattering intensity $I(\underline{\mathrm{Q}}) = |z|^2 = z\, z^*$ can therefore be written as

$$I(\underline{\mathrm{Q}}) = \iint d\underline{\mathrm{r}}_1\, d\underline{\mathrm{r}}_2\, \rho(\underline{\mathrm{r}}_1)\, \rho^*(\underline{\mathrm{r}}_2)\, e^{\imath \underline{\mathrm{Q}} (r_1 - r_2)} \quad . \quad (10.33)$$

By using the substitution $\underline{\mathrm{r}} = \underline{\mathrm{r}}_1 - \underline{\mathrm{r}}_2$ one get

$$I(\underline{\mathrm{Q}}) = \int d\underline{\mathrm{r}}\, e^{\imath \underline{\mathrm{Q}} \underline{r}} \underbrace{\int d\underline{\mathrm{r}}_1\, \rho(\underline{\mathrm{r}}_1)\, \rho^*(\underline{\mathrm{r}}_1 - \underline{\mathrm{r}})}_{\Gamma(\underline{\mathrm{r}}) = \rho(\underline{\mathrm{r}}) \circledast \rho(\underline{\mathrm{r}})} = \int d\underline{\mathrm{r}}\, \Gamma(\underline{\mathrm{r}})\, e^{\imath \underline{\mathrm{Q}} \underline{r}} \quad . \quad (10.34)$$

$\Gamma(\underline{r})$ is the autocorrelation function[8] In case of a real scattering length density eq. 10.34 is the convolution integral $\Gamma(\underline{r}) = \rho(\underline{r}) * \rho(\underline{r}) = \int d\underline{r}_1\, \rho(\underline{r}_1)\, \rho(\underline{r}_1 - \underline{r})$ of the scattering length density and is called Patterson function[9].

10.2.1. Autocorrelation function $\Gamma(\underline{r})$ and $\gamma(\underline{r})$. In the following we will make use of two simplifications. Firstly the scattering system is assumed to be isotropic. Hereby the isotropy can have its origin both in the shape of the scatterer or being a consequence of the temporal change of the particle orientation. The consequence is that $\Gamma(\underline{r})$ only depends on the modulus of r and $e^{\imath \underline{Q} r}$ can be averaged over all orientations of $\underline{r}$. (The second simplification will follow further below)

10.2.1.1. *Isotropic averages.* If α is assigned to the angle between $\underline{Q}$ and $\underline{r}$ and if all orientations α are equal probable than the probability $p_\alpha\, d\alpha$ that $\underline{Q}$ and $\underline{r}$ include the angle α is equal to $\frac{1}{2} \sin\alpha\, d\alpha$.

$$p_\alpha\, d\alpha = \frac{2\,\pi\, R\, \sin\alpha}{4\,\pi\, R^2}\, R\, d\alpha = \frac{\sin\alpha}{2}\, d\alpha \tag{10.35}$$

The average of $e^{\imath \underline{Q} r}$ over all orientations of $\underline{r}$ is

$$\begin{aligned}
\overline{e^{\imath \underline{Q} r}}^{\,\underline{r}} &= \int_0^\pi d\alpha\, \frac{\sin\alpha}{2}\, e^{\imath Q r \cos\alpha} = \frac{\sin Qr}{Qr} \qquad (10.36)\\
&= \underbrace{\int_0^\pi d\alpha\, \frac{\sin\alpha}{2}\, \cos(Q\, r\, \cos\alpha)}_{\text{symmetric to } \alpha=\pi/2} + \imath \underbrace{\int_0^\pi d\alpha\, \frac{\sin\alpha}{2}\, \sin(Q\, r\, \cos\alpha)}_{\text{antisymmetric to } \alpha=\pi/2 \Rightarrow =0}\\
&= 2\int_0^{\frac{\pi}{2}} d\alpha\, \frac{\sin\alpha}{2}\, \cos(Q\, r\, \cos\alpha) = \frac{1}{Qr}\int_0^{Qr} du\, \cos u = \frac{\sin Qr}{Qr}
\end{aligned}$$

and equation 10.34 is simplified to

$$I(Q) = \int dr\, 4\pi\, r^2\, \Gamma(r) \frac{\sin Qr}{Qr} \quad . \tag{10.37}$$

---

[8]Normally the autocorrelation function is defined as $\rho(\underline{r}) \circledast \rho(\underline{r}) = \int d\underline{r}_1\, \rho(\underline{r}_1)\, \rho^*(\underline{r}_1 + \underline{r})$, so that in fact $\Gamma(\underline{r})$ should be $\Gamma(\underline{r}) = \rho(-\underline{r}) \circledast \rho(-\underline{r})$.

[9]Here the Patterson function is defined as the autocorrelation of the scattering length density $\rho(\underline{r})$. Instead of defining the cross-section via a scattering length density as in 10.34 in neutron scattering the differential cross-section is often defined as $d\sigma_{\text{coh}}(\underline{Q})/d\Omega = (\sigma_{\text{coh}}/4\pi\, N) \int d\underline{r}\, \rho(\underline{r}) \circledast \rho(\underline{r})\, \exp(\imath \underline{Q} \underline{r})$, whereby $\sigma_{\text{coh}} = 4\pi\, \overline{b}^2$ is the coherent cross-section and $\rho(\underline{r})$ the particle number density. The Patterson function is than the autocorrelation of the particle number density. This function is independent of the scattering lengths and only dependent on the geometric arrangement of the scattering centers. The Fourier transformation of the Patterson function is therefore sometimes called Structure factor $S(\underline{Q})$ and is related in case of a static approximation to the differential cross-section by the equation $d\sigma_{\text{coh}}(\underline{Q})/d\Omega = (\sigma_{\text{coh}}/4\pi N)\, S(\underline{Q})$.

10.2.1.2. *Absence of long range order.* As a second simplification it will be assumed that long range order is absent. The consequence is that the autocorrelation $\Gamma(r)$ becomes constant for large values of r. It converges to $\bar{\Gamma} = \bar{\rho}^2 V$. $\bar{\rho}$ is the average scattering length density defined by

$$\int d\underline{\mathrm{r}}\ (\rho(\underline{\mathrm{r}}) - \bar{\rho}) = \int d\underline{\mathrm{r}}\, \eta(\underline{\mathrm{r}}) = 0 \quad . \tag{10.38}$$

Structural information is therefore only contained in a finite range of $\Gamma(\underline{\mathrm{r}})$ where it deviates from the average value $\bar{\Gamma}$. This is due to the fact that only a deviation of $\eta(\underline{\mathrm{r}})$ from the average $\bar{\rho}$ leads to a scattering contribution for $Q \neq 0$. An additional constant value $\bar{\rho}$ only contributes to the scattering at $Q = 0$ and is therefore not accessible. Consequently the average scattering length density can be subtracted without loss of generality and only deviations $\eta(\underline{\mathrm{r}}) = \rho(\underline{\mathrm{r}}) - \bar{\rho}$ have to be considered. The autocorrelation function is therefore defined as

$$\gamma(r) \;=\; \frac{1}{V}\,\overline{\eta(\underline{\mathrm{r}}) \circledast \eta(\underline{\mathrm{r}})}^{\,\underline{\mathrm{r}}} = \frac{1}{V}\,\overline{(\rho(\underline{\mathrm{r}}) - \bar{\rho}) \circledast (\rho(\underline{\mathrm{r}}) - \bar{\rho})}^{\,\underline{\mathrm{r}}} \tag{10.39}$$

$$\Rightarrow \quad I(Q) \;=\; V \int_0^\infty dr\, 4\pi\, r^2\, \gamma(r)\, \frac{\sin Qr}{Qr}. \tag{10.40}$$

$V\gamma(\underline{\mathrm{r}})$ is different from $\Gamma(\underline{\mathrm{r}})$ due to the definition of $\bar{\rho}$ (eq. 10.38) only by a constant term $\bar{\rho}^2\, V$, i.e. $V\,\gamma(\underline{\mathrm{r}}) = \Gamma(\underline{\mathrm{r}}) - \bar{\rho}^2\, V$ because

$$\Gamma(\underline{\mathrm{r}}) \;=\; \int d\underline{\mathrm{r}}_1\, \rho(\underline{\mathrm{r}}_1)\, \rho^*(\underline{\mathrm{r}}_1 - \underline{\mathrm{r}}) = \int d\underline{\mathrm{r}}_1\, (\bar{\rho} + \eta(\underline{\mathrm{r}}_1))(\bar{\rho} + \eta(\underline{\mathrm{r}}_1 - \underline{\mathrm{r}}))^* \tag{10.41}$$

$$= \bar{\rho}^2 V + \underbrace{\int d\underline{\mathrm{r}}_1\, (\bar{\rho}\, \eta(\underline{\mathrm{r}}_1) + \bar{\rho}^*\, \eta^*(\underline{\mathrm{r}}_1 - \underline{\mathrm{r}}))}_{= 0 \text{ due to def. of } \eta(\underline{\mathrm{r}}) \text{ in eq. } 10.38} + \int d\underline{\mathrm{r}}_1\, \eta(\underline{\mathrm{r}}_1)\, \eta^*(\underline{\mathrm{r}}_1 - \underline{\mathrm{r}}) \tag{10.42}$$

$$= \bar{\rho}^2 V + \gamma(\underline{\mathrm{r}})\, V. \tag{10.43}$$

10.2.1.3. *Limits $r = 0$ and $r = \infty$.* The limits $r = 0$ and $r \to \infty$ for the autocorrelation $\gamma(\underline{\mathrm{r}})$ are $\gamma(0) = \overline{\eta^2}$ and $\gamma(\infty) = 0$. The limit $r \to \infty$ is zero because $\eta(\underline{\mathrm{r}})$ is defined as the deviation of the average scattering length density $\bar{\rho}$. As long range correlation is assumed not to be present $\eta(\underline{\mathrm{r}}) \circledast \eta(\underline{\mathrm{r}})^{\,r \to \infty} = \bar{\eta}^2 = 0$. $\gamma(r)$ can be calculated by the inverse Fourier transformation of the scattering intensity $I(Q)$ (eq. 10.40)

$$V\,\gamma(r) = \frac{1}{2\pi^2} \int_0^\infty dQ\, Q^2\, I(Q)\, \frac{\sin Qr}{Qr} \quad . \tag{10.44}$$

An important special case is $r = 0$ for which equation 10.44 can be simplified to

$$V\,\gamma(0) = V\,\overline{\eta^2} = \frac{1}{2\pi^2} \int_0^\infty dQ\, Q^2\, I(Q) = \frac{\tilde{Q}}{2\pi^2} \quad . \tag{10.45}$$

The integration of the intensity $I(Q)$ in reciprocal space is therefore directly related to the average quadratic deviation of the scattering length density $\overline{\eta^2}$ but independent to the shape of the scatterers. If for example the scattering particle undergoes deformation

the scattering pattern may change drastically but the integral $\tilde{Q}$ in eq. 10.45 keeps invariant against such a deformation.

10.2.2. Volume fraction. The average quadratic deviation of the scattering length density is directly related in a two-phase system to the scattering contrast $\Delta\eta$ and volume fraction f_p of one or the other $(1 - f_p)$ phase. The average quadratic deviation of the scattering length density is defined as

$$\overline{\eta^2} = \eta_1^2 \, f_p + \eta_2^2 \, (1 - f_p), \tag{10.46}$$

whereby η_1 and η_2 are the scattering length density differences of the two phases from the average value $\bar{\rho}$ and the scattering contrast is than defined as $\Delta\eta = \eta_1 + \eta_2$. The average value $\bar{\rho}$ is given by

$$\begin{aligned} \bar{\rho} = (\bar{\rho} - \eta_1) f_p + (\bar{\rho} + \eta_2)(1 - f_p) \quad &\Leftrightarrow \quad f_p \, (\eta_1 + \eta_2) = f_p \, \Delta\eta = \eta_2 \\ &\text{or} \quad (1 - f_p) \, \Delta\eta = \eta_1 \quad . \end{aligned} \tag{10.47}$$

Replacing η_1 and η_2 in eq. 10.46 leads to

$$\overline{\eta^2} = \Delta\eta^2 \, f_p(1 - f_p). \tag{10.48}$$

The second moment of the scattering intensity, the so-called scattering invariant $\tilde{Q}$ from eq. 10.45, can therefore be related to the volume fractions of the two phases f_p and $(1 - f_p)$ by

$$\tilde{Q} = \int dQ \, Q^2 \, I(Q) = 2\pi^2 \, V \, \Delta\eta^2 \, f_p(1 - f_p) \quad . \tag{10.49}$$

Due to the Babinet principle in a scattering experiment the volume fractions can not be uniquely assigned to one or the other phase. A system with exchanged phases would have the same invariant A unique solution of eq. 10.49 for the volume fraction can only be obtained if either one already knows from somewhere else that the volume fraction of one phase is much smaller than the volume fraction of the other (dilute case) or if time resolved experiments are performed during the formation of the structure and when it is known that one phase is growing on the cost of the other one (Ostwald ripening).

10.2.3. Interparticle interferences. The square of the Fourier transformation of the scattering length density of a sample with a volume V is equal to the scattering intensity $I(\underline{\mathrm{Q}})$

$$I(\underline{\mathrm{Q}}) = \left| \int_V d\underline{\mathrm{r}} \, \rho(\underline{\mathrm{r}}) \, e^{i \underline{\mathrm{Q}} r} \right|^2 \quad . \tag{10.50}$$

The integration has to be carried out over the whole illuminated sample volume V. If the sample volume contains N particles embedded in a matrix with a constant scattering length density ρ_M and if $\underline{\mathrm{R}}_i$ defines the center of particle i with a constant scattering

length density $\rho_{P,i} = \Delta\eta_i + \rho_M$ the scattering intensity can be written as

$$\begin{aligned} I(\underline{\mathrm{Q}}) &= \left| \sum_{i=1}^{N} F_i(\underline{\mathrm{Q}})\, e^{\imath \underline{\mathrm{Q}}\, R_i} \right|^2 \\ \text{with } F_i(\underline{\mathrm{Q}}) &= \int\limits_{V_i(\underline{\mathrm{R}}_i)} d\underline{\mathrm{r}}\, \Delta\eta_i\, e^{\imath \underline{\mathrm{Q}}(\underline{\mathrm{r}}-R_i)} = \Delta\eta_i \int\limits_{V_i(\underline{0})} d\underline{\mathrm{r}}\, e^{\imath \underline{\mathrm{Q}} r} = \Delta\eta_i\, V_i\, f_i(\underline{\mathrm{Q}}). \end{aligned} \tag{10.51}$$

$V_i(\underline{\mathrm{R}}_i)$ describes the integration volume of scatterer i located at $\underline{\mathrm{R}}_i$ and $V_i(\underline{0})$ describes the integration volume of the scatterer i moved to the origin of the coordinate system. $\Delta\eta_i$ and V_i are the scattering contrast and particle volume, respectively. The square of the modulus in eq. 10.51 can be rewritten to

$$\begin{aligned} I(\underline{\mathrm{Q}}) &= \sum_{i=1}^{N} \sum_{j=1}^{N} F_i(\underline{\mathrm{Q}})\, F_j^*(\underline{\mathrm{Q}})\, e^{\imath \underline{\mathrm{Q}} \underline{\mathrm{R}}_{ij}} \\ &= \sum_{i=1}^{N} \left| F_i(\underline{\mathrm{Q}}) \right|^2 + \\ &\quad \underbrace{2 \sum_{i=1}^{N} \sum_{j>i}^{N} \left[\Re\left(F_i(\underline{\mathrm{Q}})\, F_j^*(\underline{\mathrm{Q}}) \right) \cos \underline{\mathrm{Q}} \underline{\mathrm{R}}_{ij} - \Im\left(F_i(\underline{\mathrm{Q}})\, F_j^*(\underline{\mathrm{Q}}) \right) \sin \underline{\mathrm{Q}} \underline{\mathrm{R}}_{ij} \right]}_{\Psi(\underline{\mathrm{Q}})} \end{aligned} \tag{10.52}$$

The first term for which $i = j$ the phase factor is identical to 1 and describes the sum of the scattering intensity of individual particles. The double sum in the second term describes interference effects of the scattering amplitudes scattered from different particles which depends on their relative arrangement $\underline{\mathrm{R}}_{ij} = \underline{\mathrm{R}}_i - \underline{\mathrm{R}}_j$. The scattering amplitude $F_i(\underline{\mathrm{Q}})$ is among other things dependent on the scattering contrast $\Delta\eta_i$ and on the normalized form factor $F_i(\underline{\mathrm{Q}})/\Delta\eta_i V_i = f_i(\underline{\mathrm{Q}})$, whereby $f_i(\underline{\mathrm{Q}})$ is a real-valued function with $f_i(Q = 0) = 1$. Analytical expressions for scattering intensities $i_0(Q) = \overline{|f(Q)|^2}$ of simple geometric bodies are listed in the chapter 3. In case $\Delta\eta_i$ is complex valued, i.e. the scatterer has an absorption contrast $\Delta\eta_i''$, the scattering contrast can be written as $\Delta\eta_i = \Delta\eta_i' + \imath\Delta\eta_i''$ and for the interference term we get

$$\begin{aligned} \Psi(\underline{\mathrm{Q}}) &= 2 \sum_{i=1}^{N} \sum_{j>i}^{N} f_i(\underline{\mathrm{Q}})\, f_j(\underline{\mathrm{Q}})\, V_i\, V_j \\ &\quad \times \left[(\Delta\eta_i'\, \Delta\eta_j' + \Delta\eta_i''\, \Delta\eta_j'') \cos \underline{\mathrm{Q}} \underline{\mathrm{R}}_{ij} - (\Delta\eta_i'\, \Delta\eta_j'' - \Delta\eta_i''\, \Delta\eta_j') \sin \underline{\mathrm{Q}} \underline{\mathrm{R}}_{ij} \right] \quad . \end{aligned} \tag{10.53}$$

If now all particle have an identical scattering contrast $\Delta\eta = \Delta\eta_i = \Delta\eta_j$ we get for the scattering intensity (eq. 10.51) the expression

$$\begin{aligned} I(\underline{\mathrm{Q}}) &= \sum_{i=1}^{N} V_i^2 \left(\Delta\eta'^2 + \Delta\eta''^2\right) \left|f_i(\underline{\mathrm{Q}})\right|^2 \\ &\quad + 2\sum_{i=1}^{N}\sum_{j>i}^{N} f_i(\underline{\mathrm{Q}})\, f_j(\underline{\mathrm{Q}})\, V_i\, V_j \left(\Delta\eta'^2 + \Delta\eta''^2\right) \cos \underline{\mathrm{Q}}\underline{\mathrm{R}}_{ij} \quad . \end{aligned} \tag{10.54}$$

For identical scattering contrasts there is consequently no interference between the scattering amplitude of waves scattered at the real and at the imaginary (absorption) part of the scattering contrast.

10.2.3.1. *Isotropic ensemble of particles.* In the following we assume as another simplification an isotropic ensemble of particles. Such a system of scatterer is defined as follows: If $\underline{\mathrm{R}}_i$ defines the position of any particle i and $\underline{\mathrm{R}}_{ij}$ is the difference vector between the position of particle i and j than a system of particles is called isotropic if all vectors $\underline{\mathrm{R}}_{ij}$ of the same length will take with equal probability any direction. Under this simplification the interference term $\Psi(\underline{\mathrm{Q}})$ in eq. 10.53 can be averaged over all directions $\underline{\mathrm{R}}_{ij}$. This average yield for $\overline{\sin \underline{\mathrm{Q}} R_{ij}}^{\,\underline{\mathrm{R}}_{ij}} = 0$ and for $\overline{\cos \underline{\mathrm{Q}} R_{ij}}^{\,\underline{\mathrm{R}}_{ij}} = \frac{\sin QR_{ij}}{QR_{ij}}$ (compare with eq. 10.37). The interference term can then be written as

$$\Psi(\underline{\mathrm{Q}}) = 2\sum_{i=1}^{N}\sum_{j>i}^{N} f_i(\underline{\mathrm{Q}})\, f_j(\underline{\mathrm{Q}})\, V_i\, V_j \left(\Delta\eta'_i\, \Delta\eta'_j + \Delta\eta''_i\, \Delta\eta''_j\right) \frac{\sin QR_{ij}}{QR_{ij}}. \tag{10.55}$$

Therefore also for an isotropic ensemble of scatterers no interferences between waves scatterer at the real and imaginary part of the scattering contrast disappears as already shown for systems of particles with identical scattering contrast.

10.2.4. Influence of the relative arrangement of scatterers on interparticle interferences. The expression for $\Psi(\underline{\mathrm{Q}})$ can be further simplified if the scattering system consist of identical particles which fulfill the condition that for all of them each orientation be likewise probable and furthermore the relative position of two particles do not have an influence on their orientation. The second part of the assumption is for radial symmetric particle automatically fulfilled. However, in case of a system of close packed ellipsoidal particles with half axis R, R and νR with $\nu > 1$ distance of $2R$ between the centers of the ellipsoids are possible, but for such an arrangement not all orientations of the ellipsoids are allowed anymore. That means that the relative distance has an influence on allowed orientations of the particles. The general case without the restrictions made in this paragraph are discussed by Guinier and Fournet in [**37**]. For only slightly anisotropic and not to closely packed systems the assumptions made here are at least fulfilled in first approximation. Under the made assumptions the averaging over the particle orientations can be separated from the averaging of the particle positions. As a result from the average one gets for the scattering intensity

$$\overline{I(Q)} = N\overline{|F(Q)|^2} + 2\left|\overline{F(Q)}\right|^2 \sum_{i=1}^{N}\sum_{j>i}^{N} \frac{\sin QR_{ij}}{QR_{ij}} \tag{10.56}$$

For low concentrations this averaging is in first approximation also valid for particles with a size distribution. The probability to find a particle at the position $\underline{\mathrm{R}}_i$ is in average $\frac{N}{V}\, d\underline{\mathrm{R}}_i$ and the probability to find at the same time another particle at position $\underline{\mathrm{R}}_j$ is $\frac{N}{V}\, d\underline{\mathrm{R}}_i\, \frac{N}{V}\, d\underline{\mathrm{R}}_j$. A deviation from this is considered by $P(R_{ij})$ so that the double sum in eq. 10.56 can be written as

$$\sum_{i=1}^{N} \sum_{j>i}^{N} \frac{\sin QR_{ij}}{QR_{ij}} = \int_V \int_V \frac{\sin QR_{ij}}{QR_{ij}}\, P(R_{ij})\, \frac{N^2}{V^2}\, d\underline{\mathrm{R}}_i\, d\underline{\mathrm{R}}_j \quad . \tag{10.57}$$

For isotropic media the function $P(R_{ij})$ is independent of the indices i and j and only a function of the distance R. $P(R)$ has the property to converge for large distance against one. By the substitution $P(R) = 1 - (1 - P(R))$ one gets for the interference term

$$\Psi(Q) = \left|\overline{F(Q)}\right|^2 \frac{N^2}{V^2} \int_V \int_V \frac{\sin QR_{ij}}{QR_{ij}}\, d\underline{\mathrm{R}}_i\, d\underline{\mathrm{R}}_j \tag{10.58}$$

$$- \left|\overline{F(Q)}\right|^2 \frac{N^2}{V^2} \int_V \int_V \frac{\sin QR_{ij}}{QR_{ij}} (1 - P(R_{ij}))\, d\underline{\mathrm{R}}_i\, d\underline{\mathrm{R}}_j. \tag{10.59}$$

The first term can be interpreted as the scattering of a particle with the volume V and the average scattering contrast $\overline{F(Q)}\frac{N}{V}$. As the illuminated sample volume V is relatively large this contribution is practically zero for all experimental accessible scattering angles. As for isotropic media the integration over $d\underline{\mathrm{R}}_i$ is independent from the integration over $d\underline{\mathrm{R}}_j$ and $(1 - P(R))$ quickly converges against zero the first integrationin the second term (neglecting side effects) can be written as

$$\int_0^\infty dR\, \frac{\sin QR}{QR}\, (1 - P(R))\, \frac{N^2}{V^2}\, 4\,\pi\, R^2. \tag{10.60}$$

The second integration only yields an additional multiplication factor V. Finally one gets for the scattering intensity the expression

$$\overline{I(Q)} = N \left\{ \overline{|F(Q)|^2} - \left|\overline{F(Q)}\right|^2 \underbrace{\frac{N}{V} \int dR\, 4\pi\, R^2\, (1 - P(R))\, \frac{\sin QR}{QR}}_{\Upsilon(Q)} \right\} \quad . \tag{10.61}$$

10.2.4.1. *Formula from Prins and Zernicke.* For radial symmetric identical scatterer the quare of the average form factor $\left|\overline{F(Q)}\right|^2$ and the average of the squared form factor $\overline{|F(Q)|^2}$ are the same so that one get for the expression from Prins and Zernicke [**107**] and from Debye und Mencke [**22**]

$$\overline{I(Q)} = N\, F^2(Q) \underbrace{\left\{ 1 - \frac{N}{V} \int dR\, 4\pi\, R^2\, (1 - P(R))\, \frac{\sin QR}{QR} \right\}}_{S(Q)=1-\Upsilon(Q)} \quad . \tag{10.62}$$

The problem of applying eq. 10.61 or 10.62 is the evaluation of $P(R)$. $P(R)$ depends on the geometric arrangement of the scatterer. For liquid emulsions the geometric arrangement can be related to thermodynamic quantities like concentration, temperature and interaction potential between the particles. In a theory of Raman [**82**] the geometric arrangement is associated to the interaction potential $U(r)$ in a simple way. According to his theory the potential is the sum of two-body interactions and he finds for $P(r)$ the relation $P(r) = \exp(-U(r)/kT)$. For larger concentrations many-body interactions have to be taken into account. In a more general theory of Born and Green [**13**] three-body interactions are at least considered in first approximation and they find for the scattering intensity the expression

$$\begin{aligned} \overline{I(Q)} &= N\left\{\overline{|F(Q)|^2} + \left|\overline{F(Q)}\right|^2 \frac{\chi(Q)}{\frac{V}{N}(2\pi)^{-3/2} - \chi(Q)}\right\} \qquad (10.63) \\ \text{with } \chi(Q) &= \sqrt{\frac{2}{\pi}} \int_0^\infty dr\ \left[e^{-U(r)/kT} - 1\right]\ r^2\, \frac{\sin Qr}{Qr}. \end{aligned}$$

For a simple hard sphere model with the interaction potential $U(r) = \begin{cases} 0 \text{ for } r>2R \\ \infty \text{ for } r\leq 2R \end{cases}$ the scattering intensity can be calculated analytically. According to Raman's theory Debye calculates for the scattering intensity of spheres with a radius R and a volume V_P the expression

$$\overline{I(Q)} = N\, K^2(QR)\, \left\{1 - 8\, N\, \frac{V_P}{V}\, K(2QR)\right\}, \qquad (10.64)$$

whereby $K(x)$ is the scattering function of a sphere given in section 3.1.1. Following the theory of Born and Green one gets a similar expression

$$\overline{I(Q)} = N\, K^2(QR)\, \left\{1 + 8\, N\, \frac{V_P}{V}\, K(2QR)\right\}^{-1}. \qquad (10.65)$$

Nonetheless both theories are only valid for monodisperse systems of scatterer. In practice, however, most scattering systems have a more or less pronounced size distribution and frequently also an additional variety of shapes. For such systems the interaction potential can not be expressed in a closed form. One has to introduce for each pair of particle type a separate potential [**1**] which complicates the analytical treatment a lot.

10.2.4.2. *Isolate particles.* A system of isolate particles is characterized by its property that the positions of a particle is not influenced by the positions of any other particle. For this case the interaction potential $U(r)$ and consequently also $\chi(Q)$ is identical zero. Therefore the expression for the scattering intensity simplifies to

$$I(Q) = N\,\overline{|F(Q)|^2} \quad \text{or} \quad I(\underline{Q}) = \sum_{i=1}^{N} \left|F_i(\underline{Q})\right|^2. \qquad (10.66)$$

The total scattering intensity is simply the sum of the intensity scattered by the individual particles. A system of non-interacting particles can be realized by diluting the system. Thereby the average distance between the particles is increased and the interaction potential becomes negligible small and does not influence anymore the arrangement of the scatterer.

10.2.4.3. *Polydisperse System of isolated particles.* The scattering function of a polydisperse system of isolated particles is determined by the shape and size of the particles. In a scattering experiment it is not possible to separate both quantities at the same time. In the data analysis one has to assume one of the quantities either the shape or the size distribution to get then the other quantity. Normally the shape is assumed whereby the size distribution is than obtained from the scattering curve [**34, 100**]. To get an information about the shape one normally need a system of identical particles, like for example a system of identical proteins. An additional but known size distribution would smear out the scattering too much to still allow to extract confidential information about the particle shape. The scattering intensity of a system of isolated particles of different shape and a size distribution is given by

$$I(\underline{Q}) = \sum_{\mu=1}^{M} \int N_\mu(R)\, \overline{|F_\mu(Q,R)|^2}\, dR, \tag{10.67}$$

whereby $N_\mu(R)$ is the size distribution of particles of type μ and $F_\mu(Q,R)$ its form factor. Form factor of simple objects are listed in chapter 3 and frequently used size distributions in chapter 5.

10.2.5. Influence of $N(R)$ and $F(Q,R)$ on interparticle interferences. Interparticle interferences in small angle scattering signals have been described in eq. 10.61 and 10.62 by

$$\overline{I(Q)} = N\, \overline{|F(Q)|^2} \left\{ 1 + \frac{\left|\overline{F(Q)}\right|^2}{\overline{|F(Q)|^2}} \left(S(Q) - 1\right) \right\} \tag{10.68}$$

Hereby $S(Q)$ describes the influence of the relative arrangement of the scatterers on $\overline{I(Q)}$ and can be calculated by the interaction potential between the scattering particles (eq. 10.63). Interparticle interferences depends next to the relative arrangement also on the square of the average form factor $|\overline{F(Q)}|^2$. Only for the case of identical and spherical symmetric scatterer the relation $\overline{|F(Q)|^2} \equiv |\overline{F(Q)}|^2$ is valid. In this case the interparticle interferences only depends on $S(Q)$. For particles with an irregular shape, however, the two averages are different and depends both on the size distribution as well as on the particle shape and their orientation distribution. For such systems the condition for the derivation the relation from Prins and Zernicke 10.61 namely the independency of orientation and size for higher concentrations is not anymore fulfilled. This condition allowed in eq. 10.56 to separate the averaging of the particle positions from the averaging of the form factor. Nevertheless the principle influence of a irregular particle shape and a size distribution can be made clear by the means of eq. 10.68. For judging their influence the ratio $|\overline{F(Q)}|^2/\overline{|F(Q)|^2}$ is considered.

Taking for example a system of identical but random oriented rotational ellipsoids with the half axis R, R, νR the ratio of the two averages is shown in figure 10.3 together with the scattering intensity $\overline{|F(Q)|^2}$ of the corresponding ideal dilutes system. The derivation of the formula for calculating $\overline{|F(Q)|^2}$ and $|\overline{F(Q)}|^2$ are given in appendix **??**. The figure shows that the ratio decreases for larger scattering vectors Q the more the shaper of the rotational ellipsoid is different from the ideal spherical case ($\nu = 1$).

An irregular particle shape already is sufficient to reduce the influence interparticle interferences.

Accordingly also the particle size distribution give rise to a difference in the averages $\overline{|F(Q)|^2}$ and $|\overline{F(Q)}|^2$. Figure 10.3b shows the ratio of the two averages of spherical scatterers with a lognormal size distribution of different width as a function of Q. For $Q = 0$ the ratio is given by $|\overline{F(Q)}|^2/\overline{|F(Q)|^2} = \exp(-9\sigma^2)$. One can see that the width of the size distribution strongly reduces the interference effect [**98**].

In general one can say that each kind of disorder reduces interferences. The disorder can have its origin in a random arrangement of particles (dilute systems), in an orientation distribution of irregular shaped particles, or also in a size ditsribution.

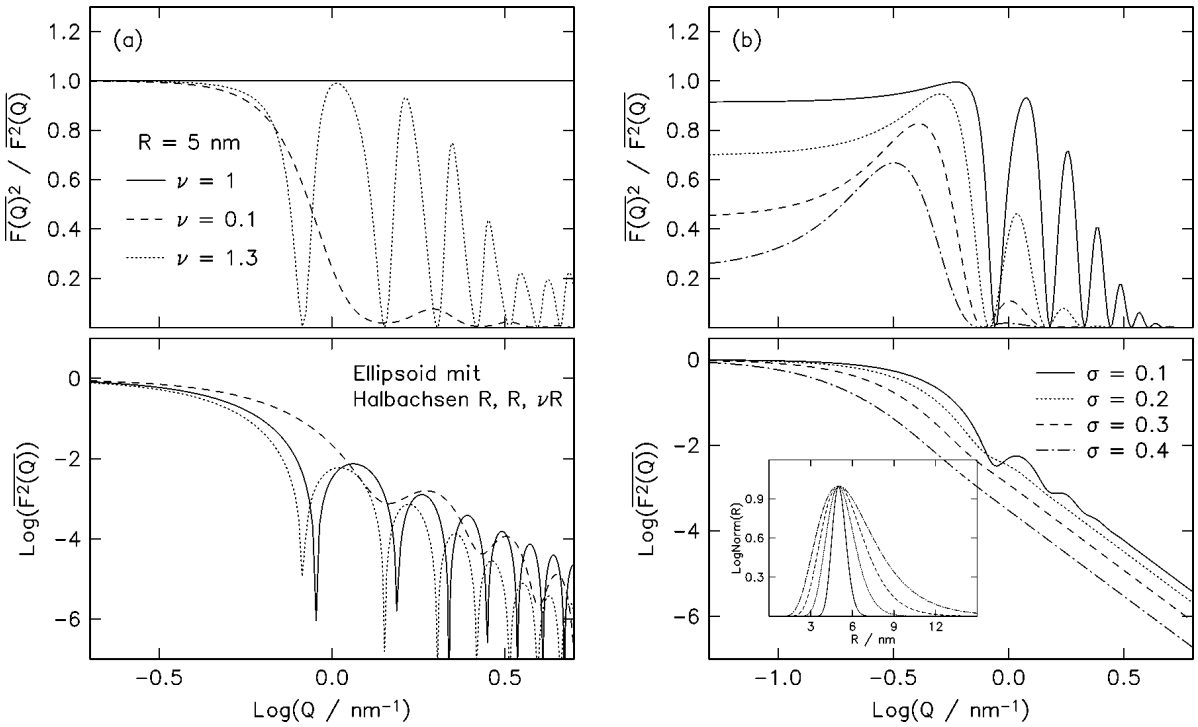

(a) The influence of irregular particle shapes on $|\overline{F(Q)}|^2/\overline{|F(Q)|^2}$ is shown for an example of random orientated rotational ellipsoids with the half axis R, R, νR for $\nu = 1$, 0.1, and 1.3.

(b) Influence of a particle size distribution $\mathrm{LogNorm}(R) = \exp\left(-(\ln\mu - \ln R)^2/(2\sigma^2)\right)$ of the widths $\sigma = 0.1$, 0.2, 0.3, 0.4 for $\mu = 5$ nm on $|\overline{F(Q)}|^2/\overline{|F(Q)|^2}$.

FIGURE 10.3. For identical and spherical symmetric scatterers the ratio $|\overline{F(Q)}|^2/\overline{|F(Q)|^2} \equiv 1$. Interparticle interferences depend then only on the relative positions of the scatterers. Size distribution and irregular shapes reduce these interference effects.

10.2.6. Scattering laws and structural parameter. In this section a series of useful scattering laws are presented, which are useful for a simple analysis of experimental data and which allow an easy determination of structural parameters. [**37**].

10.2.6.1. *Porod volume.* The ratio of the scattering intensity in forward direction $I(Q=0) = N\,V_P^2\,\Delta\eta^2$ and the scattering invariant $\tilde{Q} = 2\pi^2\Delta\eta^2\,V\,f_p(1-f_p)$ can be used to determine the particle volume V_P (V describes the illuminated sample volume). $f_p\,V = N\,V_P$ corresponds to the total volume of all scatterers whereby the particle volume V_P can be calculated by

$$\frac{V_P}{1-f_p} \overset{f_p \ll 1}{\simeq} V_P = 2\pi^2\,\frac{I(Q=0)}{\tilde{Q}}. \tag{10.69}$$

The measurement of the scattering curve in relative units is therefore sufficiant to determine the volume of a homogeneous scatterer. Sources of errors for this way of determination of particle sizes are the extrapolation into forward direction und more important the extrapolation to large scattering angles (Q^{-4}-extrapolation). Furthermore for large volume fractions f_p the particle volume has to be eventually corrected by a prefactor $1/(1-f_p)$ which is not always known.

10.2.6.2. *Radius of gyration and Guinier approximation.* The scattering intensity for small angles can be approximated in a series expansion by replacing the expression $\frac{\sin Qr}{Qr}$ in eq. 10.40 by a McLaurin series which leads to

$$I(Q) = V \int 4\pi\,r^2\,\gamma(r)\,\left[1 - \frac{Q^2r^2}{3!} + \frac{Q^4r^4}{5!} - \ldots\right] dr \quad , \tag{10.70}$$

i.e. $I(Q)$ is expanded by moments $\overline{r^n}$ of $\gamma(r)$. The first term corresponds to the scattering intensity of $Q=0$. For the second term Guinier and Fournet [**37**] have shown, that it can be related to the gyration radius of the scattering length density R_G by

$$V \int 4\pi\,r^2\,\frac{Q^2r^2}{3!}\,\gamma(r)\,dr = I(0)\,\frac{Q^2R_G^2}{3} \quad \Rightarrow \quad I(Q) = I(0)\,\left(1 - \frac{Q^2R_G^2}{3}\right) \tag{10.71}$$

with $R_G^2 = \int \eta(r)\,r^2\,dr / \int \eta(r)\,dr$. Up to the term of Q^4 this series expansion at the beginning of the scattering curve is identical to the series expansion of an exponential function which than leads to the well known Guinier approximation

$$I(Q) = I(0)\,e^{-Q^2R_G^2/3}. \tag{10.72}$$

The Guinier law is valid for any particle shape which is roughly isodiametric. For flat or elongated structures the Guinier law has to be corrected slightly [**27, 37**]. The radius of gyration for a sphere with radius R is given by $R_G = \sqrt{3/5}\,R$. The Guinier law is valid in the scattering vector interval $0 < Q < 1/R_G$.

10.2.6.3. *Correlation length.* Another characteristic quantity, which can be easily extracted from the scattering curve $I(Q)$ is the correlation length l_c. The correlation length is defined as the average width of the correlation function $\gamma(r)$:

$$l_c = \frac{2}{\gamma(0)} \int \gamma(r)\,dr. \tag{10.73}$$

Together with the definition of the scattering invariant $\tilde{Q}$ in eq. 10.49 and the relation between $I(Q)$ and $\gamma(r)$ in eq. 10.44 this results after a short calculation (changing of

integrations) to

$$l_c = \pi \, \frac{\int Q \, I(Q) \, dQ}{\int Q^2 \, I(Q) \, dQ} \quad . \tag{10.74}$$

A sphere with radius R has therefore a correlation length of $l_c = \frac{3}{2} \, R$.

10.2.6.4. *Porod law and specific surfaces.* The Porod law describes the scattering behavior at large Q values. As the scattering intensity $I(Q)$ and the correlation function $\gamma(r)$ are related via the Fourier transformation the intensity $I(Q)$ is determined at large values of Q mainly by $\gamma(r)$ at small r. For small r the correlation function $\gamma(r)$ can be expanded in a Taylor series and one gets according to Guinier and Fournet [**37**]

$$\frac{\gamma(r)}{\gamma(0)} = 1 - \frac{1}{4} \, \frac{S}{V} + \dots \quad , \tag{10.75}$$

whereby S is the total surface of all scatterer in the illuminated sample volume V. Eq. 10.75 together with 10.40 result for large Q values into the Porod law

$$I(Q) \longrightarrow \Delta\eta^2 \, \frac{2\pi \, S}{Q^4}. \tag{10.76}$$

A scaling of the scattering intensity on $\tilde{Q}$ provides an expression for the specific surface S/V of

$$\lim_{Q \to \infty} \pi \, \frac{I(Q)}{\tilde{Q}} \, Q^4 \, f_p \, (1 - f_p) = \frac{S}{V}. \tag{10.77}$$

The Porod law can be applied to all systems having sharp interfaces.

CHAPTER 11

Experimental Setup of a Small Angle Scattering Instrument

11.1. SANS-Camera

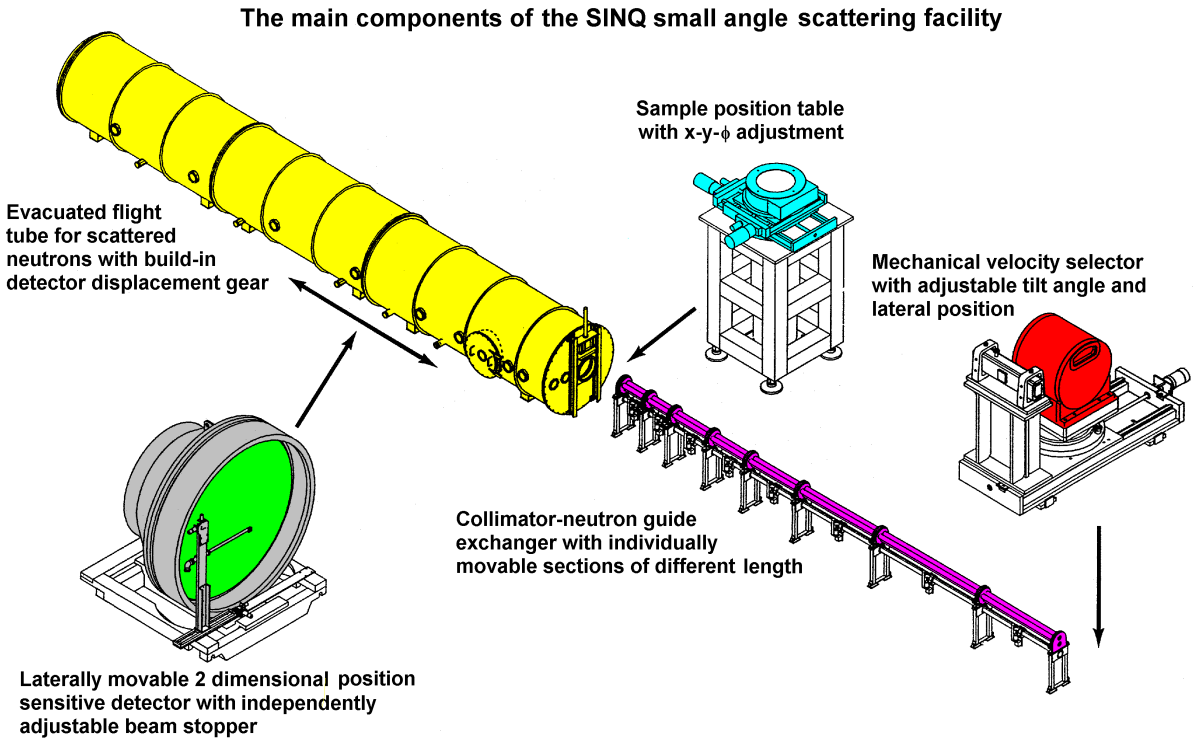

FIGURE 11.1. SANS-1 instrument at PSI, Switzerkand

11.2. SAXS-Camera

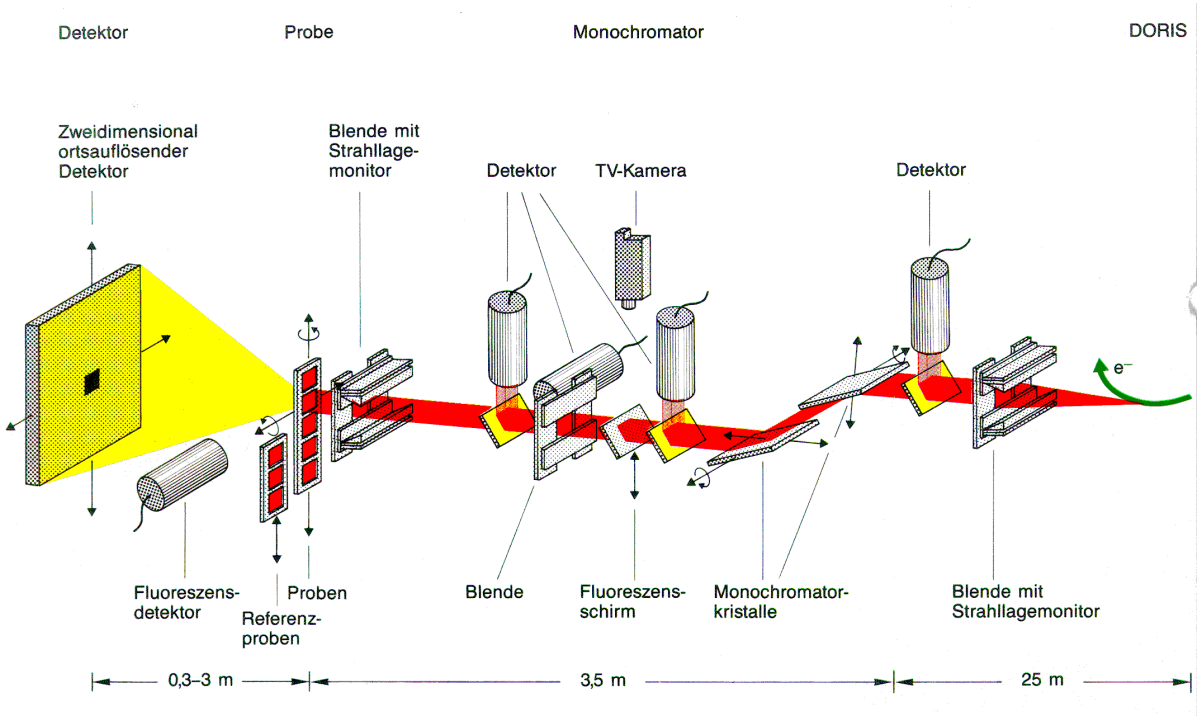

FIGURE 11.2. Small angle x-ray scattering instrument Jusifa at the synchrotron light source HASYLAB in Hamburg

CHAPTER 12

Data Reduction in SAS

12.1. Correction and Normalization of SANS-Raw data

A detector of a small angle scattering camera measures the superposition of intensities of different origin:

(1) Background noise I_B
(2) Scattering of the empty sample holder I_H
(3) scattering of the isolated sample I_S

Furthermore the detector elements can have different efficiencies ϵ_i. To determine the differential cross-section of of the sample all the different contribution to the total scattering intensity have to be considered and determined separately by different measurements. The quantity to be known is the scattering contribution of the isolated sample I_S, which in general can not be measured directly. Experimental accessible scattering contributions are the scattering of the sample in the sample holder I_{S+H}, the contribution of the empty sample holder I_H and the background noise I_B. From this experimental accessible data the wanted scattering contribution of the isolated sample has to be determined.

12.1.1. Contribution of the isolated sample. The intensity of the incident beam will be attenuated by absorption and scattering effects within the sample. Also the scattered neutrons will be further attenuated on their residual path through the sample. The measured intensity in a detector element i is given by

$$I^0_{S,i} = \int_0^d dx\, \Phi_0\, \Delta\Omega_i\, \epsilon_i\, e^{-\alpha\, x}\, A\, \rho\, e^{-\frac{\alpha(d-x)}{\cos\theta}} \left\{ \frac{d\sigma_{\rm coh}}{d\Omega} + \frac{d\sigma_{\rm inc}}{d\Omega} \right\}. \tag{12.1}$$

Hereby d describes the sample thickness in cm, Φ_0 the incident neutron flux in neutrons per cm$^2\times$sec, $d\Omega_i$ is the solid angle of the detector element i in steradian, ϵ_i the detection efficiency of detector element i and α the extinction coefficient of the sample in cm^{-1}. A the illuminated sample area in cm^2. θ describes the angle between the wave vector $\mathbf{k}_0$ of the incident neutrons and the wave vector $\mathbf{k}$ of the scattered neutrons. $\frac{d\sigma_{\rm coh}}{d\Omega}$ and $\frac{d\sigma_{\rm inc}}{d\Omega}$ are the coherent and incoherent differential cross-sections, respectively. For small angle scattering $\cos\theta \simeq 1$ and one yields after integration

$$I^0_{S,i} = \Phi_0\, \Delta\Omega_i\, \epsilon_i\, \underbrace{A\, \rho\, d}_{N_S}\, \underbrace{e^{-\alpha d}}_{T_S} \left\{ \frac{d\sigma_{\rm coh}}{d\Omega} + \frac{d\sigma_{inc}}{d\Omega} \right\}. \tag{12.2}$$

The quantity $N_S = A\,\rho\,d$ corresponds to the number of scattering atoms and $T_S = e^{-\alpha\, d} = \frac{I_{\rm trans}}{I_0}$ to the transmissions coefficient, which can be determined from the ration of the intensity of the transmitted primary beam $I_{\rm trans}$ and the intensity of the incident

beam I_0. The incoherent scattering is isotropically and equally distributed over the whole solid angle of 4π. Therefore one gets for $I^0_{S,i}$

$$I^0_{S,i} = \Phi_0 \, \Delta\Omega_i \, \epsilon_i \left\{ N_S \, T_S \, \frac{d\sigma_{\text{coh}}}{d\Omega} + A \, \frac{1 - T_S}{4\,\pi} \right\}. \tag{12.3}$$

12.1.2. Correction for sample holder and background noise. The scattering intensity of an isolated sample can practically never measured directly. The scattering of the sample is always superposed by scattering from the sample holder and by background noise. Background noise is meant to be electronic noise, cosmic radiation, and detection of neutrons, which have not passed through the sample like scattered neutrons from neighboring experiments. Because of this reasons additional measurements have to be carried out, which are a measurement of the empty sample holder I_H and a measurement with a strong absorber like Cadmium in front of the sample to measure the background noise I_B. Together with the measurement of the sample in the sample holder $I_{S+H,i}$ the scattering of the isolated sample $I^0_{S,i}$ on the detector element i can be calculated by

$$I^0_{S,i} = \left(\frac{I_{S+H,i}}{M_{S+H}} - \frac{I_{B,i}}{M_B} \right) - \frac{T_{S+H}}{T_H} \left(\frac{I_{H,i}}{M_H} - \frac{I_{B,i}}{M_B} \right). \tag{12.4}$$

The index B stands for background, H for the empty sample holder, $S+H$ for the sample in the sample holder and S for the scattering of the isolated sample. All intensities have to be normalized on the number of incident neutrons. This can be done for example by division of the measured intensity my a monitor count rate M. The factor $\frac{T_{S+H}}{T_H}$ takes account for the attenuation of the beam by the sample.

The differential cross-section in eq. 12.3 can now be calculated from the measurable intensities in eq. 12.4. Nevertheless the quantities Φ_0, $\Delta\Omega_i$ and ϵ_i still have to be known. Furthermore I^0_S is not given in physical standard units but in units per monitor count. All this can be overcome by a comparison with a standard substance St. Common standard materials are in general materials with a small coherent cross-section and a large incoherent cross-section like vanadium or water. For both of these materials the coherent cross-section is negligible small. The scattering intensities of the standard materials have to be corrected in the same way than the sample itself according to eq. 12.4. The ratio of both intensities $I^0_{S,i}/I^0_{St,i}$ leads to

$$\frac{I^0_{S,i}}{I^0_{St,i}} = \frac{T_S \, N_S \left(\dfrac{d\sigma_{\text{coh}}}{d\Omega} + \dfrac{d\sigma_{\text{inc}}}{d\Omega} \right)}{T_{St} \, N_{St} \, \dfrac{d\sigma^{St}_{\text{inc}}}{d\Omega}} \tag{12.5}$$

$$\Leftrightarrow \qquad \frac{d\sigma_{\text{coh}}}{d\Omega} + \frac{d\sigma_{\text{inc}}}{d\Omega} = \frac{I^0_{S,i}}{I^0_{St,i}} \, \frac{T_{St} \, N_{St}}{T_S \, N_S} \, \frac{d\sigma^{St}_{\text{inc}}}{d\Omega} \tag{12.6}$$

$$\text{or} \qquad \frac{d\sigma_{\text{coh}}}{d\Omega} + \frac{d\sigma_{\text{inc}}}{d\Omega} = \frac{I^0_{S,i}}{I^0_{St,i}} \, \frac{(1 - T_{St}) \, \dfrac{A_{St}}{4\pi}}{T_S \, N_S}. \tag{12.7}$$

If water is used as a standard the last formula has to be multiplied on the right side with an empirical factor $f(\lambda, \sigma_t, T) \simeq 1$. This factor corrects for the different efficiencies

of the detector for different neutron energies. This correction can become important in case of water because of it inelastic scattering behavior.

12.2. Correction and normalization of SAXS raw data

History

2013-04-30: `SASfit` 0.93.4

- In the menue for confidence intervall the non-diagonal elements of correlation matrix are shown together with the confidence interval for the fitted parameters as digonal elements.
- added some addational parameters into the fit menue useful to evaluate the goodness of a fit
- new plugin for `Parallelepiped_abc` of dimension a*b*c to be found under `[by plugins|anisotropic obj]`
- new plugin for `generalized Guinier law` to be found under `[by plugins|non-particular structures]`
- Renamed HMI format into BerSANS format and did some debugging. Now also all masked data points (negative errors) are ignored.
- added key bindings `Home`, `End`, `PgUp`, `PgDn`, `Insert`, `Delete` for going to first-last-next-previous entry or to add and remove an entry
- adding plugin with a series of form factor for strongly anisotropic structures with local planar and local cylindrical shapes
- adding a new plugin form factor for spheres with fuzzy interfaces. The existing form factors `ExpShell`, `LinShell` and `LinShell2` have been moved to this plugin.
- New plugin of `FuzzySphere` and `CoreShellMicrogel`. Also the related functions for calculating the corresponding radial profiles have been added.
- new section in the manual about absolute scale, molecular weight, etc.
- for the form factors `flat cylinder` `long cylinder`, and `Porod cylinder` the limiting case $q \equiv 0$ is now treated properly
- small bug fix in the peak function `Gamma (Area)` for checking validity of parameter
- bug fix of the resolution parameter handling in case it will be read in from a data file
- included under peak function the `Maxwell` distribution and the `generalized Maxwell` distribution
- batch fitting

2011-05-04: `SASfit` 0.93.3

- bug fix in the model `Stacked Discs`. The structure factor describing the stacking order contained a bug.
- extended plugin for stroboscopic measurements, especially for `TISANE`
- plotting: ignore negative y values on log() and sqrt() scales
- included `Pcs_homogeneousCyl` form factor
- bug fix of `ferrofluid plugin`
- added radial averaged form factor in `ferrofluid plugin`
- extended the spline plugin to be used also as form factors. In case somebody wants to fit a spline function to e.g. a TEM size distribution, this function need to be available as a form factor and not only as a size distribution.
- added configuration file `config.ini` as replacement for deprecated `sasfit_init_public.tcl`

- added switch for disabling `About` popup at start time via config file
- added checkbox (ascii options) for ignoring zero(0) intensity at the beginning of data
- removed , as data column separator
- added substitution of , ⇒ . for data columns (german decimal format to english format)
- added interface function for covariance matrix output
- covar matrix visualisation with parameter highlighting
- added a chapter about particle number densities, volume fraction and absolute intensities in the manual.
- `LogNorm_fp` size distribution is now plugin function. The new plugin is not backwards compatible. The manual explains a bit the difficulties in describing the size distribution in terms of a volume fraction.
- added scrollbars for fit parameter window

2010-07-08: `SASfit` 0.93.2

- bug fix in ferrofluid plugin
- added radial averaged form factor. Included radial averaged form factors also for SAW model
- Extended the spline plugin to be used also as form factors. In case somebody wants to fit a spline function to a size distribution, this function needs to be available as a form factor and not only as a size distribution.
- forwarding intermediate linear Guinier approximation results to the plot window (green curve)
- display of linear Guinier approximation results in `ISP` text output window
- residuum window updated with linear Guinier approximation residuum
- by default disabled, see checkbox in `ISP` window
- fixed `SLDCalculator` in source package (missing data files)
- added `KNOWN_BUGS.txt` (not complete)
- optical (layout) GUI improvements:
  - removed thick margin around text boxes for ISP/analyt results
  - added resizeable file list in `ISP` window
  - added resizeable 'merge files' list when loading data files
- added menu-¿tools-¿toggle console to show the console, it is hidden by default now
- added `OPTIM` parameter to `src/CMakeLists.txt` for optimized binary generation on the underlying hardware, use: '`cmake -DOPTIM=TRUE`'
- added configuration file `config.ini` as (working) replacement for deprecated `sasfit_init_public.tcl`
- added switch for disabling 'about' popup at start time via config file
- added switch to set the default data directory
- added checkbox (ascii options) for ignoring zero(0) intensity at the beginning of data

2010-05-13: SASfit 0.93.1

removed obsolete print menu entries and fix of textual output bug

2010-05-05: `SASfit` 0.93.0

- copy&paste-able text output, as well as `csv` export (semicolon separated) for
  - integral structural parameters (ISP) data
  - parameters of contributions
  - moments of size distribution
- improved/rewritten file selection GUI for ISP series fitting
- new and improved plugins: `Kratky Sphere`, `JuelichCoreShell` (rewritten), `Langevin`
- data is always plotted first, below the calculated lines
- error bars are drawn behind data points
- fixed wrong plotting of very large error bars
- for log-plotting on the y-axis, negative data is ignored (not plotted, was abs() before)
- fix to prevent the user from loading a `SASfit` project file as data
- fix in Form-Factor `Background` (improved numerical stability)
- bug fix for saving parameter files on windows
- bug fix in gui when selecting form factor `TwoAttachedSpheres`
- bug fix for "Singular Matrix" error

2010-01-02: `SASfit` 0.92.3

- implemented three different versions for worm like chains as described in Macromolecules 1996, 29, 7602-7612. They have been implemented as structure factors `[anistropic obj|P'(Q):local cylindrical geometry]`, so that it can be combined with different cross-section form factors of local cylindrical objects `[anisotropic obj.|Pcs(Q) for cylindrical obj.]`.
- new form factor plugin for a sphere with 3 shells
- new structure factor for a regular cluster up to maximal 5 particle (tetrahedron like)
- correction of menue entry order for magnetic shell and superparamagnetic shell
- new plugin for ferrofluid particles with a scheme similar to the one of J.S. Pedersen for Gaussian Chains attached to a spherical particle
- bug fix in `mMemberedTwistedRing`
- two more default plot: `Guinier (rods)` and `Guinier (sheets)`
- bug fix in `loglogistic` peak
- implementation of asymptotic limits for fractals, which require a numerical integration. The integration often fails for large q-values for which an asymptotic solution is available or has been constructed.
- reprogrammed `SquareWell1` structure factor for a squared well potential
- replaced `sasfit_qromb` function by `sasfit_integrate` function in the form factor for the torus. The `sasfit_qromb` routine did not work for some unknown reason. This needs to be checked.
- new structure factor for a thin square well potential
- bug fix in `BeaucageExpPowLaw2`
- Bug fix for setting plot option `Holtzer` in multiple data set tab

- public initialization file `sasfit_init_public.tcl` for setting the default working directory by the user to any path

2009-10-08: `SASfit` 0.92.2

- data reduction without data loss, after loading a project file the data reduction can be reversed
- info message about a guessed error bar is displayed only once when the ascii options are changed (not for every file)
- added tooltip for complete filenames in merge window
- color for selected fit region stays at dark grey after loading an old project file
- removed unused help buttons in file open dialogs
- fixed error loop when adding new data to previously loaded project file
- fix for a homedir being e.g. 'U:át startup on Windows
- minor correction in the routine to guess the error bar (normalization) when only two column are supplied
- fix of rare error "form factor param out of range: -1"

13th of September: `SASfit` 0.92.1

- fix for GUI problem with two plugin form factors (contribution updates). If there are two plugin model functions with a different number of parameters, you can't switch/cycle trough the contributions anymore (Next, Previous).
- fix for saving a parameter file (file creation was disabled by accident in previous version)

8.7.2009: `SASfit` 0.91.1: Since the previous version of `SASfit` (0.90.1, January 2009) there were a lot of changes to primarily improve the quality and portability of the code. Here is only a short summary of the larger changes done:

- added detailed documentation on setup and installation of `SASfit` , as well as plugin development (how to add own model functions)
- fixed some bugs in plugin framework
- added automatic determination of available plugins at build time
- enabled static building for plugins
- increasing maximum number of model parameter in GUI
- verified build compatibility for MacOS
- Extended and improved Scattering Length Density (SLD) Calculator. Now the scattering length density for x-ray energies between 1keV and 24.9 keV can be calculated.
- a few new form factor have been included: `generalized Gaussian coil`, `generalized Gaussian coil 1`, `generalized Gaussian coil 2`, `ellCylShell1`, `ellCylShell2`

12.01.2009: `SASfit` 0.90.1 : bug-fix in plugin-GUI

5.01.2009: `SASfit` 0.90: new release including full source code and binaries for windows and linux. Since the previous version of v (0.87, March 2008) there were a lot of changes to primarily improve the quality and portability of the code. Here only a short summary of the 'big' changes done (as of Dec. 17th, 2008):

(1) Structured the source code into the modules `sasfit_common`, `sasfit_sd`, `sasfit_sq`, `sasfit_ff`, `sasfit_core`.

(2) Switched to `CMake` build environment for platform independence. Build and tested `SASfit` on Linux and Windows, 32bit as well as 64bit.
(3) Replaced intensive string comparisons for model function selection in each iteration step by more reasonable selection of functions pointers at initialization time and direct call of the according function at iteration time.
(4) Fixed a lot of bugs and typos in the GUI (but there are still some)
(5) Added flexible plugin system for external model functions. This way, all model functions can be provided as plugins and though move out of the core algorithms. Also enables easy customization. In the future the modules `sasfit_sd`, `sasfit_sq`, `sasfit_ff` and `sasfit_peaks` will be converted to external plugins.
(6) Added `sasfit_peaks`, a new class of model functions containing peaks.
(7) Added capability to ship `SASfit` as standalone executable, allows running on system without the need of external libraries (e.g. Tcl, BLT, ...)

4.03.2008: (`SASfit` version 0.87) The last modification in the menu navigation still had bugs. Hopefully they are removed in this version.

28.02.2008: (`SASfit` version 0.86) The menu navigation has been debugged and optimized. Corrected a bug in calculating the polydispersity index (PDI) in DLS cumulant analysis (PDI=Gamma2/Gamma1^2)

25.01.2008: (`SASfit` version 0.85) A bug for the form factors `ROD+R^-a*` has been corrected. The implementation of the scaling approximation, partial structure factors and local monodisperse approach has been improved.

9.01.2008: (`SASfit` version 0.84) Form factor for worm-like micelles (`WORM+Chains(RW)`, `WORM+Chains(RW)_Rc`, `WORM+Chains(RW)_Nagg`) and for cluster aggregates (`Mass Fractal (Exp(-x) Cut-Off)`, `Fisher-Burford`, `MassFractExp`,`MassFractGauss`, `Mass Fractal (Exp(-x^a) Cut-Off)`, `DLCAggregation`, `RLCAggregation`, `MassFractOverlappingSph` have been implemented. Furthermore a simple scheme for importing data from the clipboard has been implemented, which e.g. allows to copy/paste data from spread-sheets directly into `SASfit`. Corrected a bug for the form factors `ROD+R^-a*`

4.10.2007: (SPHERE+Chains(RW), SPHERE+Chains(RW)_Rc, SPHERE+Chains(RW)_Nagg`SASfit` version 0.80) Next to the correction of some bugs a simulation option for multiple data sets has been implemented. Furthermore an option has been implemented to subtract a theoretical scattering contribution from the experimental data set, like e.g. a constant background signal. The format of the project files have up to now never been tested for compatibility. An attempt has been started to change this for the future versions.

20.8.2007: A couple of form factors for spherical, elliptical, cylindrical and very long rod-like micelles consisting of a homogeneous core and which are either grafted with Gaussian chains `*(RW)*`, or grafted with semi-flexible self-avoiding and interacting chains `*(SAW)*` or a corona with a power-law decaying profile $r^{-\alpha}$ `*(R^-a)*` have been implemented: `SPHERE+Chains(RW)`, `SPHERE+Chains(RW)_Rc`, `SPHERE+Chains(RW)_Nagg`, `SPHERE+Chains(SAW)`, `SPHERE+Chains(SAW)_Rc`,

SPHERE+Chains(SAW)_Nagg, SPHERE+R^-a, SPHERE+R^-a_Rc, SPHERE+R^-a_Nagg, ELL+Chains(RW), ELL+Chains(RW)_Rc, ELL+Chains(RW)_Nagg, CYL+Chains(RW), CYL+Chains(RW)_Rc, CYL+Chains(RW)_Nagg, ROD+Chains(RW), ROD+Chains(RW)_Rc, ROD+Chains(RW)_nagg, ROD+R^-a, ROD+R^-a_Rc, ROD+R^-a_nagg

30.6.2007: Rudimental copy algorithm to copy plots or parameters into window-clipboard. Everything is copied in wmf-format and the option only works fine for information in non-scrolled widgets. Copy-option can be activated with right mouse button or double click of left mouse button. A triaxial ellipsoidal (`triaxEllShell`) shell with semiaxis `a`, `b`, `c` and shell thickness `t` is available.

4.6.2007: Implementation of form factors for cylindrical shells with circular cross-section and capped ends (`CylShell2`) and without capped ends (`CylShell1`) together with an approximation for very long cylindrical shells (`LongCylShell`)

27.3.2007: Implementation of form factors for bi-continuous systems (`TeubnerStrey` and `DAB`)

23.2.2007: Implementation of the structure factor for a system of charged, spheroidal objects in a dielectric medium according to the RMSA model of Hayter and Penfold

11.11.2006: Implementation of a semiflexible polymer according to Kholodenko, some form factors with plane geometry, which are intended to be used with lamellar structure factors (`homogenousXS`, `TwoInfinitelyThinPlates`, `LayeredCentroSymmetricXS`, `BiLayerGauss`), a sphere with Gaussian chains attached `SphereWithGaussChains` and a slightly different parametrised form factor named `BlockCopolymerMicelle`. An additional option for reading ASCII data files is now available, which allows to convert values for the scattering vector from nm^{-1} into $Å^{-1}$ and vice versa.

23.10.2006: Implementation of a polydsiperse star `PolydisperseStar` and of flexible ring polymers `FlexibleRingPolymer` and `mMemberedTwistedRing`.

22.10.2006: Implementation of the form factor of a flexible polymer with Gaussian statistics (in different parameterisations `Gauss`, `Gauss2`, `Gauss3`) for a polydisperse flexible polymer with Gaussian statistics (`GaussPoly`) and a flexible ring of polymer with Gaussian statistics (`FlexiblePolymerRing`)

12.10.2006: Under the menu option `Calc/DLS...` next to a cumulant fit also a double stretched exponential decay can be selected to fit dynamic light scattering data.

5.10.2006: Implementation of a spherical shell with a diffuse (expontential) scattering length density profile inside the shell caused by solvent penetration into the shell

13.9.2006: Implementation of a form factor for spheres with gaussian chains attached.

19.7.2006: First release (current version: 0.71) at the moment only a windows version is available. The installation files for tcl/tk and blt are included in the distribution file.

Bibliography

[1] N. W. Ashcroft and L. Lenker. Structure and resistivity of liquid metals. *Physical Review*, 145(1):83–90, May 1966.

[2] B. Barboy. On a representation of the equation of state of fluids in terms of the adhesive hard-sphere model. *J. Chem. Phys.*, 61(8):3194–3196, 1974.

[3] R.J. Baxter. Percus-yevick equation for hard spheres with surface adhesion. *J. Chem. Phys.*, 49(6):2770–2774, 1968.

[4] G. Beaucage. Approximations leading to a unified exponential/power-law approach to small-angle scattering. *J. Appl. Cryst.*, 28:717–728, 1995.

[5] G. Beaucage. Small-angle scattering from polymeric mass fractals of arbitrary mass-fractal dimension. *J. Appl. Cryst.*, 29:134–146, 1996.

[6] H. Benoit. On the effect of branching and polydispersity on the angular distribution of the light scattered by gaussian coils. *J. Polym. Sci.*, 11:507–510, 1953.

[7] Ingo Berndt, Jan Skov Pedersen, Peter Lindner, and Walter Richtering. Influence of shell thickness and cross-link density on the structure of temperature-sensitive poly-n-isopropylacrylamidepoly-n-isopropylmethacrylamide coreshell microgels investigated by small-angle neutron scattering. *Langmuir*, 22(1):459–468, 2006. PMID: 16378460.

[8] Ingo Berndt, Jan Skov Pedersen, and Walter Richtering. Structure of multiresponsive intelligent? coreshell microgels. *Journal of the American Chemical Society*, 127(26):9372–9373, 2005. PMID: 15984856.

[9] Ingo Berndt, Jan Skov Pedersen, and Walter Richtering. Temperature-sensitive coreshell microgel particles with dense shell. *Angewandte Chemie*, 118(11):1769–1773, 2006.

[10] Philip Bevington and D. Keith Robinson. *Data Reduction and Error Analysis for the Physical Sciences*. McGraw-Hill, 3rd edition, 23 July 2002. ISBN-10: 0072472278, ISBN-13: 978-0072472271.

[11] A. E. Blaurock. Evidence of bilayer structure and of membrane interactions from x-ray diffraction analysis. *Biochimica et Biophysica Acta (BBA) - Reviews on Biomembranes*, 650(4):167 – 207, 1982.

[12] C.F. Bohren and D.R. Huffman. *Absorption and Scattering of Light by Small Particles*. Wiley, New York, 1983.

[13] M. Born and H. S. Green. A general kinetic theory of liquids I. The molecular distribution functions. *Proc. Roy. Soc.*, A188:10–18, 1946.

[14] W. Burchard. Statistics of star-shaped molecules. i. stars with polydisperse side chains. *Macromolecules*, 7:835–841, 1974.

[15] W. Burchard, E. Michel, and V. Trappe. Conformational properties of multiply twisted ring systems and daisy-like structures. *Macromolecules*, 29(18):5934–5939, 1996.

[16] A. Caille. X-ray scattering in smectic a. *Comptes Rendus des Seances de l'Academie des Sciences, Serie B: Sciences Physiques*, 274:891–893, 1972.

[17] G. Damaschun, H.-V. Porschel, and G. Sommer. Bestimmung der Gestalt gelöster Makromoleküle aus Röntgen-Kleinwinkeldiagrammen mit Hilfe von Gleichungssystemen. *Acta Cryst.*, A25:708, 1969.

[18] G. Damaschun and H.-V. Pürschel. Röntgen-Kleinwinkelstreuung von isotropen Proben ohne Fernordnung. I. Allgemeine Theorie. *Acta Crystallographica Section A*, 27(3):193–197, May 1971.

[19] M. Daoud and J.P. Cotton. Star shaped polymers - a model for the conformation and its concentration-dependence. *Journal de Physique (Paris)*, 43:531, 1982.

[20] W. I. F. David. Powder diffraction peak shapes. parameterization of the pseudo-voigt as a voigt function. *Journal of Applied Crystallography*, 19(1):63–64, Feb 1986.

[21] C. G. de Kruif, P. W. Rouw, W. J. Briels, M. H. G. Duits, A. Vrij, and R. P. May. Adhesive hard-sphere colloidal dispersions. a small-angle neutron-scattering study of stickiness and the structure factor. *Langmuir*, 5:422–428, 1989.

[22] P. Debye. Über die Zerstreuung von Röntgenstrahlen an amorphen Körpern. *Physik. Z.*, 28:135–141, 1927.

[23] P. Debye. Mollecular-weight determination by light scattering. *Journal of Physical and Colloid Chemistry*, 51:18–32, 1947.

[24] P. Debye, R. Anderson, and H. Brumberger. Scattering by an inhomogeneous solid. ii. the correlation function and its application. *Journal of Applied Physics*, 28(6):679, 1957.

[25] P. Debye and A.M. Bueche. Scattering by an inhomogeneous solid. *Journal of Applied Physics*, 20:518–525, 1949.

[26] W. D. Dozier, J. S. Huang, and L. J. Fetters. Colloidal nature of star polymer dilute and semidilute solutions. *Macromolecules*, 24(10):2810–2814, 1991.

[27] L. A. Feigin and D. I. Svergun. *Structure Analysis by Small-Angle X-ray and Neutron Scattering*. Plenum Press, 1987.

[28] S. Förster, N. Hermsdorf, C. Böttcher, and P. Lindner. Structure of polyelectrolyte block copolymer micelles, macromolecules. *Macromolecules*, 35:4096–4105, 2002.

[29] S. Förster, N. Hermsdorf, W. Leube, H. Schnablegger, M. Regenbrecht, S. Akari, P. Lindner, and C. Böttcher. Fusion of charged block copolymer micelles into toroid networks. *J. Phys. Chem. B*, 103:6657–6668, 1999.

[30] Peter Fratzl. Statistical model of the habit and arrangement of mineral crystals in the collagen of bone. *Journal of Statistical Physics*, 77(1-2):125–143, 1994.

[31] Thomas Frühwirth, Gerhard Fritz, Norbert Freiberger, and Otto Glatter. Structure and order in lamellar phases determined by small-angle scattering. *Journal of Applied Crystallography*, 37(5):703–710, Oct 2004.

[32] H. Furukawa. Dynamics-scaling theory for phase-separating unmixing mixtures: Growth rates of droplets and scaling properties of autocorrelation functions. *Physica A*, 123:497, 1984.

[33] Domenico Gazzillo, Achille Giacometti, Raffaele Guido Della Valle, Elisabetta Venuti, and Flavio Carsughi. A scaling approximation for structure factors in the integral equation theory of polydisperse nonionic colloidal fluids. *The Journal of Chemical Physics*, 111(16):7636–7645, 1999.

[34] O. Glatter. Data evaluation in small angle scattering: Calculation of the radial electron density distribution by means of indirect Fourier transformation. *Acta Physica Austriaca*, 47:83–102, 1977.

[35] Georg S. Greschner. Mathematical properties of polydisperse systems, 2. application to light scattering. *Die Makromolekulare Chemie*, 170(1):203–229, 1973.

[36] A. Guinier. *X-ray Diffraction*. San Francisco: Freeman, 1963.

[37] A. Guinier and G. Fournet. *Small-Angle Scattering of X-Rays*. John Wiley & Sons, Inc., 1955.

[38] W. C. Hamilton. Significance tests on the crystallographic R factor. *Acta Crystallographica*, 18(3):502–510, Mar 1965.

[39] B. Hammouda. the sans toolbox. . . . /the_SANS_toolbox.pdf.

[40] H. J. M. Hanley, C. D. Muzny, D. L. Ho, and C. J. Glinka. A small-angle neutron scattering study of a commercial organoclay dispersion. *Langmuir*, 19(14):5575–5580, 2003.

[41] J.P. Hansen and J.B. Hayter. A rescaled msa structure factor for dilute charged colloidal dispersions. *Molecular Physics*, 46:651–656, 1982.

[42] J. B. Hayter and J. Penfold. Use of viscous shear alignment to study anisotropic micellar structure by small-angle neutron scattering. *J. Phys. Chem.*, 88:4589–4593, 1984.

[43] J.B. Hayter and J. Penfold. An analytic structure factor for macroion solutions. *Molecular Physics*, 42:109–118, 1981.

[44] O. Hittmair. *Lehrbuch der Quantentheorie*. Verlag Karl Thiemig, 1972.

[45] Rex P. Hjelm, Claudio Schteingart, Alan F. Hofmann, and Devinderjit S. Sivia. Form and structure of self-assembling particles in monoolein-bile salt mixtures. *J. Phys. Chem.*, 99:16395–16406, 1995.

[46] Rex P. Hjelm, Claudio D. Schteingart, Alan F. Hofmann, and P. Thiyagarajan. Structure of conjugated bile salt-fatty acid-monoglyceride mixed colloids: Studies by small-angle neutron scattering. *J. Phys. Chem. B*, 104:197–211, 2000.

[47] Rex P. Hjelm, P. Thiyagarajan, and Hayat Alkan-Onyuksel. Organization of phosphatidylcholine and bile salt in rodlike mixed micelles. *J. Phys. Chem*, 96:8653–8661, 1992,.

[48] R. Hosemann and S.N. Bagchi. *Direct Analysis of Diffraction by Matter*. Amsterdam: North-Holland., 1962.

[49] A.J. Hurd and W.L. Flower. In situ growth and structure of fractal silica aggregates in a flame. *Journal of Colloid and Interface Science*, 122(1):178–192, 1988.

[50] T. Ida, M. Ando, and H. Toraya. Extended pseudo-voigt function for approximating the voigt profile. *Journal of Applied Crystallography*, 33(6):1311–1316, Dec 2000.

[51] Takeshi Kawaguchi. Radii of gyration and scattering functions of a torus and its derivatives. *J. Appl. Cryst.*, 34:580–584, 2001.

[52] Håkon Kaya. Scattering from cylinders with globular end-caps. *Journal of Applied Crystallography*, 37(2):223–230, Apr 2004.

[53] Håkon Kaya and Nicolas-Raphaël de Souza. Scattering from capped cylinders. Addendum. *Journal of Applied Crystallography*, 37(3):508–509, Jun 2004.

[54] A. L. Kholodenko. Analytical calculation of the scattering function for polymers of arbitrary flexibility using the dirac propagator. *Macromolecules*, 26:4179–4183, 1993.

[55] M. Kotlarchyk and S.-H. Chen. Analysis of small angle neutron scattering spectra from polydisperse interacting colooids. *J. Chem. Phys*, 79(5):2461–2489, 1983.

[56] O. Kratky and G. Porod. Diffuse small-angle scattering of x-rays in colloid systems. *Journal of Colloid Science*, 4(1):35 – 70, 1949.

[57] M.Y. Lin, H.M. Lindsay, D.A. Weitz, R.C. Ball, R. Klein, and P. Meakin. Universality of fractal aggregates as probed by light scattering. *Proc. R. Soc. Lond. A*, 423:71–87, 1989.

[58] M.Y. Lin, H.M. Lindsay, D.A. Weitz, R.C. Ball, R. Klein, and P. Meakin. Universal diffusion-limited colloid aggregation. *J. Phys.: Condens. Matter*, 2:3093–3113, 1990.

[59] M.Y. Lin, H.M. Lindsay, D.A. Weitz, R.C. Ball, R. Klein, and P. Meakin. Universal reaction-limited colloidal aggregation. *Physical Review A*, 41(4):2005–2020, 1990.

[60] Yuyan Liu, Jieli Lin, Guangming Huang, Yuanqing Guo, and Chuanxi Duan. Simple empirical analytical approximation to the voigt profile. *J. Opt. Soc. Am. B*, (5):666–672, 2001.

[61] Yulia Lyatskaya, Yufeng Liu, Stephanie Tristram-Nagle, John Katsaras, and John F. Nagle. Method for obtaining structure and interactions from oriented lipid bilayers. *Phys. Rev. E*, 63(1):011907, Dec 2000.

[62] S.V.G. Menon, V.K. Kelkar, and C. Monohar. Application of baxters model to the theory of cloud points of nonionic surfactant solutions. *Physical Review A*, 43(2):1130–1133, 1991.

[63] S.V.G. Menon, C. Manobar, and K. Srinivasa Rao. A new interpretation of a sticky hard sphere model. *J. Chem. Phys.*, 95(12):9186–9190, 1991.

[64] G. Mie. Beiträge zur Optik trüber Medien, speziell kolloidaler Metallösungen. *Annalen der Physik*, 25:377–455, 1908.

[65] J. Möller, R. Kranold, J. Schmelzer, and U. Lembke. Small-Angle X-ray Scattering Size Parameters and Higher Moments of the Particle-Size Distribution Function in the Asymptotic Stage of Ostwald Ripening. *Journal of Applied Crystallography*, 28(5):553–560, Oct 1995.

[66] R. M. Moon, T. Riste, and W. C. Koehler. Polarization analysis of thermal-neutron scattering. *Physical Review*, 181(2):920–931, May 1969.

[67] F. Müller, M. Delsanti, L. Auvray, J. Yang, Y.J. Chen, J.W. Mays, B. Dem, M. Tirrell, , and P. Guenoun. Ordering of urchin-like charged copolymer micelles: Electrostatic, packing and polyelectrolyte correlations. *Eur. Phys. J. E*, 3:45–53, 2000.

[68] Online Dictionary of crystallography. R factor. http://reference.iucr.org/dictionary/R_factor.

[69] J. J. Olivero and R. L. Longbothum. Empirical fits to the voigt line width: A brief review. *J. Quant. Spectrosc. Radiat. Transfer*, 17(233-236):1298, 1977.

[70] G. Pabst, R. Koschuch, B. Pozo-Navas, M. Rappolt, K. Lohner, and P. Laggner. Structural analysis of weakly ordered membrane stacks. *Journal of Applied Crystallography*, 36(6):1378–1388, Dec 2003.

[71] Georg Pabst, Michael Rappolt, Heinz Amenitsch, and Peter Laggner. Structural information from multilamellar liposomes at full hydration: Full q -range fitting with high quality x-ray data. *Phys. Rev. E*, 62:4000–4009, Sep 2000.

[72] J. S. Pedersen, D. Posselt, and K. Mortensen. Analytical treatment of the resolution function for small-angle scattering. *Journal of Applied Crystallography*, 23(4):321–333, Aug 1990.

[73] J. S. Pedersen and P. Schurtenberger. Scattering functions of semiflexible polymers with and without excluded volume effects. *Macromolecules*, 29:7602–7612, 1996.

[74] Jan Skov Pedersen. *Neutrons, X-Rays and Light*, chapter Modelling of Small-Angle Scattering Data from Colloids and Polymer Systems, pages 391–420. Elsevier Science, 2002.

[75] Jan Skov Pedersen and Michael C. Gerstenberg. Scattering form factor of block copolymer micelles. *Macromolecules*, 29(4):1363–1365, 1996.

[76] J.S. Pedersen. Form factors of block copolymer micelles with spherical, ellipsoidal and cylindrical cores. *Journal of Applied Crystallography*, 33(3 Part 1):637–640, Jun 2000.

[77] .S. Pedersen. Determination of size distributions from small-angle scattering data for systems with effective hard-sphere interactions. *J. Appl. Cryst.*, 27:595–608, 1994.

[78] J. K. Percus and G. J. Yevick. Analysis of classical statistical mechanics by means of collective coordinates. *Phys. Rev.*, 110(1):1–13, 1958.

[79] Horia I. Petrache, Nikolai Gouliaev, Stephanie Tristram-Nagle, Ruitian Zhang, Robert M. Suter, and John F. Nagle. Interbilayer interactions from high-resolution x-ray scattering. *Phys. Rev. E*, 57(6):7014–7024, Jun 1998.

[80] G. Porod. Die Abhängigkeit der Röntgenkleinwinkelstreuung von Form und Grösse der Kolloiden Teilchen in verdünnten Systemen, IV. *Acta Physica Austriaca*, 2:255–292, 1948.

[81] William H. Press, Saul A. Teukolsky, William T. Vetterling, and Brian P. Flannery. *Numerical Recipes. The Art of Scientific Computing*. Cambridge University Press, 3rd edition, 2007.

[82] C. V. Raman. Lxi. on the mean distance between neighbouring molecules in a fluid. *Phil. Mag.*, 47:671–679, 1924.

[83] C. Regnaut and J. C. Ravey. Application of the adhesive sphere model to the structure of colloidal suspensions. *The Journal of Chemical Physics*, 91(2):1211–1221, 1989.

[84] C. Regnaut and J. C. Ravey. Erratum: Application of the adhesive sphere model to the structure of colloidal suspensions [j. chem. phys. 91, 1211 (1989)]. *The Journal of Chemical Physics*, 92(5):3250–3250, 1990.

[85] C. Robertus, W.H. Philipse, J.G.H. Joosten, and Y.K. Levine. Solution of the percus-yevick approximation of the multicomponent adhesive sphere system to the small angle x-ray scattering from microemulsions. *J. Chem. Phys.*, 90(8):4482–4490, 1989.

[86] D. Roux and C.R. Safinya. A synchrotron x-ray study of competing undulation and electrostatic interlayer interactions in fluid multimembrane lyotropic phases. *J. Phys. France*, 49(2):307–318, 1988.

[87] K.-V. Schubert, R. Strey, S. R. Kline, and E. W. Kaler. Small angle neutron scattering near lifshitz lines: Transition from weakly structured mixtures to microemulsions. *J. Chem. Phys.*, 101:5343, 1994.

[88] S. Schwartz, J.E. Cain, E.A. Dratz, and J.K. Blasie. An analysis of lamellar x-ray diffraction from disordered membrane multilayers with application to data from retinal rod. *Biophysical Journal*, 15:1201 – 1233, 1975.

[89] R. V. Sharma and K. C. Sharma. The structure factor and the transport properties of dense fluids having molecules with square well potential, a possible generalization. *Physica A: Statistical and Theoretical Physics*, 89(1):213 – 218, 1977.

[90] B. Sjöberg. Small-angle X-ray investigation of the equilibria between copper(II) and glycyl-L-histidylglycine in water solution. A method for analysing polydispersed systems. *Journal of Applied Crystallography*, 7(2):192–199, Apr 1974.

[91] C. M. Sørensen, J. Cai, and N. Lu. Test of static structure factors for describing light scattering from fractal soot aggregates. *Langmuir*, 8:2064–2069, 1992.

[92] C. M. Sørensen and G. M. Wang. Size distribution effect on the power law regime of the structure factor of fractal aggregates. *Physical Review E*, 60(6):7143–7148, 1999.

[93] G. L. Squires. *Thermal Neutron Scattering*. Cambridge University Press, 1978.

[94] Markus Stieger, Jan Skov Pedersen, Peter Lindner, and Walter Richtering. Are thermoresponsive microgels model systems for concentrated colloidal suspensions? a rheology and small-angle neutron scattering study. *Langmuir*, 20(17):7283–7292, 2004. PMID: 15301516.

[95] Carsten Svaneborg and Jan Skov Pedersen. Form factors of block copolymer micelles with excluded-volume interactions of the corona chains determined by monte carlo simulations. *Macromolecules*, 35(3):1028–1037, 2002.

[96] M. Teubner and R. Strey. Origin of the scattering peak in microemulsions. *J. Chem. Phys.*, 87:3195, 1987.

[97] O. Toon and T. Ackerman. Algorithms for the calculation of scattering by stratified spheres. *Applied Optics*, 20(20):3657, 1981.

[98] P. van Beurten and A. Vrij. Polydispersity effects in the small-angle scattering of concentrated solutions of colloidal spheres. *J. Chem. Phys.*, 74(5):2744–2748, March 1981.

[99] H.C. van de Hulst. *Light Scattering by Small Particles*. Wiley, New York, 1957.

[100] C. G. Vonk. On two methods for determination of particle size distribution functions by means of small-angle x-ray scattering. *J. Appl. Cryst.*, 9:433–440, 1976.

[101] A. Vrij. Mixtures of hard spheres in the percus-yevick approximation. light scattering at finite angles. *J. Chem. Phys.*, 71(8):3267–3270, 1979.

[102] G. Walter, R. Kranold, T. Gerber, J. Baldrian, and M. Steinhart. Particle size distribution from small-angle X-ray scattering data. *Journal of Applied Crystallography*, 18(4):205–213, Aug 1985.

[103] C. M. Wijmans and E. B. Zhulina. Polymer brushes at curved surfaces. *Macromolecules*, 26:1214–7224, 1993.

[104] L. Willner, A. Poppe, J. Allgaier, M. Monkenbusch, P. Lindner, and D. Richter. Micellization of amphiphilic diblock copolymers: Corona shape and mean-field to scaling crossover. *EPL (Europhysics Letters)*, 51(6):628, 2000.

[105] W. Wiscombe. Mie scattering calculations–advances in technique and fast, vector-speed computer codes, ncar tech note tn-140+str. Technical report, National Center For Atmospheric Research, Boulder, Colorado, 1979.

[106] W. Wiscombe. Improved mie scattering algorithms. *Appl. Opt.*, 19:1505–1509, 1980.

[107] F. Zernike and J. A. Prins. Die Beugung von Röntgenstrahlen in Flüssigkeiten als Effekt der Molekülanordnung. *Zeitschrift für Physik*, XLI:184–194, 1927.

[108] Ruitian Zhang, Robert M. Suter, and John F. Nagle. Theory of the structure factor of lipid bilayers. *Phys. Rev. E*, 50(6):5047–5060, Dec 1994.

[109] Bruno H. Zimm. The scattering of light and the radial distribution function of high polymer solutions. *The Journal of Chemical Physics*, 16(12):1093–1099, 1948.